annual progress report

2009

ENERGY STORAGE RESEARCH AND DEVELOPMENT

EPARTMENT OF ENERGY | Energy Ef i iency & Renewable Energy

U.S. Department of Energy
1000 Independence Avenue, S.W.
Washington, D.C. 20585-0121

FY 2009
ANNUAL PROGRESS REPORT FOR
ENERGY STORAGE R&D

January 2010

Approved by David Howell, Hybrid Electric Systems Team Lead

Table of Contents

List of Figures

List of Tables

I

Introduction

A. Vehicle Technologies Program Overview

B. Energy Storage Research & Development

I. INTRODUCTION

In 2009, U.S. consumers and particularly the worldwide auto industry experienced one of the largest downturns in generations. 2009 U.S. light duty vehicle sales declined almost 26 percent compared to 2008. Sales of hybrids were on course to decline approximately 20 percent. As the auto industry rebounds overall, hybrid sales were showing continued strong performance. The U.S. government recognizes how critical a vibrant domestic auto industry is to the continued economic health of the country. As part of the American Recovery and Reinvestment Act (ARRA), on August 5, 2009, President Obama announced 48 advanced battery and electric drive projects that will receive $2.4 billion in funding[1]. These grants will accelerate the development of U.S. manufacturing capacity for batteries and electric drive components. The ARRA funding also supports PHEV and EV vehicle demonstration projects. A brief description of the battery manufacturing grants is presented in Chapter II.

In addition, several automakers announced plans to develop plug-in hybrid electric vehicles (PHEVs)[2] as well as full electric vehicles (EVs) or reconfirmed their previously announced plans. Specifically, the General Motors Chevrolet Volt PHEV40 continues on track to be released in late 2010, and Tesla, Mitsubishi and Nissan, among others, continue their development of more affordable EVs scheduled for release in 2010 or 2011.

An important step for the electrification of the nation's personal transportation is the development of more cost-effective, long lasting, and abuse-tolerant Li-ion batteries. The United States Department of Energy's (DOE's) continuing R&D into advanced batteries for transportation offers the possibility of reducing our dependence on foreign oil and the potential negative economic impacts of crude oil price fluctuations. It also supports the Administration's goal of deploying 1 million PHEVs by 2015. In FY2009, battery R&D work continued its expansion into high-energy batteries for PHEVs.

I.A Vehicle Technologies Program Overview

The DOE's Vehicle Technologies (VT) Program office works with industry, universities, and national laboratories to develop advanced transportation technologies that would reduce the nation's use of imported oil (almost 96 percent of the U.S. transportation fleet uses oil). Technologies being supported by VT include hybrid drive technologies, advanced energy storage devices (batteries and ultracapacitors), power electronics and motors, advanced structural materials, and advanced combustion engines and fuels, etc.

Collaboration with automakers enhances both the relevance and the potential for success of these programs. DOE works in partnership with the U.S. automakers through the United States Council for Automotive Research (USCAR)—an umbrella organization for collaborative research among Chrysler LLC, Ford Motor Company, and General Motors Corporation[3]. This partnership is focused on funding high-reward/high-risk research that promises improvements in critical components needed for more fuel efficient and cleaner vehicles.

I.B Energy Storage Research & Development Overview

I.B.1 Programmatic Structure

Energy storage technologies, including batteries and ultracapacitors, have been identified as critical enabling technologies for advanced, fuel-efficient, vehicles. The energy storage research and development effort within the VT Program is responsible for researching and improving advanced batteries and ultracapacitors for a wide range of vehicle applications, including HEVs, PHEVs, EVs, and fuel cell vehicles (FCVs). The office is working in close partnership with the automotive industry, represented by the United States Advanced Battery Consortium (USABC).

[1] http://www.whitehouse.gov/the_press_office/24-Billion-in-Grants-to-Accelerate-the-Manufacturing-and-Deployment-of-the-Next-Generation-of-U.S.-Batteries-and-Electric-Vehicles/

[2] http://www.greencarcongress.com/2007/07/toyota-to-obtai.html, http://www.gm-volt.com/

[3] For more information, please see http://www.uscar.org/guest/view_partnership.php?partnership_id=1.

The energy storage effort includes multiple activities – from hardware development with industry, to mid-term R&D and focused fundamental research. The activities begin by establishing technical requirements for the energy storage technologies by VT in cooperation with industry. Next, commercially available batteries are evaluated against those requirements. If requirements are unmet, additional R&D takes place, which involves either short-term directed research (applied research) by commercial developers and national laboratories, or exploratory research, generally by national laboratories and universities. The three energy storage R&D activities; *the Developer Program, Applied Battery Research*, and *Focused Fundamental Research*, are organized to complement each other.

The Developer Program's goal is to support the development of a U.S. domestic advanced battery industry whose products can meet the USABC technical goals. DOE works closely with industry to develop energy storage technologies for specific applications. The developer program includes *system development*, *technology assessments* and *benchmark testing*.

- In *system development*, DOE works with industry through cost-shared projects to develop electrochemical energy storage technologies which would meet FreedomCAR/USABC technical goals. The USABC provides technical and programmatic management of these projects, for which the cost is shared by the individual developer at a minimum level of 50 percent. The technologies include lithium-ion batteries, ultracapacitors, and separators (since separators usually contribute significantly to the total system cost). Additional R&D involves the thermal management issues for battery systems, which need to be addressed to avoid degradation in battery performance, reduced life, and greater likelihood of abusive conditions.
- *Technology assessments* are conducted on newly emerging technologies before developing full systems. The assessments typically represent 12-month projects to assess a developer's overall capabilities and are intended to validate the developer's technical claims.
- *Benchmark testing* of emerging technologies is important for remaining abreast of the latest industry developments. Battery technologies are evaluated according to the USABC Battery Test Procedures Manual (for EV batteries)[4], the Partnership for a New Generation of vehicles (PNGV) Battery Test Procedures Manual (for HEV batteries)[5], or the PHEV test procedure manual[6].

During earlier years and through FY 2008, an applied energy storage R&D activity entitled Applied Technology Development (ATD) was focused on assisting battery developers overcome the key barriers for the Li-ion battery technology in high-power HEV applications. Now Li-ion battery technologies have matured to a level where they could soon be introduced into the commercial HEV market. Therefore, ATD is now complete and the applied R&D program has now re-focused to Li-ion battery technologies for PHEV applications. This new program, denoted the *Applied Battery Research* (ABR) Program, was initiated on October 1, 2008. Its goal is to assist the industrial developers of Li-ion batteries overcome the key barriers for this technology in high-energy PHEV applications. Although this program is relatively new, there is general agreement on major barriers to using Li-ion batteries in PHEVs. Those include inadequate energy density and specific energy to meet the "charge-depleting" energy requirement, within the weight and volume constraints, for the 40-mile all-electric-range for a mid-size passenger PHEV and insufficient cycle life stability to achieve the 3,000 to 5,000 "charge-depleting" deep discharge cycles. The ABR program is headed by the Argonne National Laboratory and supported by several other national laboratories.

The *Focused Fundamental Research*, also called the Batteries for Advanced Transportation Technologies (BATT) activity, addresses the fundamental issues of chemistries and materials associated with lithium batteries. It emphasizes the identification and mitigation of failure modes, coupled with materials synthesis and evaluation, advanced diagnostics, and improved electrochemical models. Battery chemistries are monitored continuously with periodic substitution of more-promising components based on advice from within this activity, from outside experts, and from assessments of world-wide current battery R&D. The work is carried out by a team headed by the Lawrence Berkeley National Laboratory (LBNL) and involves ANL, Brookhaven National Laboratory (BNL), the National Renewable Energy Laboratory (NREL), Oak Ridge National Laboratory (ORNL), several universities, and a commercial entity.

In addition to the above, VT carefully coordinates efforts in the energy storage R&D area with other government agencies to maximize effectiveness and avoid any duplication of effort. Such efforts include membership and participation in the Chemical Working Group of the Interagency Advanced Power Group (IAPG), active participation in program

[4] United States Advanced Batteries Consortium, USABC Electric Vehicle Battery Test Procedure Manual, Rev. 2, U.S. Department of Energy, DOE/ID 10479, January 1996.
[5] U.S. Department of Energy, PNGV Battery Test Procedures Manual, Rev. 2, August 1999, DOE/ID-10597.
[6] United States Council for Automotive Research, RFP and Goals for Advanced Battery Development for Plug-in Electric Vehicles, http://www.uscar.org/.

reviews and technical meetings sponsored by other government agencies, and coordinating the participation of representatives from other government agencies in the contract and program reviews of DOE-sponsored efforts.

I.B.2 Some Recent Highlights

This section contains a few brief summaries of key technical accomplishments in FY 2009 resulting from the Energy Storage R&D effort working in partnership with the FreedomCAR and Fuel Partnership program. These accomplishments were selected from the many active projects and each represents a significant degree of accomplishment within the project, or the completion of a significant milestone, or a significant breakthrough of another kind that took place during the year.

Award of Grants under the American Recovery and Reinvestment Act of 2009 (NETL). The American Recovery and Reinvestment Act of 2009 (ARRA) (Public Law 111-5) is an economic stimulus package enacted by the 111th United States Congress in February 2009. As part of ARRA implementation, on August 5, 2009 President Obama announced $2.4 Billion in manufacturing grants to accelerate the manufacturing and deployment of the next generation of U.S. batteries and electric vehicles – by funding 48 new advanced battery and electric drive components manufacturing and electric drive vehicle deployment projects – including PHEV and EV demonstration and education projects – in over 20 states. The grantees were selected through a competitive process conducted by the DOE and are intended to accelerate the development of U.S. manufacturing capacity for batteries and electric drive components as well as the deployment of electric drive vehicles to help establish American leadership in developing the next generation of advanced vehicles. The new awards included $1.5 billion in grants to U.S. based manufacturers to produce batteries and their components and to expand battery recycling capacity, distributed over all parts of the country and these grants cover a range of manufacturing areas including those associated with material supply, cell components, cell fabrication, pack assembly, and recycling.[7]

BMW's Mild Hybrid to Use Battery Technology Developed with DOE Support, at Johnson Controls-Saft (JCS). JCS announced that it will provide lithium-ion batteries for production versions of BMW's 7 Series ActiveHybrid car, recently showcased at the Paris motor show. JCS will use new high-power cells, developed under several programs sponsored by the DOE and the USABC, in the BMW packs. The new cells are targeted for hybrid electric vehicle (HEV) and other high power applications according to a paper presented at the recent 1st International Conference on Advanced Lithium Batteries for Automobile Applications, held recently at Argonne National Laboratory. This contract is the second automotive lithium-ion production contract that uses cells developed with support of the DOE, the first being the packs for the Mercedes-Benz S400 BlueHYBRID.[8]

Completion and Publication of "Battery Life Estimator Manual" at the Idaho National Laboratory (INL). A recurring challenge to the commercialization of energy storage technologies in vehicle applications is the need to ensure their viability for the life of the vehicle, 10 or 15 years, usually too long for direct testing. The purpose of the Battery Life Estimator (BLE) Manual is to assist developers in their efforts to determine the calendar life capability of advanced battery technologies for automotive applications. Testing requirements and procedures have been previously defined in manuals published by the United States Advanced Battery Consortium (USABC). The Battery Life Estimator Manual describes a standardized method for determining battery calendar life with a high degree of statistical confidence based on models and degradation data acquired from typical battery testing. It was developed by experts from Idaho, Argonne, Sandia, and Lawrence Berkeley National Laboratories. A software package ("BatteryLife.exe") has also been developed to automate the estimation of calendar life based on the methodology.[9]

Development of New FreedomCAR/USABC Energy Storage Requirements for Lower-Energy Power Assists HEVs at the National Renewable Energy Laboratory (NREL). In support of FreedomCAR Technical Team, NREL performed analysis to show that power-assist hybrid electric vehicles (PA-HEV) can still achieve significant fuel savings with a lower-energy, higher-power energy storage system (ESS). Existing USABC targets for Energy Storage Systems (ESS) in PA-HEVs call for 300 Wh of "available" energy, which is believed to make the ESS expensive. Based on this DOE-sponsored NREL analysis, the FreedomCAR Tech Team and the USABC Management Committee created a new set of technical requirements for lower energy ESS for PA-HEVs that could be less expensive. The new requirements released in a USABC Request for Proposal, might be satisfied by ultracapacitors, asymmetric capacitors, batteries, or some other technology. [10]

[7] For more details, see section II entitled "American Recovery and Reinvestment Act of 2009."
[8] For more information, visit http://www.greencarcongress.com/2008/10/johnson-control.html
[9] For more details, see III.C.2 entitled "Battery Performance and Life Testing at INL."
[10] For more details, please visit http://www.uscar.org/commands/files_download.php?files_id=156, and see III.B.7 "Low Energy HEV Requirements Analysis (NREL)."

Commercialization and R&D100 Award for High Capacity, High Voltage Composite Cathode Material at the Argonne National Laboratory (ANL). Over the past years, ANL has developed a composite structure cathode material technology which provides much higher specific capacities (250 mAh/g) than conventional cathode materials, producing higher density batteries and longer all electric range for PHEVs. Progress this year was made in improving the rate capability of the material to 225 mAh/g at the C/2 discharge rate. Partially as a result of this, BASF, the world's largest chemical company, plans to mass produce and market the material. In addition, ANL, in collaboration with Envia Systems, was chosen as an R&D 100 Award winner for Envia Systems' lithium–ion battery which uses ANL's composite structure cathode material technology.[11]

A Molecular Dynamics Model of Charge Transfer across a Solid-Liquid Interface at the University of Utah, with Lawrence Berkeley National Laboratory (LBNL). The solid electrolyte interphase (SEI) film in Li-ion batteries serves to stabilize the anode/electrolyte interface, allowing stable cycling and a relatively long shelf life. Without that layer, Li cells would last only a few cycles. However, the SEI can also form in an unstable state, partially dissolving and re-forming with each cycle, consuming cyclable lithium, thus leading to decreased cycle life. As a first step towards an atomistic understanding of interfacial processes, this molecular dynamics (MD) modeling work has investigated carbonate electrolytes next to graphite. The simulations showed a similar Li transference energy barrier of ~12-19 kcal/mol, consistent with the experimental activation energies of 16.4-17 kcal/mol determined by R. Jow's group at Army Research Laboratory.[12]

First Principles Calculation Leads to Extremely High Rate $LiFePO_4$ at the Massachusetts Institute of Technology (MIT), with LBNL. Understanding the impact of particle composition and morphology on battery performance promises to open the path to significantly higher performance materials. Recently, Prof Gerbrand Ceder of MIT performed simulations on the Li migration barrier within and on the surface of $LiFePO_4$ and found that extremely fast charge and discharge rates should be possible. The team subsequently formulated such a material and found that its theoretical prediction were borne out by the performance of the surface treated nano-$LiFePO_4$. Although these rates might be difficult to achieve in larger cells, the ability to predict macroscopic behavior with microscopic simulations is a critical capability that may lead to new material discoveries and engineering approaches for much improved performance.[13]

World's Largest Battery Calorimeter becomes Operational at NREL. Researchers at NREL completed the fabrication and calibration of a large, advanced calorimeter for measuring heat from batteries intended for use in hybrid electric (HEVs), plug-in hybrid electric (PHEVs), and electric vehicles (EVs). The new calorimeter can test large batteries and aid developers in designing and evaluating battery thermal management systems. There are also dual power posts for testing power electronics as well as ports for liquid cooling. Recent calibration tests showed that the new calorimeter meets or exceeds industry's design specifications, which stipulate that the calorimeter has to measure heat with a resolution of better than 5 mWh and have a temperature stability of 0.01°C. This new calorimeter enhances DOE-NREL's leading-edge battery thermal R&D capabilities and is a unique addition for evaluating and designing advanced PHEV/HEV/EV battery packs.[14]

Characterization of Phosphate Cathodes for Lithium-Ion Batteries, at LBNL. Researchers in the Batteries for Advanced Transportation Technologies (BATT) Activity at LBNL found a way to substantially reduce performance problems associated with the low-cost, high voltage lithium manganese phosphate ($LiMnPO_4$) cathode material for Li-ion batteries. Although $LiMnPO_4$ has similar crystal structure as lithium iron phosphate ($LiFePO_4$), it exhibits poorer power performance and lower utilization of the active lithium. Researchers found that the factors that impede the conversion reaction during charging and discharging and result in decrepitation of the active particles can become substantially less problematic when a small portion of the manganese is substituted by magnesium, or when the particle size is reduced. [15]

Researchers Reduce Problems with Intermetallic Anodes for Li-ion Cells, at LBNL. Researchers at LBNL found that applying copper or silver coatings to the surface of intermetallic anodes (such as Si and Sn) might be beneficial in creating an effective barrier to halt unwanted reactions between the electrolyte and the electrode. The researchers studied the mechanisms of mass and charge transfer across the electrolyte/metal interface and determined that both Si and Sn electrodes form a porous, unstable surface layer which, unlike the surface layer observed on graphitic anodes, does not

[11] For more details, please visit http://www.transportation.anl.gov/publications/transforum/v9/v9n2/li-ion_battery_research.html

[12] For more information, see V.C.4 entitled "Search for New Anode Materials"and V.D.3 entitled "The Molecular Dynamics Simulation Studies of Electrolytes and Electrolyte/Electrode Interfaces."

[13] For more information, see V.B.1 entitled "First Principles Calculations and NMR Spectroscopy of Electrode Materials."

[14] For more information, see III.C.4 entitled "Battery Thermal Analysis and Characterization Activities."

[15] For more information, see V.B.3 entitled "Olivines and Substituted Layered Materials."

create an effective barrier to halt unwanted electrolyte reductions reduction processes during long-term battery operation. The copper or silver coatings make this behavior substantially less problematic and may, as a consequence, increase the cycle and calendar life of Li-ion batteries for vehicle applications.[16]

Researchers Investigate Factors Affecting Performance of Air Electrodes for High-Energy Batteries, at the Brookhaven National Laboratory (BNL). Researchers at BNL are investigating gas-diffusion electrodes, based on manganese oxide-loaded activated carbon matrices, for oxygen reduction. The matrices are made by reacting $KMnO_4$ with carbon materials and the researchers, working in collaboration with researchers at the University of Massachusetts at Boston, are using statistical design-of-experiment methods to identify the significant factors in making the matrices. Three factors: $KMnO_4$ concentration, reaction temperature, and reaction duration were tested in a two-level full-factorial design of experiment. The results indicated that reaction temperature, $KMnO_4$ concentration, and the interaction between temperature and reaction time have a significant influence on the catalytic activity of the electrodes. The results of these studies were recently published in the *Journal of Power Sources* (Vol. 185, pages 747-753, 2008).[17]

Electrolyte Cost Reduction and Performance Improvements Studied at LBNL. Researchers in the BATT Activity at LBNL are investigating various approaches to reducing the cost and improving the performance of electrolytes for lithium-ion batteries. Researchers are studying additives designed to allow the presence of some moisture in the battery components, with the goal of relaxing the stringent dry-room conditions needed during battery assembly and thereby reducing manufacturing costs. Also under study are alternative electrolyte salts that may eliminate or diminish the unwanted side reactions that reduce battery life. The third component of this research effort is the development of lithium single-ion conducting gels, which can eliminate concentration polarization effects and thereby increase battery energy density at high charge and discharge rates.[18]

Novel High-Capacity Reversible Anodes for Lithium-ion Batteries at the University of Pittsburgh. Researchers at the University of Pittsburgh have been studying new silicon-based intermetallic anodes that may provide gravimetric and volumetric energy density greater than those of graphite while exhibiting similar irreversible capacity loss and durability. High energy mechanical milling (HEMM) has been used to embed various Si morphologies and structures within graphitic and amorphous carbons to form novel Si/C hetero-structures. Systematic alloy formation studies conducted during electrochemical cycling of HEMM-derived crystalline silicon-carbon nanocomposites indicate that the conversion of crystalline Si to amorphous Si to form the high-lithium-content phase $Li_{3.5}Si$ is the primary cause of structural failure observed in crystalline Si based composites. This limiting phase transition can be bypassed by the direct generation of novel *a*-Si and C nano-composite hetero-structures exhibiting highly stable reversible capacities in excess of ~1000 mAh/g by using chemical vapor deposition and reactive mechano-chemical approaches. This research is a part of the BATT Activity managed by LBNL.[19]

Optimization of Battery Materials through Coupled Simulation and Experimentation at the University of Michigan (UM). Researchers at UM, working in the BATT Activity managed by LBNL, have developed a set of methods for simultaneously simulating temperature, pressure, and state of charge inside a battery cell during operation. The codes developed have enabled identification of shapes of cathode particles that can substantially reduce mechanical stresses inside cell's electrodes. In this way, the work is able to identify superior shapes of the materials that make up battery cells. Both battery manufacturers and automakers benefit from these analyses, and the team has most recently partnered with General Motors to form the GM/UM Advanced Battery Coalition for Drivetrains (GM/UM ABCD), which will use these models not only to predict cell performance, but also to formulate control strategies for automotive battery packs.[20]

National Lab Researchers Collaborate with Chinese Scientists to Improve Performance of Lithium-ion Batteries, at BNL. Researchers at BNL are collaborating with scientists at the Institute of Physics, Chinese Academy of Science. on research and development of advanced cathode materials to improve the energy and power capability of lithium-ion batteries for hybrid electric vehicles (HEV) and Plug-in hybrid electric vehicles (PHEV). The team is carrying out research and development on a Mn substituted $LiFe_{1-x}Mn_xPO_4$ cathode material that exhibits higher voltage plateaus

[16] For more information, see V.E.4 entitled "Investigations of Electrode Interface and Architecture."
[17] For more information, see V.B.8 entitled "Characterization of New Cathode Materials Using Synchroton-based X-ray Techniques and the Studies of Li-Air Batteries."
[18] For more information, see V.D.2 entitled "Interfacial Behavior of Electrolytes."
[19] For more information, see V.C.1 entitled "Nanoscale Composite Heterostructures: Novel High Capacity Reversible Anodes for Lithium-ion Batteries."
[20] For more information, see V.E.2 entitled "Microscale Electrode Design Using Coupled Kinetic, Thermal, and Mechanical Modeling."

during discharge than the un-substituted $LiFePO_4$. The results of these studies were presented at the 215th meetings of the Electrochemical Society held in San Francisco, CA. [21]

X-ray absorption spectroscopy reveals structural differences in battery electrodes, at BNL. Researchers at BNL are using *Ex situ* soft X-ray absorption spectroscopy (XAS) to distinguish the structural differences between the surface and bulk of electrodes. Working in collaboration with scientists at the National Institute of Science and Technology (NIST), the researchers employed both partial electron yield (PEY) and fluorescence yield detectors and showed that the surface of nickel-based compounds has a different electronic structure than the bulk. This soft X-ray XAS technique will be extended to thermal stability studies for other cathode materials with the ultimate goal of developing new materials to increase the energy density of lithium-ion batteries for PHEV applications. [21]

I.B.3 Organization of this Report

This report covers all the projects currently ongoing or starting as part of the energy storage R&D effort within the Office of Vehicle Technologies. Chapter II contains information on the projects being started which are funded under the American Recovery and Reconstruction Act (ARRA) of 2009. A list of the ARRA grant recipients is provided in Appendix A. Chapter III focuses on the developer program. Chapter IV lists all the projects which are being conducted under the Applied Battery Research activity in which the Argonne National Laboratory (ANL) has a leading role. Similarly, Chapter V lists all the projects which are part of the Focused Fundamental Research activity with a leading role by the Lawrence Berkeley National Laboratory (LBNL). A list of the individuals who contributed to this annual progress report or otherwise are collaborating with the energy storage R&D effort appears in Appendix B. A list of acronyms is provided in Appendix C. Since several figures in this report have color content, a color version of this report can be accessed at http://www1.eere.energy.gov/vehiclesandfuels/resources/fcvt_reports.html.

We are pleased with the progress made during the year and look forward to continued work with our industrial, government, and scientific partners to overcome the challenges that remain to delivering advanced energy storage systems for vehicle applications.

David Howell
Team Lead, Hybrid and Electric Systems
Vehicle Technologies Program

[21] For more information, see IV.D.2 entitled "Diagnostic Studies to Improve Abuse Tolerance and the Synthesis of New Electrolyte Materials" and V.B.8 entitled "Characterization of New Cathode Materials Using Synchroton-based X-ray Techniques and the Studies of Li-Air Batteries."

II

AMERICAN RECOVERY & REINVESTMENT ACT (ARRA) OF 2009

A. Integrated Battery Materials Production, Cell Manufacturing, and Battery Assembly Facilities

B. Battery Cell and Pack Assembly Facilities

C. Battery Materials Production Facilities

D. Battery Recycling Facilities

D.O.E. Project Manager

David Howell

II. AMERICAN RECOVERY & REINVESTMENT ACT (ARRA) OF 2009

The American Recovery and Reinvestment Act of 2009 (ARRA) (Public Law 111-5) is an economic stimulus package enacted by the 111th United States Congress in February 2009. This Act of Congress is based largely on proposals made by President Obama early during his Administration and is intended to provide a stimulus to the U.S. economy in the wake of an economic downturn. The measures are nominally worth $787 billion and include federal tax cuts, expansion of unemployment benefits and other provisions, including domestic spending in education, health care, and infrastructure, including that in the energy sector.

As part of ARRA implementation, on August 5, 2009 President Obama announced $2.4 Billion in manufacturing grants to accelerate the manufacturing and deployment of the next generation of U.S. batteries and electric vehicles – by funding 48 new advanced battery and electric drive components manufacturing and electric drive vehicle deployment projects – including PHEV and EV demonstration and education projects – in over 20 states. The grantees were selected through a competitive process conducted by DOE and are intended to accelerate the development of U.S. manufacturing capacity for batteries and electric drive components as well as the deployment of electric drive vehicles to help establish American leadership in developing the next generation of advanced vehicles. The new awards included $1.5 billion in grants to U.S. based manufacturers to produce batteries and their components and to expand battery recycling capacity, distributed over all parts of the country. As shown in Figure II- 1, these grants cover a range of manufacturing areas including those associated with material supply, cell components, cell fabrication, pack assembly, and recycling. The amounts for the individual grants are tabulated in Appendix A.

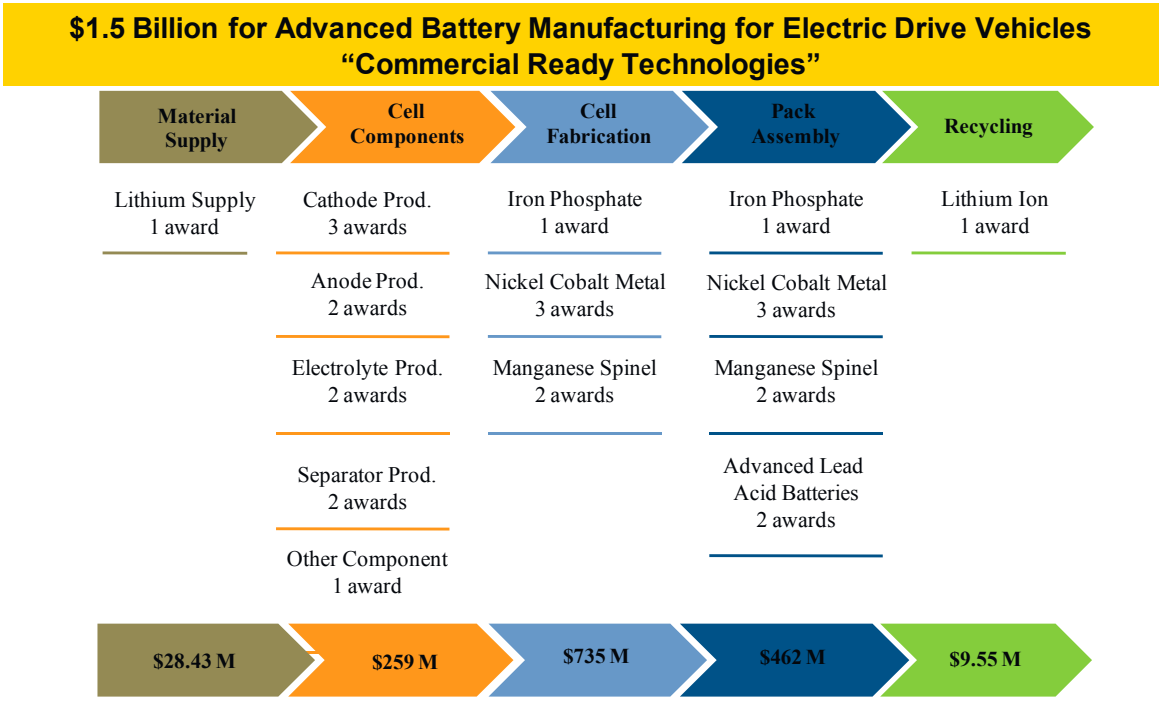

Figure II- 1: American Recovery and Reinvestment Act (ARRA) 2009 grants distribution for battery and electric drive manufacturing

The rest of this section presents a brief summary of the individual ARRA grants.

II.A. Integrated Battery Materials Production, Cell Manufacturing, and Battery Assembly Facilities

II.A.1 Johnson Controls Inc.

Build a domestic industry to manufacture Li-ion batteries for electric drive vehicles (EDVs).

Objective. The objective of this project is to establish a domestic Lithium-ion (Li-ion) battery industry with sufficient scale to be cost and technologically competitive with Asian manufacturers. The company strives to demonstrate the potential for the U.S. to become globally competitive through advanced manufacturing and leading technology creating green jobs. The plan also leverages stimulus funding to establish a U.S. supply base which will create more jobs and a sustainable business model. Johnson Controls, Inc., along with application partners Johnson Controls – Saft, Argonne National Laboratory and ENTEK, would invest $599.4 million by the end of 2012 – including $299.2 million in U.S. Government grants, matched by $300.2 million from Johnson Controls and partners.

Description. Johnson Controls will implement this project in two phases: Phase 1 of the project will create jobs upon funding award:

- Convert an existing Johnson Controls owned facility in Holland, Michigan to a state-of-the-art cell manufacturing and battery system assembly plant within 15 months.
- Expand the Engineering Development Center in Milwaukee, Wisconsin to directly support manufacturing, sales, and U.S. supplier development activities by creating a fast feedback loop between original equipment manufacturer (OEM) requests and sample products/testing data. Additionally, this expansion allows for the qualification of U.S. suppliers and manufactured materials.

Phase 2 of the project would help the U.S. Li-ion battery industry through:

- Raising an additional cell manufacturing and battery system assembly plant in Michigan
- Achieving scale and cost competitiveness relative to the Pacific Rim manufacturers

Impact. Johnson Controls will supply the automotive industry with Li-ion batteries, accelerate the development of EDVs, and stimulate the economy by creating 4,700 new green jobs in their Li-ion battery factories and associated supply chain.

II.A.2 A123Systems

"Vertically Integrated Mass Production of Automotive Class Li-ion Batteries"

Objectives

- Build the capability to support nearly 600,000 5kWh PHEVs by 2012.
- Build a stable, self-sustained enterprise, with 17% of the global market share and approximately 1/3 of the available market share, capable of competing with Asian conglomerates.
- Stimulate the economy, through the creation of 5,900 direct jobs, over 14,000 indirect jobs, and over 21,000 induced jobs.
- Help build an American battery industry infrastructure, with key materials and equipment suppliers in the U.S.

Description. A123Systems will match government funding to build a U.S.-based, vertically-integrated, high-volume automotive lithium-ion battery manufacturing system encompassing the full production process, including: the manufacture of its proprietary Nanophosphate cathode powder, electrode coating, cell fabrication, module fabrication, and the assembly of complete battery pack systems ready for vehicle integration. This three-phase plan builds upon its manufacturing experience and large customer base. It asserts it is firmly committed to providing the catalyst for the creation of a complete U.S. battery manufacturing industry. It plans to increase the percentage of raw materials and components sourced from U.S. suppliers to 70% of total content by 2014 and to invest at least 10% of its revenue in U.S.-based R&D to defend and extend technology advantage.

Impact. The program would stimulate the economy through the creation of jobs and help develop a sustained, globally-competitive U.S. battery industry. This will accelerate the development and production of electric drive systems, building upon the world's largest fleets of PHEVs and hybrid transit buses, powered by

A123's Nanophosphate lithium-ion technology. The vehicles using batteries produced by this program could reduce our nation's fuel consumption by 100 million gallons[22] and reduce CO_2 emissions by one million tons of CO_2/year[23].

II.A.3 Exide

The Exide project covers the expansion of Exide Technologies' manufacturing capacity for producing advanced batteries in existing U.S.-based battery plants. Exide has 34 plants and operations in over 80 countries, manufacturing more than 40 Gigawatt-hours of battery energy per year used in transportation, motive power, network power, and military applications. The project plan is to implement a combined incremental increase in yearly production capacity of 1.5 million additional units at two of Exide's current manufacturing locations: Columbus, Georgia, and Bristol, Tennessee.

This expansion will occur on property currently owned or controlled by the Company. Battery raw materials and component production at other key Exide locations will also be ramped up to support this project. One such regional location is in Eastern Pennsylvania which includes a centralized plastic container, cover, and vent molding operation in Lampeter; as well as a production complex in Reading including recycling and formation operations, and a large distribution center.

These advanced battery technologies are targeted to have an accelerated near-term impact (in high volume) for micro-hybrid vehicles, idle reduction commercial vehicles, and other strategic market segments. This expansion involves two of Exide's global technologies: a Spiral Wound Absorbed Glass Mat (AGM) design and a Flat Plate AGM design, both of which will be manufactured with advanced carbon technology as required by customer specific advanced vehicle applications.

The spiral wound battery product is currently in production at an Exide battery plant in Europe. When the planned technology transfer to the United States takes place, which will be accelerated by the federal grant, the Tennessee Exide production operation will be the only Spiral Wound lead acid battery "made in America" focused on the transportation market segment. Furthermore, this production capacity will serve both an existing market of 2 million units, and also enable development of advanced spiral wound designs for upcoming new micro-hybrid and mild hybrid applications. Thus, the Exide project would fulfill the job creation goals of the advanced battery program and also promote the enhanced use of hybrid vehicles, thereby achieving energy saving.

These expansion projects will create approximately 320 new U.S. manufacturing jobs and will help retain existing jobs by enhancing the advanced technology base at the designated production sites. The project will also create additional jobs in the supply chain, generating a job multiplier effect to further advance the economic stimulus goals of the advanced battery grant program. It will also result in the creation of many construction jobs at project sites in Tennessee and Georgia during the 3-year project period.

[22] 580,000 PHEVs driving 12,000 miles a year that get miles per gallon vs. a standard vehicle with 30 miles per gallon would save 200 gallons per vehicle every year, or a total of 116 million gallons of fuel per year.

[23] CO_2 emissions from a gallon of gasoline = 2,421 grams x 0.99 x (44/12) = 8,788 grams = 8.8 kg/gallon = 19.4 pounds/gallon from Environmental Protection Agency fact sheet, "Emission Facts: Average Carbon Dioxide Emissions Resulting from Gasoline and Diesel Fuel", http://www.epa.gov/OMS/climate/420f05001.htm

II.A.4 East Penn

Objective. East Penn Manufacturing Co. (East Penn) will expand its production capacities to manufacture high volumes of Advanced Valve Regulated Lead-Acid (VRLA) batteries and the UltraBattery, both commercially viable technologies. East Penn has 63 years of battery manufacturing experience, a modern recycling infrastructure, and exclusive licenses for its UltraBattery technology, and it will scale up production to over 2.8 million batteries annually by 2013 then run at that capacity or above. The Company's current customers are already supporting the demand for these advanced batteries with commitments of over 4.2 million batteries between 2009 and 2012.

In order to service these customers with the essential battery products needed for HEV applications and to create 400 more U.S. jobs, East Penn applied for the DOE grant supporting the production capacity increase of the current U.S. based manufacturing plant facilities. With DOE assistance, East Penn plans to become the leading United States source of Advanced VRLA and UltraBattery power serving the global vehicle market with a viable, safe, cost effective, and highly recyclable alternative to currently foreign-controlled technologies like nickel metal hydride and lithium-ion.

Description. In order to scale up production to over 2.8 million batteries annually by 2013 and to continue to run at that capacity or above thereafter, East Penn will use a recently constructed 739,000 sq. ft. manufacturing plant that will be populated and fully developed with specialized equipment including: electrode fabrication, assembly, formation, and finishing equipment. Additional capacity for electrode materials (lead oxide) as well as related manufacturing infrastructure will be added. East Penn is the sole project coordinator with some subcontract work projected.

Impact. Over 4.2 million advanced batteries (representing 1.1 million kWh available energy) will be produced over the next four years and over 2.8 million advanced batteries (600,000 kWh) will be produced annually thereafter. The substantial number of batteries projected to be produced will help preserve and create hundreds of jobs. This commercially viable alternative can save approximately 200 million gallons of petroleum over the next four years with projections showing cumulative savings of 1.2 billion by 2020. East Penn has the potential to establish itself as a leading U.S. supplier for alternative battery power providing the U.S. with a viable and practical alternative to imported Nickel Metal Hydride and Li-ion battery power.

II.B. Battery Cell and Pack Assembly Facilities

II.B.1 Kokam/Dow, Midland Battery Park

Objective. Design, build, and operate a Superior Lithium Polymer Battery (SLPB) manufacturing plant to produce an annual capacity of 1.2 Billion Wh or 60,000 Electric Vehicle Batteries with 20 kWh battery systems.

Description. Dow Kokam will construct a 772,078 SF SLPB manufacturing plant that will produce batteries for the advanced vehicle market that are affordable, safe, powerful, and long lasting.

Impact. The manufacturing plant is designed and "shovel-ready" for immediate impact on the economy and area employment. Additionally, the Project will employ approximately 900 people to operate the plant. In the long-term, the Project could have a significant impact for the electric vehicle and hybrid electric vehicle industry by making the electric vehicle more affordable, since the battery represents a significant fraction of the cost of the electric vehicle. As the cost of electric vehicle becomes more affordable to the consumer, more electric vehicles will be sold, replacing internal combustion engines and reducing U.S. dependence on foreign oil.

II.B.2 CPI/LG Chem

Objective. Construct a new battery manufacturing facility in Michigan to supply lithium-ion battery cells for automotive use.

The completion of this effort would result in validated production capability for advanced automotive battery cells in an all-new U.S. facility. LG Chem (LGC)/CPI, an established global supplier in high volume Lithium-ion battery cells and packs for various applications, has demonstrated product capability to meet General Motor's performance specifications and has been awarded production responsibility for the

Chevrolet Volt, first volume production Extended Range Electric Vehicle (EREV) or Plug-In Hybrid Electric Vehicle in the U.S.

The overall objective is to replicate production of Li-ion battery cells from Ochang, Korea into a new manufacturing facility in Michigan. The project would meet this objective and provide a foundation for the emergence, growth and success of electric and hybrid electric Vehicles in the U.S. automobile market. When in full production, the proposed facility will create more than 440 jobs and will produce over 18 million cells (3.75V, 15Ah) annually. After starting assembly operations in 2012, an expansion of production capability will continue through 2013 with the addition of a mega-electrode manufacturing line and more assembly lines.

Description. The start of production of Li-ion cells in the Michigan plant will involve siting and construction of a new facility, the installation of new equipment and staffing the plant with operators, engineers and administrative staff.

Detailed studies of candidate sites will be completed to make a final site selection. The building construction will be done in two phases, the first in 2011 to begin assembly operations, and the second in 2012 as an expansion to accommodate high volume electrode manufacturing as well as more than doubling assembly capacity.

In the first phase of the project, to meet customer timing requirements, two assembly lines will begin operation in the 2nd quarter in 2012 utilizing electrodes made in LGC's Korean based plant to produce 5 million cells in 2012. This permits timely supply and also provides an opportunity for experienced technical experts to fully develop the manufacturing equipment and processes that will ultimately be duplicated in Michigan. Concurrent with the start of assembly production, the new building will be expanded to accommodate new electrode manufacturing and added assembly equipment that will bring the capacity to 18 million cells per year by the end of 2013. This project could bring valuable technology, manufacturing capability and jobs to the U.S. to serve the automotive industry and potentially many other future applications.

II.B.3 EnerDel

Description. EnerDel produces large-format lithium-ion batteries and has end-to-end production facilities based in the United States. It expects to accelerate the U.S. transition to electric drive vehicles by producing 60,000 Li-ion auto battery packs per year by 2013. The proposed project would also create approximately 1,700 new jobs at its two Indiana plants and increase investments and job creation among its many U.S.-based suppliers. EnerDel envisions to drive the United States toward international leadership in lithium-ion battery manufacturing and supply and expects to rapidly advance toward its vision by fulfilling the first phase of its business expansion plan. The goal of this project is to significantly expand EnerDel's advanced battery manufacturing capacity and help establish the domestic resources for automobile-grade lithium-ion batteries that U.S. based battery manufacturers must have in order to compete.

EnerDel expects to achieve this goal by fulfilling four concrete objectives. The first objective will be purchasing and expanding existing site locations and equipment capacity. This will ensure the physical resources necessary for producing 60,000 EV batteries per year. For its second objective, EnerDel will expand its competitive mass production and engineering capability. EnerDel will add more high-volume, high-speed automated production lines for both cell manufacturing and battery system assembly. EnerDel will also continuously recruit and train an anticipated workforce of approximately 1,700 new U.S. based employees. The third objective will be enhancing EnerDel's supply chain and promoting cost competiveness of base materials. This will be accomplished by identifying key suppliers and materials for domestic sourcing; and conducting the necessary qualification processes. EnerDel will also strive to promote U.S. jobs by working with domestic and international suppliers to achieve supply, quality and pricing standards that meet or exceed current offshore suppliers. Finally, the fourth objective will be to achieve the third-party certifications necessary to be positioned as a Tier 1 supplier to automakers. With these certifications in place, EnerDel will become the first U.S. based end-to-end manufacturer of automotive grade lithium-ion batteries that meet or exceed OEM quality standards.

In addition to enabling EnerDel to reach a manufacturing capacity of 60,000 batteries per year, achieving EnerDel's several project goals will permit realizing the potential for these batteries which compare favorably to current NiMH batteries. EnerDel plans to make batteries which: (i) weigh less and occupy less space; (ii) provide more power in HEV applications; (iii) provide more energy in EV and PHEV applications; (iv) provide a longer life when compared to today's NiMH batteries; and (v) provide equal or better safety characteristics due to excellent thermal properties of our chemistry. EnerDel expects to reach each of these goals and current data indicates these goals are going to be met. Specifically,

EnerDel has increased safety by developing its own lithium titanate anode material in collaboration with Argonne National Laboratory for HEV applications. EnerDel has also developed a hard carbon anode Li-ion battery for PHEV/EV applications. Both chemistries show extremely positive safety and cycle life performance in comparison with graphite-based Li-ion batteries. Also, an innovative Li-ion flat stack prismatic cell design is used that reduces battery size and maintenance, lowers production costs, has improved heat dispersion characteristics compared to cylindrical designs, and improves overall performance.

The overriding goal is to create a United States based supply chain and manufacturing industry so that, as the auto industry moves toward lithium-ion batteries, EnerDel can help the U.S. reclaim a leadership role in battery design.

II.B.4 General Motors (GM)

GM Li-ion Battery Pack Manufacturing. GM leverages more than a decade of company investment in electric drive vehicles. It will use the Recovery Act funds to accelerate the deployment of battery pack manufacturing capabilities, enabling high volume production of GM's first-to-market extended-range electric drive vehicle – the Chevrolet Volt. Two additional battery pack programs are also targeted after the initial Volt acceleration and production.

Objectives

- Deliver domestically produced, affordable, and environmentally sound energy sources to substantially reduce petroleum consumption.
- Aid in the nation's economic recovery by creating U.S.-based manufacturing jobs.
- Accelerate development and production of Electric Drive Vehicle Systems by manufacturing General Motors' Li-ion battery packs.
- Develop reliable, quality battery packs that can be cost-effectively produced in high volume.

Description. The project will create and retain jobs in at least four areas: manufacturing of pre-production battery packs; design, construction, and installation of production machinery and equipment, tooling, and supporting operations; production and quality improvement during the product lifecycle; and creation of production jobs in the on-going operation.

This project will deliver production capability for GM's Li-ion battery packs to serve electric drive vehicles. It will finalize designs for construction, installation and validation of machinery, equipment, tooling, and key staff and facilities. The principal methods of the project are 1) program management and planning; 2) pre-production and low volume process validation; and 3) high volume battery pack manufacturing, refurbishing, and recycling facilities.

The Volt's battery pack design is directly coupled with the vehicle design to assure complete integration between the battery pack and the vehicle. This integrated approach assures both performance and efficiency of the overall vehicle, to meet final customer expectations. Future programs will follow the same strategy.

Impact. Investment in this project will drive innovation cycles and move the battery pack technology down the cost curve. The project will accelerate U.S. manufacturing capabilities for commercially viable extended-range electric drive vehicles; and create U.S. leadership in automotive applications of new generation battery technologies. The project will expand the U.S. workforce trained in automotive battery pack manufacturing technologies, creating and retaining green jobs at GM and its suppliers.

The project will contribute to national goals for reducing petroleum dependence and improving carbon footprint. It will enable high-volume production of electric drive vehicles (EDVs) and strengthen U.S. contribution to global CO_2 reduction. This capacity will significantly contribute to the Administration's goal of having one million plug-in EDVs by 2015.

II.B.5 Saft

Saft Factory of the Future for high-volume Li-ion batteries for military hybrid vehicles, smart grids, renewable energy storage, broadband, and defense & aerospace applications.

Saft's Factory of the Future for Lithium-ion battery manufacturing for DOE will provide a showcase of environment friendly and energy efficient design concepts to employ hundreds of people in well-paid jobs and will enable electric drive applications such as military hybrid vehicles, broadband, grid stabilization, green, renewable energy, space, mobility and aviation batteries to be broadly adopted in the world markets to achieve significantly reduced carbon emissions and fuel savings.

Description. Saft proposes to use its considerable experience in building factories for Lithium-ion cell and battery manufacturing and expertise in Lithium-ion technology to build a Factory of the Future capable of manufacturing and delivery high quantities of Li-ion cells,

modules, and batteries to the military hybrid vehicle, industrial energy, electric drive markets, other defense and aerospace markets.

Methods to be employed. Saft will invest immediately, along with DOE, in establishing the factory and manpower to support manufacturing which will be used in delivery of Lithium-ion cells and batteries in high volumes. Saft will create up to 800 jobs within three years of beginning the project, with the first year job creation starting at approximately 200 new jobs. Saft will use LEAN manufacturing techniques to ensure that the factory is established with consideration for cost savings. Also, Saft will employ risk mitigation and risk management practices which will assure being able to provide on-time schedule and technical performance.

Saft will use the Earned Value Management System of assigning and managing project costs in respect to financial objectives of the program. It will use LEED® green factory initiatives in the buildings, power usage, and waste management; all of which will be complemented by its recycling plan for batteries once used. The decision to use LEED® techniques in designing the Factory of the Future is consistent with the markets intended to be addressed which are green energy related.

Potential impact of the project. The projected outcome of establishing this factory is to be ready to provide cost competitive, high volume Lithium-ion cells, modules, and batteries to the military vehicle, defense and industrial markets in anticipation of those market needs.

The benefits to the U.S. will be to establish domestic capability for Lithium-ion batteries which are cost competitive, more environment-friendly, and employ U.S. workforces. This new domestic capability will lower fuel costs for electric drive applications, reduce carbon footprint, create hundreds of jobs, and enable solar and wind power renewable energy systems, as well as Smart Grid power stations to improve energy reliability and costs.

II.C. Battery Materials Production Facilities

II.C.1 Celgard

Celgard: Celgard U.S. Manufacturing Facilities Initiative for Li-ion Battery Separator. Celgard, LLC is a global leader in the production of lithium-ion battery separators and one of the largest global suppliers to the industry. Its separators are primarily used in rechargeable lithium-ion batteries for consumer electronic devices such as notebook computers, mobile telephones, digital cameras, power tools, reserve power and electricity grid storage systems, and electric drive vehicles (EDVs).

Celgard proposes to expand its separator production capacity in the United States to produce an additional 80 million square meters of separator per year. Based on forecast demand, this quantity of separator will be necessary to supply domestic lithium-ion battery manufacturers participating in the EDV industry.

Celgard plans to use a phased approach for its separator production capacity expansion. This approach will make separators available in early 2010. Phase 1 production capacity will be increased in line with growing domestic demand for separator required by U.S. advanced battery manufacturing. Phase 2 production capacity will be initiated at a facility in another state in 2009 and completed in 2012.

The Celgard Project will meet an important objective of the American Recovery and Reinvestment Act of 2009 by creating 251 direct jobs and 1,200 indirect jobs in the U.S, starting in 2009.

II.C.2 Toda

Advanced Cathode Material Production Facility. Toda America Incorporated (Toda) is a cathode materials supplier to Li-ion battery manufacturers worldwide. Its principal objective is to establish a high-volume Advanced Battery Supplier Manufacturing Facility in the U.S., in collaboration with diverse stakeholders including industry, university, and government entities and to become a strong and supportive strategic supply partner to the U.S. advanced battery industry.

As a first step, Toda is preparing to invest an initial $70.1 million (total capital investment) to establish its U.S. plant, as part of a longer-term U.S. commitment. This facility will develop and produce oxide materials for cathodes to serve both existing Toda customers and emerging players in this industry. Phase 1 and 2 will each contain two lines for a total of four lines for the proposed facility. For Phase 1, the facility's capacity is 1,800 tons/yr, determined by the two continuous flow kilns, each with a capacity of 900 tons/yr. For Phase 2, Toda expects to install kilns with a capacity of 2,000

tons/yr. Total production volume at this facility will equal 3,800 tons of cathode materials per year, which is sufficient to supply batteries for around 450,000 HEVs or 125,000 PHEVs. (HEV batteries emphasize power over energy storage while PHEV batteries emphasize energy storage capacity over power. Material consumption is approximately 8 kg for a HEV and approximately 30 kg for a PHEV battery.) In addition, Toda has robust R&D capabilities, and is currently working to commercialize the next-generation of Li-ion battery materials using the latest technology licensed from ANL. Toda already produces several distinct materials using proprietary Li-metal oxide combinations and technologies.

Toda Kogyo currently operates seven manufacturing facilities, including several that produce Li-ion cathode material. It is anticipated that the facility that will be used for this project will be built in South Carolina. It will incorporate equipment identical to that currently being used in Toda Kogyo's facility in Japan. Production of cathode material for shipment to customers is scheduled to start on March 31, 2011, approximately 18 months after the award is granted. Toda's existing U.S. customers purchasing cathode material from its Japanese plant have committed to buy cathode material from its South Carolina plant.

Toda is planning for substantial further investment in the U.S. over the next 10-15 years, paced with the expected growth of the U.S. battery manufacturing industry. Toda intends to collaborate closely with federal, state, and local stakeholders and to engage in creative industrial partnering options and is poised to serve as a key contributor in the development of a robust advanced battery manufacturing industry in the U.S.

II.C.3 Chemetall Foote

Battery Grade Li Carbonate and Li Hydroxide Manufacturing Expansion. The expansion will provide a long-term cost-effective domestic source of lithium carbonate and lithium hydroxide for battery applications. Advanced lithium rechargeable battery cells are currently in use and many new applications are being developed. Lithium based rechargeable batteries are being developed for such applications as HEV, PHEV, and EV cars in addition to the traditional uses in cell phones, laptops and power tools. Lithium has the advantage of high energy density / weight ratio which is important especially in automotive applications.

The starting materials of choice for rechargeable lithium batteries are lithium carbonate and lithium hydroxide. Chemetall Foote Corp. is recognized around the world as a leader in lithium technology and is currently the only domestic source of lithium carbonate/lithium hydroxide. The company operates a lithium carbonate and lithium hydroxide plant in Silver Peak, NV, a lithium metal and lithium salt operation at Kings Mountain, NC and has two other lithium production plants in the United States. For these sites to be viable suppliers to the battery industry over the long-term overall production costs need to be reduced and product quality needs to be improved. This is needed to successfully compete internationally.

Description. The company will expand the Silver Peak, NV lithium carbonate facility and convert to geothermal based electricity; build a state of the art battery grade lithium hydroxide manufacturing plant in Kings Mountain, NC. At Silver Peak, expansion and conversion to geothermal energy will make the plant competitive with foreign producers of lithium carbonate. The state of the art facility at Kings Mountain will provide battery grade lithium hydroxide and position the facility to take advantage of new technology to produce lithium hydroxide as it is developed.

Impact. By expanding Silver Peak lithium carbonate and converting it to geothermal based electricity Chemetall Foote expects to significantly reduce the production cost of battery grade lithium carbonate and be competitive compared to South American and Asian suppliers. The new lithium hydroxide facility in Kings Mountain will be competitive from a quality and cost standpoint with any facility in the world. The U.S. automotive industry and other U.S. battery manufactures will be able to depend on a reliable domestic source of battery grade lithium salts that apply high quality standards.

These projects will enable Chemetall Foote to hire additional employees at all levels for Battery Grade lithium operations as. All construction, engineering, and equipment for the project will be supplied by U.S. companies.

II.C.4 Honeywell

High-Volume Manufacturing of $LiPF_6$. Honeywell proposes to build a U.S. manufacturing facility to produce the critical Li-ion battery material – lithium hexafluorophosphate, $LiPF_6$. Honeywell's $LiPF_6$ project directly supports the DOE's objective to build and validate production capability of battery materials in

the U.S. This project will result in the first U.S. manufacturing facility for $LiPF_6$, establish a secure domestic supply for this critical material in the Electric Drive Vehicle (EDV) supply chain, and form the foundation of a sustainable domestic Li-ion battery industry.

Description. All Li-ion batteries require $LiPF_6$, a material that is not currently made in the U.S. and was in short supply in 2008. Leveraging its capabilities as the world's largest HF manufacturer, Honeywell developed a novel process to prepare high-purity $LiPF_6$ as demanded for high-quality lithium-ion batteries. Honeywell initiated plant design and engineering work in 2008, the proposal is "shovel ready" and can create immediate jobs for Americans.

The project will create 151 direct engineering and construction jobs to build the facility, as well as additional jobs with American equipment suppliers. Honeywell will also add 34 long-term professional and manufacturing jobs to manufacture this strategic Li-ion battery material.

Honeywell's experience in developing manufacturing processes and facilities, combined with its history in the industry and relationships with battery customers, can help ensure the technical and commercial success of the project and advance the national objective to increase the availability and affordability of EDVs. The project will leverage significant existing assets and know how, to enable bringing $LiPF_6$ to market quickly. It is imperative that the U.S. based Li-ion battery industry have secure access to the highest quality $LiPF_6$ to avoid disruptions in supply and/or quality from foreign sources.

Potential Impact of the Project. This project will help enable the successful commercialization of EDVs by providing a secure, reliable supply of $LiPF_6$ to the U.S. market. Honeywell's manufacturing process is expected to be environmentally sound, eliminating a hazardous by-product typically produced in alternate processes. All domestic Li-ion battery manufacturers, and their EDV customers, will benefit from this secure and cost-effective supply of $LiPF_6$.

II.C.5 BASF

BASF: The Chemical Company – Li-ion Battery Cathode Production Plant in Elyria, Ohio.

The specific cathode material has been licensed from ANL and has been shown to be a material of choice among the largest North American and Asian cell manufactures actively engaged in providing lithium-ion battery solutions to the automotive marketplace.

When completed, the BASF facility is expected to be the largest cathode material facility in North America. The impacts of such a facility are anticipated to be significant in three areas: First, the facility construction and staffing will have a positive economic impact for Ohio; second, the facility will attract more ancillary businesses to North America; and finally, the commitment of BASF to this project will shift the high technology field of lithium-ion batteries from Asia, where it currently rests, to the United States of America. BASF has several cell manufacturing partners as well as support from raw material suppliers that will enable it to be fully successful in this effort.

II.C.6 EnerG2

Nanoengineered Ultracapacitor Material. EnerG2, Inc. and its partner Oregon Freeze Dry, Inc. (OFD) will build a facility for the commercial scale production of nanostructured, synthetic, high-performance carbon electrode material. The plant will be completed on an 18-month fast track basis by March 2011 and produce proprietary NC-Series electrode carbon for use in ultracapacitors for EDV energy storage systems. The project cost will be $28.4M. EnerG2 and OFD will each contribute $3.55M for a combined cost share of $7.1M or 25% of the total project cost. The DOE contribution will total $21.3M.

EnerG2, Inc. engineers new materials for energy storage. Founded in 2003, EnerG2 has collaborated with the University of Washington on novel energy storage technologies based on synthetic nanostructured carbons. Oregon Freeze Dry, (OFD), the world leader in contract freeze-drying, has been an EnerG2 R&D partner since 2006. The manufacturing facility will be based in OFD's industrial park in Albany, OR, to take advantage of OFD's expertise in freeze drying, the key production process.

The global market for electrical double layer capacitors (EDLC) or "ultracapacitors" is currently over $600M including applications such as electric rail and heavy hybrids. Large-scale adoption of ultracapacitors in "light" EDVs has been hindered by cost and performance of one key ingredient, electrode carbon.

Carbon provides an electrolyte interface with massive surface area required to store high charge density. EnerG2's NC-Series carbon overcomes fundamental limitations of conventional carbon sources (e.g. coal, coconut husks). EnerG2's improved cost/performance will accelerate the adoption of ultracapacitors for EDVs, and in turn make EDVs more attractive to consumers. EnerG2 and OFD are in pilot scale production today and are ready to grow production to meet global demand.

To prepare for the product launch, EnerG2 has partnered with leading ultracapacitor manufacturers. These manufacturers view an NC-Series carbon based ultracapacitor as the next stage innovation in conventional hybrids and the enabling technology required for plug-in hybrids to succeed. They will be prepared to integrate EnerG2 materials into their ultracapacitor products as scale production comes on line. As demand rises beyond 2011, EnerG2 will expand its operations and/or license its technology to other electrode manufacturers.

Other attractive features of ultracapacitors include their long cycle life (millions of charge/discharge cycles), inherently simple design, and environmentally benign components. EnerG2's manufacturing process will utilize carbon feedstocks derived from resins also used in wood products, meaning related jobs will be saved in the hard-hit U.S. specialty chemicals industry. This project will directly create 50 construction jobs and 35 manufacturing jobs in Albany, Oregon, a rural community with one of the highest unemployment rates in the country.

Beneficiaries from this project will include the global automotive industry, the state of Oregon, and consumers worldwide who will enjoy higher performing and potentially safer hybrid and electric drive vehicles, reduced dependence on oil, and a cleaner environment.

II.C.7 Novolyte

Production of electrolytes for lithium-ion batteries. Novolyte Technologies, Inc. is an independent company carved out of the Ferro Fine Chemicals Group in November 2008. Ferro Fine Chemicals began operations in 1958 as Grant Chemical Company, Inc. It is headquartered in Cleveland, OH and has operations in Zachary, LA and Suzhou, China. Novolyte is a global manufacturing and technical leader in the area of electrolyte solutions for lithium batteries, lithium-ion batteries and ultracapacitors. Electrolyte mixtures are mixtures of lithium salts, organic solvents and other additives that provide functionality to the battery system. Electrolyte mixtures are a key component in Li-ion batteries.

The goal of Novolyte Technologies' project is to expand its electrolyte capacity in the United States while retaining existing employees and creating new employment opportunities. It intends to do so by expanding the existing electrolyte manufacturing facility and by installing solvent recycling capabilities at its facility in Zachary, LA. Once completed, the expanded facility will have enough capacity to supply the amount of electrolyte necessary to make a minimum of 100,000 PHEV batteries (or an equivalent amount of Electric Drive Vehicle batteries).

The expansion component of the proposed project is expected to be completed over the next three years and will consist of the installation of new buildings, bulk chemical storage, materials handling, purification equipment, and reactors in order to efficiently manufacture electrolyte solutions, a key component of lithium batteries, Li-ion batteries and ultracapacitors. Also, packaging and quality control/quality assurance capabilities consistent with current and expected market requirements will be installed as part of the project. The project will be completed in two phases. Phase one will expand existing capacity and be complete in year 1 while phase two will include the build out of a new green field electrolyte manufacturing facility on the Zachary site.

From this expansion Novolyte expects to create 66 project related jobs during the installation of the new capacity over the next 24 months and 18 new full time Novolyte positions supporting the manufacturing and business growth objectives.

II.C.8 FutureFuel

Commercial Production of Graphite Anode Materials for High Performance Lithium-ion Batteries. FutureFuel Chemical Company (FFCC) will design, install, and operate a commercial-scale plant to produce Intermediate Anode Powder exclusively for ConocoPhillips (COP) at its specialty chemical and biofuel manufacturing facility located in Batesville, Arkansas. Intermediate Anode Powder is a coated and stabilized graphite powder that is the starting material for CPreme® Anode Material.

CPreme® Anode Material is a high power anode material invented, developed, commercialized, and marketed by COP. CPreme® Anode Material meets the challenge of high rate lithium-ion battery applications, including power tools, defense, utility load management, and hybrid-electric and electric vehicles.

II.C.9 Pyrotek

Pyrotek is a privately owned U.S. based company founded in 1956, in Spokane, WA. It manufactures and sells a vast array of products for use in high temperature environments, and is a world leader in the handling, processing, and filtration of molten aluminum. Metaullics Systems, a Division of Pyrotek, Incorporated ("Pyrotek"), utilizes graphite furnaces to heat treat materials to extremely high temperatures, known as graphitization.

Pyrotek is a strategic partner of ConocoPhillips in the production of a high performance anode material, marketed and sold by ConocoPhillips as CPreme® Anode Material (CPreme®). Its role in the production of this high performance anode material is to graphitize specially treated material provided by ConocoPhillips. This is the final step in producing CPreme®.

ConocoPhillips is the leading domestic manufacturer of high performance anode materials for lithium-ion batteries. CPreme® has been adopted for use in power tool, defense, automotive and utility load management applications. It is based on patented technology and proprietary processing developed by ConocoPhillips, and has been shown to provide superior performance over industry benchmark anode materials. Two leading domestic battery manufacturers, A123Systems and Johnson Controls, Inc., have strategic business relationships with ConocoPhillips to utilize the CPreme® product within their automotive applications. This project dramatically expands the production of CPreme®, which will significantly advance the efforts to develop and produce high-performance EVs.

II.C.10 H&T Waterbury

New Metal Li-ion Battery Container Manufacturing. H&T Waterbury, Inc. (H&T) of Waterbury, Connecticut proposes to develop a unique U.S.-based manufacturing process which will produce metal outer shell containers for lithium-ion batteries for use in sustainable products in the automotive and other industries. The operation is designed to expand H&T's staff through the creation of 12 professional, semi-skilled and skilled technical positions in Waterbury, Connecticut during the grant period. Operations are projected to begin within 6 months of award.

The project will be implemented in a step-wise fashion. Phase One includes the development of a pilot scale plant that will install a used press for the purposes of trial runs for tooling and customer approvals. Subsequent phases include the hiring of skilled staff and the build out of additional presses, cleaning machines and packaging systems.

Impacts. Upon implementation, this project will establish a reliable, long-term manufacturing plant in Waterbury, Connecticut for the production of deep drawn cylindrical metal containers for rechargeable (Li-ion) cell and battery producers who wish to establish U.S.-based manufacturing capability. This would alleviate the current dependence on Asian manufacturers exclusively for these cells and batteries. Establishing this U.S. manufacturing supply chain would fulfill critical needs of the associated energy saving technologies including electric/hybrid automobiles, energy storage, and other technologies. A reliable source for these materials in the United States will be available to support local consumer interests and auto industries. The project will create 12 professional, semi-skilled and skilled positions and support 950 new positions at customers' proposed facilities (SAFT America, Johnson Controls- SAFT).

II.D. Battery Recycling Facilities

II.D.1 Toxco

Objectives. The Toxco Incorporated proposed project would expand the domestic recycling capacity for large format advanced Li-ion batteries used in electric drive vehicles (EDVs) – including hybrid electric, electric, and plug-in hybrid electric vehicles by designing and building a state of the art recycling facility to operate in conjunction with its existing EDV battery recycling facility in Ohio. Successful completion of this project will provide renewable raw materials to

the battery OEM's and ensure the proper environmental management of the end of life batteries.

Specific project objectives include:

- Customer validated management of spent EDV batteries to include the environmentally friendly recycling of those "end of life" batteries by the processing of the recovered components back to battery grade products and other relevant resource aftermarkets.
- The refurbishment of certain batteries as electrochemical energy storage devices.
- Increased recycling capacity for EDV battery recycling up to 100,000 PHEV Li-ion battery packs per year.
- Building three lines to specifically recycle the following Li-ion battery chemistries: $LiCoO_2$, $LiFePO_4$, $LiMnO_2$, and mixed oxides.

The successful completion of this project will result in a comprehensive, fully permitted, environmentally friendly EDV battery recycling facility in the U.S.

Description. Toxco Ohio is currently situated on a 35 acre lot and possesses an 180,000 sq ft facility for battery recycling. Activities at this facility include the recycling of EDV type NiMH batteries as well as consumer type and industrial batteries. This project will add a 50,000 sq. ft building on site with the capability to recycle 9,000,000 lbs (or almost 100,000 batteries per year – assuming a 5kWh per battery at 120Wh per kg and 91 lbs per battery) per year of advanced Li-ion batteries used in EDV applications. The 50,000 sq ft building will house three process lines dedicated to the recycling of three types of advanced Li-ion: $LiCoO_2$, $LiFePO_4$, and Lithium Mixed Metal Oxides. These chemistries represent the anticipated battery technologies used by the automotive OEMs in their proposed EDVs. This facility will incorporate processing equipment for the evaluation of and refurbishment of EDV batteries for re-use in alternative secondary power markets. Lastly, this facility will have equipment to extract and refine the electrolyte solutions, cathode material and carbon from spent batteries for use in the battery market as a feedstock material.

Benefits. This project could significantly advance U.S. capability to recycle current and future EDV lithium-ion batteries, including those batteries from PHEVs. Specific project benefits include:

- Lower cost raw materials for the battery manufacturing industry thereby reducing the manufacturing cost of advanced batteries and facilitating market acceptance of EDV automobiles.
- Extending the life cycle of batteries through refurbishment
- Proving an environment friendlier alternative to land filling of battery waste.
- Additionally, the project will support the Recovery Act goals of job creation by providing new construction jobs and over 40 new long-term manufacturing and management jobs in an economically depressed area.

Toxco Incorporated, a leading battery recycling company in North America, has been in the business of lithium battery recycling since 1993 and currently works with multiple battery and automotive OEMs. Toxco companies recycle over 75 million batteries total per year at multiple permitted battery recycling facilities throughout the United States and Canada.

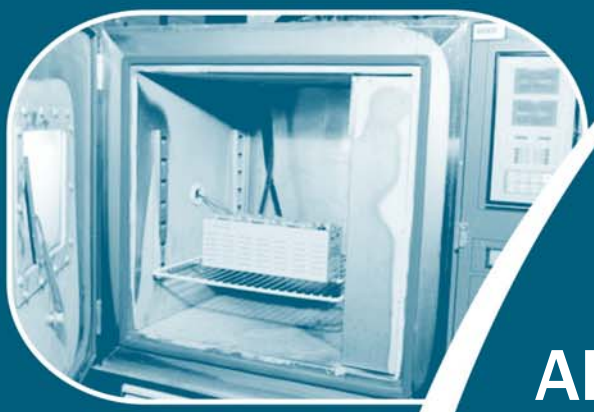

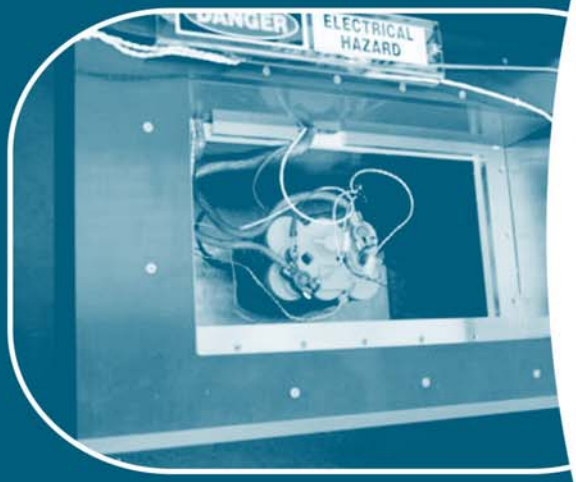

III

ADVANCED BATTERY DEVELOPMENT, SYSTEMS ANALYSIS, AND TESTING

A. System and Materials Development

B. Systems Analysis

C. Battery Testing Activities

D.O.E. Project Manager

David Howell

III. ADVANCED BATTERY DEVELOPMENT, SYSTEMS ANALYSIS, AND TESTING

One of the primary objectives of the Energy Storage effort is the development of durable and affordable advanced batteries and ultracapacitors for use in advanced vehicles, from start/stop to full-power HEVs, PHEVs, and EVs. The battery technology development activity supports this objective through projects in several areas:

- System and materials development of full battery systems and advanced materials for those systems,
- Systems analysis which includes thermal analysis and simulation, various simulations to determine battery requirements, life modeling, recycling studies and other studies,
- Testing of batteries being developed with DOE support and of emerging technologies to remain abreast of the latest industry developments and to validate developer claims,
- International activities which DOE supports in order to remain abreast of technology and policy developments around the world, and
- Small Business Innovative Research (SBIR) to fund early-stage R&D for small businesses/entrepreneurs.

III.A. System and Materials Development

Objectives

- By 2010, develop an electric drive train energy storage device with a 15-year life at 300 Wh with a discharge power of 25 kW for 18 seconds and a cost of $20/kW.
- By 2014, develop a PHEV battery that enables a 40 mile all-electric range and costs $3,400

Technical Barriers

- **Cost** – The current cost of Li-based batteries (the most promising chemistry) is approximately a factor of three-five too high on a kWh basis for PHEVs and approximately a factor of two too high on a kW basis for HEVs. The main cost drivers being addressed are the high costs of raw materials and materials processing, cell and module packaging, and manufacturing.
- **Performance** – The performance advancements required include the need for much higher energy densities to meet the volume and weight requirements, especially for the 40 mile PHEV system, and to reduce the number of cells in the battery (thus reducing system cost).
- **Abuse Tolerance** – Many Li batteries are not intrinsically tolerant to abusive conditions such as a short circuit (including an internal short circuit), overcharge, over-discharge, crush, or exposure to fire and/or other high temperature environments. The use of Li chemistry in the larger (PHEV) batteries increases the urgency to address these issues.
- **Life** – The ability to attain a 15-year life with 300,000 HEV cycles or 5,000 EV cycles is unproven and is anticipated to be difficult.

Technical Targets

- Focus on the small-scale manufacture of cells, batteries, and advanced materials for high-power applications (HEVs and 42 Volt start/stop systems) and high-energy applications (e.g., PHEVs).
- Attempt to meet the summary requirements for PHEVs and HEVs developed with industry as shown in Table III-1 and Table III-2.

Table III-1: Summary Requirements for PHEV Batteries[24]

Characteristics at EOL (End of Life)		High Power/Energy Ratio Battery	High Energy/Power Ratio Battery
Reference Equivalent Electric Range	miles	**10**	**40**
Peak Pulse Discharge Power (2 sec/10 sec)	kW	**50/45**	**46/38**
Peak Regen Pulse Power (10 sec)	kW	**30**	**25**
Available Energy for CD (Charge Depleting) Mode, 10 kW Rate	kWh	**3.4**	**11.6**
Available Energy in CS (Charge Sustaining) Mode	kWh	**0.5**	**0.3**
CD Life	Cycles	**5,000**	**5,000**
CS HEV Cycle Life, 50 Wh Profile	Cycles	**300,000**	**300,000**
Calendar Life, 35°C	year	**15**	**15**
Maximum System Weight	kg	**60**	**120**
Maximum System Volume	Liter	**40**	**80**
System Recharge Rate at 30°C	kW	**1.4 (120V/15A)**	**1.4 (120V/15A)**
Unassisted Operating & Charging Temperature	°C	**-30 to +52**	**-30 to +52**
Survival Temperature Range	°C	**-46 to +66**	**-46 to +66**
Maximum System Price @ 100k units/yr	$	**$1,700**	**$3,400**

[24] For more details and for additional goals, see http://www.uscar.org/guest/view_team.php?teams_id=11.)

Table III-2: Energy Storage Targets for Power Assist Hybrid Electric Vehicles

Characteristics	Minimum value	Maximum value
Pulse discharge power (kW)	25 (for 10 seconds)	40 (for 10 seconds)
Maximum regenerating pulse (10 s; kW)	20 (50 Wh pulse)	35 (97 Wh pulse)
Total available energy (kWh)	0.3	0.5
Cycle life (cycles)	300k 25-Wh cycle (7.5 MWh)	300k 50-Wh cycle (15 MWh)
Cold-cranking power at −30ºC (three 2-sec pulses, 10-s rests between; kW)	5	7
Calendar life (years)	15	15
Maximum weight (kg)	40	60
Maximum volume (liters)	32	45
Production price @ 100k units/year ($)	500	800
Operating temperature (ºC)	−30 to +52	−30 to +52
Survival temperature (ºC)	−46 to +66	−46 to +66

Accomplishments

- The PHEV research and development activity is now fully underway with multiple systems development contracts being conducted, and numerous advanced materials and components contracts through the National Energy and Technology Laboratory (NETL). All system development for light duty vehicles is conducted in collaboration with industry through the USABC. All of the USABC subcontracts are awarded competitively and are cost-shared by the developer at a minimum of 50 percent.
- The following subsections highlight the battery and materials development activities for 2009.

III.A.1 High Energy PHEV Systems

III.A.1.1 Advanced High-Performance Batteries for Plug-In Hybrid Electric Vehicle Applications (Johnson Controls – Saft)

Renata Arsenault (USABC Program Manager)

Subcontractor:
Johnson Controls-Saft, Inc.

Scott Engstrom (Program Manager)
5757 N. Green Bay Road
Glendale, WI 53209
Phone: (414) 524-2357; Fax: (414) 524-2008
E-mail: scott.engstrom@jci.com

Start Date: June 16, 2008
Projected End Date: April 29, 2011

Objectives

- Develop a prismatic battery cell which will meet program Gap Chart targets at system and cell levels.
- Develop and build a PHEV battery system capable of a 20-mile all-electric drive range (AER) using cells developed for this program.
- Develop and deliver a paper design for a 40-mile all-electric range PHEV battery system design using the 20-mile cell.

Technical Barriers

- Improving pack level volumetric and gravimetric energy density
- Cycle-life in charge-depleting and charge-sustaining modes
- Characterization and improvement of the abuse tolerance behavior
- Meeting performance goals within the projected price target
- Developing prismatic mechanical design to include suitable vent and current interrupt device (CID)

Technical Targets

- Available energy in charge depleting mode: 5.8 kWh for 20-mile system and 11.6 kWh for 40-mile system
- Specific Energy: 122 Wh/kg for 20-mile and 142 Wh/kg for 40-mile system
- Energy Density: 183 Wh/L for 20-mile and 230 Wh/L for 40-mile system
- 20-mile System Cost: $2,200

Accomplishments

- Alternative high melting point separators and their suppliers were identified. Parts were procured and initial evaluations were conducted with some success.
- Abuse testing results for overcharge, short-circuit and nail penetration (both sharp nail and blunt rod)
- The energy density of high-energy cylindrical cells was improved by about 3%, based on mechanical cell changes to improve packaging efficiency.
- A baseline 10 mile PHEV system using 88 cells was delivered in December, 2008. National Lab evaluation is underway to verify performance.
- Alternate cathode technologies were developed and evaluated. Although not fully optimized, Iron-Phosphate (LFP) was found to provide some improvement to abuse tolerance. However, performance and life are not compliant to the USABC goals. The performance was compared with and summarized against Nickel-Cobalt-Aluminum (NCA) technology.
- Nickel-Manganese-Cobalt (NMC) technology had been under investigation in cylindrical cells.
  - Early prototype cathodes were built for evaluations in cylindrical cells (9Ah).
  - Prismatic hard-shell mechanics were developed and released for a 4th quarter build
  - A proof-of-concept build with off the shelf (OTS) hardware was completed, evaluation is currently underway.
- Surrogate test cell developed for abuse testing.
- Conducted >2000 CD cycles using the baseline cells.
- Conducted manufacturing efficiency studies on alternatives to the electrode slitting process and to reduce the amount of fasteners. Results have been shared with the USABC body.

✧ ✧ ✧ ✧ ✧

Introduction

Achieving the DOE cost targets will require improved cell-level energy density and system level packaging efficiency without conflicting with other performance goals and product abuse tolerance. In the interest of improving packaging efficiency, it was agreed to execute a scope shift from existing cylindrical cell optimization toward new prismatic cell development after the first year of development. This also shifted the cathode technology focus from NCA toward NMC development, along with other compatible materials.

Approach

The approach for this PHEV development program has always been to leverage, reuse and optimize improvements to existing technology and system components and sub-assemblies as an efficient use of resources and means of maintaining lower assembly costs. On the system side, this is still primarily the case. The development of PHEV software, core battery management system and pursuit of improved cell and system assembly processes are still on track to be utilized as core pieces of the developed system.

At the program's mid-point, further improvements in the volumetric packaging efficiency and resulting system form factor were determined to be better accomplished with an as yet undefined prismatic cell. This decision also dictates the need to develop NMC cathode technology, which affords reduced levels of out-gassing, thereby reducing the pressure on the larger prismatic faces. The first phase in NMC development will be to begin to select the appropriate material supplier as well as the mix of materials using a known cylindrical cell form, which has previously been used to evaluate improvements in NCA and LFP technologies. The second phase of this development will be to optimize the cathode technology in the chosen prismatic size factor. JCS will procure development cell manufacturing equipment toward finalizing the best combination of cell mechanics and internal chemistry. Initially, JCS was able to leverage existing electrode stacking equipment through their partner Saft in use at one of their locations.

Results

PHEV Baseline System Characterization. A 10-mile AER baseline system (Figure III-1) using 88 high-energy to power ratio cells was shipped to Argonne National Labs. The cells used are in the latter stages of development and are intended for inclusion in the JCS cell portfolio. The unit met the DOE target for available energy, Figure III-2, but it does not meet mass or volume goals.

Figure III-1: Baseline PHEV 10-mile development system shipped to Argonne National Labs

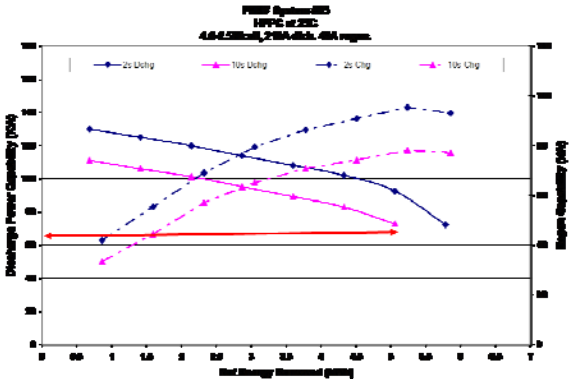

Figure III-2:. Baseline PHEV system available energy at 25°C.

NMC Cathode Development. Prior to submitting the program change proposal to USABC, JCS began work to develop NMC cathode technology in 2008 using pouch packaging. In addition, JCS's partner, Saft, has studied NMC technology over the past ten years and much of that knowledge was leveraged as a starting point. Cylindrical cells have now been built for evaluation and JCS has been working with multiple suppliers of advanced cathode materials toward selecting the appropriate formulation.

Comparison Summary of LFP and NCA Cell Performances. JCS has advanced their LFP technology over the past several years to a level which was deemed ready to begin characterization.

The main limitation of LFP chemistry was demonstrated to be capacity loss during calendar life. At 40°C storage at 100% state-of-charge (SOC) after about 140 days, NCA retains over 95% of its capacity, while LFP retained about 75%, Figure III-3. According to JCS's most recent assessment, it is expected that this result could be improved to about 85-90% with further development. However, even with these improvements, the LFP chemistry would still not meet USABC life targets. The development of LFP cathodes continues, but is no longer part of this DOE development program.

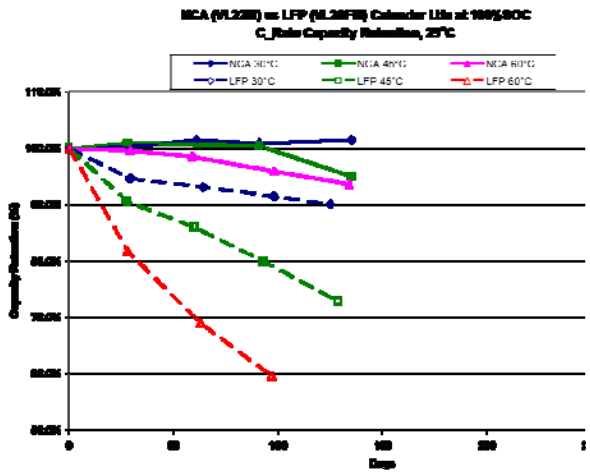

Figure III-3: Capacity Retention of LFP vs. NCA at about 140 days.

Abuse Tolerance Testing. Recent abuse tolerance testing has focused on identifying potential improvements by substituting advanced separator materials into a variety of standard cell configurations. Ceramic-filled, ceramic-coated and higher melting-point materials have been tested. A combination of the ceramic-coated and higher melting point separators has produced better results. This has been demonstrated through oven tests on separator samples but has not yet been demonstrated at the cell level. Testing the various sizes also demonstrated that smaller diameter cylindrical cells yielded better results. This will carry over to the prismatic form factor as thinner cells should yield better abuse tolerance results, as well as exhibit better thermal management at the cell level by conducting heat away from hot spots more readily. However, it was demonstrated that cell-level overcharge protection requires a current interrupt device (CID). Since the application of a CID in pouch cell format is extremely difficult to design, JCS chose to develop a hard case prismatic cell, Figure III- 4.

Prismatic vs. Cylindrical Packaging Study. Although still in a preliminary stage with the final cell size not yet determined, a packaging study is being conducted in conjunction with thermal analysis profiles in use on other JCS systems. Initial results have concluded that while there will be some improvement in system packaging density, there will be more benefit from the thermal management and potential reduced system height.

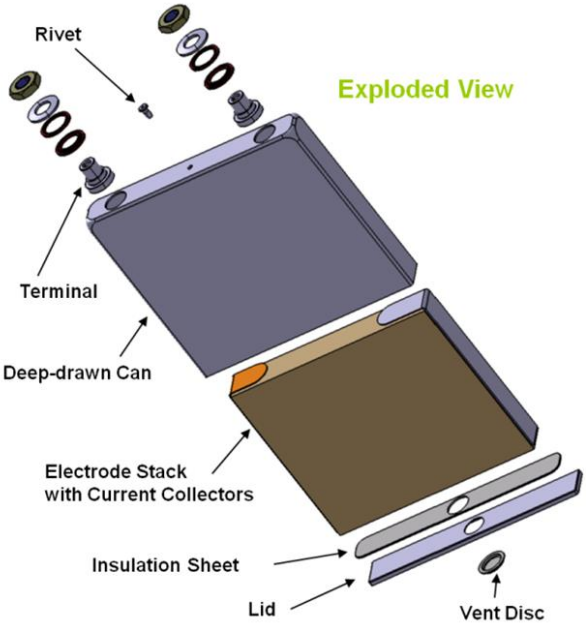

Figure III- 4: Preliminary prismatic cell mechanical design.

Conclusions and Future Directions

In the near-term, JCS will continue to evaluate NMC cathode technologies. Once the cathode active material formulation has been selected, cylindrical cells will be built for National Lab evaluation and comparison. These cells along with prismatic baseline cells will be submitted over the next year of the program. PHEV system development for a 20-mile all-electric range will commence in the first quarter of 2010. With very aggressive timing, prismatic cells that have been optimized and produced on JCS development equipment will be built into systems and delivered to USABC in the first half of 2011. The Advanced Manufacturing team will continue to study and implement improvements to the assembly processes in conjunction with the cell design team and the electrochemical team.

The program for the development of a PHEV-suitable prismatic cell and system has been extended by the DOE in the third quarter of 2009, following a proposal from JCS in the second quarter. With that change, development efforts for cylindrical cell mechanics, NCA and LFP were removed from the new scope of the USABC program. The goal of the redefined and extended program is to demonstrate improved packaging on an entirely new system, thereby improving system-level energy density, while maintaining projected low costs.

FY 2009 Publications/Presentations

1. Presentation to the 2009 DOE Annual Merit Review Meeting.

III.A.1.2 PHEV Battery Development (EnerDel)

Dawn Bernardi (USABC Program Manager)

Subcontractor: Enerdel, Inc.

Cyrus N. Ashtiani (Program Manager)
8740 Hague Road, Building 7
Indianapolis, IN 46256
Phone: (317) 585-3400; Fax: (317) 585-3444
E-mail: cashtiani@ENERDEL.com

Subcontractor:
Argonne National Laboratory, Argonne, IL

Start Date: March 2008
Projected End Date: September 2010

Objectives

- Design, build, and test $Li_4Ti_5O_{12}$ /$LiMn_{1.5}Ni_{0.5}O_4$ (LTO/LMNO) cells utilizing positive active material synthesized by Argonne National Laboratory (ANL).
- Develop and evaluate a stable high-voltage electrolyte system that is compatible with the LMNO/LTO cell.

Technical Barriers

One of the challenges of the LTO/LMNO system is that the LMNO positive active material is newly developed and lacks commercial availability. ANL will need to synthesize this material in a large quantity with consistent characteristics to provide EnerDel with material to develop and produce cells. The LMNO positive material operates at a potential that is higher than typical positive active materials. Therefore a new electrolyte system may be required in order to operate at these higher potentials.

Technical Targets

- Develop a cell to meet the 10-mile PHEV goal.
- Obtain a positive-electrode material that can operate in the high-potential range (4V – 5V *vs.* Li/Li^+) while still achieving approximately 130 mAh/g of capacity.
- Develop and utilize a high-potential, stable electrolyte system that can operate in the temperature range of -30°C to 55°C.

Accomplishments

- Demonstration of over 1500 room-temperature, full cycles with 100% capacity retention in 1-mAh LTO/LMNO coin cells.
- Development of a LMNO coating that increased capacity retention from 30% to 80% over 500 cycles in coin cells at 55°C.
- Successful synthesis of LMNO positive active material (with and without coating) in consistent batches of more than 10 kg each.
- Development of 3.1-V, 2.7-Ah LTO/LMNO cells that showed up to 80% capacity retention at 6C. Six cells comprised the program's 1st deliverable and were sent to Idaho National Laboratory for further evaluation.

Introduction

EnerDel proposed to develop a new battery system based on a novel high-voltage positive chemistry that could meet the 10-mile PHEV requirements while maintaining long life, excellent safety, and low cost. The main candidate for this new high-voltage positive is a stable $LiMn_{1.5}Ni_{0.5}O_4$ (LMNO) spinel that can theoretically provide 147 mAh/g of capacity at an operating voltage of 4.8 V *vs.* Li/Li^+. The proposed negative electrode for this system is the LTO material that EnerDel has already adopted for use in HEV batteries in combination with the $LiMn_2O_4$ positive material (at 4.0 V *vs.* Li/Li^+). The combination of LTO with LMNO allows the benefits of the LTO negative electrode to be utilized in a high-energy battery with an operating voltage of 3.2 V. The inherent safety of LTO relative to current carbon-based negatives is well recognized and relates to LTO being a comfortable 1.5 V away from dangerous lithium dendrite formation (graphite, for example, sits very close at 0.08 V.) Both LMNO and LTO can avoid large volume changes during operation and therefore hold the promise of long life. Relatively abundant raw materials for the production of both LMNO and LTO indicate the potential for low cost; additionally, LTO does not require formation. The LTO/LMNO system enables EnerDel to achieve a battery that has the safety characteristics from the LTO material and the energy density necessary for the PHEV goals from the LMNO material.

Approach

EnerDel is working with ANL to obtain the novel, 5-V LMNO spinel material. ANL has experience developing positive active materials and currently has equipment capable of producing batches of material that are approximately 10-kg in size. The expertise of ANL is leveraged to obtain large quantities of this material. The large volume is necessary in order for EnerDel to optimize the electrode fabrication process. EnerDel has experience

developing lithium-ion cells with novel chemistries such as the $LiMn_2O_4/Li_4Ti_5O_{12}$ HEV cell. EnerDel will demonstrate the capability of the LMNO/LTO cell in a prismatic design with a capacity of approximately 3 Ah.

Results

Material. EnerDel has received a total of 11 batches of LMNO material from ANL (Table III-3). Each batch has had consistent material properties and capacity (Figure III-5).

Table III-3: LMNO material deliverable dates and quantity from ANL.

Lot	Amount (kg)
August 2009	11
July 2009	11
May 2009	11
April 2009	5.5
February 2009	8.5
December 2008	8.5
September 2008	6
July 2008	3
June 2008	4
Small batch	1

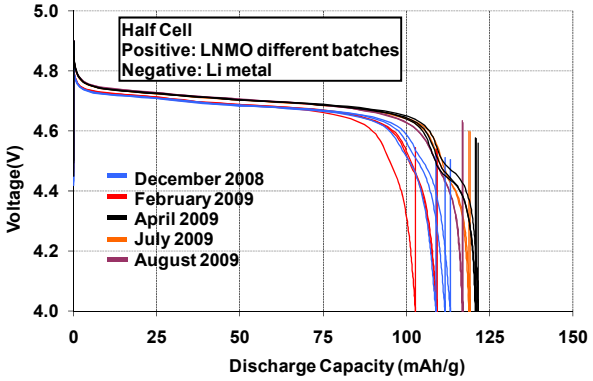

Figure III-5: 1C discharge capacity of LMNO half cells made from material received from ANL.

Electrolyte Development. EnerDel has evaluated alternatives to the conventional liquid electrolyte solutions for the high-voltage spinel system. Among the alternatives included were ionic liquids and alternative solvent systems such as sulfone solvents.

Ionic liquids are more stable at higher voltages, but are typically too viscous to provide high rate. EnerDel has investigated the effect of mixing ionic liquids with conventional solvents in order to reduce the viscosity while still maintaining the benefits of the ionic-liquid system. Current results show that more optimization for the ratio of ionic liquid to conventional solvent is necessary.

Sulfone systems are currently being developed by ANL. EnerDel has received one sample of this solvent system from ANL. Further evaluation is necessary as more sulfone solvent becomes available.

Cell Development. 2.7-Ah sized cells have been developed and shipped to Idaho National Laboratory for testing according to the USABC PHEV manual.

Power tests (HPPC) were conducted on the cells with a 10-second discharge/charge pulse. Figure III-6 shows the pulse power capability and Figure III-7 shows the resistances calculated from the voltage profiles. The attractive power capability of these cells is related to nearly constant resistance from 100% down to 30% state-of-charge. The cells also showed good rate capability; 60% to 80% coulombic capacity retention was obtained at 6C.

EnerDel continues to develop these cells in order to improve the rate capability and energy density of the system. Improved cells will be delivered to Idaho National Laboratory for further testing at the completion of the program.

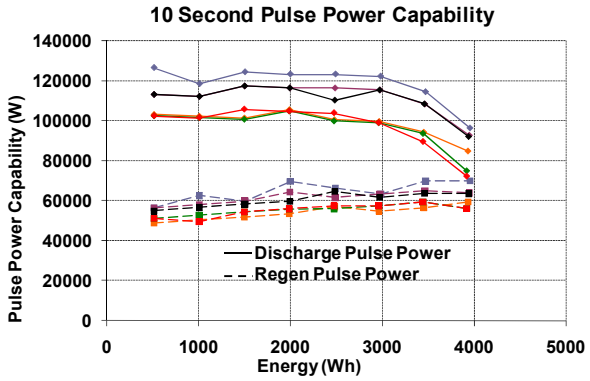

Figure III-6: HPPC results of CD sized cells delivered to INL for testing.

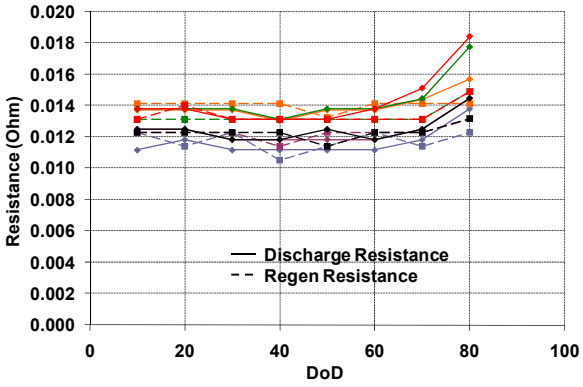

Figure III-7: 10 second resistance values calculated from the HPPC test.

Conclusions and Future Directions

EnerDel has received 11 batches of LMNO material from ANL. The latest batches have been approximately

10-kg in size which will allow EnerDel to complete the optimization of the electrode fabrication process. This will allow EnerDel to produce the final set of deliverables for the program. The last deliverable is a set of 40, 3-Ah cells which will be delivered to Idaho National Laboratory at the end of November. These cells will incorporate the optimal electrolyte/solvent combination along with the most recent batch of coated LMNO material delivered from ANL.

EnerDel would like to continue its development of the LMNO/LTO chemistry to further improve the performance of this system. This system allows the benefits of the LTO to be utilized in a higher energy density system.

FY 2009 Publications/Presentations

1. 2009 DOE Annual Peer Review Meeting Presentation.

III.A.1.3 Development of High-Performance PHEV Battery Pack (CPI – LG Chem)

Harshad Tataria (USABC Program Manager)

Subcontractor: Compact Power, Inc.

Mohamed Alamgir (Program Manager)
1857 Technology Drive
Troy, MI 48083
Phone: (248) 291-2375; Fax: (248) 597-0900
E-mail: alamgir@compactpower.com

Subcontractor: LG Chem, Seoul, South Korea

Start Date: January 1, 2008
Projected End Date: March 31, 2010

Objectives

- This is a 27 month program aimed primarily at developing and demonstrating a Li-ion cell for PHEV10 applications to meet the energy, power and life requirements of the USABC program. A 15-yr calendar-life and 5,000 charge depleting cycles are the targets for this cell. While addressing these key issues, we will also focus on evaluating their abuse-tolerance and low-temperature performance.
- The above cell work will be supplemented by studies related to modules leading to the development, testing and delivery of packs to the USABC. These studies will be directed at finding a design solution that maximizes the effectiveness of the enclosed cells in terms of performance, life and abuse tolerance, while minimizing system weight, volume, and cost. In order to achieve these goals, the proposed pack development work will involve analysis, design and testing of a pack that is scalable and efficient with respect to manufacturing and validation.

Technical Barriers

The project focuses on addressing the following technical barriers.

(A) Demonstrate cycle-life of over 5,000 cycles

(B) Demonstrate calendar-life of over 15 years

(C) Cold-cranking power of 7kW

(D) Develop a pack that is mechanically and electrically efficient and meets the USABC cost target of $1,700.

Technical Targets

- Demonstrate cell cycling capability of over 5,000 cycles
- Show data to demonstrate 15 years of calendar-life
- Develop a novel cooling system that is electrically and mechanically efficient
- Develop a pack design that is modular, easy to manufacture and is close to the cost target of USABC.

Accomplishments

- We have demonstrated that our high power baseline cell is easily capable of meeting the 5000 cycle-life as well as the 15-year calendar-life targets of the USABC under the PHEV cycling conditions.
- Two generations of high specific energy PHEV cells have been fabricated which allowed us to identify design factors critical for the life of these cells. These results have now been incorporated into the design of cells to be delivered to and tested at the National Labs.
- The cells have been characterized thermally at National Renewable Energy Labs (NREL). Thanks to laminated/plate design, the cells demonstrate lower and uniform heating during cycling.
- Abuse-tolerance tests have been carried out at Sandia National Labs showing attractive results.
- We have developed a pack that is mechanically efficient using an advanced cooling system and is being built for delivery and testing at the National Labs.

✧ ✧ ✧ ✧ ✧

Introduction

Development of a cost-effective, high performance battery is a prerequisite for the successful introduction of electric vehicles. With that objective in mind, we are working to develop a spinel-based Li-ion battery using laminated packaging.

Approach

To achieve the USABC objective, we have developed a cell chemistry based on spinel, our patented Safety

Reinforcing Separator (SRS), and a laminated packaging design. The objective is to optimize the mixed cathode, anode and electrolyte compositions in order to meet the USABC targets for cycle- and calendar-life. Evaluation of other critical factors such as anode to cathode ratios, effect of binders and electrolyte additives is also an important task. In addition, compositions of the various components have been altered to improve the cold-cranking power of the cells.

We have developed a pack design which is mechanically, electrically and thermally efficient. Since our cells are based on laminated packaging, work was focused on developing unique cell restraint and interconnect mechanism, especially involving welding. To achieve an efficient thermal system, a new type of cooling system has also been designed.

Results

Development of an optimized cathode system. We have varied the compositions of the cathode with respect to power, energy, abuse-tolerance and cost in order to optimize the composition of the cathode system.

Development of anode system. Using a matrix of selection criteria, we have identified an anode composition which is optimum with respect to energy, power, cold-cranking capability as well as life and cost.

Development of electrolyte system. The composition of the electrolyte appears to play a critical role in dictating the life and cold-cranking power of our cell. As expected, electrolyte compositions determine the quality of the SEI which, in turn, affects the cycle- and calendar- lives of the cell.

Cycle-life. Our baseline cell developed under the HEV program was at first used to generate cycle-life using the PHEV cycling conditions. The data demonstrate that the cell is capable of demonstrating over 5000 cycles without showing any significant loss in energy and power. The cycle-life of the high energy PHEV cell shows stronger dependency on cell components than its HEV counterpart. Based on these data, we have tailored the cell compositions to enhance the cycle-life. These cells will be delivered to the National Labs to validate our observations.

Calendar-life Testing. While calendar-life of the baseline cell has been well-characterized in our HEV program, relative data similar to cycle-life were also obtained with our baseline HEV cell and the first generation of our high energy PHEV cell with respect to calendar-life. The effect of cell components especially those of the anode and electrolyte is being extensively studied for this purpose over a large temperature range.

Thermal Characterization of Cell. The cell has been characterized thermally at NREL. The cell shows efficient thermal characteristics; not only does the cell show lower heat output, it also shows more uniform temperature across the cell body. This is due to the plate design and thin format of the cells.

Abuse-Tolerance Characteristics. The cells have been subjected to a number of key abuse-tolerance tests such as short-circuit, nail-penetration, thermal stability and overcharge. The data demonstrate the efficacy of our proprietary separator in preserving a high degree of abuse-tolerance for these high energy PHEV cells.

Development of Pack. Considerable effort was directed at designing a mechanically robust pack. This involved finding an optimum cell restraint system for our laminated cell as well as fabrication conditions for the interconnect system, especially the terminal to terminal welding.

Development of an efficient cooling system. A focus of our pack development work was the development of an efficient cooling system. A total of 10 potential cooling systems were evaluated based on a number of key parameters such as the ability to remove heat from cells, uniform performance across all the cells in the pack, energy required to run the cooling system, simplicity of manufacturing, and cost. This was followed by the development of flexible cell retention system which could be used in any cooling methods. From this, the refrigerant-to-air cooling system was selected and then necessary components were developed and sized. These were then tested and optimized for efficiency using the parameters listed above.

Conclusions and Future Directions

Key factors determining the energy, power, life and cold-cranking capability of our cells have been identified and optimized. Extensive abuse-testing of the cells has also been carried out with very attractive results. Considerable design iterations have been carried out on the pack system with the development of a new cooling system.

Based on the current cell data, 2nd generation of cells have been fabricated and will be delivered. These will be subjected to cycle- and calendar-life testing as well as abuse-testing and thermal characterization.

Packs and modules are now being built to be delivered to the National Labs for performance, life and abuse-tolerance testing. The packs will incorporate the new cooling system we have developed.

FY 2009 Publications/Presentations

1. Presentation to the 2008 DOE Annual Peer Review Meeting.
2. Presentation at FL International Seminar on Li batteries, Ft Lauderdale, March 2009.

III.A.1.4 Nanophosphate for PHEV Applications: A Multi-Generational Approach (A123Systems)

Ron Elder (Program Manager)

Subcontractor: A123Systems

Leslie Pinnell, (Program Manager)
321 Arsenal Street
Watertown, MA 02472
Phone: (617) 778-5577; Fax: (617) 778-5749
E-mail: lpinnell@a123systems.com

Start Date: October 11, 2009
Projected End Date: March 1, 2011

Objectives

- Design, build and test cells and modules for PHEV battery systems that will achieve the DOE / USABC FreedomCAR performance and cost targets.
- Develop and demonstrate performance and cost impact from innovative smart materials.

Technical Barriers

This project addresses the following technical barriers for performance and cost: (A) Cell Cycle Life, (B) Calendar Life, (C) System Weight and Volume, and (D) System Cost

Technical Targets

- Demonstrate cell performance which can meet FreedomCAR PHEV 10 Mile (minimum) and 40 mile (maximum) targets.
  - Develop technology which enables achievement of USABC cost targets, of $1,700 / 10 mile PHEV system and $3,400 / 40 mile PHEV system.
- Conduct testing to allow estimation of 15 years in-use calendar life.

Accomplishments

- Developed a 19Ah prismatic cell which can meet power and energy targets for 10 mile and 40 mile PHEV targets.
- Locked the first generation AP4 PHEV cell design, which has achieved over 2,500 cycles to 87% capacity in 100% DOD 1C, 2C cycling.
- Demonstrated 90 days storage at 55°C, at 100% state of charge, with 90% retained and recovered capacity.
- Developed a next generation (Gen 1.5) 20 Ah prismatic cell which is targeted for design lock in January, 2010, and has achieved 600 cycles to 98% capacity in 1C, 2C 100% DOD cycling.
- Scaled up nanocomposite separator (NCS) coating equipment and processes to enable preliminary evaluation in 20 Ah prismatic cells. Smaller prismatic test cells with NCS separator have shown over 4,000 cycles in 100% DoD 1.5C, 2.5C cycling to date, currently at 80 – 90% capacity.
- A three year joint development program was initiated with ORNL to scale up NCS process development.
- Developed higher energy nanophosphate cathode material "M1x" which achieved targeted capacity of 150 mAh/g and which provides much higher voltage than the current LFP chemistry.
- Testing of the new M1x cathode in cylindrical 28650 cells resulted in >160 cycles to 97% capacity at 100% DoD and 23°C, and ~400 cycles to 80% capacity at 60°C.

✧ ✧ ✧ ✧ ✧

Introduction

Achievement of USABC FreedomCAR goals will require cells and battery modules which successfully deploy technologies with high energy and efficient design. The most significant challenge in developing this system is cost. Cost estimates for both 10 mile and 40 mile PHEV systems have dropped significantly over the past year due to improved performance, streamlined module design and optimized designs with lower cost materials. Cost estimates at the beginning of the PHEV program, in March 2008, were roughly 3.5 times the Minimum Freedom Car PHEV target - currently that gap has been reduced to 50% over target. Additional improvement from the Smart Materials program are expected to further decrease this gap and bring the A123 system to within 30% of the FreedomCAR minimum PHEV cost objective. Performance of this system has also improved, as shown by reduced BSF estimate from 110 at the program start, to a current end of program estimate of 81.

Approach

A123 has developed a 19Ah prismatic cell, which has power and energy projected to meet most of the USABC FreedomCAR targets. Continued challenges lie in ongoing and aggressive cost reduction, and demonstration of cycle and calendar life. As the A123 nanophosphate cathode material has inherently lower voltage than most other Li-ion systems, cold crank response is also a challenge due to increased impedance at -30°C. The development approach to close the gap on these performance objectives has been to continue to incrementally increase energy and power for lower BSF, thus lower cost, and to develop materials with higher energy and lower cost per Wh. The module has been designed to further enhance cycle and calendar life of the A123 prismatic cells by adopting a low volume compression system to ensure continuous and optimal pressure on each cell.

Results

10 Mile (Minimum) PHEV. End of program estimates for the 10 mile PHEV modules show that most FreedomCAR goals can be achieved or exceeded, Figure III-8. The A123 nanophosphate system strength is its power capability, therefore the focus has been on optimizing energy for this lower voltage Li-ion cell. Cycle life and calendar life estimates have not yet been provided as testing using USABC-specific protocol has just recently started. Internal development tests using 1C / 2C 100% DOD cycling indicate that progress has been significant over the past year, doubling the cycle life during that timeframe.

A123 PHEV packs vs. FreedomCAR Energy Storage System End-of-Life Performance Goals

Characteristics	Units	A123 BOP (16Ah)	Q3 2009 (20Ah)	EOP 100K (20Ah)	2014 100K (20Ah)	FreedomCar 10-mile goal
Reference Equivalent Electric Range	miles	10.4	10.0	10.1	10.0	10
Peak Pulse Discharge Power, 2s	kW	88	114	108	102	50
Peak Pulse Discharge Power, 10s	kW	70	92	88	83	45
Peak Regen Pulse Power, 10s	kW	53	80	76	71	30
Maximum Current, 10s	A	300	300	300	300	300
Available Energy for Charge Depleting Mode, 10 kW rate	kWh	3.5	3.4	3.4	3.4	3.40
Available Energy for Charge Sustaining Mode	kWh	0.67	0.64	0.64	0.64	0.50
Minimum Round-Trip Energy Efficiency for USABC HEV cycle	%	>90	>90	>90	>90	>90
Cold Crank power at -30'C, 3x 2s pulses	kW	5	4	4	3	7
Charge-depleting cycle life	Cycles					5000
Charge-depleting discharge throughput	MWh					17
Charge sustaining PHEV cycle life, 50 Wh profile	Cycles					300k
Calendar Life, 35'C	year					15
Max system weight	kg	84	81	80	74	60
Max system volume	Liter	54	52	52	50	40
Max operating voltage	V	418	323	308	289	400
Min operating voltage	V	220	170	162	152	>0.55 x Vmax
Max self discharge	Wh/day	<20	<20	<20	<20	50
System recharge rate at 30'C	kW	1.4	1.4	1.4	1.4	1.4
Unassisted operating and charging temperature range	'C	-30 to +52	-30 to +52	-30 to +52	-30 to +52	-30 to +52
Survival temperature range	'C	-46 to +66	-46 to +66	-46 to +66	-46 to +66	-46 to +66
Max system production price @ 100k units/yr	$	6060	4219	2402	2159	1700
# of cells in series		110	85	81	76	
# of cells in parallel		1	1	1	1	
BSF (assuming 20% energy/power loss)		110	85	81	76	

Figure III-8: Gap Analysis for 10 Mile (Minimum) PHEV Cell

System level cost estimates have been reduced by almost 1/3 during the first 18 months of the project, due to increasing cell energy (thus decreasing pack BSF), reducing materials cost through external contracts and internal processing improvements, and designing a "minimalist" module system for improved volumetric and gravimetric efficiency.

40 Mile (Maximum) PHEV. End of program estimates for the 40 mile PHEV application (Figure III-9) are closer to FreedomCAR goals, generally due to the larger BSF, see the improved power capability at cold temperatures, for example. The one exception to this is production pricing, where the large BSF becomes a significant cost challenge. Efforts to reduce cost on a cell and module basis have resulted in reductions of approximately 50% during the first 18 months of the program, but this is still 2X the program goal. Continued efforts to drive the cost down to within 1.5X is focused on development of more innovative materials concepts which are covered under the Smart Materials program objectives.

A123 PHEV packs vs. FreedomCAR Energy Storage System End-of-Life Performance Goals

Characteristics	Units	A123 BOP (16 Ah)	Q3 2009 (AP4 20Ah)	EOP 100K (AP5,20Ah)	2014 100K (20 Ah)	FreedomCar 40-mile goal
Reference Equivalent Electric Range	miles	40.0	40.3	40.2	40.3	40
Peak Pulse Discharge Power, 2s	kW	>100	388.8	368.7	348.7	46
Peak Pulse Discharge Power, 10s	kW	>100	316.1	299.8	283.6	38
Peak Regen Pulse Power, 10s	kW	>100	139.7	132.5	125.3	25
Maximum Current, 10s	A	300.0	300.0	300.0	300.0	300
Available Energy for Charge Depleting Mode, 10 kW rate	kWh	11.7	11.7	11.7	11.7	11.60
Available Energy for Charge Sustaining Mode	kWh	1.5	1.5	1.5	1.5	0.30
Minimum Round-Trip Energy Efficiency for USABC HEV cycle	%	>90	>90	>90	>90	>90
Cold Crank power at -30˚C, 3x 2s pulses	kW	16.0	12.8	12.1	11.5	7
Charge-depleting cycle life	Cycles					5000
Charge-depleting discharge throughput	MWh					58
Charge sustaining HEV cycle life, 50 Wh profile	Cycles					300k
Calendar Life, 35˚C	year					15
Max system weight	kg	204	180	165	147	120
Max system volume	Liter	120	105	98	92	80
Max operating voltage	V	423.5	339.5	395.6	374.1	400
Min operating voltage	V	242.0	194.0	184.0	174.0	>0.55 x Vmax
Max self discharge	Wh/day	<20	<20	<20	<20	50
System recharge rate at 30˚C	kW	1.4	1.4	1.4	1.4	1.4
Unassisted operating and charging temperature range	˚C	-30 to +52	-30 to +52	-30 to +52	-30 to +52	-30 to +52
Survival temperature range	˚C	-46 to +66	-46 to +66	-46 to +66	-46 to +66	-46 to +66
Max system production price @ 100k units/yr	$	15950	14429	8180	7407	3400
# of cells in series		121	97	92	87	
# of cells in parallel		3	3	3	3	
BSF (assuming 20% energy/power loss)		363	291	276	261	

Figure III-9: Gap Analysis for 40 Mile PHEV Cell

A study to evaluate the impact of compression, rate and temperature on the prismaticAP4 cells' performance in various module designs was conducted. The results show that cycle life is improved when cells are subjected to continuous compression, Figure III-10. A 30% increase in the number of cycles was achieved in a 100% DOD 1C, 2C screening test when applying constant 8 psi of pressure to the cycling cells.

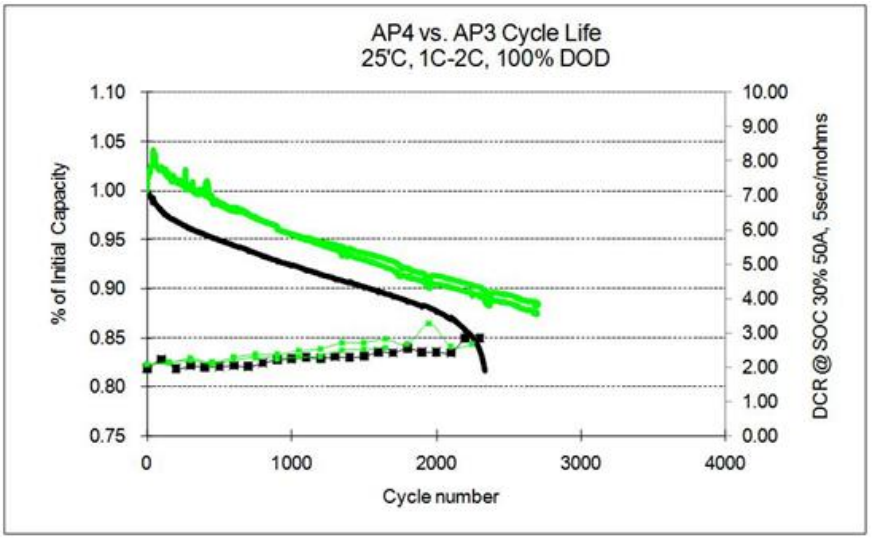

Figure III-10: Cycle Life Screening Test to Evaluate Compression

Calendar life screening tests show improvements in high temperature storage with the use of modified cell design. The newer cells retained 90% of their capacity after storage for 85 days at 55°C at 100% SOC, see Figure III-11.

Validation (DVP&R) testing of the AP4 design has been initiated. Meanwhile, a newer generation of prismatic cell, AP5, is under development and testing is underway to confirm optimal design and materials selection.

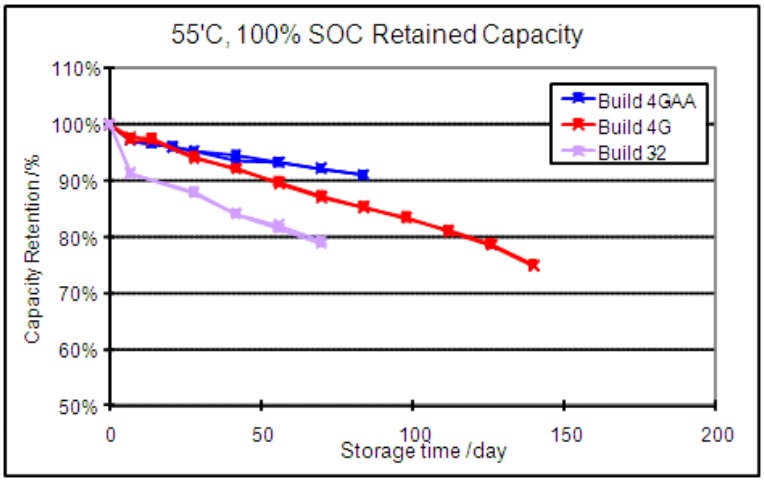

Figure III-11: Storage of AP4 Prismatic Cells at 55°C

Smart Materials

Separator

A novel separator is under development to reduce materials and processing costs and improve safety. This material has been designed to provide parity (with existing commercial separators) plus power and cycle life. The challenge has been in the process scale-up, to enable a volume cost of <$1.00 / m^2.

Anode Powder

New anode materials and formulations were evaluated for process capability, capacity, cycle life, storage, and cost, in preparation for AP5. Three viable candidates have been built into full size 20Ah cells, and HPPC, cycle life and storage life testing is in progress.

Cathode Powder

A new nanophosphate cathode material was developed, which has higher voltage, and therefore increased energy vs. the current material. Over 10% higher energy was achieved at a 2C discharge rate and over 20% higher energy was achieved at a 20C discharge rate. High temperature stability, which has been a vulnerability of this material to date, was improved significantly.

A synthesis process was developed with key unit operations and processing parameters identified. Synthesis was scaled up to the 20kg level, and two rounds of commercial grade 18650 cell builds and testing were conducted (18650 format, co-funded by Tardec). Cells showed good room temperature 1C/2C cycle life (ongoing, >1,800 cycles predicted).

Program next steps are to confirm high temperature cycling performance at 45°C, scale up synthesis, and conduct production trial runs in Q4'09.

PHEV Module Design

The module development program objective is to evaluate optimal configurations for PHEV modules which accommodate different series-parallel configurations and minimizes design and manufacturing costs. Effort has been increasingly focused on creating a flexible, modular structure to meet a wide range of customer applications with a standard set of design elements. Technical challenges include managing the tradeoff between volumetric energy density and cooling, cell to cell thermal management and SOC balancing, and assembly simplicity for lowest cost.

Significant progress was made in the area of Design Validation and UNDOT testing of the Prismatic Module A-Phase design through Q2'09. Notable accomplishments include:

- UNDOT altitude simulation, thermal cycling, vibration, shock, short circuit and overcharge test on three module configurations (6S3P, 11S3P, 16S3P).
- Design validation testing at the "mini-module" level (1S3P) including nail penetration, overcharge, short circuit, thermal stability per USABC FreedomCAR

test methods. All the results fell into EUCAR level 4 rating or lower

- Additional testing was performed to acquire data relative to "Customer testing." A "-20°C drive away" thermal test was performed on a 22S3P module to simulate a consumer using an EV after the car has reached equilibrium at -20°C overnight. The current, voltage and temperature response was recorded until the battery was completely discharged providing a transient thermal response of the module along with electrical performance.

Program next steps are to continue to develop a robust, low cost manufacturing process.

Conclusions and Future Directions

A123Systems' PHEV program is on track for delivering 55 test samples of a 20 Ah prismatic cell by September, 2010, which meet energy and power FreedomCAR goals for the selected BSFs, for both 10 mile and 40 mile PHEV applications. Cycle life and calendar life have not yet been determined using USABC-protocol tests, therefore these goals cannot be estimated until results are available, in Q2-Q3 of next year. Cost is the most challenging target, and has received heightened focus. Development and eventual implementation of Smart Materials in this project have the capability of significantly reducing overall system cost, and closing the gap between current estimates and FreedomCAR goals.

FY 2009 Publications/Presentations

1. Presentation to the 2009 DOE Annual Peer Review Meeting.

III.A.2. High Power/HEV Systems

III.A.2.1 Lithium Titanate / Manganese Spinel HEV System (EnerDel)

Euthemios Stamos (USABC Program Manager)

Subcontractor: Enerdel, Inc.

Cyrus N. Ashtiani (Program Manager)
8740 Hague Road, Building 7
Indianapolis, IN 46256
Phone: (317) 585-3400; Fax: (317) 585-3444
E-mail: cashtiani@ENERDEL.com

Subcontractor: Argonne National Laboratory, Argonne, IL

Start Date: August 1, 2007
Projected End Date: July 30, 2009

Objectives

- Design, build and scale up Mn-spinel/Lithium Titatate (LTO) system EnerDel developed during the initial phase of the program from 2Ah to a full size 4~4.5Ah prismatic pouch cell for a 25kW HEV system
- Demonstrate performance, cycle, and calendar life particularly at elevated temperatures (45°C+)

Technical Barriers

The challenge of LMO/LTO system is that at elevated temperatures it is prone to gassing and a correspondingly higher power fade.

Technical Targets

In this program, also referred to as phase II, two broad objectives were set for successful completion. One objective was to scale up and optimize the 2Ah CD-size cell, to the final HEV full size, named 'A5' cell, estimated at the time to fall between 4.0 to 4.5Ah. The second objective was to do a thorough root-cause analysis of power-fade at elevated temperatures and to find and implement the most cost-effective ways of mitigating the problem.

Accomplishments

The most critical accomplishment of this program was a thorough investigation of the LTO/LMO chemistry at elevated temperatures. The investigations not only identified that gas generation was the root cause of power fade, but also led to effective means of mitigating the gas generation through a combination of electrolyte and process modifications. In addition, EnerDel scaled up and optimized the cell to a full-size HEV format named 'A5' with a battery scaling factor (BSF) of 48 which is suitable for an HEV 25kW USABC application.

Introduction

The advantages of lithium titanate as an anode material for Li-ion batteries are well-documented in the literature. Chief among these are, best-in-class safety, and superior cycle life resulting from a robust anode in the presence of electrolyte and the fact that LTO undergoes insignificant volumetric expansion-contraction during charge-discharge cycles compared to carbonaceous and other types of anodes..

In the first phase of this program, EnerDel successfully scaled up and optimized its LMO/LTO pouch cell from a 100mAh reference cell to a 2.0Ah pouch cell in the so called "CD" size format. This cell showed excellent performance characteristics and met all USABC-HEV 25kW application targets. In particular, it met the cold-cranking requirement at -30°C which is the toughest performance criteria for other Li-ion chemistries often resulting in a significant overdesign. Although the CD size LMO/LTO cells met or exceeded the USABC performance targets, in the area of life, they showed high power fade at elevated temperatures. Independent tests at INL projected a calendar life of about 13 years at RT in spite of negative impact of the elevated temperatures on life.

In phase II; the current program, two broad objectives were set. The first objective was to scale up and optimize the CD-size cell, to the final HEV full size cell, also referred to as the "A5" format.

The second objective was to do a thorough root-cause analysis of power-fade at elevated temperature and then

find the most cost-effective ways of mitigating the problem.

Approach

EnerDel adopted a two-prong parallel approach to meet the program goals. On one front it proceeded to design and optimize the full size A5-format cell, and on the other it proceeded with a thorough root-cause analysis of the LMO/LTO system at elevated temperatures. The scale-up of the cell also involved material process scale up at our subcontract Argonne National Lab so that manufacturing of the larger format cells on production-grade equipment becomes feasible.

Results

Cell Scale-up & Optimization. EnerDel successfully scaled-up and optimized the LMO/LTO pouch cells from CD-size to A5-size format. Figure III-12 shows the HPPC performance test results of the CD-size cells with a BSF of 111 in red. The HPPC test results of an earlier version A5-size design with a BSF of 48 are shown in the same figure in blue. A diminished performance in the order of ~10% is observed in this non-optimized A5-size cell. After optimizing the A5 cell, the HPPC data were re-examined and can be observed on the same figure in green (same BSF=48). The resulting optimized cell has the same or better Pulse-Power performance characteristics.

Calendar Life at Elevated Temperature. EnerDel identified and demonstrated that the major cause of the cell power fade at elevated temperatures was excessive gas generation. It then proceeded through a series of Design of Experiments, electrochemical, physical, & analytical tools to identify the cause of gas-generation by the process of elimination. In the end, after identifying the root-cause and testing for multiple solution paths, it chose a combination of electrolyte modification and proprietary process adjustments as the most cost-effective way of addressing the premature power-fade at elevated temperature.

Figure III-13 shows a comparison between the power-fade during calendar life testing between the final cells and the cells at the beginning of the program. Cells were stored at 100%SOC and 60°C ambient temperature.

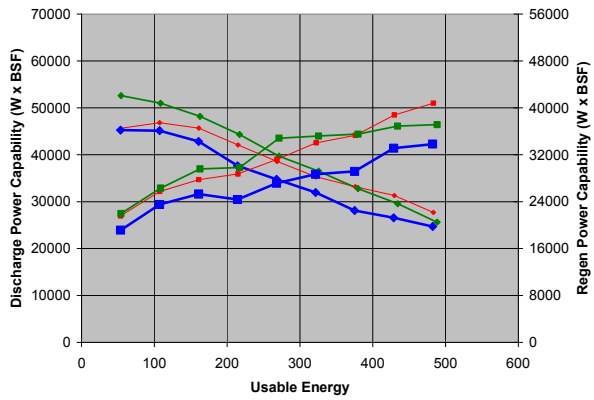

Figure III-12: HPPC Data of (RED, middle crossing point)-CD-size Cell (BLUE, bottom-most crossing point)-Initial A5 cells, (GREEN, top most cross point) Final A5 Cells

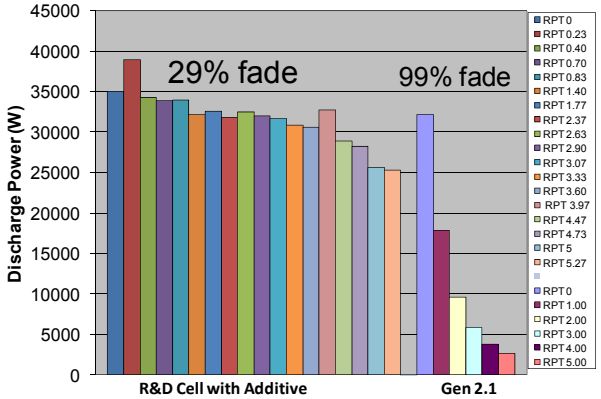

Figure III-13: RPT tests of modified and pre-modified cells stored at 100%SOC and 60°C

Conclusions and Future Directions

This program met its two primary objectives of scaling up to a full-size cell, determining the primary aging factors at elevated temperatures and mitigating the problem of aging at elevated temperatures. In the end, the program enabled EnerDel to bring the LTO/LMO technology to the HEV market. The next steps will involve development of the complete HEV battery systems tailored to this chemistry and some additional effort in reducing the cost of the technology, in materials, cell design & manufacturing process.

FY 2009 Publications/Presentations

1. 2009 DOE Annual Peer Review Meeting Presentation.

III.A.2.2 A Novel Nanophosphate-based Li-ion Battery for 25 kW Power-assist Applications (A123Systems)

Ron Elder (Program Manager)

Subcontractor: A123Systems

Terri Sacco (Program Manager)
A123Systems, Inc.
321 Arsenal Street
Watertown, MA 02472
Phone: (617) 393-4124; Fax: (617) 924-8910
E-mail: tsacco@a123systems.com

Start Date: December 2006
Projected End Date: June 2010

Objectives

- Design, build, and test cells and modules for HEV battery systems that will achieve the DOE / USABC performance and cost targets.
- Develop and demonstrate performance and cost impact from innovative, smart materials and designs.

Technical Barriers

This project addresses the following technical barriers for performance and cost:

(A) Cell Cycle Life

(B) Calendar Life

(C) System Weight and Volume

(D) System Cost

Technical Targets

- Demonstrate cell performance which can meet FreedomCAR HEV targets.
- Develop technology which enables achievement of USABC cost targets of $500 system production price @ 100k units/yr
- Conduct testing to allow estimation of 15 years in-use calendar life.

Accomplishments

- Produced a production-ready 32113 cell which can meet USABC HEV power and energy targets
- Optimized the 32113 cell design for robustness by implementing a can-positive design
- Created a 6Ah HEV prismatic cell to greatly improve on cost, energy, and power targets.
- Developed a 10-cell 32113 HEV prototype module

✧ ✧ ✧ ✧ ✧

Introduction

Achievement of USABC FreedomCAR goals requires cells and battery module technologies with high power and efficient design. The most significant challenge in developing this system is cost. Cost estimates have dropped significantly since the beginning of the program due to improved performance, optimized designs, and lower cost materials. Cost estimates at the beginning of the HEV program were almost 3 times the USABC target. Now, with the optimized 6Ah prismatic cell design, the projected cost is at, or only slightly above, target.

Approach

A123 has developed a 32113 cylindrical cell, whose power and energy meet most of the USABC FreedomCAR targets. Continued challenges lie in ongoing and aggressive cost reduction and cold crank performance. As the A123 Nanophosphate cathode material has inherently lower voltage than most other Li-ion systems, cold crank response is also a challenge due to increased impedance at -30°C. The development approach to close the gap on these performance objectives was to optimize the cell materials, design, and performance, while simultaneously developing a new, high power prismatic cell, resulting in a lower BSF needed to meet the targets, and therefore, much lower cost.

Results

32113 Cell

Gen 1 32113

The Gen 1 cell was the first 32113 cell produced to meet the HEV USABC targets. This cell meets all targets, with the exception of cold crank and cost.

25Wh cycle life testing is well underway with this cell with a total of >170k cycles completed. The cell is expected to reach the 300k USABC target by the end of the program.

The USABC calendar life testing is on track and has yielded positive results. The test will complete by the end of the program. A model was developed by A123 Systems to project long-term calendar life. The Gen 1 cells are on track to pass the projected USABC requirement of 15 years. See Table III-4 for the Gen 1 Gap Analysis and the Figures Figure III-14 and Figure III-15 for the 25Wh Cycle life capacity fade and impedance growth. Figure III-16 illustrates Gen 1 calendar life data and life projections.

Table III-4: Gap Analysis for Gen 1, 32113 Cell

Characteristics	Units	A123 Gen 1 BOL	Gen 1 100k Cycle	Gen 1 170k Cycle Sept '09	A123 EOP Goal	FreedomCar 25 kW goal
Discharge Pulse Power (10s)	kW	**38.1**	**34.4**	**33.6**	25 (20% loss or 30 for BOL)	25
Present Regenerative Pulse Power (10s)	kW	**33.5**	**30.3**	**29.8**	20 20% loss or 24 for BOL)	20
Total BOL available energy	kWh	**0.51**	TBD	TBD	0.30	0.30
Round trip energy efficiency	%	**95**			>90	>90
Cycle Life number of 25Wh cycles		N/A	100k	170k	300k	300k
Cold Cranking Power @ -30 *C	kW	**3.2**			**5**	5
Calendar Life	years	TBD	TBD	TBD	15	15
Maximum System Weight	kg	**24**			21	40
Maximum System Volume	liters	**18**			15	32
Operating Voltage Limits (max, min)	V	**240**			190	400
Operating Voltage Limits (max, min)	V	**132**			105	0.55 Vmax
Production price @ 100k/yr		**1218**			**780**	500
Maximum allowable self-discharge rate	Wh/day	**0.8**			<3.3	50
Equipment operation	*C	**30 to +52**			-30 to +52	-30 to +52
Equipment survival	*C	**46 to +66**			-46 to +66	-46 to +66
Cell type		32113 Gen-1				
Capacity	Ah	3.6				
BSF		63			50 (32113)	

Gen 2 32113

The Gen 2 cell was developed as a higher power cell which also incorporates a more robust, can-positive design. The Gen 2 cell design enabled the BSF to be reduced, while still meeting the USABC power and energy requirements, resulting in overall system cost reduction. See Table III-5 for the Gen 2 Gap Analysis and the Figure III-14 and Figure III-15 for the 25 Wh cycle life capacity fade and impedance growth.

Abuse Test Results

Abuse tests results were positive for both Gen 1 and Gen 2 cells, achieving EUCAR Level 3 and below for all tests. Table III-6 is a summary of all USABC abuse tests conducted and the results.

6Ah HEV Prismatic Cell

A 6Ah HEV prismatic cell is under development. Prototype cells will be provided to USABC before the end of the program. Initial performance tests have proven this to be a very high power cell, enabling a significant cost reduction, resulting in a projected cost that will meet or be only slightly above USABC HEV cost targets. It is important to note that this BSF is calculated using the power delivered when the current is not limited. In an actual application, there may be a current limitation, due to the system electronics capability, which may limit the current allowed to pass through the system. In that case, the BSF may need to be increased to deliver the same power, which would increase the system cost. Table III-7 is the Gap Analysis for this cell.

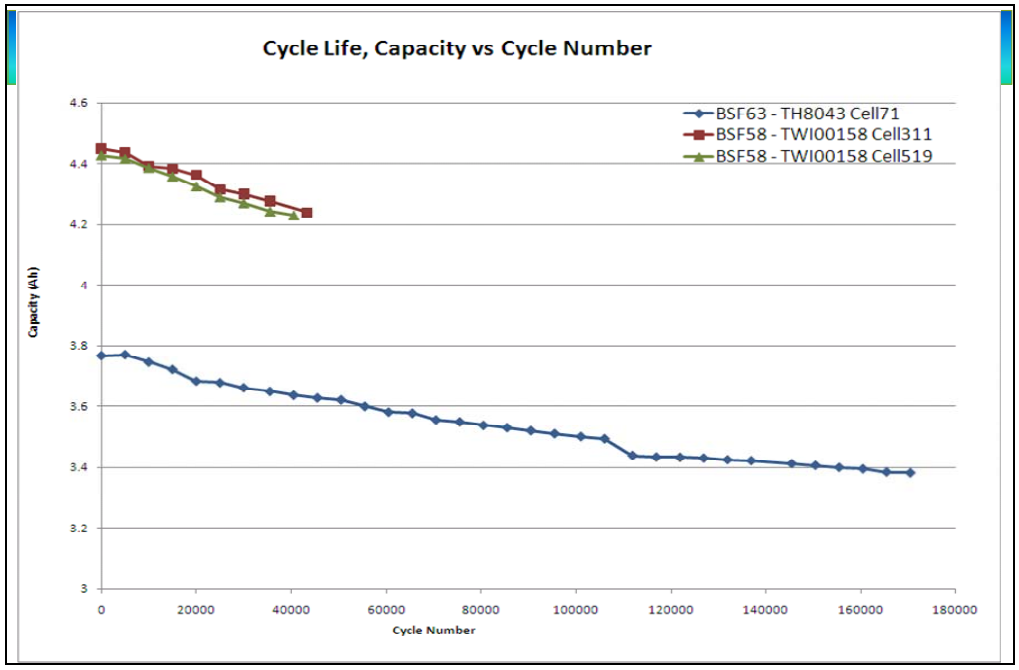

Figure III-14: 25Wh Cycle Life Capacity - 32113 Gen 1 & Gen 2 Cells

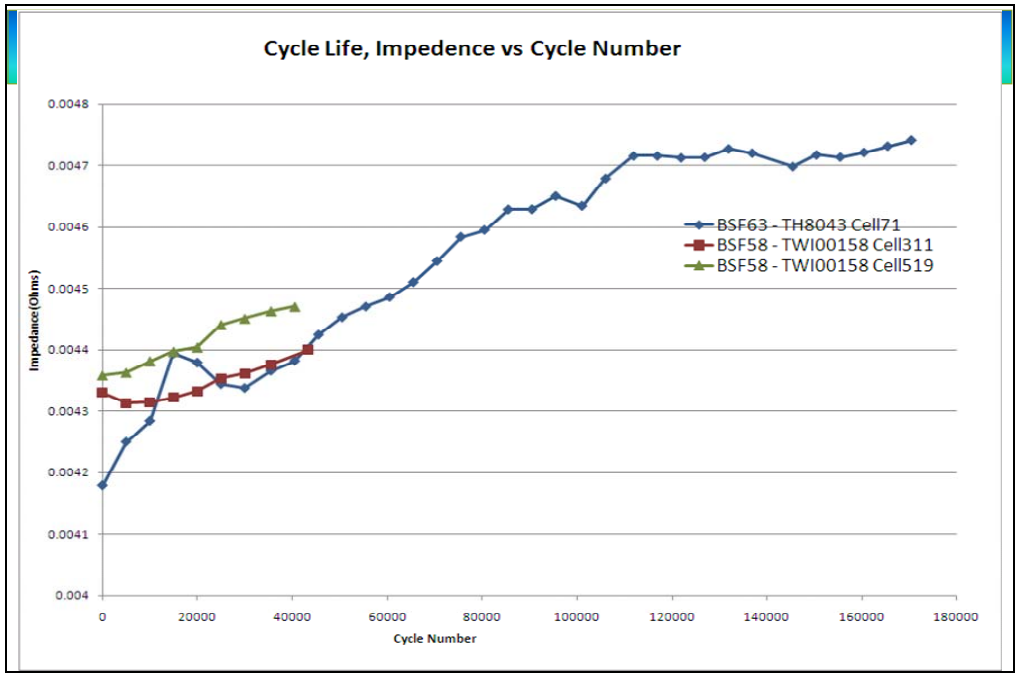

Figure III-15: 25Wh Cycle Life Capacity - 32113 Gen 1 & Gen 2 Cells

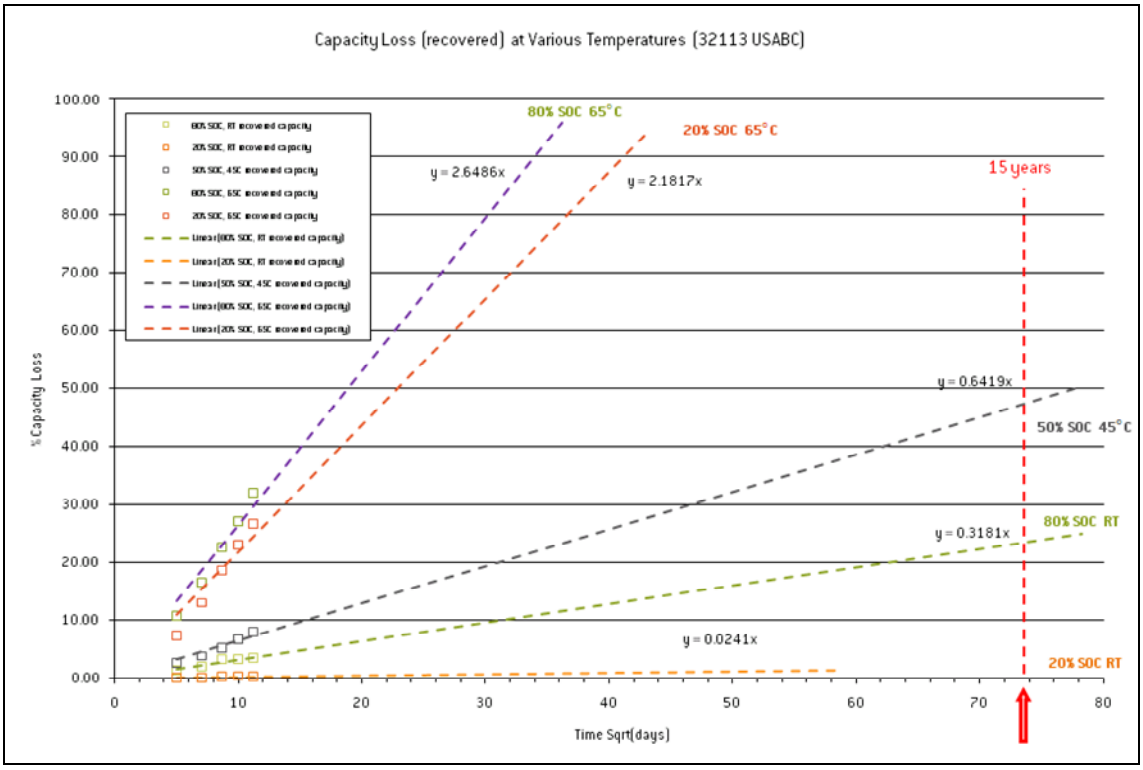

Figure III-16: USABC Gen 1 Calendar Life Data and Life Extrapolations

Table III-5: Gap Analysis for Gen 2, 32113 Cell

Characteristics	Units	Gen 2 B0.1 BOL	Gen 2 40k Cycles Sept '09	A123 EOP Goal	FreedomCar 25 kW goal
BOL Discharge Pulse Power (10s)	kW	**33.9**	**33.3**	25 (20% loss or 30 for BOL)	25
Present Regenerative Pulse Power (10s)	kW	**29.7**	**28.7**	20 20% loss or 24 for BOL)	20
Total available energy	kWh	**0.51**	TBD	0.30	0.30
Round trip energy efficiency	%	**95**		>90	>90
Cycle Life number of 25Wh cycles		N/A	40k	300k	300k
Cold Cranking Power @ -30 °C	kW	**3.2**		**5**	5
Calendar Life	years	TBD	TBD	15	15
Maximum System Weight	kg	**24**		21	40
Maximum System Volume	liters	**18**		15	32
Operating Voltage Limits (max, min)	V	**220**		190	400
Operating Voltage Limits (max, min)	V	**121**		105	0.55 Vmax
Production price @ 100k/yr		**1149***		**780**	500
Maximum allowable self-discharge rate	Wh/day	**0.8**		<3.3	50
Equipment operation	°C	**-30 to +52**		-30 to +52	-30 to +52
Equipment survival	°C	**-46 to +66**		-46 to +66	-46 to +66
Cell type		32113 Gen-2 B0.1			
Capacity	Ah	4.4			
BSF		58		50 (32113)	

Table III-6: USABC Abuse Test Results

USABC Test Summary			
Tests	Spec/Procedure/Notes	Gen 1 Status	Gen 2 Status
Abuse Testing			
Short Circuit Test	USABC	4 EUCAR 2, 1 EUCAR 4	EUCAR 2
Overcharge Test	USABC (4.7V, 32A, 200%)	EUCAR 2	EUCAR 2
Overdischarge Test	USABC	EUCAR 2	Planned for B1
Thermal Stability Test	USABC (modife temp to 150C)	EUCAR 2	Planned for B1
Nail Penetration Test @RT	USABC (w/ blunt steel nail 8mm dia. @ 8cm	EUCAR 3	3 = EUCAR 4, 2 = EUCAR 3
Nail Penetration Test @55°C	USABC (w/ blunt steel nail 8mm dia. @ 8cm	Delayed until Gen2	2 Cells = EUCAR 3
Crush Test (in X & Y axis)	USABC	EUCAR 2	Planned for B1
Mechanical Shock Test	USABC	EUCAR 2	Planned for B1

Table III-7: Gap Analysis for 6 Ah Prismatic HEV Cell

Characteristics	Units	A123 HEV Prismatic	A123 EOP Goal	FreedomCar 25 kW goal
Discharge Pulse Power (10s)	kW	30	25 (20% loss or 30 for BOL)	25
Present Regenerative Pulse Power (10s)	kW	24	20 20% loss or 24 for BOL)	20
Total available energy	kWh	>>0.30	0.30	0.30
Round trip energy efficiency	%	>90	>90	>90
Cycle Life number of 25Wh cycles		N/A	300k	300k
Cold Cranking Power @ -30 *C	kW	**5**	**5**	5
Calendar Life	years	TBD	15	15
Maximum System Weight	kg	<<40	21	40
Maximum System Volume	liters	<<32	15	32
Operating Voltage Limits (max)	V	**103**	185	400
Operating Voltage Limits (min)	V	**57**	102	0.55 Vmax
Production price @ 100k/yr		**$500 -$650**	**780**	500
Maximum allowable self -discharge rate	Wh/day	**0.8**	<3.3	50
Equipment operation	*C	**30 to +52**	-30 to +52	-30 to +52
Equipment survival	*C	**46 to +66**	-46 to +66	-46 to +66
Cell type		Prismatic HEV		
Capacity	Ah	6 Ah		
BSF		27*	50 (32113)	

***Note: This BSF is calculated using the power delivered when the current is not limited. In an actual application, there may be a current limitation, due to the system electronics capability, which may limit the current allowed to pass through the system. In that case, the BSF may need to be increased to deliver the same power.**

HEV Module Design

A prototype module was developed and samples will be provided to USABC for testing in April of 2010. Figure III-17 shows a schematic of the module.

Figure III-17: A123 10-cell Module Design

Conclusions and Future Directions

A123Systems' HEV 32113 Gen 2 cells have proven to meet the energy and power USABC goals outlined at the beginning of the program. Abuse test results were positive. Cycle life and calendar life testing on the 32113 cells are close to completion and the cells are on track to pass long-term USABC targets. Ten-cell modules prototypes were made from the 32113 cells and will be ready for USABC testing in April of 2010. Moving forward, cost is the most challenging target. The 6Ah Prismatic cell was developed to overcome this challenge and better meet the cost targets. Prototypes of this cell will be delivered to USABC in January of 2010, before the close of the HEV Program.

III.A.3. Advanced Materials and Processing

III.A.3.1 HTMI Separator Development (Celgard)

Amy Paik (USABC Program Manager)

Subcontractor: Celgard, LLC.

Ron Smith (Project Manager)
13800 South Lakes Dr.
Charlotte, NC 28078
Phone: (704) 587-8565; Fax: (704) 588-7393
E-mail: ronsmith@celgard.com

Start Date: October 1, 2008
Projected End Date: March 30, 2010

Objectives

- Determine the attributes that make up high temperature melt integrity (HTMI) of a Li-ion battery separator.
- Demonstrate a material that best meets that described attributes of HTMI.

Technical Barriers

There are no currently accepted standards for measuring and reporting HTMI in Li-ion battery separators. As such, an acceptable standard must be determined to effectively measure HTMI properties in battery separators and its effectiveness in Li-ion batteries.

Materials and manufacturing methods that best utilize the characteristics identified in the standard may not be widely in use today. Further work may be required to completely commercialize an acceptable technology.

Technical Targets

- The initial target is the determination of a standard measurement system for HTMI with a focus on reducing internal shorts.
- Technical focus in the separator will be placed on reducing shrinkage, z direction stability and internal short resistance at high temperature
- The development of a separator product that best meets these targets.

Accomplishments

- Standard Setting
- A literature survey was completed to evaluate the industry perspective on the key elements of HTMI. Numerous examples were found claiming benefits of "High Temperature Melt Integrity". The benefits were found to fall in three main categories
  - Reduction in shrinkage
  - Z direction stability
  - Internal short resistance at high temperatures
- Confirmation testing in batteries to demonstrate the linkage between the three main characteristics and battery performance are ongoing.
- An overview of material selection was conducted to determine what materials could be used in conjunction with the battery environment and currently available manufacturing methods.
- Prototype materials trying to maximize the benefits of the HTMI characteristics have been produced. Several approaches have been evaluated to determine the maximum benefit in battery performance.

✧ ✧ ✧ ✧ ✧

Introduction

Reducing the occurrence and propagation of internal shorts are important goals of the USABC. An important function of the separator is to prevent internal shorts by preventing electrical contact of the anode and cathode materials. Improving this function can potentially increase the durability and functional temperature range of a cell.

Approach

- Evaluation of existing materials to determine the current state of the technology
- Determine film testing methods to determine
  - Shrinkage
  - Z direction stability

  - Internal short resistance
- Correlate film testing results to battery level testing results
- Develop standard test for HTMI
- Develop material to best support HTMI

Results

Development of a standard. An industry overview was conducted to determine where the focus of the industry has been in the creation of HTMI materials. The overview clearly shows that the battery industry has focused on the key areas stated in the Approach section.

An array of test methods has been proposed and developed with appropriate conditions to measure HTMI characteristics. A baseline study has been completed with commercial separators focusing on the key areas as mentioned in the Approach section. Correlation of film properties to the battery benefits has begun. Initial correlation studies indicates that high temperature stability in X, Y, and Z direction and minimal propagation in response to a hot spot are the most significant film characteristics that will best determine improved cell performance under abuse conditions.

Several tests make up the evaluation of these film categories. Future work must still be done to verify the exact tests that link to battery performance improvements. Continued development of an advanced material to this standard is also important for verifying the proposed tests.

Development of a material. A study of materials capable of meeting the demanding environment of a battery was completed. The SEM of typical Celgard battery separator material is shown in Figure III-18. The result of this work has focused the efforts around high temperature filling agents that can be used in battery separators. The evaluation has included both polymeric and inorganic materials.

The material development portion of the work has also been evaluating the method for combining advanced materials into known manufacturing methods. Several approaches have been under evaluation. Future work will determine the best method for manufacturing.

Trade-offs between increased complexity of manufacturing methods and cost of these advanced materials are also under consideration.

Conclusions and Future Directions

Film properties of interest for battery separators have been narrowed to

- Shrinkage
- Z Direction Stabiltiy
- Internal Short Resistance

Further work is required to validate the correlation between the film testing results and the benefits in a battery. Once this work is complete a standard will be proposed for the measurement of HTMI in battery separators.

A range of materials available to develop an HTMI separator have been explored along with manufacturing methods necessary to produce appropriate films. Lab and prototype scale development will continue to be carried out to produce acceptable film using multiple methods. A final method must still be selected and full scale trials and commercialization must still be completed.

The cost of manufacturing an HTMI separator is still under investigation. Advanced manufacturing methods and materials may require additional research and development to completely commercialize.

FY 2009 Publications/Presentations

1. Presentation to the 2009 DOE Annual Funding Review

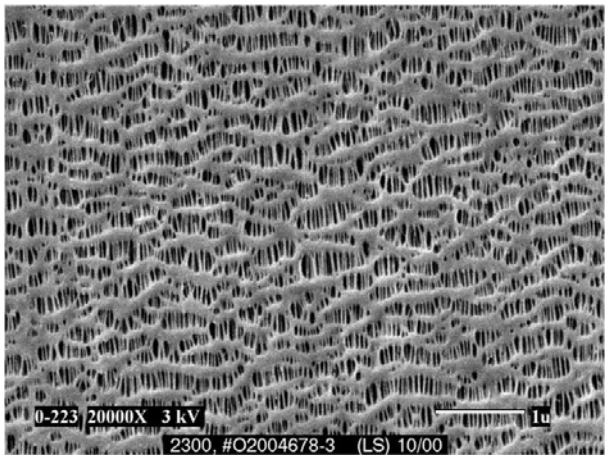

Figure III-18: SEM of typical Celgard battery separator material

III.A.3.2 Highly Filled and/or Cross-linked Li-ion Battery Separators for HEV/PHEV Applications (ENTEK)

Harshad Tataria (USABC Program Manager)

Subcontractor: ENTEK Membranes LLC

J. Emanuel, R. Waterhouse, and R.W. Pekala
250 N. Hansard Ave.
Lebanon, OR 97355
Phone: (541-259-3901), Fax: (541-259-8016)
E-mail: rpekala@entek-membranes.com

Start Date: October 1, 2008
Projected End Date: December 31, 2009

Objectives

- Produce a lithium-ion separator having a high loading level of inorganic filler and/or cross linked polymer that exhibits excellent high temperature melt integrity, but no shutdown characteristics.
- Deliver sample rolls for HEV / PHEV cell build (using automated assembly equipment) to at least one USABC cell developer.

Technical Barriers

This project addresses conflicting separator requirements, technical barriers and manufacturing issues:

(A) Thermal stability and puncture strength show opposite trends with filler loading level.

(B) In plant recycling of cross linked polymers.

(C) Uniform filler dispersion in thin films

Technical Targets

- Thickness: less than 25 µm
- Permeability: MacMullin Number less than 11
- Wettablity: wets out in electrolytes
- Pore Size: less than 1 µm
- Puncture Strength: greater than 300 gf / 25.4 µm
- Thermal Stability at 200°C: less than 5% shrinkage
- No high temperature shut down
- Tensile Strength: Less than 2% offset at 1000 psi

Accomplishments

- Porous films were made with eight different types of inorganic fillers. Four of these types were from different manufactures and included more than one grade. Two of these types included grades with different types of surface treatments.
- Porous films were made with four different types of polyethylene, including ultrahigh molecular weight polyethylene (UHMWPE), high density polyethylene (HDPE), cross linkable polyethylene (XLHDPE) and blends of these polymers.
- Porous films were produced from fifty-nine different formulations on the Entek pilot line using a simultaneous biaxial orientation (Process A).
- Porous films were produced using a sequential biaxial orientation process (Process B).
- Films were produced with:
  - MacMullin Number less than 11
  - Less than 5% shrinkage at 200° C
  - Less than 2% offset at 1000 psi
  - No high temperature shut down
- Cell build samples were delivered to a USABC cell developer**.**

✧ ✧ ✧ ✧ ✧

Introduction

For small commercial lithium-ion cells under abuse conditions, such as external short circuit or overcharging, the separator is required to shutdown at temperatures well below where thermal runaway can occur. Shutdown results from collapse of the pores in the separator due to softening or melting of the polymer, thus slowing down or stopping ion flow between the electrodes. Nearly all Li-ion battery separators contain polyethylene as part of a single- or multi-layer construction so that shutdown begins at ~130°C, the melting point of polyethylene. For larger cells such as those used in hybrid or plug-in hybrid electric vehicles (HEV, PHEV), the utility of the shutdown characteristic has been called into question. Much of the safety and abuse tolerance for failure modes in which separator shutdown might play a role is handled at a system level. Failures of batteries in the field have demonstrated that shutdown is not a guarantee of safety.

The principle reason is that, after shutting down, residual stress and reduced mechanical properties above the polymer melting point can lead to shrinkage, tearing, or pinhole formation. The goal of this project is a separator with low impedance and excellent high temperature, mechanical and dimensional stability.

Approach

To achieve these goals, the following approaches were used: (1) incorporation of inorganic fillers into a polyolefin separator at high loading levels during extrusion (filled separators), (2) use of silane-grafted polyethylene to crosslink the polymer matrix in highly filled separators (cross-linked separators), and (3) annealing of biaxially-oriented, highly filled separators above the melting point of the polymer matrix to reduce residual stress while maintaining high porosity.

Results

Thermal Stability of Highly Filled Films Without Heat Treatment. Table III-8 summarizes thermal stability data for highly-filled films made by process A in the Entek pilot plant. Films were tested for thermal stability at 200ºC under argon for 60 min. These films were not annealed or heat treated prior to testing. After testing, all three films could be folded without cracking. MD = machine direction, XMD = cross direction.

Table III-8: Thermal Stability Data for Highly-filled Films Made by Process A

Filler / Polymer	Thickness µm	Shrinkage @ 200ºC	
		% MD	%XMD
Filler1 / UHMWPE / HDPE	31	3.6	2.9
Filler1 / UHMWPE / XLHDPE	38	3.2	2.2
Filler 2 / UHMWPE / HDPE	24	2.8	3.3

Effect of Annealing Temperature on High Thermal Stability. Figure III-19 summarizes thermal stability data of a film tested at 200ºC in argon for 60 min. The film was made by process B. Process conditions were the same for all films. The films are all the same formulation with filler 3 and UHMWPE 3. The films were then heat treated under Ar at 120°, 145°, 165° and 185°C. For this film, heat treatment temperatures above 165°C were required to reduce both MD and TD (XMD) shrinkage to less than 5%.

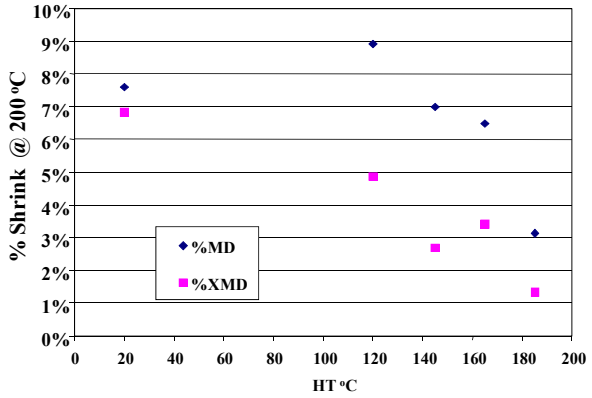

Figure III-19: Shrinkage @ 200°C for Different HT Temps

2% Offset Yield for Highly Filled Films by Process B. Table III-9 summarizes 2% off set yield for films made by process B, under different process conditions and with different degrees of heat treatment. The films are all the same formulation with filler 3 and UHMWPE 3. With respect to automated cell assembly equipment, the MD stress is the more important property.

Table III-9: Heat Treatment and 2% Offset Yield

Process Conditions	Heat Treatment° C	MD stress @ 2% offset Yield, psi	XMD stress @ 2% offset Yield, psi
1	none	829	463
1	165	662	
2	none	3,967	375
2	125	5,850	508
2	145	6,994	536

MacMullin Number. Table III-10 summarizes electrical resistance data (MacMullin Number) for a highly filled film made by process B, and an unfilled separator film Teklon HPIP (made by Entek). The filled film contains filler 3 and UHMWPE 3. Resistance measurements were made in an electrolyte consisting of 1M LiPF6 in 1:1 EC:DEC

Table III-10: MacMullin Numbers for a highly filled film by process B, and an unfilled separator film Teklon HPIP

	Thickness	Resistivity	MacMullin Number
Description	mm	Ω-cm	
Process B	0.0373	153	2.28
HPIP	0.0247	909	8.57

High Temperature Shut Down. Shutdown testing was conducted on separators wet out with an electrolyte. The sample was placed between wetted carbon electrodes

positioned between metal platens which were heated at a constant rate of 50°C/min. As the temperature is ramped from 25°C to 200°C, the separator impedance at 1 kHz is continuously measured using an LCR meter. The impedance at 100°C is noted and the temperature at which a 1,000 fold increase occurs is considered to be the shutdown temperature.

Figure III-20 shows shut down curves for an un-filled polyethylene separator (black curve), a separator made by process A, containing filler 1 (red curve) and a blank consisting of electrolyte only (green curve). Note that the resistance of an unfilled competitor separator peaks (shuts down) at 140°C and then drops starting at 160°C. The filled separator resistance shows little change up to 200°C. The filled separator does not shut down or rupture.

Conclusions and Future Directions

- Highly filled battery separators for use in high power and high energy lithium-ion and lithium polymer batteries for HEV/PHEV applications have been produced by two different processes, with two different fillers, and different polyethylene blends. These separators have:
- Very low MacMullin numbers
- Good wet out in electrolyte
- Good thermal stability
- No high temperature shut down
- Less than 2% off set at 1000 psi
- Thermal stability and tensile properties can be improved by heat treatment.

Sample separator material in roll stock form was processed successfully in automated battery assembly equipment.

During the remainder of the project ENTEK will optimize both processes, optimize formulations and gain additional experience in a production environment.

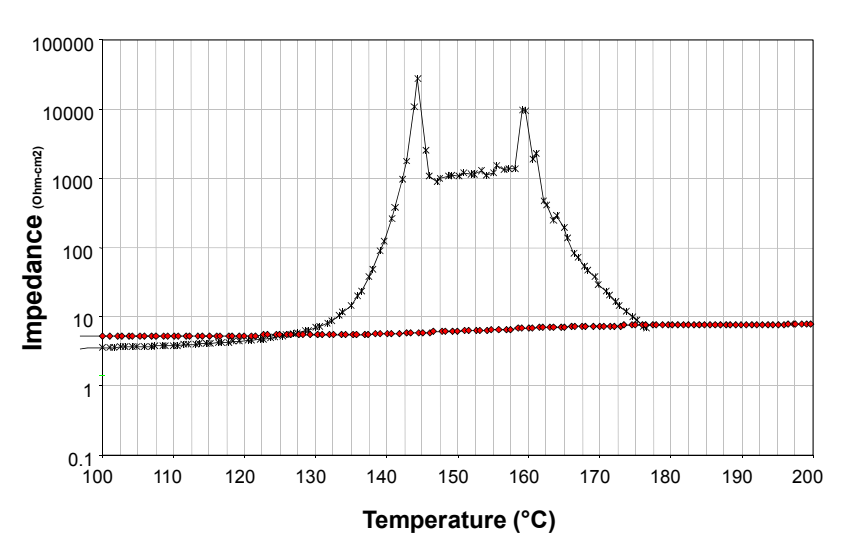

Figure III-20: Shut down curves for several separators

III.A.3.3 Advanced Cathode Materials with High Energy, Power, and High Thermal Stability for PHEV Applications (3M)

Harshad Tataria (USABC Program Manager)

Subcontractor: 3M

Junwei Jiang (Program Manager)

3M Electronics Markets Materials Division
3M Company, Bldg 209-2c-26
St. Paul, MN, 55144
Phone: (651) 733-8504; Fax: (651) 736-7478
E-mail: Jjiang9@mmm.com

Start Date: March 1, 2009

Projected End Date: August 31, 2010

Objectives

- Design and optimize a new cathode material that has better performance and lower cost than commercial $LiNi_{1/3}Co_{1/3}Mn_{1/3}O_2$ material.
- Demonstrate the manufacturing capability of the new cathode material in 3M pilot plant (~ 100kg level) and demonstrate superior performance in 18650-size cell.

Technical Barriers

This project addresses the following technical barriers from the design and optimization of new cathode materials, scaling up in pilot scale (~ 100kg batch level), 18650-size cell design to demonstrate the superior performance of new designed material:

(A) Performance of $LiNi_{1/3}Co_{1/3}Mn_{1/3}O_2$ material

(B) Design new cathode materials

(C) Optimization of new material in lab scale (~ 20g level)

(D) Pilot capability to scale up (~ 100kg level)

(E) 18650-size cell design with new optimized material

(F) Thermal stability characterization of cathode materials

Technical Targets

- New material with approximately 5 ~ 10% capacity improvement compared to commercial $LiNi_{1/3}Co_{1/3}Mn_{1/3}O_2$ material.
- Approximately 10% cost reduction.
- Similar or higher thermal stability than commercial $LiNi_{1/3}Co_{1/3}Mn_{1/3}O_2$ material.

Accomplishments

- Finished the basic physical and electrochemical performance test on benchmark cathode material ($LiNi_{1/3}Co_{1/3}Mn_{1/3}O_2$), which demonstrates good capacity (~156mAh/g at 4.3V) and excellent thermal stability (exothermic peak temperature ~315°C in DSC at 4.3V vs. Li).
- Optimized the 18650-size cell design with commercial $LiNi_{1/3}Co_{1/3}Mn_{1/3}O_2$ material. Two tabs were used per electrode. The optimized 18650 cell has a low internal impedance of approximately 40mΩ.
- Completed the physical and electrochemical performance tests on 12 different cathode compositions and identified the promising composition range for a new cathode material design.
- Set-up and ran 2 liter co-precipitation reactor to study the metal hydroxide morphology control. The key parameters have been identified.
- Set-up and ran a 300 liter reactor to study how to control the hydroxide particle growth and morphology.

✧ ✧ ✧ ✧ ✧

Introduction

Achieving the USABC PHEV goals may require higher energy, lower cost materials. This project is proposing a new material with an improved capacity of ~165mAh/g at 4.3V. In order to meet the cost reduction of ~10% compared to $LiNi_{1/3}Co_{1/3}Mn_{1/3}O_2$, the Co composition in the new cathode material needs to be as low as possible, since Co price governs the raw material cost in Li-Ni-Co-Mn-O layered cathode materials. The new cathode material also needs to have a balanced high capacity, low cost, and high thermal stability, which will be potentially ideal for automotive applications.

Approach

To meet the USABC-3M target of 5 ~ 10% capacity improvement compared to $LiNi_{1/3}Co_{1/3}Mn_{1/3}O_2$, we need to optimize Ni and Co content, since they are both electrochemically active. In order to meet the 10% cost reduction target, we need a lower amount of Co than 20%.

Based on the above considerations, we planned to characterize 12 different compositions of cathode material, where Co is ~10% or 20% with Ni ranging from 25% ~ 75% and Mn ranging from 10% ~ 40%. The results will help to map out the new material composition range in order to meet USABC-3M cathode program goal.

Results

Commercial $LiNi_{1/3}Co_{1/3}Mn_{1/3}O_2$ (NCM) Characterization. The commercial NCM cathode material is used as a benchmark. The physical, thermal, and electrochemical performances of $LiNi_{1/3}Co_{1/3}Mn_{1/3}O_2$ have been characterized. The material has an average particle size of 11.1μm and tap density of 2.55g/cm^3. The first discharge capacity from 4.3V to 2.5V vs. Li is ~156mAh/g. The thermal stability of charged $LiNi_{1/3}Co_{1/3}Mn_{1/3}O_2$ (4.3V vs. Li) has been characterized by ARC and DSC. The onset temperature in ARC is ~180°C and the exothermic reaction peak in DSC is ~315°C.

18650-size Cell Optimizations. We optimized the 18650-size cell system with $LiNi_{1/3}Co_{1/3}Mn_{1/3}O_2$ cathode material and graphite anode material, such as electrode loading from 1.0mAh/cm^2 to 2.0mAh/cm^2, PVDF binder amount from 1.5% to 4%, conductive carbon amount from 1.5% to 4%, cathode electrode density from 2.7g/cm^3, 3.0 g/cm^3, to 3.3 g/cm^3, the electrode tab numbers, etc. The final optimized 18650-size cell with $LiNi_{1/3}Co_{1/3}Mn_{1/3}O_2$ cathode has a good cycle life and also low internal impedance around 40mΩ. The charge-depleting cycle life characterization is underway.

Cell Design using Battery Design Studio (BDS). BDS is a software tool used to design cells and systems. We used it to optimize the cell system, such as internal impedance, cell capacity, and rate performance with $LiNi_{1/3}Co_{1/3}Mn_{1/3}O_2$ cathode and graphite anode.

New Cathode Material Design and Optimization. Based on our past experience and understanding of layered cathode materials, in order to design a cathode material that has higher capacity, lower cost, and comparable or higher thermal stability than $LiNi_{1/3}Co_{1/3}Mn_{1/3}O_2$, we need to keep Co as low as possible for cost reduction and Mn as high as possible for thermal stability improvement. The 12 different cathode compositions that were chosen are shown in Figure III-21 in a ternary phase diagram, $xLiMn_{1/2}Ni_{1/2}O_2 \bullet y\ LiNiO_2 \bullet z\ LiCoO_2$ ($x + y + z = 1$), where Co content is around 10% or 20%. The 12 cathode materials have been synthesized and optimized in terms of sintering conditions. The physical, thermal, and electrochemical performances of the 12 materials have been characterized. For example, Figure III-22 shows the thermal stability characterization, by DSC, of 6 charged cathode materials with different amount of Ni content from 45%, 50%, 55%, 60%, 65%, to 70% and Co around 20%. The data clearly show that the cathode material with higher amount of Ni or lower amount of Mn has lower DSC exothermic peak temperature indicating lower thermal stability. One of the above cathode compositions shows good thermal stability and also high capacity. A cathode material around this composition could be very promising.

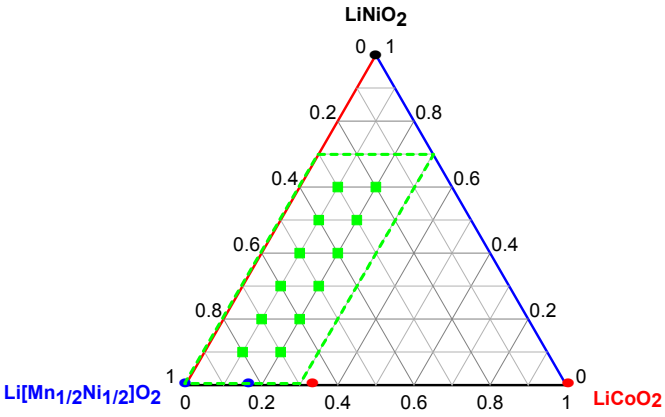

Figure III-21: 12 New Cathode Materials Indicated in Green in Ternary Phase Diagram, $xLiMn_{1/2}Ni_{1/2}O_2 \bullet y\ LiNiO_2 \bullet z\ LiCoO_2$ ($x + y + z = 1$), where Co content is around 10% or 20%.

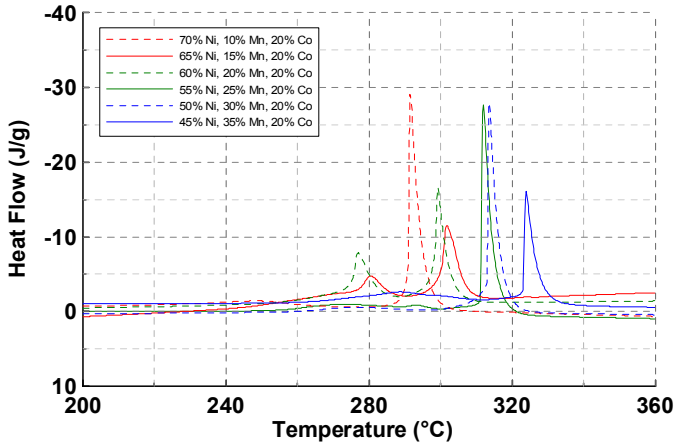

Figure III-22: DSC of 6 Charged New Cathode Material at 4.3V vs. Li metal ($LiNi_{0.45}Co_{0.2}Mn_{0.35}O_2$ in solid blue, $LiNi_{0.5}Co_{0.5}Mn_{0.3}O_2$ in dashed blue, $LiNi_{0.55}Co_{0.2}Mn_{0.25}O_2$ in solid green, $LiNi_{0.6}Co_{0.2}Mn_{0.2}O_2$ in dashed green, $LiNi_{0.65}Co_{0.2}Mn_{0.15}O_2$ in solid red, and $LiNi_{0.7}Co_{0.2}Mn_{0.1}O_2$ in dashed red).

2L and 300L Reactor Setup and Run. A 2 liter reactor was designed to study the effects of key parameters, such as reacting temperature, reactant concentrations, chelating agent addition, PH value, etc. on the metal hydroxide (cathode precursor) morphology (size, shape, density, porosity, etc). Figure III-23 shows a schematic of the metal hydroxide co-precipitation reactor. We have completed the condition studies in the 2L reactor and know the mechanism to control particle morphology. So far, we have done 2 trials in the 300L reactor to

synthesize $Ni_{1/3}Co_{1/3}Mn_{1/3}(OH)_2$, a precursor to the $LiNi_{1/3}Co_{1/3}Mn_{1/3}O_2$ cathode material.

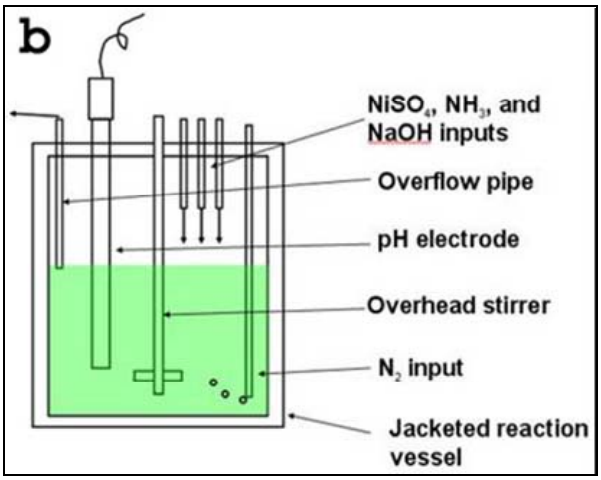

Figure III-23: Schematic Drawing of a Co-precipitation Reactor for Metal Hydroxide Synthesis.

Conclusions and Future Directions

The initial studies on 12 new cathode materials in $xLiMn_{1/2}Ni_{1/2}O_2 \bullet y\ LiNiO_2 \bullet z\ LiCoO_2$ ($x + y + z = 1$) ternary phase diagram show how capacity and thermal stability vary with Ni composition. In summary, at 20% Co, the cathode material with higher amount of Ni gives higher capacity up to 190mAh/g at 4.3V but lower thermal stability shown in DSC measurements. The final optimization and selection of the new composition cathode material is underway.

In the next step, we will choose the cathode material composition based on the studies according to the USABC-3M cathode program goal by the end of October, 2009. By the end of April, 2010, we will optimize the hydroxide precursor of the chosen cathode composition using the 300L reactor and then sinter out the new cathode material at high temperature around 1000°C. The optimized cathode material will be used to fabricate 18650-size cell for studies according to FreedomCAR Battery Test Manual for PHEVs.

III.A.3.4 Advanced High-Energy Anode Materials (3M)

Chris Johnson (NETL Program Manager)

Subcontractor: 3M.

Mark Obrovac (Principal Investigator)
3M Electronics Materials Marketing Division
3M Center
St. Paul, MN 55144
Phone: (651) 733-0050; Fax: (651) 736-7478
E-mail: mobrovac@mmm.com

Start Date: January 5, 2009
Projected End Date: June 22, 2010

Objectives

- Identify, synthesize, and characterize new high energy density alloy anode material for use in advanced lithium-ion batteries for PHEVs.
- Optimize alloy manufacturing processes to demonstrate scalability.
- Use 18650 test cells to optimize alloy coating formulations, electrolyte formulations and cell designs for PHEV electrochemical performance and abuse tolerance.

Technical Barriers

This project addresses the following technical barriers associated with the use of alloy negative materials:

(A) Low cycle life

(B) High irreversible capacity, leading to low overall cell energy density

(C) High manufacturing costs associated with the production of nanostructured alloys

(D) Accommodation of the large volume expansion of alloy negative materials in electrochemical cells

(F) Thermal stability issues associated with the use of alloy anodes.

Technical Targets

- Enable a 15-20% improvement in energy density over conventional cells containing graphite anodes.
- Enable at least 300 cycles with 20% fade when cycled with a capacity swing of 70%.
- Demonstrate manufacturability on a pilot scale (>3 kg)
- Demonstrate thermal stability: (150ºC hot block test, no thermal runaway, <5°C overshoot)
- Demonstrate a rate capability of 2C/0.2C > 90%

Accomplishments

- Identified two candidate silicon-based alloy compositions (L-19725 and L-20772) for this project as described in Subtask 1.1.
- Demonstrated manufacturing viability of alloy candidates as described in Subtask 1.2.
- Optimized the manufacturing processes for both alloy candidates to deliver consistent alloy characteristics as described in Subtask 1.2.
- Developed high-loading electrode formulations that demonstrate good cycling at the coin cell level for both alloy candidates, as described in Subtask 1.2.
- Synthesized kg quantities of both candidate alloy materials to enable 18650 cell testing as described in Subtask 1.3.
- Developed large-scale slurry formulation for both candidate alloys as described in Subtask 1.3.
- Developed high loading densified double-sided coatings for 18650 sized cells as described in Subtask 1.3 for both candidate alloys.
- Demonstrated 300 100% DOD charge/discharge cycles with less than 20% capacity fade in 18650 cells as described in Subtask 1.3.
- Demonstrated alloy thermal stability with low overshoot temperature in hotbox tests as described in Subtask 1.3.
- Demonstrated rate capabilities in 18650 cells with rates of 0.2C/2C exceeding 90% as described in Subtask 1.3.
- Developed improved electrolyte formulations that increase alloy cell performance as described in Subtask 2.
- Identified key causes of electrode volume expansion during cycling as a key part of meeting the goals in Subtask 3.

Introduction

The main focus of this DOE funded research is to develop anode materials that can increase the energy density of PHEV batteries significantly beyond what current Li-ion technology can provide. Considerable achievements have been made towards meeting the objectives set out in this program. As a result of our

ambitious research program most targets for the first budgetary period have already been met including alloy composition, manufacturing viability, coating formulation, electrolyte development, and cycling performance targets.

Approach

The purpose for this research program is to develop practical anode materials for PHEV power sources. Therefore in addition to the performance requirement objectives of this project there are other restrictions that need to be met in order for the materials developed in this program to have practical use. Specifically, the following approach towards materials development was taken:

- Raw materials cost must be kept low.
- Inexpensive existing manufacturing processes that can result in high-volume production should only be considered.
- Coatings should preferably be from aqueous slurries and must be coated using existing slurry coating procedures.
- Cell assembly must be performed using existing manufacturing procedures.

Without meeting the above specifications it is our opinion that the likelihood of adoption of any new battery materials is low.

It is widely recognized that Si or Sn-based alloys are the only alloy materials that can deliver significant gains in energy density over graphite. With the above guidelines in mind, research in this project focused on Si-based alloys, since the raw-materials cost of Sn-based alloys was deemed too high for PHEV applications. The design of the alloy was based on the active/inactive alloy concept described in reference 1, with a target volumetric capacity of 1500 mAh/cc. At this capacity the alloy is expected to have a volumetric expansion of 100% during lithiation [1] and increase the energy density of a Li-ion cell by 15-20%, depending on the cathode formulation.

Results

Subtask 1.1: Initial Characterization.

Two candidate alloy compositions previously developed by 3M were chosen for this project:

L-19725 Alloy
Morphology: 4.2 g/cc; D50 = 7μm; 1.0 m^2/g
Capacity: 816 mAh/g; 1590 mAh/cc
Irreversible capacity: 15%
Average voltage: 0.45 V

L-20772 Alloy
Morphology: 4.1 g/cc; D50 = 2.5 μm; 4.5 m^2/g
Capacity: 860 mAh/g; 1600 mAh/cc
Irreversible capacity: 9%
Average voltage: 0.45 V

Both alloys are silicon-based. The alloys also contain tin, but only in small amounts to improve kinetics during cycling. All other components comprise low cost raw materials.

Both alloys exceed the capacity targets of this program and demonstrate little capacity fade in coin cells tests, shown in Figure III-24. The small capacity fade observed in coin cells is thought to be due to the poor stack pressure in the 3M coin cell design, since 18650 cell testing shows much less fading (see section describing Subtask 1.3 below). Because of this, the observed fading is thought to be a hardware issue and not a material issue. Therefore the coin cell cycling requirements specified in Subtask 1.1 were deemed satisfied by these materials.

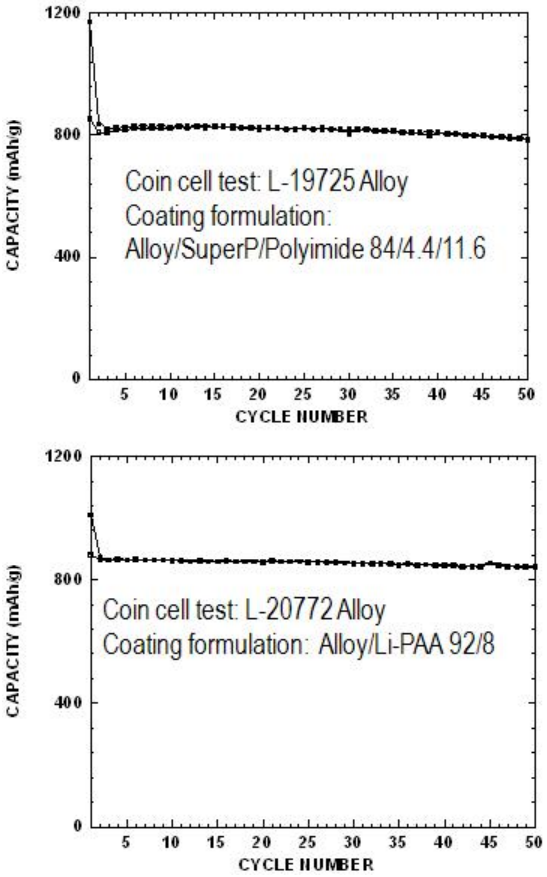

Figure III-24: Coin cell cycling tests of L-19725 and L-20772 alloys chosen for development in this project. Coin cells were cycled between 5 mV and 0.9 V at a rate of C/4.

To determine alloy reactivity with the electrolyte, as specified in this subtask, coin cells were disassembled after 50 cycles and the alloy coatings examined with SEM. This study found that significant SEI growth on the alloy particles had formed after 50 cycles, caused by electrolyte decomposition during cycling. This is a significant issue

that needs to be solved for the successful implementation of these materials. Solving this issue is currently a major focus of this project.

Subtask 1.2: Manufacturability/Viability Analysis.

Alloys L-19725 and L-20772 were chosen in part because their manufacture is based on established industrial processes. Both alloys can be made in our lab in batch sizes exceeding that required in Subtask 1.2. As a result many kilograms of these materials can be made monthly to enable large-scale coating optimization and 18650 cell evaluation of alloy anodes.

Viable manufacturing processes must reliably produce materials within our specifications for each batch of material. At the beginning of this project, this was not the case and the following significant issues existed:

- standard operating procedures not established
- material capacity batch/batch variation > 10%
- particle batch/batch size variation > 10%
- particle sizing method not established
- reactivity of particles with water after sizing

Considerable effort has been made during this DOE funded research into optimizing manufacturing processes. This effort has resolved all of the above issues, resulting in batch/batch variations of less than 5%. As a result the goals described in Subtask 1.2 to demonstrate manufacturing viability have been met.

Electrode coatings with loadings from 3-4 mAh/cm^2 comprising both L-19725 and L-20772 were formulated with 33-70% graphite. The addition of graphite allows alloy electrodes to be calendered to low porosity and results in higher energy density than coatings with no graphite. Many different graphites, formulations and dispersion processes were tested in order to optimize electrode coating performance. This work resulted in electrode coatings with capacities of 900 mAh/cm^3 that when tested in coin cells had no capacity fade within the error range of our coin cell experiments. These results completely satisfy the requirements as described in Subtask 1.2.

Subtask 1.3: 18650 Cell Performance Testing.

Sufficient quantities of both alloy materials were synthesized according to the methods developed in Subtask 1.2 to enable the coating of 18650 cell electrodes. Electrode coatings were also formulated according to the coating development results obtained in Subtask 1.2. As specified in the Project Objectives, 18650 cells were assembled using an MNC cathode.

Considerable development work has taken place under this DOE contract to optimize coatings, electrolytes and 18650 cell assembly to meet the performance targets outlined in the Project Objectives. Aqueous slurry formulations and their methods of preparation were developed so that their viscosity and dispersion quality were compatible with commercial coating systems. Full-sized coating runs were then undertaken in which the coating and drying conditions were optimized. The resulting coatings were then slit, calendered and wound into prototype 18650 cells. Many 18650 prototype cells were made to test different electrode formulations, electrolyte formulations, electrode loadings, current collector thicknesses, and other cell design parameters.

As a result of this testing we have demonstrated 68% capacity retention after 500 cycles for 18650 cells containing alloy L-19725 anodes (shown in Figure III-25) and 70% capacity retention after 500 cycles for 18650cells containing alloy L-20772 anodes. Rate capability and thermal stability targets outlined in the Project Objectives have also been exceeded with 18650 cells using both alloys. In fact all performance targets outlined in the Project Objectives have been achieved. However, each target has been met using a different cell design, not by the same cell.

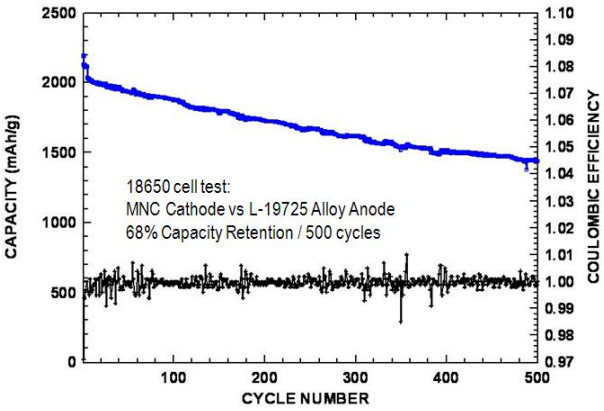

Figure III-25: 18650 cycling test of MNC vs. L-19725 alloy, showing a capacity retention of 68% after 500 cycles. The coulombic efficiency of this cell was 99.96% averaged over the 500 cycles shown. This cell was cycled between 2.6V and 4.2V (100% DOD) at a cycling rate of C/2.

Now that it is understood how to reach the goals outlined in the Project Objectives with different cell designs, what remains is to make a single cell design that meets all requirements. In addition, although the thermal stability requirements were satisfied after a few charge/discharge cycles it needs to be demonstrated if good thermal stability will be maintained after many hundreds of cycles. Experiments are underway to address these remaining objectives for this Subtask.

Subtask 2 - Electrolyte Optimization.

Significant electrolyte development work was done to achieve the 18650 cycling performance described in Subtask 1.3. It was found that at least 40% fluoroethylene carbonate (FEC) content was required in the electrolyte for good cycling to be obtained. Without FEC, only about 50-100 cycles were achievable, after which it was found that all of the electrolyte had been consumed during cycling.

It was also found that certain electrolyte additives strongly enhance the thermal stability characteristics of 18650 cells comprising alloy anodes. The same additives were found to enhance cycling performance. It is believed that these additives contribute to forming a stable SEI layer on the alloy surface.

As a result of this work a multi-component electrolyte formulation was developed that combines good cycling and good thermal stability characteristics and resulted in the 18650 performance described in Subtask 1.3. Nevertheless the fade that exists in the 18650 cells is thought to be due to slow electrolyte decomposition on the alloy surface during cycling. Further work on electrolyte optimization will take place to resolve this issue.

Subtask 3 - Cell Development for the Accommodation of Anode Volume Expansion.

Prior to the start of this project it was discovered that blending alloy coatings with graphite significantly reduces the volume expansion of alloy coatings from about 115% for pure alloy coatings to less than 50% expansion for an alloy/graphite blend. As explained in Subtask 1.2 such alloy/graphite blends also can be calendered to high density, making their energy density higher than alloy coatings containing no graphite. It was found that the volume expansion of such alloy/graphite blends is easily accommodated in an 18650 cell without any modification of the cell design.

As mentioned in previous sections, the decomposition of electrolyte on the alloy surface occurs during cycling. This decomposition reaction consumes lithium and is responsible for the linear fade observed in the 18650 cells, shown in Figure III-25. The reaction was also found to result in the formation of a thick SEI layer on the alloy particles, which grows in thickness after every cycle. Surprisingly the cell impedance and rate capability are not affected by the formation of this SEI layer. However after many cycles the volume occupied by the electrolyte decomposition products becomes significant and causes electrode swelling much higher than that caused by the expansion of the alloy. It is believed that after many hundreds of cycles the cell will no longer be able to accommodate this swelling, resulting in the crushing of the separator and shutdown of the cell.

Therefore the objective to accommodate the volume expansion in Subtask 3 will concentrate on eliminating the growth of this SEI layer. This should also have the effect of reducing cycling fade, which is also caused by SEI growth. We have observed that the addition of FEC drastically reduces the growth of the SEI layer. Therefore one area of research will be further electrolyte development to understand the reactions that cause SEI growth and modifying electrolyte formulations to halt it. Other experiments related to the alloy itself will also be conducted.

Conclusions and Future Directions

This DOE/3M funded research program has resulted in many significant breakthroughs in alloy anode performance. Many of the performance targets outlined in the Program Objectives have nearly been reached. As a result it is our assessment that the performance of the alloy materials and cells developed during this research program is far superior to any alloy cells reported by other research groups. Furthermore, unlike many other studies, the materials developed here were demonstrated in real commercial-sized cells and are made with inexpensive raw materials utilizing established manufacturing methods. These methods allow the rapid scale-up of large volumes of practical materials that can compete in the marketplace.

Although the materials performance shown here likely is already suitable for consumer electronic applications, further improvements are required for PHEV applications. The elimination of electrolyte decomposition reactions is now a major focus of Phase 1 of this research. The solution of this problem is likely to both increase cycle life and reduce electrode swelling. Further improvements to achieve PHEV performance targets will follow as described in the Phase 2 objectives of this project, pending approval of subsequent budget periods.

FY 2009 Publications/Presentations

1. M.N. Obrovac, L. Christensen, D.B. Le, J.D. Singh, “New Alloy Anodes for Commercial Li-ion Cells”, Presented at the 216th Meeting of the Electrochemical Society, October 7, 2009.

References

1. M.N. Obrovac, L. Christensen, D.B. Le and J.R. Dahn, J. Electrochem. Soc., 154, A849-A855 (2007).

III.A.3.5 Stabilized Li Metal Powder (FMC)

Chris Johnson (NETL Program Manager)

Subcontractor: FMC Corporation

Marina Yakovleva (Principal Investigator/Project Dir.)
FMC Corporation, Lithium Division
Seven LakePointe Plaza
2801 Yorkmont Road, Suite 300
Charlotte, NC 28208
Phone: (704) 868-0891; Fax: (704) 868-5496
E-mail: Marina.Yakovleva@fmc.com

Dr. Yuan Gao (Co-Principal Investigator/Project Dir.)
FMC Corporation, Lithium Division
Seven LakePointe Plaza
2801 Yorkmont Road, Suite 300
Charlotte, NC 28208
Phone: (704) 868-5503; Fax: (704) 868-5387
E-mail: Yuan.Gao@fmc.com

Start Date: May 1, 2009
Projected End Date: April 30, 2012

Objectives

- Objective 1: Develop a process and a prototype unit for the commercial production of dry stabilized lithium metal powder (SLMP).
- Objective 2: Develop a process and design a commercial unit to scale-up the production of SLMP dispersion.
- Objective 3: Explore the use of an alternative pilot scale unit to produce dry SLMP powder directly from battery quality lithium metal.
- Objective 4: Integrate SLMP Technology into a Li-ion cell for PHEV application.

Technical Barriers

This project addresses the following technical barriers

(A) Develop PHEV technologies capable of 40 mile electric range

(B) Substantial petroleum displacement

(C) Improved air quality

Technical Targets

- Make available commercial quantities of SLMP, an independent source of lithium that will enable higher energy, safer, environmentally friendlier and lower cost lithium batteries and to mitigate the dependence on cobalt availability and price.
- Expedite the development of cost-effective manufacturing processes for SLMP to support high volume production of Li-ion Batteries.
- Evaluate, design and acquire pilot-scale unit for alternative production technology to further decrease the cost of production by cutting the number of process steps and increasing the volume of production by using a continuous process.
- Develop process technology for the integration of SLMP into Li-ion battery systems and demonstrate the benefits relative to a state-of-the-art baseline.

Accomplishments (05/01/09-09/30/09)

- Engineering design of the prototype unit for dry powder production has been the primary focus during this time period. The design is complete and the vendor will commence material procurement and vessel fabrication shortly
- The vendor for the commercial unit for production of lithium dispersion was selected and the engineering design of this dispersion unit is almost complete
- Procurement, qualification and selection of the electrode materials to be used for the demonstration of the SLMP technology in the full Li-ion pouch cell is complete.

✧ ✧ ✧ ✧ ✧

Introduction

Achieving the DOE technical and cost targets for HEV/PHEV batteries will require development and use of new electrode materials. SLMP technology provides an independent source of lithium for Li-ion systems, removes the current limitation that all lithium has to come from the cathode and, thus, allows the use of non-lithium providing cathode materials with potentially larger capacities. These new cathode materials are expected to be more overcharge tolerant and could be used with high capacity advanced anodes with high irreversible capacities.

Approach

Currently, there is not one cathode/anode system that can satisfy the safety, cost and performance requirements of the PHEV application. Industry currently uses $LiMn_2O_4$ or $LiFePO_4$, for example, that are the primary cathodes

considered to be safer and less expensive than $LiCoO_2$. Unfortunately, these cathodes are inferior to the energy density of the conventional $LiCoO_2$ cathode and, when paired with the advanced anode materials, such as silicon composite material, the resulting cell will still not meet the energy density requirements. However, SLMP™ technology may be used to compensate for the irreversible capacity in the anode and thus improve efficiency of the cathode utilization.

Based on the current trend of oil prices, we believe the demand for PHEVs will be ahead of the technology development. In other words, the launch of PHEVs will be mainly limited by the technology development cycle, which will likely require another five years. The main hurdle is still safety, followed by cost and calendar life. To satisfy the critical national needs of reducing our dependence on imported oil, it is critical to develop and validate revolutionary technologies, such as SLMP technology, and to establish the manufacturing base for the production of the advanced battery materials to meet the nation's needs.

Results

In general, lithium metal is a flammable solid that reacts violently with moisture to create flammable hydrogen and corrosive lithium hydroxides. Molten metal is especially reactive and given that the auto ignition point is essentially the same as the melting point, can spontaneously ignite in air. The reactivity of lithium increases with temperature and surface area. Therefore, molten metals or dispersions require special care in handling. Thus, significant effort was made during the first five months of this program to identify and select vendors capable of fabricating equipment that meets technical and safety requirements. Engineering design of the prototype dry powder production unit has been completed and fabrication will begin shortly. The design of the dispersion unit is almost complete and fabrication will start upon approval of the drawings.

Significant effort was made to source $LiMn_2O_4$, the material of choice for the positive electrode to be used in our electrochemical system. We have sourced material from leading Asian suppliers and have conducted some initial screenings. Figure III-26 shows the electrochemical behavior of spinel materials in the half cells at room temperature, Figure III-27 compares cycle-ability of the same materials at 60°C and Figure III-28 shows the rate capability of the selected spinel from supplier T. Each spinel material was formulated into a slurry in NMP with the following composition: $LiMn_2O_4$ (90%) + Super P carbon black (5%) + Kynar 761 PVdF (5%). This formulation was used based on both the vendor's suggestions and our experience. The coin cells were assembled using Ferro 1M $LiPF_6$ /EC+DEC (1:1) electrolyte. The cell test protocol is: constant current charge at 0.5 mA/cm^2 to 4.3 V followed by 4 hours constant voltage charge at 4.3 V and constant current discharge at 0.5 mA/cm^2 to 3.0 V. We used an Arbin BT2000 battery cycler for these tests. Based on the test results and considerations such as material availability at the commercial levels, the spinel from supplier T was selected as a cathode material for the electrochemical system to be used for the demonstration of the SLMP technology.

We have also completed characterization of the graphite anode materials, MCMB 25-28. The slurry containing MCMB had the following formulation: 90% MCMB, 5% PVdF, 5% conductive carbon (Super P). The cell testing protocol is as follows: Discharge: constant current at 0.1 mA/cm^2 to 0.01 V, constant voltage at 0.01 V until the current reaches 0.01 mA/cm^2. Charge: constant current at 0.1 mA/cm^2 to 1.5 V. The irreversible capacity for this material was calculated to be 8.7%. This material was selected as the anode material for the demonstration of SLMP Technology in electrochemical system #1.

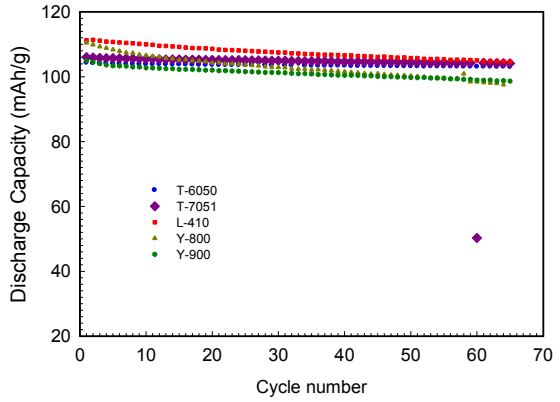

Figure III-26: Comparison of the cycle-ability tests results for the $LiMn_2O_4$ materials at room temperature

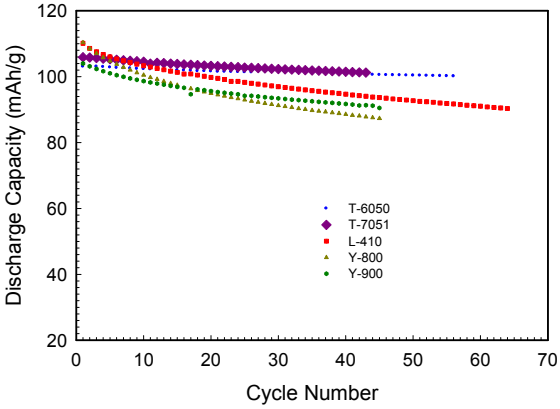

Figure III-27: Comparison of the cycle-ability tests results for the $LiMn_2O_4$ materials at 60°C

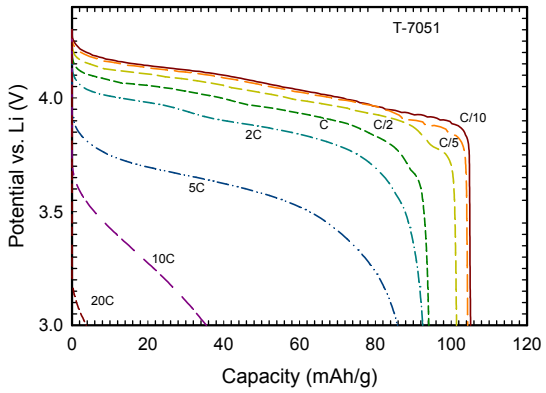

Figure III-28: Rate capability of $LiMn_2O_4$ from supplier T

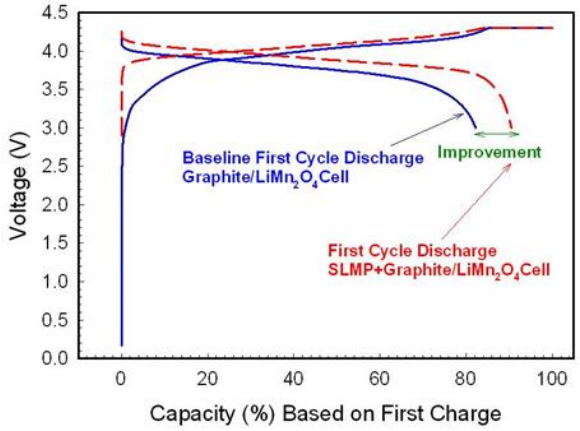

Figure III-29: First cycle efficiency improvement in $LiMn_2O_4$/MCMB system using SLMP Technology.

Upon completion of the characterization/qualification tests, we have transitioned to a larger format pouch cells with a 49 cm^2 electrode size. Figure III-29 demonstrates first cycle efficiency improvement in the Li-ion pouch cell. The spinel material has been formulated as a slurry with the following composition: $LiMn_2O_4$ (90%) + carbon black (5%) + PVdF (5%) in NMP and then manually casted on the Al current collector; the graphite has been formulated as a slurry with the following composition: MCMB-25-28 (90%) + carbon black (3%) + PVdF (7%) in NMP and then casted on the Cu current collector. The anode was purchased from a supplier M. Both cathode and anode electrodes were dried in a vacuum oven at 100°C overnight. Surface application technique was used to apply SLMP in xylene slurry onto the prefabricated MCMB electrodes. Upon solvent evaporation, the MCMB electrodes were calendared at 200 lbs/cm^2. The pouch cells were assembled and we used Ferro 1M $LiPF_6$ /EC+DEC (1:1) electrolyte. The cells were pre-conditioned for 5 hours and then cycled using the following test protocol: constant current charge at 0.25 mA/cm^2 to 4.3 V, constant voltage charge at 4.3 V for about 7 hours; constant current discharge at 0.25 mA/cm^2 to 3.0 V; we used a Maccor battery cycler for these tests. It is important to note that electrodes were not matched in these cells and we are currently working with the vendor to obtain the matched electrode sheets to proceed with our further experimental plans. However, as one can see in Figure III-29, the improvement of almost 10% was demonstrated in the overall cell efficiency.

Conclusions and Future Directions

We have completed all the tasks scheduled for the first five months of this project. We are expecting the delivery of the equipment for the dry powder production in December of 2009, followed by the installation of the unit and initiation of the design of experiments as disclosed in our proposal.

The dispersion unit fabrication will start upon design completion and drawings approval later this year. The evaluation of the alternative technology is scheduled according the proposed plan.

The benefits of the SLMP technology have been demonstrated on the electrochemical system $LiMn_2O_4$/MCMB. We are working with the vendors to obtain matched electrodes to proceed with the technology optimization experiments.

FY 2009 Publications/Presentations

No publications/presentations were made in FY 2009; we have currently completed tasks for the first five months out of the 36 months of this project.

III.A.3.6 Develop and Improve Lithium Sulfur Cells for EV Applications (Sion Power)

Chris Johnson (NETL Program Manager)

Subcontractor: Sion Power

Yuriy Mikhaylik (Project Manager)
Sion Power Corporation.
2900 East Elvira Rd
Tucson, AZ 85756
Phone: (520) 799-7609; Fax: (520) 799-7501
E-mail: ymikhaylik@sionpower.com

Start Date: Ongoing
Projected End Date: TBD

Objectives

- Phase 1: Applied Research. Develop metallic lithium anode stabilized with dual-phase electrolyte system and demonstrate anode electrode specific capacity exceeding 750 mAh/g over 50 full charge-discharge cycles in laboratory scale Li-S cells.
- Phase 2: Technology Development. Develop large format prototype Li-S cells with lithium anode stabilized with dual-electrolyte system and demonstrate >350 Wh/kg and enhanced cycle life using USABC test conditions.
- Phase 3: Technology Validation. Manufacture large format production cells, perform performance evaluation using USABC test procedures and abuse tolerance testing and demonstrate improvement by making the cell more thermally stable – increasing the runaway temperature to >165°C.

Technical Barriers

This project addresses the following technical barriers:

(A) Materials for dual-phase electrolyte sufficiently inhibiting detrimental side reactions on the Li anode

(B) Gel-polymer coating for dual-phase electrolyte compatible with high speed production.

(C) Hardware for coating dual-phase electrolyte components.

(D) Hardware for dual-phase electrolyte experimental and large format prototype cell manufacturing and testing.

Technical Targets

- Optimization of dual-phase system constructs
- Selection of method to create a dual-phase system in the cell
- Dual-Phase electrolyte formulation and mass balance optimization
- Laboratory scale cell design, manufacturing and test: demonstration of anode unit specific capacity to exceed 750 mAh/g over 50 full charge/discharge cycles.
- Gel polymer mixing/coating hardware system development
- Gel polymer coating process optimization to achieve ~20 m/min web-speed.
- Large format cell design, optimization and manufacturing
- Large format production cell manufacturing, test & evaluation- full scale USABC test performance evaluation and abuse tolerance test

Accomplishments

- Selected over 10 solvents, all showed immiscibility with polysulfide solutions formed at the sulfur cathode –promising components of dual-phase system.
- Selected polymers showing gel-electrolyte formation, high conductivity and solvent partition.
- Performed lab-scale Li anode gel-electrolyte coating, experimental Li-S cells assembled and tested.
- Demonstrated improved thermal stability with gel-polymer electrolyte coating.
- Designed, purchased and installed high speed gel-polymer coater.
- Demonstrated gel-polymer coating process compatibility with high speed web-coating
- Designed, purchased and installed slitter for gel-polymer coated Li anodes to produce large format negative electrodes. Performed slitter evaluation with experimental gel-polymer coated Li anodes.

✧ ✧ ✧ ✧ ✧

Introduction

Achieving the DOE cell performance targets for electric vehicle applications will require improved Li anode chemical stability (safety), cycle-ability and capacity. It also requires high specific energy and must be compatible with high volume manufacturing.

Approach

To meet the DOE targets, SION Power will develop a unique electrolyte providing two liquid phases having good Li+ conductivity, self-partitioning and immiscibility, serving separately the cathode and anode electrodes. A self-partitioning multi-phase electrolyte will enable us to tailor the electrolyte composition at each electrode to provide the optimum chemical stability. This innovative approach will be applied to develop a stabilized high energy metallic lithium anode. While this approach could be applied to any Li metal or Li-ion rechargeable cell, SION Power will use a lithium sulfur rechargeable battery system to demonstrate the two liquid phases concept.

Results

Materials for dual-phase electrolytes. The main components of the dual-phase electrolyte system are solvents with self-partitioning or immiscibility and gel-polymers to immobilize the immiscible anode solvent. We have identified over 10 solvents exhibiting the desired properties. We also identified several polymers forming gel-electrolytes with ionic conductivity exceeding 10^{-4} S/cm. These polymers are web-coating compatible and can be formed during monomers polymerization on the anode surface or can be coated from polymer solution.

Cell testing. Gel-polymer coated anodes have been combined with sulfur cathodes in experimental cells. Preliminary test results showed that gel-polymer coating reduced detrimental polysulfide/Li reactions leading to higher charge efficiency. Gel-polymer anode coating also substantially improved the thermal stability of small Li-S cells, with runaway temperatures exceeding 165°C.

Hardware for gel-polymer coating and anode electrode slitting. A large scale gel-polymer coater and anode electrode slitter have been designed, purchased and installed in the dry room (Figures Figure III-30, Figure III-31). The coater is an atmospheric, gravure, roll-to-roll coater, with both UV polymerization and convection drying capabilities. The gel coater also removes the inter-leaf prior to coating, and inserts another inter-leaf upon wind-up after coating. After the coating, the anode on substrate can be slit to the required width (Figure III-31). Both hardware units have been evaluated with previously selected gel-polymer materials and demonstrated compatibility with the high speed process.

Figure III-30: New prototype production gravure Gel coater, incorporating both UV polymerization and convection drying.

Figure III-31: New anode slitting station.

Conclusions and Future Directions

The initial dual-phase electrolyte materials tests showed their potential to improve Li anode stability. New hardware trials also showed compatibility of selected materials with high speed production. This progress creates the basis for targeting an anode electrode specific capacity exceeding 750 mAh/g over 50 full charge-discharge cycles in the laboratory scale Li-S cells.

New hardware also creates the basis for further technology development of large format prototype Li-S cells with lithium anode stabilized by the dual-electrolyte system.

III.A.3.7 High Volume, Low Cost, Manufacturing Techniques for Cathode Materials (BASF)

Chris Johnson (NETL Program Manager)
Subcontractor: BASF Catalysts, LLC

Anthony M Thurston
BASF Catalysts, LLC
23800 Mercantile Road
Beachwood, OH 44122
Phone: (216) 360-5043; Fax: (216) 464-5780
E-mail: anthony.thurston@basf.com

Subcontractor: Farasis Energy, Hayward CA

Start Date: September 15, 2009
Projected End Date: February 25, 2012

Objectives

- Successfully produce two low cost cathode materials, suitable for PHEV applications.
- Validate that quality targets are achieved through cell testing and battery pack testing
- Work closely with a Tier 1 auto supplier and/or automotive OEM.

Technical Barriers

This project addresses the following objectives of the Vehicle Technology Program for renewable energy research and development

(A) Development of LIB cathode materials for PHEV applications

(B) Scale up of manufacturing process for LIB cathode material

(C) Reduction of production costs

(D) Achieve USABC target and quality requirements

Technical Targets

- Synthesis of NMC in semi-batch laboratory scale process
- Production of NMC at the pilot plant level to fully address scalability issues
- Production trials for NMC at a production plant level to validate process, quality and cost targets are achieved.
- Development of a secondary LIB cathode material through the pilot plant level

Accomplishments

- Successful synthesis of NMC at the laboratory level that meets currently available NMC material targets for quality and performance.
- Evaluation of various process parameters to reduce processing time and production costs while maintaining a consistent and acceptable product quality and performance
- Successful testing of samples at the coin cell level

✧ ✧ ✧ ✧ ✧

Introduction

The production of low cost cathode materials is dependent upon the proper selection of raw materials coupled with a cost effective production process. However, this alone is not enough; there are also many specific requirements for chemical purity, physical characteristics and electrochemical performance that must be achieved and cannot be sacrificed.

Approach

To meet the USABC targets, BASF will use a systematic approach in the development and scale up for the production of cathode materials using our background and knowledge of materials chemistry and expertise. The effort will be focused on minimizing or eliminating expensive starting materials and the incorporation of low cost processing steps that do not require exotic conditions such as high pressure or expensive solvents.

Results

To date we have been able to produce cathode materials at the pilot plant scale that meet or exceed current specifications, see sample results in Figures Figure III-32 and Figure III-33. As a result of initial results from a design of experiments program, we have been able to identify key elements that are critical for the end product performance. Further work on the variation of these key elements is necessary in order to determine the minimum requirements necessary to meet the customer's product expectations.

Analytical and electrochemical test results have shown that BASF's product development process is capable of preparing LIB cathode materials with characteristics that can be measured with enough precision such that cause and effect relationships can be distinguished and corrections can be made in order to obtain acceptable product quality.

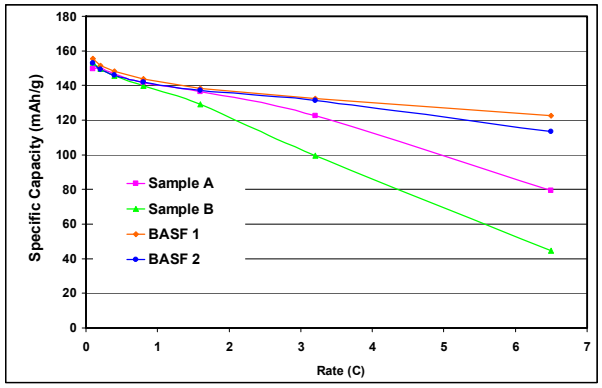

Figure III-32: Rate capability of BASF and commercial samples

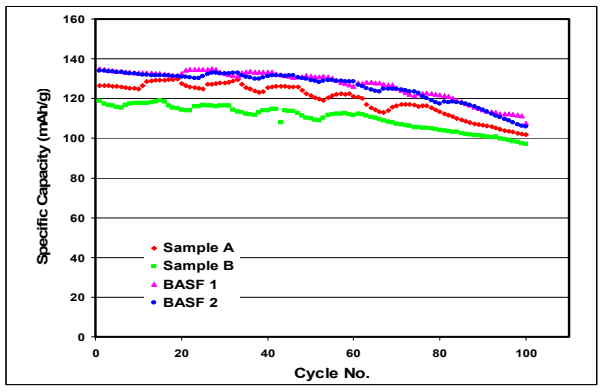

Figure III-33: Cycle capacity of BASF and commercial samples

Conclusions and Future Directions

Future work will be devoted to refining the critical process parameters in an effort to minimize processing steps and time while maximizing productivity.

We have produced 111 NCM in the pilot plant that has comparable capacity, power, and rate capability with lower impurities than commercial cathode. This gives us the advantage of better cycle life.

Further cost reduction via lowering cobalt content and process development through additional optimization of the critical and costly parameters will provide BASF with a reproducible low cost process for the domestic production of LIB cathode materials

Several prominent LIB automotive cell producers are currently evaluating / qualifying our NMC product.

III.A.3.8 Small Business Innovative Research Projects (SBIR)

James A. Barnes (Technical Manager, Energy Storage Topics)

EE-2G, U.S. Department of Energy
1000 Independence Ave., SW
Washington, DC 20585
Phone: (202) 586-5657; Fax: (202) 586-2476
E-mail: James.Barnes@ee.doe.gov

Start Date: Continuing Effort
Projected End Date: September 30, 2010

Objectives

Use the resources available through the Small Business Innovation Research (SBIR) and Small Business Technology Transfer (STTR) programs to conduct research and development of benefit to the Energy Storage effort within the Vehicle Technologies Program Office.

Introduction and Approach

The Energy Storage effort of the Vehicle Technologies Program Office supports small businesses through two focused programs: Small Business Innovation Research (SBIR) and Small Business Technology Transfer (STTR). Both of these programs are established by law and administered by the Small Business Administration. Grants under these programs are funded by set asides from all Extramural R&D budgets; 2.5% of these budgets is set aside for SBIR and 0.3% for STTR. These programs are administered for all of DOE by an SBIR Office within the Office of Science. Grants under these programs are awarded in two phases: a 6 – 9 month Phase I with a maximum award of $100K and a 2 year Phase II with a maximum award of $750K. Both Phase I and Phase II awards are made competitively. Energy Storage participates by writing a topic which is released as part of the general DOE solicitation. A typical topic focuses on a broad area and will contain several focused sub-topics. Grant applications are solicited in response to these sub-topics. The Energy Storage sub-topics are written to address technical barriers to the successful commercialization of advanced energy storage systems (batteries and ultracapacitors) for use in electric drive vehicles (HEVs, PHEVs, and EVs). Each year, areas of focus are identified by DOE staff based on technical challenges to meeting the goals of the Program. Sub-topics are written to address these challenges within the scope of the SBIR process. The grant process places the following constraints on the drafting of these sub-topics:

- The scope of work must be appropriate for a small business.
- The sub-topic must be broad enough to attract five to seven proposals.
- The sub-topic must be narrow enough to attract no more than twelve to fifteen proposals.
- The scope of work must be appropriate given the funding limitations of the SBIR/STTR programs.

Phase II Awards Made in FY 2009

Under the SBIR/STTR process, Companies with Phase I awards that were made in FY 2008 are eligible to apply for a Phase II award in FY 2009.

The FY 2008 subtopics were as follows:

a. Technologies that Result in Cells with Increased Energy Density by developing technology that will "stabilize" the surface of a lithium metal electrode in a rechargeable system

b. Development of Separators for Lithium-Ion Cells with High Temperature Melt Integrity

c. Development of "High Voltage" Electrolytes for Use in Advanced Lithium-Ion Cells

d. Development of "High Voltage" Positive Electrode Materials for Use in Advanced Lithium-Ion Cells

Five Phase I awards were earlier made in FY 2008 that resulted in the following three Phase II awards in the summer of FY 2009:

Subtopic b.

Development of High Temperature Melt Integrity Seperators for Lithium-Ion Cells (MaxPower, Inc., 141 Christopher Lane, Harleysville, PA 19438). A major safety concern related to the lithium-ion battery is the possibility of an internal short-circuit due to the shrinkage of its separator when exposed to high temperatures. This project will develop an electrospinning apparatus for the production of high-melt-integrity separators for lithium-ion batteries. Physical properties such as thickness and porosity will be measured, and to ensure safety, the electrospun separators will be characterized for thermal and electrochemical stability

Development of Separators for Lithium-Ion Cells with High Temperature Melt Integrity (Policell Technologies, Inc., 160 Liberty Street, Building #4, Metuchen, NJ 08840). This project will develop a thermally stable separator for lithium-ion batteries. These

separators will be used to make batteries offering improved safety and reliability and suitable for use in HEVs, and PHEVs.

Subtopic c.

High Voltage Electrolyte for Lithium-Ion Cells (TIAX, LLC, 15 Acorn Park, Cambridge, MA 02140). This project will develop technology to improve performance and reduce costs of batteries for HEVs and PHEVs. The improved batteries will make these vehicles more commercially viable, and thus increase the likelihood that they will yield significant environmental, economic, and political benefits.

Phase I Awards Made in FY 2009

Subtopics in FY 2009 were included in two major topics; they were as follows:

14 d. Development of Nanoparticle-sized, "High Voltage" Positive Electrode Materials for Use in Advanced Lithium-Ion Cells

15 a. Technologies to Assess the Behavior of a Lithium-Ion Cell Containing an Internal Short Circuit

15 b. Development of Asymmetric Electrochemical Capacitors

15 c. Development of Lithium-ion Cells that Do Not Require the Positive Electrode to Provide the Lithium that Is Cycled

15 d. Additives to Reduce the Flammability of Materials Vented from a Lithium-ion Cell

Awards made under 14d:

Nanostructured High Voltage Cathode Materials for Advanced Lithium-ion Batteries (ADA Technologies, Inc., 8100 Shaffer Parkway, Suite 130, Littleton, CO 80127-4107). High performance and long lifetime energy storage devices are critical for zero-emission advanced transportation technologies. This project proposes to develop high performance electrode materials and combine them with environmentally benign electrolytes to develop advanced lithium-ion batteries to fulfill this requirement.

Nanoparticle-Sized, High-voltage Cathode Materials for Use in Advanced Lithium-Ion Cells (Aegis Technology Inc., 3300 A Westminster Avenue, Santa Ana, CA 92703). The successful development and application of high-power, reliable Li-ion batteries for future PHEVs will significantly improve energy efficiency, reduce emissions and dependence on petroleum, and improve the competitiveness of U.S. manufacturing in global market of HEVs. The development of advanced nanomaterials for positive electrodes is an essential step to achieve these benefits.

Nanocomposite High Voltage Cathode Materials for Li-ion Cells (NEI Corporation, 400 Apgar Drive, Suite E, Somerset, NJ 08873). This project will develop and implement a new class of 5V high voltage Li-ion battery cathode material for next generation PHEVs.

Award made under 15a:

Implantation, Activation, Characterization and Prevention/Mitigation of Internal Short Circuits in Lithium-Ion Cells (TIAX, LLC, 15 Acorn Park, Cambridge, MA 02140-2301). This project will develop technology to improve the safety of batteries for PHEVs and HEVs, making these vehicle technologies more commercially viable, and thus increasing the likelihood that they will yield their potential environmental, economic and political benefits.

Awards made under 15b:

3-D Nanofilm Asymmetric Ultracapacitor (Ionova Technologies, Inc., 182 Thomas Johnson Drive, Suite 204L, Frederick, MD 21702). This project will apply advances in nanotechnology to create a new type of ultracapacitor energy storage device. Resulting ultracapacitors will be capable of storing significantly greater amounts of energy than commercially available devices while providing dramatic improvements in safety, cost, environmental impact and in other important metrics. This is an STTR award.

Asymmetric Electrochemical Capacitors for Hybrid Vehicle Technology (Luna Innovations Incorporated, 1 Riverside Circle, Suite 400, Roanoke, VA 24016). This project will develop high energy and high power capacitors suitable for use in hybrid electric vehicles. Novel carbon nanomaterials will be used to advance capacitor technology in order to implement these energy storage devices in commercial vehicles.

Nanocomposite Positive Electrode for Asymmetric Electrochemical Capacitors (Metamateria Partners, LLC, 1275 Kinnear Road, Columbus, OH 43212). Nanostructured positive electrode will be developed for energy storage devices for HEVs and PHEVs. These will improve energy and power density of supercapacitors and may lead to commercialization of electric vehicles.

Awards made under 15c:

Novel, High Performance Li-ion Cell (Farasis Energy, Inc., 23575 Cabot Blvd., Suite 206, Hayward, CA 94545). This project will develop a novel approach to increasing the performance and capacity of Li-ion cells. Use of the technology could accelerate the adoption of efficient distributed power systems and EVs by greatly increasing the life of the battery systems.

Reciprocal Lithium-ion Cell with Novel Lithium-Free Cathode and Pre-Lithiated Carbonaceous Anode (Yardney Technical Products, Inc., 82 Mechanic Street, Pawcatuck, CT 06379). This project will develop an inexpensive and environmentally benign lithium-ion cell

with novel cathode and pre-lithiated carbon anode. The essential feature of the developing cell is that it is in a charged state while being assembled while the traditional lithium-ion cell must pass a so-called "formation step" (few charge-discharge cycles lasting about a week) after assembling.

Award made under 15d:

Flameproof Additives for Automotive Li-ion Batteries (EIC Laboratories, Inc., 111 Downey Street, Norwood, MA 02062). This project will develop liquid additives to large lithium-ion batteries to be used in electric vehicles. The additives will suppress flammability that may be brought about by an accident or electrical failures.

FY 2009 Publications/Presentations

1. Presentation to the 2008 DOE Annual Peer Review Meeting.
2. B. Meyer, M. Salomon, D. Bansal, and M. Morgan, MaxPower, Inc., High Temperature Electrospun Separators for Lithium-Ion Batteries, 216th Meeting of the Electrochemical Society, Vienna, Austria, October, 2009.

III.B. Systems Analysis

Battery thermal analysis and characterization and requirements, cost and other analyses are performed in support of system development activities. These activities address issues related to battery thermal control and improving the thermal performance of energy storage devices through thermal characterization and testing, measuring thermal properties, modeling, analysis, and control strategies. Cost analyses are performance in an attempt to identify areas most needing advances to reduce system cost. Finally, ANL has performed a battery recycling study to understand the impact of battery recycling on material availability issues. The following projects are described below.

III.B.1 PHEV Battery Cost Assessments (TIAX)

Brian Barnett

TIAX LLC
15 Acorn Park
Cambridge, MA 02140
Phone: (617) 498-5307; Fax: (617) 498-7012
E-mail: Barnett.b@tiaxllc.com

Start Date: April 24, 2008
Projected End Date: March 31, 2009

Objectives

- Assess battery cost implications of selected cathode material chemistries being considered for PHEV applications.
- Identify factors with significant impact on cell/pack costs; develop insight into the relative benefits of alternative cathode chemistries; identify areas where more research could lead to significant reductions in battery cost.

Technical Barriers

- Not applicable

Technical Targets

- Not applicable

Accomplishments

- Estimates were developed for the cost of lithium-ion PHEV batteries employing four different cathode active materials, at two electrode loading levels, and two fade levels.
- Factors with significant impact on cell costs were identified and quantified.
- Areas where more research could lead to significant reductions in battery cost were identified.

✧ ✧ ✧ ✧ ✧

Introduction

TIAX's established cost model for PHEV batteries assumes a vertically integrated manufacturing process from cell fabrication through completed battery system. For cell production, the TIAX cost model yields estimates for the cost of goods sold (COGS), i.e., manufacturing cost, including capital cost. Materials and manufacturing cost estimates were based on production of cylindrical format cells in high volume. All supplied materials, e.g., cell materials, packaging components, are treated as outside-purchased and include supplier mark-ups. No supplier mark-up is included in in-process goods, e.g., cells to be assembled into packs.

The TIAX cost model was used to assess the implications to cost of a 5.5 kWh-usable Li-ion PHEV battery pack for the following cost modeling factors and conditions:

- Cathode materials (4): NCA, NCM, $LiFePO_4$, and $LiMn_2O_4$
- Anode material (1): graphite
- Electrode loading (2): low (1.5 mAh/cm^2) and high (3.0 mAh/cm^2)
- Fade (2): 0%, 30%

These cost modeling factors produced sixteen different scenarios to be considered. Each scenario was based on a SOC range of 80%. Costs were to be estimated at a production volume of 500,000 vehicles/year.

Approach

TIAX employed a parametric approach in which TIAX's cost model was applied many times with different sets of input parameters. Inputs included:

- Battery chemistries
- SOC range
- Electrode loadings
- Material costs
- Equipment costs
- Equipment throughput
- Fade
- Nominal battery pack voltage
- Energy required (20 mile range)

Individual cost input variables were identified and a likely range of values established for each. Cell designs were built up from specific electrode properties. Since Li-ion batteries of the size and design considered in this study have not been manufactured and tested, key assumptions were made about battery performance, including:

- Power output: peak power (40 kW for 2 seconds, or 20 kW for 100 seconds) is available from the battery even at low SOC. Low temperature performance was not considered.
- Power input: the battery can be recharged at the peak rate (30 kW) except when the battery is at a high SOC.
- SOC range: 10-90%, i.e., battery size is 6.9 kWh nominal to deliver 5.5 kWh usable.

It should be noted that it is not certain that target power and fade levels can actually be met at the electrode loadings modeled and over the SOC range modeled for all cathode active material chemistries.

Both single and multi-variable sensitivity analyses were performed for the purpose of identifying key factors influencing costs, particularly those factors with potential high leverage to reduce battery cost.

Results

The PHEV battery configurations modeled in this study resulted in battery costs (COGS) ranging from \$264/kWh to \$710/kWh, or \$1452 to \$3905 for 5.5 kWh usable energy.

Cost of cathode active material is a somewhat less important factor in battery system cost than might have been thought. There is significant overlap in battery costs among the four cathode classes evaluated, with wider variation within each chemistry than between chemistries.

Upfront cell design is a critical factor in battery cost. Electrode loading (i.e., electrode length) seems to be more significant than cathode active material cost within the ranges evaluated. Manufacturing process speed also has a significant impact on battery cost.

The projected costs for PHEV batteries in this study are consistent with what might be expected from consideration of 18650-based Li-ion battery costs. 18650 cells represent a standardized Li-ion design currently produced in volumes approaching one billion cells/year worldwide, using the most highly automated processes currently available in the industry. This production volume corresponds to about 10 GWh/year, or enough volume in terms of materials and electrode area to yield about one million PHEVs/year. Current Li-ion OEM 18650 cell costs are in the \$200-\$250/kWh range.

Conclusions and Future Directions

The PHEV battery configurations modeled in this study resulted in battery costs (COGS) ranging from \$264/kWh to \$710/kWh, or \$1452 to \$3905 for 5.5 kWh usable energy. There is significant overlap in battery costs among the four cathode classes evaluated, with wider variation within each chemistry than between chemistries.

Doubling the speed of all manufacturing processes noticeably decreased battery cost in most scenarios. Separator cost and coater speed are significant factors in battery system cost.

The ability to utilize a wide SOC range contributes significantly to reducing energy storage costs. Lower fade and wider SOC range both reduce cost by resulting in lower required nominal battery energy and smaller battery size. Therefore, materials that support a wide SOC range should help to reduce overall battery costs. Other specific areas of research with potential to yield reductions in battery cost include materials that provide minimal fade, impedance growth and calendar aging. Also, chemistries and/or electrode designs that permit shorter, thicker electrodes while meeting target requirements for power and energy should yield cost reductions in the battery. In general, chemistries and designs that enable lower overall electrode area per battery and minimize battery size will reduce cost. Fundamentally different electrode preparation processes could result in favorable battery manufacturing cost impact, both capital and operating. Also, identification and adoption of advanced processing technologies to increase coater speed and/or other unit operations significantly are a potential source of cost reduction.

FY 2009 Publications/Presentations

1. Presentation to the 2009 DOE Annual Peer Review Meeting.

III.B.2 Battery Pack Requirements and Targets Validation (ANL)

Danilo J. Santini
Argonne National Laboratory
9700 South Cass Avenue
Argonne, IL 60439
Phone: (703) 678 7656; Fax: (630) 252-3443
E-mail: dsantini@anl.gov

Subcontractor: Electric Power Research Institute
Partner: IEA HEV & EV Implementing Agreement

Start Date: Oct. 2006
Projected End Date: Sept. 30, 2010

Objectives

- Examine Li-ion plug-in hybrid (PHEV) battery chemistries
- Evaluate parallel, split and series powertrains
- Evaluate PHEVs designed for blended vs. all-electric charge depletion
- Determine cell power and energy cost trade-offs, for four chemistries
- Determine best charge depletion attributes to maximize electricity-for-gasoline substitution
- Estimate real world PHEV fuel & electricity use
- Determine likely early U.S. market for PHEVs
- Estimate PHEV well to wheels (WTW) emissions and energy use

Technical Barriers

This project addresses the following technical barriers in the choice of battery chemistry and battery pack configuration in support of maximum market success of electric drive supported by grid electricity.

A. Initial costs of providing both power and energy in plug-in hybrid batteries
B. Establishing a cost effective balance/mix of mechanical and electric drive
C. Achieving battery life cycle net benefits, given low U.S. gasoline prices, considering trade-offs among:
   - Initial cost
   - Cycle life
   - Calendar life
   - Energy and power densities

Technical Targets

- Maximization of net present value benefits per kWh of grid electricity used. Evaluate chemistries, powertrains, pack kW and kWh, by target market.
- Determination of cost effectiveness of battery power and kWh energy storage relative to charging infrastructure costs (high kWh per pack and few charges/day vs. less kWh per pack with more charges)
- Determination of fuel saved per kWh used during charge depletion, by chemistry and powertrain type

Accomplishments

Publications from the study to date include estimates supporting the following points:

- To successfully market electrification of drivetrains, PHEVs are far superior to EVs.
- Car (or small crossover)-based series or split PHEVs with moderate power (50-70 kW) and energy (~ 6-10 kWh) are most cost effective
- Suburbs are the target market for PHEVs
- HEV and PHEV powertrains are complements, not competitors (HEV for urban street driving, PHEV for urban/suburban arterial driving).
- PHEVs should be compared to conventional drivetrains in suburban driving conditions, not to HEVs
- Drivetrain electrification via PHEVs can most cost effectively reduce GHGs and extend fuel resources (enhance sustainability)
- PHEVs may never be a universal powertrain, will take time to cut oil use
- Best Li-ion chemistries for PHEVs may be different than for HEVs

✧ ✧ ✧ ✧ ✧

Introduction

Achieving currently stated DOE cost and technical performance targets for electric drive vehicles (HEVs, PHEVs, EVs) may be sufficient to support cost effective near-term introduction of electric drive. However, by examining the market into which the various kinds of battery packs will "fit" (powertrain type, charge depletion strategy, vehicle size and function, driving behavior of probable purchasers, charging costs and

availability), the advisability of adjusting cost and technical targets is investigated.

Approach

There are four candidate battery chemistries under evaluation to achieve DOE technical and cost targets for near-term use in light duty passenger vehicles.

(1) $LiNi_{0.8}Co_{0.15}Al_{0.05}O_2$/graphite (NCA-G),

(2) $LiFePO_4$/graphite (LFP-G)

(3) $Li_{1.06}Mn_{1.94}O_4/Li_4Ti_5O_{12}$ (LMO-TiO) and

(4) $Li_{1.06}Mn_{1.94}O_4$/graphite (LMO-G).

This study includes development of a production cost model for these four chemistries.

There are three major powertrain options under development for plug-in hybrids. These are: (1) power split, (2) parallel, (3) series range extender. For each it is possible to configure the powertrain with varying shares of electric energy and power provided, relative to gasoline or diesel fuel. This study includes assessment of production costs for each of the powertrain options, taking into account the battery pack cost trade-offs identified in the battery cost model, and considering different choices of power and energy in battery packs installed in these powertrains.

For near-term introduction, the charging infrastructure is divided into three categories, level 1 (ubiquitous 120 V, 15 amp circuits), level 2 (240 V, 20-70 amp circuits), and level 3 (480V, 70+ amp circuits). This study primarily considers the benefits of designing PHEVs to make the greatest use of level 1 charging, taking into consideration the potential to upgrade to level 2. Level 3 charging for electric vehicles is a secondary concern.

This study takes into account level 1 "plug availability" in proximity to parked vehicles (garage and carport locations) and the related patterns of vehicle use by households with readily accessible level 1 charging.

Results

Target Market for PHEVs. In general, it has been shown that the market advantage for PHEVs in comparison to EVs and HEVs is at an average driving speed faster than for these powertrains. When combined with considerations of household income and garage/carport ownership, this implies that PHEVs will be most competitive in relatively low density suburbs.

For HEVs, the dominant powertrain type is the split hybrid. The parallel HEV powertrain is not currently found in light duty vehicles, but is used in medium duty trucks and may be introduced by Nissan in light duty passenger vehicles within the next five years. PHEV "spin-offs" of such HEVs are anticipated to be designed to have a power capability sufficient for all electric neighborhood and city core driving, but otherwise operate in "blended mode". For such PHEVs, simulation has been used to demonstrate that the distance to depletion will generally increase as driving speed increases. However, importantly, it has been noted that the time to depletion will generally drop as speed increases (Figure III-34). Average time in the vehicle per day for U.S. households is relatively constant, regardless of location. These facts mean that PHEVs "spun-off" from HEVs will enjoy an increasing opportunity for multiple charges per day as average speed driven increases.

Battery pack costs for HEVs vs. PHEVs. For "spin-off" PHEVs, cost-effectiveness analysis, the initial version of the battery cost model, has demonstrated very sharply dropping $/kWh costs for relatively small charge depletion distance (pack kWh) values. The initial version of the battery cost model also implies relatively small differences in cost for the four chemistries under evaluation. The initial interpretation of these results is that attributes other than first cost (cycle life, calendar life, useable capacity,

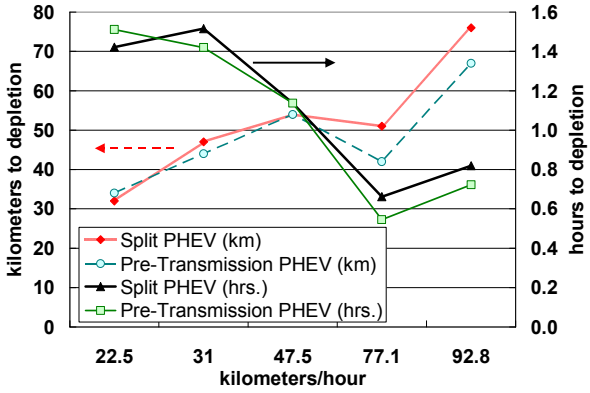

Figure III-34: Distance and time to charge depletion of the chosen PHEVs, by driving cycle

safety, energy and/or power density) will be the keys to eventual success of the different chemistries (Figure III-35). Put another way, creation of high W/Wh batteries for HEVs drives up $/kWh costs dramatically relative to an energy oriented battery pack design (low W/Wh) suitable for PHEVs and EVs.

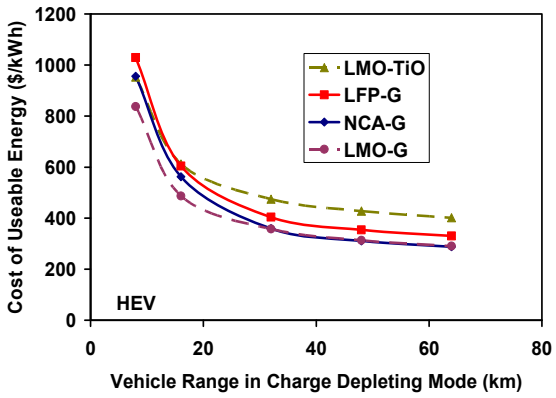

Figure III-35: Cost per kWh for "spin-off" PHEV battery packs, holding pack kW constant and increasing kWh

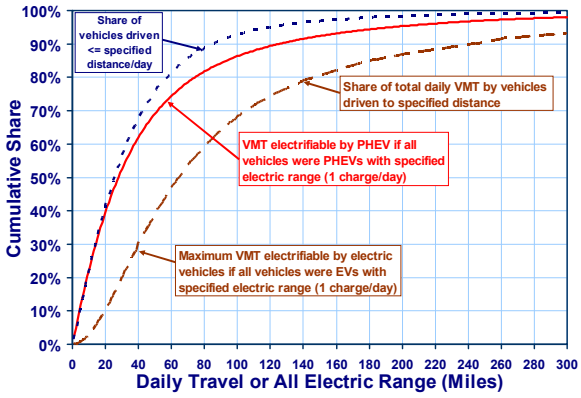

Figure III-36: NHTS one-day travel data and maximum technical potential electrified VMT by PHEV vs. EV

Technical Potential for Electric Drive via PHEVs vs. EVs. The technical potential to substitute miles driven electrically via PHEVs vs. EVs was estimated, under the assumption that every household owned the vehicle of specified design as a replacement for a conventional vehicle, charging the pack once per day. The National Household Travel Survey (NHTS) pattern of daily vehicle use was utilized (Figure III-36). Theoretical PHEVs and EVs with varying ranges (charge depletion distances) were hypothesized, despite the lack of realism of this assumption for high ranges. All electric range capability was assumed in each case.

Multiple interpretations of the graphic created are possible. For example, if one is interested in evaluating the potential of a PHEV with 20 miles of range compared to an EV with such range, the chart implies that four times as many miles could be electrified with the PHEV. Should the value be 40 miles, then twice as many miles can be electrified with a PHEV instead of an EV with similar range. One interpretation is that with small amounts of battery kWh per vehicle much larger potential for miles of electrification exists if those packs are in PHEVs instead of EVs. Short to medium range blended mode PHEVs are very effective in miles electrifiable potential. The chart implies that a 20 mile range could achieve 2/3 of the electrification of miles that a 40 mile range could accomplish.

On the other hand, one might compare an EV with 100 miles of range to a PHEV with 40 miles, and conclude that the EV has greater potential to electrify miles. Probably coincidentally, since this chart was published, a number of announcements of EVs with approximately 100 miles of range have been announced. The drawback of this chart is that it addresses hypothetical technical potential ignoring costs of the vehicles.

Accordingly, for PHEVs, a relatively simple market concept was developed to try to help engineers and scientists without economic backgrounds (those who had developed charts of the type used in Figure III-36) to understand the limitations of the methodological foundation for the former chart. The crude "heart of the market" revision illustrated what would happen if consumers proved unwilling to purchase vehicles with all electric range that exceeded their daily driving distance, a decision that is economically logical in light of the high costs of energy storage in battery packs (Figure III-36).

This analysis addressed the question of best choice of all electric range for a PHEV in the event that all development resources were to go into only one PHEV design. It implied indifference for an all-electric range from about 20 miles to 50 miles, with about the same share of miles theoretically electrifiable. Expressed in this fashion, extension of range from 50 to 100 miles is estimated to be counter-productive (result in a loss of market share), because too many households would not drive enough to make the battery pack range investment worthwhile.

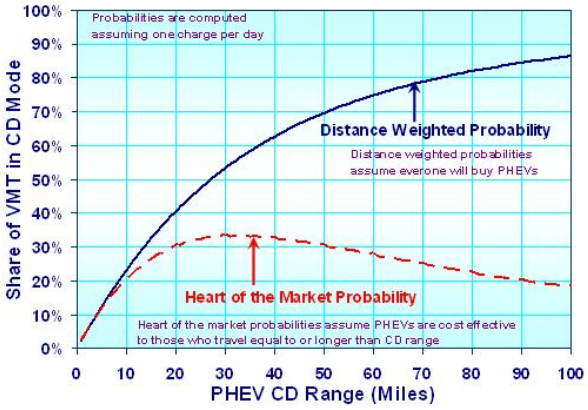

Figure III-37: Miles electrifiable if only one PHEV technology were available, with specified range, with no purchases by households driving less miles per day.

A logical extension of this line of reasoning is to determine the most cost effective PHEV configuration among those capable of 20-40 miles of all-electric range. Further, there is a question of market viability of provision of all electric range vs. blended mode charge depletion operation, due to the costs of higher power requirements in the former case Figure III-37, along with FY 2009's battery cost findings, suggests FY 2010 comparison of PHEVs with 15-20 miles of blended mode charge depletion distance accomplishing more than one charge per day, to those with 30-40 miles and up to one charge per day. Also suggested is evaluation of jointly determined competitive market potential of multiple types of PHEV powertrains in combination with city EVs.

GHG emissions and sustainability. Analysis of the GHG emissions and net WTW feedstock energy use per mile indicated that charge depleting electric drive was the most effective light duty vehicle fossil-fueled powertrain option when grid-electric power is provided with a natural-gas-fueled combined-cycle power plant. For renewables, the results also indicated that charge depleting electric drive is the most effective renewable option when renewables converted to electricity - wind, solar and hydro – are used to create miles of service.

Conclusions and Future Directions

The near-term target market for light duty PHEVs is the suburbs. Appropriate evaluation of PHEVs requires prediction of the driving behavior of most probable owners. For a given amount of battery capacity per vehicle, if all consumers were to purchase vehicles with electric drive from plugging into the grid, the most miles electrifiable per kWh of packs produced would be obtained if the packs were in PHEVs rather than EVs. Battery pack costs per kWh drop very sharply when one compares a PHEV to an HEV, but drop much less sharply when one compares an EV to a PHEV. If only one PHEV design were available and was purchased only by those households that consistently drove beyond its range, estimates imply that medium range (20 miles) would be nearly as effective as a 40 mile range.

Since multiple types of PHEVs are coming to market, as well as city EVs, more sophisticated examinations of probable market segments for each type of plug-in vehicle are necessary. Now that a battery cost model has been developed, plans are to use the battery cost model with other OVT cost and vehicle simulation models to examine relative cost effectiveness of HEVs, PHEVs and city EVs in "real world" city, suburban, rural, and inter-city driving. The trade-off between purchases of — (1) more kWh of battery pack capacity with few charges versus (2) less kWh of capacity with more charges — will be investigated. The battery cost model will be documented and used to support other OVT assessments of the desirability of electric drive.

Since recent claims by corporate FCV proponents contradict the WTW finding that charge depleting PHEVs can use less natural gas and create less GHGs than hydrogen fueled FCVs using hydrogen from reformed natural gas, our 2009 result must be re-examined.

Further, the recommended WTW and cost effectiveness comparisons as a function of four patterns of driving (city, suburban, rural, inter-city) will be compiled.

FY 2009 Publications/Presentations

Publications

1. Vyas, A., D. Santini and L. Johnson. *Plug-In Hybrid Electric Vehicles' Potential for Petroleum Use Reduction: Issues Involved in Developing Reliable Estimates. Paper and poster presentation.* Proceedings of the 88th Annual Meeting of the Transportation Research Board, Washington DC Jan. 11-15, 2009 (shortened version appears in Transportation Research Record, 2009)

2. Nelson, P., D. Santini and J. Barnes. *Factors Determining the Manufacturing Costs of Lithium-Ion Batteries for PHEVs*. Proceedings of the 24th International Battery, Hybrid and Fuel Cell Electric Vehicle Symposium and Exposition, Stavenger Norway. May 13-16, 2009

3. Santini, D.J. *Highway Vehicle Electric Drive in the United States: Current Status and Issues*. Paper presented at the Clean Cities Strategy Workshop, Office of Vehicle Technologies, Energy Efficiency and Renewable Energy, U.S.

Department of Energy, Washington DC. Sept. 22-23, 2009

Presentations

4. Santini, D.J. *Battery Pack Requirements and Targets Validation: FY 2009 DOE Vehicle Technologies Program* Presentation at the Annual U.S. Department of Energy Office of Vehicle Technologies Merit Review, Arlington VA. May 21, 2009.
5. Santini, D.J. *Comparing Four Battery Cost Models, 2001-2009.* Presentation at Plug-in 2009. Long Beach CA. Aug. 10-13, 2009.
6. Nelson, P. *Modeling Manufacturing Costs of Lithium-Ion Batteries for PHEVs.* Presentation at Plug-in 2009. Long Beach CA. Aug. 10-13, 2009.
7. Vyas, A., D. Santini, and A. Moawad. PHEV Modeling: Daily Usage Pattern and Cost Effectiveness. Presentation at Plug-in 2009. Long Beach CA. Aug. 10-13, 2009.

III. B. 3 Battery System Life and Cost Modeling (NREL)

Kandler Smith
National Renewable Energy Laboratory
1617 Cole Blvd
Golden, CO 80401
Phone: (303) 275-4423; Fax: (303) 275-4415
E-mail: kandler.smith@nrel.gov

Start Date: March, 2007
Projected End Date: September 30, 2010

Objectives

- Develop and validate battery life models that account for multiple degradation factors relevant to automotive applications, e.g., age, cycles, depth of discharge of cycles, and temperature exposure.
- Use the degradation life models in trade-off studies for battery performance, life, and cost to minimize cost of plug-in hybrid electric vehicle (PHEV) & electric vehicle (EV) battery systems while meeting performance goals at end of life.

Technical Barriers

This project addresses the following technical barriers to the development of advanced batteries for PHEVs and EVs:

(A) High cost of PHEV & EV battery systems

(B) Uncertainties in predicting battery life

(C) Geographic and consumer usage scenario analysis

Technical Targets

The requirements for PHEV batteries as determined by DOE and the USABC are as follows:

- PHEV with 10 mile electric range: 45 kW pulse power for 10 seconds, 3.4 kWh usable energy, mass less than 60 kg, volume less than 40 L, cost less than $1,700
- PHEV with 40 mile electric range: 38 kW pulse power for 10 seconds, 11.6 kWh usable energy, mass less than 120 kg, volume less than 80 L, cost less than $3,400
- Calendar life: 15 years at 35°C
- Cycle life: 5,000 deep discharge (EV) cycles and 300,000 shallow (HEV) cycles.

Accomplishments

- Developed an empirical degradation model for predicting the capacity and power fade of a Li-ion battery. The model captures dominant effects relevant to automotive applications, i.e., age, number cycles, depth of discharge of cycles, temperature exposure, and voltage or state-of-charge exposure.
- Compiled degradation data collected by other laboratories for various Li-ion cells with graphite/nickel-cobalt-aluminum chemistry. Fit empirical model to data to achieve a representative model of this chemistry.
- Conducted performance/life/cost trade-off analysis to identify optimal power to energy ratio and excess energy margin to meet life and performance requirements with minimum cost. Showed the significance of temperature exposure on battery life and cost.
- Extended the model to analyze arbitrary temperature fluctuation and charge/discharge cycling scenarios. Applied the model to quantify the impact of different charging scenarios (once per night, vs. multiple times per day) on battery life.
- Incorporated the degradation model into NREL's pre-existing multi-scale multi-dimensional electrochemical/thermal model for predicting non-uniform degradation in large-format PHEV cells caused by thermal and cycling non-uniformities.

✧ ✧ ✧ ✧ ✧

Introduction

The high cost of Li-ion battery systems hinders the market penetration of clean EVs and PHEVs. Today's HEV and PHEV batteries are oversized in order to meet life goals. For batteries to last 10 to 15 years, the total beginning-of-life energy content is often two to five times greater than that actually used. Mathematical models that describe battery performance, cost, and life are needed to quantify trade-offs and identify the research priorities and engineering solutions needed to achieve long-life, low-cost battery systems.

Approach

While performance and cost modeling of batteries is fairly well established, life modeling is not. Depending on the needs of a particular analysis, battery

performance models can either be physics-based (describing lithium transport and electrochemical kinetics) or empirical (matching current/voltage behavior with a circuit model). Battery cost models typically consist of accounting spreadsheets combining component costs with manufacturing cost estimates.

Predicting battery life is highly complex. Li-ion battery degradation is driven by numerous interacting effects, such as

- solid-electrolyte interfacial (SEI) film layer growth,
- fracturing (and regrowth) of the SEI film layer due to expansion/contraction or mechanical stress of cycling,
- formation of a resistive solid film layer near the active surface during cycling, and
- fracturing and isolation of active material due to the mechanical stress of cycling.

Each of those mechanisms causes battery resistance growth and capacity loss, depending on the time spent at temperature and voltage (or state of charge, SOC), and the number of cycles at a given depth of discharge. At present, no physics-based model exists that simultaneously describes the influence of all of these important degradation effects.

Given the lack of a comprehensive physical model, NREL chose an empirical approach. NREL's empirical life model fits physically justifiable equations to capacity fade and resistance growth for various accelerated cycling and storage conditions. The graphite/nickel-cobalt-aluminum (NCA) chemistry was chosen for the FY09 life model development given the (i) popularity of the chemistry due to its good performance and life characteristics and (ii) 5+ years of publicly available data showing its aging characteristics under a variety of conditions.

Results

NCA Li-ion Life Model Development. Numerous factors can influence battery life, requiring a prohibitively large test matrix to fully exercise each factor and determine its influence on battery capacity fade and resistance growth. Such large datasets are rarely collected and almost always proprietary. To develop a comprehensive life model, NREL compiled the results of many NCA chemistry life-cycle datasets from DOE national laboratories (ANL, INL), Boeing, NASA-JPL, Saft, and Southern California Edison (SCE).

Although results vary depending on the cell design, the data show that the NCA chemistry can exhibit relatively low capacity fade under a variety of cycling or storage conditions, but often high resistance growth, sometimes in excess of 100% for cells stored at moderate-to-high temperatures and/or cycled to deep depths of discharge. Figure III-38 shows an example of the life model fit [1] to published Boeing data for a 40 Ah Saft VES-140 cell designed for satellite applications. While datasets such as Boeing's were instructive as to decoupling the influence of various factors—including depth of discharge (DOD), end-of-charge voltage (EoCV) and number of cycles—it is possible that the satellite cell is not fully representative of present-day PHEV cell designs. For this reason, the final model parameters [3] were adjusted to reflect recent results from DOE and SCE labs with NCA chemistry cells designed for PHEV applications.

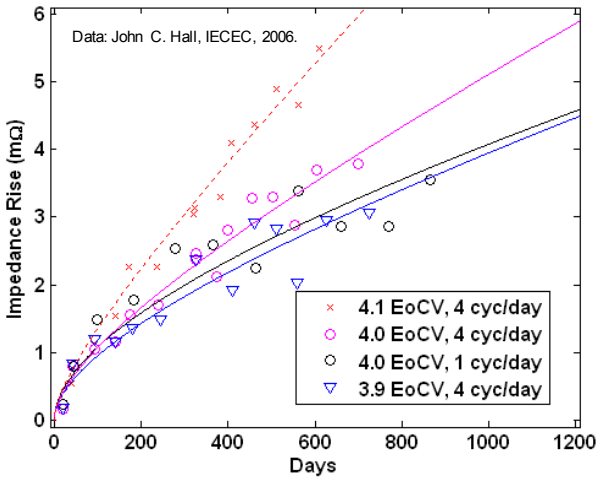

Figure III-38: Impedance rise or resistance growth of a 40 Ah Li-ion NCA cell under different low earth orbit satellite cycling conditions. Data (symbols) fit by NREL life model (lines).

Performance/Life/Cost Trade-off Analysis. Coupled performance, life, and cost models were used to sweep the battery system design space to identify low-cost designs that meet DOE/USABC performance goals at the end of life for PHEV10, PHEV20, and PHEV40 vehicles [6]. Figure III-39 shows trade-offs for a PHEV10 design. For this representative NCA technology, the lowest cost system results when the cell is designed with a power/energy ratio of 15 hr^{-1}. If the cell is designed with less power, the system must include substantial excess energy and be cycled within a narrow DOD in order to meet the life goal. In general, excess energy comes at great cost because of the expense of additional active material. In practical situations, where one must select from pre-existing cell designs, for example, it is generally preferable to oversize a battery with too much power rather than too little. Excess power costs relatively little in comparison to excess energy. Excess power enables a larger fraction of battery stored energy to be used and generally results in a smaller, lighter battery.

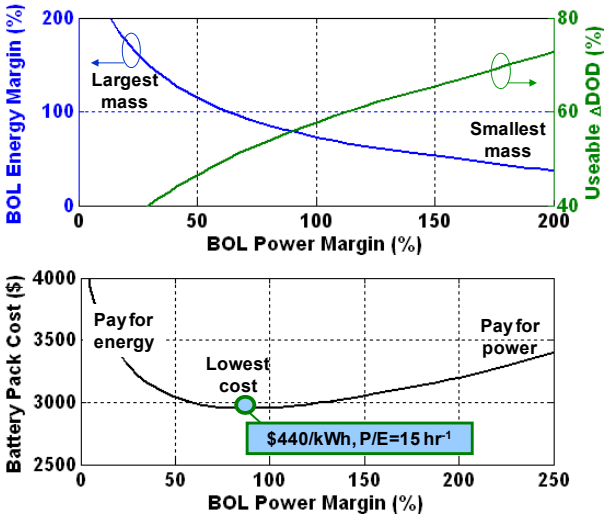

Figure III-39: Performance and cost trade-offs for a PHEV10 battery sized for 10-year life at 30°C with 1 deep discharge cycle/day. The lowest cost design has roughly 80% excess power at beginning of life and uses only 55% of stored energy. The lowest cost pack is projected to cost $2,950, which is reflective of today's technology costs at high-volume production.

Consumer Use and Geographic Scenario Analysis. The degradation rate of Li-ion batteries can be highly dependent upon how they are used by the consumer. Consumers might cycle PHEV batteries with one deep discharge per day and fully recharge them at night. But for consumers that have access to recharge during the day (at work or while shopping, for example) deep discharge cycling can occur more frequently. The effect of such charging scenarios on battery degradation and trade-offs with fuel consumption were explored in Ref. [3].

Batteries also degrade on storage, that is, even if the hybrid or electric vehicle is never driven. This "calendar" or storage life is highly dependent upon temperature, and batteries in hot climates will degrade more quickly than those in cold climates. Figure III-40 gives an example of differences in power loss for a battery stored in various climates. The typical practice is to size an automotive battery system for a 10- or 15-year life in a worst-case hot climate, e.g., as in Phoenix, AZ. But this practice results in a larger, more costly battery than may be necessary in cooler climates. An alternative to oversizing PHEV batteries for worst-case hot climates is to design battery cooling systems that are active while vehicles are parked and grid-connected.

Large-Format Battery Non-uniform Degradation. The trend in the automotive industry is toward larger cells to reduce the number of parts and increase the energy for PHEV and EV designs. A consequence of large cells, however, is non-uniform working potential distributed throughout electrode foils due to long internal current paths, and non-uniform temperature due to long thermal conduction paths that carry away heat. Both effects contribute to non-uniform cycling of large cells with uncertain consequences for the longevity of large cells. The NCA chemistry degradation model was integrated into NREL's multi-physics, multi-scale, multi-dimensional (MSMD) electrochemical/thermal model to explore these effects [4, 5]. Figure III-41 shows the distribution of cycling imbalance that occurs late in life for a 20 Ah cylindrical cell undergoing the more aggressive US06 cycling profile. Early in life the imbalance is negligible; late in life, the inner core of the cell and areas closest to cell terminals degrade (localized areas with less capacity and higher resistance), and are used less than the rest of the cell. The multi-dimensional electrochemical- thermal-degradation model will help designers answer crucial questions with respect to large-cell thermal, electrical, and electrochemical design and explore the implications of long-term cell use under severe cycling conditions.

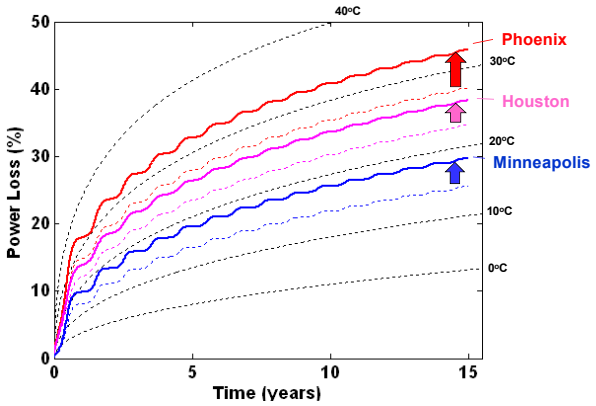

Figure III-40: Power loss for an NCA battery stored for 15 years in various ambient conditions. For the three cities, arrows show the additional battery degradation that occurs due to heating of the passenger cabin, which also indirectly heats the battery.

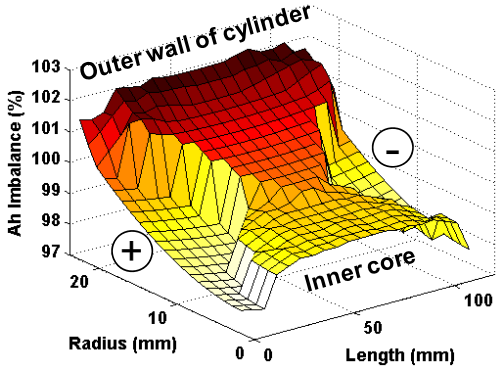

Figure III-41: Cycling Imbalance predicted by MSMD electrochemical/ thermal model of a cylindrical 20 Ah PHEV10 cell after 16 Months of accelerated Us06-CD cycling.

Conclusions and Future Directions

Considering the numerous factors contributing to Li-ion battery degradation, the life model developed in FY09 has several important applications in component design, system design, and analysis of the market feasibility of a specific battery technology. We found that for a PHEV-10 with the NCA/graphite chemistry- due to the effect of battery degradation with temperature - a large battery (almost $1,000 more expensive) is needed in Phoenix, AZ compared to a battery needed in Minneapolis, MN. Future efforts will continue to explore trade-offs in life and cost to better understand the capabilities and optimize the today's technology as well as highlight research that is needed to improve the life and lower the cost of tomorrow's technology. Moving forward, the model will be continually validated against real-world experience in the field and improved where necessary. The model will also be expanded to other Li-ion chemistries beyond graphite/NCA.

FY 2009 Publications/Presentations

1. K. Smith, T. Markel, A. Pesaran, Battery Seminar, FL, March 2008.
2. A. Pesaran, presentation at the 2009 DOE Annual Merit Review Meeting, Washington D.C., May 2009.
3. T. Markel, K. Smith, A. Pesaran, "Improving Petroleum Displacement Potential of PHEVs Using Enhanced Charging Scenarios," EVS-24, Stavanger, Norway, May 13-16, 2009.
4. K. Smith, G.-H. Kim, A. Pesaran, "Modeling of Nonuniform Degradation in Large-Format Li-ion Batteries," 215th Electrochemical Soc. Mtg., San Francisco, CA, May 25-29, 2009.
5. K. Smith, G.-H. Kim, A. Pesaran, "Modeling of Nonuniform Degradation in Large-Format Li-ion Batteries," Advanced Automotive Battery Conference, Long Beach, CA, June 10-12, 2009.
6. A. Pesaran, K. Smith, T. Markel, "Impact of the 3Cs of Batteries on PHEV Value Proposition: Cost, Calendar Life, and Cycle Life," Advanced Automotive Battery Conference, Long Beach, CA, June 10-12, 2009

III.B.4 Battery Lease Analysis – Project Better Place (NREL)

Michael P. O'Keefe
National Renewable Energy Laboratory
1617 Cole Blvd.
Golden, CO 80401-3393
Phone: (303) 445-9036; Fax: (303) 445-9036
E-mail: Michael.Okeefe@nrel.gov

Start Date: October 1, 2008
Projected End Date: September 30, 2010

Objectives

- Evaluate the concept of electric vehicle (EV) service providers, such as the business model proposed by the company Better Place. Specifically, investigate the economic and energy benefits of such a system as well as the implications on the battery.
- Build a computer tool that can evaluate scenarios such as the EV service provider concept to give feedback on the overall cost/benefit of each scenario as well as the implications to the battery in terms of required cost targets, expected duty cycle, and technical requirements.

Technical Barriers

The major technical barriers to the adoption of electric vehicles are the cost of the battery and low energy density leading to limited electric driving range. To address the cost and limited range, this project identifies the system implications for batteries used in new vehicle systems, such as an EV Service Provider network (our focus this year). In addition, we are working to identify the relationship between battery economics, performance, and life to provide guidance on required R&D cost and performance targets related to the various scenarios we investigate.

Technical Targets

The long-term targets for EV batteries are specific energy of 200 Wh/kg, cost of $150/kWh, and life of 10 years with 1,000 deep cycles. This project focuses on how an EV service provider could reduce the initial battery cost for consumers.

Accomplishments

- Developed a "Battery Ownership Model" which allows us to simulate the usage and life of various battery technologies in different EV business and engineering scenarios. Preliminary results have been obtained.
- Applied the "Battery Ownership Model" to simulate the EV Service Provider concept similar to Better Place and contrast that with conventional vehicles, hybrid electric vehicles, plug-in hybrid electric vehicles, and direct-ownership electric vehicles.

✧ ✧ ✧ ✧ ✧

Introduction

Electric vehicles (EVs) have long been regarded for their significant energy benefits: the ability to completely replace petroleum, the ability to be fueled by electricity that is ubiquitous and capable of being generated from a diversified mix of resources, and their potential to drastically reduce greenhouse gas emissions and other emissions if coupled to a clean electric utility grid. Other attributes of EVs such as their high-tech image, their quiet operation, and their ability to be refueled from home or other areas outside a gas station are valued by some consumers as well.

Despite these alluring positive attributes, however, electric vehicles have failed to become a mainstream option, largely because of their high costs when compared to other vehicle technologies. The up-front cost is especially high as a result of the expense of the battery. Furthermore, although electricity is easily accessed in most areas of the United States, a robust vehicular charging infrastructure for EVs does not currently exist. This has implications for the available range of travel for a consumer direct-owned EV and might require a larger battery for an acceptable range. Finally, the consumer must take on the added risk that batteries may not last the life of the car. This significantly affects the economic proposition of EVs.

One company, Better Place, has proposed a new concept of EV ownership that involves an "EV Service Provider." The EV Service Provider takes on all of the recharging and infrastructure needs of EV ownership in exchange for a subscription fee. Specifically, in the EV Service Provider model, as proposed by Better Place, the Service Provider—

- owns all of the EV batteries
- installs and maintains a distributed network of charge points for use by their subscribers (and nonsubscribers, for a fee)
- installs and maintains a battery swapping station for customers who require a "quick refueling" for

occasions in which they must drive longer than their EV's range on a single trip

- provides on-vehicle intelligence and coordination with a command and control center to manage the electrical charging of all vehicles on the system, which lowers the impact on the utility grid and meets consumer-specific needs (such as an EV owner who needs priority recharging).

Traditional direct-ownership of an EV is depicted in Figure III-42. In this ownership model of an EV, the consumer has to pay the substantial up-front costs of an EV purchase. Additionally, the consumer may have to pay for a replacement battery at some point. Also, there is no infrastructure available for this EV owner.

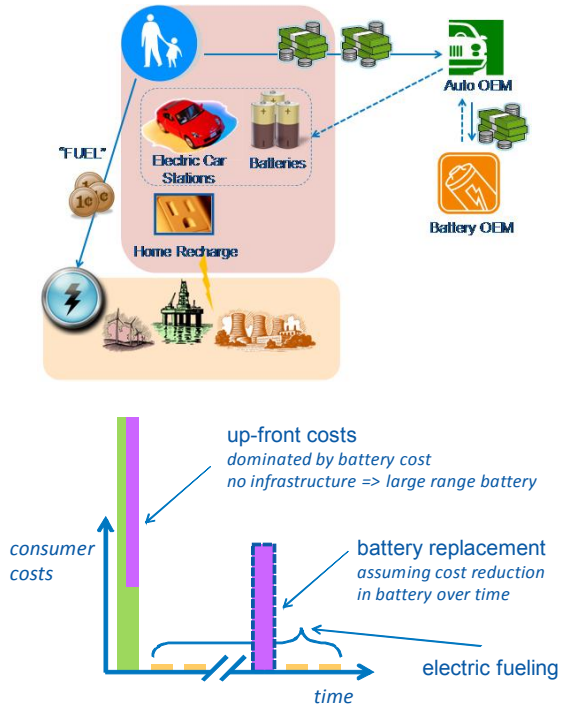

Figure III-42: Traditional EV Direct Ownership

A contrasting EV Service Provider system is displayed in Figure III-43. Here, the EV Service Provider allows the consumer to purchase an EV at a lower up-front cost. The consumer then gets full access to the network of recharging services in exchange for a subscription fee.

We are currently investigating the economic and energy implications of this model.

Approach

In situations in which the scale and/or scope of testing is prohibitive (because of a lack of time, money, equipment, or capability), it is often helpful to construct a computational model of a system of interest and study the model as a surrogate for the real system. Such a model can help the researcher discover relationships between a myriad of potential input parameters and the sensitivities of output parameters to various inputs.

This is the approach we took for this project. The model we created is called the "Battery Ownership Model," which has a focus on evaluating various usage and ownership scenarios for advanced battery technology in a transportation context.

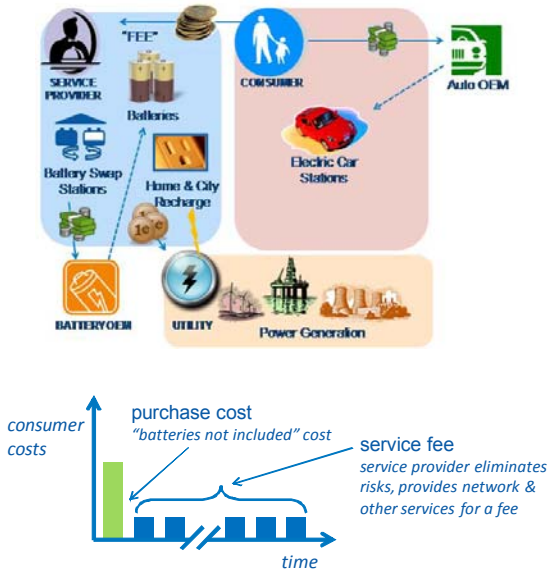

Figure III-43: EV Service Provider Concept

When evaluating a sufficiently complex system involving new vehicle powertrain technologies that can interface with the electric utility grid, it is important to sufficiently capture the critical elements of all of the relevant subsystems. For the EV Service Provider system, it quickly became apparent that many different subsystems and critical elements span various engineering disciplines. Therefore, we formed a multidisciplinary team to develop our model. The team members' expertise includes vehicle systems analysis, software construction, finance and economics, robust design and optimization, reliability and battery life prediction, governmental and economic policy, deployment issues, carbon markets, and knowledge of vehicle-to-electric-utility interfaces and related challenges.

Our model consists of several different modules that were constructed by the respective domain experts. The module system for the Battery Ownership Model is depicted in Figure III-44.

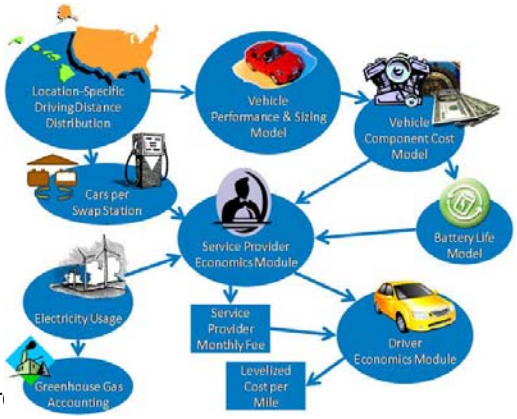

Figur

The model contains the following modules:

- Location-specific energy cost forecasts and location-specific driving data that yields a probability density function for distance driven per day
- A vehicle performance module to predict the fuel consumption of conventional vehicles, hybrid electric vehicles, plug-in hybrid electric vehicles, and electric vehicles
- A parametric vehicle cost model that predicts the cost of the advanced technology vehicles based on their component sizes
- A battery life model that predicts battery degradation due to usage
- A swap-station infrastructure module that predicts the number of cars that can be serviced by a single swap station at the same convenience level as today's gasoline-powered vehicles. This module predicts the amount of swap station infrastructure needed
- A service provider economics module that accounts for all of the fixed and variable costs of running a service provider business
- An electricity usage module that predicts the electrical energy needed to recharge EVs from charge points and/or swap stations
- A greenhouse gas accounting and carbon market module that calculates the greenhouse gas emissions for each option and optionally assesses a price for carbon pollution based on existing carbon markets.
- A driver economics module to calculate the total costs to the consumer for each technology.

Results

Following are some preliminary results from our modeling that show insightful trends.

Early analysis shows that the Service Provider can economically compete with conventional ICE vehicles on a net present cost basis under the following qualitative conditions:

- consumer vehicle-miles traveled per year is above average
- battery costs are low (near DOE technical targets)
- battery life is high (near DOE technical targets)
- Service Provider return on equity is not excessive.

We also recognize that there are additional benefits to the service provider system that are not currently being reflected in the costs, such as fewer required trips to the gasoline station, environmental image, and so on.

One of our initial questions was, "What makes up a majority of the EV Charge Provider's infrastructure costs: charge points, swap stations, or batteries?" We found that the answer is batteries, for a large range of costs based on estimates for the number and costs of charge points and swap stations. This trend is shown in Figure III-45

. The Department of Energy's technical target for PHEV battery cost is $300/kWh. As one can see, for battery costs of $300/kWh and above, batteries constitute over 75% of the cost of the installed infrastructure for the service provider.

We used levelized cost per mile as a metric to compare different vehicle options. A comparison of results for our internal combustion engine conventional small car versus data reported by AAA and others appears in Figure III-46. The NREL cost model for the conventional small car compares favorably with similar predictions by AAA.

We investigated the daily driving patterns and trip frequency of U.S. drivers using the latest National Household Transportation Survey dataset. From that dataset, we were able to estimate how often people might have to use "swap stations" to switch their depleted batteries for a fully charged battery if driving patterns stay constant. Depending upon the availability of charge points located throughout a region, consumers will be able to recharge from only once per day to as frequently as after every trip (if there is a charging receptacle at each parking space). Depending on those inputs, we calculated the "swap percent" or the percent of recharging events that must come from swap stations. The results appear in Figure III-47.

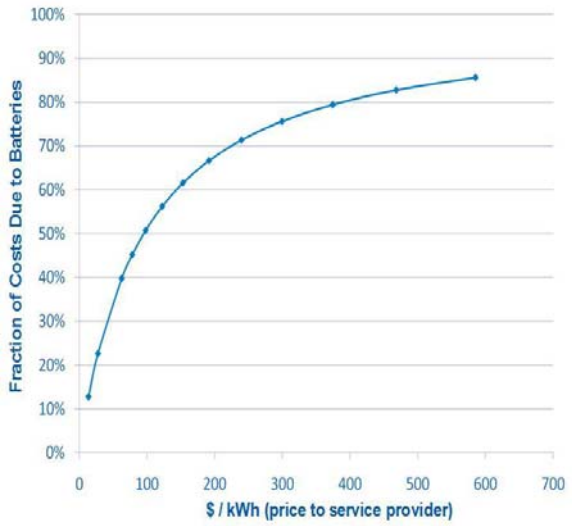

Figure III-45: Battery Fraction of Service Provider Infrastructure Costs

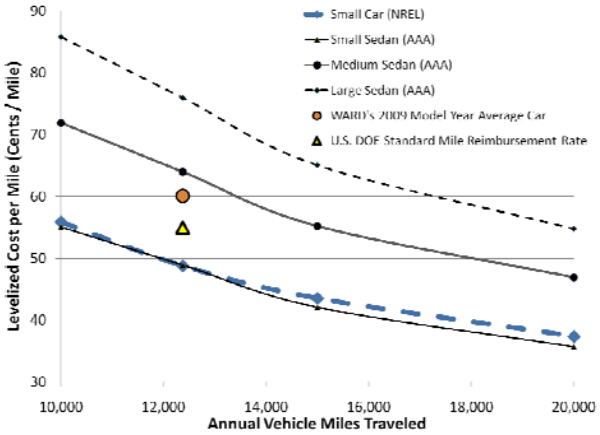

Figure III-46: Levelized Cost per Mile Predictions

We also studied how the "category" of driver affects the results. As can be seen, a suburban driver would require fewer swapping events than the national average driver—a population that includes rural drivers who travel long distances at a time (and would thus require considerable swap station usage). Based on this analysis, the percentage of recharging events that would be from swap stations is forecasted to be from as much as 1 in 10 to as infrequent as 1 in 100.

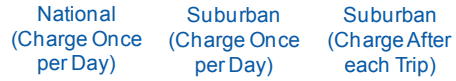

Figure III-47: Swap Percentage Based on Driving Distribution

Conclusions and Future Directions

We developed a battery ownership model to evaluate various EV business scenarios. Preliminary results show that, on a direct economic basis, there are situations in which the EV Service Provider scenario is economically competitive with other options. More study is necessary to confidently confirm these findings. Early results show that battery cost is forecasted to be the major cost component of the Service Provider's infrastructure cost and that, based on the latest National Household Transportation Database, swap stations will not be used excessively.

In FY10, we intend to continue to explore the EV Service Provider scenario as well as other scenarios for EV infrastructures using alternative methods such as fast charging, charge-spots only, battery-leasing only, and vehicle swapping. Furthermore, we intend to investigate further the secondary use of batteries and how they can affect the economics and usage of energy projects (such as renewable energy). Also, we will be looking at how the different options studied by our tool compare on a "cost per petroleum barrel reduced" and "cost per ton-equivalent of CO_2 reduced" basis. Finally, we recognize that consumer purchase decisions are not made solely on the basis of economics. Therefore, we will be investigating consumer choice modeling in an attempt to forecast how different vehicle technologies and business scenarios may be valued and adopted by consumers.

FY 2009 Publications/Presentations

1. NREL Milestone Report for U.S. Department of Energy: "Evaluation of EV Battery Miles/Swap Concept," September 2009

III.B.5 PHEV Battery Secondary Use Study (NREL)

Ahmad Pesaran
National Renewable Energy Laboratory
1617 Cole Blvd., Golden, CO 80401-3393
Phone: (303) 275-4441
E-mail: Michael.OKeefe@nrel.gov

Start Date: October 1, 2008
Projected End Date: September 30, 2010

Objectives

- Initiate scoping out a program and technology roadmap to evaluate the potential value of reusing so-called "end-of-life", or "second-life" batteries from plug-in hybrid electric vehicles (PHEVs) and electric vehicles (EVs) for other applications.
- Interact with others interested in PHEV battery secondary use to identify potential partners.

Technical Barriers

The barriers to the secondary use of PHEV and EV batteries are as follows:

- Lack of understanding of the value of PHEV or EV batteries for secondary-use applications
- Lack of knowledge and data on the performance of PHEV and EV batteries for other applications
- Too many different PHEV and EV battery sizes, shapes, voltages, chemistries, and configurations, as well as differences in end of life performance
- Potential low cost of other energy storage devices, such as lead acid batteries.

Technical Targets

Part of this secondary use of end-of-life PHEV batteries project, which was recently established, is an effort to establish technical targets. Therefore, we have proposed the following targets:

- Identify the top five most profitable applications and/or opportunities for reusing so-called "end-of-life" batteries from PHEVs and EVs for secondary applications.
- Provide validated tools and data to industry for implementation of those applications and opportunities.

Accomplishments

- Developed initial scope of a program for PHEV battery secondary use and reviewed it with DOE and other experts
- Identified the elements of the PEHV battery secondary use program and obtained buy-in from stakeholders
- Established the major elements of the battery secondary-use program: define goals, identify applications, test both control and second-life batteries, perform a cost-benefit analysis, and conduct demonstration projects to evaluate the merits
- Discussed the scope of the PHEV battery secondary use with staff at the University of California at Davis, California Energy Commission, Johnson Controls Inc., and Nissan; all expressed interest in collaborations
- University of California, with funding from California Energy Commission, expressed interest in a cost-shared project with NREL/DOE
- Drafted a statement of work for requesting proposals from U.S. companies to evaluate potential of battery secondary use for other applications.

✧ ✧ ✧ ✧ ✧

Introduction

The high cost of lithium ion (Li-ion) battery systems hinders the development and market penetration of clean electric and plug-in hybrid electric vehicles. One of the ways to reduce the initial cost of the battery is to recover its cost by using so-called "end-of-life" batteries for other applications. It is a common belief that Li-ion batteries in PHEVs and EVs reach the end of their useful life when their capacity, energy, and/or power capabilities drop by 20% to 30%. This belief is based on wanting the vehicle to perform in roughly the same manner at both the beginning and the end of the life of the battery. At the battery's end of life, a supposedly "depleted" PHEV or EV Li-ion battery may still have reasonable energy capabilities for other applications, such as stationary use. The residual value of second-use battery applications could be their potential to offset the initial high cost of PHEV and EV batteries and to help make electric drive vehicles more affordable.

The new interest in PHEV and EV springs from the renewed strong interest in reducing emissions and dependence on imported oil. These in turn have led to an expansion in the development and resurgence in the development of batteries for PHEVs and EVs. The technical advances in Li-ion batteries have resulted in longer life and better performance, but they are still high in cost. The secondary use of batteries could potentially have a value that could be used to lower the high cost. The use of renewable solar and wind technologies to produce electricity is growing, and their increased market penetration requires energy storage to mitigate the intermittency of wind and solar energy. New trends in utility peak load reduction, energy efficiency, and load management

also need energy storage. Smart grid, grid stabilization, low-energy buildings, and utility reliability require energy storage as well, such as batteries. There is currently a large investment in in the United States for battery manufacturing for the new green economy. As a result, the DOE Energy Storage Program is interested in establishing a new project activity for secondary use of batteries. NREL was assigned to this project because of its extensive expertise and capabilities in energy storage for transportation and in distributed grids, advanced vehicles, utilities, solar energy, wind energy, grid interfaces, and understanding the dynamics of the stakeholders.

Approach

We searched the literature to identify the previous studies on battery secondary use. A 1997 ANL study sponsored by USABC found that nickel metal hydride (NiMH) batteries at the end-of-life are still useful for some low-power applications. A 2002 Sentech study sponsored by Sandia National Laboratories (SNL) and DOE investigated several applications for second use. The 1997 ANL study sponsored by USABC indicated that NiMH batteries at the end of life are still useful for other applications. The 2002 Sentech study sponsored by SNL and DOE identified several potential stationary applications for battery secondary use. None of the studies demonstrated the end-of-life batteries for second use applications. After discussion with stakeholders, we identified the following benefits for secondary use of batteries:

- Reducing the (first) cost of batteries for PHEV and EV applications
- Reducing the cost and environmental impacts of recycling and disposal of batteries before their "true" end of life
- Providing advanced batteries for non-vehicle applications such as renewable electricity and home use.

A need for scoping out a new program for secondary-use applications was identified. We identified the following potential applications:

- Stationary applications
  - Grid
    - Local substation support or substation management
    - Load leveling and grid stabilization
    - On-grid residential/commercial buildings peak shaving
    - Rapid response energy storage system and high response services
    - Smart grid and efficiency implementation
    - Home energy use for demand control
  - Non-grid
    - Telecommunications backup
    - Emergency power backup (UPS)
    - Off-grid home with renewables
    - International – developing countries
    - Other mobile applications
  - Refurbished batteries for low-mileage PHEVs & EVs
  - Off-road vehicles
  - Lift trucks
  - Heavy-duty vehicles
  - Trolleys
  - Buses
  - Recreational or occasional-use vehicles, ATVs, electric boats, etc.

In order to scope out a program and define a roadmap, we came up with a list of questions to be addressed in a secondary-use battery program. The questions were divided into two categories:

1. Questions to help decide whether battery secondary use has merit
   - How is the "end-of-life" in a vehicle battery defined?
   - What would we like to know? What unknowns need to be studied?
   - What are the performance (energy and power) needs and remaining life of end-of-life or second-life batteries for various applications?
   - How do end-of-life batteries compare with new lead acid batteries?
   - What are the safety and liability issues associated with reusing end-of life batteries?
   - What are the conditions of cells or modules in a pack when they are at the end-of-life in vehicles? Should they be dismantled or recycled?
   - How do we calculate present value of end-of-life batteries?
   - What are the applications most suited for end-of-life or second-life batteries?
   - What are the costs and benefits of secondary use of end-of-life batteries?
   - What are the barriers to the second use of batteries?
   - What analysis needs to be performed to evaluate if secondary use could be successful?
2. Questions to answer if it is decided that secondary use has merit
   - What are the mechanisms for collection, screening, distribution, and field implementation of end-of-life batteries?
   - Who is going to do the collection, screening, distribution, etc?

- Who is taking the risk in owning the end-of-life batteries? What is the value? Who should own end-of-life batteries?
- What practices or standards are needed in designing battery systems for eventual secondary use and for ease of disassembly or integration?

Results

We identified the following barriers to the secondary use of PHEV/EV batteries:

- Low cost of unused lead acid batteries
- Uncertainty in valuation of used batteries at end of first life
- Too many cells in a pack – disassembly vs. use as whole
- Separation of a poor cell or module from the rest
- Too many cell types, chemistries, and voltages
- Too many sizes and shapes of cells and batteries
- Uncertainty about a used battery's life and performance – how good is it?
- Voltage and size matching for different applications
- The need for battery management system will add cost
- Special equipment to adapt Li-ion batteries to existing applications
- Equalization
- Balancing
- Safety issues of used Li-ion batteries
- Regulations
- Hazardous material handling
- Shipping requirements
- Liabilities
- Warranty costs.

We scoped out a program for secondary battery use and identified the following elements for roadmapping:

- Define and refine goals and objectives
- Gather information on batteries, life, end-of life performance and applications
- Obtain industry input through one-on-one interviews and at workshops, later
- Identify and rank potential stationary and mobile applications.
- Develop energy storage requirements for potential applications
- Develop testing protocols for characterizing second-life batteries for these applications
- Perform characterization tests to evaluate battery conditions at end of life versus control batteries
- Identify practical barriers and refine the roadmap for addressing them
- Perform a cost-benefit analysis
- Collaborate and partner with stakeholders (car and battery manufacturers, utilities, states, universities, other)
- Conduct demonstration and deployment projects
- Evaluate processes and infrastructure for reuse
- Design and develop standards and methods for uniform battery fabrication for ease of eventual reuse
- Disseminate and share information
- Conduct annual reviews.

The program elements are described in more detail below.

Define Goals and Objectives. We recommend the goal to be to identify the top five profitable applications/opportunities for reuse of end-of-life batteries from PHEVs and EVs for secondary applications and provide validated tools and data to industry for implementation. These are the objectives:

- Establish a program (and a roadmap) for identifying the top five applications and opportunities for battery secondary use
- Reduce the initial cost of batteries to make PHEVs and EVs more affordable
- Reduce the disposal and recycling of end-of-life batteries before their "true end-of-life" to reduce environmental impacts and operational costs.

Gather Information. The program will obtain data on the state of the art of different batteries, vehicle types, battery sizes, and power profiles; gather information on any existing practices for secondary use of conventional batteries; collect information on utility and home applications; and look at trends in energy storage use and applications. We will also survey various industries to identify potential complementary applications to increase the use of batteries.

Identify and Evaluate Potential Applications. The program will evaluate the potential of non-PHEV and EV applications that require energy storage and currently use lead acid batteries; identify the requirements for energy storage for different applications; estimate the value of energy storage for stationary grid-renewable applications in terms of local substation support, load leveling, and grid stabilization. We will also evaluate the potential of on-grid residential/commercial buildings peak shaving, rapid-response energy storage systems, and high-response services; study the smart grid applications and potential to increase energy efficiency; estimate the value of energy

storage in the stationary non-grid and telecommunication backup, emergency power backup (UPS), and off-grid home use with renewables and whether end-of life PHEV batteries have a potential role. We will estimate the value and requirements of energy storage in other mobile applications, including off-road vehicles such as lift trucks, heavy-duty vehicles such as trolleys and buses, recreational vehicles and ATVs, and vehicles for occasional use. And we will match performance and cost requirements for energy storage in these applications using end-of-life batteries (size, energy, voltage, and discharge time) as well as rank the potential of these applications.

Perform Characterization and Testing. We need to understand the potential characteristics (performance and life) of end-of-life batteries for potential second-use applications. As part of this, we will define targets/requirements and testing procedures/protocols for different second-use applications, including energy or capacity, power, self-discharge, response time, calendar and cycle life, and state of health. We need to understand and differentiate the above characteristics and parameters for cells, modules, and packs. The program needs to acquire appropriate equipment for conducting tests and secure end-of-life batteries for characterization and testing. We need to obtain end-of life batteries from field testing or demonstrations in projects across the United States. We need to perform accelerated PHEV and EV aging tests to take them to end of life and then perform tests to characterize end-of-life and fresh batteries according to the specific test procedures for the identified applications.

Perform Cost-Benefit Analysis. We need to develop analysis tools based on existing models and use existing and enhanced battery life predictions. We will adapt existing utility-grid-energy storage analysis capabilities at various organizations, including NREL. We will estimate the required/desired cost of energy storage for each application and identity the values and benefits of secondary use of PHEV batteries for different applications. We will propose valuation methods to estimate the value of the "depleted" batteries (present vs. future) and identify the costs associated with collection, characterization, disassembly, packaging and distribution of depleted batteries. Life vs. cost trade-off analysis will be performed, and risks and rewards of ownership of an end-of-life battery will be evaluated.

Identify Barriers and Define a Roadmap. We need to identify barriers to making "depleted" Li-ion batteries competitive with other energy storage systems. To do this, we will identify uncertainty in the performance and value of end-of-life batteries; perform tests and develop tools to estimate values; determine how to identify whether there are too many small cells in a pack; and evaluate the merits of disassembly vs. use as a whole. Initially, there will be too many cells of different types, chemistries, sizes and shapes, and voltages; therefore, we need to define sorting and matching processes and infrastructure or standards and the need for special equipment to adapt to existing hardware. We will also identify battery management systems; address safety concerns associated with Li-ion batteries; implement early diagnostics and protection systems; determine regulations for handling and shipping hazardous batteries; work with regulation agencies and policy makers; and identify liabilities and warranty costs by working with suppliers and users.

Obtain Industry Input. The program will conduct one-on-one interviews with stakeholders to collect information on car makers, battery manufacturers, and integrators; cell and module developers; material suppliers; battery recyclers; utility and grid analysts; solar and wind energy experts; experts at the national labs and universities; amd state and federal agencies; regulators (hazardous materials and shipping). We will also conduct one or two workshops with various stakeholders to finalize the roadmap and review any analysis and roadmap for feedback.

Refine Roadmap and Program Plan. The program will conduct demonstrations of actual applications, including demonstrating and deploying second-life batteries in some real applications to obtain data and gain experience and identifying some potential applications and sites for demonstrating end-of-life batteries in the field. We will also secure end-of-life batteries for applications; obtain end-of-life batteries from field programs; and perform accelerated PHEV and EV tests to take them to end-of-life. We will install second-life and control batteries in the applications and obtain data on the performance and reliability of the systems. We will also compare the performance and reliability of the systems with control new energy storage systems (such as new lead acid batteries).

Reuse Processes and Infrastructure. The program will evaluate and define potential processes and infrastructure for collection, evaluation, disassembly, sorting, reassembly, packaging, and distribution of spent batteries. We will also address these questions:

- Who defines end-of-life and what method should be used to determine it?
- Who determines if it is the battery's end-of-life or a need for service, and how?
- How do we differentiate between bad cells and bad packs?
- How do we determine whether to send the battery for service, recycling or reuse?
- Should bad cells be separated from a pack?

  Should packs be disassembled into smaller modules?

- How do we sort cells/modules/packs for a particular application?
- How are the batteries reassembled?
- What are the packaging needs and control systems?
- How are the reassembled packs distributed to their final destinations?
- Is it better to have a few central locations for distribution around the country or many smaller distributed locations?
- Who owns the spent battery, and who will be responsible for the testing, evaluation, disassembly, reassembly, distribution, and sales?

Design Common Practices/Standards for Reuse. Having too many different cell sizes, shapes, capacities, voltages, and chemistries makes battery reuse difficult. Having too many types of modules with different sizes and shapes, capacities, cell-cell connection types, fastening types (welding versus mechanical) makes reuse difficult in multiple applications. Therefore, we need to do the following:

- Identify a small number of standard sizes and voltages to make it easier to establish a reuse infrastructure
- Implement a particular battery design to accommodate later disassembly of cells or modules for reuse in a particular application
- Ask car makers, battery developers, and integrators to begin the design of cells/modules/packs with reuse in mind
- Evaluate automated disassembly and repackaging vs. manual methods.

Collaborate, Disseminate, and Review. We will collaborate and partner with industry, universities, states, policy makers, and other stakeholders as part of this effort. We will disseminate information to the research and stakeholder community through the Internet, meetings, workshops, and focused conferences. As part of this effort, we will conduct annual program reviews and refine plans as needed.

Conclusions and Future Directions

Recent developments and dynamics have generated significant interest in programs for secondary use of batteries that will become available from plug-in hybrid electric and electric vehicles at their so-called "end-of-life." We propose a phased program for FY09-FY11 for the secondary use of these batteries. The major elements of program planning are to define goals, identify applications, conduct tests of control and second-life batteries, perform a cost-benefit analysis, and conduct demonstration projects to evaluate the merits. We have drafted a statement of work for cost-shared collaborations with industry. In FY10, we plan to request proposals for demonstrations of second-use batteries in one or two promising applications. We will work with industry to obtain end-of-life batteries and start testing them to evaluate their suitability for different applications. We will also conduct a workshop to obtain feedback from stakeholders.

FY2009 Presentations and Publications

1. Ahmad Pesaran, "Draft Program Scope for PHEV Battery Secondary Use," NREL Presentation to DOE Energy Storage Team, Washington, DC, July 2009.

III.B.6 Battery Recycling (ANL)

Linda Gaines
Center for Transportation Research
Argonne National Laboratory
9700 S. Cass Ave.
Argonne, IL 60439
Phone: 630/252-4919, Fax: 630/252-3443
E-mail: lgaines@anl.gov

Start: spring 2008

Projected Completion: fall 2011

Objectives

- Estimate material demands for Li-ion batteries
  - Identify any potential scarcities
- Calculate theoretical potential for material recovery
- Evaluate real potential for recovery using current recycling processes
- Determine potential for recovery via process development
- Develop improved process(es) to maximize material recovery

Barriers

- Scarcity could increase costs for battery materials
  - Recycling could increase effective material supply and keep costs down
  - Current processes recover cobalt, use of which will decline
  - Recycling economics in doubt
- Process data are not published

Technical Goals

- Characterize current battery recycling processes
- Determine current production methods for other materials
- Estimate impacts of current recycling processes
- Estimate energy use/emissions for current material processes
- Estimate energy use/emissions for current battery processes
- Evaluate alternative strategies for additional material recovery
- Develop improved recycling processes

Accomplishments

- Selected promising battery chemistries
- Designed battery packs for each chemistry and vehicle type
- Estimated materials use for optimistic EV demand scenario
- Compared U.S. and world lithium demand to reserves
- Presented lithium demand estimates at battery and plug-in vehicle conferences
- Determined current production methods for lithium and batteries

✧ ✧ ✧ ✧ ✧

Introduction

Use of vehicles with electric drive, which could reduce our oil dependence, will depend on lithium-ion batteries. But is there enough lithium? Will we need to import it from a new cartel? Are there other materials with supply constraints? We project the maximum demand for lithium and other materials if electric-drive vehicles expanded their market share rapidly, estimating material demand per vehicle for four battery chemistries. Total demand for the United States is based on market shares from an Argonne scenario that reflects high demand for electric-drive vehicles, and total demand for the rest of the world is based on a similar International Energy Agency (IEA) scenario. Total material demand is then compared to estimates of production and reserves, and the quantity that could be recovered by recycling, to evaluate the adequacy of supply. We identify producing countries to examine potential dependencies on unstable regions or future cartels. As plug-in hybrid vehicles and possibly pure electrics enter the automotive market, use of lithium in batteries will rise rapidly. Recovery of material from spent batteries will be a key factor in alleviating potential material supply problems. We examine battery recycling processes that are available commercially now or have been proposed. The processes will be compared on the basis of energy saved and emissions reductions, suitability for different types of feedstock, and potential advantages.

Approach

We are answering these questions to address material supply issues.

- How many electric vehicles will be sold in the U.S. and world-wide?
- What kind of batteries might they use?
- How much lithium would each use?

- How much lithium would be needed annually?
- How does the demand compare to the available resources?
- How much difference can recycling make?
- What recycling processes are available?
- Could other materials become scarce?

Results

Vehicle Demand. To estimate U.S. sales of vehicles with electric drive, we extended the Energy Information Administration (EIA) projections of light vehicle sales for the United States from 2030 to 2050. Only moderate growth is projected between now and 2050, and most of that is in the light truck market. We took the most optimistic scenario for the penetration of vehicles with electric drive into the U.S. market from the DOE Multi-Path Study (Phase 1). In this scenario, 90% of all light-duty vehicle sales are some type of electric vehicle by 2050. This is an extreme-case scenario, not a projection, representing the maximum percent of U.S. sales that could be accounted for by hybrid and electric vehicles.

We relied on an IEA scenario for world demand. IEA is developing scenarios of what would need to be done to meet IPCC CO_2-reduction goals, based on World Bank economic and UN population projections, and the relationship between these and car ownership. Figure III-48 shows our U.S. scenario, as well as IEA's projection of world LDV sales.

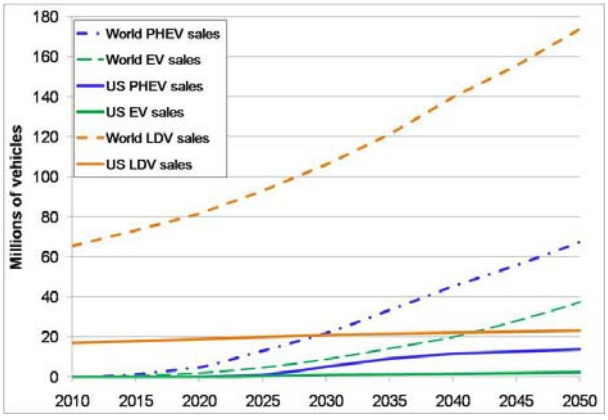

Figure III-48: Light-Duty Vehicle Sales Projection to 2050

Batteries. We chose three promising chemistries, in addition to the current NCA graphite, to compare on the basis of material usage. These are defined in Table III-11. All contain lithium in the cathode active material and a lithium salt ($LiPF_6$) in the electrolyte solution. One also uses a lithium titanate material, instead of the standard graphite, in the anode. For each battery chemistry analyzed, all materials in the electrodes and the electrolyte were tabulated to give total material required.

From (1) the mass percent of each element in the active compounds and (2) the mass required of each compound in the batteries, we calculated the quantities of lithium and other materials required per battery pack. For lithium, the total is the sum of lithium from the cathode, the electrolyte, and the anode (for the cells with titanate anodes). The total requirement of lithium (on an elemental basis) for each car is shown in Table III-12. The electric vehicle battery requirement is based on an assumed 100-mile range. Four batteries were designed — one for each of the chemistries chosen — for each of three automobile all-electric ranges.

Total Lithium Requirements and Reserves. Once the total quantities of material required per vehicle by type were determined, they were multiplied by the annual vehicle sales by type to provide an estimate of the material demanded. Figure III-49 shows the U.S. results for lithium, assuming that all vehicles used the current NCA-Graphite chemistry. It also shows how potential U.S. demand compares to historical world production and U.S. consumption. The U.S. consumption is perhaps misleading, since it only accounts for direct purchases of lithium compounds by U.S. firms and omits indirect consumption in imported batteries and products containing batteries. U.S. demand for lithium for automotive batteries has a very long way to go before it strains current production levels, with U.S. demand, even under this aggressive penetration scenario, not reaching current production levels until after 2030.

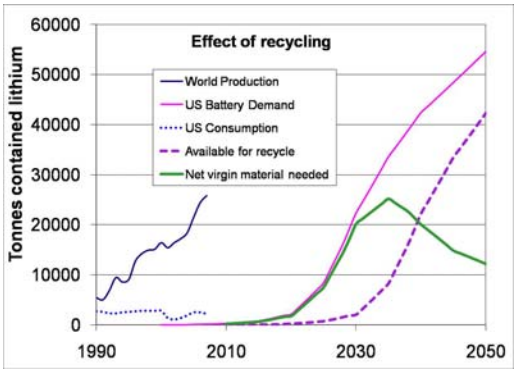

Figure III-49: Future U.S. Lithium Demand Compared to Historical Production

We then considered the potential impact of recycling on net demand for materials. Figure III-49 also shows the demand curve lagged by 10 years (assumed average battery life) to approximate material that would be available for recycling if all lithium were recycled. Finally, the graph shows the difference between the gross material demand and the potentially recyclable material. This represents the net quantity of virgin material that would be required if all battery material could be recycled. This curve turns over, meaning that the quantity of virgin material required

actually declines after about 2035. This demonstrates the importance of recycling.

Table III-11: Battery Chemistries Included in the Analysis

System→ Electrodes	NCA Graphite	LFP (phosphate) Graphite	MS (spinel) Graphite	MS TiO
Positive (cathode)	$LiNi_{0.8}Co_{0.15}Al_{0.05}O_2$	$LiFePO_4$	$LiMn_2O_4$	$LiMn_2O_4$
Negative (anode)	Graphite	Graphite	Graphite	$Li_4Ti_5O_{12}$

Table III-12: Total Lithium Required per Passenger Automobile

	Battery Type															
Parameter	NCA-G				LFP-G				LMO-G				LMO-TiO			
Range (mi) @ 300 Wh/mile	4	20	40	100	4	20	40	100	4	20	40	100	4	20	40	100
Total Li in pack (kg)	.4	1.5	3.0	7.4	.2	.9	1.9	4.7	.2	.7	1.4	3.4	0.6	2.5	5.1	12.7

World demand could be considerably lower than the maximum shown in Figure III-50. Smaller cars with smaller batteries than IEA assumed (12–18 kWh) are likely to be used. And, it can be argued that hybrids are more attractive than battery electric cars. Further, many of the vehicles could be electric bicycles or others that require less than 10% as much lithium per vehicle. With smaller batteries and recycling, net world demand in 2050 can be kept to four times current production.

We estimated cumulative battery demand for lithium under the assumption that all batteries were produced using a single chemistry. Total potential world lithium demand is shown in Table III-13. (This was done for each of the four chemistries; NCA graphite is shown.) This total was then compared to several estimates of the world reserve base. The maximum demand (double the quantity shown) would occur if all batteries were made by using titanate anodes, since this chemistry uses the most lithium per battery. Only in that case does total demand exceed the USGS conservative reserve base estimate. However, by taking care with battery size and taking advantage of material that could be made available from recycling, enough lithium is available to use while we work toward an even more efficient, clean, and abundant means of supplying propulsion energy.

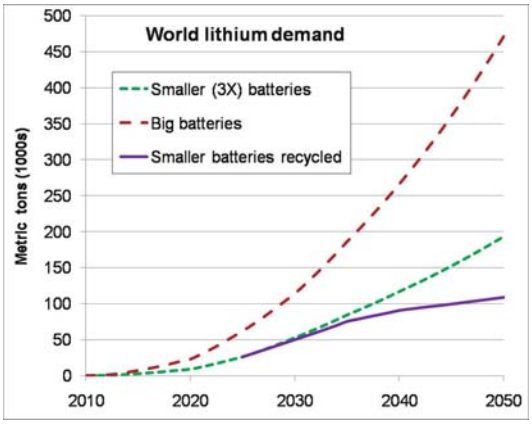

Figure III-50: Future World Lithium Demand Scenarios

Table III-13: World Lithium Demand and Reserves

Item	Cumulative Demand to 2050 (contained lithium, 1,000 metric tons)
Large batteries, no recycling	6,474
Smaller batteries, no recycling	2,791
Smaller batteries, recycling	1,981
USGS Reserves	4,100
USGS Reserve Base	11,000
Evans and others	30,000+

Chile dominates current production, with Australia second. Bolivia has huge untapped reserves, and China is rapidly developing its production capacity. The United States has limited reserves, and so it is likely to remain a materials importer, although batteries could certainly be produced here from these imported materials. The United States has relatively stable relationships with the major lithium-producing countries, and so significant supply problems are not anticipated.

Other Materials. We also estimated the potential demand for nickel, cobalt, and aluminum for NCA-graphite batteries; iron and phosphorus for LFP batteries; manganese for the LMO-G; and titanium for the LMO-TiO. These quantities were then compared to USGS reserve data for each material, if appropriate. For some materials, such as iron, the quantity available is sufficiently large that another measure was used for comparison. Table III-14 compares material availability to potential cumulative U.S. light-duty battery demand[25] to 2050 and estimates the percent that could be required. A potential constraint was

[25] Assuming that all batteries were made by using only the chemistry requiring the material

identified for cobalt. If NCA-G were the only chemistry used, batteries use could impact the reserve base by 2050. Approximately 9% of the world reserve base could be required for U.S. light-duty vehicle batteries. World demand would be a factor of four larger. Of course, recycling would significantly alleviate this pressure, as would the expected shift away from NCA-G to other chemistries.

The U.S. does not produce any cobalt, and so we must depend entirely on imports[26]. Cobalt is produced in many other countries, so it is unlikely that any one country or group could manipulate supply or price. Similarly, the U.S. does not produce any nickel, except for a small amount as a by-product of copper and platinum/palladium mining, so we import from a diversity of producers that suggests security of supply. The remaining battery materials are all abundant.

Recycling Processes. Recycling can recover materials at different production stages, all the way from basic building blocks to battery-grade materials. At one extreme are smelting processes that recover basic elements or salts. These are operational now on a large scale and can take just about any input, including different battery chemistries (such as Li- ion, Ni-MH, etc.) or mixed feed. Smelting takes place at high temperature, and organics, including the electrolyte and carbon anodes, are burned as fuel or reductant. The valuable metals (Co and Ni) are recovered and sent to refining so that the product is suitable for any use. The other materials, including lithium, are contained in the slag, which is now used as an additive in concrete. The lithium could be recovered by using a hydrometallurgical process.

At the other extreme, recovery of battery-grade material has been demonstrated. Such processes require as uniform feed as possible, because impurities in feed jeopardize product quality. The components are separated by a variety of physical and chemical processes, and all active materials and metals can be recovered. It may be necessary to purify or reactivate some components to make them suitable for reuse in new batteries. Only the separator is unlikely to be usable, because its form cannot be retained. This is a low-temperature process with a low energy requirement. Almost all of the energy and processing to produce battery-grade material from raw materials is saved. Large volumes are not required.

Conclusions

Shortages have often been forecast without adequate exploration or consideration of incentives rising prices might provide. In the case of materials for lithium-ion batteries, it appears that even an aggressive program of vehicles with electric drive can be supported for decades with known supplies, if recycling is instituted. Reliance on pure electrics could eventually strain supplies of lithium and cobalt.

Table III-14: Comparison of U.S. Light-Duty Battery Demand to Material Availability

Material	Availability (million tons)	Cumulative Demand	Percent Demanded	Basis
Co	13	1.1	9	World reserve base
Ni	150	6	4	
Al	42.7	0.2	0.5	U.S. capacity
Iron/steel	1,320	4	0.3	U.S. production
P	50,000	2.3	~0	U.S. phosphate rock production
Mn	5,200	6.1	0.12	World reserve base
Ti	5,000	7.4	0.15	

FY2009 Presentations and Publications

Presentations

1. *Potential Demand for Lithium in Automotive Batteries*, IEA Annex 10 Meeting on Lithium Supply, Charlotte, NC (December 4, 2008).
2. *Lithium-Ion Batteries: Possible Material Demand Issues*, 13th Battery Materials Recycling Seminar & Exhibit, Fort Lauderdale, FL (March 17, 2009).
3. *Lithium-Ion Batteries: Material Demand and Recycling Issues*, Plug-In 2009, Long Beach, CA (August 2009).

Papers

1. L. Gaines and P. Nelson, *Lithium-Ion Batteries: Possible Materials Issues*, proceedings of the 13th Battery Materials Recycling Seminar & Exhibit, Fort Lauderdale, FL (2009).

[26] A fraction of current supply comes from the stockpile and recycling, but any new supply will be imported.

III.B.7 Low Energy HEV Requirements Analysis (NREL)

Jeff Gonder and Ahmad Pesaran
National Renewable Energy Laboratory
1617 Cole Blvd.
Golden, CO 80401
Phone: (303) 275-4441; Fax: (303) 275-4415
E-mail: Jeff.gonder@nrel.gov
ahmad.pesaran@nrel.gov

Start Date: April 2007
Projected End Date: September 2009

Objectives

- Evaluate the relationship between the energy storage system (ESS) capabilities (particularly in vehicle energy us) in a hybrid electric vehicle (HEV) and the vehicle's fuel consumption.
- Support the United States Advanced Battery Consortium (USABC) "Alternate HEV ESS Workgroup" in establishing lower energy ESS targets relative to the current set of requirements for power-assist HEVs.

Technical Barriers

This project addresses the following technical issues raised in the Electrochemical Energy Storage Technical Team technology development roadmap:

- Ambitious efficiency, weight, volume and affordability goals.
- Establish targets to provide clear goals for the development and research community.

Technical Targets

- Two-second/10-second discharge pulse power: 56 kW/20 kW for the new targets (previously 25 kW for 10 seconds)
- Two-second/10-second regen pulse power: 40 kW/30 kW for the new targets (previously 20 kW for 10 seconds)
- "Available" energy over which both power requirements are simultaneously met: 26 Wh (previously 300 Wh)
- Energy window for vehicle use: 165 Wh (previously 425 Wh)
- Selling price/system @ 100,000 systems/yr: $400 (previously $500)

Accomplishments

- Demonstrated via simulation that most HEV fuel savings can be realized with ESS energy windows for vehicle use of <165 Wh.
- Analyzed chassis dynamometer test data on standard drive cycles to confirm that current production HEVs use ESS energy windows in this range.
- Determined the ESS pulse power performance (over standard tests) required to satisfy the HEV power demands on the ESS during driving.

✧ ✧ ✧ ✧ ✧

Introduction

The USABC ESS performance goals for power-assist HEVs were last published in November 2002. Those goals call for an HEV ESS to possess 300 Wh of "available" energy (at a minimum) over which the ESS charge and discharge power requirements are simultaneously met. Adding the energy swept by the 10-sec charge and discharge power requirements to either end of this region results in an energy window for vehicle use of 425 Wh. An energy requirement this large has been found to increase the cost of HEV energy storage. In order to evaluate cost-saving opportunities, the USABC requested an investigation of the relationship between HEV fuel use and the ESS in-use energy window.

Approach

A generic midsize parallel HEV was modeled using the DOE-managed Powertrain System Analysis Toolkit (PSAT) software program. The modeling included three different degrees of hybridization (DOH) cases (the ratio between the power of the electric motor and the engine in the HEV). For each DOH case, the ESS energy content was swept over six cases from a high to a low. Simulating each configuration over multiple drive cycles revealed trends in fuel consumption and ESS usage between the various designs. In order to isolate the impact of the ESS on the vehicle's fuel use, the vehicle mass and all other platform characteristics were held constant for all of the configurations.

To provide a sanity check for the simulation results, the study also analyzed data from controlled testing on production hybrid vehicles and observed the ESS in-use energy window over standard drive cycles.

Results

Fuel Consumption Trends from Simulations. Figure III-51 shows some of the simulation results over a

city-type drive cycle. The vertical axis on the figure shows the vehicle fuel use (lower on the figure is better). The horizontal axis shows the in-use energy window for the ESS during the drive cycle. The point that falls on the left axis (with an energy window of zero Wh) represents the fuel use of a comparable conventional vehicle. All the other data points in the figure represent a different HEV configuration. Each of the three sets of colored lines represents a different DOH, with the higher DOH (higher electric motor power and smaller engine) cases resulting in lower fuel use. This is largely due to the fact that the smaller engine is able to operate at high efficiency levels a greater amount of the time relative to a larger engine.

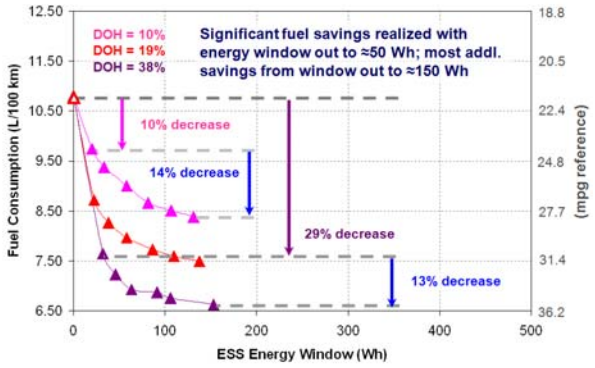

Figure III-51: Simulation Results over the Urban Dynamometer Driving Schedule (UDDS) Driving Cycle

In addition to showing a fuel savings benefit from higher electric motor/ESS power, the figure shows a fuel savings trend with increasing ESS energy window. Across all three DOH cases, significant fuel savings occur in the first roughly 100 Wh, with additional albeit tapering fuel savings thereafter. Most additional fuel savings occur with energy windows to 165 Wh.

Comparison with Production HEV Test Data. Figure III-52 presents a similar graph based on analysis of production HEV test data over standard drive cycles. This analysis confirms the ability of existing HEVs to operate using energy windows within roughly 165 Wh.

Power Pulse Analysis. The next requested analysis was to determine the desired pulse power capability of the lower energy ESS device. This was done by examining the pulse power characteristics of the different simulated HEV configurations over the standard city-type drive profile as well as over a high-speed and acceleration drive cycle. Ultimately, the power pulse characteristics of the most aggressive case (the largest DOH vehicle operating on the high-speed and acceleration drive cycle) were selected for establishing the new targets. Figure III-53 plots all the ESS pulses during this drive cycle case with respect to each pulse's duration in seconds and magnitude in kW. The envelope drawn above and below the pulse distribution was used to establish the ESS targets for discharge (+55 kW for 2 seconds and +20 kW for 10 seconds) and charge, such as from HEV regenerative braking (-40 kW for 2 seconds and -30 kW for 10 seconds).

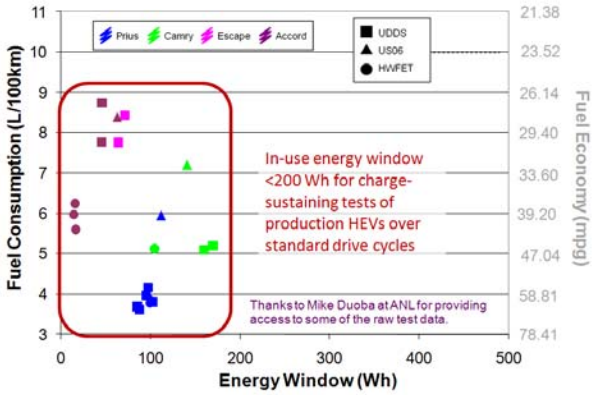

Figure III-52: Production HEV Data Analysis

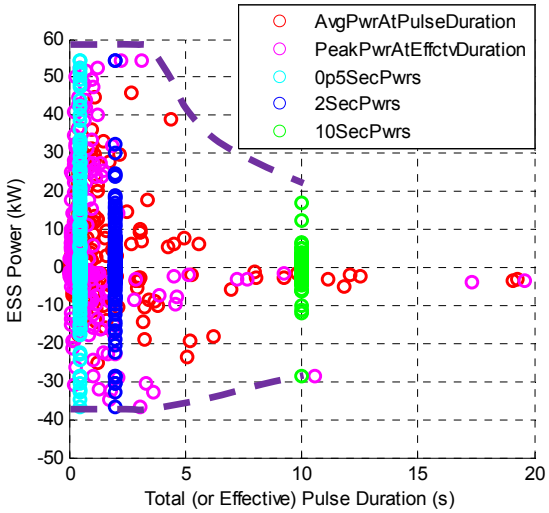

Figure III-53: Distribution of Power Pulses vs. Duration for the Highest DOH HEV Case over the High-Speed and Acceleration US06 Drive Cycle

Conclusions and Future Directions

NREL performed vehicle and energy storage analysis to establish relationship between vehicle fuel economy, and the energy storage power and energy capabilities for a power assist HEV. Based on the analysis, the USABC has established a new set of lower energy ESS targets for power-assist HEVs that could support the development of cost-effective, fuel-saving HEVs. Systems satisfying the new targets could be based on symmetric or asymmetric capacitors, batteries, or some other device.

The process of developing the new targets also helped improve our understanding of the difference between the "available" energy over which the discharge and charge

power requirements are simultaneously met and the energy window for vehicle use (which includes the energy swept by the 10-second pulse power requirements at either end of the simultaneously met region). This distinction will be important to keep in mind going forward when comparing standardized testing of devices against the established targets with in-use observations of ESS devices in vehicles.

FY 2009 Publications/Presentations

1. J. Gonder, A. Pesaran, J. Lustbader, H. Tataria, "Fuel Economy and Performance of Mild Hybrids with Ultracapacitors: Simulations and Vehicle Test Results," Proceedings of the 5th International Symposium on Large EC Capacitor Technology and Application in conjunction with Advanced Automotive Battery Conference, Long Beach, CA, June 2009.
2. Pesaran, A.; Gonder, J.; Keyser, M. "Ultracapacitor Applications and Evaluation for Hybrid Electric Vehicles," Proceedings of the Advanced Capacitors World Summit 2009, La Jolla, CA, April 1, 2009.
3. Presentation to the 2009 DOE Annual Merit Review Meeting, Washington DC, May 2009.

III.C. Battery Testing Activities

III.C.1 Battery Performance Testing at ANL

Ira Bloom (Primary Contact)
John Basco, Panos Prezas, Lee Walker
Argonne National Laboratory
9700 South Cass Avenue
Argonne, IL 60439
Phone: (630) 252-4516; Fax: (630) 252-4176
e-mail: ira.bloom@anl.gov

Contract Number: DE-AC02-06CH11357

Start Date: Ongoing
Projected End Date: September 30, 2010

Objectives

- Provide DOE, USABC, and battery developers with reliable, independent and unbiased performance evaluations of cells, modules and battery packs.
- Benchmark battery technologies which were not developed with DOE/USABC funding to ascertain their level of maturity.

Technical Barriers

This project addresses the following technical barriers as described in the USABC goals [1, 2]:

(A) Performance at ambient and sub-ambient temperature

(B) Calendar and cycle life

Technical Targets

- 15-y calendar life
- 300,000 HEV cycles
- 5,000 PHEV charge-depleting cycles
- End-of-life target of 25 kW at 300 Wh (HEV) or 45 kW at 500 Wh / 3.4 kWh charge-depleting energy (PHEV)
- 5-kW cold cranking power at -30°C

Accomplishments

Tested battery deliverables from many developers:

- HEV batteries: Tested battery technologies from A123 Systems, Johnson Controls-SAFT (in progress)
- PHEV batteries: Validated the new test manual using prototype cells. Provide comments to Idaho National Laboratory to refine the test manual. Tested contract deliverables from Johnson Controls-SAFT (in progress)
- Benchmarked battery technologies for vehicle applications. Tested deliverables from SK Energy, G4 Synergetics, Mitsui Mining and Smelting, Samsung, Firefly Energy (in progress).

✧ ✧ ✧ ✧ ✧

Introduction

Batteries are evaluated using standard tests and protocols which are transparent to technology. Two protocol sets are used: one that was developed by the USABC [1, 2], and another which provides a rapid screening of the technology.

Approach

The batteries are evaluated using standardized and unbiased protocols, allowing a direct comparison of performance within a technology and across technologies. For those tested using the USABC methods, the performance of small cells can be compared to that of larger cells and full-sized pack by means of a battery scaling factor [1, 2].

The accelerated screening test protocols were designed to accrue many cycles on a battery quickly and to work with high-energy and high-power cells. The point of these tests is to determine how stable the performance of the battery is in a short amount of time. It should be noted that these are not USABC hybrid-electric or plug-in hybrid-electric vehicle tests.

Results

The battery technology from one developer was sampled at two different times, 2006 and 2008, and subjected to the accelerated screening test protocols. The test consisted of initial characterization using C/1 capacity measurements and the hybrid pulse-power characterization

test at the low current value (HPPC-L) and 100% DOD life cycling at the C/1 rate at 40°C. After every 50 cycles, the batteries were cooled to 30°C and recharacterized in terms of C/1 capacity and HPPC-L tests. In both cases, the batteries successfully completed 500 cycles and testing was voluntarily ended.

The changes in cell resistance vs. cycle count from the HPPC-L tests are shown in Figure III-54. As can be seen from the figure, the cell resistance increases with cycle count in both cases. However, the rate and the amount of resistance increase is significantly less in cells 1 and 2. The difference probably reflects changes in their cell chemistry which affect cell resistance growth.

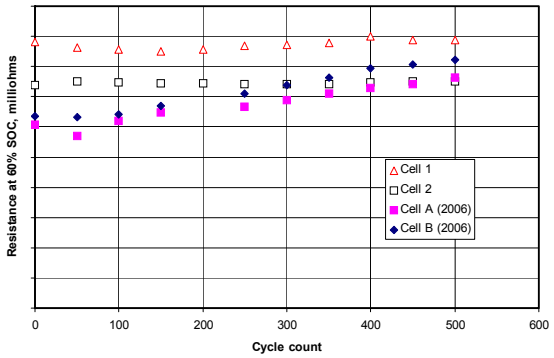

Figure III-54: Resistance vs. cycle count for two samples. Cells A and B represent technology that is two years older than that in Cells 1 and 2.

The effect of these changes can also be seen in the plot of C/1 capacity vs. cycle count (Figure III-55). The C/1 capacity decreases with cycle count in both cases, but, in the newer cells (cells 1 and 2) the rate of capacity decline is less.

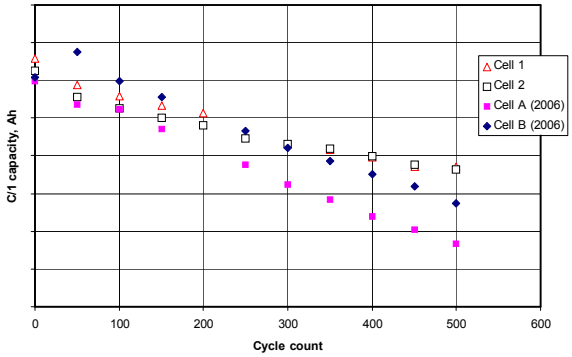

Figure III-55: C/1 capacity vs. cycle count for two samples of a developer's technology. Cells A and B represent technology that is years older than that in Cells 1 and 2.

An important question that occurs in the area of PHEV battery testing is the effect of SOC on battery life during CD+CS (charge depleting plus charge sustaining) cycling. Two PHEV cells were cycled at 30°C using a combined charge-depleting/charge-sustaining profile. The CS portion was performed at two states of charge, 60% and 30%, representing HEV and PHEV modes of operation. In this work, 60% SOC was reached after about 3 CD profiles and 30% SOC after about 5 CD profiles. An example of the cycling profile is shown in Figure III-56.

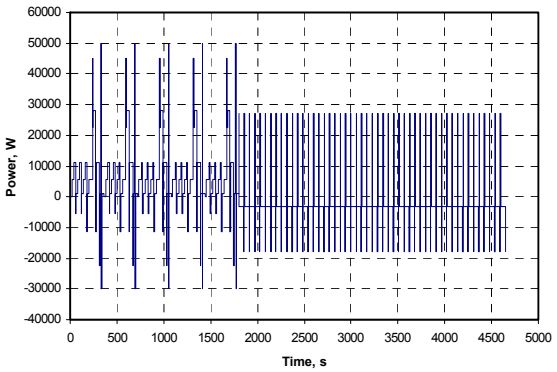

Figure III-56: CD+CS combined cycle profile consisting of 5 CD profiles and 50 CS profiles.

As expected, the total available energy of the cells decreased with cycle count. Figures Figure III-57 and Figure III-58 show the effect of SOC on CS and CD energy.

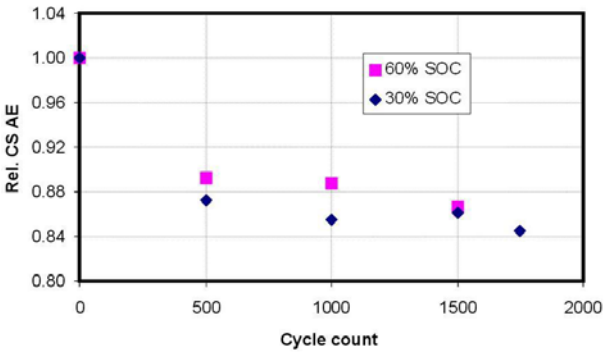

Figure III-57: Effect of SOC used for CS cycling on CS energy.

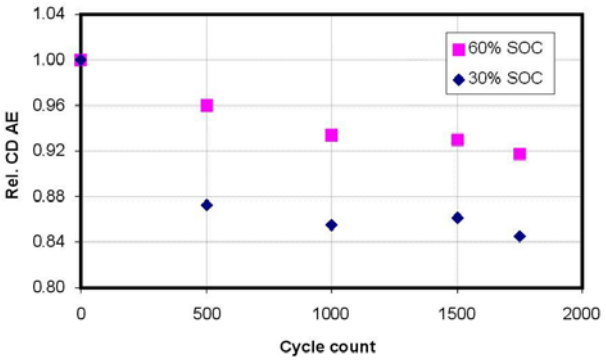

Figure III-58: Effect of SOC used for CS cycling on CD energy at the 10-kW rate.

From Figure III-57, there was very little, if any, effect of SOC on CS available energy. On the other hand, there was a large difference in CD available energy which depends on SOC. The lower the SOC, the higher the CD decrease was. The difference between the two can be correlated with energy throughput. There was higher energy throughput in the cell to get to the lower SOC.

Conclusions and Future Directions

Accelerated screening testing has been shown to be a useful way to gauge the state of a developer's technology and to determine the effect of any improvements that are made. In the area of PHEV testing, the SOC at which charge-sustaining cycling occurs has a pronounced effect on the charge-depleting available energy.

For the future, we plan to:

- Continue testing HEV contract deliverables
- Start testing PHEV contract deliverables
- Continue acquiring and benchmarking batteries from non-DOE sources
- Aid in refining standardized test protocols
- Upgrade and expand test capabilities to handle increase in deliverables

List of Abbreviations

AE: available energy
CD: charge depleting
CS: charge sustaining
HEV: hybrid electric vehicles
PHEV: plug-in hybrid electric vehicles
SOC: state-of-charge
USABC: United States Advanced Battery Consortium (DOE, GM, Chrysler and Ford)

FY 2009 Publications/Presentations

1. Presentation to the 2009 DOE Annual Peer Review Meeting.

References

1. FreedomCAR Battery Test Manual for Power-Assist Hybrid Electric Vehicles, DOE/ID-11069, October 2003.
2. FreedomCAR Battery Test Manual for Plug-In Hybrid Electric Vehicles, March 2008.

III.C.2 Battery Performance and Life Testing at INL

Jeffrey R. Belt
Idaho National Laboratory
P.O. Box 1625, Idaho Falls, Idaho 83415-2209
Phone: (208) 526-3813, Fax (208) 526-0690
Email: Jeffrey.belt@inl.gov

Start Date: FY 2008/2009 INL Testing
Projected End Date: Open task

Objectives

The purpose of this activity is to provide high-fidelity performance and life testing, analyses, modeling, test procedures and methodologies development, reporting and other support related to electrochemical energy storage devices under development by the Department of Energy's Vehicle Technologies Program.

Technical Barriers

This project supports the primary technical barriers: performance, life, abuse tolerance and cost.

Technical Targets

Target applications include power-assist hybrid electric vehicles (HEVs), Plug-in Hybrid Electric Vehicles PHEVs, and Electric Vehicles (EVs). Testing targets include conventional benchmarking activities as well as diagnostic testing, which is designed to explore more mechanistic-level issues of device performance.

Accomplishments

534 cells, 14 modules, and two vehicle system-level Li-ion battery packs were tested during the FY 2008/2009 reporting period.

The Battery Life Estimator Manual, INL-EXT-08-15136 was published in August 2009.

Introduction

The development of advanced batteries for automotive applications requires that developmental, diagnostic and validation testing be performed to support development goals and to characterize performance against technical targets established for HEVs (including Ultracapacitors), PHEVs, EVs, and other electric drive system applications.

Approach and Results

Validation and review of the Battery Test Manual For Plug-In Hybrid Electric Vehicles, INL/EXT-07-12536 continued throughout the fiscal year. Several proposed modifications and additions were accepted in FY 2009 and will be included in Revision 1 expected by September 2010. Figure III-59 is an example of the power and energy capability for a representative PHEV cell tested in FY 2009.

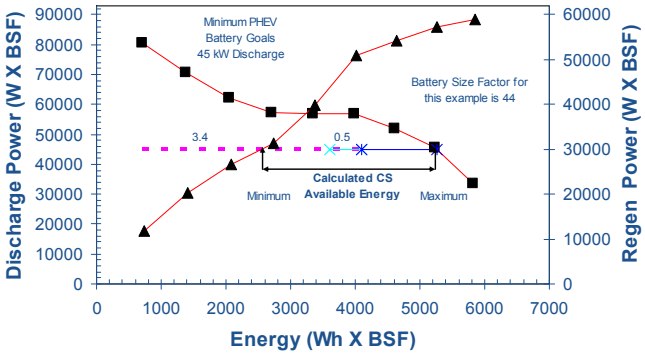

Figure III-59: Typical power and energy capability for PHEV cells under test.

In addition, work began in FY 2009 to develop technical targets for additional HEV designs. INL is collaborating with NREL and the DOE on this project.

Deliverables tested at INL are detailed for each of three DOE development programs assigned to the INL. In addition, status information is provided on benchmark test hardware, including ultracapacitor testing activities, and the INL Smart Battery Status Monitor project.

Several deliverables were tested from Johnson Controls - Saft. The first is a 24-cell study that focused on combined calendar/cycle life testing and was initiated in FY 2001 (with cells from Saft, prior to creation of the JCS joint venture). The Li-ion cells were designed for the HEV application. The second set of deliverables consists of a 32-cell study that focused on low temperature performance, as well as separate calendar and cycle life testing of the new VL7P technology from FY 2006/2007. The Li-ion cells incorporated design process improvements for cost reduction for the Maximum Power Assist HEV application. The third set of deliverables consists of a 3-cell study that focused on cycle life testing of the VL7P Technology from FY 2008. These Li-ion cells were designed for the Maximum Power Assist HEV

application. The fourth set of deliverables consists of two VL7P battery packs that focused on cycle life testing, Figure III-60. The 344-Volt Li-ion packs were designed for the Maximum Power Assist HEV application.

Figure III-60: JCS 344-Volt battery pack

Three sets of deliverables are being tested from EnerDel. The first set of deliverables consists of a 20 cell study that is focused on calendar and cycle life testing. The Li-ion cells were designed for the Minimum Power Assist HEV application. The second set of deliverables consists of a 3-cell study that focused on cycle life testing. The Li-ion cells were designed for the PHEV10 application. The third set of deliverables consists of a 6-cell and 6-module study that focused on cycle life testing. The Li-ion cells were designed for the Minimum Power Assist HEV application.

Three sets of deliverables were tested from Compact Power. The first set of deliverables consists of a 12-cell study that is focused on calendar life testing of a FY 2007 technology. The Li-ion cells were designed for the Minimum Power Assist HEV application. The second set of deliverables consists of a 20-cell study that focused on calendar and cycle life testing of a FY 2008 technology. The Li-ion cells were designed for the Minimum Power Assist HEV application. The third set of deliverables consists of a 40-cell study that focused on cycle life testing. The Li-ion cells were designed for the PHEV10 application.

General results from the above projects suggest some Li-ion designs exhibit a temporary increase in power with time at 30°C. This mechanism generally diminishes after a year of calendar life testing. However, the general trend, shown in Figure III-61, is for increased power fade with increased temperature. Diagnostic testing on specific technologies will further elucidate the mechanisms involved in temperature related power and capacity fade.

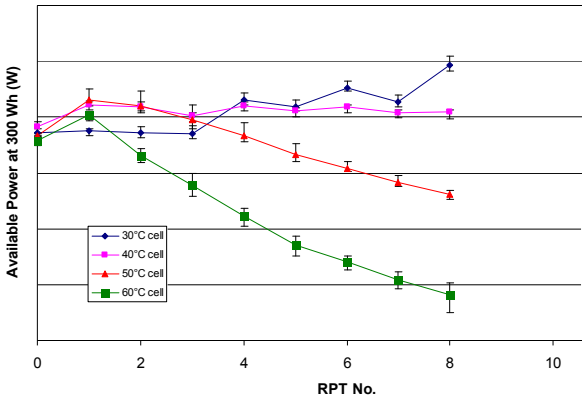

Figure III-61: Typical effect of temperature on Li-ion battery power fade.

One set of ultracapacitor deliverables were tested from Nesscap based on their FY 2006/07 technology. The focus of the 8-cell and 2-module study was aimed at the effect of temperature on performance for calendar life testing. Example ultracapacitor test results shown in Figure III-62 indicate that in general, the energy fade increases with increasing temperature.

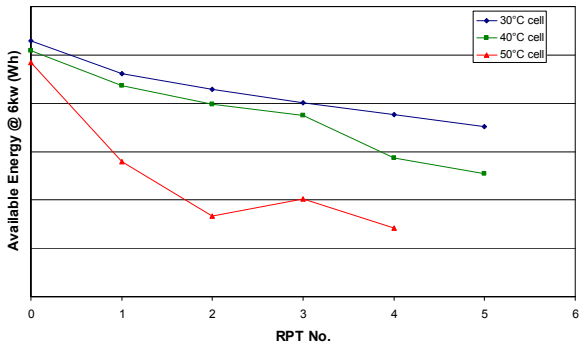

Figure III-62: Typical effect of temperature on Ultracapacitor energy fade.

Benchmarking Activities. INL also performs benchmark testing, wherein various electrochemical energy storage devices are tested to evaluate their performance and potential for focused development activities. The INL tested several devices during FY 2008/2009. NLE provided two 48-volt Li-ion modules for calendar and cycle life testing based on a Power Assist HEV design. Sanyo provided 350 18650-size cells of various power to energy ratios for calendar and cycle life testing that are applicable to Power Assist and Plug-In HEV designs. The large number of test cells will allow several focused diagnostic studies aimed at identifying performance limiting mechanisms (see below). Altairnano provided Li-ion cells using novel materials for both the Power Assist and PHEV designs. One set of 20 3.5-Ah cells are undergoing calendar and cycle life testing at

various temperatures. Another set of 20 cells are undergoing charge depleting cycle life testing. Additionally, the Furukawa Battery Company provided two Ultrabattery modules for cycle life testing. The Ultrabattery uses, a unique lead acid-carbon high capacity electrode configuration aimed at micro-hybrid applications.

Diagnostic Testing (DT). Well designed test protocols can be aimed at answering more fundamental (mechanistic) questions of battery performance. This is done at the INL for various aspects of cell performance, including issues of temperature-related constraints regarding power goals, interfacial phenomena, charge/discharge limitations, aging rates and related mechanisms, path dependence of cell aging, kinetics, etc.

An example of such DT is polarization data, where, in the case of commercial 18650 Sanyo Y test cells, Figure III-63 readily shows charge-limiting behavior and both current and temperature limitations on capacity. These are important measures for defining the boundary of cell operation within a given application.

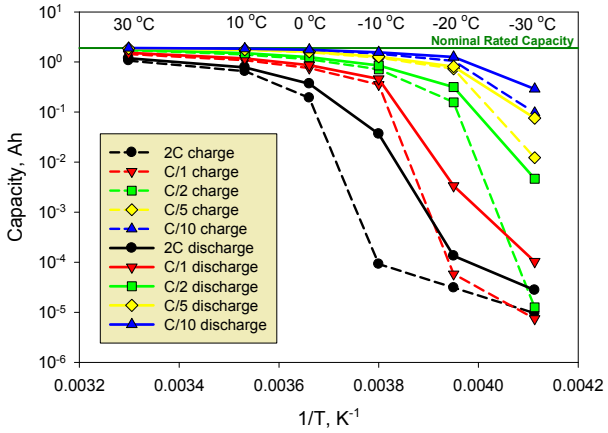

Figure III-63: Polarization study results for a representative Sanyo Y cell operated from C/10 to 2C and -30 to 30 °C.

EIS measurements are an indispensable DT tool for investigating interfacial impedance and aging effects. Figure III-64 shows beginning-of-life EIS measurements for Sanyo Y cells at 70% SOC and 30°C. The data shows not only the magnitude of the interfacial impedance, but also cell-to-cell variability. Included as part of a periodic RPT, EIS will reveal information regarding aging mechanisms and how these affect cell variability over time.

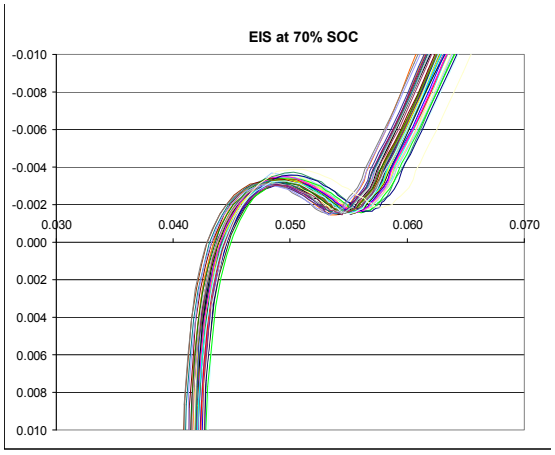

Figure III-64: EIS of 51 Sanyo Y cells at 70% SOC and 30 °C, showing low beginning-of-life interfacial impedance and low cell variability.

Technology Life Verification Testing (TLVT). INL continues to collaborate with ANL, SNL, and LBNL on TLVT. This work focuses on accelerated testing and modeling for life prediction. The techniques are described in a Battery Life Estimator Manual published in September 2009. Testing in support of this project will continue in FY 2010.

Smart Battery Status Monitor. This project continues to be developed under a collaborative effort between INL, Montana Tech, and Qualtech Systems. The method, when combined with a library of life models, performance data, and prognostic tools, will quickly and accurately predict the remaining life of an energy storage device using rapid in-situ impedance measurement techniques. Several joint patents have been awarded and three new invention disclosures have been submitted for real-time estimation of battery impedance. The validation testing began in May 2009 wherein the on-board impedance monitoring will be compared with standard HPPC/EIS measurements.

Conclusions and Future Directions

Testing has identified the technologies that suffer from temperature dependent power and capacity fade, and has quantified such behavior under well-defined protocols applied within controlled laboratory conditions, resulting in determinable data uncertainty. Focused diagnostic testing will further become a central tool for elucidating performance-hindering mechanisms, e.g., to help identify mechanisms responsible for accelerated fade at higher temperatures. Testing has also established baseline performance and helped to track improvements made during the development programs. We will continue to expand and improve our testing methods and protocols to match the increasing needs within DOE.

III.C.3 Battery Abuse Testing at SNL

E. Peter Roth
Sandia National Laboratories
PO Box 5800 MS0614
Albuquerque, NM 87109
Phone: (505) 844-3949; Fax: (505) 844-6972
E-mail: eproth@sandia.gov

Start Date Oct. 1, 2008
Projected End Date: September 30, 2009

Objectives

- Provide an independent abuse test laboratory for DOE and USABC
- Perform abuse testing on cells and modules delivered by USABC contractors as part of their contract deliverables
- Develop new abuse characterization tests

Technical Barriers

- Abuse tolerance of energy storage devices is identified as a barrier in USABC and DOE battery development programs.

Technical Targets

- Perform abuse testing of cells and modules from contractors to USABC and report results to USABC Tech Team and developers
- Continue to develop improved abuse test techniques and protocols to help in evaluation of safe operating limits

Accomplishments

- Abuse tests were performed on all USABC contractor deliverables and final reports have been issued, including:
- **Johnson Controls-Saft.**
  - HEV cell level tests completed (2 groups of 6 cells)
- **Compact Power Inc.-LG Chem.**
  - HEV cell and module level tests completed (6 cells, 6 modules)
  - PHEV cells delivered and testing completed (12 Cells)
- **A123.**
  - HEV cell level tests completed (8 cells)
- **EnerDel.**
  - PHEV cells and modules delivered (11 cells, 4 modules) and testing started.
  - Developed new cell-level high-voltage separator integrity test for evaluating separator response during shutdown in a series string configuration.
  - Developed a new Pressure Induced Internal Short Circuit Test protocol for evaluation of full cell response to internal shorts due to failure of separator or electrodes.

✧ ✧ ✧ ✧ ✧

Introduction

Abuse tests are designed to determine the safe operating limits of full HEV\PHEV energy storage devices. The tests are performed to yield quantitative data on cell\module\ pack response to allow determination of failure modes and help guide developers toward improved materials and designs. Standard abuse tests are performed on all devices to allow comparison of different cell chemistries and designs. New tests and protocols are developed and evaluated to more closely simulate real-world failure conditions.

Approach

Abuse\Characterization tests are performed which evaluate the response to expected abuse environments.

- Test to failure of energy storage device.
- Documentation of conditions that cause failure.
- Evaluate failure modes and abuse conditions using destructive physical analysis (DPA)
- Provide quantitative measurements of cell/module response.
- Document improvements in abuse tolerance.
- Develop new abuse test procedures that more accurately determine cell performance under most likely abuse conditions

Possible tests that can be performed cover three main categories of abuse conditions:

- Mechanical Abuse
  - Controlled Crush
  - Penetration

  - Drop
  - Water Immersion
  - Mechanical Shock
- Thermal Abuse
  - Thermal Stability
  - Simulated Fuel Fire
  - Elevated Temperature Storage
  - Rapid Charge/Discharge
  - Thermal Shock Cycling
- Electrical Abuse
  - Overcharge/Overvoltage
  - Short Circuit
  - Overdischarge/Voltage Reversal
  - Partial Short Circuit

The Core Abuse Tests that are usually performed include:

- Overcharge: (4 cells)
  - Rates: 1C and 3C
  - Flammability test: with and without external ignition source (spark)
  - Monitor heat generation rate and evolved gas species
- Short-Circuit: (2 cells)
  - Hard short (1 mohm)
  - Intermediate short (10 mohm or resistance comparable to cell internal resistance)
- Thermal Ramp: (4 cells)
  - Ramp to 250°C or failure (5°C/min)
  - Two states of charge (100%SOC, 50%SOC)
  - Flammability test: with and without external ignition source (spark)
  - Monitor heat generation rate and evolved gas species
- Separator Shutdown Integrity: (2 cells)
  - Heat to slightly above separator shutdown temperature and hold
  - Apply external voltage (20V) and monitor for separator breakdown
  - Repeat at 10°C higher temperature
- Pressure Induced Internal Short Test (2 cells)
  - Room Temperature (100%SOC, 50%SOC)

Results

The actual test results from the USABC testing are Battery Protected Information and cannot be released publicly. However, our generalized test response data is shown below for test cells that have been fabricated in our laboratory and show many of the properties seen in the larger cells.

Representative Short-Circuit Data. Short circuit testing is performed on a fully charged cell\module\pack under two load conditions: hard short (1 mohm) and moderate short (~10 mohm). The hard short tests for cell and interconnect failure under worst case conditions while the moderate short tests for more realistic short conditions. The moderate short often is more abusive to the cell because cell continuity is maintained throughout the shorting period resulting in more energy release by the cell. Shorting in a multi-cell pack often results in a cascading failure of the cells. A single cell initially gets hot enough to activate the internal shutdown separator and becomes a high-impedance element in the string. A high reverse potential then appears across that cell from the other active cells and then the cell can undergo separator shorting leading to re-establishment of a current path. The energy released from that cell can then cause the next cell to go into shutdown and follow the same failure path. This cascading failure can proceed throughout the pack resulting in catastrophic failure. Figure III-65 shows the voltage profile for such a failure while Figure III-66 shows the accompanying current and integrated discharge capacity. This 12 cell pack eventually caught fire and was destroyed.

Representative Overcharge Data. Overcharge testing is performed at two rates, a 1C rate and a high rate, usually 3C. Charging begins at 100%SOC and continues until at least 200%SOC or cell failure. During the test, cell voltage, current and multi-location temperatures are measured. Real-time gas analysis is also performed using FTIR and mass spectrometry. Overcharge often results in increased gas generation and new gas species, especially hydrogen. Heat generation during overcharge often results in the cell reaching the separator shutdown temperature and restricting the flow of current. A high potential can then appear across the cell from the power supply increasing to its upper compliance limit. This high potential can cause separator failure and thermal runaway of the cell. Figure III-67 shows the voltage\ temperature profile for a single cell during overcharge which underwent such a failure.

Figure III-68 shows the same data as a function of %SOC showing that the cell underwent failure at about 180%SOC.

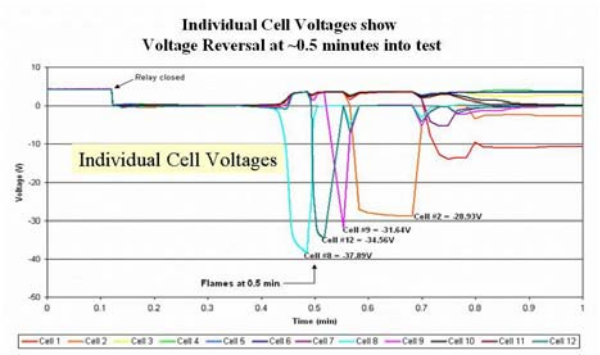

Figure III-65: Voltage profile for 12 cell pack during hard short circuit test showing cascade failure of the cells.

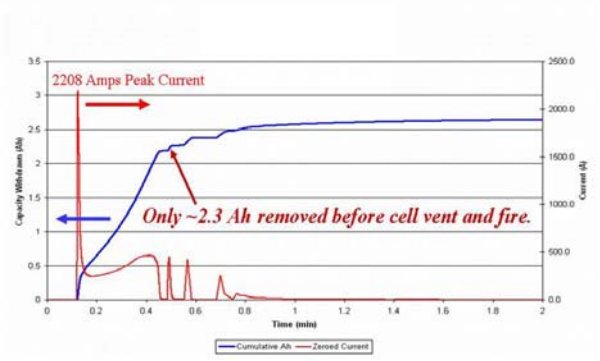

Figure III-66: Current and integrated capacity profiles for 12 cell pack during hard short circuit test showing cascade failure of the cells.

Representative Over-Temperature Data

Electrical storage devices (cells\modules\packs) are thermally ramped at a fixed heating rate to temperatures resulting in venting and thermal runaway. An upper limit of 250°C is usually sufficient to result in failure. The cells are measured at 100%SOC and 50%SOC. Voltage, temperature and gas evolution are measured throughout the run. Temperature difference between the device and the heating block is used to calculate the cell heating rate in excess of the block temperature. Flammability of the vent gases can be tested by using spark ignition sources in the enclosure as shown in Figure III-69. The cell and block temperatures are shown in Figure III-70 while calculated cell heating rate is shown in Figure III-71. Thermal runaway is often seen to occur in three stages corresponding to reactions beginning first at the anode and progressing to involve the anode and cathode at higher temperatures, eventually resulting in a high-rate thermal runaway. This runaway profile is highly dependent on cell chemistry.

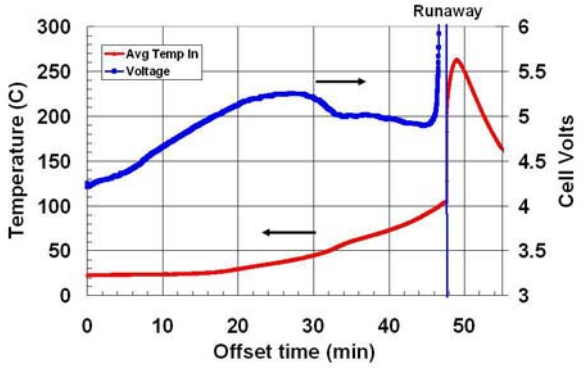

Figure III-67: Voltage\temperature profile during overcharge of a single cell showing separator shutdown and failure leading to thermal runaway.

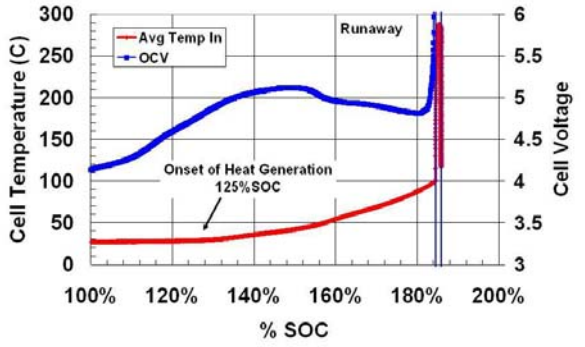

Figure III-68: Voltage\temperature profile as a function of %SOC during overcharge of a single cell showing separator shutdown and failure leading to thermal runaway

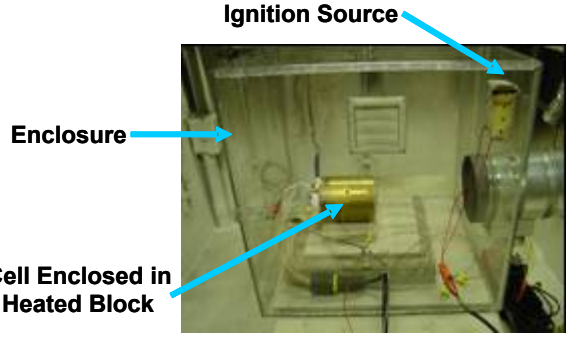

Figure III-69: Picture of cell thermal ramp setup inside Lexan enclosure box.

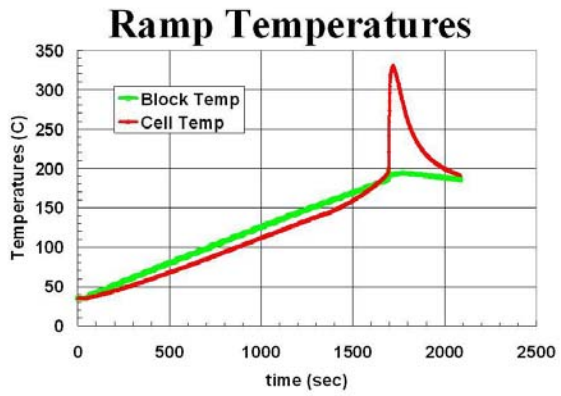

Figure III-70: Cell and heater block temperatures during thermal ramp.

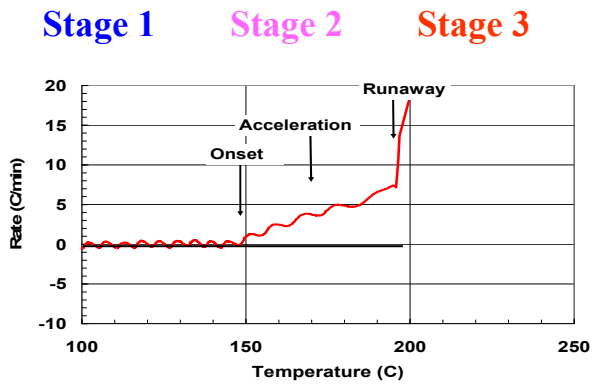

Figure III-71: Cell heating rate during thermal ramp showing three stages of thermal runaway leading to explosive loss of the cell.

Separator Shutdown Integrity Test

A new test was developed to characterize the response of cells which incorporate a shutdown separator. It was observed that cell failure often occurs at the shutdown temperature of the separator when higher potentials can appear across the cell. This test takes the cell to a temperature slightly above the shutdown temperature and then applies a potential (20V) across the cell while monitoring the cell current, voltage and temperature. Shorting of the cell can be readily measured as a function of time and temperature. The cell is considered to pass this test if it remains stable for a minimum of 30 minutes. Figure III-72 shows the data for a cell which passed the test but did eventually fail after 45 minutes.

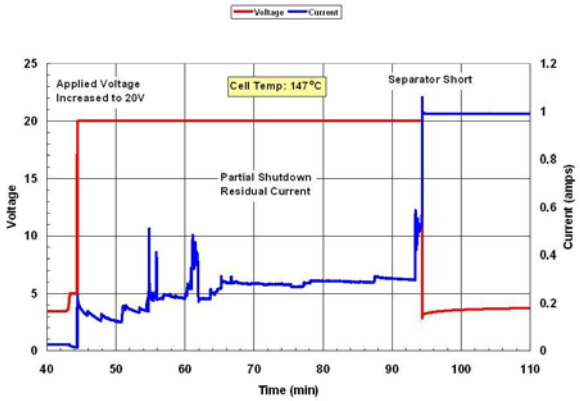

Figure III-72: Cell voltage and current monitored above the shutdown temperature with an applied 20V potential.

Conclusions and Future Directions

Cell and module abuse testing has provided critical information to the USABC cell developers that has aided in development of improved abuse tolerant cell and module designs. This information is necessary for an objective evaluation of these cells and designs by the DOE and the U.S. car manufacturers.

Testing in the coming FY will shift from HEV designs to the higher energy PHEV cells and modules. Modifications of testing procedures and facilities may be necessary for safe evaluation of these highly energetic devices.

FY 2009 Publications/Presentations

The information produced for the USABC is protected and cannot be published or presented in an open public forum. Presentation of the testing results is limited to quarterly Tech Team meetings consisting of the car manufacturers and DOE personnel.

1. 2009 DOE Annual Peer Review Meeting.

III.C.4 Battery Thermal Analysis and Characterization Activities (NREL)

Matt Keyser
National Renewable Energy Laboratory
1617 Cole Boulevard
Golden, Colorado 80401
Phone: (303) 275-3876; Fax: (303) 275-4415
E-mail: matthew.keyser@nrel.gov

Start Date: October 1, 2008
Projected End Date: September 30, 2009

Objectives

- Use NREL's unique test equipment to thermally evaluate PHEV and HEV cells developed by FreedomCAR battery developers.
- Support FreedomCAR developers with electro-thermal analysis of energy storage devices for assessing and improving the thermal design of their electrochemical devices for enhanced life and performance.

Technical Barriers

This project addresses the following energy storage research and development technical barriers identified by the Vehicle Technologies Program:

- **Cost** – The current cost of Li-based batteries (the most promising chemistry) is approximately a factor of three to five times too high on a kWh basis.
- **Performance** – The performance barriers include the need for much higher energy densities to meet volume and weight requirements and to reduce the number of cells in the battery (thus reducing the system cost).
- **Life** – The ability to attain a 15-year life—300,000 HEV cycles or 5,000 EV cycles—is unproven and anticipated to be difficult. Specifically, the impact of combined EV/HEV cycling on battery life is unknown, and extended time at high state of charge (SOC) is predicted to limit battery life.

Technical Targets

- By 2010, develop an electric drive train energy storage device with a 15-year life at 300 Wh with a discharge power of 25 kW for 18 seconds and a cost of $20/kW.
- Develop hardware for specific applications that can be tested against respective performance targets and used for subsystem benchmarking.
- Develop a battery for PHEV-40 with the following requirements: 38 kW pulse power for 10 seconds, 11.6 kWh usable energy, mass less than 120 kg, volume less than 80 L, cost less than $3,400.

Accomplishments

- Thermally evaluated the Johnson Control Saft (JCS) VL22M, the JCS VL41M, the A123 32113 Gen 2 lithium iron phosphate HEV cell, and the CPI PLG1 pouch cell and performed electrical and thermal characterization of JSR Micro's asymmetrical Li-ion capacitor and the Nesscap ultracapacitor module.
- Initiated testing of the A123 32113 Gen 2 B1 HEV cell, the Gen 3 EnerDel HEV cell, and the Gen 3 EnerDel HEV module.
- Finished the design and fabrication phases of the large calorimeter at NREL. The new large calorimeter is six times the volume of NREL's existing calorimeter but can measure similar magnitudes of heat effects—as low as 15 joules (J). We have tested PHEV and HEV cells in the large calorimeter, and the results compared favorably to those of our existing calorimeter.

✧ ✧ ✧ ✧ ✧

Introduction

The operating temperature is critical in achieving the right balance among performance, cost, and life for both Li-ion batteries and ultracapacitors. At NREL, we have developed unique capabilities to measure the thermal properties of cells. We also use our electro-thermal finite element models to analyze the thermal performance of battery systems in order to aid battery developers with improved thermal designs. Finally, we calibrated and began using NREL's new large calorimeter to measure the heat generation of PHEV cells.

Approach

Using NREL's unique calorimeters and infrared thermal imaging equipment, we obtain thermal characteristics (heat generation, heat capacity, and thermal images) of PHEV and HEV batteries and ultracapacitors developed by FreedomCAR manufacturers and other industry partners. NREL supports the Energy Storage Technical Team by participating in the JCS, CPI, A123, EnerDel, and other workgroups.

Results

Thermal Evaluation of the JCS VL22M and VL41M PHEV Cells. The objective of NREL's effort was to measure the thermal characteristics of the JCS VL41M and VL22M cells. In FY08, NREL initiated thermal imaging of the cells and found no areas of thermal concern. In FY09, NREL expanded upon the thermal testing completed in FY08. Figure III-73 shows a thermal image of three VL41M cells under PHEV charge-depleting (CD) and charge-sustaining (CS) cycles. The charge-depleting portion of the cycle is more thermally aggressive than the charge-sustaining cycle and, as expected, the terminals of the cells are the hottest part of the cell. We also tested the cells in NREL's calorimeter to determine their heat generation and efficiency as a function of current and temperature. The cells were tested at -15°C, 0°C, and 30°C. The efficiency of the VL41M PHEV cell at 30°C was greater than 91% for all RMS discharge currents below 150 A. The efficiency of the VL22M PHEV cell at 30°C was greater than 87% for all RMS discharge currents below 110 A.

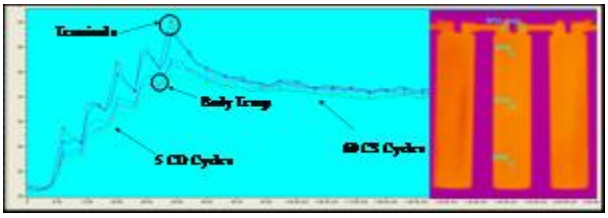

Figure III-73: JCS VL4M under 5 CD and 60 CS cycles

Thermal Evaluation of the A123 32113 Gen 2 HEV Cell. NREL evaluated the heat generation and efficiency of the A123 32113 Gen 2 HEV cell at -15°C, 0°C, and 30°C.

Figure III-74 compares and contrasts the Gen 1 and Gen 2 A123 HEV cells. Essentially, the efficiency and heat generation between the 3.6 Ah Gen 1 cell and the 4.4 Ah Gen 2 cell are approximately the same. Note that the cells have the same volume and package style—32113. Under the 25 Wh HEV cycle at 30°C, the Gen 2 cell has an efficiency of 96.7%, whereas the efficiency decreases to 94.0% under the 50 Wh HEV cycle at the same temperature.

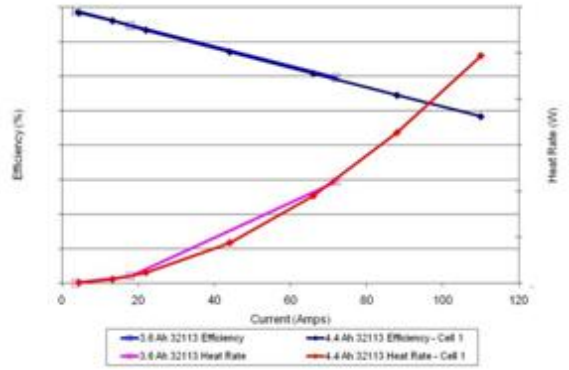

Figure III-74: Efficiency and heat generation comparison of the Gen 1 and Gen 2 A123 HEV cells

Thermal Evaluation of the CPI/LG Chem PLG1 Pouch Cell. In FY09, NREL tested a PLG1 pouch cell from Compact Power, Inc., a U.S. subsidiary of LG Chem of South Korea. The cell was designed and evaluated for PHEV10 application. Prototype cells were built at LG Chem and tested by CPI and DOE under the USABC program. NREL performed thermal characterization testing of the cell. Tests included thermal imaging of the cell under high-rate discharge and aggressive vehicle power profile (US06) cycling, – as shown in Figure III-75. The cells showed reasonable thermal uniformity, with no significant hot spots of concern. In PHEV10 applications, maximum temperature is reached at the end of charge-depletion EV-type cycling. Charge-sustaining HEV-type cycles generate far less heat and thus require less cooling from the thermal management system to maintain the desired battery temperature. Heat generation measurements were conducted using NREL's calorimeter at 30°C, 0°C, and -15°C for a range of constant current discharge/charge and vehicle power profiles.

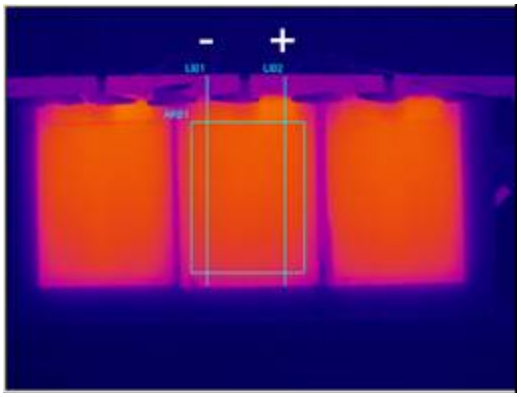

Figure III-75: Infrared image of the CPI PLG1 pouch under US06 cycling

JSR Micro's Asymmetrical Li-ion Capacitor. NREL electrically and thermally evaluated JSR Micro's Li-ion capacitor. This capacitor consists of an activated carbon positive electrode and a lithium-doped carbon negative electrode with a proprietary electrolyte developed by JSR Corporation.

The electrical testing of the cell included cycling the cell at 10 A, 50 A, and 100 A and then performing a low and high current HPPC at 30°C. The discharge capacity of the cell was 0.97 Ah, 0.84 Ah, and 0.74 Ah at 10, 50, and 100 A, respectively. The discharge capacity was evaluated over a voltage range from 3.8 V to 2.2 V. The LIC cells were also subjected to a low current, 10 A, and a high current, 50 A, HPPC. The impedance of the cell is slightly higher than comparable lithium and ultracapacitor cells. NREL also evaluated the heat generation and efficiency of the cell at 30°C. Figure III-76 shows the calorimeter response to constant current discharge and regen currents. Of note, the cell is completed endothermic for regen currents up to 70 A. The LIC cell is approximately 78% efficient at a discharge current of 80 A. Furthermore, NREL thermally images the cells and found that the temperature difference across the cell is less than 2.5°C for a discharge current of 100 A.

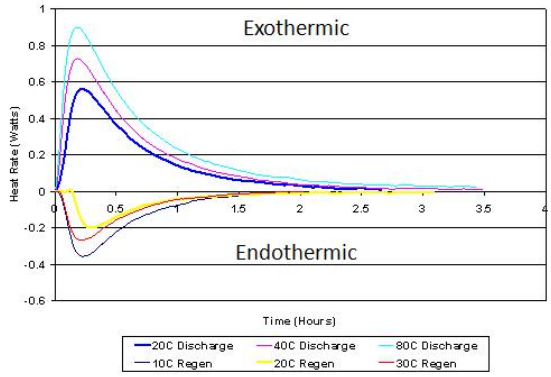

Figure III-76: JSR Micro's LIC cell under constant current regen and discharge currents

Thermal Evaluation of the Nesscap Ultracapacitor Module. NREL thermally evaluated the performance of the Nesscap 18 cell ultracapacitor module. We measured the temperature rise and difference between corresponding cells as well as the voltage of each cell. Testing was done at an initial ambient temperature of 0°C, 30°C, and 45°C using an enhanced or aggressive Toyota Camry US06 power profile. As expected, the center cells were the hottest ones within the module. The temperature gradually decreased from the middle cells to the external cells. The temperature difference between the cells after 12 US06 cycles was less than 4.0°C. The balancing board, internal to the Nesscap ultracapacitor module, was aggressive in regulating voltages when any cell voltage exceeded 2.6 V. Therefore, the balancing resistors radiated heat to the cells surrounding the balancing board and thus had a thermal effect on the nearby cells, as shown in Figure III-77.

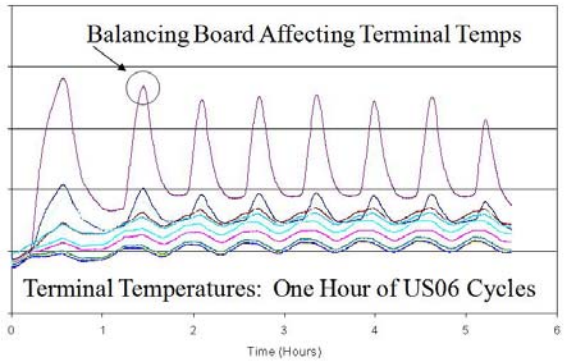

Figure III-77: Nesscap cell temperatures and balancing board temperature during US06 cycling

Development of NREL's Pack Calorimeter. We finished the design and fabrication phases of the pack calorimeter at NREL. The new pack calorimeter measures 60 cm x 40 cm x 40 cm, or six times the volume of NREL's existing calorimeter, and can measure similar magnitudes of heat effects—as low as 15 J. We also completed the shakedown and calibration phases for the large calorimeter. And we tested a limited number of cells in the large calorimeter; the results compared favorably to those of our existing calorimeter. The new calorimeter is shown in Figure III-78.

Figure III-78: NREL's battery pack calorimeter

Conclusions and Future Directions

Although there is variation between lithium chemistries, the efficiency of these cells is typically greater than 85% at 30°C. However, further research needs to be performed with regard to pack design to ensure that the cell-to-cell temperature difference is less than 2–3°C to ensure a 15-year life. The data provided

by NREL's unique test equipment aides in the development of innovative thermal designs to achieve this goal.

In FY10, NREL will continue to thermally evaluate PHEV and HEV cells to meet the Vehicle Technologies Program's goals and objectives.

FY 2009 Publications/Presentations

1. Presentation at the 2009 DOE Annual Merit Review Meeting, Washington DC. May 2009.
2. Presentations to the FreedomCAR Electrochemical Energy Storage Technical Team and each of the individual USABC battery manufacturer workgroups.
3. Pesaran, A.; Kim, G.-H.; and Keyser, M., "Integration Issues of Cells into Battery Packs for Plug-in and Hybrid Electric Vehicles," Proceedings of the EVS-24 International Battery, Hybrid and Fuel Cell Electric Vehicle Symposium, Stavanger, Norway, May 13-16, 2009.
4. Smith, K.; Markel, T.; Pesaran, A., "PHEV Battery Trade-Off Study and Standby Thermal Control," Proceedings of the 26th International Battery Seminar & Exhibit, Fort Lauderdale, Florida, March 16-19, 2009.

III.D Energy Storage R&D Collaborative Activities with the International Energy Agency (IEA)

David Howell, Team Leader

Hybrid and Electric Systems
EE-2G, U.S. Department of Energy
1000 Independence Ave., SW
Washington, DC 20585
Phone: (202) 586-3148; Fax: (202) 586-2476
E-mail: David.Howell@ee.doe.gov

Alternate Point of Contact:

James A. Barnes
James.Barnes@ee.doe.gov
Phone: (202) 586-5657

Start Date: Continuing Effort
Projected End Date: September 30, 2010

Objective

Use the resources available through the International Energy Agency's (IEA) Implementing Agreement on Hybrid and Electric Vehicles (IA-HEV) to facilitate the exchange of information on relevant technologies and governmental activities within the international community and to study relevant issues.

Introduction and Approach

The International Energy Agency (IEA) is an autonomous body that was established in November 1974 within the framework of the Organization for Economic Co-operation and Development (OECD) to implement an international energy program. It carries out a comprehensive program of energy co-operation among twenty-six of the OECD's thirty member countries. Much of the IEA's work is done through over 40 Implementing Agreements. The Hybrid and Electric Systems Team is very active in the IA-HEV. This IA has 13 member countries: Austria, Belgium, Canada, Denmark, Finland, France, Italy, Netherlands, Spain, Sweden, Switzerland, Turkey, the United Kingdom, and the United States. In turn, the IA-HEV functions through seven annexes (working groups) that focus on relevant areas of interest. These include Information Exchange (I), Electrochemical Systems (X), Electric Cycles (XI), Heavy-duty Hybrid Vehicles (XII), Fuel Cells for Vehicles (XIII), Lessons Learned (XIV), and Plug-in Hybrid Electric Vehicles (XV). The United States is a member of all of these annexes and provides organizational leadership for Annexes I, X, and XIV.

Results

Annex X: Electrochemical Systems. Annex X is most relevant to the focus of the Energy Storage effort within Vehicle Technologies. It functions by sponsoring informal, focused workshops to address technical or informational issues important to batteries for vehicles. In FY 2009, it held a meeting on the World's Supply of Lithium in Charlotte, North Carolina in early December 2009. The location was chosen because Charlotte is the home of two of the world's major lithium companies. The decision to hold the workshop was prompted by the fact that there has been extensive discussion about whether there is enough lithium in the world to allow the use of lithium-ion batteries in a significant number of Hybrid Electric Vehicles (HEVs), PHEVs, and Electric Vehicles (EVs). Some of the discussions that suggested that the world's supply of lithium was not sufficient were available on public internet sites, but many negative comments were made in informal settings. Examples that were mentioned to the organizers of the meeting included a venture capital company who questioned a battery company's business plan because "there would not be enough lithium to make a significant number of batteries." In another meeting, a company marketing a non-lithium battery asserted that their technology should be adopted because "the world was going to run out of lithium." The goals of the workshop were to collect data on the world's lithium supply, allow for interested parties to discuss the issue, and to encourage follow-on analysis and publications on the subject.

In order to allow for effective discussions, attendance at the workshop was limited. Invitations were sent to companies supplying lithium, battery companies, vehicle manufacturers, the recycling industry, and representatives of governments and universities. Over 25 people attended the two-day meeting. Attendees represented the following groups and companies:

- Governments and national laboratories: Canada, UK, U.S.
- Universities: Sweden
- Large lithium suppliers: Chemetall/Foote (U.S.), FMC Lithium (U.S.), and SQM (Argentina)

- Smaller lithium suppliers: Simbol Mining (U.S.), Avalon Ventures (Canada)
- Battery manufacturers: A123Systems (U.S.), EnerDel (U.S.), Johnson Control/Saft (U.S./France), EaglePicher (U.S.), Saft (U.S./France), MaxPower (U.S.).
- Vehicle manufacturers: GM (U.S./global)
- Battery Recycling Industry: RSR Technologies (U.S./global).

Topics that were discussed included:

- Current supply of lithium
- Potential sources of lithium, not now being exploited
- Current uses of lithium
- Impact of HEVs, PHEVs and EVs on lithium market
- Impact of recycling on lithium supply.

A brief summary of the information discussed at the meeting includes the following items:

- The world's current production capacity for lithium exceeds current demand.
- Current production capacity can be increased significantly.
- Increasing capacity at a given site can require several years.
- Lithium reserves exist around the world
  - Europe
  - North America
  - South America
  - Asia
- The technology for exploiting these reserves exists today.
- Some of these technologies may be marginally more expensive than the brine-based technologies used today.
- As lithium-ion batteries are used in more vehicles, recycling of lithium metal and lithium compounds could become a significant part of the supply stream.
  - About 85% of the lead in lead/acid batteries is recycled.
- The world's supply of lithium is sufficient to allow for the use of lithium-ion batteries in all appropriate HEVs, PHEVs, and EVs likely to be produced in the next several decades.
- Some HEVs will not use lithium-ion batteries.
  - Micro (Stop/Start) hybrids will probably use lead/acid batteries.

A scenario that projects ALL light, passenger vehicles in the world being EVs using lithium-ion batteries was mentioned. This situation would require significant increases in lithium production and might require turning to new ores and other sources.

Since this meeting, several groups and individuals have completed more detailed analyses of the situation based on the data and discussions from the meeting. Among these studies is one done by Dr. Linda Gaines of Argonne National Laboratory. She may be reached at lgaines@anl.gov.

FY 2009 Publications/Presentations

1. Presentation to the 2008 DOE Annual Peer Review Meeting.
2. 2008 Annual Report of the Implementing Agreement on Hybrid and Electric Vehicles, April, 2009. (Copies of this report are available from James Barnes at the address given at the beginning of this section.)

IV

APPLIED BATTERY RESEARCH

D.O.E. Project Manager

David Howell

Technical Lead

Gary Henriksen

Argonne National Laboratory

IV. APPLIED BATTERY RESEARCH

IV.A Introduction

The Applied Battery Research (ABR) for Transportation program is being conducted in support of the FreedomCAR and Fuel Partnership which is targeting more fuel-efficient light duty vehicles that can reduce U.S. dependence on petroleum, without sacrificing performance. There is an emphasis on developing and improving critical component technologies; and energy storage technologies are included among those critical components. In PHEVs, energy storage devices provide the primary power source for a number of "all-electric" miles, after which the vehicles again operate in the conventional HEV mode. They enhance the efficiency of the prime power source (currently an internal combustion engine) in HEVs by leveling the load and capturing regenerative braking energy. Better energy storage systems are needed to help expand the commercial markets for HEVs and to help make PHEVs commercially viable. The energy storage requirements for various vehicular applications were presented in Section III.

The ABR program is focused on materials and cell couples for high energy PHEV batteries for use in light-duty vehicles. The key barriers associated with PHEV batteries are:

- High cost
- Limited calendar and cycle life,
- Insufficient tolerance to abusive conditions,
- Insufficient energy density to meet 40-mile all-electric range, and
- Operation between -30ºC and +52ºC.

The program is seeking to develop higher energy materials, higher voltage electrolytes, and more optimal cell chemistries that are more chemically, structurally, electrochemically, and thermally stable in the cell environment; as well as possessing cost advantages over current materials. Conventional high-energy Li-ion batteries, of the type used in consumer electronics, employ sophisticated and relatively expensive electronic controls that limit their exposure to abusive conditions. The program has focused on both understanding and enhancing the inherent abuse tolerance of the individual materials, components, and cell chemistries, which will help reduce the level of sophistication of the electronic control system and thereby realize cost savings.

Seven DOE national laboratories are collaborating in the program. Argonne National Laboratory (ANL) provides coordination of the program activities for DOE. The other six participating DOE laboratories are Brookhaven National Laboratory (BNL), Idaho National Laboratory (INL), Lawrence Berkeley National Laboratory (LBNL), the National Renewable Energy Laboratory (NREL), Oak Ridge National Laboratory (ORNL), and Sandia National Laboratories (SNL). As part of this program, ANL researchers maintain close communications and (in some cases) collaborations with a large number of international material supply companies, through which they gain access to the latest advanced electrode and electrolyte materials for evaluation.

The Applied Battery Research for Transportation program is organized into three main tasks to address the issues associated with PHEV and HEV energy storage technologies:

Battery Cell Materials Development—focuses on research, development, and engineering of higher energy advanced materials and cell chemistries that simultaneously address the life, performance, abuse tolerance, and cost issues.

Calendar & Cycle Life Studies—deals with understanding the factors that limit life in different Li-ion cell chemistries, which are used as feedback to Task 1. This task also deals with the establishment of in-program cell fabrication capabilities for use in these life studies.

Abuse Tolerance Studies—deals with understanding the factors that limit the inherent thermal and overcharge abuse tolerance of different Li-ion cell materials, components, and cell chemistries, as well as developing approaches for enhancing their inherent abuse tolerance.

The subtask breakdown for the program is provided in Figure IV- 1.

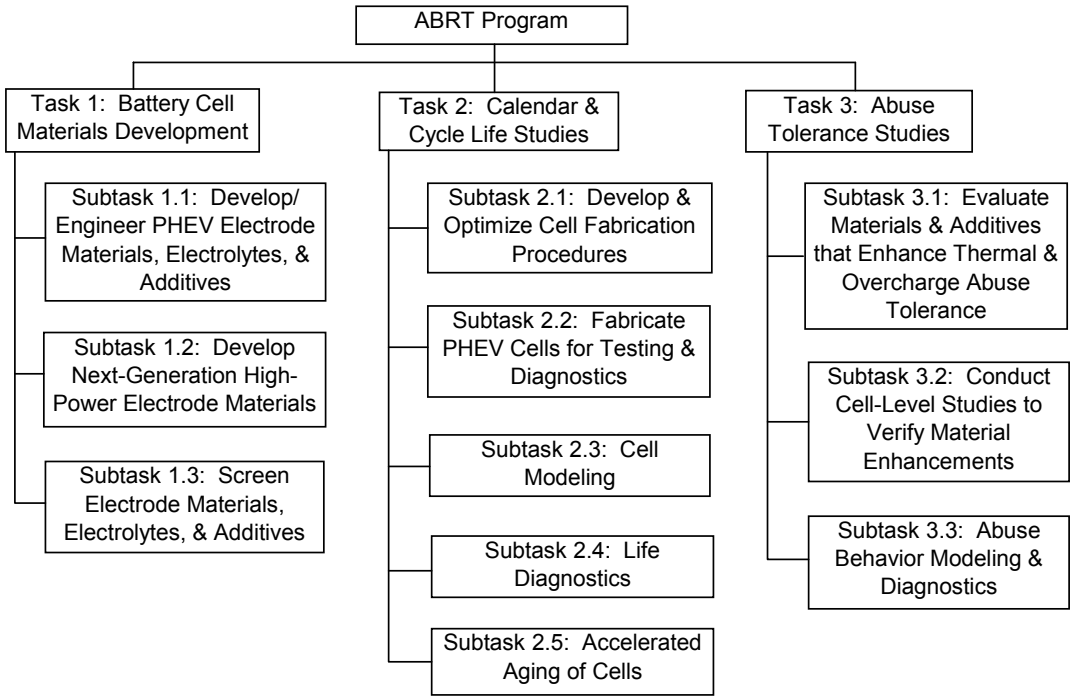

Figure IV- 1: Task and subtask breakdown for the Applied Battery Research for Transportation Program in FY 2009.

The remainder of this section provides technical highlights and progress on the Applied Battery Research program for FY 2009. The information provided is representative only and detailed information is available from publications cited in each project overview.

IV.B. Materials Development

The objectives of the materials development effort are numerous. Researchers are screening new materials, optimizing Li-ion electrolytes, and working to develop and improve specific new materials. The goal is to enable affordable, safe 40 mile PHEV batteries that are free from many of the abuse tolerance shortcomings inherent in today's chemistries. In addition, researchers are looking for breakthrough high power materials to enable a revolutionary reduction in HEV cost.

IV.B.1 Screen Electrode Materials and Cell Chemistries (ANL)

Wenquan Lu

Argonne National Laboratory (ANL)
9700 S. Cass Ave.
Argonne, IL 60439
Phone: (630) 252-3704; Fax: (630)972-4414
E-mail: luw@anl.gov

Collaborators :
Andrew Jansen (ANL)
Sun-Ho Kang (ANL)
Dennis Dees (ANL)
Khalil Amine (ANL)
Gary Henriksen (ANL)

Subcontractor:
Illinois Institute of Technology, Chicago, IL

Start Date: Oct. 1st, 2008
Projected End Date: September 30, 2010

Objectives

- To identify and evaluate low-cost cell chemistries that can simultaneously meet the life, performance, and abuse tolerance goals for Plug-in HEV applications.
- To enhance the understanding of advanced cell components on the electrochemical performance and safety of lithium-ion batteries.

Technical Barriers

An overwhelming number of materials are being marketed by vendors for Lithium-ion batteries. It is a challenge to down select and screen these materials effectively.

On the other hand, there is no commercially available high energy material to meet the 40 mile PHEV application established by the FreedomCAR and Fuels Partnership. Search and identification of potential electrode materials is the primary goal for this project.

Determining the impact of formulation and fabrication on performance of electrode materials with a broad variation of chemical and physical properties is also a challenge.

Technical Targets

- High energy density materials identification and evaluation.
- Low cost cell components identification and characterization.

Accomplishments

The material screening test protocol is developed for PHEV application using the "Battery Test Manual for Plug In Hybrid Electric Vehicle" (Mar. 2008). The simplified test procedure addressed the pulse power, regen power, and charge depleting energy, major issues for PHEV application at the coin cell level. The energy density requirement of the electrode materials to meet the requirement of PHEV application is also calculated using Argonne's battery design model.

Various cathode and anode materials were obtained from vendors for evaluation. The high energy materials include high energy density graphite, $LiMnPO_4$, and $LiNi_xCo_yMn_zO_2$ materials. Beside high energy materials, some high power materials, such as $LiMn_2O_4$, are also investigated for HEV applications.

Other than the electrode materials, the other cell components of the Li-ion batteries, such as separators, are also characterized for low cost and better thermal properties.

✧ ✧ ✧ ✧ ✧

Introduction

The identification and evaluation of the high energy density electrode materials, which will meet the volume and weight requirements of the Li-ion batteries for 40 mile all electric range (AER) PHEVs, is the focus of this project. Currently, no commercial electrode material can meet this requirement. The search for high energy density material is challenging. Beside high energy density electrode materials, other cell components will be evaluated to address the performance, safety, and cost issues.

Approach

In order to identify the electrode materials to meet the PHEV requirements, the electrode material screening activity will include not only the commercially available materials, but also the potential high energy density materials under research and development. The cost issue will be addressed by avoiding the rare elements, expensive precursors, or elaborate processing.

The selected electrode materials will be evaluated in controlled conditions following established protocols. Coin cells (2032 size) will be used for initial screening studies. If promising results are obtained with coin cells, then larger laboratory cells will be used such as the 32 cm² stainless steel planar test fixture or simple single-stack pouch cells. Accelerated aging studies will be performed at 55°C of promising materials to give a preliminary indication of life. Where appropriate, the thermal abuse response will be studied using a differential scanning calorimeter. Materials that show characteristics favorable to PHEV batteries will be recommended for further life evaluation in Task 2 and rigorous abuse tolerance testing in Task 3.

Other than the electrode materials, other cell components, such as separator, binder, current collector, etc., will be searched and evaluated to address their electrochemical performance, thermal safety, and cost.

Results

Test Protocol Development for Material Screening. The energy storage system performance targets for PHEVs are summarized in Chapter 2 of this report. However, those requirements are for large format batteries. A simplified test protocol was developed for material research and development and material screening purposes. Corresponding to 40 mile PHEV requirements in the manual, the pulse power and charge depleting (CD) rate of the battery system for PHEV is calculated and listed in Table IV-1 below. The calculated CD rate and pulse power rate can be directly applied to any size cell without considering the battery size factor (BSF). The result in the table has taken a 30% energy margin into consideration.

Table IV-1: HPPC and CD rate for material screening

Available Energy	Pulse	Regen	Crate,CD
%	C	C	C
50	1.3	0.83	0.3
60	1.5	0.99	0.4
70	1.8	1.16	0.5

Energy Density Requirement of Electrode Materials for 40 mile PHEV. From the test manual, 40 mile PHEV requires at least 180 Wh/kg (with consideration of a 30% energy margin and 70% energy usage) at the battery system level. If we translate this energy density requirement to material level, the specific capacity of cathode and anode should be 170 and 350 mAh/g, respectively, even at the beginning of life (BOL).

Figure IV- 2 shows the capacity requirement to meet 40 mile PHEV using Argonne's battery design model. In this model, all the properties of battery, other than the specific capacity values, are kept same as the Gen 2 chemistries, $LiNi_{0.8}Co_{0.15}Al_{0.05}O_2$, MAG-10 graphite, and 1.2M $LiPF_6$ EC/EMC (3/7) electrolyte. The specific capacity of anode and cathode could be lower if the battery system is further optimized. Nevertheless, the current electrode materials cannot meet this goal under the normal operating conditions. Figure IV- 2 also indicates that the easiest way to meet the 40 miles PHEV is to improve the specific capacity of both anode and cathode active materials. Obtaining the specific capacity improvement from only one electrode will be very difficult.

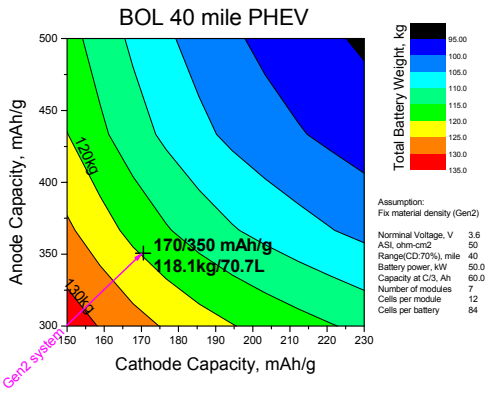

Figure IV- 2: Specific capacity requirements for anode and cathode electrode of Li-ion battery

High Energy Density Graphite from Hitachi Chemical Co. Compared to soft and hard carbons, graphite has a higher specific capacity, 372 mAh/g, and is the anode material of choice for PHEV applications. However, the cycle and calendar life need to be addressed due to the high activity of the lithiated graphite. Hitachi Chemical Co. has developed the surface modified graphite by carbon coating. The carbon coated graphite still has

more than 350 mAh/g reversible capacity up to 10 wt.% carbon coating shown in Figure IV- 3. The carbon coated graphite shows not only the high energy density, but also comparable or lower area specific impedance (ASI) than that of Gen2 baseline system.

The carbon coated graphite can further improve the thermal stability. As shown in Figure IV- 4, the heat flow is clearly depressed with increasing the carbon coating. The depressed heat flow implies the less heat generation from the cell under abuse conditions and safer battery system. The depressed heat flow is apparently due to the carbon coating, which might provide a barrier between graphite and electrolyte and reduce the reduction reaction of electrolyte by the lithiated graphite.

High Energy Density $LiMnFePO_4$ from High Power Lithium (HPL). $LiMnFePO_4$ can deliver up to 170 mAh/g, similar to $LiFePO_4$, but operates as high as 4.1 volts. This makes $LiMnPO_4$ a promising high energy density cathode material to be used for PHEV applications. The nanosize C-$LiMnPO_4$ composite developed by HPL was obtained and evaluated at Argonne. Similar to $LiFePO_4$, $LiMnFePO_4$ is intrinsically safe with lower cost. Also the power capability is addressed by making a nanosize carbon composite. The material is tested using Li/$LiMnFePO_4$ half cell. Test result indicates that there is almost 170 mAh/g capacity (Figure IV- 5) at C/20 rate in the very first charge cycle. Only 10% reversible capacity loss is observed in the following discharge cycle. Beside of its high specific capacity, the cycling performance of the Li/$LiMnFePO_4$ half cell is also very good at C/2 rate at room temperature as shown in Figure IV- 6.

PVDF based Separator from Porous Power Technologies (PPT). The separator is a major component in Li-ion batteries, contributing almost 20% of the total material cost. A high porosity separator developed by Porous Power Technologies (PPT) was obtained and evaluated. The PPT separator is PVDF-based, which has as high as 80% porosity (as shown in Figure IV- 7). In this study, the thickness of PPT separator is 25 µm.

The electrochemical performance of PPT separator was evaluated using Gen 2 chemistries. Because of its extremely high porosity, the Li-ion diffusion in PPT separator is fast, resulting into low resistance and high power. The higher power capability of the Li-ion cell using PPT separator is demonstrated in Figure IV- 8, which shows less area specific impedance (ASI) during high pulse power characterization (HPPC) test.

The thermal analysis of PPT separator was carried out using DSC. The result indicates that the PPT separator is more thermally stable due to its lower heat generation and higher on-set temperature to melt down. Furthermore, the shrinkage of PPT separator (shown in Figure IV- 9) is much less than conventional PP- or PE-based separators.

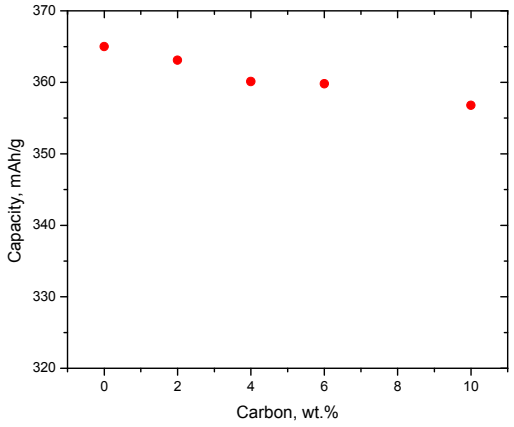

Figure IV- 3: Specific capacity of carbon coated graphite

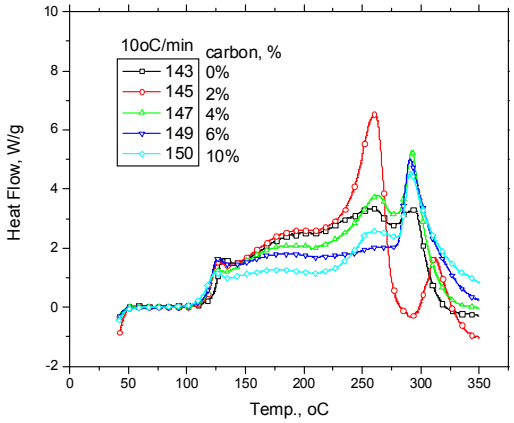

Figure IV- 4: DSC result of carbon coated graphite

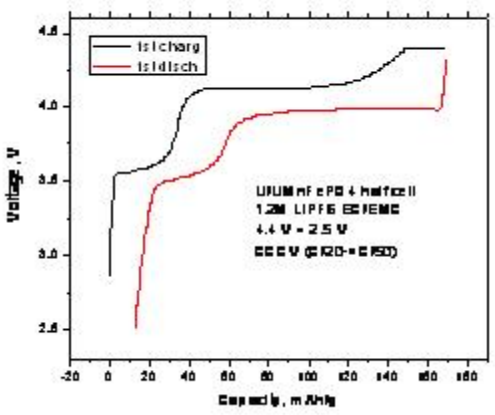

Figure IV- 5: Voltage profile of Li/$LiMnFePO_4$ half cell

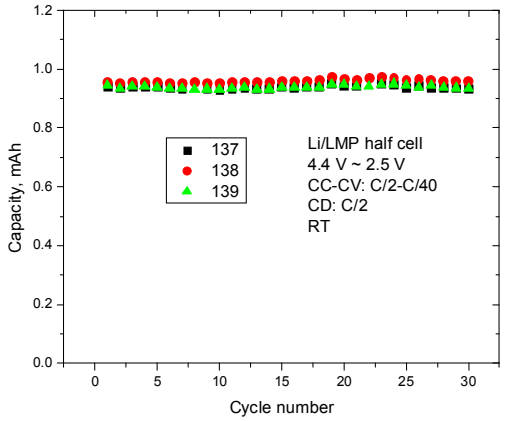

Figure IV- 6: Cycle performance of $LiMnPO_4$

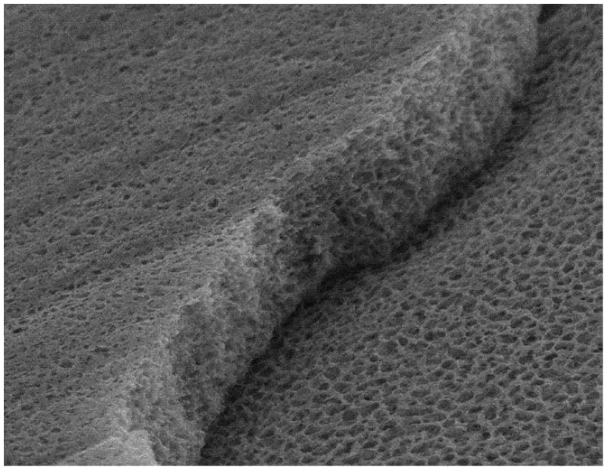

Figure IV- 7: SEM image of PVDF based separator by Porous Power Technologies

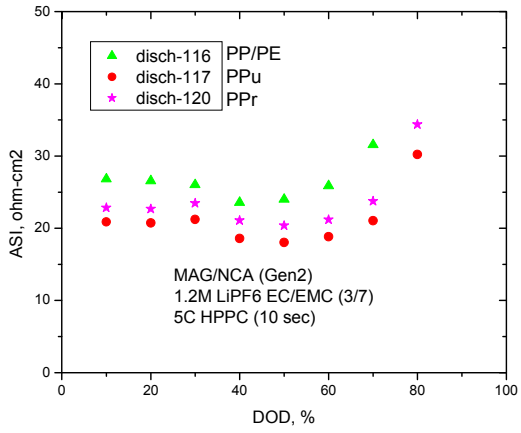

Figure IV- 8: ASI of Gen 2 cell using PPT separator

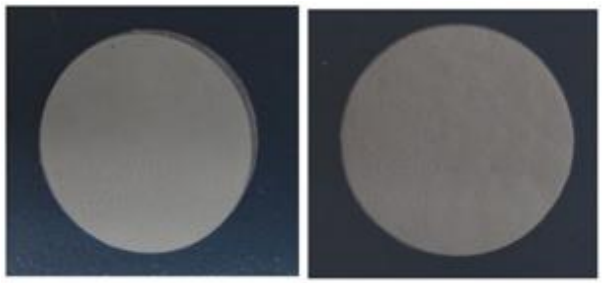

Figure IV- 9: Shrinkage test of PP/PE (left) and PPT (right) separators

Conclusions and Future Directions

A test protocol for material screening purpose has been developed corresponding to the requirements of 40 mile PHEV application. The simplified procedure will be applied to all future material screening tests. According to Argonne's battery design model, the required specific capacities of anode and cathode materials are at least 350 mAh/g and 170 mAh/g. Therefore, the electrode material searching will be very challenging. The material search will not be limited to commercially available materials only, but will extend to materials under R&D.

Surface modified graphite (SMG) from Hitachi Chemical Co. has been evaluated. All Hitachi SMG samples have high specific capacity – above 350 mAh/g. The power capability improvement is noticed by carbon coating according to the half cell HPPC. The exothermic heat of lithiated graphite is reduced by carbon coating, which indicates good thermal stability.

The HPL $LiMnFePO_4$ can deliver high specific capacity: above 160 mAh/g. Iron dopant is electrochemically active in $LiMnFePO_4$. Under half cell condition, there is about 80% capacity retention at 2C rate. $LiMnFePO_4$ shows good cycling performance at room temperature under half cell condition. The total heat generation from fully charge $LiMnFePO_4$ is less than nickel base cathode materials, indicating better thermal stability.

The PVDF-based separators from Porous Power Technologies show power improvement due to high porosity. Another advantage of this separator is small shrinkage compared to PP or PE based separators. In the future, other components of Li-ion batteries, such as separator, binder, and current collector, etc., will be searched and evaluated in order to address the cost issue.

FY 2009 Publications/Presentations

1. Presentation to the 2009 DOE Annual Peer Review Meeting.

IV.B.2 Streamlining the Optimization of Li-ion Battery Electrodes (ANL)

Wenquan Lu and Sun-Ho Kang
Argonne National Laboratory
9700 S. Cass Ave.
Argonne, IL 60439
Phone: (630) 252-3704; Fax: (630)972-4414
E-mail: luw@anl.gov

Collaborators:
Dennis Dees, Argonne National Laboratory
Jansen Andrew, Argonne National Laboratory
Daniel Abraham, Argonne National Laboratory
Center for Nanoscale Materials, Argonne National Laboratory

Start Date: Oct. 1, 2008
Projected End Date: September 30, 2010

Objectives

To establish the scientific basis needed to streamline the lithium-ion electrode optimization process.

- To identify and characterize the physical properties relevant to the electrode performance at the particle level.
- To quantify the impact of fundamental phenomena associated with electrode formulation and fabrication (process) on Li-ion electrode performance.

Technical Barriers

Development of a safe cost-effective lithium-ion battery for a PHEV with a 40 mile all electric range that meets or exceeds all performance goals.

- Establishing the interdependence of Li-ion electrode performance and the specifics of the fabrication process.
- Reducing the complexity of the optimization process resulting from the broad range of active materials, additives, and binders.
- Quantifying the impact of fundamental phenomena on electrode performance.

Technical Targets

- To correlate the electronic conductivity and electrochemical performance of the electrode.
- To develop a model to quantify the impact of electronic conductivity on cell performance.

Accomplishments

- A new approach to streamline the optimization of an electrode is identified. The electrode materials will be investigated at the particle level. The chemical and physical properties of the particle and their concomitant effect on the electronic conductivity of the electrode will be studied.
- The significant impact of electrode processing on the electrochemical performance of Li-ion batteries is demonstrated. The calendering effect on the electrode conductivity is observed for a $LiFePO_4$ electrode.
- Electronic conductivities of various active electrode materials (powder) were carried out using an in-house developed apparatus.
  - The conductivity ranges of various active electrode materials were examined. Variation in electronic conductivity between different electrode materials indicates different electrode formulations are needed for optimized electrodes.
  - The conductivity of $LiFePO_4$ carbon blends was determined. Results indicate that < 5 wt.% percolation threshold is required, even for a poor electronic conductor such as $LiFePO_4$.

✧ ✧ ✧ ✧ ✧

Introduction

In general, the performance of lithium-ion electrodes is highly dependent upon the specific fabrication process. Electrode performance optimization is further complicated by the broad range of active materials (e.g. oxides, phosphates, graphites, carbons, and alloys) and inactive materials (polymer binders, conductive additives). Such extensive material variability results in lengthy development efforts in order for new electrode compositions to be fully optimized, often resulting in promising materials being discarded. Quantifying the impact of fundamental phenomena related to electrode formulation and fabrication on electrode performance should drastically reduce the optimization process for new electrode active materials. The goal of this work is to establish the scientific basis needed to streamline the lithium-ion electrode optimization process.

Approach

The common approach to electrode optimization for new electrode active materials is to follow a set of

heuristics familiar to lithium-ion battery developers that is essentially little more than an Edisonion study. New electrode active materials are generally judged on their electrochemical properties, but it is often their chemical and physical properties (e.g. primary particle size, secondary particle size and extent of agglomeration, and surface characteristics) that can dictate their overall performance. Interactions of the active material with the solvent, polymer, and carbon additive during the mixing, coating, drying, and calendering can potentially have a significant influence on the electrode microstructure, which is critical to the electrode electrochemical performance. This effort will determine the significant interactions, as well as the methodology for predicting their influence on performance.

The initial focus of this effort will be on optimizing the electronic conductivity of the electrode. The factors affecting the distribution of binder and conductive additive throughout the composite matrix will be systematically investigated at the particle level, as well as their effect on overall electrode performance. Some modeling work will be carried out to help quantify the impact of fundamental phenomena on electrode performance.

Results

New approach to streamline the optimization of electrode. The general approach has been to optimize the electrode by varying the conductive additive and binder to overcome the percolation threshold at the laminate level. New electrode materials are generally judged on their electrochemical properties. This method, generally adopted by industrial manufacturers, requires lengthy development efforts to fully optimize even single materials and sometimes causes promising materials to be discarded. Streamlining the optimization of electrodes requires a new approach to establish the scientific basis at the particle level.

The new approach will focus on correlating the chemical and physical properties (e.g. primary particle size, secondary particle size and extent of agglomeration, and surface characteristics, see Figure IV- 10) with electrode performance and determining how subsequent processing steps are also influenced by these fundamental particle characteristics.

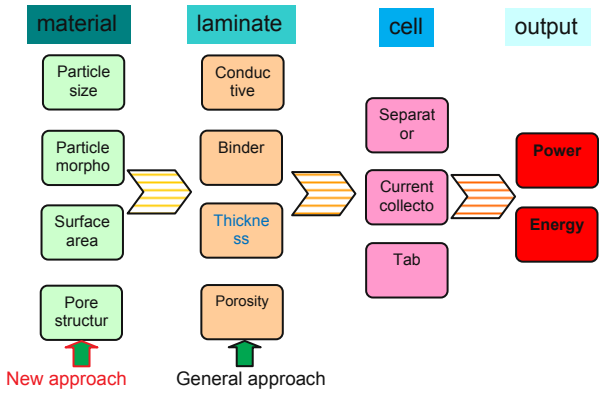

Figure IV- 10: Schematic diagram of streamlining the optimization of electrode

Process effect on electrochemical performance of electrode. Figure IV- 11 shows the area specific impedance (ASI) of $LiFePO_4$ electrodes as a function of porosity, with all other electrode parameters held constant. It can be clearly seen that impedance is significantly reduced by increased calendering of the electrode. Improvements in the power capability are also seen in high rate (5C) HPPC 1st pulse discharge tests. These improvements can be attributed to the reduction of the interfacial impedance. This is further supported by SEM images, which indicate increased physical (and thus electronic) contact between particles in the lower porosity electrodes.

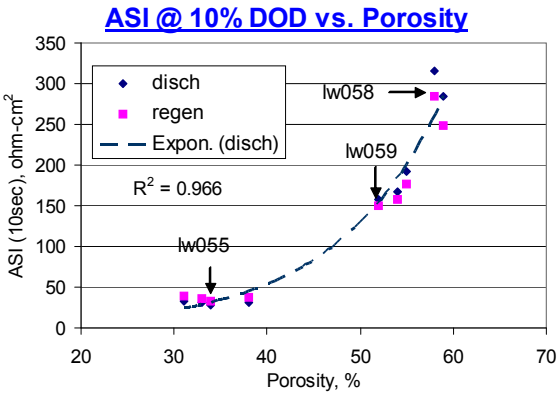

Figure IV- 11: Calendering effect on the impedance of $LiFePO_4$ electrode

Electronic conductivity of powder. The initial focus of this study is to optimize the electronic conductivity of the electrode. In order to investigate the electronic conductivity of electrodes at the particle level, an apparatus to measure the powder conductivity was developed (Figure IV- 12, left.). The apparatus consists of an insulating compartment, which is filled with powder. The powder is pressed by the metal plugs at the top and bottom. The resistivity of the powder is measured at various pressures.

As shown in Figure IV- 12 (right), the measured powder resistivity varies less than an order-of-magnitude over the range of pressures studied. Several electrode materials, such as $LiMn_2O_4$, $LiCoO_2$, and $LiNi_{0.8}Co_{0.15}Al_{0.05}O_2$, $LiNi_{1/3}Co_{1/3}Mn_{1/3}O_2$, and $LiFePO_4$, have been evaluated using this apparatus. The measured conductivities of electrode materials are consistent with literature results.

By using the electronic conductivity measurement apparatus, the conductive carbon additive effect on $LiFePO_4$ was investigated (see Figure IV- 13). As can be seen, the electronic conductivity of the mixture increases with additional additive, especially at low additive compositions. The powder conductivity of uncoated $LiFePO_4$ can be dramatically increased from ~10^{-7} to ~10^{-3} S/cm using as low as 5 wt.% carbon additive. These results indicate that for even extremely poor electronic conductors such as $LiFePO_4$, the percolation threshold is less than 5 wt%. Future studies will investigate the influence of the binder on the percolation threshold of $LiFePO_4$.

Electronic and ionic conductivity impacts on battery performance. Other than the electronic conductivity of the electrode, the ionic conductivity of the electrolyte is another factor that affects the power performance of electrodes. The relationship between electronic and ionic conductivity is currently being modeled by Dees at Argonne. Figure IV- 14 shows the ASI of $LiNi_{1/3}Co_{1/3}Mn_{1/3}O_2$ as function of the electronic conductivity of the electrode. When the electronic conductivity is much greater than the ionic conductivity (>0.01 S/cm), electronic conductivity does not impact electrode impedance. When the electronic conductivity is much less than the ionic conductivity (<0.001 S/cm), the electronic conductivity significantly impacts electrode impedance. When the electronic conductivity is comparable to the ionic conductivity (0.001-0.01 S/cm), both electronic conductivity and ionic conductivity play a role on the electrode impedance during pulse discharge. Therefore, the composition of the conductive additive should be tailored to meet the power and energy requirements of Li-ion batteries.

Conclusions and Future Directions

The focus of this investigation is to correlate the chemical and physical properties of electrode materials with the resulting electrochemical performance. This new approach will be used to establish the scientific basis for streamlining the optimization of electrodes.

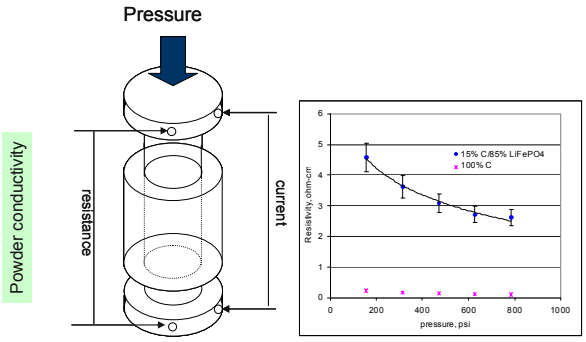

Figure IV- 12: Powder conductivity measurement apparatus

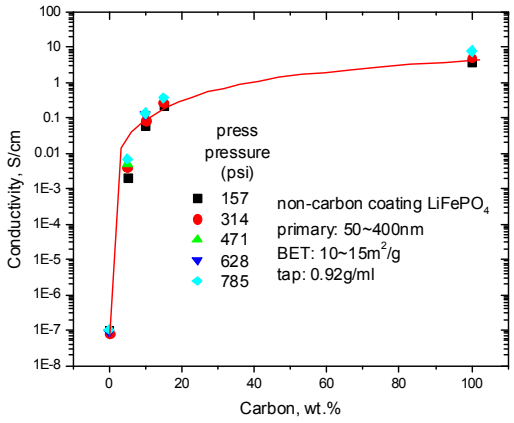

Figure IV- 13: Carbon Additive Effect on Conductivity of $LiFePO_4$/Carbon Blend

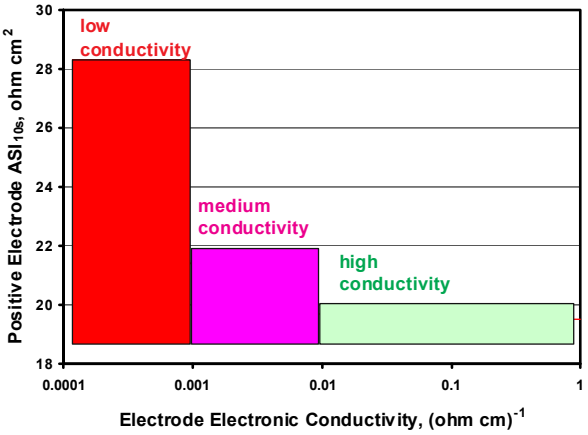

Figure IV- 14: Electrode Electronic Conductivity Impact on ASI

An apparatus for measuring the electronic conductivity of powders was developed. This apparatus has been used to investigate the conductive additive (carbon) effect on the electronic conductivity of a $LiFePO_4$ and carbon mix. It is found that the percolation threshold of very insulating $LiFePO_4$ is less than 5 wt.% without PVDF binder.

Previous modeling results for $LiNi_{1/3}Co_{1/3}Mn_{1/3}O_2$ correlated the electrode electronic conductivity and electrolyte ionic conductivity. The streamlining work should consider both factors to tailor the conductivity of electrode to meet the specific application requirement.

In the future, the particle conductivities, inter-particle interactions and interactions with conductive additives and binders will be studied.

FY 2009 Publications/Presentations

1. Presentation to the 2009 DOE Annual Peer Review Meeting.

IV.B.3 Applied Battery Research on Anodes

IV.B.3.1 Developing a New High Capacity Anode with Long Life (ANL)

Khalil Amine
Argonne National Laboratory
9700 South Cass Avenue
Argonne, Il 60439
Phone: (630) 252-3838; Fax: (630) 252-4176
E-mail: amine@anl.gov

Start Date: September 1, 2008
Projected End Date: September 30, 2010

Objectives

- Develop new anode materials that provide very high gravimetric and volumetric energy density for plug-in hybrid vehicles.
- Explore ways for preparing nanosize TiO_2 having different structural arrangements and exhibiting a suitable morphology for lithium batteries.
- Develop ways to overcome the barrier of the insulating properties of these materials.
- Demonstrate the applicability of TiO_2 in full lithium-ion cells.

Technical Barriers

- Overcome the inherent safety issue of graphite.
- Extend the life of the lithium-ion battery.

Technical Targets

- Develop a safe and high-capacity anode based on a TiO_2 compound that can theoretically generate 335 mAh/g. (The operating voltage of TiO_2 is around 1.5 V and therefore prevents any safety concern as opposed to the graphite anode).
- Develop a suitable electrode morphology to achieve high volumetric capacity.
- Demonstrate the life and safety of cells fabricated with TiO_2 anode combined with high-potential cathodes.

Accomplishments

- Developed a new aqueous method to prepare nanosize TiO_2 materials based on low cost precursors.
- Developed processes to isolate different TiO_2 polymorphs (anatase, rutile, and brookite) by tuning the synthesis conditions.
- Directly synthesized the anatase form by the thermolysis reaction of an aqueous oxysulfate solution, the rutile and an oxalate hydrate phase by addition of oxalate species, and brookite form by thermal decomposition of the oxalate hydrate phase.
- Determined that the morphology of TiO_2 brookite is unique, with nano-domains of TiO_2 embedded in large micron-size particles and a high specific surface area of 255 m^2/g.
- Determined that the TiO_2 brookite phase exhibited the highest columbic efficiency compared to the anatase and rutile phases.
- Determined that the TiO_2 brookite exhibits stable cycling behavior, with the retention of 155 mAh/g capacity after 20 cycles at C/10. The volumetric capacity was 165 mAh/cm^3, which is significantly higher than most TiO_2 nano-materials because they display lower packing density, i.e., around 0.5-0.8 g/cm^3.

✧ ✧ ✧ ✧ ✧

Introduction

Beyond their wide use in small electronic devices, lithium-ion batteries are now facing the challenge of meeting the energy and power requirements for plug-in hybrid vehicles and electric vehicles. Our research has focused on the development of new electrode materials that could provide higher power and energy, longer cycle life, lower cost, and enhanced safety. Titanium oxide (titania) is an interesting alternative anode to graphite due to its operating voltage (~1.5 V), which may enable extended cycle life as well as enhanced safety. Additionally, titanium is abundant, non-toxic, and inexpensive. These characteristics are of great importance with regard to the production of batteries in large scale. However, the practical capacity (~170-200 mAh/g) achieved by the TiO_2 anode is much lower than the theoretical one (335 mAh/g) based on the Ti^{4+}/Ti^{3+} redox couple and still needs to be sustained over long-term cycling. This capacity stability can be achieved by the use of nano-structured titania materials. In general, the project aims to develop high-capacity anodes for lithium-ion batteries, and as an early stage, TiO_2 compounds are being investigated as safe and long-life advanced anodes.

Approach

- Develop a simple synthesis route to prepare nano-size TiO_2 materials using low-cost salts.
- Eliminate safety concerns because the high voltage of TiO_2 reduces the chances of solid-electrolyte interface (SEI) formation.
- Explore coating TiO_2 with nanosize conductive carbon layers to improve conductivity and increase active particle utilization to achieve higher energy densities.

Results

The thermolysis reaction of the low cost salt titanium oxysulfate with and without the presence of additives has been thoroughly investigated in an aqueous medium. Three forms of TiO_2 have been successfully prepared: anatase, rutile, and brookite. The anatase has been prepared by a thermolysis reaction of the oxysulfate solution at 90°C for 4 h without any additives. The use of oxalate species ($C_2O_4^{2-}$) has led to the successive isolation of a titanium oxalate hydrate, $Ti_2O_3(H_2O)_2(C_2O_4)\bullet H_2O$ (for $[C_2O_4^{2-}]/[Ti^{4+}] = 1$), and the rutile phase (for $[C_2O_4^{2-}]/[Ti^{4+}] = 2$). The isolation of TiO_2 rutile by using a high concentration of oxalate emphasized the chelating properties of this anion.

A detailed investigation of the thermal behavior of $Ti_2O_3(H_2O)_2(C_2O_4)\bullet H_2O$ has shown that it decomposes into the TiO_2 brookite form at a temperature as low as 300°C. Profile matching of the X-ray diffraction pattern (Figure IV- 15) attested to the brookite phase purity.

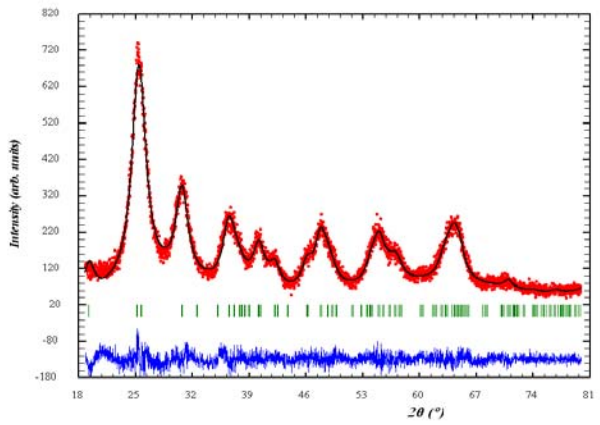

Figure IV- 15: Profile matching of the X-ray pattern of TiO_2 brookite prepared by thermal decomposition of the titanium oxalate at 300°C. Red curve: experimental; black curve: calculated; and blue curve: difference between experimental and calculated curves.

The TiO_2 anode materials retained the morphology of the oxalate precursor, i.e., 3-µm particles with an eggshell morphology (Figure IV- 16). N2 adsorption/desorption revealed a type IV isotherm (Figure IV- 17), indicating that the prepared TiO_2 brookite is mesoporous. The surface area calculated by the BET method was 255 m^2/g, which can only be explained by the existence of significant porosity created at the level of the eggshell micron-size particles. The mesopore size was centered at 3.4 nm, and the total porous volume was 0.25 ml/g. Based on the high surface area and porosity numbers associated with the broadness of the diffraction lines, TiO_2 brookite obtained after decomposition of the titanium oxalate hydrate consists of nano-domains embedded in micron-size particles.

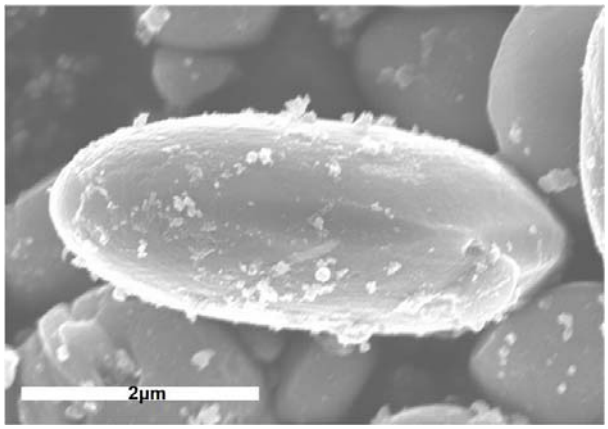

Figure IV- 16: Scanning electron microcopy image of TiO2 brookite obtained by thermal decomposition.

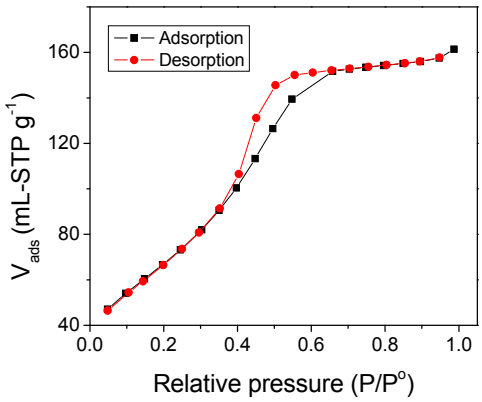

Figure IV- 17: N_2 adsorption isotherms of TiO_2 brookite.

The morphology displayed by TiO_2 brookite appears to be of interest in lithium-ion batteries for several reasons. Firstly, in terms of electrode fabrication, spherical particles exhibit better dispersibility, important during the coating process of the material on the current collector. Secondly, the mesoporosity provides a higher surface contact between the material and the electrolyte, which enhances the electrochemical activity. Finally, this morphology can provide high volumetric energy density in a battery. For instance, most nano-materials dedicated to Li-ion battery

applications suffer from low packing density, which, despite the enhancement of their electrochemical performances, compromises the overall energy density of the battery. In our case, the titanium oxalate hydrate provides a tap density of 1.2 g/cm^3, which slightly decreases upon annealing, to 1.05 g/cm^3.

The cycle-ability of TiO_2 brookite performed at the C/10 rate is presented in Figure IV- 18. Both gravimetric (mAh/g) and volumetric (mAh/cm^3) capacities are reported; the volumetric capacity was calculated from the tap density. The TiO_2 brookite exhibited stable cycling behavior, with the retention of 155 mAh/g after 20 cycles. The volumetric capacity was around 165 mAh/cm^3, which is significantly higher than most nano-TiO_2 materials since they display lower packing density, i.e., around 0.5-0.8 g/cm^3.

The evolution of the capacity of TiO_2 brookite with increasing rates has been studied and is displayed in Figure IV- 19.

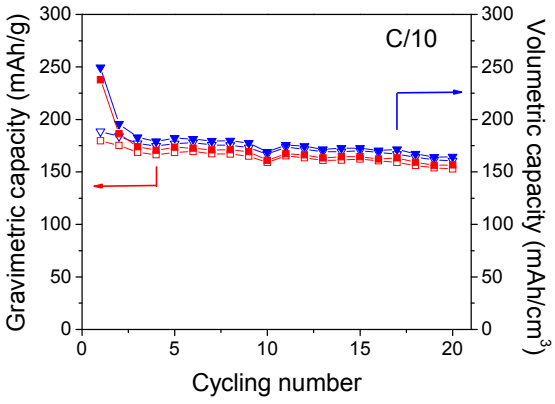

Figure IV- 18: Cycle-ability of TiO_2 brookite performed at C/10 (33.5 mA/g) as function of the gravimetric and volumetric capacity. Empty symbols refer to the charge; filled symbols, to the discharge.

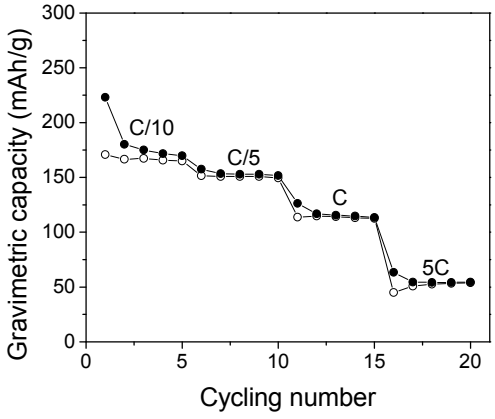

Figure IV- 19: Rate capability of TiO_2 brookite.

The TiO_2 brookite displayed a specific discharge capacity of 170 mAh/g, which was reduced to 152, 113, and 55 mAh/g at the C/5, C, and 5C rates, respectively. Such a decrease of capacity while increasing the current density can be ascribed to the insulating character of TiO_2-based materials. Nevertheless, there are several ways to improve the electronic conductivity of insulating materials, including the use of conductive additives such as carbonaceous-like phases, use of metal and metal oxide coatings, and or particle size reduction. Future work will focus on improving the rate capability of the TiO_2 material, as well as investigating other advanced high-capacity anodes.

Conclusions and Future Directions

Using a simple aqueous precipitation method based on a low-cost titanium oxysulfate precursor, three TiO_2 polymorphs have been prepared: anatase, rutile, and brookite. While the anatase form can be directly obtained from the thermolysis reaction of an oxysulfate solution, the rutile and the brookite have been prepared by the addition of oxalate species. Depending on the concentration, the oxalate anions have been shown to act either as a ligand with the stabilization of a titanium oxalate hydrate, $Ti_2O_3(H_2O)_2(C_2O_4)\bullet H_2O$, or as a chelating agent with the isolation of the rutile phase. The brookite form was obtained by thermal decomposition of the oxalate hydrate at a temperature as low as 300°C. The resulting solid consisted of nano-domains of TiO_2 brookite embedded in large micron-size particles and exhibited a high specific surface area of 255 m^2/g due to the mesoporosity arising from the removal of water from the oxalate species. This morphology is of interest for lithium-ion batteries because of an easier coating process and a higher surface contact between the electrode material and the electrolyte that enhances the electrochemical activity. Finally, based on electrochemical characterizations, TiO_2 brookite provided higher volumetric energy density than comparable nanomaterials.

The future plan for this work includes the following:

- Optimize the TiO_2 brookite morphology.
- Explore new synthesis route using a continuously stirred tank reactor that can provide higher packing density materials.
- Improve the capacity and the rate capability by means of doping and/or coating.
- From the synthesis, characterization, and electrochemical standpoints of these materials, evaluate their possible applicability in high-energy-density Li-ions batteries.
- Investigate other high capacity anodes with the aim to stabilize their reversible capacities.

FY 2009 Publications/Presentations

1. Poster to the DOE Annual Peer Review Meeting, Washington DC, May 18-22, 2009.
2. D. Dambournet, I. Belharouak, and K. Amine, "Nanosized TiO_2 Anatase, Rutile, and Brookite Anodes for Li-ion Batteries," presented at 215th Electrochemical Society Meeting, San Francisco, California, May 24-29, 2009.
3. D. Dambournet, I. Belharouak, and K. Amine, "Tailored Preparation Methods of TiO2 Anatase, Rutile, Brookite: Mechanism of Formation and Electrochemical Properties," Paper submitted to *Chemistry of Materials*.

IV.B.3.2 Develop Improved Methods of Making Inter-metallic Anodes (ANL)

Andrew N. Jansen
Argonne National Laboratory
9700 South Cass Avenue
Argonne, IL 60439-4837
Phone: (630) 252-4956; Fax: (630) 972-4461
E-mail: jansen@anl.gov

Collaborators:
Jack Vaughey, Argonne National Laboratory
Dileep Singh, Argonne National Laboratory
Dennis Dees, Argonne National Laboratory
Paul Nelson, Argonne National Laboratory
Nick Veselka, Argonne National Laboratory
Chris Joyce, Argonne National Laboratory

Start Date: October, 2008
Projected End Date: September, 2010

Objectives

- Make electrodes based on intermetallic alloys such as Cu_6Sn_5 using a wide selection of binders with a particular emphasis on binders that are able to accommodate relatively large volume expansions.
- Develop methods to determine and control the optimum particle size, composition, and morphology of Cu_6Sn_5 based intermetallic alloys.

Technical Barriers

Plug-in hybrid electric vehicles (PHEVs) need a high energy density battery to meet the 40 mile range target in 120 kg (80 L) battery size. Intermetallic alloys have the potential to be high capacity anode materials, but the following issues must be addressed

1. Low cycle life
2. Large volume expansion upon lithiation.

Technical Targets

- Determine the influence of binder on Cu_6Sn_5 cycle life.
- Explore methods of controlling particle size and morphology.
- Produce an intermetallic electrode with 200 cycles and 80% capacity retention.

Accomplishments

- Developed blending and coating process to make electrodes with varying thickness of Cu_6Sn_5 to establish baseline.
- Identified metals supplier to help in development of intermetallic alloys of varying particle size and morphology.
- Evaluated the influence of conductive and resistive additives to electrode powder mix in an attempt to minimize copper migration.
- Expanded Argonne's Battery Design Model to assess the benefit of using intermetallic alloys in PHEV batteries.
- Obtained numerous samples of electrode binders for binder optimization study.
- Initiated particle critical size investigation.

✧ ✧ ✧ ✧ ✧

Introduction

Previous work from the BATT program has shown that doped-Cu_6Sn_5 materials have reversible capacities similar to graphite. Their voltage profile (Figure IV- 20) is approximately 100 mV above graphite, which should enhance safety but not significantly affect energy. When their high material density is taken into account the volumetric capacities are nearly 3X that of an optimized graphite based electrode as can be seen in Figure IV- 21. This will enable the use of much thinner negative electrodes; resulting in smaller batteries for same energy.

Work on the Li_xSi system by 3M has shown that using binders more appropriate for the volume expansion of the Li_xSi system can greatly enhance cycle life. It is hoped that with proper binder selection and particle size and morphology Cu_6Sn_5–based materials will find success as lithium-ion anodes.

Approach

The general approach in this subtask will be to explore alternative methods of making electrodes based on intermetallic alloys such as Cu_6Sn_5. The goal is not necessarily to develop new classes of active materials but rather, to employ materials already being developed in the BATT Program.

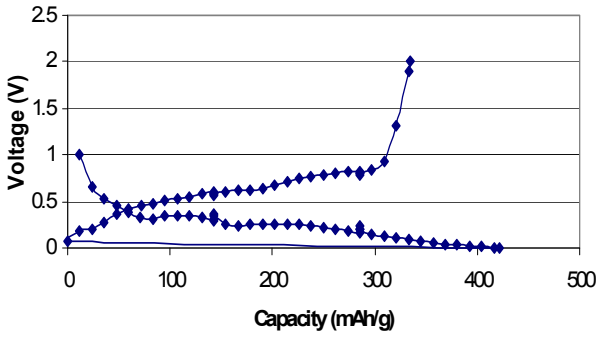

Figure IV- 20: Charge and discharge voltage profile of Cu_6Sn_5 versus lithium.

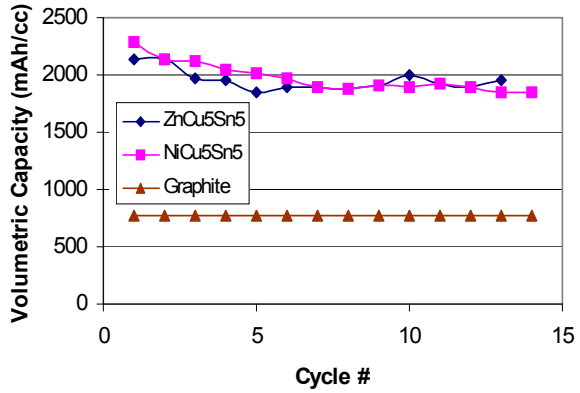

Figure IV- 21: Volumetric capacity density of Cu_6Sn_5-based intermetallic alloys compared against graphite.

Success will be achieved upon development of an electrode that can accommodate the large volume expansion and contraction during deep discharge cycling, and can prevent the excluded metal (such as copper) from agglomerating into an inert mass during cycling. Likely solutions to these problems will involve the proper choice of binders and methods of controlling the particle size and morphology during production, and during repeated cycling.

Results

Need for Elastic Binders. Binders and electrode recipes have been optimized for graphite, but little effort has been applied to intermetallic anode materials.

The typical binders used in anode systems were developed for graphite/carbon as the active material, which experience approximately 10% volume expansion upon lithiation, whereas intermetallic anodes and silicon anodes can experience a volume expansion that can be as high as 450% upon complete lithiation.

Certainly, part of the capacity fade of intermetallic anodes is related to the binder not holding the electrode together as the particle volume fluctuates between charge and discharge. Recent evidence in literature regarding silicon based anodes suggests that the binder is an important variable that must be optimized for these new anode systems.

Several classes of commercial binders have been identified and samples have been obtained for evaluation with a commercially prepared sample of Cu_6Sn_5 powder. The binders include PVDF-based polymers with functional groups tailored for anodes and cathodes over a range of molecular weights, and a few aqueous based binders.

Several methods of making electrode slurry were made including an initial step of dry blending the Cu_6Sn_5 powder with acetylene black carbon and SFG-6 graphite on a roller mill. Figure IV- 22 shows an SEM image of this dry blend. Note the Cu_6Sn_5 particle size of nearly 10 microns, which will be discussed in a later section.

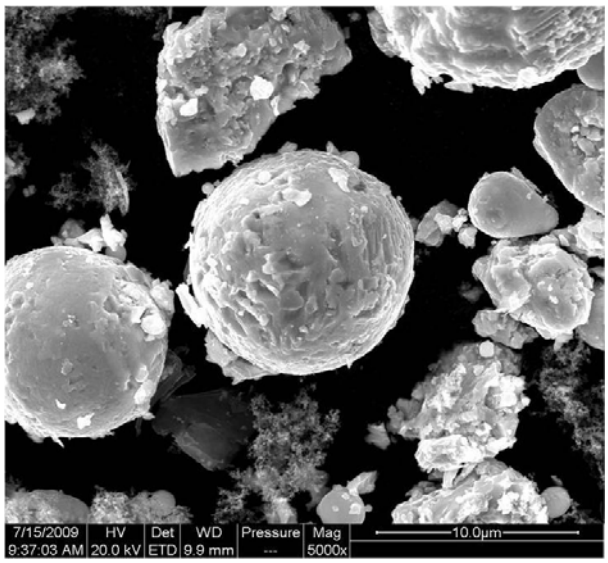

Figure IV- 22: SEM photo of Cu_6Sn_5 powder blended on roller mill with acetylene black carbon and SFG-6 graphite.

The results of this binder study are summarized in Figure IV- 23, where the cycle life of each binder electrode was determined from coin cells made with lithium counter electrodes in 1 M $LiPF_6$ in EC:EMC (3:7 w/w) and a cutoff voltage of 0.1 V on discharge (lithiation). The capacity of these electrodes ranged from 210 to 260 mAh/g, with the higher utilization occurring with binders based on PVDF tailored for anode use. Higher utilization can be obtained with a cutoff voltage of 0 V. As can be seen from these results, the choice of binder did not significantly affect the capacity loss rate of these electrodes. This result was not expected and a search was begun to determine the cause of this excessive capacity loss.

Inert Additives to Extend Life. The discharge mechanism for the $Li_xM_yCu_5Sn_5$ electrode materials can be

related to the $Na/NiCl_2$ and $LiAl/FeS_2$ battery systems. Previous electrode optimization work on these materials has identified the main culprit in capacity fade is due in part to diffusion of the displaced metal (Cu, Ni, Al) from the reaction center. By adding high surface area secondary components to the electrode, (e.g. MgO in LiAl and S in $NiCl_2$), this diffusion can be controlled resulting in significant enhancements in performance.

Earlier studies on the $FeCu_5Sn_5$ type electrode have highlighted a similar capacity fade mechanism. Recent work on the addition of extra tin to the electrode active material mix has shown some positive results. The extra tin may act as a sponge for the copper extruded that cannot make it back to the Li_2CuSn before the battery completes the following discharge.

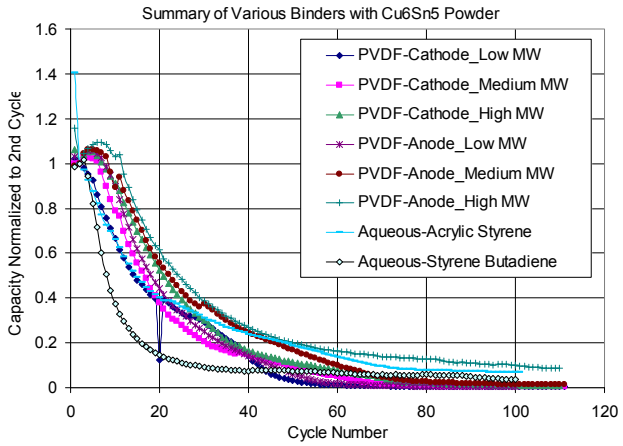

Figure IV- 23: Capacity loss rate for various binders with Cu_6Sn_5 with 4 wt.% acetylene black and 4 wt.% SFG-6 graphite. Capacity was normalized to 2nd cycle capacity.

A plan was initiated to study the controlled addition of inactive secondary phases to the electrode mix. It is hoped that this will help to prevent the metal diffusion (Cu and its substitutes) away from the active tin. Since Cu_6Sn_5-based electrode have such high volumetric capacities, additions of even 20% inert phases would still represent a significant enhancement in cell capacity.

Electrodes were made with Cu_6Sn_5 and acetylene black as the baseline mix, into which graphite, MgO or alumina powder was added. Cycle life studies were done with these electrodes and the results are presented in Figure IV- 24. It is clear that for this baseline Cu_6Sn_5 material, the addition of metal oxide additives to the bulk electrode does not appear to prevent capacity fade in these thick electrode designs. New electrode processing methods are being explored, but in light of this study and the binder study it appears that the baseline Cu_6Sn_5 material may not have the necessary properties for long cycle life. A new study was initiated to determine the appropriate particle size and is discussed in the next section.

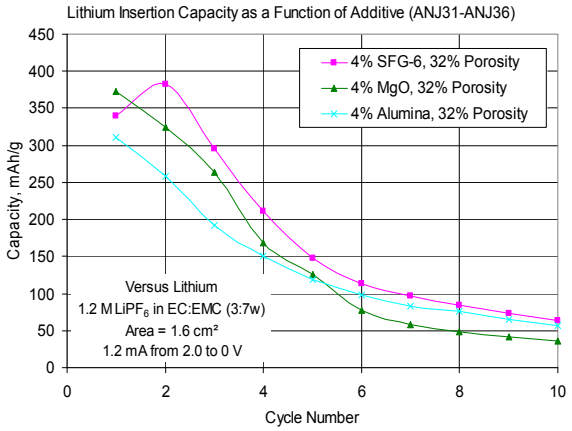

Figure IV- 24: Capacity loss rate for various binders with Cu_6Sn_5 with 4 wt.% acetylene black and 4 wt.% of either SFG-6 graphite, MgO, or alumina.

Volume Expansion Is a Concern. Full lithiation of Cu_6Sn_5 may not be practical due to the large volume expansion and contraction that occurs during electrochemical cycling. The unit cell volume was calculated for Cu_6Sn_5 and for its lithiated products, and is shown in the following Table IV-2. This volume expansion must be designed into the particle so that it does not crack upon repeated cycling.

Table IV-2: Unit Cell Volume calculated for Cu_6Sn_5 and its lithiated products

Phase	Unit Cell(s)	Volume of Unit Cell, Å³	Volume per Sn Atom, Å³
Cu_6Sn_5	$Cu_{24}Sn_{20}$	782	39.1
Li_2CuSn + Cu	$Li_8Cu_4Sn_4$ + 0.8Cu	245 +0.8(11.75)	63.6
$Li_{17}Sn_4$ + Cu	$Li_{340}Sn_{80}$ + 96Cu	7634 +96(11.75)	109.5

The modeling work of Huggins and Nix[27] provide some useful insight into the problem of Sn particle cracking upon lithiation. They developed a simplified model based on the modulus and fracture toughness of the bulk Sn material. The results of this model can be represented by the following equation:

$$h_c \approx \frac{23}{\pi}\left(\frac{3K_{Ic}}{Be_T}\right)^2$$

[27] R.A. Huggins and W.D. Nix, "Decrepitation Model For Capacity Loss During Cycling of Alloys in Rechargeable Electrochemical Systems", *Ionics* **6** (2000) p. 57-63.

where

h_c is critical size in μm
K_{Ic} is fracture toughness in MPa -m½
B is elastic modulus in GPa
e_T is strain dilation (ΔV/V)

From this model, Huggins suggests that an appropriate particle size for a pure tin electrode is on the order of 0.2 μm. This is nearly two orders of magnitude smaller than the 10 micron particle size used in this study to date. Smaller particle size Cu_6Sn_5 based intermetallic alloys are being sourced at present.

The mechanical properties of $Li_xM_yCu_5Sn_5$ electrode materials are not known in literature. Efforts were initiated in late FY09 to determine these properties for Cu_6Sn_5 and its alloys. This opens up a new approach to searching for optimal intermetallic anode materials. Find metallic and intermetallic alloys that are capable of being lithiated and then determine their bulk mechanical properties to determine a critical particle size. If the particle size is too small then try to increase the fracture toughness and decrease the elastic modulus of the metal anode material through alloying with additional metals and phases. This is the approach that will be explored in FY10.

Conclusions and Future Directions

It became clear in this year's effort that the commercially obtained Cu_6Sn_5 baseline material was not ideal for use in a lithium-ion battery. No binder or inert additive was found that could compensate for the large volume expansion that occurs upon lithiation. Repeated cycling caused the particle to crack and split into smaller particles that are no longer connected to the conductive electrode matrix. Modeling work in literature suggests that the particle cracking problem can be avoided by starting with a particle that is less than a critical size.

Work will continue on the subject of critical particle size based on Huggins' work. Alloys and their lithiated products will be casted and their mechanical properties will be evaluated using Universal Materials Testing Machine (Instron) tension testing for modulus and Single Edged Notched Bend (SENB) testing for fracture toughness, among other tests.

Samples of $Li_xM_yCu_5Sn_5$ powders will be either made in house or obtained from commercial vendors as a function of particle size to prove the results of Huggins' model as applied here. A high priority will be given to those alloys that have a high fracture toughness and low elastic modulus.

Lower level efforts will include a continued search for additives that promote copper (or metal species) retention at the particle level and electrode level, and a search for better binders with high adhesion to metals and high elasticity. A study on electrolyte additives to enhance SEI formation on intermetallic electrodes may be initiated.

FY 2009 Publications/Presentations

1. Poster presentation at the DOE Vehicles Technology Program 2009 Annual Merit Review Meeting.

IV.B.3.3 Lithium Metal Anodes (ANL)

John T. Vaughey

Chemical Sciences and Engineering Division
9700 S Cass Ave
Argonne National Laboratory
Lemont, IL 60439
Phone: (630) 252-8885
E-mail: vaughey@anl.gov

Collaborators :
Carmen M. Lopez
Dennis W. Dees

Start Date: October 1, 2007
Projected End Date: September 30, 2010

Objectives

- To overcome the well known problems with the metallic lithium electrode - stability, safety, and cycling efficiency - that continue to block its implementation into advanced lithium batteries for PHEVs.
- Characterize the morphological evolution of the lithium electrode on cycling
- Develop and characterize coating technologies that will withstand the lithium cell environment

Technical Barriers

This project addresses the following technical barriers from the Energy Storage section of the DOE Vehicle Technologies Program Multi-Year Research, Development and Demonstration Plan:

(A) 40 mile range for PHEVs

(B) Abuse tolerance

(C) Cell life

Technical Targets

- Synthesize, design and characterize polymer-alloy composite films deposited on the surface of a lithium electrode.
- Utilize characterization tools available at the National Electron Microscopy Center and Center for Nanoscale Materials to investigate the changes in morphology that occur on cycling for a lithium metal anode.
- Investigate new types of surface coatings with better surface adhesion.

Accomplishments

- Studied the morphological changes in the lithium electrode as a function of cycling rate and time. Identified three distinct types of lithium in a cycled electrode whose ratio varied with electrochemical history.
- Determined loss of electrolyte solvent to side reactions with the lithium metal was a key limiting cell lifetimes.
- Loss of direct contact by the lithium with the current collector was a major factor in a dramatic rise in cell impedance seen at end-of-life.
- Showed that early cycling history was a key element in formation of a stable surface film. Very slow charging rates allowed for gases formed during SEI formation to build up beneath the surface. Eventually these bubbles would pop, resulting in numerous nucleation points for dendrite growth and cell failure.
- Identified new conformal coating method for lithium metal based on a simple surface reaction involving the natural passivation layer of lithium metal.
- Various silane-coated materials were synthesized and shown to dramatically increase stability of the metal surface to the electrolyte. For coatings based on small chain silanes, no increase in resistance was observed (by EIS) for 2 weeks in an electrochemical cell versus a 6-fold increase for the control.

✧ ✧ ✧ ✧ ✧

Introduction

Achieving the DOE 40 mile range target for PHEVs will require several improvements in current lithium-ion battery technology. For studies involving anode materials, the focus has been on safety, the passivation (SEI) layer, and the effects of electrode nano-structuring. Whereas most studies have been done on carbon or other alternative anode materials, switching from a graphitic carbon anode to lithium metal would have many advantages. Notably 10X anode capacity, increased options for cathode materials, faster kinetics with no lithium diffusion would allow for a planar electrode geometry, and a factor of 4 reduction in coating volume. Historically however significant safety issues have limited the appeal of lithium in commercial cells. Previous work has identified poor electrodeposition characteristics and electrolyte instabilities as major causes of the safety issues.

Approach

To meet the DOE targets, we have undertaken a study of the lithium metal anodes in order to develop a better understanding of their failure mechanisms and to propose new solutions to make them a viable alternative to graphite for PHEV battery systems.

We are studying methods to establish a stable, dense, and uniform lithium/electrolyte interface exhibiting good electrochemical performance.

- Analyze the failure mechanism of various Li-metal electrode coatings previously postulated in the literature to be stable for various lengths of time.
- Develop conformal stable coatings using newly developed solution-based silane chemistry.
- Evaluate nanocomposite polymer/Li-ion conductor coatings to break the materials problem into its components.
- Use some of the latest microscopic and spectroscopic characterization equipment to characterize the lithium/electrolyte interface.

Results

Lithium Metal Coatings. Coating lithium metal has been a well studied approach to extending the life of the electrode. Early studies focused on electrolyte decomposition products and complex additives. Initial success in this research direction was found by Aurbach and co-workers who identified the electrolyte 1M $LiAsF_6$ in 1,3 dioxolane as viable. Systematic studies indicated that the active coating was in fact a composite of the Zintl phase Li_3As (from the salt) and a conductive PEO-like polymer derived from the solvent. The system fails at rates over C/2 owing to inadequate lithium-ion conduction resulting in a very porous lithium electrode. To build on this concept, we extensively studied a series of composites based on the fast Li-ion conductors Li_3Sb and $Li_{4.4}Sn$ co-deposited with vinyl ethylene carbonate (VEC) and vinyl carbonate (VC), common artificial SEI-formers employed in the battery industry. We identified several systems who were capable of cycling at rates in excess of 2C for extended times. At end-of-life (250-300 cycles) cells were disassembled and the lithium electrodes evaluated. Selected data is shown in Figure IV- 25. Common failure mechanisms included significant increases in resistance owing to electrolyte loss (solvent side-reactions), instability of the polymer (degradation) after extended periods in contact with lithium metal, and loss of effectiveness for the Zintl additive owing to SEI build-up. Figure IV- 26 shows before and after pictures of a lithium electrode coated with a $Li_{4.4}Sn$/VEC composite coating. Continued work on this class of coatings has focused on understanding the role of the lithium migration thru the coating and how the $Li_{4.4}Sn$ clusters effect dendrite nucleation and growth.

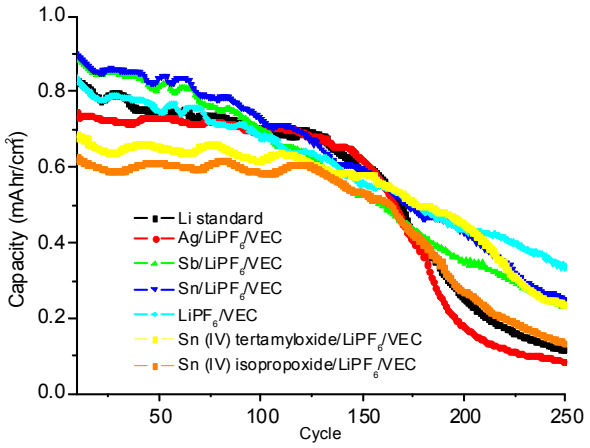

Figure IV- 25: Fast (2C) cycling of a lithium metal electrode coated with various Zintl-VEC composite coatings.

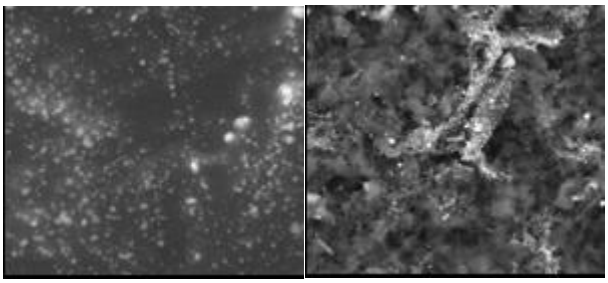

Figure IV- 26: Fate of a lithium metal electrode coated with $Li_{4.4}Sn$ -VEC composite coatings. Initial coating (left) shows good dispersion of nanoscale $Li_{4.4}Sn$ clusters within the VEC matrix. After 200 cycles (right) particles have moved away from lithium metal surface into dendritic layer, concentrating on the top of electrode.

Conformal Coatings. To better adhere the coating to the surface we have initiated studies utilizing atomic layer deposition (ALD)-type chemistry with simple silanes. In these studies we take advantage of the naturally hydroxlated surface of lithium metal and selectively react it with a small chain silane to produce a monolayer coverage of the desired material.

Preliminary studies of the coatings show them to be very stable in the battery environment and successful in protecting the lithium surface from electrolyte reactions. A series of EIS Spectra is shown in Figure IV- 27. A study on the stability of the coated materials shows, for small chain silanes, excellent long-term stability in a typical electrolyte environment with only small increases in resistance. For comparison, a clean Li electrode studied under the same conditions showed a 6-fold increase in impedance owing to electrolyte reactions.

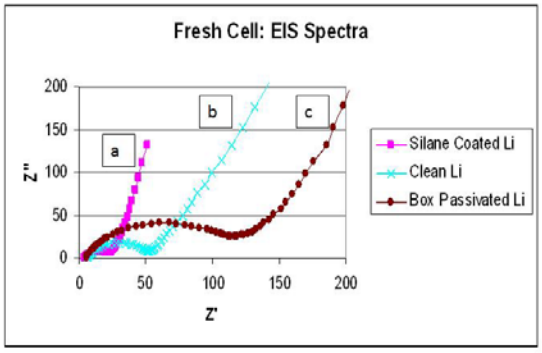

Figure IV- 27: Impedance spectra of lithium metal (a) silane-coated Li , (b) clean lithium, (c) lithium tested as received and passivated by the dry box atmosphere..

Morphological Studies. In 1996, EIS studies by Aurbach et al. had indicated that on cycling a lithium metal electrode developed several distinct layers. The structures or composition of the layers detected by EIS modeling were not within the scope of their publication. Because most structural analysis of lithium electrodes reported in the open literature is performed at cell death, we initiated a study to monitor the evolution of these layers and various electrochemical variables that influenced them. Initial studies centered on identifying the role of cycling rate on SEI formation. As lithium interacts with its electrolyte environment, it forms a passivation coating. However, it was not known how the evolution of this layer is affected by charging. We were able to show that at low rates, the layer was created before the electrode finished evolving gas. This resulted in surface bubbling and rapid surface degradation when the bubbles 'popped'. The material keeps growing macroscopically and uncontrollably until it breaches the separator, contacts the cathode and shorts the cell. Cell failure from shorting occurred as early as 25 cycles. No evidence of dendritic growth was detected under these conditions. A typical electrode is shown in Figure IV- 28.

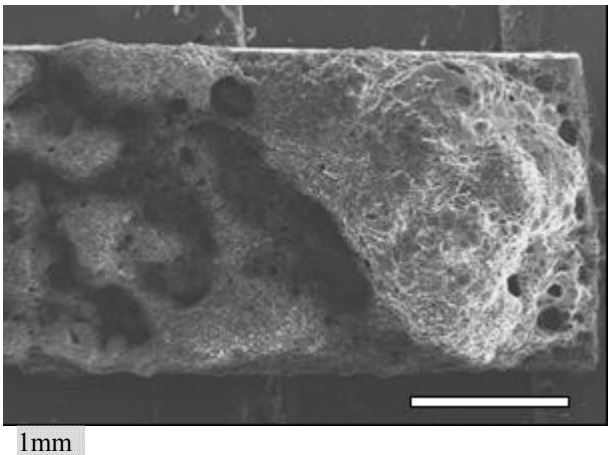

Figure IV- 28: SEM of the surface of a lithium metal electrode charged/discharged at a slow rate.

Additional cross sectional SEM studies of the electrode also enabled us to monitor the rate of growth of each layer as a function of cycle life. In these studies it can be shown (see Figure IV- 29) that the dendritic layer on the surface of the lithium metal electrode is very thin, consistently about 15 microns thick. The porous layer grows at a relatively constant rate and can be characterized by high surface area and high solvent reactivity. The base layer of dense lithium has the best connection to the current collector and upon its loss the cell typically fails. The low density lithium deposited during cycling appears to have some but small activity in the cell.

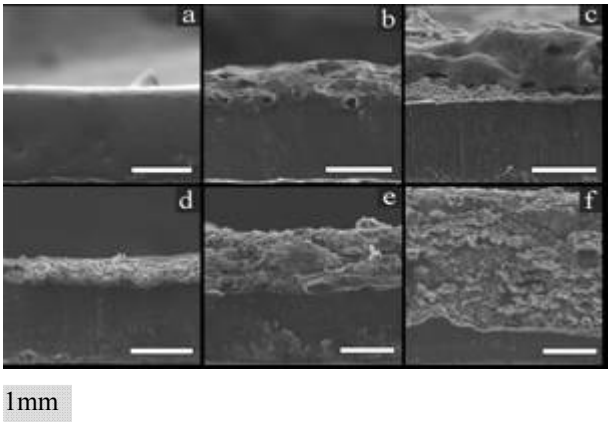

Figure IV- 29: SEM images (a) before cycling (with SEI layer), and (b) 2 cycles, (c) 10 cycles, (d) 50 cycles, (e) 125 cycles and, (f) 250 cycles. *The scale bars represent 100 microns.*

Cell failure can result owing to actions by any of the three layers – dendritic shorting in extreme cases, loss of solvent owing to reactions with the porous layer lithium, or loss of good contact with the current collector when the base lithium is depleted.

Conclusions and Future Directions

- Zintl metal / composite polymer coatings (Li_xM) form extend cycle life but a gradual impedance rise (polymer degradation) reduces rate capability while long-term stability is hindered by migration of Zintl layer at the rates utilized.
- Cycled lithium metal anodes have a complex morphology that lays at the heart of the lifetime problems. Dendritic lithium tends to form as a surface layer (~15 μm) on top of the metal anode on cycling with a porous lithium bulk.
- Gradual loss of *good* contact between the porous lithium anode and the current collector results in a large impedance rise and eventual cell failure.
- Continue studies of silane and related materials coatings on lithium metal surface. Conformal

coatings may have higher stability and extend cell lifetime.

- Continue studies of polymer/lithium-ion conductor nanocomposites and assess the relationship between their composition and cell lifetimes.

FY 2009 Publications/Presentations

Publications

1. Carmen M. Lopez, John T. Vaughey, Dennis Dees "Morphological Transitions on Lithium Metal Anodes" *J. Electrochem. Soc.*, *J. Electrochem. Soc.*, 156, A726 (2009)

Presentations

2. C. M. Lopez, J. T. Vaughey, D.W. Dees "Systematic Investigation of Morphological Transitions on Lithium Metal Anodes" 1st International Conference on Advanced Li-ion Batteries for Automotive Applications, Argonne, IL September 2008.
3. C. M. Lopez, J. T. Vaughey, D.W. Dees "Systematic Investigation of Morphological Transitions on Lithium Metal Anodes" Argonne National Laboratory Postdoctoral Research Symposium, Argonne, IL, September, 2008.
4. C. M. Lopez "Morphology-Property Relationships in Electrode Materials for Energy Generation and Storage" A123 Systems, October 2008.
5. C. M. Lopez "Morphology-Property Relationships in Electrode Materials for Energy Generation and Storage" Department of Chemistry and Biochemistry, University of Texas at Arlington, February 2009.
6. C. M. Lopez, J.T. Vaughey, D.W. Dees "Morphology-Performance Relationships in Metallic Lithium Anodes" 215th Meeting of the Electrochemical Society, San Francisco, CA, May, 2009.
7. J. T. Vaughey, C. M. Lopez, D. Dees "Lithium Metal Anodes" DOE Hydrogen Program and Vehicle Technologies Program Annual Merit Review, Washington, DC, May, 2009.

IV.B.3.4 New High Power $Li_2MTi_6O_{14}$ Anode Material (ANL)

Khalil Amine
Argonne National Laboratory
9700 South Cass Avenue
Argonne, Il 60439
Phone: (630) 252-3838; Fax: (630) 252-4176
E-mail: amine@anl.gov

Start Date: September 1, 2008
Projected End Date: September 30, 2010

Objectives

- Develop new anode materials that provide very high power capability and outstanding safety.
- Explore ways for preparing pure and nanosize $MLi_2Ti_6O_{14}$ (M= Sr or Ba) with high capacity.
- Investigate the applicability of $MLi_2Ti_6O_{14}$ as the anode for the Li-ion battery.

Technical Barriers

- Overcome the inherent safety issue of the graphite anode.
- Improve the power density of the battery.
- Increase the cycle and calendar life of the battery.

Technical Targets

- Develop safe and high-power anode materials based on the open-structure $MLi_2Ti_6O_{14}$. The operating voltage of these materials lies in the electrolyte stability window but is lower than that of the commercial $Li_4Ti_5O_{14}$ anode, providing safety and high-energy density.
- Develop a suitable electrode morphology to achieve high capacity.
- Demonstrate the life and safety of cells fabricated with $MLi_2Ti_6O_{14}$ anodes combined with high-potential cathodes.

Accomplishments

- Developed a sol-gel method to prepare pure $MLi_2Ti_6O_{14}$.
- Completed a comparative study of $MLi_2Ti_6O_{14}$ based on its structural and electrochemical characteristics.
- Developed a Sr-based $MLi_2Ti_6O_{14}$ electrode that exhibited high capacity and very promising rate capability.

✧ ✧ ✧ ✧ ✧

Introduction

Lithium-ion batteries are being considered to power a new generation of clean vehicles. Battery life span, cost, and safety are still major barriers. With regard to safety, the issues associated with the formation of the solid-electrolyte interface (SEI) at the graphitic electrode can be overcome through the development of alternative anodes that can operate within the electrochemical stability zone of conventional electrolytes. This region is generally known to be above the potential (~1 V) of SEI formation and below the potential (~4.3 V) of electrolyte oxidation. The voltage profiles of tetravalent titanium-based materials such as $LiTi_2(PO_4)_3$, TiO_2, and $Li_4Ti_5O_{14}$ fall within this region. Their operating voltages are 2.5, 1.7, and 1.5 V, respectively, vs. metallic lithium. These variations are primarily due to the difference of structures and the iono-covalent character of Ti-O bonds though the Ti^{4+}/Ti^{3+} redox couple. In general, it is possible to tailor the energy of a given electrochemical couple based on structural considerations and the chemical bonding involved. $MLi_2Ti_6O_{14}$ (M = Sr or Ba) compounds are new Li-ion insertion anodes that have shown lower operating voltage and lower resistivity compared to commercial $Li_4Ti_5O_{14}$. In general, the project aims to develop a high power anode for lithium-ion batteries, and $MLi_2Ti_6O_{14}$ (M = Sr, Ba) compounds have been chosen based on its above-mentioned properties.

Approach

Our approach is as follows:

- Develop a new synthesis route to prepare pure $MLi_2Ti_6O_{14}$.
- Demonstrate the reduced safety concerns and higher energy density expected with $MLi_2Ti_6O_{14}$ electrodes.
- Develop a conductive coating to improve conductivity and thus rate capability.

Results

We have synthesized $MLi_2Ti_6O_{14}$ by a sol-gel method. Lithium acetate hydrate, “M” acetate, and titanium isopropoxide were used as precursors and dissolved in a solution containing anhydrous ethanol and acetic acid. The formed gel was heated at 200°C overnight to complete the removal of the solvents. Finally, after grinding, the dry

gel was annealed at 900°C for 12 h under an air atmosphere. The X-ray patterns of the prepared $MLi_2Ti_6O_{14}$ materials are shown in Figure IV- 30 and indicate high phase purity. The $MLi_2Ti_6O_{14}$ structure is built upon edges and corners sharing TiO_6 octahedra, resulting in a three-dimensional network. The lithium atoms are located in tetrahedral sites, forming tunnels within the structure. The Sr and Ba atoms are located in 11-fold positions.

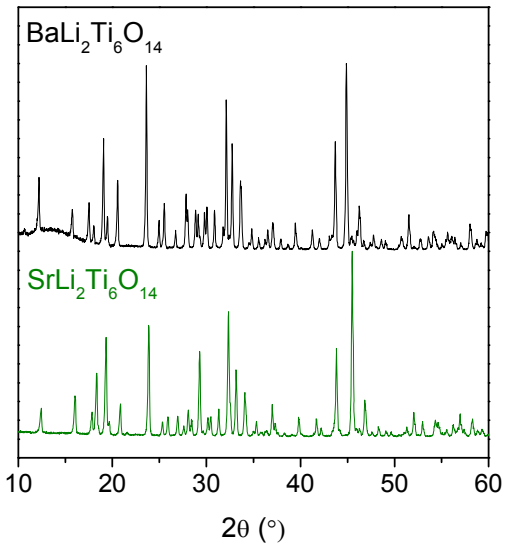

Figure IV- 30: X-ray diffraction powder patterns of $MLi_2Ti_6O_{14}$ prepared by sol-gel method.

Figure IV- 31 shows the cyclic voltammetry curves of the $MLi_2Ti_6O_{14}$ materials in the voltage range between 0.5 and 2 V under a similar scan rate. In all cases, the data demonstrate that the reduction process that occurs at the electrodes during the initial cathodic sweep is different from that of subsequent cycles. The observed peaks remain more or less constant starting from the second cathode sweep. The $SrLi_2Ti_6O_{14}$ and $BaLi_2Ti_6O_{14}$ materials exhibited two main cathodic peaks: for the former material, 1.31 and 1.0 V; and for the latter material, 1.27 and 1.07 V.

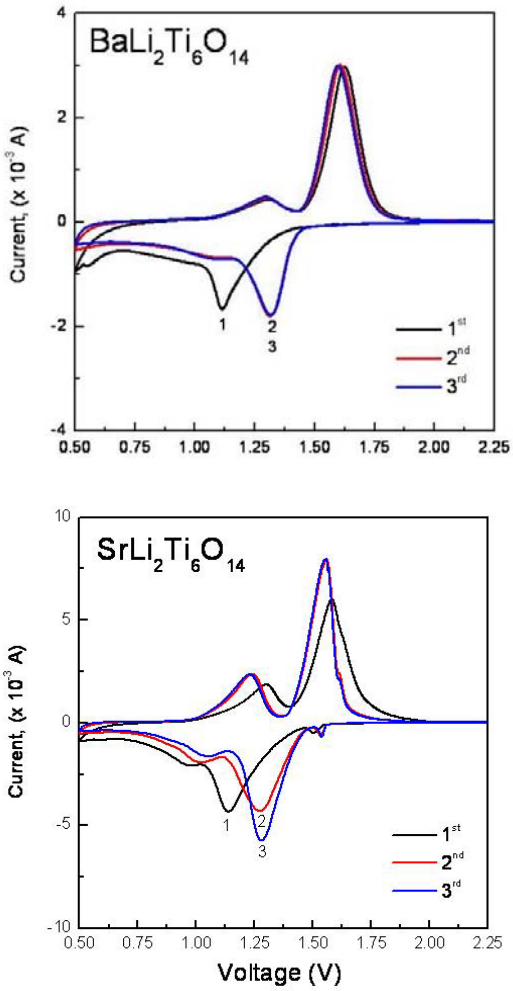

Figure IV- 31: Cyclic voltammograms of $MLi_2Ti_6O_{14}$ series performed at 0.5 mV/s for three cycles.

Figure IV- 32 shows typical voltage profiles of lithium cells with $MLi_2Ti_6O_{14}$ electrodes over 20 cycles. The discharge and charge curves were recorded between 0.5 and 2 V under the same gravimetric current density of 10 mA/g. The initial discharge capacities for the $SrLi_2Ti_6O_{14}$ and $BaLi_2Ti_6O_{14}$ electrodes were 145 and 118 mAh/g, respectively, which correspond to 3.3 and 2.9 Li-ion uptake (Figure IV- 32). The corresponding coulombic efficiencies were 85% and 79%. The voltage profiles and specific capacities at selected cycle numbers (1st, 2nd, and 20th) are also shown in Figure IV- 32. The capacity (75 mAh/g and 45 mAh/g, respectively) that arises from the first plateau at 1.4 V was stable with cycling. The capacity of the plateaus below 0.8 V was not reversible upon cycling. At the completion of the 20th cycle, the discharge capacities of the $SrLi_2Ti_6O_{14}$ and $BaLi_2Ti_6O_{14}$ electrodes were 115 and 88 mAh/g, respectively, which translate to 21% and 25% loss from the initial capacities.

Figure IV- 33 shows the cycling performance of $Li/MLi_2Ti_6O_{14}$ electrodes under discharge current of 10 mA/g. Both materials exhibited stable cycling.

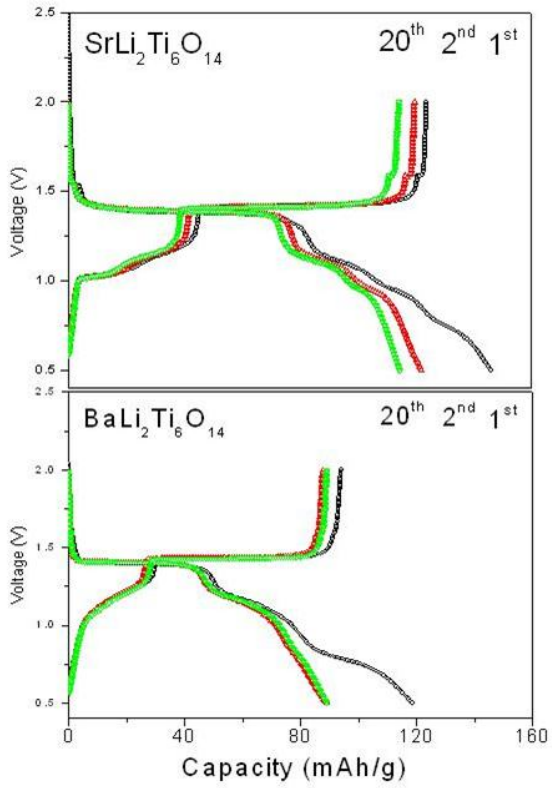

Figure IV- 32: Charge/discharge voltage profiles of $MLi_2Ti_6O_{14}$ cells cycled between 0.5 and 2 V under 10 mA/g.

Figure IV- 34 shows the rate capability of the Sr-based materials cycled under 100, 200, 400, and 800 mA/g. The Sr-based compound showed very promising rate capability performance: 92 mAh/g within 15 minutes, *i.e.*, 800 mA/g.

Conclusions and Future Directions

Open-structure $MLi_2Ti_6O_{14}$ (M = Sr or Ba) materials have been synthesized by a sol-gel method. The initial discharge capacities obtained for $SrLi_2Ti_6O_{14}$ and $BaLi_2Ti_6O_{14}$ were 145 and 118 mAh/g, respectively. The corresponding coulombic efficiencies were 85% and 79%. The two compounds showed stable cycle life. Finally, $SrLi_2Ti_6O_{14}$ exhibited promising rate capability.

The future plan for this work includes the following:

- Improve the capacity and the rate capability by means of doping and/or coating the electrode material.
- Investigate the stability of the electrode materials by conducting aging tests.
- Explore new synthesis route to reduce the electrode particle size.
- Investigate the cycle life, calendar life, and safety of the cell based on this anode.

Publications/Presentations

1. Poster to the DOE Annual Peer Review Meeting, Washington DC, May 18-22, 2009.
2. D. Dambournet, I. Belharouak, and K. Amine, "$MLi_2Ti_6O_{14}$ Lithium Insertion Materials: A Comparative Study," paper to be submitted to *Journal of the Electrochemical Society*.

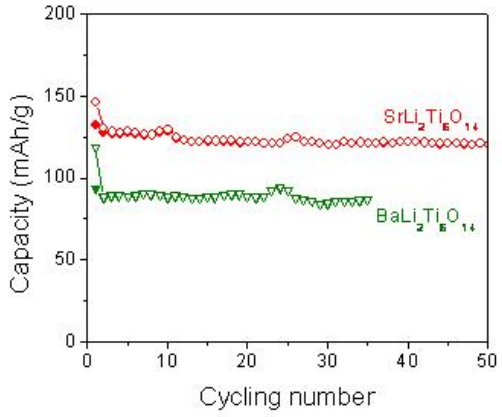

Figure IV- 33: Cycle-ability of $MLi_2Ti_6O_{14}$ performed at 0.5-2 V under 10 mA/g.

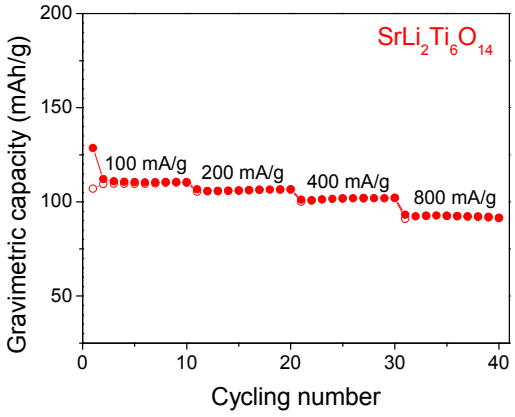

Figure IV- 34: Rate capability of $SrLi_2Ti_6O_{14}$ performed at 0.5-2 V.

IV.B.4 Applied Battery Research on Cathodes

IV.B.4.1 Engineering of High Energy Cathode Material (ANL)

Khalil Amine
Argonne National Laboratory
9700 South Cass Avenue
Argonne, Il 60439
Phone: (630) 252-3838; Fax: (630) 252-4176
E-mail: amine@anl.gov

Start Date: September 1, 2008
Projected End Date: September 30, 2010

Objectives

- Enable the Argonne high energy composite layered cathode $xLi_2MnO_3 \bullet (1-x)LiNiO_2$ for 40 miles PHEV
- Optimize suitable composition and engineer the material to improve its packing density and rate capability for PHEV applications
- Explore surface protection to enable high capacity and long cycle life at high voltage (4.6V)

Technical Barriers

- Poor continuous charge and discharge rate capability
- High electrode impedance
- Low pulse power
- Low packing density which translate to low volumetric energy density
- High reactivity with the electrolyte at high voltage

Technical Targets

- Improve the rate capability. Our target is to increase the rate capability from C/10 to 1C ~ 2C.
- Improve the tap density of the material to 2~2.4g/cc
- Stabilize the surface of the particles to significantly improve the calendar and cycle life of the material

Accomplishments

- Developed a carbonate based co-precipitation process that provides spherical particle morphology.
- Optimized the carbonate based co-precipitation process to obtain high packing density cathode materials.
- Optimized composition to provide high energy, high packing density and 1C rate capability

✧ ✧ ✧ ✧ ✧

Introduction

To meet the high-energy requirement of 40-miles electric drive P-HEV, it is necessary to develop very high energy cathodes and anodes that offer 5,000 charge-depleting cycles, 15 years calendar life as well as excellent abuse tolerance. These challenging requirements make it difficult for conventional cathode materials to be adopted in P-HEVs. Here, we report on very high energy cathodes based on layered lithium rich nickel manganese oxide composites as potential cathode candidates for PHEV and EV applications. This material exhibits over 200mAh/g capacity, relatively good stability and improved safety characteristics.

Approach

- Develop a process that leads to very dense material to increase the electrode density and therefore the electrode capacity.
- Investigate ways of obtaining spherical particle with high homogeneity.
- Investigate the nano-coating of the material with metal fluoride, phosphate and oxide to reduce the initial interfacial impedance and stabilize the cathode interface in order to improve the cycle life at elevated temperature.
- Investigate the effect of making 3 micron secondary particle and 50 nm secondary particles that are distributed in dense configuration (limited pores) on the rate capability of the material.
- Investigate new ways of coating oxides with carbon to improve conductivity of the material.

Results

Improving the packing density of high energy composite electrode. In the initial stage, and in order to prepare a pure phase of high energy composite electrode, we used a sol-gel process where the mixing of the different precursors was done at the molecular level using ionized water as solvent. The resulting material after gellation and calcinations at high temperature shows a highly pure material with capacities at C/5 of 250mAh/g. However,

this material exhibits very high surface area of 32m^2/g and very low packing density of 0.8g/cc. As a result the volumetric energy density of the material was very low. In order to increase the packing density of the material, we developed and patented a new carbonate based co-precipitation using a continuous stirring reactor to prepare the carbonate precursors first. Figure IV- 35 shows a schematic set up of the reactor. The Mn, Co, and Ni sulfate solution were pumped to the reactor. The pH of the solution was controlled by adding ammonia and the co-precipitation took place when adding $NaCO_3$. After the seeding process the precursor that was recovered in a continuous way from the reactor, was filtered, washed and dried. The precursor was then mixed with Li_2CO_3 and calcined at 900°C to form a final high energy composite electrode. The materials made from process shows packing density of 1.8 to 2.1g/cc.

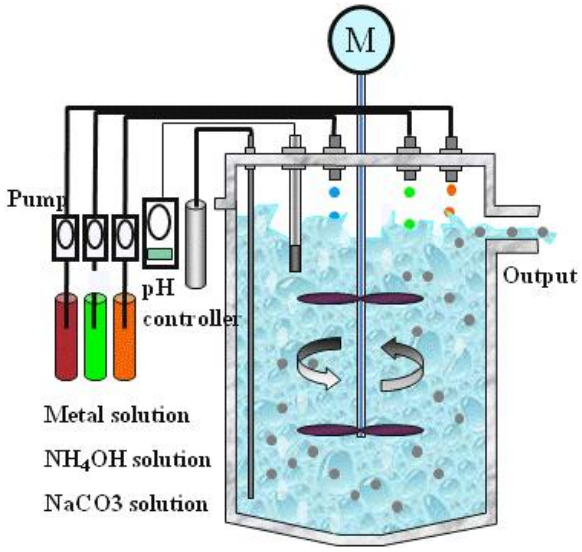

Figure IV- 35: Continuous stirring reactor used to make Ni-Mn-Co-carbonate precursors.

Improving the rate capability of the High Energy Composite cathode. To improve the rate capability of the composite electrode, we targeted the preparation of a material that had a micron size spherical morphology that incorporate nano-phased primary particles for fast lithium diffusion and thus improved rate capability. For this purpose, we synthesized several composite electrode compositions with different lithium excess and investigated the role of lithium excess on particle morphology and power capability. Several excess lithium $Li_{(1+x)}Ni_{0.25}Mn_{0.75}O_{(2.25+x/2)}$ composite materials with ($0.32 \le x \le 0.65$) using a $Ni_{0.25}Mn_{0.75}CO_3$ carbonate precursor prepared via a coprecipitation method in a continuous stirred tank reactor.

Figure IV- 36 shows the XRD patterns of the lithiated $Li_{(1+x)}Ni_{0.25}Mn_{0.75}O_{(2.25+x/2)}$ compounds:

(a) $Li_{1.32}Ni_{0.25}Mn_{0.75}O_{2.41}$,

(b) $Li_{1.375}Ni_{0.25}Mn_{0.75}O_{2.4375}$,

(c) $Li_{1.5}Ni_{0.25}Mn_{0.75}O_{2.5}$,

(d) $Li_{1.575}Ni_{0.25}Mn_{0.75}O_{2.5375}$, and

(e) $Li_{1.65}Ni_{0.25}Mn_{0.75}O_{2.575}$.

Note that these notations have been somewhat simplified in the literature in order to reflect a specific structural order. For instance, a material such as $Li_{1.5}Ni_{0.25}Mn_{0.75}O_{2.5}$ (spectrum c) could be written as $Li_{1.2}Ni_{0.2}Mn_{0.6}O_2$ by dividing by a factor of 1.25 to reflect the notation $Li(Li_{0.2}Ni_{0.2}Mn_{0.6})O_2$ that is consistent with the structural order of the layered α-$NaFeO_2$ ($R\bar{3}m$). An advanced notation has been widely adopted to reflect the structural complexity and the composite character of these materials. For example, $Li_{1.5}Ni_{0.25}Mn_{0.75}O_{2.5}$ could be written as $[1/2Li_2MnO_3 \cdot 1/2LiNi_{0.5}Mn_{0.5}O_2]$ to show that two layered components (*C2/m* and $R\bar{3}m$) can be structurally integrated to form a composite compound.

Figure IV- 37 shows SEM images of the lithiated samples a-e. The, primary particles that construct the secondary particles underwent significant size change after lithiation, namely, from around 80 nm (sample a) to around 200-500 nm for samples with the highest lithium content (d and e). The images also show that the primary particles that compose the surface of samples a and b form a much denser and smoother surface than that of the other samples, with much more pronounced roughness for the samples containing higher lithium concentrations (Figure IV- 37d and Figure IV- 37e). These morphological observations were accompanied by a gradual drop of the packing density from the highest value of 2.1 gcm^{-3} (samples a and b) to the lowest value of 1.7 gcm^{-3} (samples d and e). The lower the lithium content, the smaller the primary particles and the higher the compact ability.

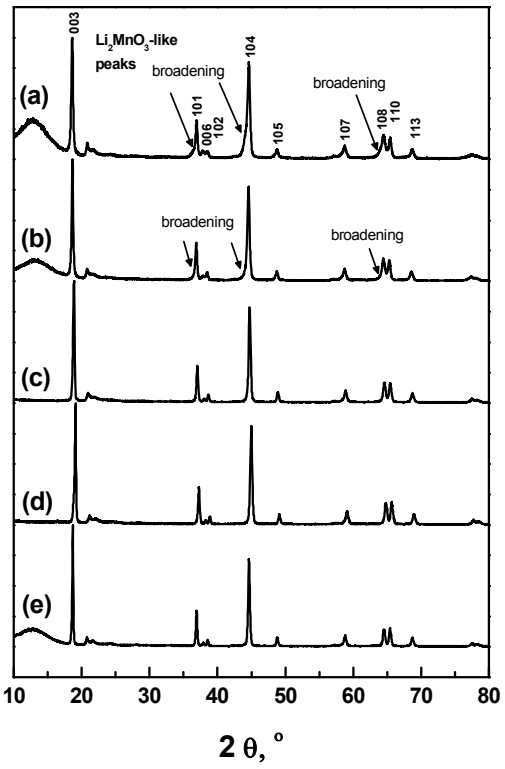

Figure IV- 36: XRD patterns of $Li_{1.32}Ni_{0.25}Mn_{0.75}O_{2.41}$ (a), $Li_{1.375}Ni_{0.25}Mn_{0.75}O_{2.4375}$ (b), $Li_{1.5}Ni_{0.25}Mn_{0.75}O_{2.5}$ (c), $Li_{1.575}Ni_{0.25}Mn_{0.75}O_{2.5375}$ (d), $Li_{1.65}Ni_{0.25}Mn_{0.75}O_{2.575}$ (e)

Figure IV- 38 shows the voltage profiles of cells constructed with cathodes of samples a-e. The cells were galvanostatically charged and discharged according to the following procedure: initial charge from the open-circuit voltage to 4.9 V and then discharge to 2 V under a 23 $mA.g^{-1}$ current density (first cycle); further charge and discharge between 2 and 4.6 V for three cycles under the same current density (cycles 2 to 4); and within the same voltage window, cycle three times while doubling the current density to 46 $mA.g^{-1}$ (cycles 5 to 7), which was repeated until the current density reached 230 $mA.g^{-1}$ or ten times the initial value (cycles 11 to 13). Note that we prefer to use the mass current density instead of C-rate because of the confusion that the latter can create between researchers.

Among all studied materials, the electrochemistry of cathodes with samples a and b has unique characteristics. First, cells with these cathodes showed the largest charge and discharge capacities under all rates, with sample b delivering the highest discharge capacity under 230 $mA.g^{-1}$ current density (Figure IV- 38a and Figure IV- 38b). Indeed, its 210 $mAh.g^{-1}$ capacity is, to the best of our knowledge, the highest achieved discharge capacity under such a high current density for an advanced composite cathode material, in addition to the benefit of being cobalt free.

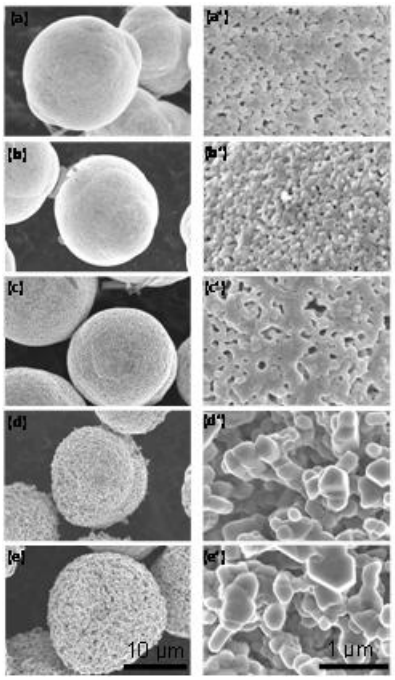

Figure IV- 37: SEM images (left side: secondary particles; right side: primary particles) of $Li_{1.32}Ni_{0.25}Mn_{0.75}O_{2.41}$ (a), $Li_{1.375}Ni_{0.25}Mn_{0.75}O_{2.4375}$ (b), $Li_{1.5}Ni_{0.25}Mn_{0.75}O_{2.5}$ (c), $Li_{1.575}Ni_{0.25}Mn_{0.75}O_{2.5375}$ (d), $Li_{1.65}Ni_{0.25}Mn_{0.75}O_{2.575}$ (e).

Figure IV- 39 shows the cycling performance of the nano-sized structured $Li_{1.375}Ni_{0.25}Mn_{0.75}O_{2.4375}$ (sample b) in a cathode-limited cell configuration with $Li_4Ti_5O_{12}$ as the negative electrode. In this case, $Li_4Ti_5O_{12}$ was selected as the anode to eliminate the possibility of cycle life fade that could arise from the use of metallic lithium or graphite. The $Li_4Ti_5O_{12}/Li_{1.375}Ni_{0.25}Mn_{0.75}O_{2.4375}$ cell was cycled between 0.5 and 3.1 V under a current density of 73 $mA.g^{-1}$. The cell showed excellent cycling performance and more than 220 $mAh.g^{-1}$ capacity for at least 200 cycles with very high efficiency.

We also investigated the safety characteristics of the $Li_{1.375}Ni_{0.25}Mn_{0.75}O_{2.4375}$ material. The DSC results are given in Figure IV- 40. In the presence of 1.2M $LiPF_6$-EC-EMC electrolyte, the charged material exhibited a single exothermal peak with an onset temperature of 275°C. The total amount of heat generated during the thermal decomposition of the material was 830 Jg^{-1}. The high onset temperature and low heat associated with the electrolyte and charged $Li_{1.375-x}Ni_{0.25}Mn_{0.75}O_{2.4375}$ clearly confirm that this material has suitable thermal stability for practical cell utilization, especially for PHEVs and EVs.

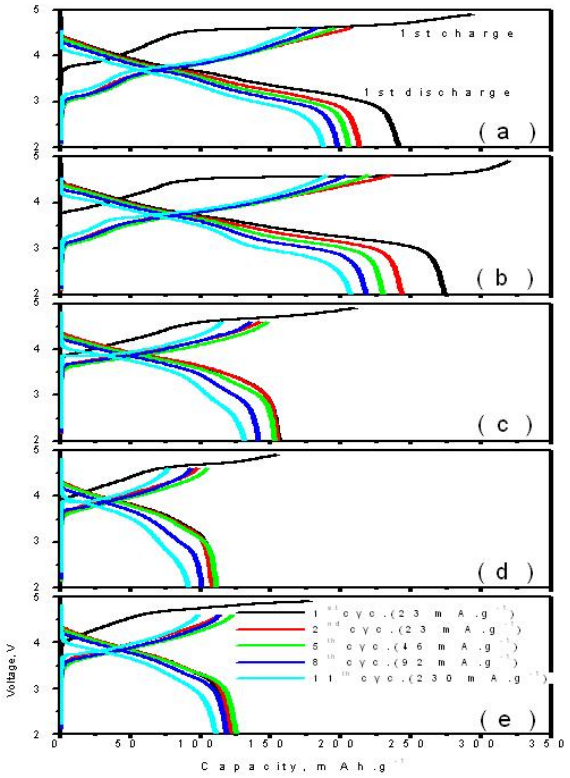

Figure IV- 38: Voltage profiles (left side) at increased current rates of $Li_{1.32}Ni_{0.25}Mn_{0.75}O_{2.41}$ (a), $Li_{1.375}Ni_{0.25}Mn_{0.75}O_{2.4375}$ (b), $Li_{1.5}Ni_{0.25}Mn_{0.75}O_{2.5}$ (c), $Li_{1.575}Ni_{0.25}Mn_{0.75}O_{2.5375}$ (d), $Li_{1.65}Ni_{0.25}Mn_{0.75}O_{2.575}$ (e); corresponding differential capacities vs. voltage.

FY 2009 Publications

1. H. Deng, I. Belharouak, Y.K. Sun, and K. Amine, **J. Mater. Chem.,** 19 (26), 4510-4516, 2009.
2. J.-H. Lim,H. Bang,K.-S. Lee,K. Amine and Y.-K. Sun, Electrochemical characterization of Li_2MnO_3-, ***Journal of Power Sources***, 189 (1): 571-575 (**2009**)
3. H. Park; S. H. Kang; I. Belharouak; Y. K. Sun and K. Amine, Journal of Power Sources, 2008, 177 (1): 177-183.
4. H. B. Kim; B. C. Park; S. T. Myung; K. Amine; J. Prakash and Y. K. Sun, **Journal of Power Sources**, 2008, 179 (1): 347-350.
5. H. Deng, I. Belharouak, H. Wu, R. Cook, Y-K. Sun, and K. Amine, **J. Amer. Chem. Soc**., Peer Review, 2009.

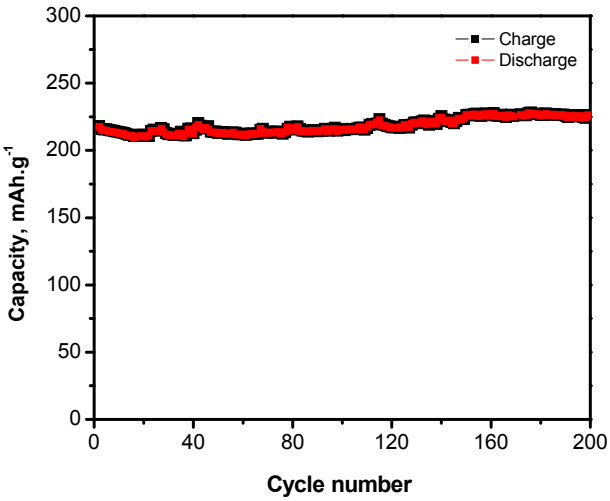

Figure IV- 39: Cycling performance of $Li_4Ti_5O_{12}$/ $Li_{1.375}Ni_{0.25}Mn_{0.75}O_{2.4375}$ (sample b) cell under 73 $mA.g^{-1}$ current density.

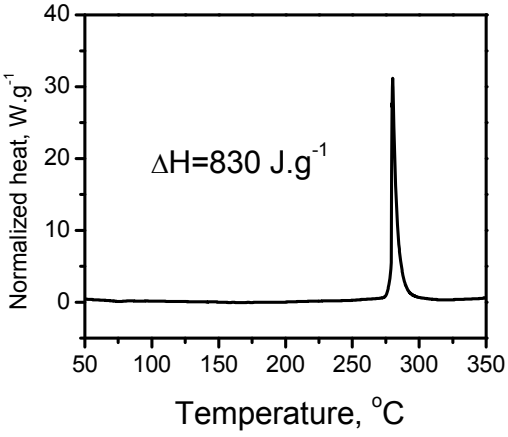

Figure IV- 40: DSC curve of $Li_{1.375}Ni_{0.25}Mn_{0.75}O_{2.4375}$ (sample b) in the presence of 1.2M $LiPF_6$-EC-EMC electrolyte

IV.B.4.2 Developing New High Energy Gradient Concentration Cathode Material (ANL)

Khalil Amine
Argonne National Laboratory
9700 South Cass Avenue
Argonne, IL 60439
Phone: (630) 252-6551; Fax: (630) 972-4451
E-mail: amine@anl.gov

Start Date: October 1, 2008
Projected End Date: September 30, 2014

Objectives

Develop a new high energy cathode material for PHEV applications that provides:

- Over 200mAh/g capacity
- Good rate capability
- Excellent cycle and calendar life
- Good abuse tolerance

Technical Barriers

(A) 15 years calendar life
(B) 5000 cycle life
(C) High cost
(D) Poor safety

Technical Targets

- Develop a cathode that offers over 200mAh/g with very high rate capability, good cycle life and improved safety
- Develop a process that make spherical and uniform particles with high packing density and high homogeneity
- Stabilize the surface of the particles to significantly improve the calendar and cycle life of the material

Accomplishments

- Developed a co-precipitation process that provides small quantities of a high energy gradient concentration precursor and cathode material.
- Characterized the material and demonstrate that the material has a gradient concentration with changing concentration of Ni, Mn and Co within each particle.
- Demonstrated that the gradient concentration cathode material provides high capacity

✧ ✧ ✧ ✧ ✧

Introduction

Layered lithium nickel-rich oxides, $Li[Ni_{1-x}M_x]O_2$ (M = metal), have attracted significant interest as the cathode material for rechargeable lithium batteries due to their high capacity, excellent rate capability, and low cost. However, their low thermal-abuse tolerance and poor cycle life, especially at elevated temperature, prohibit their use in practical batteries. Here, we report on a new concentration-gradient cathode material for rechargeable lithium batteries based on a layered lithium nickel cobalt manganese oxide. In this material, each particle has a central bulk that is rich in nickel and a manganese-rich outer layer with decreasing Ni concentration and increasing Mn and Co concentrations as the surface is approached. The former provides high capacity, while the latter improves the thermal stability.

Approach

- Develop a novel high-capacity and safe cathode material, in which each particle consists of bulk material $Li[Ni_{0.8}Co_{0.1}Mn_{0.1}]O_2$, that provide over 200mAh/g capacity, surrounded by a concentration-gradient outer layer where nickel ions are gradually replaced with manganese ions to provide outstanding cycle life and safety. The resulting surface composition is $Li[Ni_{0.46}Co_{0.23}Mn_{0.31}]O_2$, which is much more stable in contact with the electrolyte than is the bulk composition.
- Investigate ways of obtaining spherical particle with high homogeneity.
- Investigating the nano-coating of the material with metal fluoride, phosphate and oxide to reduce the initial interfacial impedance and stabilize the cathode interface in order to improve the cycle life at elevated temperature.

Results

Here, we report on a novel high-capacity and safe cathode material with an average composition of $Li[Ni_{0.68}Co_{0.18}Mn_{0.18}]O_2$, in which each particle consists of bulk material surrounded by a concentration-gradient outer layer. As illustrated in Figure IV- 41, the bulk is a nickel-rich layered oxide ($Li[Ni_{0.8}Co_{0.1}Mn_{0.1}]O_2$) to satisfy the

high energy and power requirement for P-HEVs. In the outer layer, the reactive Ni ions are gradually replaced with Mn ions to provide outstanding cycle life and safety. The resulting surface composition is $Li[Ni_{0.46}Co_{0.23}Mn_{0.31}]O_2$, which is much more stable in contact with the electrolyte than the bulk composition.

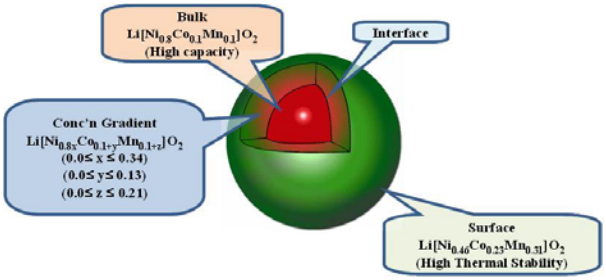

Figure IV- 41: Schematic representation of gradient concentration cathode material

We prepared cathode materials composed of these particles by a newly developed co-precipitation method involving the precipitation of hydroxide particles from solutions of varying Ni:Mn:Co ratios. Spherical $Li[Ni_{0.8}Co_{0.1}Mn_{0.1}]O_2$ particles were also synthesized by the co-precipitation process for comparison. The total average chemical composition of the concentration-gradient particle was determined by atomic absorption spectroscopy (AAS) to be $Li[Ni_{0.64}Co_{0.18}Mn_{0.18}]O_2$. The lattice parameters for the compound determined from X-ray diffraction data are a = 2.871(2) Å and c = 14.247(3) Å, with the values slightly lower than those of $Li[Ni_{0.8}Co_{0.1}Mn_{0.1}]O_2$ [a = 2.879(2) Å and c = 14.262(3) Å].

To determine the local composition in the bulk and at the surface, and to track the compositional change within the particles of the synthesized material, we performed electron-probe X-ray micro-analysis (EPMA) and scanning electron microscopy (SEM) on both the precursor hydroxide and the final lithiated oxide with a concentration gradient, as shown in Figure IV- 42. The diameter of the spherical hydroxide particle is about 14 µm (Figure IV-42a); its Ni-rich central bulk occupies about 10 µm. As can be deduced from Figure IV- 42b, the concentrations of the transition metal elements (Ni, Co, and Mn) for the hydroxide remained almost constant, $[Ni_{0.8}Co_{0.1}Mn_{0.1}](OH)_2$, from the center to 5 µm toward the interface; after this point, the Ni concentration decreased abruptly from 80% to 40% toward the surface of the particle, while the Co and Mn concentrations increased from 10% each to approximately 30%, resulting in a surface composition of $[Ni_{0.40}Co_{0.29}Mn_{0.31}](OH)_2$.

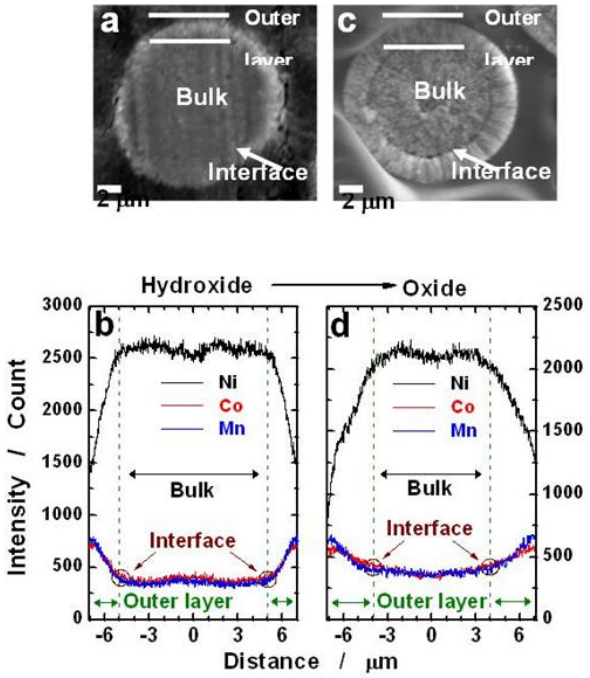

Figure IV- 42: Scanning electron microscopy (SEM) and electron-probe X-ray micro-analysis (EPMA) results; (a) SEM photograph and (b) EPMA line scan of precursor hydroxide; (c) SEM photograph and (d) EPMA line scan of the final lithiated oxide $Li[Ni_{0.64}Co_{0.18}Mn_{0.18}]O_2$. In both cases, the gradual-concentration changes of Ni, Mn, and Co in the interlayer are clearly evident. The nickel concentration decreases and the Co and Mn concentrations increase toward the surface.

After the lithiation at high temperature, the particle diameter was still 14 µm; however, the Ni-rich bulk shrank and the outer layer expanded, as shown by Figure IV- 42c. This change occurred because of the inter-diffusion of Ni, Co, and Mn during the calcination at the interface between the bulk and the outer layer. As can be deduced from Figure IV- 42d, the Ni, Co, and Mn concentrations remained nearly constant from the center to 4 µm toward the interface. After that point, the Ni concentration decreased gradually from 80% to 56% at the bulk/outer layer interface, while the Co and Mn concentrations increased from 10% to approximately 22% each at the interface. Between the interface and the surface of the particle, the Ni concentration continued to decrease while the Co and Mn concentrations increased. Because of the inter-diffusion of the metal ions, the steepness of this concentration change is less sharp than in the case of the precursor hydroxide (compare Figure IV- 42b and Figure IV- 42d). The composition at the surface of the particles appeared to be $Li[Ni_{0.46}Co_{0.23}Mn_{0.31}]O_2$ according to the EPMA. As per our design, the intentionally induced Ni, Co, and Mn concentration difference in the hydroxide precursor resulted in a final lithiated oxide with a concentration-gradient that started at the interface and continued toward the surface of the particle.

We characterized the battery performance by comparison of the $Li[Ni_{0.8}Co_{0.1}Mn_{0.1}]O_2$ and the concentration-gradient cathode materials. As seen in Figure IV- 43a, the $Li[Ni_{0.8}Co_{0.1}Mn_{0.1}]O_2$ material delivered a discharge capacity of approximately 212 mAh $(g\text{-oxide})^{-1}$. A slight decrease in capacity (209 mAh g^{-1}) was observed for the concentration-gradient material. To assess the stability of our new material, we selected an aggressive test profile where the cells were charged up to 4.4 V and cycled at 55°C (Figure IV- 43b). Both cells based on $Li[Ni_{0.8}Co_{0.1}Mn_{0.1}]O_2$ and our concentration-gradient material show high initial capacity of approximately 209 mAh g^{-1}, which could meet the energy requirement needed for P-HEVs. However, the cell based on the bulk $Li[Ni_{0.8}Co_{0.1}Mn_{0.1}]O_2$ composition retained only 67% of its initial capacity after 50 cycles, while our material showed excellent capacity retention of 96% during the same cycling period, which is similar to the cell based on the surface-composition only $Li[Ni_{0.46}Co_{0.23}Mn_{0.31}]O_2$. This result clearly indicates that our cathode material can provide high capacity with long cycle and calendar life even at high temperature and high cut-off voltage.

Figure IV- 43c shows the capacity retention of the $Li[Ni_{0.8}Co_{0.1}Mn_{0.1}]O_2$ and our concentration-gradient material using Al-pouch full cell with graphite as negative electrode. While the cell based on $Li[Ni_{0.8}Co_{0.1}Mn_{0.1}]O_2$ retained only 80.4% of its initial value after 500 cycles, our concentration-gradient material showed much higher capacity retention of over 96.5%. The poor cycling performance of $Li[Ni_{0.8}Co_{0.1}Mn_{0.1}]O_2$ could originate from a structural transformation at the particle surface because of the high reactivity of the Ni ions with the electrolyte, which, in turn, could increase the charge-transfer resistance between the cathode and the electrolyte upon cycling (5, 18-21). By reducing the Ni concentration and increasing the Mn concentration in the outer layer, we were able to stabilize the near surface region of the material and thus limit its reactivity with the electrolyte. Also, the concentration-gradient within the particle prevents the formation of micro-cracks and the segregation that can occur at the interface between the bulk and the outer layer, especially if there is a sharp variation of the composition at that point.

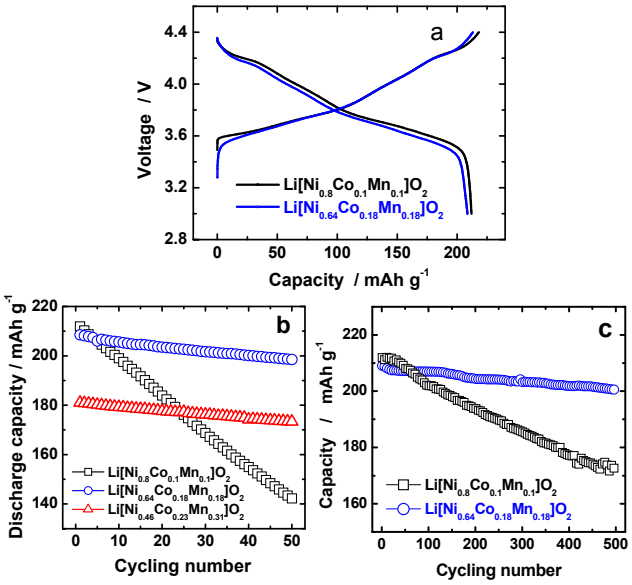

Figure IV- 43: Charge-discharge characteristics of $Li[Ni_{0.8}Co_{0.1}Mn_{0.1}]O_2$, $Li[Ni_{0.46}Co_{0.23}Mn_{0.31}]O_2$, and concentration-gradient $Li[Ni_{0.64}Co_{0.18}Mn_{0.18}]O_2$; (a) initial charge and discharge curves of $Li[Ni_{0.8}Co_{0.1}Mn_{0.1}]O_2$ and concentration-gradient material at 55°C obtained from 2032 coin-type half cell using Li metal as the negative electrode (current density: 0.5-C rate corresponds to 95 mA g^{-1}); (b) cycling performance of half cell based on $Li[Ni_{0.8}Co_{0.1}Mn_{0.1}]O_2$, $Li[Ni_{0.46}Co_{0.23}Mn_{0.31}]O_2$, and concentration-gradient material cycled between 3.0 and 4.4 V at 55°C by applying a constant current of 0.5-C rate (95 mA g^{-1}); and (c) cycling performance at 1-C rate (75 mA corresponds to 190 mA g^{-1}) of laminated-type lithium-ion batteries with an Al-pouch full cell (75 mAh) employing MCMB graphite as the negative electrode and either $Li[Ni_{0.8}Co_{0.1}Mn_{0.1}]O_2$ or concentration-gradient material as cathode (upper cut-off voltage of 4.2 V).

The thermal stability and safety of cathode material during charging are important concerns in judging the suitability of the material for use in Li-ion battery for practical applications such as P-HEVs. Figure IV- 44 shows the differential scanning calorimetry (DSC) profiles of $Li_{1-\delta}[Ni_{0.8}Co_{0.1}Mn_{0.1}]O_2$ and our concentration-gradient material charged to 4.3 V in the presence of 1 M $LiPF_6$/ethylene carbonate-diethyl carbonate electrolyte. For the $Li_{1-\delta}[Ni_{0.8}Co_{0.1}Mn_{0.1}]O_2$, the onset temperature of the exothermic reaction occurred at approximately 180°C, with a peak at 220°C. The reduced content of Ni in layer $LiMNiO_2$ (M = Co, Mn) gives rise to reduced heat generation, but doesn't improve the thermal stability, significantly. However, our concentration-gradient material shows higher onset temperature and reduced heat generation compared to the bulk composition $Li[Ni_{0.8}Co_{0.1}Mn_{0.1}]O_2$. We propose that the stability of this material originates from the Mn^{4+} in the surface region. For example, the onset temperature of the exothermic reaction was 270°C for the concentration-gradient $Li[Ni_{0.64}Co_{0.18}Mn_{0.18}]O_2$; thus, the reaction with the electrolyte was delayed by approximately 90°C compared with $Li_{1-\delta}[Ni_{0.8}Co_{0.1}Mn_{0.1}]O_2$, due to the high stability of

the outer surface composition $Li[Ni_{0.46}Co_{0.23}Mn_{0.31}]O_2$ in our gradient-concentration material which shows an onset temperature of over 305°C. The total generated heat was 2,303 J g^{-1} with our material, which is 31% lower than that determined for $Li_{1-\delta}[Ni_{0.8}Co_{0.1}Mn_{0.1}]O_2$ (3,346 J g^{-1}).

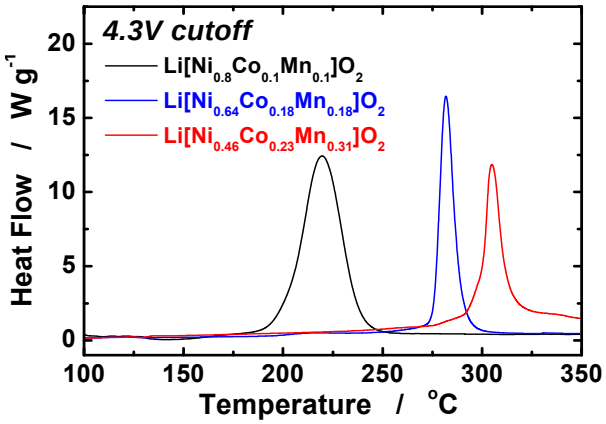

Figure IV- 44: DSC traces showing heat flow from the reaction of the electrolyte with $Li_{1-\delta}[Ni_{0.8}Co_{0.1}Mn_{0.1}]O_2$, gradient material $Li_{1-\sigma}[Ni_{0.64}Co_{0.18}Mn_{0.18}]O_2$, and $Li_{1-\sigma}[Ni_{0.46}Co_{0.28}Mn_{0.31}]O_2$ charged to 4.3 V.

FY 2009 Publications/Presentations

1. Y.-K. Sun, S.-T. Myung, B.-C. Park, J. Prakash, I. Belharouak, and **K. Amine***, *Nature Materials,* **Vol 8, pp324, April 2009.**
2. K. Amine*, S. Myung and Y. K. Sun, *Advanced Functional Materials , under review (2009)*

IV.B.4.3 Design and Evaluation of Novel High Capacity Cathode Materials (ANL)

Michael Thackeray
Argonne National Laboratory
9700 South Cass Avenue
Argonne, IL 60439
Phone : (630) 252-9184 ; Fax : (630) 252-4176
E-mail: thackeray@anl.gov

Collaborators:
C. S. Johnson, Argonne National Laboratory
S. H. Kang, Argonne National Laboratory
M. Balasubramanian, Argonne National Laboratory
S. V. Pol, Argonne National Laboratory

Start Date: October 1, 2008
Projected End Date: September 30, 2010

Objectives

All the cathode materials being exploited in today's commercial lithium-ion cells, viz., layered $LiCoO_2$ and its derivatives, e.g., $LiNi_{0.80}Co_{0.15}Al_{0.05}O_2$ (NCA) and $LiNi_{0.333}Mn_{0.333}Co_{0.333}O_2$ (NMC), spinel $LiMn_2O_4$ (LMO) and olivine $LiFePO_4$ (LFP) do not provide a sufficiently high capacity to satisfy the energy requirements of batteries for 40-mile all-electric-range PHEV applications. The objective of this project is to design, evaluate and screen high capacity, low cost and safe cathode materials to meet this goal.

Technical Barriers

- Low energy density
- High cost
- Low abuse tolerance

Technical Targets (USABC - End of life)

- 142 Wh/kg, 317 W/kg (PHEV 40 mile requirement)
- Cycle life: 5,000 cycles
- Calendar life: 15 years
- Improved abuse tolerance

Accomplishments

- Synthesized and evaluated Li_5FeO_4 as a lithium-rich cathode precursor for loading the graphite anode of lithium-ion cells.
- Used the excess lithium to discharge a high capacity $Li_{1.2}V_3O_8$ cathode component in the cathode that offers 372 mAh/g if discharged (at an average ~2.5 V) to the composition $Li_5V_3O_8$.
- Investigated structural changes in chemically-delithiated Li_5FeO_4 samples by X-ray absorption spectroscopy (XAS), which demonstrated that lithium extraction from Li_5FeO_4 was accompanied by oxygen loss (net loss = Li_2O) without any significant change to the Fe oxidation state.
- Compared the data with C_6/Li_2MnO_3-$Li_{1.2}V_3O_8$ lithium-ion cells in which Li_2MnO_3 acts in an analogous manner to Li_5FeO_4 as a source of lithium for loading the graphite anode.

✧ ✧ ✧ ✧ ✧

Introduction

The application of charged cathodes, such as MnO_2, V_2O_5 or $Li_{1.2}V_3O_8$ that offer high theoretical capacities (300-440 mAh/g) in conventional lithium-ion cells with graphite anodes is prohibited because there is no, or insufficient, lithium in the cathode to lithiate the anode during the first charge. It has recently been demonstrated that Li_2MnO_3 ($Li_2O \bullet MnO_2$) with a layered rock salt structure and structurally-integrated materials containing an Li_2MnO_3 component, such as $xLi_2MnO_3 \bullet (1\text{-}x)LiMO_2$ (M=Mn, Ni, Co), can be electrochemically charged by removing Li_2O to yield an active MnO_2 component. Because oxygen is irreversibly lost from the Li_2MnO_3 structure during this process, only one of the two lithium ions can be reintroduced into the residual MnO_2 structure during the reverse reaction to yield the corresponding rocksalt stoichiometry, $LiMnO_2$. The surplus lithium loaded into the anode can therefore be used either to compensate for irreversible capacity loss effects at carbon, metal (e.g., Sn), intermetallic (e.g., Cu_6Sn_5) or metalloid (e.g., Si) anodes or, alternatively, to lithiate a charged component in the parent cathode material. We have extended this concept to investigate cathode precursor materials with significantly higher Li_2O content such that they can be used effectively in combination with a charged high capacity component in the cathode.

Approach

Our approach is to explore the possibility of using materials with a very high lithium content, such as anti-fluorite Li_5FeO_4 ($5Li_2O•Fe_2O_3$), as cathode precursors for loading a graphite anode during the initial charge of lithium-ion cells. A charged, high capacity, cathode component, such as MnO_2 (308 mAh/g) or $Li_{1.2}V_3O_8$ (372 mAh/g) is used in combination with the cathode precursor to make use of the excess lithium loaded into the anode. This approach is an attractive alternative to 1) using commercial lithium metal powder or foil as a means to prelithiate graphite anodes when lithium-ion cells are loaded in the charged state, e.g., with MnO_2 or $Li_{1.2}V_3O_8$, or 2) having to lithiate such charged cathodes chemically prior to cell assembly in the discharged state. Lithium-ion cells with Li_5FeO_4 cathode precursors were compared with cells containing a Li_2MnO_3 ($Li_2O•MnO_2$) cathode precursor, which has a low Li_2O content relative to Li_5FeO_4 ($5Li_2O•Fe_2O_3$).

Results

Li_5FeO_4 has a defect anti-fluorite structure in which one Fe^{3+} ion substitutes for three Li^+ ions in Li_2O; it can be represented as $Li_5Fe\square_2O_4$, or $[Li_{1.25}Fe_{0.25}\square_{0.50}]O$, in which □ is a vacancy. Li_5FeO_4 has orthorhombic symmetry (Pbca) with lattice parameters of 9.218, 9.213 and 9.153 Å, each of which is essentially double that of the '*a*' lattice parameter of cubic Li_2O (Fm-3m, a=4.610 Å). The X-ray diffraction pattern of the as-prepared Li_5FeO_4 sample, after standing in air for 8 hours, as well as the JCPDS reference pattern (to 37.5 °2θ) and a schematic illustration of the structure are shown in Figure IV- 45. The X-ray pattern shows a minor amount of Li_2CO_3 impurity (<5%), as indicated by the weak peaks between 30 and 32 °2θ. The Fe^{3+} ions in the Li_5FeO_4 structure reside in isolated FeO_4 tetrahedra, the lithium ions occupying 5/7 of the remaining tetrahedral sites. The interstitial tetrahedral and octahedral sites provide an energetically favorable pathway for fast Li^+-ion diffusion.

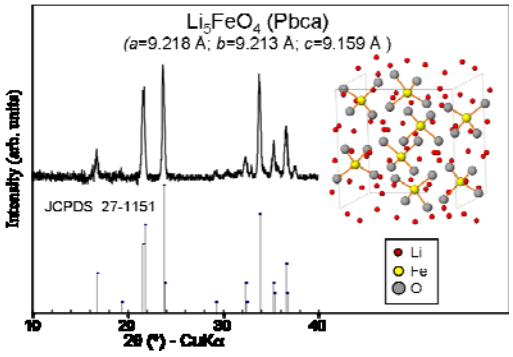

Figure IV- 45: X-ray diffraction pattern and schematic structural representation of Li_5FeO_4.

C_6/Li_5FeO_4, C_6/Li_2MnO_3 and Li/LiV_3O_8 Cells. C_6/Li_5FeO_4, C_6/Li_2MnO_3 and Li/LiV_3O_8 cells were constructed to evaluate the electrochemical performance of the individual Li_5FeO_4, Li_2MnO_3 and LiV_3O_8 cathode components. The electrochemical profile of the initial charge/discharge cycle of a C_6/Li_5FeO_4 cell is compared with that of a C_6/Li_2MnO_3 cell in Figure IV- 46. In the absence of electrolyte effects, the capacity withdrawn from the Li_5FeO_4 electrode (498 mAh/g) corresponds to the removal of approximately 3 Li per Fe (519 mAh/g) i.e., 60% of the theoretical capacity (867 mAh/g).

In-situ Fe K-edge XAS experiments of chemically-dilithiated Li_5FeO_4 conducted at Sector 20 bending magnet beamline (20 BM) of the Advanced Photon Source at Argonne National Laboratory revealed that lithium extraction between 3.5 V and 4.8 V does not appear to occur with any significant change to the iron oxidation state; we therefore attribute the capacity on the initial charge of Li/Li_5FeO_4 cells predominantly to the simultaneous removal of lithium and oxygen (net loss = Li_2O) that would maintain an Fe^{3+} oxidation state. Preliminary analyses of the XAS data suggest that Li_2O removal from Li_5FeO_4 is accompanied by a condensation of isolated FeO_4 tetrahedra to a polyhedral linkage of edge–shared FeO_6 octahedra.

Discharge of the C_6/Li_5FeO_4 cell takes place in two steps, the first between 2.6 and 1.5 V (~125 mAh/g) and the second between 1.5 and 0.8 V (107 mAh/g). The first step is attributed to lithium insertion into the delithiated $(5-\delta)Li_2O•Fe_2O_3$ ($\delta<3$) structure with a concomitant reduction of trivalent to divalent iron; the second step is attributed to the extrusion of metallic iron.

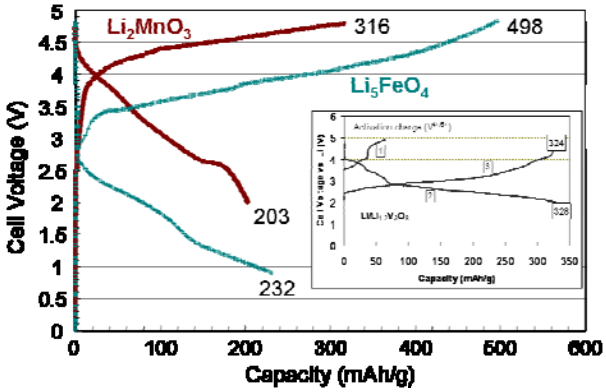

Figure IV- 46: Initial charge and discharge profiles of C_6/Li_5FeO_4, C_6/Li_2MnO_3 and Li/LiV_3O_8 (inset) cells.

Lithium extraction from Li_5FeO_4 (as Li_2O) occurs at a significantly lower voltage than it does from Li_2MnO_3 (Figure IV- 46). In the latter case, only 316 mAh/g, which corresponds to the removal of ~1.38 Li per Mn, (i.e., 69% of the theoretical value for complete Li_2O removal, 459 mAh/g) was withdrawn from the electrode between 3 V

and 4.8 V. On discharge to 2 V, the delithiated Li_2MnO_3 electrode delivered 203 mAh/g, which corresponds to the reinsertion of 0.9 Li per Mn.

The charge/discharge profile of a $Li/Li_{1.2}V_3O_8$ lithium half cell, provided as an inset in Figure IV- 46, shows the expected voltage response and capacity of a $Li_{1.2}V_3O_8$ electrode. After an initial charge to oxidize all the vanadium ions to the pentavalent state, >300 mAh/g was delivered reversibly by the $Li_{1.2}V_3O_8$ electrode between 4.5 and 2.0 V. The data demonstrate that if 300 mAh/g can be withdrawn from a Li_5FeO_4 or Li_2MnO_3 cathode precursor, and if this capacity can be recovered by the activated precursor and a charged cathode component such as $Li_{1.2}V_3O_8$ during discharge, then it should be possible to engineer lithium-ion cells with blended and balanced Li_5FeO_4 (Li_2MnO_3) and $Li_{1.2}V_3O_8$ cathode components that together deliver at least 150 mAh/g between 4.8 and 1.5 V.

C_6/Li_5FeO_4-$Li_{1.2}V_3O_8$ and C_6/Li_2MnO_3-$Li_{1.2}V_3O_8$ Lithium-Ion Cells. The electrochemical cycling profiles for the 1st, 2nd and 10th cycles of C_6/Li_5FeO_4-$Li_{1.2}V_3O_8$ and C_6/Li_2MnO_3-$Li_{1.2}V_3O_8$ cells are shown in Figure IV- 47a and b, respectively. A Li_5FeO_4:$Li_{1.2}V_3O_8$ molar ratio of 1:1 was selected for the C_6/Li_5FeO_4-$Li_{1.2}V_3O_8$ cell, whereas a Li_2MnO_3:$Li_{1.2}V_3O_8$ molar ratio of 0.74:0.26 was selected for the C_6/Li_2MnO_3-$Li_{1.2}V_3O_8$ cell to compensate for the lower Li_2O content in the Li_2MnO_3 precursor relative to Li_5FeO_4.

The electrochemical profiles of the initial charge/discharge cycles of the lithium-ion cells in Figure IV- 47a and b are a combination of the C_6/Li_5FeO_4, C_6/Li_2MnO_3 and $Li/Li_{1.2}V_3O_8$ voltage profiles shown in Figure IV- 46. In Figure IV- 47a, taking into consideration 1) the individual capacities from the blended Li_5FeO_4-$Li_{1.2}V_3O_8$ components when charged to 4.8 V, 2) the relative masses of the components, and 3) probable electrolyte oxidation effects above 4.5 V, the initial charge capacity of 220 mAh/g is in good agreement with the expected capacity of 205 mAh/g. When subsequently discharged to 2 V, lithium insertion into the activated Li_5FeO_4 and $Li_{1.2}V_3O_8$ components provides a capacity 160 mAh/g. Thereafter, when cycled between 3.8 and 1.5 V, cells lose capacity steadily, yielding 140-120 mAh/g over the next 10 cycles. The loss in capacity is attributed to irreversible iron extrusion from the iron-oxide component towards the end of discharge, highlighting the importance of tailoring the upper and lower voltage limits to optimize the performance of cathodes containing Fe-based metal oxides.

The electrochemical cycling behavior of the C_6/Li_2MnO_3-$Li_{1.2}V_3O_8$ lithium-ion cell is shown in Figure IV- 47b. In this case, using the electrochemical data in Figure IV- 46 as a guide, notably 1) the level of lithium extraction from the Li_2MnO_3 precursor, i.e., 1.38 Li per Li_2MnO_3 unit and 2) the corresponding capacity from the $Li_{1.2}V_3O_8$ electrode, then a maximum 187 mAh/g would be expected from the composite cathode when charged to 4.7 V, in good agreement with the experimentally obtained value (200 mAh/g, Figure IV- 47b). When discharged to 1 V at 0.05 mA/cm^2 on the subsequent two cycles, the activated Li_2MnO_3-$Li_{1.2}V_3O_8$ cathode delivers >150 mAh/g. Because this cathode delivered no significant capacity between 2 and 1 V, the lower voltage limit was raised to 2 V for further cycling, which was conducted at double the rate (0.1 mA/cm^2). Despite the narrower voltage range and slight decrease in discharge voltage due to polarization, the cathode provided a steady 150 mAh/g for the next 8 cycles, demonstrating the superior electrochemical properties of the Li_2MnO_3-$Li_{1.2}V_3O_8$ cathode over Li_5FeO_4-$Li_{1.2}V_3O_8$. What is remarkable is that our results demonstrate that the Li_2MnO_3 component shows enhanced cycling stability when blended with $Li_{1.2}V_3O_8$, relative to its poor cycling efficiency as an independent electrode.

Conclusions and Future Directions

Li_5FeO_4 and Li_2MnO_3 have been evaluated as cathode precursors to load the graphite anode of C_6/Li_5FeO_4-$Li_{1.2}V_3O_8$ and C_6/Li_2MnO_3-$Li_{1.2}V_3O_8$ lithium-ion cells, in which a charged $Li_{1.2}V_3O_8$ component in the parent cathode is used to accommodate the surplus lithium provided to the anode during the initial charge of the cells. These composite lithium metal oxide electrodes containing manganese, vanadium and iron provide a capacity of at least 150 mAh/g, when cycled between 4.7 and 2 V; they offer the possibility of designing alternative cathode materials without costly cobalt- and nickel components that are unstable in their charged states.

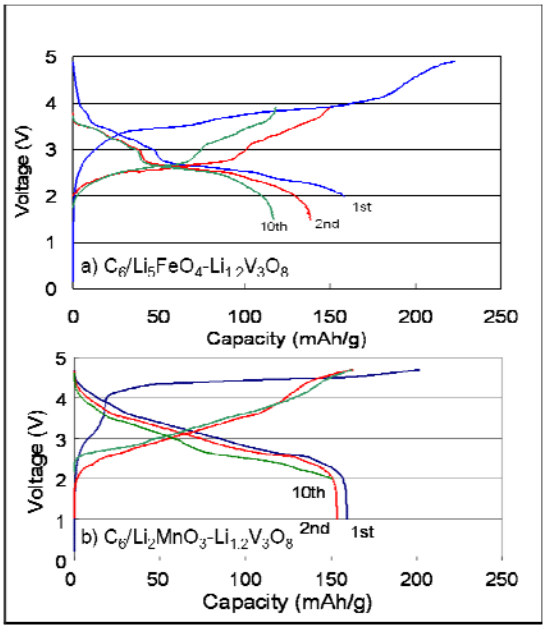

Figure IV- 47: Cycling performance of a) C_6/Li_5FeO_4-$Li_{1.2}V_3O_8$ and b) C_6/Li_2MnO_3-$Li_{1.2}V_3O_8$ lithium-ion cells.

Based on these initial studies, we propose 1) to expand our exploration of other lithium-rich materials with an antifluorite-type structure, such as Li_6MnO_4, as a source of lithium for loading lithium-ion cells in combination with other charged cathode materials, e.g., MnO_2, and 2) to advance our understanding of the complex delithiation and relithiation reactions of these precursor materials.

Our results raise the possibility of exploiting Li_2O extraction/Li_2O reformation reactions in Li-air cells.

FY 2009 Publications/Presentations

1. "Li_2O removal from Li_5FeO_4 – a cathode precursor for lithium-ion batteries" C. S. Johnson et al. Chemistry of Materials. Submitted (2009).
2. Presentation to the 2009 DOE Annual Peer Review Meeting in Washington D.C.

IV.B.4.4 Development of High-Capacity Cathode Materials with Integrated Structures (ANL)

Sun-Ho Kang
Argonne National Laboratory
9700 S. Cass Avenue
Argonne, IL 60439
Phone: (630) 252-4212; Fax: (630) 252-4176
E-mail: sunho.kang@anl.gov

Collaborators :
Mahalingam Balasubramanian (ANL)
Vilas G. Pol (ANL)
Christopher S. Johnson (ANL)
Michael M. Thackeray (ANL)

Start Date: October 1, 2008
Projected End Date: September 30, 2010

Objectives

Plug-in hybrid-electric vehicles (PHEVs) require lithium-ion batteries with higher energy densities than those adopted in HEVs. Safety and cost also need to be improved because of the larger size of PHEV battery packs. The current commercial cathode materials, such as $LiCoO_2$, $LiNi_{0.8}Co_{0.15}Al_{0.05}O_2$, $LiNi_{1/3}Co_{1/3}Mn_{1/3}O_2$, $Li_{1+x}Mn_{2-x}O_4$, $LiFePO_4$, do not meet those requirements particularly for PHEVs with a 40-mile all-electric range (PHEV 40). The objective of this effort is to develop low-cost, high-energy, and thermally-stable cathode materials with acceptable power capability to meet the performance requirements for a PHEV 40.

Technical Barriers

The primary technical barrier is the development of a safe and cost-effective PHEV battery with a 40 mile all electric range that meets or exceeds all performance goals. Specific barriers for this project include:

(A) Low energy density

(B) High cost

(C) Thermal abuse limitations

Technical Targets

- Development of Mn-based oxide cathode materials with integrated structures (spinel-layered)
- Specific capacity of ~200 mAh/g at 1C rate

Accomplishments

- Synthesized $(Ni_{0.25}Mn_{0.75})CO_3$ precursor with spherical morphology by coprecipitation
- Synthesized $Li_{1.2}(Ni_{0.25}Mn_{0.75})O_y$ with integrated spinel-layered ($LiMO_2$)-layered (Li_2MnO_3) structures
  - Achieved ~250 mAh/g of reversible, stable capacity at slow rates (~C/23)
  - Achieved ~200 mAh/g of discharge capacity at ~C/1 rate without Co substitution
- Studied the effect of Co on the structure and electrochemical properties of $Li_{1.2}(Ni_{0.25}Mn_{0.75})O_y$

✧ ✧ ✧ ✧ ✧

Introduction

Li- and Mn-rich oxides with 'layered-layered' intergrown structures, $xLi_2MnO_3•(1-x)LiMO_2$ (M=Mn,Ni, Co), can deliver a very high capacity (>200 mAh/g) when charged to high voltages (>4.4 V *vs.* Li^+/Li). However, these cathode materials generally show a relatively poor rate capability which presents a limitation for practical applications. This limitation is attributed to poor electronic/ionic conductivity in the oxide bulk as well as at the particle surface. Other limitations include a poor ionic conductivity at the particle surface that arises from damaging reactions with the electrolyte at high voltages and leads to a high interfacial impedance. To overcome the intrinsic rate-limitations of high-capacity $xLi_2MnO_3•(1-x)LiMO_2$ (M=Ni,Co,Mn) cathodes, efforts have been made to create spinel components in the layered-layered structure.

Approach

Lithium metal oxides with a spinel-type structure are well known to exhibit fast Li-ion diffusion through a three-dimensional interstitial space. It is, therefore, anticipated that the rate performance of 'layered-layered' cathode materials could be enhanced, should a structurally-compatible spinel component be introduced into the intergrown structure.

$LiNi_{0.5}Mn_{1.5}O_4$ with a spinel-type structure and $Li_{1.2}Ni_{0.2}Mn_{0.6}O_2$ with an integrated layered-layered structure have the same nickel-to-manganese ratio (Ni/Mn=1/3) but different lithium-to-transition metal

(TM=Ni+Mn) ratios (Li/TM=0.5 and 1.5, respectively). Therefore, by simply varying the Li content, it is expected that electrode materials with different structures and electrochemical properties could be prepared. In this work, in order to create a spinel component in the layered-layered structure, the Li/TM ratio was varied between 1.0 and 1.5; the crystal structures and electrochemical properties of the electrode materials were examined.

Results

Preparation of Mn-Ni carbonate by coprecipitation. A $(Ni_{0.25}Mn_{0.75})CO_3$ precursor material was prepared by coprecipitation. A 2M aqueous solution of Mn-sulfate and Ni-sulfate was added to a 2M solution of Na_2CO_3 and NH_4OH at 50 °C under constant stirring. The coprecipitated $(Ni_{0.25}Mn_{0.75})CO_3$ powder was filtered, washed, and dried in air at 100 °C. The X-ray diffraction (XRD) pattern and morphology of the powder are shown in Figure IV- 48a and b, respectively.

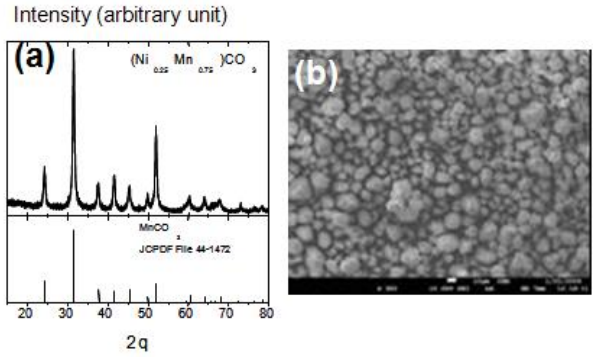

Figure IV- 48: Powder XRD pattern (a), and SEM image (b) of coprecipitated $(Ni_{0.25}Mn_{0.75})CO_3$ powder.

Synthesis of $Li_x(Ni_{0.25}Mn_{0.75})O_y$ (0.5≤x≤1.5). $Li_x(Ni_{0.25}Mn_{0.75})O_y$ was synthesized by mixing $(Ni_{0.25}Mn_{0.75})CO_3$ and Li_2CO_3 and calcining the mixture at 700-900 °C in air for 12 h. XRD patterns of the oxide powders synthesized at 900 °C are given in Figure IV- 49. The two end members (x=0.5 and 1.5) showed well-known spinel and layered-layered structures, respectively, as expected. The XRD patterns of materials with intermediate Li contents (x=1.0 and 1.2) exhibited mixed characters of layered ($LiMO_2$), cation ordering (Li_2MnO_3, denoted with red circles), and spinel (LiM_2O_4, denoted with •), which indicates that the spinel component was successfully created in the layered-layered matrix.

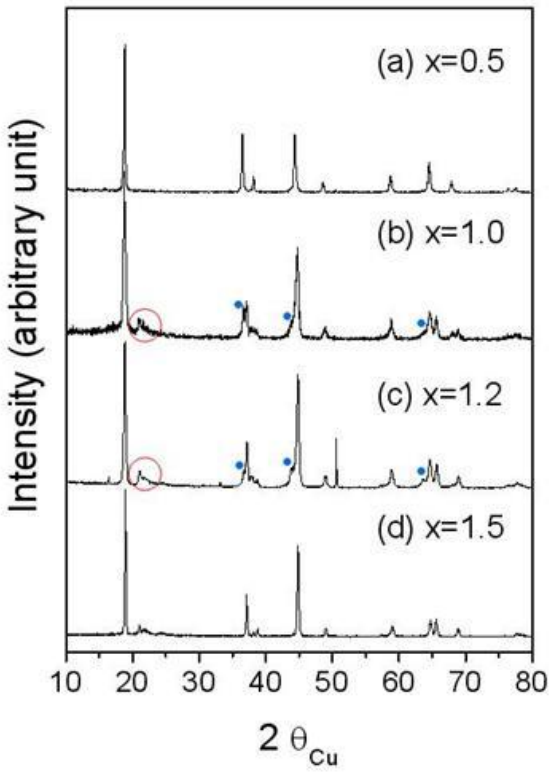

Figure IV- 49: Powder XRD patterns of $Li_x(Ni_{0.25}Mn)O_y$ (0.5≤x≤1.5) synthesized at 900 °C.

Electrochemical Testing Initial charge/discharge profiles of lithium half-cells containing $Li_{1.2}(Ni_{0.25}Mn_{0.75})O_y$ prepared at 700-900 °C are given in Figure IV- 50a; corresponding differential capacity plot of 900 °C sample is shown in Figure IV- 50b. The positive electrode consisted of 80 wt% $Li_{1.2}(Ni_{0.25}Mn_{0.75})O_y$, 10 wt% carbon, and 10 wt% PVDF binder on aluminum foil. The electrolyte was 1.2 M $LiPF_6$ in EC:EMC (3:7 by volume). The cells were cycled between 2.0 and 4.95 V at 10 mA/g. Figure IV- 51 shows capacity variation with cycling of lithium cell containing $Li_{1.2}(Ni_{0.25}Mn_{0.75})O_y$ electrodes. Rate capability was also examined by increasing discharge current from 10 to 200 mA/g; voltage profiles of $Li_{1.2}(Ni_{0.25}Mn_{0.75})O_y$ at different discharge currents are shown in Figure IV- 52. All the electrochemical testing was carried out at room temperature. The cells delivered very high initial capacity (Figure IV- 50a, >220 mAh/g). As indicated in Figure IV- 50b, the electrode material exhibited electrochemical signatures from all of the structural components that appeared in the XRD pattern: Li_2MnO_3 activation at ≥ 4.5 V during the first charge, $LiNi_{0.5-\delta}Mn_{1.5+\delta}O_4$-type spinel, and $LiMO_2$-type layered phase. In spite of the extremely high charge voltage (4.95 V), the lithium cells showed excellent cycling stability (Figure IV- 51) and cycling efficiency (>99%). Excellent rate capability was also observed (Figure IV- 52): 210

mAh/g at C/2 rate and 200 mAh/g at C/1 rate. Little change in plateau voltage and length at 4.8 V in Figure IV-52 (circled, contribution from spinel) regardless of current rate demonstrates beneficial impact of the integrated spinel phase (high-rate tolerance).

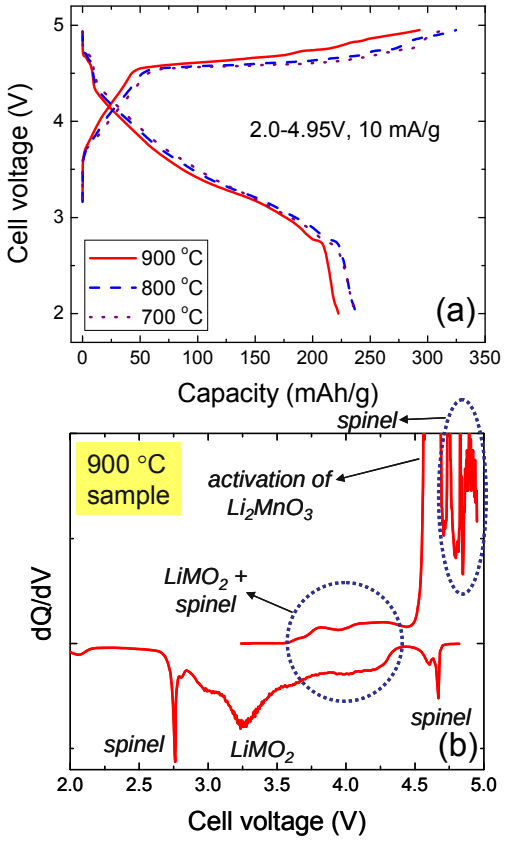

Figure IV- 50: (a) Initial charge/discharge profiles of lithium cells containing $Li_{1..2}(Ni_{0.25}Mn_{0.75})O_y$ prepared at 700-900 °C. The cells were cycled between 2.0 and 4.95 V at 10 mA/g. (b) Corresponding differential capacity plot of the first cycle for the 900 °C sample.

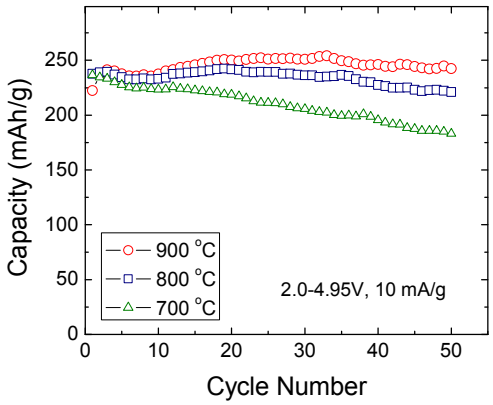

Figure IV- 51: Capacity variation against cycle number of lithium cells containing $Li_{1..2}(Ni_{0.25}Mn_{0.75})O_y$ electrodes.

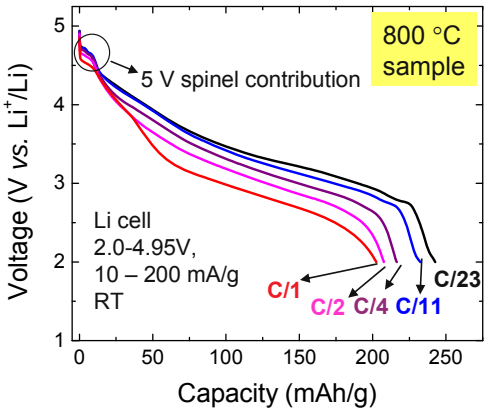

Figure IV- 52: Discharge profiles of $Li/Li_{1.2}(Ni_{0.25}Mn_{0.75})O_y$ cells at various discharge currents.

Structural analysis using X-ray absorption spectroscopy. A more detailed structural study was carried out using X-ray absorption spectroscopy at Sector 20 bending magnet beamline of the Advanced Photon Source at ANL. Figure IV- 53a and b show initial results on Mn XANES and EXAFS for the $Li_{1.2}(Ni_{0.25}Mn_{0.75})O_y$ sample prepared at 800 °C. The Mn XANES and XAFS data show that $Li_{1.2}(Ni_{0.25}Mn_{0.75})$ O_y is close in structure to $Li_{1.5}(Ni_{0.25}Mn_{0.75})O_{2.5}$ (layered-layered) and very different from $Li_{0.5}(Ni_{0.25}Mn_{0.75})O_2$ (spinel). The Li^+ ions in the TM layers are clustered preferentially around Mn in both $Li_{1.2}(Ni_{0.25}Mn_{0.75})O_y$ and $Li_{1.5}(Ni_{0.25}Mn_{0.75})O_{2.5}$. Further detailed, quantitative analysis of the XANES and EXAFS spectra is under way.

Conclusions and Future Directions

Cathode materials with three-component 'composite' structures have been successfully designed and synthesized. $Li_{1.2}Ni_{0.25}Mn_{0.75}O_y$ showed electrochemical features from the three integrated components (spinel, Li_2MnO_3, $LiMO_2$) and exhibited very high initial capacity (>225 mAh/g, ~C/23 rate). Excellent cycling efficiency and stability in wide voltage windows (2.0-4.95 V) and good rate performance (200 mAh/g at C/1 rate) were also observed.

In the future, further optimization in terms of Li:TM ratio will be done and the effects of various dopants on the structure and electrochemical properties will be studied. Electrochemical performance of these electrode materials in full lithium-ion cell configuration and thermal stability will also be investigated.

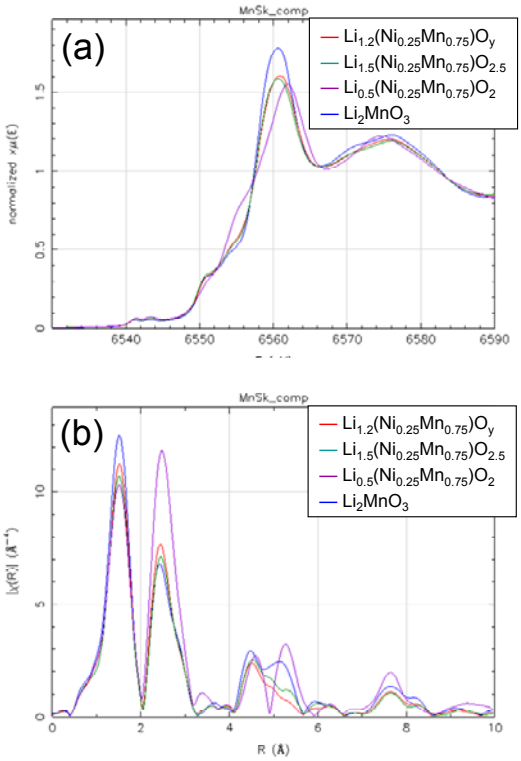

Figure IV- 53: Mn XANES (a) and EXAFS (b) spectra of $Li_{1.2}(Ni_{0.25}Mn_{0.75})O_y$ sample prepared at 800 °C.

FY 2009 Publications/Presentations

1. Presentation at the 2009 DOE Annual Merit Review Meeting, May 19, 2009, Washington D.C.

IV.B.4.5 Evaluation of Li_2MnSiO_4 Cathode (ANL)

Ilias Belharouak
Argonne National Laboratory
9700 South Cass Avenue
Argonne, Il 60439
Phone: (630) 252-4450; Fax: (630) 252-4176
E-mail: belharouak@anl.gov

Start Date: September 1, 2008
Projected End Date: September 30, 2010

Objectives

- Develop new preparation methods to synthesize high purity Li_2MnSiO_4 materials.
- Understand the structure of these materials at the local and bulk levels.
- Check whether these materials pertain to the concept of 2-lithium ions extraction and insertion cathode materials.
- Develop ways to overcome the barrier of the insulating properties of these materials.
- Achieve an overall evaluation of these materials from the structural and electrochemical standpoints with regard to their possible applicability in high-energy density Li-ion batteries.

Technical Barriers

This project addresses the following technical barriers:

- Energy density of available Li-ion battery technologies, weight, volume, and affordability.
- Abuse tolerance of energy storage systems must be intrinsically tolerant of abusive conditions

Technical Targets

- Develop a two-electron high-energy density cathode: extraction and insertion of 2-Li ions from/in the host structure is possible because manganese ions can oxidize and reduce reversibly from 2 to 4 oxidation states, with the generation of 333mAh/g theoretical capacity according to the following scheme: $Li_2Mn^{2+}SiO_4 \leftrightarrow Mn^{4+}SiO_4 + 2Li^+ + 2\bar{e}$
- Develop a safer cathode: strong covalent Si-O bonds will translate into very stable electrochemical and enhanced safety characteristics.
- Develop an inexpensive cathode: low cost of manganese

Accomplishments

- Sol-gel preparation method has been found to be appropriate for obtaining Li_2MnSiO_4 having the highest purity ever reported.
- The structure of Li_2MnSiO_4 was resolved, it exhibits lithium ions that reside within channels and that are available for extraction and insertion. Rietveld structural refinement analysis has confirmed the structure of Li_2MnSiO_4 that is a derivative of Li_3PO_4-type structure.
- Squid and EPR measurements confirmed that the electronic configuration and magnetic behavior are those of Mn^{2+} ions.
- Li_2MnSiO_4 was found to be constituted by large agglomerates that are made of nanosized particles.
- High-energy ball milling was found to be an effective way to breakdown the large agglomerates without inducing damage to the atomic scale arrangement of the material.
- Initial carbon coating and ball milling experiments were found to significantly improve the capacity of Li_2MnSiO_4.

✧ ✧ ✧ ✧ ✧

Introduction

Since the strategy of reducing the inactive materials at the battery pack level has been exhausted over the last decade, the only route to surmount the energy density shortfall is the development of higher specific capacity materials and/or higher cell voltage. Silicate family (Li_2MSiO_4, where M = Fe, Mn, and Co) has been introduced because its high theoretical capacity may be exploited if the transition metal ions can be oxidized and reduced reversibly from their lowest oxidation state (2+) to a higher oxidation state (4+). This condition requires the extraction/insertion of two lithium ions from the host structure, with the generation of 333-mAh/g theoretical capacity. The manganese ($Mn^{2+}/^{4+}$) redox couple is of particular interest because it exhibits a high potential (vs. Li°), and resources to prepare the material are plentiful and clean. The preparation of Li_2MnSiO_4 material is, however,

not trivial due to the possible presence of mixed phases and/or impurities. The aim of the present work is to report on a new synthesis route by an all-acetate sol/gel method that was found to be successful in preparing high-purity Li_2MnSiO_4. Carbon coating and particle size reduction by high-energy ball milling were found to be effective ways to enhance the electrochemical activity of this material.

Approach

- Li_2MnSiO_4 can be iso-structural to certain forms of Li_3PO_4: Mn^{2+} ions are present within a $[SiO_4]$ anionic silicate network that replaces $[PO_4]$ anionic phosphate network, and 2-Li ions are available in 3-dimentional channels.
- Strong covalent Si-O bonds will translate into very stable electrochemical and enhanced safety characteristics.
- The extraction/insertion of 2-Li ions from/in the host structure is possible because manganese ions can oxidize and reduce reversibly from 2 to 4 oxidation states, with the generation of 333mAh/g theoretical capacity according to the following scheme: $Li_2Mn^{2+}SiO_4 \leftrightarrow Mn^{4+}SiO_4 + 2Li+ + 2\bar{e}$
- $Mn^{2+/4+}$ redox couple is preferred because of its higher potential vs. Li°, so high energy-density can be achieved.
- Manganese based cathode are low cost materials.

Results

Li_2MnSiO_4 was synthesized by a sol-gel method from lithium acetate, manganese acetate, and silicon acetate precursors. The gel product was dried at 100°C and then heated to 600, 700, and 800ºC for 24 h under He/H_2 (3.5 %) gas flow. Carbon-coated Li_2MnSiO_4 was prepared by adding cellulose to the initial mix.

X-ray patterns of Li_2MnSiO_4 samples prepared at 600, 700, and 800°C are shown in Figure IV- 54. The figure also shows the agreement between these patterns and the calculated X-ray diagram of Li_2MnSiO_4 (uppermost spectrum), whose structural model is a derivative of an orthorhombic form of Li_3PO_4 (S.G. $Pmn2_1$). The sample prepared at 700°C seemed to be the most pure phase. An overlap exists between the stability domains of the main and impurity phases, so that it is very difficult to isolate an impurity-free Li_2MnSiO_4 phase. Li_2MnSiO_4 partially decompose according to the following schemes: $Li_2MnSiO_4 \rightarrow Li_2SiO_3 + MnO$ and/or $Li_2MnSiO_4 \rightarrow ½\ Li_4SiO_4 + ½\ Mn_2SiO_4$.

Figure IV- 55 shows the temperature dependence of the molar magnetic susceptibility $\chi_m(T)$ for Li_2MnSiO_4 prepared at 700°C. $\chi_m(T)$ is typical for an antiferromagnetic material. The magnetic susceptibility shows a maximum at the Néel temperature (T_N = 12 K), below which χ_m increased with temperature, and above which the material is typically paramagnetic, following the Curie-Weiss law.

The Curie and the Weiss constants, after deduction from the linear fitting of the $1/\chi_m$ vs. T data, were found to equal 4.54 emu·K·mol^{-1} and -29 K, respectively.

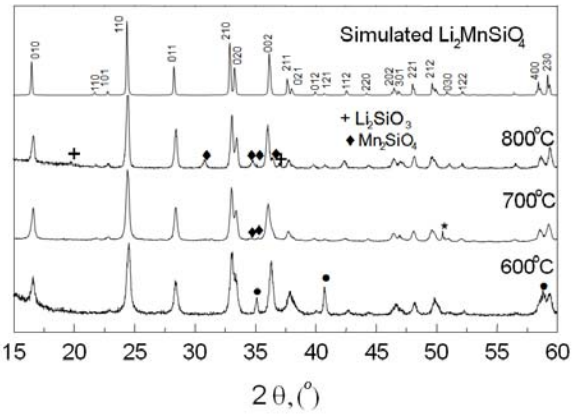

Figure IV- 54: X-ray patterns of Li_2MnSiO_4 prepared at 600, 700, and 800°C under reducing atmosphere. Calculated pattern also shown at top.

Therefore, the experimental paramagnetic effective moment was μ_{eff} = 6.0 μ_B, which is consistent with the spin-only calculated paramagnetic moment of Mn^{2+} ions (μ_{eff} = 5.92 μ_B). This result clearly confirms that the observed magnetic behavior is that of Mn^{2+} (d^5) ions located in tetrahedral sites. Indeed, according to crystal field theory, a high spin configuration is always expected in tetrahedral sites due to the weakness of the surrounding field.

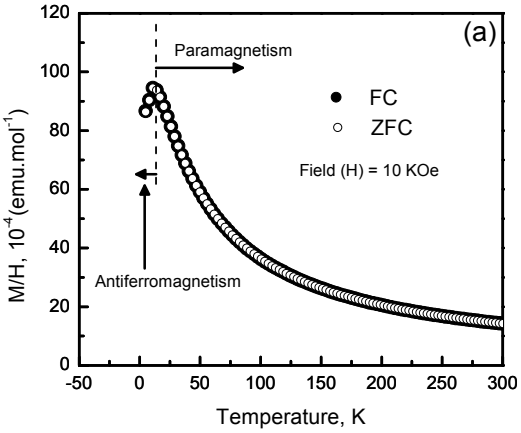

Figure IV- 55: Temperature dependence of (a) the magnetic susceptibility

Figure IV- 56 shows the SEM photographs of the Li_2MnSiO_4 materials prepared at 700°C. Large aggregates (10 to 50 μm) are observed for the as-prepared material

(Figure IV- 56a). These aggregates are made of nanosized particles (100-200 nm) that were cemented together during the calcination of the material (Figure IV- 56b). The observed morphology may not be suitable to achieve the full theoretical capacity. On one hand, Li_2MnSiO_4 itself is an insulating material; on the other hand, despite the presence of carbon black additive, only the small particles at the surface of the large agglomerates can be electrochemically active. The core of the large aggregates, however, is insufficiently conductive to allow for rapid and full lithium extraction and insertion. Therefore, methods such as carbon coating and high-energy ball milling were considered to enhance the electronic conductivity and shorten the pathways for lithium mobility. By use of a cellulose precursor, Li_2MnSiO_4 was coated with carbon on the surface of the large particles (Figure IV- 56c). After 4 h of ball milling, the large agglomerates had broken into smaller particles without inducing a noticeable structural change (Figure IV- 56d).

Figure IV- 57 shows the charge/discharge profiles of the as-prepared (a), carbon-coated (b), ball-milled (c) and Li_2MnSiO_4 cathode materials in coin cells. All cells were assembled with lithium metal as the negative electrode and were tested in the voltage range of 1.5-4.8 V under a current density of 10 mA/g. Due to its large aggregates and insulating characteristics, the as-prepared Li_2MnSiO_4 was almost electrochemically inactive despite the presence of 15 wt.% carbon black, where specific capacities of only 10 and 4 mAh/g were achieved in the first charge and discharge, respectively. When coated with 7 wt.% carbon (but 15 wt% total carbon in the electrode), the charge and discharge capacities were much improved, 190 and 135 mAh/g, with a coloumbic efficiency of 71%. The capacity and electrochemical activity also improved when the material was subjected to ball milling in the presence of 15 wt.% carbon black. However, only 172 and 115 mAh/g capacities were obtained in this case.

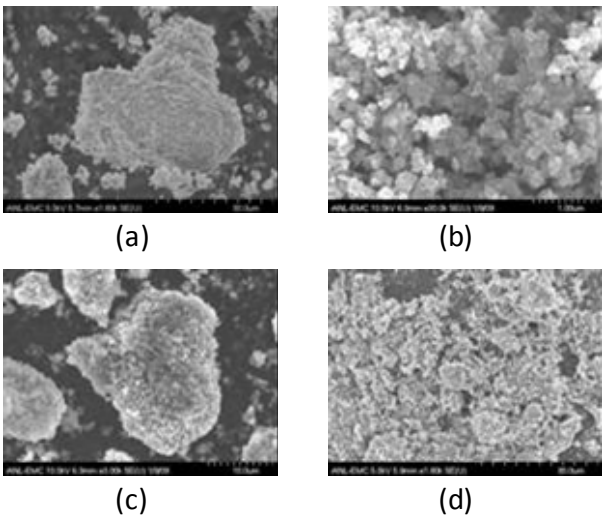

Figure IV- 56: Scanning electron microscopy images of (a) and (b) as-prepared Li_2MnSiO_4, (c) carbon-coated Li_2MnSiO_4, and (d) high-energy ball-milled Li_2MnSiO_4.

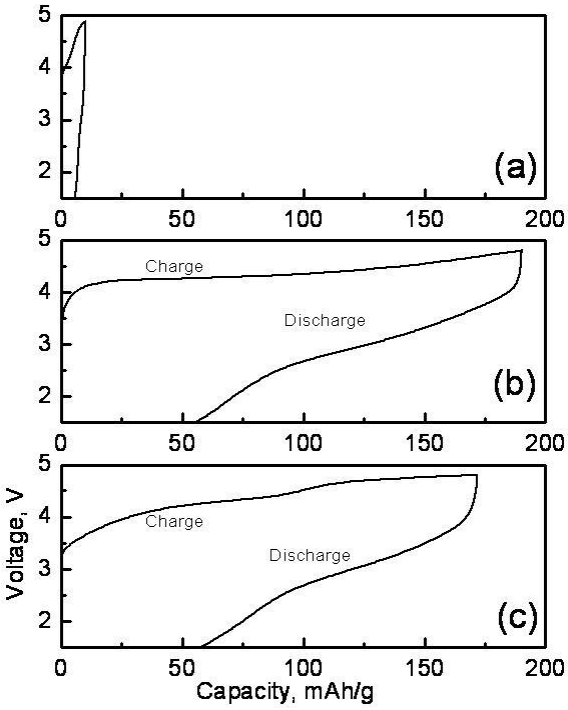

Figure IV- 57: Voltage profiles of (a) as-prepared Li_2MnSiO_4, (b) carbon-coated Li_2MnSiO_4, and (c) high-energy ball-milled Li_2MnSiO_4..

Conclusions and Future Directions

An all-acetate precursor sol/gel method has been used to produce Li_2MnSiO_4 with a minimal level of impurities and with sub-micron particle sizes. Despite the agglomeration of the nanosize particles during calcination, carbon coating and high-energy ball milling enhanced the electronic conductivity and reduced the lithium diffusion pathways of the material, resulting in relatively high

capacities. From this study we infer two needs before Li_2MnSiO_4 material can achieve practical high-energy battery utilization. First is overcoming the insulating properties of this silicate material. By applying the same strategies as used in the case of $LiFePO_4$ olivine, carbon coating and particle size reduction, we have been able to partially activate the material electrochemically. However, extraction/insertion of only one lithium ion appears to be at work, given the partial achievement of the 333-mAh/g theoretical capacity for Li_2MnSiO_4. Second is a need to better understand the structure of Li_2MnSiO_4. A close examination of this structure suggests the possibility of a cationic mix between Mn^{2+} and Li^+ ions, since both ions are located in tetrahedral sites and possess close ionic radii (0.59 Å for Li^+ and 0.66 Å for Mn^{2+}, compared with 0.26 Å for Si^{4+}). This cationic mixing would likely cause the blocking of the pathways available for lithium ion diffusion in an ideal Li_3PO_4 ($Pmn2_1$) type structure and thus reduce the capacity. The same observation can be also made in the case of $LiMnPO_4$ olivine, where coating and particle reduction attempts were not found as successful as in the case of $LiFePO_4$.

The future plan for this work includes the following:

- Develop experimental preparation methods based on a sol-gel process that will inhibit the aggregation of Li_2MnSiO_4 nano-particles into large agglomerates.
- Continue the effort of achieving full capacity of the material using: carbon coating using carbonaceous additives; High-energy ball milling; and gas phase carbon coating reaction.
- The information learned from the study of Li_2MnSiO_4 will be used to investigate the compositions with iron and cobalt as the electrochemically active ions.
- Achieve an overall evaluation of these materials from the structural and electrochemical with regard to their possible applicability in high-energy density Li-ions batteries.

FY 2009 Publications/Presentations

1. Poster to the DOE Annual Peer Review Meeting, Washington DC, May 18-22 (2009).
2. Structural and Electrochemical Characterization of Li_2MnSiO_4 Cathode Material I. Belharouak, A. bouimrane, and K. Amine Paper Accepted to the Journal of Physical Chemistry

IV.B.5 Applied Battery Research on Electrolytes

IV.B.5.1 Novel Electrolytes and Electrolyte Additives for PHEV Applications (ANL)

Daniel P. Abraham

Argonne National Laboratory
9700 South Cass Avenue
Argonne, IL 60439-4837
Phone: (630) 252-4332; Fax: (630) 972-4406
E-mail: abraham@anl.gov

Collaborators:
B. Lucht, University of Rhode Island

Start Date: October, 2008
Projected End Date: September, 2010

Objectives

The performance, calendar-life, and safety characteristics of Li-ion cells are dictated by the nature and stability of the electrolyte and the electrode-electrolyte interfaces. Desirable characteristics for these electrolytes include stability in the 0 to 5V vs. Li range, excellent lithium ion conductivity, wide temperature stability range, non-reactivity with the other cell components, non-toxicity and low cost. Our goal is to develop novel electrolytes and electrolyte additives to meet the cost, calendar life and safety requirements of batteries for PHEV applications.

Technical Barriers

This project addresses the following technical barriers to the development of a PHEV battery with a 40 mile all electric range that meets or exceeds all performance goals.

- Cell Performance
- Cell Calendar and Cycle Life
- Cell Safety/Abuse Tolerance

Technical Targets

- Develop novel electrolytes with electrochemical stability in the 0 to 5V vs. Li voltage range.
- Develop additives to conventional electrolytes that improve cell shelf and cycle life by 50%. Cell performance and thermal abuse characteristics should stay the same or be enhanced by these additives.

Accomplishments

- Glycerol carbonates (GC) and solvents derived from this compound are being examined as low cost alternatives to conventional electrolytes.
  - Electrochemical tests conducted with GC obtained commercially show poor performance. Techniques to dry/purify GC are being developed.
  - Techniques to prepare variants of GC, i.e., replacing the OH group with other species are also under development.
  - Initial electrochemical tests conducted with these GC and GC-variant electrolytes show promising results.
- Additives designed to react on and protect the positive electrode surface are being examined.
  - Initial data show that small additions of 2,3 dihydrofuran (DHF), 2,5 DHF and vinylene carbonate (VC) to conventional electrolytes improves cell life.
- Electrochemical experiments with ionic liquids have been initiated.
  - Electrolytes with N-propyl-N-methylpyrrolidinium bis(fluorosulfonyl)imide (P_{13}FSI) and FSI salt cycle well in graphite//Li cells.
  - Electrolytes with N-butyl-N-methylpyrrolidinium bis(trifluoromethanesulfonyl)imide (P_{14}FSI) and TFSI salt cycle well in oxide//Li cells in the 3-4V voltage window.

✧ ✧ ✧ ✧ ✧

Introduction

Recent advances in cathode and anode materials have refocused attention on electrolytes as the technological bottleneck limiting the operation and performance of lithium-battery systems. Whereas, attributes such as cell potential and energy density are related to the intrinsic property of the positive and negative electrode materials, cell power density, calendar-life and safety are dictated by

the nature and stability of the electrolyte and the electrode-electrolyte interfaces. A wide electrochemical window, wide temperature stability range, non-reactivity with the other cell components, non-toxicity, low cost, and a lithium-ion transference number approaching unity are, in general, desirable characteristics for lithium battery electrolytes. In addition, the electrolyte should have excellent ionic conductivity to enable rapid ion transport between the electrodes, and be an electronic insulator to minimize self-discharge and prevent short-circuits within the cell. Research on electrolytes and on functional electrolyte additives to improve cell life, thermal abuse behavior and low-temperature (<0°C) performance of high-power lithium-ion cells is being conducted at Argonne National Laboratory (Argonne) and is intended to spur commercialization of lithium-ion batteries for a wide range of vehicle applications, including hybrid-electric vehicles (HEVs), plug-in HEVs and battery electric vehicles (EVs).

Approach

Our approach is to (i) develop novel electrolytes that include glycerol carbonate, and modifications thereof, (ii) examine electrolyte additives that can enhance cell life by protecting the electrode surfaces, (iii) investigate the use of ionic liquids, and mixtures of ionic liquids and carbonate solvents, to enable high-safety batteries. Glycerol carbonate (GC) can be a potential low-cost substitute for currently used lithium-battery solvents. Our approach is to dry/purify GC obtained from a commercial manufacturer and examine its performance in lithium-ion cells. Furthermore, we've developed techniques to replace the H (in the OH) group of GC with other alkyl species to form methyl ethers, ethyl ethers, and oligoethylene oxide ethers that will be examined as potential solvents. The electrolyte additives to generate passivation films at the positive and negative electrode surfaces are being determined by theoretical (molecular orbital) calculations on the electrolyte component to examine oxidation and reduction voltages. Some of the ionic liquids under consideration are ones reported to show promise in the lithium-battery literature.

Results

Glycerol Carbonate based electrolytes. The GC solvent was obtained from a commercial manufacturer. Electrochemical tests conducted with electrolytes prepared with this as-received solvent showed relatively poor performance. This poor performance may be attributed to the low purity of the GC solvent. According to the manufacturer's specifications, the as-received GC was only 93.5% pure; the remaining 6.5% impurities may include alcohols and moisture, which are known to be detrimental to lithium and lithium-ion cells. We have developed techniques to dry/purify commercially-obtained GC (see Figure IV- 58).

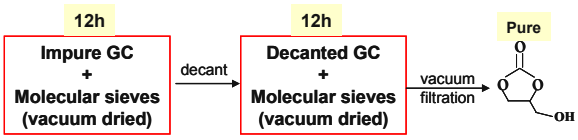

Figure IV- 58: GC drying/purification procedure conducted in an Ar-atmosphere glove box.

The FTIR spectrum of the dried and purified GC (see Figure IV- 59) shows O-H, C=O and C-O features that are characteristic of the GC compound.

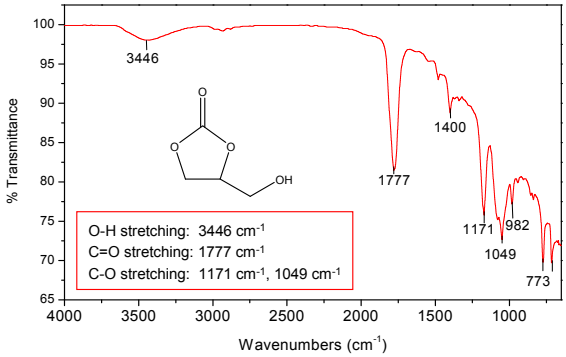

Figure IV- 59: FTIR spectrum of glycerol carbonate.

Electrochemistry data from a Mag10-graphite//Li cell containing a GC-based electrolyte is shown in Figure IV-60. Figure IV- 60 shows that graphite electrodes can be cycled in GC-based electrolytes. The cycling data were obtained at 55°C because the electrolyte viscosity was higher than that of conventional EC-based electrolytes. Figure IV- 60 shows that (i) solvents containing OH groups can be used in lithium battery systems, and (ii) a solid electrolyte interphase (SEI) layer forms on the graphite and protects it from solvent intercalation.

Additives for conventional electrolytes. An ideal electrolyte additive should passivate and protect the electrode surfaces from further reactions with the electrolyte. The PHEV testing conditions include wider voltage windows and greater SOC-swings (than HEV test conditions). Hence, reactions at the positive electrode-electrolyte interface are expected to have a significant impact on cell performance and life. We are investigating the effect of additives that are designed to react on the surface of the cathode to produce a thin lithium-ion conductive layer that stabilizes the electrolyte against further oxidation. Some of these additives are shown in Figure IV- 61.

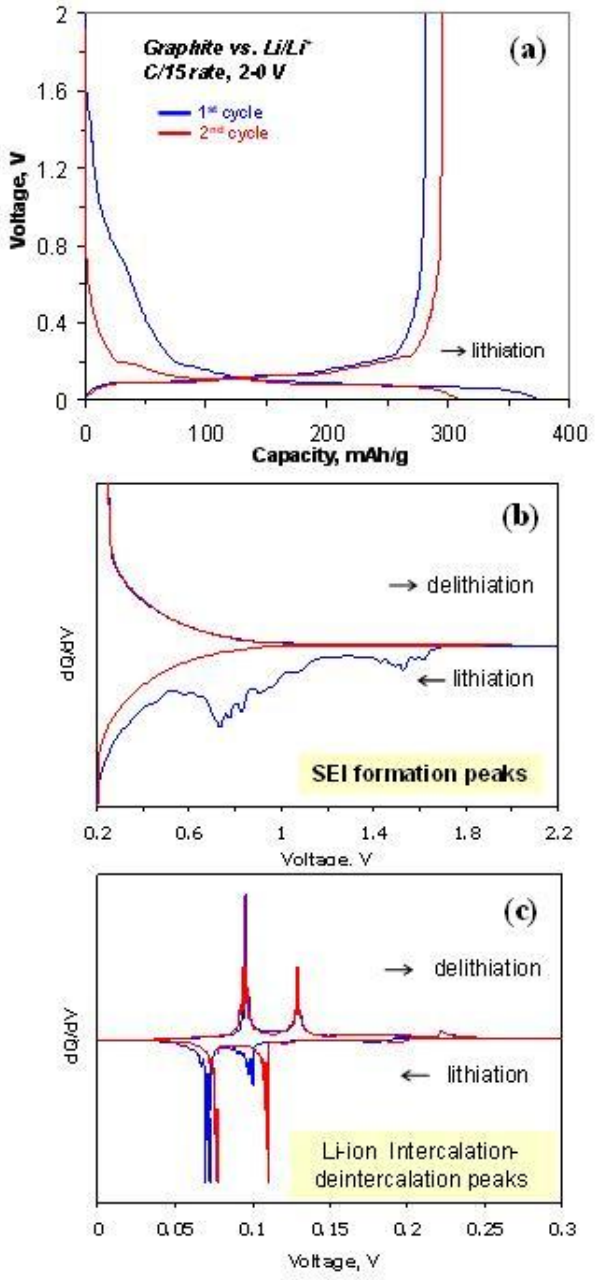

Figure IV- 60: (a) Graphite vs. Li data in cell containing GC-based electrolyte. dQ/dV data showing peaks corresponding to (b) electrolyte reduction, SEI formation, (c) Li-ion insertion and extraction.

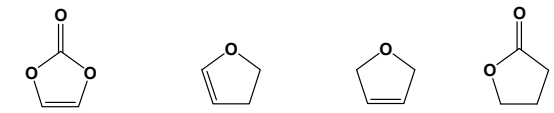

Figure IV- 61: Some of the electrolyte additives being considered to enhance cell calendar and cycle life.

Some initial electrochemistry data with cells containing these additives are shown in Figure IV- 62. The data in Figure IV- 62 were acquired in cells containing a $LiNi_{0.8}Co_{0.2}O_2$-based (NCA) positive electrode, graphite-based negative electrode; the baseline electrolyte was EC:DEC:DMC + 1M $LiPF_6$. Cell cycling was conducted between 3 and 4.5V to increase the rate of electrolyte oxidation at the positive electrode. These initial data indicate that small additions of 2,5 DHF, 2,3 DHF and VC to the baseline electrolyte can improve cell life. Long-term aging experiments are currently in progress.

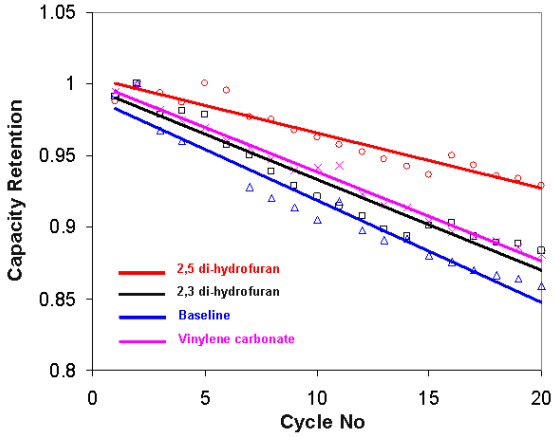

Figure IV- 62: Cells containing the additives show better capacity retention than the baseline electrolyte.

Electrolytes based on ionic liquids. We have initiated tests with room-temperature ionic-liquids (RTIL), and mixtures of RTIL and organic electrolytes, to enable high-safety, high-performance batteries (Figure IV- 63). Some of these tests are being conducted in collaboration with Dr. Adam Best, CSIRO, Australia.

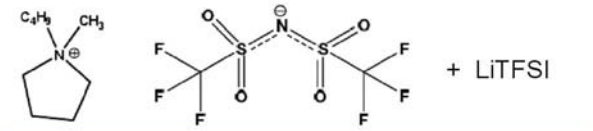

$P_{14}TFSI$ = N-butyl-N-methylpyrrolidinium bis(trifluoromethanesulfonyl)imide

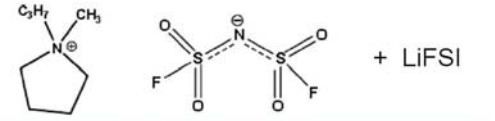

$P_{13}FSI$ = N-propyl-N-methylpyrrolidinium bis(fluorosulfonyl)imide

Figure IV- 63: Some ionic liquid based electrolytes being studied for lithium batteries.

Figure IV- 64 is a representative example of electrochemical experiments being conducted with electrolytes based on ionic liquid solvents.

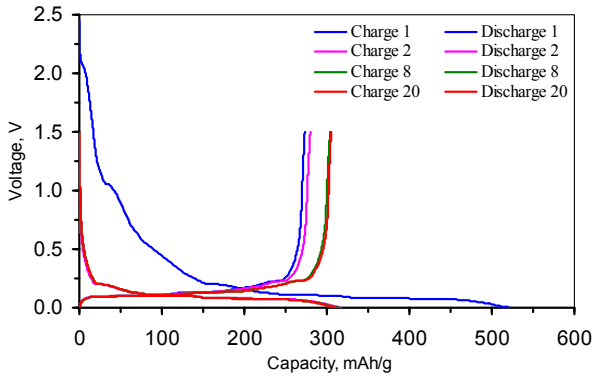

Figure IV- 64: Cycling behavior of graphite//Li cell containing $P_{13}FSI$ + LiFSI tested at 55°C.

The first cycle data shows a high irreversible capacity. But cell efficiency continues to increase with cycling and was >99.9% at and beyond 20 cycles. However, NCA(+)//Li cells containing the $P_{13}FSI$ + LiFSI electrolyte showed very poor cycling behavior. On the other hand, NCA(+)//Li cells containing the $P_{14}TFSI$ + LiTFSI electrolyte cycled well in the 3-4V voltage range and displayed expected capacities. However, graphite//Li cells with this electrolyte showed capacities that were less than half that of the expected values.

Conclusions and Future Directions

Novel electrolytes need to be developed to meet the cost, calendar life and safety requirements of batteries for PHEV applications. These batteries may be deep-discharged >5,000 times during the lifetime of the automobile and should have a calendar life of more than 10 years. Our approach is to (i) develop novel electrolytes that include glycerol carbonate (GC), and modifications thereof, (ii) examine electrolyte additives that can enhance cell life by protecting the electrode surfaces, (iii) investigate the use of ionic liquids to enable high-safety batteries. Our initial studies have focused on developing techniques to prepare high-purity glycerol carbonate. Electrochemical data obtained with these GC-based electrolytes appear promising. We will continue investigating the cycling behavior and performance of electrolytes based on these compounds; properties such as electrochemical stability window, temperature stability, etc. of "promising" electrolytes will be determined.

Our experiments with electrolyte additives designed to protect the positive electrode show promise. In addition to conducting more extensive tests with the current additives, we expect to identify new electrolyte additives that can enhance cell life by protecting the electrode surfaces from reactions with the electrolyte. Effects on cell performance, life, and safety from use of these new additives will be determined. We have also initiated with various electrolytes based on liquids; data from various tests conducted with these electrolytes will be reported in the coming years.

FY 2009 Publications/Presentations

1. Poster presentation at the DOE Vehicles Technology 2009 Annual Merit Review Meeting.
2. "Effect of electrolyte composition on initial cycling and impedance characteristics of lithium-ion cells", *J. Power Sources 180 (2008) 612*.

IV.B.5.2 Development of Electrolyte Additives (ANL)

Khalil Amine
Argonne National Laboratory
9700 South Cass Avenue
Argonne, Il 60439
Phone: (630) 252-3838; Fax: (630) 252-4176
E-mail: amine@anl.gov

Start Date: July 1st, 2009
Projected End Date: September 30, 2010

Objectives

Our first objective is to stabilize the interface of Li-ion batteries by investigating functional electrolyte additives that forms a very stable passivation film at the carbon anode. Stabilizing the interface has proven to be key in improving significantly the cycle and calendar life of lithium batteries for HEV and PHEV applications. The second objective is to develop advanced new stable salt different from the conventional $LiPF_6$ based salt that hydrolyzes and forms HF acid which causes cell performance degradation.

Technical Barriers

- Calendar life
- Cycle life
- Abuse tolerance

Technical Targets

- Develop several new and stable electrolyte additives that form a robust passivation film at the carbon anode to improve cycle and calendar life
- Develop several new and stable electrolyte additives that form a robust passivation film at the oxide cathode to improve cycle and calendar life\
- Quantify the role of these additives in different cell chemistries

✧ ✧ ✧ ✧ ✧

Introduction

For the past decade, the U.S. Department of Energy has been supporting the development of advanced batteries for power assist Hybrid Electric Vehicle (HEVs) and Plug in Hybrid Electric Vehicle (PHEV). These batteries are based on conventional lithium-ion systems with limited calendar and cycle life (less than 2 years). One of the primary life-limiting factors is the high reactivity between the electrolyte and the electrodes at the interface. These surface reactivities lead usually to high cell impedance and significant cell capacity loss.

Approach

To stabilize the interface of Li-ion batteries, we propose to investigate functional electrolyte additives that can be added to the electrolyte and that can either polymerize or be reduced at voltages higher than 1.1 V during the initial formation charging to prevent any conventional passivation film from taking place first at the anode. In the case of the cathode, the additive must be oxidized at voltages above 4V to allow for stable film formation at the interface of the cathode. These additives must form a thin and a uniform film made of one stable single component that protects the interface of both electrodes.

Argonne has identified about a dozen additives that have unsaturated bond needed for polymerization at the surface of the anode. In this project, we will focus on synthesizing some of these additives, carrying out full characterization of the additives before investigating their effect on both cycle and calendar life. The most promising additives will be mixed with the electrolyte in different ratios to determine the most suitable ratio that has a better effect on the cell electrochemical performance. Once an appropriate ratio of the additive has been determined, a full cell study with the additive will be carried out to quantify the impact on cell life and safety by carrying out extensive calendar and cycle life at high temperature as well as well as DSC to check the impact of the additives on carbon anode safety.

This project began late in 2009; therefore the results will be presented during the 2010 Annual Merit Review and the FY 2010 annual progress report.

IV.B.5.3 High Voltage Electrolytes for Li-ion Batteries (ARL)

Kang Xu, Arthur von Cresce, Jan L. Allen,
T. Richard Jow (Technical Point of Contact)

U.S. Army Research Laboratory
2800 Powder Mill Road
Adelphi, MD 20783
Phone: (301) 394-0340; Fax: (301) 394-0273
E-mail: taiguang.richard.jow@us.army.mil

Start Date: August 15, 2008
Projected End Date: September 30, 2010

Objectives

- Develop high voltage electrolytes that enable the operation of Li-ion batteries with high voltage cathodes at higher voltages for enhanced energy density for plug-in hybrid electric vehicles (PHEV).

Technical Barriers

This project addresses the following technical barriers of today's Li-ion batteries:

- State-of-the-art electrolytes made of $LiPF_6$ in carbonate solvent mixtures decompose at voltages above about 4.2 V.
- Electrolytes containing sulfone based solvents are anodically stable up to about 5.8 V but lack ability for forming protective SEI at the anode.
- Commercially available sulfones such as dimethyl sulfone and sulfolane are viscous.
- High voltage cathode materials today do not have suitable high voltage electrolytes for realizing their capacity and achieving long cycle and storage life.

Technical Targets

- Synthesize improved sulfone based solvents with and without unsaturated bonds and evaluate their electrochemical properties.
- Formulate, test and evaluate electrolytes containing synthesized sulfone based solvents in Li half cells.
- Select promising formulations, test and demonstrate in complete cells in button cell or in prototype cell configurations.

Accomplishments

- Synthesized asymmetric sulfone, ethyl methyl sulfone, and sulfones with unsaturated bonds including methyl allyl sulfone (MAS) and methyl propargyl sulfone (MPS).
- Synthesized also carbonate solvents with unsaturated bonds including methyl allyl carbonate (MAC), methyl propargyl carbonate (MPC) and linear cyclic carbonate (LCC).
- HOMO and LUMO of the above newly synthesized solvents were calculated suing QM method (by Professor J. Klauda, U. of Maryland). The correlation coefficients between LUMO and reductive potential and that between HOMO and oxidative potentials are -0.968 and -0.919 for HF/6-31++g(d,p), respectively.
- Using 3-electrode cell with Pt as working and Li as counter and reference electrodes, an oxidation limit of about 6 V vs. Li/Li^+ was observed for electrolytes of $LiPF_6$ in EC-MAS (1:1) and $LiPF_6$ in MAS.
- Comparing to $LiPF_6$ in EC-EMC (3:7 w/o) electrolyte, the ARL sulfone based electrolyte allowed more reversible and higher current response under slow linear voltage scan (at a rate of 0.01 mV/s) up to 4.90 V on $LiNi_{1/3}Mn_{1/3}Co_{1/3}O_2$ working electrode with Li as counter and reference electrodes.
- $LiNi_{1/3}Mn_{1/3}Co_{1/3}O_2$ vs. Li half-cell has been shown a smaller capacity fading when cycling in the ARL sulfone based electrolyte than in $LiPF_6$ in EC-EMC (3:7) electrolyte between 2.5 and 4.9 V.

✧ ✧ ✧ ✧ ✧

Introduction

Achieving higher energy density using the new generation of high voltage cathodes with voltages from 4.5 to 5.0 V such as $LiNi_{1.5}Mn_{0.5}O_2$, $Li_{1+x}Ni_{1/3}Mn_{1/3}Co_{1/3}O_2$, and $LiCoPO_4$ for Li-ion batteries for PHEV will need compatible high voltage electrolytes. The state-of-the-art electrolytes made of $LiPF_6$ in carbonate solvent mixtures decompose at voltages above about 4.2 V and are unable to realize the higher energy density and achieve long cycle and storage life. Compatible high voltage electrolytes are urgently needed to be developed.

Approach

Instead of using the state-of-the-art carbonate based solvent systems, our approach is to explore the use of sulfone based solvent systems. It has been reported that the electrolytes containing sulfone based solvents are anodically stable up to about 5.8 V. However, they lack ability for forming protective SEI at the anode.

Furthermore, the commercially available sulfones such as dimethyl sulfone and sulfolane are viscous. To allow the high voltage operation of the high voltage cathode materials, we will develop electrolytes based on improved sulfone based solvents.

To improve the sulfone based solvent systems, our approaches include the following:

- Explore asymmetric sulfone with different functional groups for lower melting points and low viscosity.
- Explore sulfone solvents with functional groups containing un-saturated bonds.
- Explore the use of sulfone based solvents as additives in combination with other solvent systems such as carbonates and other additives such as vinylene carbonate (VC) for improved performance.

Results

Improved Sulfone Solvents Development. Asymmetric sulfone, ethyl methyl sulfone, and sulfone with unsaturated bonds including methyl allyl sulfone (MAS) and methyl propargyl sulfone (MPS) were successfully synthesized for tests and evaluations.

Evaluation of ARL Sulfone Based Electrolytes Using Cyclic Voltammetry. A number of electrolyte formulations containing sulfone based solvents were evaluated in 3-electrode cells with $LiNi_{1/3}Mn_{1/3}Co_{1/3}O_2$ as working electrode and Li as counter and reference electrodes using cyclic voltammetric technique. The voltage was scanned to 4.90 V vs. Li/Li^+ at a scan rate of 0.01 mV/s. The electrolyte of 1 m $LiPF_6$ in EC-EMC (3:7 w/o) was also evaluated in the same manner as a baseline for comparison. As shown in Figure IV- 65, the $LiNi_{1/3}Mn_{1/3}Co_{1/3}O_2$ electrode has achieved better reversibility and higher current response using one of the sulfone based electrolyte formulations.

4.9 V Cycling Test of ARL Sulfone Based Electrolytes. The capacity of the $LiNi_{1/3}Mn_{1/3}Co_{1/3}O_2$ electrode cycled against Li versus cycle number in the selected sulfone based electrolyte formulation using CR2032 button cell as a test platform is shown in Figure IV- 66. In the first two cycles, the cell was cycled only to 4.2 V to stabilize the interface. The cell was then cycled between 2.5 and 4.9 V. The same electrode tested using the baseline 1 m $LiPF_6$ in EC-EMC (3:7 w/o) electrolyte under the same conditions is also included in this figure for comparison. This figure indicates that the $LiNi_{1/3}Mn_{1/3}Co_{1/3}O_2$ electrode was cycled with a slower capacity fading rate in the sulfone based electrolyte than in carbonate based electrolyte.

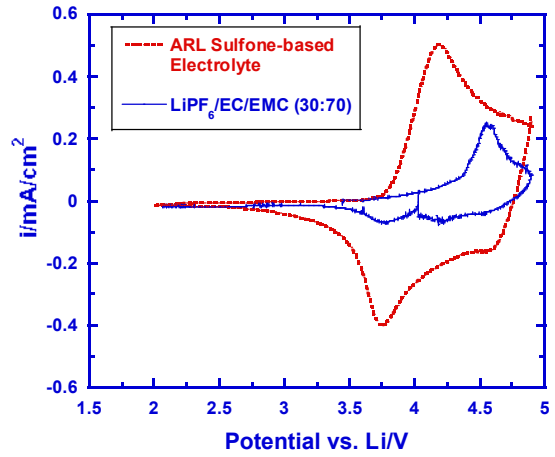

Figure IV- 65: Slow scan (0.01 mV/s) cyclic voltammogram of electrolytes on surface of $LiNi_{1/3}Mn_{1/3}Co_{1/3}O_2$: three electrode configuration, Li as counter and reference; $LiNi_{1/3}Mn_{1/3}Co_{1/3}O_2$ as working.

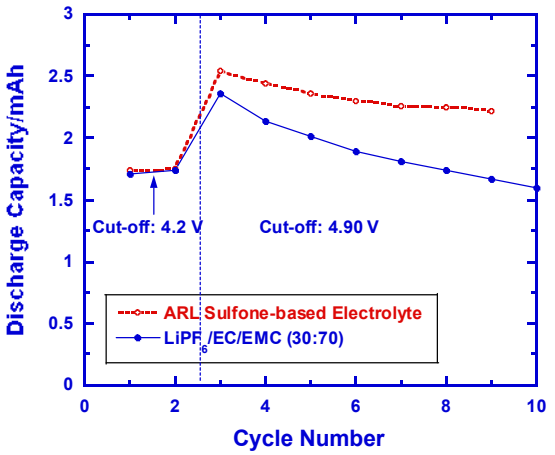

Figure IV- 66: Galvanostatic (0.103 mA/cm^2) cycling of electrolytes on surface of $LiNi_{1/3}Mn_{1/3}Co_{1/3}O_2$: two electrode configuration in CR2032 coin cell; 1st two cycles were cut-off at lower potential to stabilize the surface.

Conclusions and Future Directions

We have identified sulfone–based electrolyte formulations that showed higher stability at the $LiNi_{1/3}Mn_{1/3}Co_{1/3}O_2$ electrode than $LiPF_6$ in EC-EMC (3:7) electrolyte at voltages of as high as 4.9 V. Smaller capacity fading has also been achieved for cycling $LiNi_{1/3}Mn_{1/3}Co_{1/3}O_2$ electrode versus Li in ARL sulfone–based electrolytes than in LiPF6 in EC-EMC (3:7) electrolyte. Our works in progress include the following.

- Further enhance stability of ARL electrolyte formulation on cathode surface: additives (cathode additive) found and under development for extensive long cycling.

- Identified additive (anode additive) that confers stability on graphitic anode while maintaining stability of > 5 V.
- Integration of electrolyte systems for full cell testing.

FY 2009 Publications/Presentations

1. Poster Presentation to the May 2009 DOE Annual Merit Review Meeting.

IV.B.5.4 Development of Novel Electrolytes for Use in High Energy Lithium-Ion Batteries with Wide Operating Temperature Range (JPL)

Dr. Marshall C. Smart
Electrochemical Technologies Group
Device Research and Application Section
Jet Propulsion Laboratory
California Institute of Technology
4800 Oak Grove Drive, M/S 277-207
Pasadena, CA 91109-8099
(818) 354-9374 (Phone)
(818) 393-6951 (Fax)
E-Mail : Marshall.C.Smart@jpl.nasa.gov

Start Date: Oct 1, 2009
Projected End Date: September 30, 2010

Objectives

- Develop a number of advanced Li-ion battery electrolytes with improved performance over a wide range of temperatures (-30 to +60°C) and demonstrate long-life characteristics (5,000 cycles over 10-yr life span).
- Improve the high voltage stability of these candidate electrolyte systems to enable operation up to 5V with high specific energy cathode materials.
- Define the performance limitations at low and high temperature extremes, as well as, life limiting processes.
- Demonstrate the performance of advanced electrolytes in large capacity prototype cells.

Technical Barriers

This project addresses the following technical barriers associated with the development of PHEVs:

(A) Narrow operating temperature range

(B) Limited life

(C) Poor abuse tolerance.

Technical Targets

- The technology development program is focused up enabling 10 s discharge power, and is associated with a number of technical targets, including:
  (a) 750 W/kg (10 mile) and 316 W/kg (40 mile)
  (b) Cold cranking capability to -30°C,
  (c) Cycle life: 5,000 cycles (10 mile) and 3,000 cycles (40 mile)
  (d) Calendar life: 15 years (at 40°C);

Accomplishments

- This is a new project with a projected start date of October 1, 2009

✧ ✧ ✧ ✧ ✧

General Approach

The development of electrolytes that enable operation over wide temperature range, while still providing the desired life characteristics and resilience to high temperature (and voltage) remains a technical challenge. To meet the proposed objectives, the electrolyte development will include the following general approaches: (1) optimization of carbonate solvent blends, (2) use of low viscosity, low melting ester-based co-solvents, (3) use of fluorinated esters and fluorinated carbonates as co-solvents, (4) use of novel "SEI promoting" and thermal stabilizing additives, (5) use of novel non-fluorine based salts (with Materials Methods and LBNL). Many of these approaches will be used in conjunction in multi-component electrolyte formulations (i.e., such as the use of low viscosity solvents and novel additives and salts), which will be targeted at improved operating temperature range while still providing good life characteristics.

Electrolyte Characterization Approach:

The candidate electrolytes will be characterized using a number of approaches, including performing ionic conductivity and cyclic voltammetry measurements, and evaluating the performance characteristics in experimental ~ 400 mAh three electrode cells. Initially, these cells will be fabricated with either (a) MCMB /$LiNi_{0.8}Co_{0.2}O_2$ or (b) graphite /$LiNi_{1/3}Co_{1/3}Mn_{1/3}O_2$ electrode couples. Other electrode can be evaluated depending upon availability from collaborators. In addition to performing charge/discharge characterization over a wide range of temperatures and rates on these cells, a number of electrochemical characterization techniques will be employed, including: (1) Electrochemical Impedance Spectroscopy (EIS), (2) DC linear (micro) polarization, and (3) Tafel polarization measurements. The

electrochemical evaluation in proven three electrode test cells enables electrochemical characterization of each electrode (and interface) and the identification of performance limiting mechanisms. Electrodes are easily harvested from these test cells and samples will be delivered to collaborators (i.e., URI and LBNL). In addition to evaluating candidate electrolyte in spirally round experimental cells, studies will be performed in coin cells, most notably in conjunction with high voltage cathode materials.

Performance Demonstration

Performance testing of large capacity prototype cells containing candidate advanced electrolytes will be performed and evaluated under a number of conditions (i.e., assessment of wide operating temperature capability and life characteristics). JPL has on-going collaborations with a number of battery vendors and the capabilities to perform extensive testing. The type of prototype cells that will be considered include (i) Yardney 7 Ah prismatic cells, (ii) Quallion prismatic cells (0.300Ah size), and (iii) A123 2.2 Ah cylindrical cells. Cells will be procured and obtained through on-going collaborations

Collaborations

We intend to collaborate with a number of institutions, including: (a) Univ. Rhode Island (Brett Lucht: perform analysis of harvested electrodes, on-going collaborator), (b) Argonne Nat. Lab (Khalil Amine: source of electrodes, on-going collaborator), (c) Material Methods, LBNL (John Kerr) (evaluation of novel salt, ex-situ analysis), (d) A123 Systems, Inc. (electrolyte development, on-going collaborator), (e) Quallion, LCC. (electrolyte development, on-going collaborator), (f) Yardney Technical Products (electrolyte development, on-going collaborator), (g) Saft America, Inc. (collaborator, industrial partner under NASA program), and (f) NREL (Smith/Pesaran) (supporting NREL in model development by supplying data).

IV.C. Calendar and Cycle Life Studies

In the calendar and cycle life studies area, researchers are developing and applying novel diagnostics and modeling tools to understand cell behavior, including the cause of capacity and power fade under cycling and calendar aging. Causes of fade being investigated include mechanical fatigue, SEI instability, high voltage breakdown of cathode and electrolyte materials, among others. Also, a group at ANL is developing the ability to make PHEV sized cells for intermediate term testing and diagnostics studies (6 month to 1 year cells).

IV.C.1. Diagnostics and Modeling

IV.C.1.1 Electrochemistry Cell Model (ANL)

Dennis W. Dees
Argonne National Laboratory
9700 South Cass Avenue
Argonne, IL 60439-4837
Phone: (630) 252-7349; Fax: (630) 972-4520
E-mail: dees@anl.gov

Collaborators:
Daniel Abraham, Argonne
Sun-Ho Kang, Argonne
Andrew Jansen, Argonne
Wenquan Lu, Argonne
Kevin Gering, INL

Start Date: October, 2008
Projected End Date: September, 2010

Objectives

The objective of this work is to correlate analytical diagnostic results with the electrochemical performance of advanced lithium-ion battery technologies for PHEV applications.

- Link experimental efforts through electrochemical modeling studies.
- Identify performance limitations and aging mechanisms.

Technical Barriers

The primary technical barrier is the development of a safe cost-effective PHEV battery with a 40 mile all electric range that meets or exceeds all performance goals.

- Interpreting complex cell electrochemical phenomena.
- Identification of cell degradation mechanisms.

Technical Targets

- Develop an efficient parameter fitting technique for model.
- Initiate electrochemical modeling studies on PHEV lithium-ion battery technologies.
- Develop improved electrochemical model for two-phase active materials.

Accomplishments

- Equivalent circuit interfacial model developed for streamlining electrode parameter determination.
  - Parameter estimation remains the primary challenge for examining new intercalation active material electrodes.
- Initiated examination of changes in general battery characteristics and testing protocols going from HEV to PHEV battery studies (e.g. thicker electrodes, different operating currents, wider state-of-charge swings, controlled power testing, etc.).
  - Conducted electrode thickness cell performance simulations.
- Developed new phase-transition reaction-diffusion lithium transport model for two-phase electrode active materials (e.g. LiC_6, $LiFePO_4$, $LiMn_2O_4$, $Li_4Ti_5O_{12}$).
  - Integrated new two-phase active material model into electrochemical cell model and examined graphite negative electrode as test case.
  - Compared new model to earlier shell-core two-phase model.

✧ ✧ ✧ ✧ ✧

Introduction

The electrochemical modeling effort is aimed at associating electrochemical performance measurements with post-test diagnostic studies conducted on lithium-ion cells. The methodology for the electrochemical model is described in detail in the literature.[28,29,30] Two versions of the model are utilized in this effort. One version of the electrochemical cell model is used to simulate the cell response from Electrochemical Impedance Spectroscopy (EIS) studies, and the other model version is utilized for examining DC studies, such as controlled current or power cycling and diagnostic HPPC tests. The underlying basis for both models is the same, as well as their parameter set.

The general methodology for the electrochemical model follows the work of Professor Newman at Berkeley. Continuum based transport equations using concentrated solution theory describe the movement of salt in the electrolyte. Volume-averaging of the transport equations accounts for the composite electrode geometry. Electrode kinetics, thermodynamics, and diffusion of lithium in the active material particles are also included. The detailed theoretical description of the active material/electrolyte interface, commonly referred to as the solid electrolyte interphase or SEI, is based on post-test analytical diagnostic studies. The SEI region is assumed to be a film on the active material and layer at the surface of the active material. The film is taken to be an ill-defined mixture of organic and inorganic material through which Li-ions from the electrolyte must diffuse and/or migrate across to react electrochemically at the surface of the active material. The lithium is then assumed to diffuse through the surface layer and into the bulk active material in the particle. Capacitive effects are incorporated into the model at the electrochemical interfaces and a localized electronic resistance between the current carrying carbon and the oxide interface can also be included. The model can also accept multiple particle fractions with unique characteristics.

Approach

The approach for electrochemical modeling activities is to build on earlier successful HEV characterization and modeling studies in extending efforts to PHEV technologies. The HEV studies involved developing a model based on the analytical diagnostic studies, establishing the model parameters, and conducting parametric studies with the model. The parametric studies were conducted to gain confidence with the model, examine degradation mechanisms, and analyze cell limitations. Efforts this year have focused on expanding and improving the model's data base and capabilities.

Results

Streamlining Electrode Interfacial Parameter Determination. Estimating the parameters for the electrochemical model is a very time intensive effort. The electrolyte parameters are efficiently provided by Kevin Gering at INL utilizing his Advanced Electrolyte Model. However, the interfacial and active material parameters are determined by fitting the AC impedance electrochemical model to experimental EIS electrode data. An equivalent circuit model of the interfacial phenomena was developed to streamline this process.

The dominance of the interfacial impedance in most lithium-ion battery technologies results in a relative uniform current distribution throughout the electrodes. This observation suggests that the interfacial parameters can be fit separately without using the full impedance model. While it is not possible to fully simulate all the interfacial phenomena with a standard equivalent circuit model, a reasonably good approximation was developed that utilizes existing standard EIS fitting programs. Good agreement to full model determined interfacial parameters were obtained for Gen2 NCA (see Figure IV- 67) and Gen3 NMC positive electrodes. This equivalent circuit model interfacial parameter fitting method should considerably shorten the parameter development time for new lithium-ion battery technologies being examined. However, a full impedance model optimization program is needed to efficiently fit the active material parameters associated with the low frequency impedance.

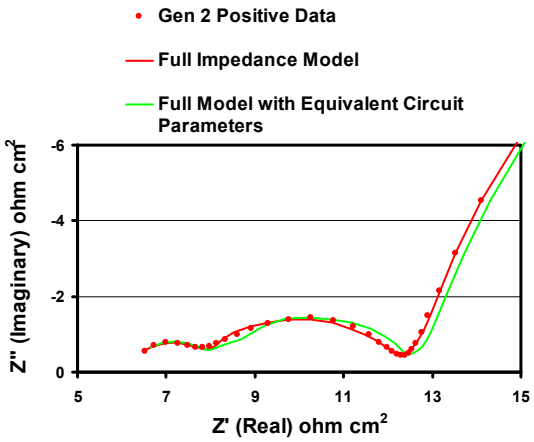

Figure IV- 67: Equivalent circuit model utilized to determine Gen2 NCA positive electrode interfacial parameters

[28] D. Dees, E. Gunen, D. Abraham, A. Jansen, and J. Prakash, *J. Electrochem. Soc.*, **152** (7) (2005) A1409.

[29] D. Abraham, S. Kawauchi, and D. Dees, Electrochim. *Acta*, **53** (2008) 2121.

[30] D. Dees, E. Gunen, D. Abraham, A. Jansen, and J. Prakash, *J. Electrochem. Soc.*, **155** (8) (2008) A603.

Transition from Modeling HEV to PHEV Lithium-Ion Battery Technologies. Generally speaking, there are two types of model changes required for the transition from HEV to PHEV studies. First, there are the straight forward modifications such as thicker electrodes, wider state-of-charge swings, and new testing protocols. Second, there are the more extensive modifications that involve fundamental changes in the active material and/or interfacial portion of the electrochemical model such as coated active materials, two-phase reaction active materials, and new degradation mechanisms. The PHEV electrode thickness studies conducted on a series of NCA positive electrodes provided an excellent opportunity to utilize the previously established Gen 2 HEV electrochemical model for these PHEV studies.

Taking advantage of the previously established Gen 2 NCA positive electrode parameters, the impedance of positive electrode half-cells (i.e. lithium metal electrode/separator/positive electrode) was simulated with the electrochemical model, as shown in Figure IV- 68. The generally good agreement between the model and experiment is a strong indicator that the model is accurately accounting for the effects of the electrode thickness changes. An example of this is the rapid increase in electrode impedance as thickness and active area approach zero. The consistently high experimental values at low electrode loadings can be attributed to the partial breakdown of volume averaging assumption (i.e. the electrode thickness and the active particle size are becoming comparable). The spread in experimental results at high electrode loadings is probably related to the stability of lithium counter electrode.

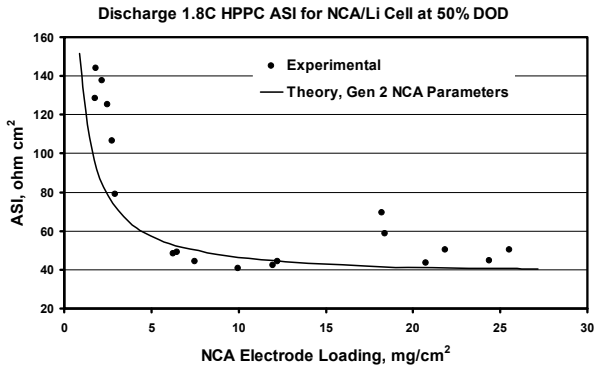

Figure IV- 68: NCA positive electrode loading study: half-cell experimental impedance compares favorably to electrochemical model with Gen 2 electrode parameters

New Lithium Transport Model for Two-Phase Electrode Active Materials. A new phase-transition reaction-diffusion lithium transport model was developed for two-phase electrode active materials (e.g. LiC_6, $LiFePO_4$, $LiMn_2O4$, $Li_4Ti_5O_{12}$). Earlier development of a modified shell-core two-phase active material model that focused on describing the graphite active material was able to adequately account for cell potential changes associated with the transport of lithium in the graphite, but the relatively slow phase transition rate suggested that the two-phase boundary may occur over a region rather than at an interface. Further, literature studies suggest that the shell-core model is not generally correct for lithium-ion active materials.[31]

The new lithium transport model includes lithium diffusion in both phases of the active material and equilibrium at the interfaces between active phases. Volume averaged transport equations are used inside the particle and the well known Avrami phase growth equation[32] (see Equation 1) with a lithium concentration dependent rate constant (k in Equation 1) is used to describe the phase transition. In Equation 1 ε_S is the volume fraction of the phase, t is time, and n is related to the dimensionality of the phase change.

$$\varepsilon_{S2} = 1 - e^{-(kt)^n} \qquad [1]$$

The Avrami, equilibrium, and diffusion equations were integrated into full electrochemical cell model in such a way to add only one variable to the overall model.

As a natural extension to earlier investigations and based on its importance to the lithium-ion battery technology, graphite was selected as a test case for the new model. Staged lithium intercalation into graphite is well studied in the literature with its open circuit voltage curve shows regions of single and two-phase reactions. Also, Galvanic Intermittent Titration Technique (GITT) studies were used to help establish model parameters and compare the new two-phase active material model to earlier shell-core two-phase model. As in the case of the earlier modeling studies the new model was able to accurately simulate the GITT studies as shown in Figure IV- 69.

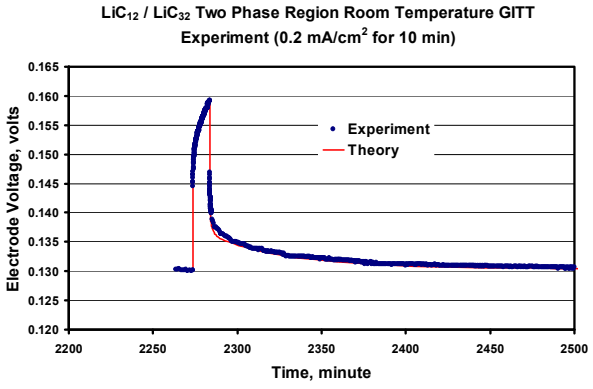

Figure IV- 69: Comparison between simulation and experiment of a graphite negative electrode voltage change during GITT experiment

[31] J. Allen, R. Jow, and J. Wolfenstine, Chem. Mater. **19** (2007) 2108.

[32] Phase Transformations in Metals and Alloys, D. Porter and K. Easterling, New York: Van Nostrand Reinhold, 1981.

However, unlike the shell-core modeling studies the new model indicates (see Figure IV- 70) that as current is passed there is a slow change in the phase distribution throughout the particle. Further, the phase distribution continues to change after current is halted as the lithium concentration gradients in the cell relax. At higher currents (see Figure IV- 71) the phase change occurs faster and closer to the surface. Finally, the phase distribution mirrors the lithium concentration distribution because the phase transition rate is driven by lithium concentration gradients in the particle.

It is interesting to note the changes in the phase distribution within the particle as the phase growth rate is artificially increased. As one may expect, the model's behavior approaches that of the shell-core model at very fast phase change rates. Increasing the phase growth rate narrows the phase change region in the particle. Increasing the phase growth rate also reduces the electrode voltage rise and impedance during discharge. At low currents the slow voltage rise of the electrode follows the inverse of the lithium concentration at the surface of the active material. Increasing the phase growth rate reduces lithium concentration gradients at the surface of the active material, because of the increasing rate that lithium is being released by the phase change.

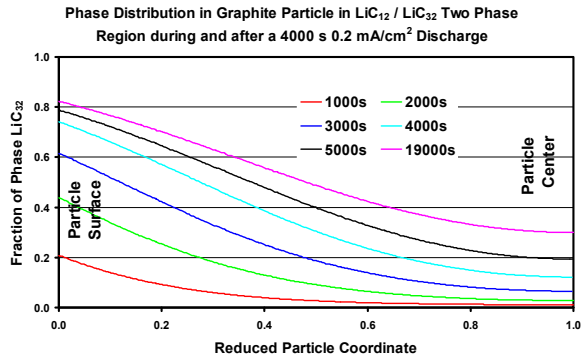

Figure IV- 70: Phase distribution in graphite particle during GITT experiment

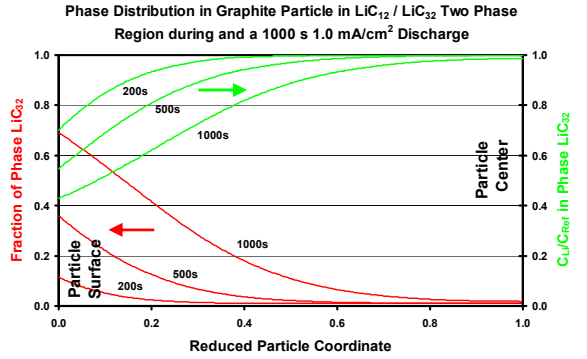

Figure IV- 71: Phase and concentration distributions in graphite particle at higher discharge rate

Conclusions and Future Directions

The equivalent circuit interfacial model should greatly streamline electrode parameter estimation for the full cell electrochemical model. However, a full impedance model optimization program is needed to efficiently fit the active material parameters associated with the low frequency impedance.

The electrode thickness cell performance simulations helped show that the electrochemical model could adequately account for geometric changes in cell designs and as such represented a good first step in the transition to PHEV focused electrochemical models. Obviously, continued development of these electrochemical models is needed such as examining alternative materials, additives, and testing protocols.

With most lithium-ion PHEV technology battery packs having excess power, the primary concern for performance degradation becomes capacity loss. Integration of capacity loss degradation mechanisms into the electrochemical model will be initiated. There also remains needed improvements in the DC electrochemical model such as including non steady-state interfacial effects and adding the capability for multiple active material particle fractions, which will be addressed at a lower priority to other developments.

The new lithium transport model for two-phase active materials adds much to the understanding of these materials while at the same time not increasing greatly the complexity of the complete cell electrochemical model. Further development work needs to be done with the model such as applying it to systems where three phases are present as for the case of graphite at high currents. Also, the EIS version of the phase change electrochemical model needs to be developed. Finally, the model should be exercised on several lithium-ion battery technologies.

FY 2009 Publications/Presentations

1. Poster presentation at the DOE Vehicles Technology Program 2009 Annual Merit Review Meeting.
2. "Analysis of the Galvanostatic Intermittent Titration Technique (GITT) as Applied to a Lithium-Ion Porous Electrode," *J. Power Sources*, **189** (2009) 263-268.

IV.C.1.2 Diagnostic Studies on Li-Battery Cells and Cell Components (ANL)

Daniel P. Abraham

Argonne National Laboratory
9700 South Cass Avenue
Argonne, IL 60439-4837
Phone: (630) 252-4332; Fax: (630) 972-4406
E-mail: abraham@anl.gov

Collaborators:
S.-H. Kang, Argonne National Laboratory
D. Dees, Argonne National Laboratory
A. Jansen, Argonne National Laboratory
I. Petrov et al., University of Illinois at Urbana-Champaign
B. Lucht, University of Rhode Island

Start Date: October, 2008
Projected End Date: September, 2010

Objectives

Battery systems based on lithium-ion technology are being extensively investigated at Argonne. Studies on batteries for hybrid electric vehicles (HEVs) were conducted under the Advanced Technology Development (ATD) program and studies on batteries for plug-in hybrid electric vehicles (PHEVs) are being conducted as part of the Advanced Battery Research (ABR) for Transportation program. The objective of this study is to identify factors that contribute to cell performance degradation (capacity fade, impedance rise) on long-term storage/cycling. Identifying sources of cell performance degradation is an important step towards modifying the cell chemistry to attain the 15y life goal for these cells (for example, by electrolyte additives that modify the electrode surfaces).

Technical Barriers

This project addresses the following technical barriers to the development of a PHEV battery with a 40 mile all electric range that meets or exceeds all performance goals.

- Cell Performance
- Cell Calendar and Cycle Life

Technical Targets

- Determine sources of performance degradation in ATD Generation 3 cells.
- Identify species in graphite SEI layer and determine mechanisms of SEI formation.

Accomplishments

Some highlights from our studies on ATD Generation 3 are as follows:

- The negative electrode is the main contributor to cell impedance rise in cells containing the $LiF_2BC_2O_4$ additive
- The additive improves cell performance by inhibiting impedance rise at the positive, and reducing capacity loss at the negative electrode
- The positive electrode capacity loss on aging is very small. The negative electrode showed measurable capacity loss that apparently results from pore-clogging or particle isolation.
- Increase in negative electrode impedance has been correlated to accumulation of transition metals at this electrode upon cell aging.
- Inhibition of positive electrode impedance rise has been correlated to presence of B-bearing oligomers, arising from $LiF_2BC_2O_4$, at the electrode surface.

Some conclusions from our SEI layer studies on binder-free graphite electrodes cycled in cells containing various electrolytes include the following:

- LiF and phosphate compounds, such as lithium alkyl phosphates $Li_xPO_yR_z$ (R=CH_3, etc), and lithium oxyfluorophosphates $Li_xPO_yF_z$ are important components of the graphite SEI formed in the $LiPF_6$ electrolyte.
- LiF, alkyl borates, such as $B(OMe)_3$, lithium borates Li_xBO_y and lithium fluoroborates $Li_xBO_yF_z$ are prominent in the graphite SEI formed in the $LiBF_4$ electrolyte. The reduction products of the $LiBF_4$ salt are less soluble in EMC than the related reduction products of $LiPF_6$. The insoluble B containing species may include inorganic/polymer compounds (-B-O-) with or without cross-linking.
- A significant quantity of LiF, $Li_xBO_yF_z$ and lithium oxalate (or alkyl esters of oxalic acid) is present in the SEI of graphite formed in $LiF_2BC_2O_4$ electrolyte. Our data also support the presence of organic species/oligomeric compounds that decompose at elevated temperatures.
- Lithium oxalate (or alkyl esters of oxalic acid), Li_xBO_y, tri-coordinated borates and various oligomeric compounds are present in the graphite SEI formed in LiBOB. These compounds appear to be insoluble in EMC, and decompose at temperatures above 200°C. The graphite SEI may be fairly thick

because graphite peaks are not observed in the XPS data and abundant organic decomposition products are found in the TGA data.

- Lithium alkoxides, such as CH_3OLi, and possibly small amounts of lithium alkyl carbonates, such as lithium diethylene carbonate, may also be present in the graphite SEI but these species are washed off during electrode rinsing. Our data does not support the presence of Li_2CO_3 in any of the graphite SEI.

✧ ✧ ✧ ✧ ✧

Introduction

Testing of the third generation ATD cells (i.e., Gen3 cells) is currently in progress. These cells contain a $Li_{1.05}(Ni_{1/3}Co_{1/3}Mn_{1/3})_{0.95}O_2$-based positive electrode, and an MCMB-10 graphite based negative electrode. The baseline electrolyte is 1.2 M $LiPF_6$ in 3EC:7EMC (by wt.); most cells also contain 2-3 wt% $LiF_2BC_2O_4$ as an electrolyte additive, which appeared to improve cell longevity. The Gen3 cells are being tested using both calendar (pulse-per-day) and cycle (continuous cycling) life profiles with periodic interruptions for reference performance tests to gage cell capacity and impedance changes as a function of aging.

Approach

We typically employ electrochemical and physicochemical techniques for our diagnostic studies. Our electrochemical measurements are conducted in cells that include coin cells, pouch cells, and reference electrode cells to determine cell performance, performance degradation characteristics, and degradation sources. Our physicochemical examinations employ a combination of spectroscopy, microscopy, diffraction and chemical analysis techniques that include scanning and transmission electron microscopy, energy dispersive spectroscopy, electron energy loss spectroscopy, X-ray diffraction, X-ray photoelectron spectroscopy, Fourier Transform Infrared spectroscopy (FT-IR) with Attenuated Total Reflectance (ATR), and Nuclear Magnetic Resonance (NMR) Spectroscopy.

Results

Cell Disassembly and Electrochemistry Experiments. Electrochemical cycling and aging data on cells with Gen3 electrodes were obtained from 2032-type coin cells (1.6 cm^2 electrodes), pouch cells (25 cm^2 electrodes) and from larger cells (32 cm^2 electrodes) that incorporated a Li-Sn reference electrode (RE). These cells were made with fresh electrodes or with electrodes harvested from 0.4 Ah pouch cells with an average electrode active area of ~377 cm^2 (see Figure IV- 72). These pouch cells were disassembled in an Ar-atmosphere glovebox with very low oxygen and moisture contents. The electrodes, both from formed and aged cells appeared wet when harvested, which indicated that sufficient electrolyte was present in the cells. For all electrodes the composite coating remained adhered to the current collector, i.e., no delamination was observed even for electrodes from aged cells. Figure IV- 72 shows that the separator color was white on both positive and negative electrode sides for electrodes from the formed cells. In contrast, separators from aged cells were brown on the side facing the positive electrode.

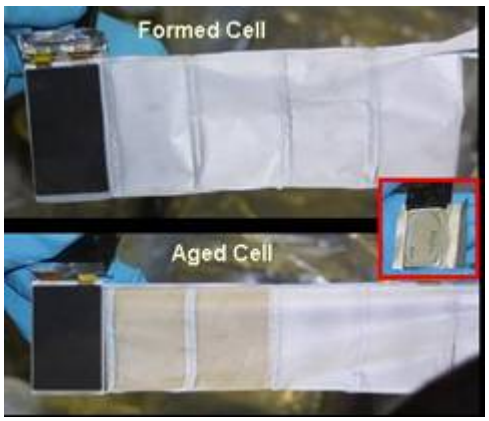

Figure IV- 72: Electrodes harvested from cells after formation cycling and after long-term aging (4V, 38 wks at 55°C); the inset shows a pouch cell image.

The aging studies conducted in the RE cells showed that both positive and negative electrodes contribute to impedance rise, when the cell contains the baseline electrolyte. Cells containing the $LiF_2BC_2O_4$ electrolyte-additive showed lower capacity-fade and impedance-rise, i.e., the additive had a beneficial effect on cell performance. In these cells, the negative electrode was the main contributor to cell impedance rise. Furthermore, the impedance rise was observed in the frequency regime associated with electrode-electrolyte interfacial processes, which indicated that the negative electrode SEI layer becomes more resistive during cell aging. The $LiF_2BC_2O_4$ additive appeared to inhibit interfacial impedance rise at the positive electrode. The impedance rise for this electrode was mainly in the frequency regime associated with electronic processes in electrode, and was probably associated with degradation of contact between oxide particles and the electron-conducting carbons.

Coin cells prepared with aged positive electrodes vs. Li showed capacities similar to that of the fresh electrode at slow cycling rates, i.e., positive electrode capacity loss on accelerated aging was small. However, the aged electrode cells showed greater polarization on discharge, which was consistent with their higher impedance. On the other hand, coin cells containing aged negative electrodes

vs. Li showed significantly lower capacities than that of the fresh electrode (see Figure IV- 73). This capacity loss may be due to several factors that include pore-clogging and/or particle isolation. The $LiF_2BC_2O_4$ additive was seen to be effective in reducing capacity loss. DMC-rinsing of negative electrodes before cell preparation did not help recover "original" electrode capacity.

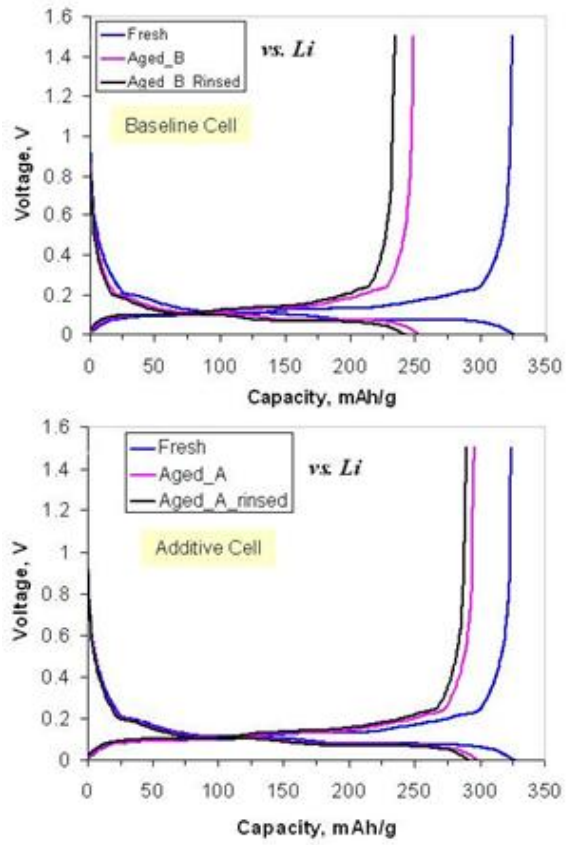

Figure IV- 73: Capacity fade from coin cells containing electrodes harvested from fresh and aged (4V, 38 wks at 55°C) pouch cells.

Diffraction, Microscopy and Spectroscopy. X-ray diffraction (XRD) data on harvested electrode showed no obvious damage to the electrode active materials (oxide-positive, graphite-negative). However, Scanning Electron Microscopy (SEM) images showed a thin surface layer on the oxide electrode after formation cycling which thickened on aging. The images indicated thicker surface films on aged positive electrodes from cells containing the $LiF_2BC_2O_4$ electrolyte additive. X-ray photoelectron spectroscopy (XPS) spectra showed that the composition of positive electrode surface films changes with cell age (see Figure IV- 74). The carbon and binder peaks observed in the fresh positive electrode data were absent in data from aged electrodes indicating an overlying surface film. The aged sample spectra suggested the presence of various species, including ethers (ROLi), carbonates ($ROCO_2Li$), $Li_xPF_yO_z$ and $Li_xBF_yO_z$. Boron-bearing oligomers, arising from $LiF_2BC_2O_4$, may inhibit electrode impedance rise by forming a protective layer on the oxide.

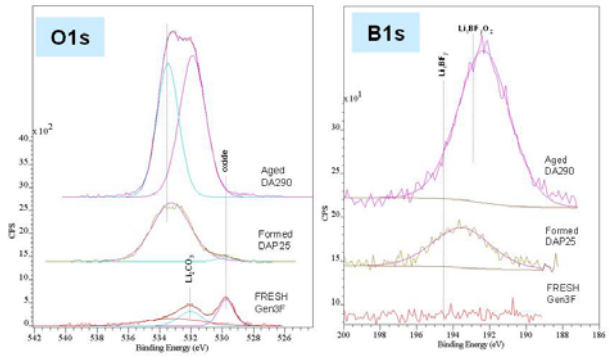

Figure IV- 74: O1s and B1s XPS data from fresh, formed and aged (4V, 38 wks at 55°C) pouch cells show significant differences.

SEM micrographs from harvested negative electrodes showed that the graphite and carbon fibers are covered by a very thin SEI after formation cycling but thicker "surface films" after cell aging (Figure IV- 75). The aged-SEI was relatively smooth on carbon fibers from additive cells and rougher on fibers from baseline cells. XRD data show no changes to the bulk graphite structure. Data obtained by dynamic SIMS and chemical analysis measurements have shown that transition metals accumulate at the graphite electrode on aging (~100 ppm). The higher impedance of the aged graphite anodes may be the result of SEI modification induced by this accumulation of transition metals.

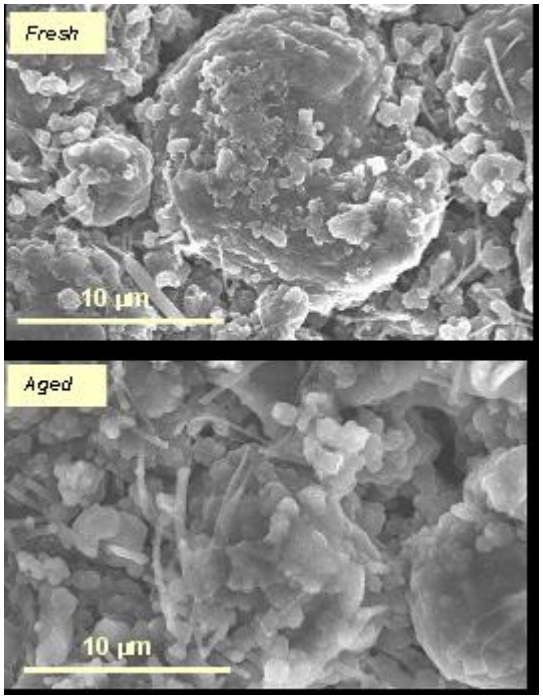

Figure IV- 75: SEM micrographs on graphite electrodes from fresh and aged (4V, 38 wks at 55°C) pouch cells.

Conclusions and Future Directions

We've been studying the performance degradation of ATD Generation 3 cells containing $Li_{1.05}(Ni_{1/3}Co_{1/3}Mn_{1/3})_{0.95}O_2$,-based positive electrode, graphite-based negative electrode, and 1.2 M $LiPF_6$ in 3EC:7EMC (by wt.) electrolyte with and without $LiF_2BC_2O_4$ as an electrolyte additive. Our data indicate that impedance rise is lower for cells containing the $LiF_2BC_2O_4$ additive, which appears to form boron-bearing films that form a protective layer on the oxide electrode. We've shown that the negative electrode is the main contributor to impedance rise in these cells, and have correlated this rise to the accumulation of transition metals at this electrode upon cell aging. In addition, we have characterized the SEI layers that form on graphite electrodes cycled in cells with 1.2M $LiPF_6$, 1M $LiF_2BC_2O_4$, 1M $LiBF_4$, and 0.7M LiBOB salts in 3EC:7EMC (by wt.) solvent, and have postulated reaction mechanisms to explain the presence of the SEI constituents.

In the coming year, we will examine performance and performance degradation of materials and cells tested under PHEV relevant conditions. These cells may contain (a) electrode materials that are new or modified versions of current chemistries, (b) novel electrolytes, or additives to current electrolytes, to enhance cell performance and life, (c) changes in cell testing conditions that include wider voltage windows and greater state-of-charge (SOC) swings, etc. The degradation mechanisms associated with various cell chemistries and testing conditions needs to be identified to determine suitable electrode-electrolyte combinations that will meet the target goals of PHEV batteries. We will also continue examination of electrode surface films after formation cycling in cells containing various electrolytes and electrolyte additives. Some of these experiments will be conducted on model electrodes, such as binder-free graphite electrodes and binder- and carbon-free oxide electrodes.

FY 2009 Publications/Presentations

1. Poster presentation at the DOE Vehicles Technology 2009 Annual Merit Review Meeting.
2. "Examining the Solid Electrolyte Interphase on Binder-Free Graphite Electrodes", *J.Electrochemical Soc. 156 (2009) A318*.
3. "Evidence of Transition-Metal Accumulation on Aged Graphite Anodes by SIMS", *Electrochemical and Solid-State Letters 11 (2008) A226*.
4. "First cycle irreversibility of layered Li-Ni-Co-Mn cathode", *Electrochimica Acta 54 (2008) 684*.
5. "Effect of electrolyte composition on initial cycling and impedance characteristics of lithium-ion cells", *J. Power Sources 180 (2008) 612*.

IV.C.1.3 Structural Investigations of Layered Oxide Materials for PHEV applications (ANL)

Daniel P. Abraham

Argonne National Laboratory
9700 South Cass Avenue
Argonne, IL 60439-4837
Phone: (630) 252-4332; Fax: (630) 972-4406
E-mail: abraham@anl.gov

Collaborators:
J. Bareno, Argonne National Laboratory
S.-H. Kang, Argonne National Laboratory
M. Balasubramanian, Argonne National Laboratory
I. Petrov et al., University of Illinois at Urbana-Champaign
N. Karan et al., University of Puerto-Rico

Start Date: October, 2008
Projected End Date: September, 2010

Objectives

The structure and structural rearrangements in manganese-based oxides, which show anomalously high-capacities when cycled at high-voltages, have a significant effect on cell performance, calendar-life, and safety. The objective of this work is to obtain a detailed structural understanding of the $Li_{1+a}(Mn_xNi_yM'_z)O_2$ family of materials: M' is typically Co, but in order to reduce material cost, other elements such as Fe, Cr, Al, Ga, and Nb are being studied as replacements for Co.

Technical Barriers

This project addresses the following technical barriers to the development of a PHEV battery with a 40 mile all electric range that meets or exceeds all performance goals.

- Oxide/Positive Electrode/Cell Performance
- Cell Calendar Life
- Oxide Stability/Cell Safety

Technical Targets

Our experiments are designed to answer various questions that include the following:

- What are the local atomic arrangements in the as-prepared oxides and how are these arrangements influenced by composition?
- What are the charge compensation mechanisms during oxide delithiation & lithiation, i.e., during electrochemical cycling?
- What phase transformations result on cycling/aging? How does this affect the oxide's capacity and rate performance?
- Do all these oxides lose oxygen during the first high-voltage charge cycle?
- Does the excess Li help or hinder oxide rate performance? Why?
- What are the correlations between the composition, structure, and performance for the various oxides?

Accomplishments

- From data acquired on $Li(Li_{0.2}Mn_{0.6}Ni_{0.2})O_2$ samples we have determined the following:
- In addition to occupying the Li-layers, Li atoms occupy the TM-layers in an ordered manner following a Li-TM-TM-Li sequence.
- A probe of the local Mn-environment indicates a dearth of TM atoms, which suggests that Li atoms preferentially surround (i.e., order around) Mn forming $LiMn_6$-like areas.
- Structural changes result when the oxides are delithiated at voltages greater than 4.5V.
- From data acquired on $Li(Mn_{0.5-x}Ni_{0.5-x}Cr_{2x})O_2$ samples ($0 \leq x \leq 0.2$) we have determined that:
- Partial exchange of Li and Ni among the sites (i.e., cation mixing) decreases with increasing Cr content.
- As-prepared samples contain Ni^{+2}, Cr^{+3}, and Mn^{+4}. Charge compensation on delithiation is accomplished by simultaneous oxidation of Ni^{+2} and Cr^{+3}.

✧ ✧ ✧ ✧ ✧

Introduction

Lithium-bearing manganese-based layered oxides are promising positive electrode active material candidates to achieve high energy and power density lithium-ion batteries. However, the performance and calendar life of existing materials needs to be improved before widespread applications in, plug-in hybrid (PHEV) and fully-electric vehicles (EV) can be realized. Despite considerable materials research over the last decade, the structure of

common cathode materials, as well as their evolution upon cycling, and the atomistic mechanisms responsible for these changes remains the subject of debate.

This project combines advanced structural characterization techniques, including X-ray diffraction (XRD), X-ray absorption spectroscopy (XAS), and analytical electron microscopy (AEM) to investigate atomistic rearrangements in lithium-bearing layered oxide materials during and after electrochemical cycling. Fundamental insights into the tradeoffs between oxide performance and stability will help define new design strategies for the next-generation of high-performance long-lasting batteries.

Approach

We have embarked on a multi-institution effort to synthesize, characterize, and model these complicated oxide structures. After oxide synthesis, structure examination by XRD, and initial electrochemical performance examination, we conduct both *ex situ* and *in situ* XAS measurements on the samples. These XAS studies, conducted at Argonne's Advanced Photon Source (APS) provide information on transition metal (TM) oxidation states, coordination characteristics around the TM atoms, and changes in these parameters during electrochemical cycling. Because the information obtained by XAS is an average over several grains, the data provides a snapshot of the oxide bulk that is used as a guide for analytical electron microscopy (AEM) study, which provides information on the local (<2 nm) structure and composition in the oxides. The AEM study includes electron diffraction and high angle annular dark field (HAADF) electron microscopy to examine the oxide's crystal structure at near-atomic spatial resolution and electron energy loss spectroscopy to examine composition variations in the 1 to 10 nm scale range.

Results

Study of $Li(Li_{0.2}Mn_{0.6}Ni_{0.2})O_2$ samples. The $Li(Li_{0.2}Mn_{0.6}Ni_{0.2})O_2$ compound was synthesized by firing a mixture of $(Ni_{0.25}Mn_{0.75})CO_3$ and Li_2CO_3 at 900°C for 6 h in air. Most peaks in the XRD pattern of the as-synthesized oxide could be indexed based on the α–$NaFeO_2$ (R-3m) structure, with lattice constants a=0.2854 nm and c=1.4225 nm in the hexagonal representation. In addition to the reflections derived from the R-3m structure, a set of small, relatively broad peaks were visible in the range from 2θ = 20° to 25º. These peaks are characteristic of cation ordering in the TM layers, as occurs between the lithium and manganese ions in Li_2MnO_3.

Figure IV- 76 shows charge-discharge cycling data from a $Li_{1.2}Ni_{0.2}Mn_{0.6}O_2$//Li cell. During the first charge cycle, the voltage increases monotonically until ~4.5V corresponding to the oxidation of Ni^{+2} to Ni^{+4}. The long plateau observed, starting at ~4.5V, has been attributed to simultaneous removal of lithium and oxygen from the oxide. The 200 mAh/g first cycle discharge capacity is much larger than the 128 mAh/g value calculated from the oxidation of Ni^{+2} to Ni^{+4}. The ~4.5V plateau is not observed after the first charge cycle. The intensity of XRD peaks in the 20° to 25º 2θ range diminished significantly after cycling at voltages > 4.5V.

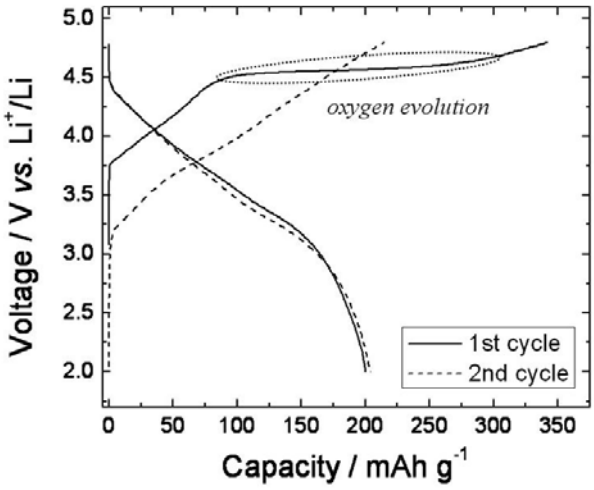

Figure IV- 76: Charge-discharge cycling data from a $Li(Li_{0.2}Mn_{0.6}Ni_{0.2})O_2$//Li cell.

Figure IV- 77 shows selected area electrode diffraction (SAED) patterns from an as-synthesized sample. The [11-20] zone axis pattern shows only the expected reflections from the R-3m structure, while the [10-10] zone axis pattern shows additional streaks at the n/3 (11-20) positions, which suggests ordering in the TM-planes. The presence of streaks (not individual spots) indicates a small ordered-domain size and a lack of domain-periodicity along the c-axis (the direction of the streak).

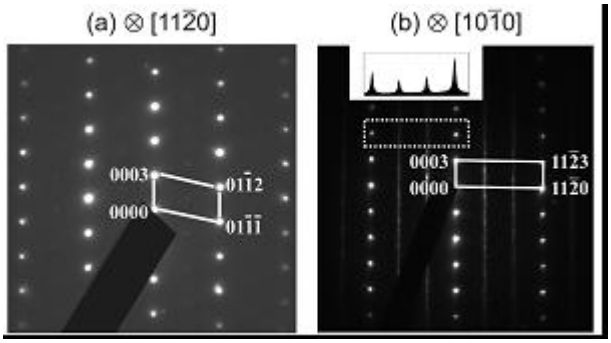

Figure IV- 77: SAED patterns from $Li(Li_{0.2}Mn_{0.6}Ni_{0.2})O_2$ recorded along [11-20] and [10-10] zone axes.

In HAADF images (also known as Z-contrast images) the intensity in each pixel is proportional to the average atomic number Z of the projected atomic column. Thus,

TM-rich atomic columns appear significantly brighter than either Li-rich or O columns. HAADF images obtained along the [10-10] zone axis showed a distinct dot pattern of two bright columns followed by a dark column (see Figure IV- 78). This dot pattern is a direct consequence of the atomic arrangement in the transition metal plane that follows a sequence of two TM-rich columns (higher Z, brighter) and one Li-rich column (lower Z, darker). The TM planes followed several stacking sequences, bounded by stacking faults along the c-axis. Meshes with distinct rectangular (R) and parallelogram (P) periodicity were observed.

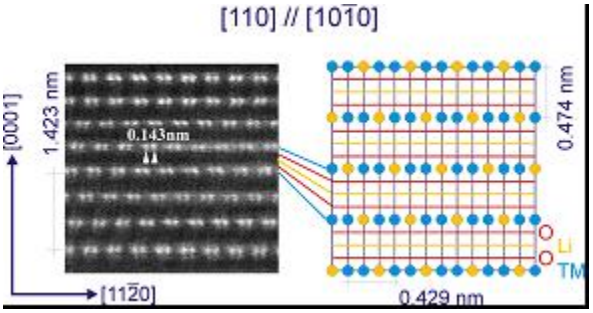

Figure IV- 78: HAADF micrograph showing the Li-TM-TM-Li sequence at TM-planes.

Study of $Li(Mn_{0.5-x}Ni_{0.5-x}Cr_{2x})O_2$ ($0 \le x \le 0.2$) samples.

Layered $Li[Mn_{0.5-x}Cr_{2x}Ni_{0.5-x}]O_2$ ($0 < 2x < 0.2$), (Mn/Ni = 1) samples were synthesized by a chemical solution route. XRD patterns of as-prepared powders are shown in Figure IV- 79. All major diffraction peaks could be indexed based on a hexagonal unit cell (α-$NaFeO_2$ type structure) with space group R-3m. Weak peaks between 2θ = 20 - 25° arise from cation ordering in the transition metal layers. The lattice parameter and peak intensity data indicated that the extent of Li and Ni intermixing decreased with increasing Cr content in the oxide.

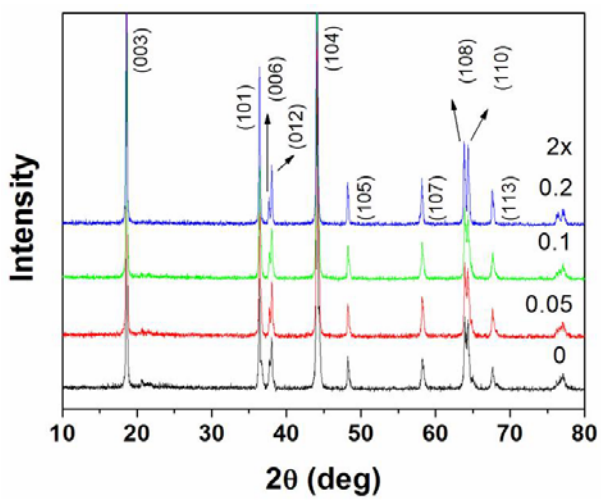

Figure IV- 79: XRD patterns of as-prepared $Li(Mn_{0.5-x}Cr_{2x}Ni_{0.5-x})O_2$ samples.

Electrochemical cycling data in the 3 to 4.3 V range vs. Li/Li^+ showed that charge capacity of the oxides increased with increasing Cr content. The discharge capacity, however, showed a maximum value for the 2x = 0.05 oxide, and was lower for the 2x = 0.1 and 0.2 compositions.

Normalized Ni K-edge XANES spectra for as-prepared $LiMn_{0.5-x}Cr_{2x}Ni_{0.5-x}O_2$ samples are shown in Figure IV- 80. The edge positions and shapes are similar for all samples indicating that predominately divalent Ni is present in all the as-prepared oxides. Corresponding Cr K-edge spectra showed predominately trivalent Cr and Mn K-edge spectra showed predominately tetravalent Mn in all the as-prepared samples.

On electrochemical delithiation (~145 mAh/g capacity), charge compensation in $Li(Mn_{0.5-x}Cr_{2x}Ni_{0.5-x})O_2$ samples is accomplished by the simultaneous oxidation of Ni^{+2} and Cr^{+3} ions, while the oxidation state of the manganese ions remained unchanged. The Ni K-edge in all the $Li(Mn_{0.5-x}Cr_{2x}Ni_{0.5-x})O_2$ samples shifted rigidly to higher energies (see Figure IV- 80), which indicated an increase in the average oxidation state of nickel. The Cr K-edge edge positions also showed a rigid shift to higher energies and a significant increase in the pre-edge peak intensity. These observations indicated that on delithiation some of the Cr^{+3} ions were oxidized to Cr^{+6}.

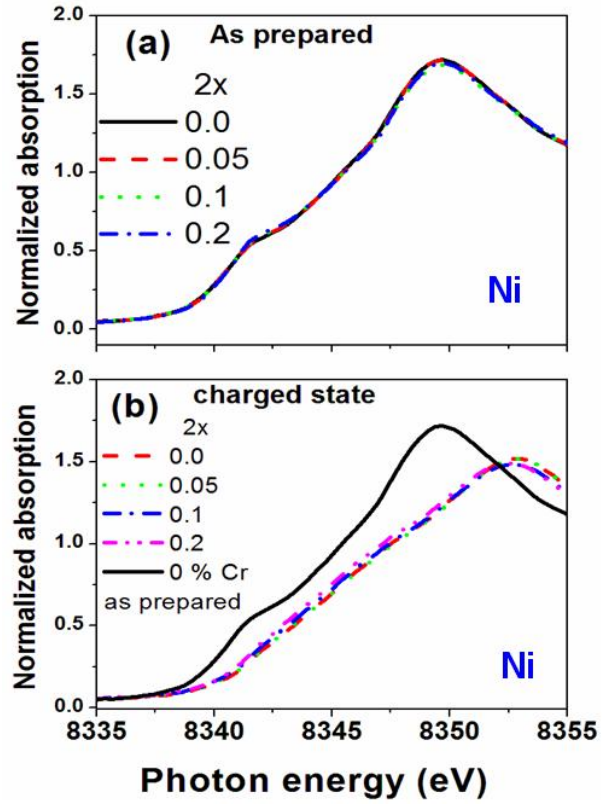

Figure IV- 80: Normalized Ni K-edge XANES spectra of (a) as-prepared, and (b) electrochemically-delithiated $Li(Mn_{0.5-x}Cr_{2x}Ni_{0.5-x})O_2$ samples.

Conclusions and Future Directions

Through a combination of analytical microscopy, X-ray absorption spectroscopy, and electrochemistry techniques we have begun to unravel the complicated local structures in the $Li_{1+a}(Mn_xNi_yM'_z)O_2$materials. The *state of the art* microscopy techniques provides direct access to the atomic arrangement in the layered materials. In particular, HAADF reveals the ordering of Li in the TM planes through contrast modulation due to the significant difference in atomic number between Li and TM atoms.

The small probe size (≃0.1 nm) of aberration-corrected instruments, together with the wide field-of-view range, allow us to bridge the gap between extremely local (XAS, NMR) techniques and long-range (XRD) techniques while maintaining atomic lateral resolution.

Our studies on $Li(Li_{0.2}Mn_{0.6}Ni_{0.2})O_2$ samples show that Li atoms are ordered both in, and normal, to the transition metal planes in the as-synthesized oxide. These results are in agreement with the XAS study, which suggest very local ordering of Li around Mn, resulting in $LiMn_6$-like areas, in the TM planes. The XAS data also show that the Ni atoms are surrounded by transition metal atoms, i.e., there is no indication of Li-ordering around Ni. Studies on cycled electrodes indicate loss of lithium ordering in the TM planes after high-voltage cycling (> 4.5V). Examination of $LiMn_{0.5-x}Cr_{2x}Ni_{0.5-x}O_2$ (2x=0, 0.05 0.1, 0.2) compounds showed that nickel, chromium and manganese are present predominantly in the divalent, trivalent and tetravalent state, respectively in the as-prepared samples. On electrochemical delithiation (~ 145 $mAhg^{-1}$ capacity), charge compensation in the oxide structure is accomplished by the simultaneous oxidation of Ni^{+2} and Cr^{+3} ions, while the oxidation state of the manganese ions remained unchanged.

We are currently examining the structures of other oxides including Li_2MnO_3, $Li_{1.2}Mn_{0.4}Co_{0.4}O_2$ and $Li_{1.2}Mn_{0.4}Cr_{0.4}O_2$ to answer the questions listed in our objectives. These investigations include the following:

- Analytical electron microscopy study of Li_2MnO_3; regions with and without "defects" are being analyzed
- Examination of $LiMn_{0.5-x}Cr_{2x}Ni_{0.5-x}O_2$ charged at voltages >4.5V, i.e., beyond the oxygen evolution regime. Initial data show significant structural rearrangements that affect oxide performance.
- Studies on $Li_{1.2}Mn_{0.4}Co_{0.4}O_2$ and $Li_{1.2}Mn_{0.4}Cr_{0.4}O_2$. Initial data show that the structure and electrochemical performance of Co- and Cr- bearing oxides are different from those of Ni-bearing oxides.

FY 2009 Publications/Presentations

1. "Local structure and composition studies of $Li_{1.2}Ni_{0.2}Mn_{0.6}O_2$ by analytical electron microscopy", *J. Power Sources 178 (2008) 422.*
2. "Structural Characteristics and Electrochemical Performance of Layered $Li[Mn_{0.5-x}Cr_{2x}Ni_{0.5-x}]O_2$ Cathode Materials", *J. Power Sources 187 (2009) 586.*
3. "Structural investigations of layered oxides for PHEV applications", presentation at Lithium Battery Discussion (LiBD 2009), Archachon, France, Sept. 20-25, 2009.
4. Poster presentation at the DOE Vehicles Technology 2009 Annual Merit Review Meeting.

IV.C.1.4 Electrochemistry Diagnostics at LBNL

Frank McLarnon
Environmental Energy Technologies Division
Lawrence Berkeley National Laboratory
Berkeley, CA 94720
Phone: (510) 486-4636; Fax: (510) 486-4260
E-mail: frmclarnon@lbl.gov

Start Date: October 1, 2008
Projected End Date: September 30, 2010

Objectives

- Carry out diagnostic evaluation of ABR Program lithium battery chemistries *via* post-test cell characterization, and investigate cell degradation mechanisms.
- Minimize irreversible cell capacity losses (ICL) *via* synthesis and evaluation of novel carbon-metal composites.
- Develop a reliable, inexpensive, self-actuating mechanism for overcharge protection in high-energy Li-ion batteries for PHEV applications.
- Identify new materials in the BATT Program that are ready for enhanced screening diagnostics.
- Scale-up BATT Program materials and initiate more-enhanced analysis and testing for PHEV applications.

Technical Barriers

This project addresses the following technical barriers facing the battery technology development effort in the DOE Office of Vehicle Technologies:

- Inadequate Li-ion battery energy, lifetime, and safety for PHEV applications
- Need for new advanced battery materials with acceptable specific energy, durability, costs, and safety characteristics
- High ICL during cell formation cycles
- Unacceptable safety problems that accompany inadvertent Li-ion cell overcharge.

Technical Targets

- Determine the specific changes in ABR Program test cell components that accompany battery power fade, capacity fade, and/or catastrophic failure.
- Identify electrode and electrolyte processes that are significantly influenced by various cell-formation protocols.
- Evaluate electroactive polymer morphologies to optimize rate capability and cycle life of overcharge-protected Li-ion cells.

Accomplishments

- Demonstrated that carbon disordering increases anode surface reactivity and causes SEI layer reformation, which shifts the cathode to a higher SOC and accelerates cathode degradation.
- Showed that complete delithiation of graphitic anodes accelerates structural disordering and must be avoided in order to extend Li-ion cell lifetimes.
- Carried out X-ray diagnostic analyses that revealed little electrode degradation of a Gen-3 cell with significant capacity and power loss, suggesting that loss of available Li and/or electrolyte starvation are likely cell fade mechanisms.
- Prepared oriented nanotubes of electroactive polymers with uniform distribution by deposition in the pores of an alumina membrane. These structures will be evaluated for enhanced overcharge protection performance.
- Identified materials from the BATT program that are ready for scale-up and evaluation.

✧ ✧ ✧ ✧ ✧

Introduction

A primary aim of this project is to use advanced diagnostic techniques to characterize ABR Program cell components that are being developed for use in PHEV applications. The diagnostic results are used to determine cell failure mechanisms, as well as suggest new approaches to design more-stable cell components. Another aim is to develop new materials that enhance cell performance and safety, for example by evaluating new electroactive polymers that provide cell overcharge protection. In addition, selected materials discovered in the BATT Program are being evaluated for scale-up and testing for possible PHEV applications.

Approach

This project employs specific research approaches to support development activities in three separate areas:

- **PHEV Electrodes, Materials, and Additives:** (a) fabricate anodes with novel compositions and/or structures that reduce the charge required to form stable SEI layers, and (b) investigate pretreatment regimens for electrodes and/or electrolytes with the goal of reducing capacity losses due to non-SEI-forming side reactions.
- **PHEV Electrode Material Development:** (a) use electroactive polymers as internal overcharge protection agents; (b) maximize protection through the optimization of polymer composite morphology and cell configuration; (c) determine which BATT Program materials are ready for scale-up, testing, and diagnostic evaluation in full cells; (d) decide on the best approach for increasing the quantity of the material to ~200 g; and (e) design full cells and perform long-term cycling.
- **Life Diagnostics:** use advanced spectroscopic and microscopic techniques in conjunction with electrochemical methods to characterize components harvested from fresh and tested PHEV cells, model thin-film cells, and special cells used to evaluate SEI formation processes.

Results

PHEV Electrodes, Materials, and Additives: ***Strategies to Minimize ICL*** **(R. Kostecki and T. Richardson).** We have previously shown that the graphite anodes suffer severe surface structural damage upon prolonged cycling in rechargeable Li-ion batteries. This is evidenced in the Raman spectra of graphite anodes from tested Li-ion cells by the increased prominence of the D-band (~1330 cm^{-1}) with respect to the G-band (1580 cm^{-1}). This effect has been reported for Mag-10 and KS-15 graphite anodes and appears to occur generally in all graphitic carbons.

During the past year we investigated the origin of the surface structural damage in graphite, its implications on the electrochemical performance of graphitic anodes and possible remedies.

Thin-film Mag-10 composite anodes [graphite 92%, PVDF 8%] were assembled into sealed coin cells with a Li metal counter and reference electrodes, a Celgard 2500 separator, and filled with 1.2 M $LiPF_6$, EC:DEC (1:2, by wt%) electrolyte. After three formation cycles at C/25, cycling experiments were carried out galvanostatically at C/5 between the following three potential limits: 1–0.18, 0.098–0.23 and 0.005–0.15 V, all *vs.* Li/Li^+. The respective compositions were $0 \leq x < 0.1$, $0.1 < x < 0.5$ and $0.3 < x \leq 1.0$, where x represents the mole fraction of Li in the Li_xC_6 compound. A total of 200 cycles were carried out. The cells corresponding to these cycling protocols will be referred to as C1, C2 and C3, respectively. C1 cell was cycled between pure graphite and dilute stage-4, C2 cell was cycled between stage-4 and stage-2 compositions and C3 was cycled between stage-3 and stage-1 compositions

Raman mapping of anodes from cycled cells show that the average intensity ratio of disordered to ordered graphite peaks (I_D/I_G ratio) increased from 0.3 for a fresh electrode to 0.45 for C3 cells, 0.58 for C2 cells and 0.61 for C1 cells. Representative Raman maps from all cycled cells display a wide distribution of the I_D/I_G ratio with a large contribution from the disordered graphite. This result suggests that the initial Li-ion intercalation into graphite (*ca.* $Li_{0.05}C_6$) causes the most damage to the graphite surface structure.

Electrochemical impedance spectroscopy (EIS) measurements of the cycled cells support spectroscopic results. All three cells show a significant increase in the impedance in the mid and high frequency sections of the impedance spectrum where Li^+ transport across the SEI film, charge-transfer resistances and/or contact resistances between the graphite particles usually contribute to the anode impedance. The observed impedance increase is the highest in C1 cell followed by C2 and C3 cells. This is in concert with the extent of structural disorder observed by Raman in cycled cells. The more disordering induced in the graphite surface, the more charge is consumed in the SEI reformation, which leads to thicker surface deposits and higher interfacial resistance. The low-frequency behavior, which corresponds to the potential-dependent solid-state diffusion of Li-ion into graphite, is relatively unaffected.

It has been previously reported that intercalation of large anions (*e.g.,* 1-ethyl-3-methylimidazolium) cause more structural disorder in microcrystalline graphite than smaller ions (*e.g.,* L^+). To explain the observed surface disordering in graphite upon cycling one must assume a highly non-equilibrium conditions upon Li^+ insertion/deinsertion, which create large Li^+ concentration gradients between the graphite edge sites and the bulk of graphene domains and induce a significant stress into the graphene planes (Figure IV- 81).

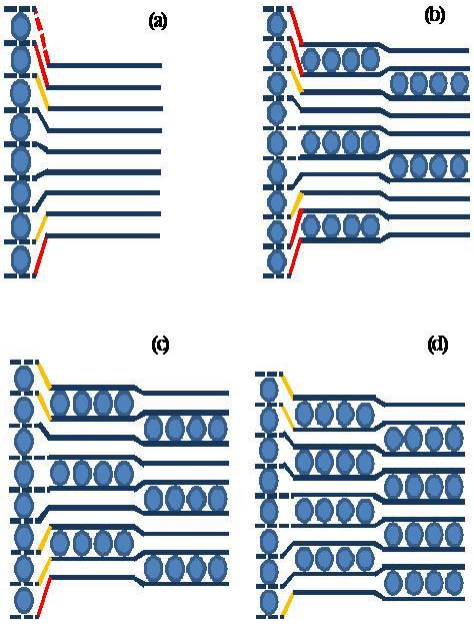

Figure IV- 81: Schematic representation of various stages of Li^+ intercalation (a) graphite, (b) stage-4, (c) stage-3 and (d) stage-2 and the corresponding stress induced in the graphene crystalline lattice.

The largest amount of stretching-bending induced at the edges of the graphene sheets occurs during initial stages of intercalation, *i.e.*, formation of diluted, stage-4 and stage-3 phases. The concentration-gradient between the edge and bulk sites and the corresponding stress gradually decreases during the formation of stage-3, stage-2 and stage-1 compounds, respectively.

PHEV Electrode Material Development: ***Overcharge Protection*** **(G. Chen and T. Richardson).** Electroactive polymers have been shown to provide reversible, internal overcharge protection when incorporated into battery separators. The rate capability and cycle life of the protection mechanism, however, fall far short of what is expected from the intrinsic properties of the polymers. The performance was found to be largely controlled by the morphology of the composite membrane, which determines the utilization of the polymer as well as the effectiveness of the electronic conduction path established between the cathode and the anode upon overcharge. In addition, the normal cell performance could be affected by the reduced porosity of the composite membrane.

To improve the efficiency of the protection, a composite morphology with uniform, continuous polymer distribution through the separator pores is desirable. One approach is to use an array of electrodeposited polymer nanowires or nanotubes to directly connect the anode and cathode. This would maximize the current density through the composite during overcharging, while reducing the separator area required for the conducting polymer. Such a structure was fabricated by electrochemical polymerization of 3-butylthiophene within the uniform, cylindrical pores of a commercially available porous alumina membrane (Anodisc 25, Whatman Corp.). This membrane, which has a pore size of 20 nm, was first coated with a 10 nm Au layer to provide electrical contact for the growing the polymer deposit. Electrodeposition of poly(3-butylthiophene) was achieved through electro-oxidation of the monomer dissolved in 1.0M $LiPF_6$ in propylene carbonate (PC) and dimethyl carbonate (DMC) electrolyte (1:2). Figure IV- 82 shows the nanostructured polymer obtained after 30 cycles, after removal of the alumina template. The polymer deposit consists of aligned nanotubes 20 nm in diameter, extending the full 60 μm thickness of the template, so that each polymer nanotube is capable of providing an overcharge current path upon oxidation. Cells will be fabricated to test the overcharge protection performance of these composites.

Commercially available membrane templates with different porosities, pore sizes, and compositions will also be used. The approach will be applied to a range of electroactive polymers for the preparation of composite separators.

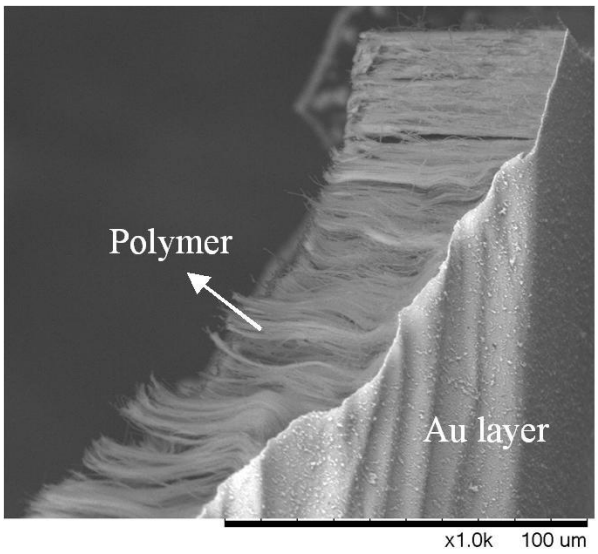

Figure IV- 82: SEM image of electrodeposited poly(3-butylthiophene) nanotubes.

PHEV Electrode Material Development: ***Scale-up of BATT Program Materials for Evaluation*** **(V. Battaglia).** In mid-May we received our first allocation of resources to start this new project in BATT materials scale-up. On June 24, a visiting scholar from Tianjin University, Jin Chong, arrived and has assumed research leadership of the project. One of the first tasks we accomplished was to survey the BATT Program for new materials. We received several responses. Table IV-3

provides the list of contributors, the material they intend to provide, and the status.

Table IV-3: List of Research Contributors

Investigator	Material	Status
G. Ceder	High-rate $LiFePO_4$	Will visit Nov. 30
M. Thackeray	High-capacity NCM	Waiting for materials
N. Dudney	$LiFePO_4$-impregnated carbon mat	Waiting for materials
M. Doeff	Al-doped NCM	Waiting for materials
P. Kumta	Si-C nano-composite	Waiting for materials
K. Zaghib	$LiFePO_4$	Laminates arrived 10/1/09
B. Lucht	$LiPF_4C_2O_4$	Arrived 9/10/09

As we waited on the results of the survey, Mr. Chong familiarized himself with our electrode fabrication and cell testing techniques. He worked on a new polymer system based on poly acrylic acid (PAAH) which was initiated based on certain promising results from Japan. This is a water soluble binder system. We have been testing the acid form as well as the Li, Na, and K substituted forms. Preliminary results showed that during the mixing step, the slurry with cation substituted polymers contained a large number of dispersed bubbles, which resulted in laminates with macroscopic holes. We also found agglomerated acetylene black in the cast films. In addition, the dried films were very brittle, with thicker films showing cracks; full cells could only be made from electrodes with PAAH, PAALI, and PAALI and acetylene black. Cathodes of $LiFePO_4$ and the new binder were also cast. Cells were also made using PVdF and acetylene black as a comparison. We found that the electrodes with PAALi showed the best reversible capacity and improved first cycle ICL. Cycling performance showed that the electrode with PAALi and acetylene black had the best rate performance and the best cycle-ability.

Life Diagnostics: *Diagnostic Evaluation of ABR Battery Chemistries* (R. Kostecki and T. Richardson). Gen3 cell components from cell number G3A.60L45.I105.23.64.54.G.T were received from ANL following 64 weeks testing at 45°C in which the cell suffered 20% capacity loss and 54% power fade. The electrodes were examined by SEM/EDX, XRD, and *ex situ* cycling. The cathode was found to have 100% of its initial C/25 capacity. XRD of a cathode sample following rapid charging and rinsing to remove electrolyte showed only very small relaxation, indicative of little or no particle isolation in the electrode (Figure IV- 83). Anodes appeared to be in good condition, although small deposits of transition metal oxides were found with highly varying metal ratios, indicating that they were not dislodged particles from the cathode.

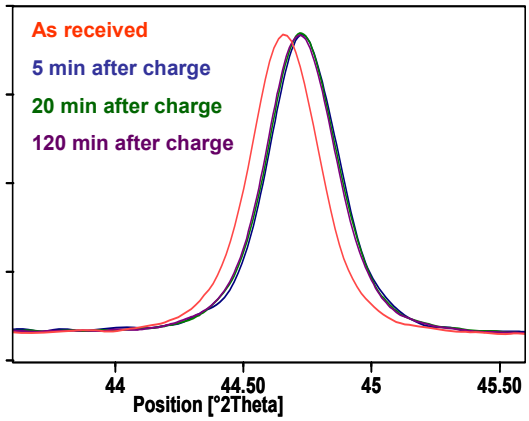

Figure IV- 83: XRD patterns of fresh and fast-charged Gen3 cathode.

Conclusions and Future Directions

Avoiding complete delithiation and/or shallow cycling of graphite anodes close to the fully discharge state can minimize the extent of graphite disordering. Consequently, the contribution from the irreversible processes involved in the SEI layer reformation and the associated loss of cyclable lithium in the battery can be reduced and the battery life extended. This negative effect is likely to be intensified at higher cycling rates and/or elevated temperatures where faster charge transfer kinetics result in a greater disparity of Li concentration between the surface and bulk.

More detailed analysis of the Li_xC composition-dependent electrochemical stress, including its temperature and rate dependence, are currently underway. A more quantitative analysis of this phenomenon, as well as the roles of elastic and electrostatic interactions in intercalation and staging, is currently being pursued from both experimental and computational perspectives.

More work needs to be done to determine the cause of and then eliminate the agglomeration of acetylene black and the macroscopic holes. We are in the process of testing cells with the $LiPF_4C_2O_4$ salt from Prof. Lucht. We are ordering the materials and equipment for synthesizing the $LiFePO_4$ from Prof. Ceder. We are planning a trip to MIT to work in Prof. Ceder's lab as part of the tech transfer of making their materials. We shall soon test the laminates from HQ.

Overcharge protection separators with a variety of morphologies will be investigated, with the aim of optimizing protection while minimizing the impact on normal cell performance, cost, and complexity.

FY 2009 Publications/Presentations

1. Presentation to the 2009 DOE Annual Peer Review Meeting.
2. L. J. Hardwick, M. Marcinek, L. Beer, J. B. Kerr, R. Kostecki, "An Investigation of the Effect of Graphite Degradation on the Irreversible Capacity in Lithium-ion Cells," *J. Electrochem. Soc.* **155**, A442 (2008).
3. L.J. Hardwick, V. A. Sethuraman V. Srinivasan, R. Kostecki, "A Study of the Mechanism of Graphite Structural Degradation in Lithium-ion Cell Anodes," 214th ECS Meeting, Oct. 12-17, Honolulu, HI.

IV.C.1.5 Investigate Mechanical Fatigue in Cycled Electrodes (ORNL)

Claus Daniel
Oak Ridge National Laboratory
1 Bethel Valley Rd.
P.O. Box 2008, MS-6083
Oak Ridge, TN 37831-6083
Phone: (865) 241-9521; Fax: (865) 241-5531
E-mail: danielc@ornl.gov

Start Date:	January 2, 2009
Projected End Date:	September 2010

Objectives

- Establish a fundamental understanding of (1) crack initiation, growth, and particle fracturing and (2) the role of mechanical degradation in capacity fade
- Develop "fatigue-like" models to predict lifetime and to guide the development of electrode microstructure
- Establish a laboratory-scale methodology for using acoustic emission (AE) for monitoring degradation in Li-ion batteries.
- Develop the tools and procedures needed to combine AE with X-ray diffraction (XRD). The correlation between emission parameters and structural changes in electrode materials will be explored.

Accomplishments

- Develop procedures for electrode fabrication, cell cycling, and AE collection from Li-ion half cells.
- Test cells with various electrode materials, including mesocarbon microbeads (MCMB), and determine any initial correlation of AE with degradation processes in the materials.

✧ ✧ ✧ ✧ ✧

Introduction

Intercalation compounds in batteries experience volume changes during cycling. Related stress and strain can cause mechanical degradation. The role of mechanical degradation on capacity fade is debated. A fundamental understanding of the accumulation of point defects, the initiation of cracks, crack growth, and particle fracture and sliding is needed in order to understand their roles on capacity fade. An understanding of those mechanisms in different intercalation compounds can furthermore be developed in "fatigue-like" models in order to create better lifetime predictions and guidance for microstructural design of advanced electrodes.

Approach

Acoustic emission spectroscopy is utilized to detect, sort, and classify mechanical events such as crack initiation, crack growth, particle or coating fracturing, and particle loosening and sliding during cycling. Additional characterization methods (such as XRD, Raman spectroscopy, and various microscopy techniques) are planned to be performed in situ in order to link acoustic signatures to "real" events. This will allow for a further fundamental understanding of those mechanisms and their contributions to capacity fade. In a later stage of the project, "fatigue-like" models will be developed that can predict cycle life and guide advanced microstructure development for improved mechanical performance.

Results

Initially, MCMB electrodes were studied. Future studies will include a variety of other electrode materials. Several classes of events were identified from the AE data. Type 1 emissions may result from crack initiation or propagation in the solid-electrolyte interphase (SEI) layer that develops on and around individual MCMB particles. Other authors have associated emissions similar to Type 2 with gas formation. Because CO_2 is a by-product of SEI formation, the formation of CO_2 bubbles is a likely source of this emission type. A Type 3 emission is characteristically very similar to a Type 2, but with a less-defined waveform and frequency peak average and duration. The source of this event type is unclear but may result from shifting of the MCMB particles past one another as they expand and contract or from tearing of the composite film.

Events were manually sorted into class types and were put in a scatter plot to establish grouping trends. The values of an event's duration, amplitude, and frequency centroid parameters proved particularly important in discriminating between different event types. Amplitude was very useful in filtering electromagnetic interference events that showed very regular emission amplitudes. The duration, amplitude, and frequency centroid proved to be statistically different between Type 1, 2, and 3 emissions based on Student's t-tests with 95% confidence. Figure IV-84 shows a scatter plot matrix of these three parameters.

An SEM image of the cycled electrode showed the presence of a fractured SEI layer (see Figure IV- 85). The formation of these cracks is the most likely source of Type

1 events. SEM images of the electrodes in cross-section showed a 28% increase in thickness, from 25 to 32 µm, as a result of cycling. This may indicate a loosening of the composite film as cycling proceeds, which may allow for an increased amount of particle shifting and hence the observed increase in Type 3 emissions as cycling proceeds.

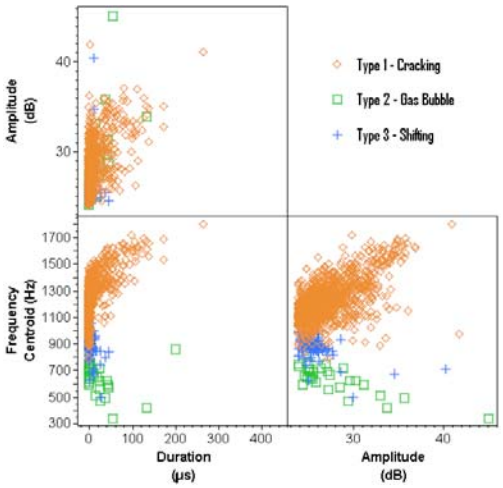

Figure IV- 84: Scatter plot of duration, amplitude, and frequency centroid showing grouping of emissions useful for identifying event types.

Conclusions and Future Directions

The use of AE to identify and monitor various processes inside a cycling Li-ion half cell has been demonstrated. This demonstrates the ability of AE to provide not only information of when events occur during cycling within the system, but also information about their nature. Knowing the source of emissions and how to identify their characteristics from MCMB composite electrodes in half cells may allow for their identification in more complex commercial cells, where additional sources of AE may exist. The inherent in situ nature of AE may allow for its combination with other characterization techniques. Work is currently under way to develop a combined AE-XRD technique to allow correlation between AE and atomic structure in active electrode materials. Furthermore, AE cycling experiments are currently under way on Si as well as other materials, such as $LiCoO_2$, $LiMnO_2$, and Sn.

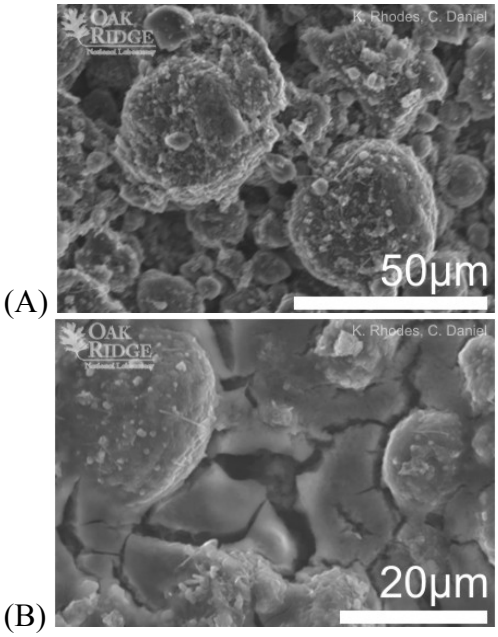

Figure IV- 85: SEM of (A) a fresh MCMB electrode and (B) the electrode after cycling, showing a fractured SEI layer.

FY 2009 Publications/Presentations

1. K. J. Rhodes, C. Daniel, N. Dudney, E. Lara-Curzio, Acoustic Emission from MCMB Electrodes in Li-ion Half Cells, J. Electrochem. Soc. (submitted)
2. K. Rhodes, C. Daniel, E. Lara-Curzio, N. Dudney, Characterization of Fatigue Behavior of Electrode Materials for Li-ion Batteries using Acoustic Emissions, 215th Electrochemical Society Meeting, San Francisco, CA, May 24-29, 2009
3. K. Rhodes, C. Daniel, E. Lara-Curzio, N. Dudney, Degradation and Fatigue of Active Electrode Materials for Li-ion Batteries, Oak Ridge Chapter of ASM Educational Symposium, Materials for Megawatts, Oak Ridge, TN, April 22, 2009 (Poster talk; 2nd place for outstanding student research)
4. K. Rhodes, C. Daniel, N. Dudney, E. Lara-Curzio, Analysis of Cycling Induced Fatigue in Electrode Materials for Li-ion Batteries, Materials Science & Technology 2009, Oct. 25-29, 2009, Pittsburgh, PA
5. C. Daniel, Materials and Processing for Lithium-Ion Batteries, Materials Science & Technology 2009, Oct. 25-29, 2009, Pittsburgh, PA (invited)

IV.C.2. Cell Fabrication and Testing

IV.C.2.1 Fabricate PHEV Cells for Testing & Diagnostics (ANL)

Andrew N. Jansen

Argonne National Laboratory
9700 South Cass Avenue
Argonne, IL 60439-4837
Phone: (630) 252-4956; Fax: (630) 972-4461
E-mail: jansen@anl.gov

Collaborators:
Dennis Dees, Argonne National Laboratory
Wenquan Lu, Argonne National Laboratory
Sun-Ho Kang, Argonne National Laboratory
Paul Nelson, Argonne National Laboratory
Chris Joyce, Argonne National Laboratory
Johnson Controls-SAFT
Mobius Power
Media-Tech (Korea)

Start Date: October, 2008
Projected End Date: September, 2010

Objectives

- Several new battery chemistries are being proposed for PHEV batteries that must be evaluated in cell formats that are larger than a few mAh in capacity. The main objective of this task is to obtain trial cells for calendar and cycle life studies in pouch cell or rigid cell (*e.g.* 18650) formats from industrial battery vendors.
- Electrode designs must be developed that are appropriate for PHEV batteries.
- Argonne will develop the capability to fabricate in-house trial cells in its new dry room facility.

Technical Barriers

- Newly developed battery materials for PHEVs need to be tested in limited batch size before larger scale industrial commitment.
- Validation tests are needed in cell formats with at least 0.4 Ah in capacity.

Technical Targets

- Produce graphite and NCA electrodes of varying thickness and test performance.
- Use thickness performance data to design PHEV battery.
- Place order with qualified vendors to make electrodes and pouch/18650 cells for ABR.
- Distribute vendor cells to ABR for testing and diagnostics.
- Design and install facility for making in-house 18650 and pouch cells at Argonne.

Accomplishments

- Made cathode and anode electrodes of varying thickness to determine influence of electrode thickness on impedance and active material utilization.
- Determined optimum PHEV battery parameters using Battery Design Model with baseline electrode results as input.
- Ordered baseline PHEV electrodes from vendor.
- Identified cell making vendor willing to make 18650 cells using baseline PHEV electrodes.
- Completed design and installation of new dry room that will be used to fabricate future lithium-ion prototype cells.
- Ordered 18650 and pouch cell making equipment that will occupy new dry room after extensive discussions with Asian vendors.

✧ ✧ ✧ ✧ ✧

Introduction

The previous ATD program required cells designed for HEV applications, which used thin electrodes. The performance of thicker PHEV electrodes must be determined and verified in a baseline cell build using NCA and Mag-10 graphite, which were the baseline materials known as Gen2 in the ATD program. Subcontracts will be established with battery developers to produce flexible or rigid cells based on

materials from the vendor screening subtask or from materials developed in the ABR and BATT programs. This will occur while Argonne's in-house cell making capability is being developed, and also for several months after the in-house capability is established. Comparisons will then be made between developer-made cells and cells made in-house. Once the in-house cells are deemed to be reliable, the developer subcontracts will be reduced and the ABR Program will rely on Argonne for cell builds.

Approach

Promising new exploratory materials are often developed in small coin cells, which may or may not scale up well in large PHEV battery designs. For this reason, pouch cells or rigid cells such as 18650s will be used for testing new materials in the capacity range of 0.4 to 2 Ah.

It is anticipated that pouch cells will be used for initial evaluations of long-term exploratory materials. Pouch cells are an efficient method of determining the stability of a cell system during calendar and cycle life aging. If the chemistry is not stable, it is likely that gassing will occur inside the cell. This will result in the pouch cell bulging or rupturing if the gassing is significant. More established materials and chemistries (or those that pass the pouch cell evaluation) will be used in rigid cells (*e.g.* 18650s).

Concurrent to the fabrication of PHEV cells by industrial vendors, Argonne will develop the capability to fabricate pouch cells and 18650 cells at Argonne. Key to this is the installation of a new dry room facility and acquisition of required cell making equipment. It is expected that in-house trial cells will be produced at Argonne during FY10.

In the mean time, trial cells will be purchased from battery developers through subcontracts. Subcontracts will be established with battery developers to produce these cells based on screened materials from suppliers and from the ABR and BATT programs. Electrode-making equipment will be installed based on arrival of purchased equipment and completion of dry room. Once in-house cells are deemed to be reliable, the developer subcontracts will be reduced.

Results

Negative Electrode Thickness Study. Single-sided negative electrodes were made with varying thickness using Argonne's mini-coater. The active loading was 92 wt.% Mag-10 graphite from Hitachi Chemical with 8 wt.% PVDF binder (Kureha KF9130). A relationship between total material loading and calendered thickness was established as shown in Figure IV- 86. Half cell studies were performed to establish specific capacity of the graphite as a function of total material loading. These results are presented in Figure IV- 87, which indicate that utilization is not significantly affected by thickness (at low current rate). Electrodes above ~11 mg/cm² loading had relatively poor adhesion. For reference, the total material loading for the ATD Gen2 negative was 4.8 mg/cm².

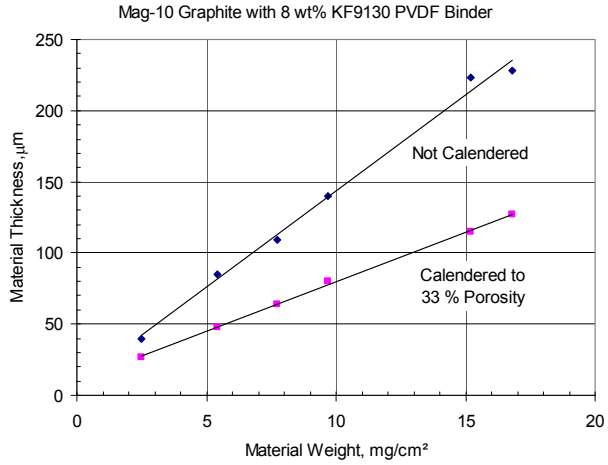

Figure IV- 86: Relationship between material thickness and total material loading for Mag-10 graphite negative electrode.

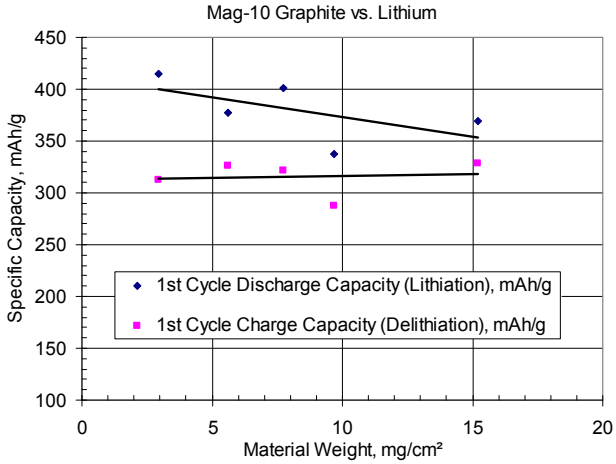

Figure IV- 87: Specific capacity of Mag-10 graphite (vs. lithium) at 0.25 mA/cm² as a function of total material loading.

Positive Electrode Thickness Study. Single-sided positive electrodes were also made with varying thickness using Argonne's mini-coater. The active loading was 84 wt.% $LiNi_{0.8}Co_{0.15}Al_{0.05}O_2$ (NCA) from Toda with 8 wt.% PVDF binder (Kureha KF1120) and 4 wt.% SFG-6 graphite (Timcal) plus 4 wt.% acetylene black (Chevron ABC-55). The total material loading versus thickness is shown in Figure IV- 88. The specific capacity of the NCA as a function of total material loading is presented in Figure IV- 89. (The electrolyte used in all these studies was 1.2 M $LiPF_6$ in EC:EMC (3:7 w/w)). A slight decrease in specific capacity is seen as thickness increases. For reference, the total material loading for the Gen2 positive was 8.8 mg/cm².

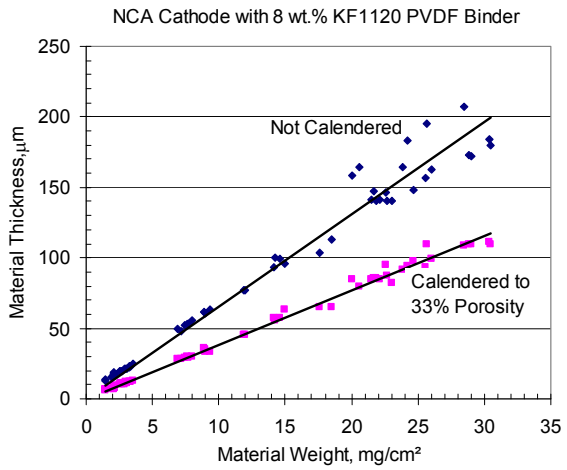

Figure IV- 88: Relationship between material thickness and total material loading for NCA positive electrode.

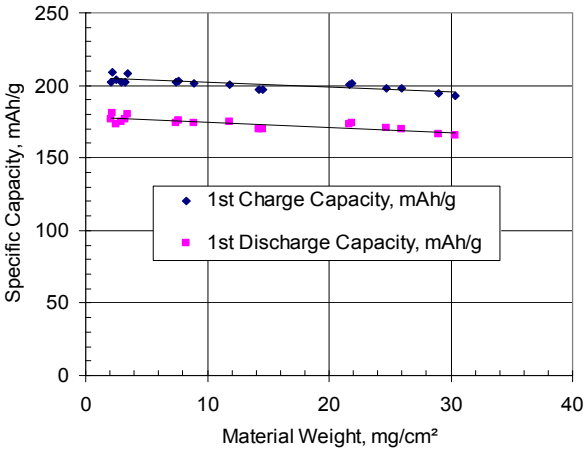

Figure IV- 89: Specific capacity of NCA (vs. lithium) at C/10 rate as a function of total material loading.

Investigations were also performed to assess the impact of material loading density on HPPC impedance. These results are shown in Figure IV- 90 for the case of NCA versus CGP-G8 graphite from ConocoPhillips, where the negative to positive ratio was held between 1.1 to 1.3 and the porosity was between 30 and 35%. The impedance is very high for thin electrodes and decreases sharply as the thickness increases. It eventually levels off after approximately 7 mg/cm² total material loading for the positive electrode, very near the loading of the Gen2 system. This apparently surprising result was actually predicted by the modeling work of Dees[33]. Essentially, the cell ASI decreases with increasing electrode thickness due to the increase in electrochemically active area per geometric electrode area. Thus, the move to thicker electrodes for PHEV batteries should not pose a significant challenge regarding electrode impedance, as long as the electrolyte is able to support the higher current densities.

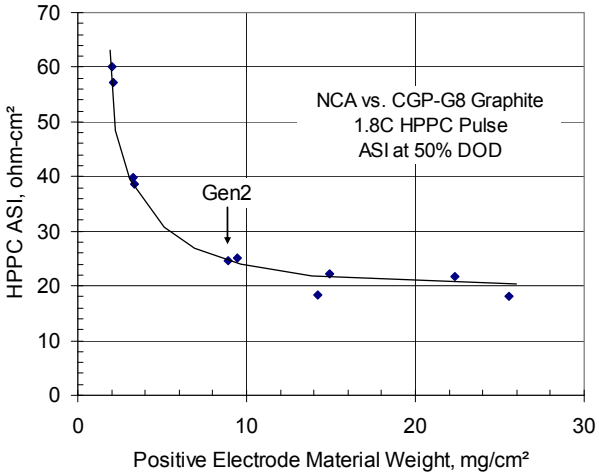

Figure IV- 90: HPPC impedance for NCA positive electrode vs. graphite negative electrode as a function of positive electrode material loading.

A rate study was also performed with these matched electrodes and is summarized in Figure IV- 91. Cells with thicker electrodes deliver less capacity utilization at higher discharge rates, above 1C. This suggests that the positive electrode should not exceed 100 µm material thickness (~27 mg/cm²) for PHEV use.

Baseline PHEV Electrode Design. Based on the above results regarding performance as a function of electrode thickness, a preliminary design was created for the baseline PHEV electrode build as follows:

Cathode

84 wt. % $LiNi_{0.8}Co_{0.15}Al_{0.05}O_2$ (NCA) (~160 mAh/g)
8 wt. % PVDF binder (Kureha 1120)
4 wt. % Acetylene Black Carbon
4 wt. % SFG-6 Graphite (Timcal)

Anode

95 wt. % Mag-10 Graphite (~310 mAh/g)
5 wt. % SBR/CMC Aqueous Binder

[33] D. Dees, E. Gunen, D. Abraham, A. Jansen, and J. Prakash, "Electrochemical Modeling of Lithium-Ion Positive Electrodes during Hybrid Pulse Power Characterization Tests", *JES* **155** (2008) p. A603-A613.

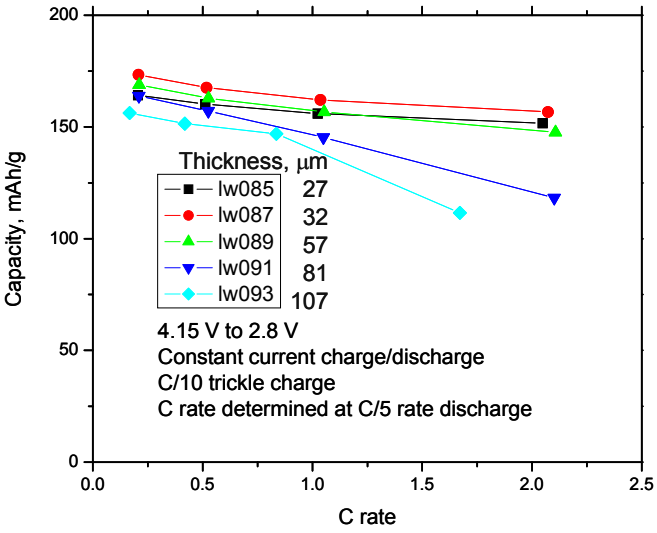

Figure IV- 91: Rate study for NCA positive electrode vs. graphite negative electrode. Negative-to-positive ratio maintained between 1.1 and 1.3.

Electrodes

~33 % porosity (calendered)

Negative-to-positive ratio ~1.1

Cathode:

total material thickness (each side) ~75 µm

total weight (each side): 19 mg/cm² (2.6 mAh/cm²)

Anode:

total material thickness (each side) ~80 µm

total weight (each side): 10 mg/cm² (2.9 mAh/cm²)

Calculated PHEV Battery Design Using Baseline Electrode Parameters. An estimate of the PHEV battery parameters were made using the Battery Design Model developed at Argonne by Paul Nelson and are presented in Table IV-4. These values will improve as more data is obtained from the baseline cells.

Table IV-4: PHEV Parameter Estimates using the Battery Design Model

Battery Power	45 kW
Battery Weight	110 kg
Battery Volume	67 L
Battery Energy	15.5 kWh
C/3 Capacity	45.4 Ah
Number of Modules	8
Cells per Battery	96
Battery Voltage	347 V
Vehicle Range	40 miles

Installing New Dry Room Facility. Laboratory space was made available to the battery department at Argonne for a new dry room. The room was cleared of all cabinets, flooring, HVAC, electrical, plumbing, ventilation, and interior walls to create an empty shell into which the dry room was built – essentially a room within a room. Bid estimates were obtained from two dry room vendors. Final contract was awarded to

Scientific Climate Systems to install a room that is ≤100 PPMv moisture (-42°C dew point), ~500 ft^2 area, with 6 persons, and 750 SCFM exhaust capability. Project oversight, site preparation, and utility upgrade costs were much higher than anticipated (i.e. more than doubled the cost of the dry room). The dry room became operational in August 2009. Work then began on cabinetry and utilities inside.

Two Asian vendors were located that deal with manufacturing of pilot scale lithium-ion cell making equipment. Extensive discussions were held with them to determine the best equipment for ABR Program's needs. Bid estimates were received with the final contract for the pouch cell making equipment and the 18650 equipment both being award to Media Tech of Korea. This equipment will begin to arrive in late CY2009.

Conclusions and Future Directions

Much effort was spent in FY09 to determine the influence of electrode thickness on electrochemical performance. Baseline electrodes were designed and ordered from an industrial vendor and should arrive at the start of FY10. These electrodes will then be used in an 18650 cell build by another vendor and distributed to members of the ABR Program for evaluation.

Future work will center on having advanced materials made into pouch cells and/or 18650 cells for evaluation and comparison against baseline chemistry. These cells will be built by industrial vendors and eventually by Argonne in its new cell building facility once it becomes fully operational. Cell making equipment will be installed in the new dry room and training will be provided by Media Tech in early 2010.

FY 2009 Publications/Presentations

1. Poster presentation at the DOE Vehicles Technology Program 2009 Annual Merit Review Meeting.

IV.C.2.2 Statistical Design of Experiment for Li-ion Cell Formation Parameters using "Gen3" Electrode Materials: Final Summary (INL, ANL)

Kevin L. Gering, PhD
Idaho National Laboratory (INL)
P. O. Box 1625
Idaho Falls, ID 83415-2209
Phone: (208) 526-4173; Fax: (208) 526-0690
E-mail: Kevin.Gering@inl.gov

Contributors (INL): Jeffrey Einerson, Binh Pham
(ANL): Daniel Abraham

Start Date: October 1, 2005
End Date: December 31, 2008

Objectives

- To apply proven statistical methods to design an experimental matrix that will explore single and interactive effects of key parameters on the cell formation process, using the DOE-ATD Gen3 chemistry as a test case.
- Determine best and worst formation conditions, as judged from capacity and interfacial conductance data over accelerated cycle-life conditions.
- Based on a thorough statistical evaluation of test data, perform an optimization study to determine the least amount of time required during formation to meet a minimum performance goal of 50% capacity retention at end of life.

Technical Barriers

The SEI formation process is vital toward surface passivation of electrodes in Li-ion cells, and thus it is a very important first step in producing stable cells that will exhibit good power and energy characteristics over long life. However, formation is regarded as chemistry-specific, and formation parameters must be optimized on a case-by-case basis. There remains much to be learned about improving the formation protocol to achieve optimized SEI characteristics.

Technical Targets

- Utilize a design-of-experiment (DOEx) approach to investigate the foremost formation parameters for Gen3 cells, using button cells spread over three stages. Formation parameters include temperature (T), upper cutoff voltage (UCV), charge and discharge cycling rates (C_{ch}, C_{dis}), time at open circuit voltage between cycle legs (t_{OCV}), and the total number of formation cycles (n_{cyc}). The experimental matrix covered 31 distinct formation test conditions.
- Utilize standard statistical analysis tools to determine the relative influence of parameters on cell performance, and utilize the statistical results to interpolate within and extrapolate past the test conditions to enable time optimization of the formation protocol.

Accomplishments

- Three stages of formation studies were completed that encompassed 31 unique test conditions, and involved over 180 button cells.
- Statistical analyses were completed based on representative capacity and cell interfacial conductance values for each test condition, looking at beginning and end of test life.
- Best and worst formation conditions were determined.
- Derived and validated a sigmoidal-based response variable expression that provides robust treatment of interpolated and extrapolated test conditions.
- A time-optimization study was performed to determine the least amount of time required for satisfactory formation of Gen3 cells.
- A draft paper that covers this work is in final preparation, and will be submitted for journal review by the end of 2009.

✧ ✧ ✧ ✧ ✧

Introduction

Conventional lithium-ion cells rely on passivation films at electrode surfaces to provide long-term stability of operation over time and voltage regimes. These films are commonly referred to as surface-to-electrolyte interphase (SEI) films, and are formed in the earliest cycling history of a cell. Attributes of SEI films are crucial factors in determining the efficiency, safety and life of lithium-ion cells, and include such factors as SEI thickness, resistance, capacitance, permittivity, porosity, electrostatic signature, chemical composition, and spatial variations thereof.

Using a statistical design-of-experiment approach spanning three stages, this work investigated the formation

process for "Gen3" electrode materials comprised of a $LiMn_{1/3}Ni_{1/3}Co_{1/3}O_2$ cathode and a meso carbon microbead (MCMB) 10-28 anode, while the electrolyte was EC-EMC (3:7, mass) + 1.2M $LiPF_6$. Under the DOEx, this investigation follows a systematic and statistically-based evaluation of the foremost formation parameters, which include temperature, upper cutoff voltage, charge and discharge cycling rates, time at open circuit voltage between cycle legs, and the total number of formation cycles.

Approach

- The experimental matrix was statistically designed to accommodate a satisfactory two-level screening study of the six formation parameters in Table IV-5. The approach chosen is based on a ¼ fraction of a 2^6 factorial, resulting in 2^{6-2} (16) core conditions. Added to this core matrix are the necessary conditions to investigate a full 3×3 matrix of the T and UCV parameters, one replicate condition (all parameters set at defaults), one control group, and five supplemental conditions deemed necessary after completing Stages 1 and 2.

Table IV-5: Summary of test parameters and their values.

Parameter	Values		
Temperature (T), °C	0	30*	50
Upper Cutoff Voltage (UCV)	3.7	4.0*	4.2
Charge Cycling Rate (C_{ch})	$C_1/24$		$C_1/10$*
Discharge Cycling Rate (C_{dis})	$C_1/24$		$C_1/10$*
OCV rest after each UCV and LCV taper time (t_{OCV})	None*		4 hours
Total number of complete formation cycles (n_{cyc})	2*		3
* default values			

- The generalized formation cycle procedure is given below, where items *in italic font* are formation parameters shown at their default values. These values were changed for each test condition according to the parameter assignments within the matrix. Amperage values given are for Gen3 materials, assuming button cell dimensions.
  1. Thermally soak cells for two hours at the specified temperature of *30 °C* and maintain this temperature throughout formation.
  2. Perform full charge at a *$C_1/10$* rate (*0.19 mA* for Gen3 button cells) to *4.0 V*, and hold at constant voltage taper charge until $I \le I_{ch}/10$.
  3. Provide *zero hour* rest at OCV.
  4. Perform full discharge at a *$C_1/10$* rate to 3.0 V.
  5. Provide *zero hour* rest at OCV.
  6. Repeat Steps 2 through 5 once for a total of two complete formation cycles.
  7. Bring cells to 30 °C and maintain at that temperature for initial characterization.
- Initial characterization (immediately following formation) consisted of the following:
  - $C_1/1$ static capacity (one current, charge and discharge), and related electrochemical efficiency at $C_1/1$.
  - L-HPPC (FreedomCAR basis)
  - Battery size factor (BSF) for each cell.
  - EIS at 80% SOC. Performed at 10 kHz to 10 mHz (in some cases 250 kHz to 10 mHz).
  - Self-discharge test (cells charged to 4.0 V then left at OCV for two days).
- The procedure for cycle-life testing (cycL) was based on constant power charge and discharge pulses per the PNGV 25-Wh Power Assist profile, where the target SOC was 80% SOC (3.82V). All cycL testing was performed at the elevated temperature of 50 °C. This testing also included a daily low-current mini-pulse (SRPT) at SOC_{ref} to track the changes in ohmic response over time for each cell. For the overall cycL scenario, each cell underwent approximately 1150 cycles per day. The overall cycL protocol was designed to impose at least 45,000 cycL cycles on each cell. Cells were removed from test if they experienced obvious early failure (e.g., cannot complete cycle profile). Characterization during cycL testing included a daily SRPT at 80% SOC, and a weekly (about every 7,500 cycles) $C_1/1$ static capacity test (one current, charge and discharge).
- Final characterization contained the same elements as initial characterization, minus the L-HPPC and BSF determination (we saw that many of the cycL-aged cells could not complete L-HPPC profiles at the end of their test life).
- Both linear and non-linear forms of the response variable expression (RVE) were tried in finding a single form suitable for regression, interpolation, and extrapolation of test conditions. A sigmoidal form was found to be superior.

Results

Results involving stage-wise data have been reported earlier and will not be mentioned here. The focus of this report is the final determination of preferred formation conditions from the statistical analyses and a time-optimized formation protocol for the Gen3 chemistry.

Robust Generalized RVE. As mentioned above, a non-linear RVE was adopted to perform the final analyses:

$$y = y_{ref}\left[\frac{1}{1+\exp\left\{y_o+\sum_i a_i x_i+\sum_i\sum_j a_{ij}x_i x_j+\sum_i e_i\right\}}\right]$$

which provided robust regression of in-matrix data and properly bounded extrapolation of off-matrix conditions. Figure IV- 92 shows the goodness-of-fit for using this expression on capacity and conductance data for all 31 test conditions. The predicted values (filled dots) are mostly within the standard error range. The fitting residuals are scattering around zero also indicate non-bias fitting model.

Case Study: Optimization of Formation Protocol to Minimize Formation Time. In the battery production world, time is money, and the more time required for battery formation, the more expense involved and throughput is decreased. With this in mind the following formation optimization problem was addressed: *What cell formation protocol for the Gen3 chemistry done at 40 ℃ and upper cutoff voltage of 4.2V will yield the shortest formation time while producing cells that maintain at least 50% of their initial capacity and/or 50% of their initial conductance by the end of their life?* That is, we wish to produce cells that by end-of-life will have a capacity and/or conductance ratio (final to initial) of at least 0.5, an arbitrary goal that is easily changed to reflect application requirements. In answering this optimization question, all the time-related processes (cycling rates, t_{ocv}, n_{cyc}, and their interactions) needed to be collectively minimized. The above sigmoidal RVE was used as the predictor for investigating numerous combinations of variables (many of them off-matrix) that would yield predicted cell capacity and conductance for the conditions relevant to minimization of formation time.

The results are summarized in Figure IV- 93. Here we have computed initial and mean capacity and conductance of cells done at selected conditions of T=40°C and UCV=4.2V and for all time-related variables and their first order interactions C_{ch}=C_{dis}=1/(2,4,8,16,24,32); t_{OCV}=0,1,2,3,4,5,6,7,8 hr; and n_{cyc} =1,2,3,4,5, giving 270 total conditions considered in the optimization matrix.

Figure IV- 93 shows all surface plots of resultant capacity and conductance ratios (predicted final to reference) plotted against total formation time and formation cycling rate for values of t_{OCV} and n_{cyc}. The red dots represent all formation protocols that meet cells formation requirements of total formation time less than 100 hours and capacity (or conductance) final-to-reference ratio greater than 0.5 and the blue dots represent formation protocols that have capacity (or conductance) final-to-reference ratios greater than 0.5, but total formation time is greater than 100 hours. The black dots represent conditions where neither criterion is met. There are cases of less than 50 total hours formation, which generally arise for faster cycling rates (C/4 to C/8), while having more total formation cycles (at least 4) and moderate to high t_{ocv}.

Conclusions and Future Directions

Overall results from the statistical optimization exercise indicate that total formation times between two to three days are feasible for Gen3 if the cycling rates are increased while increasing both t_{ocv} and the total number of formation cycles. Future work should continue utilizing the DOEx approach for new cell chemistries to establish a defensible scientific basis for quantifying the effects of formation parameters on cell performance and life.

FY 2009 Publications/Presentations

1. K. L. Gering, *Statistical Design of Experiment for Li-ion Cell Formation Parameters using "Gen3" Electrode Materials: Final Summary*, DOE-EERE Merit Review Meeting (May 19, 2009, Arlington, VA).

Capacity	Conductance
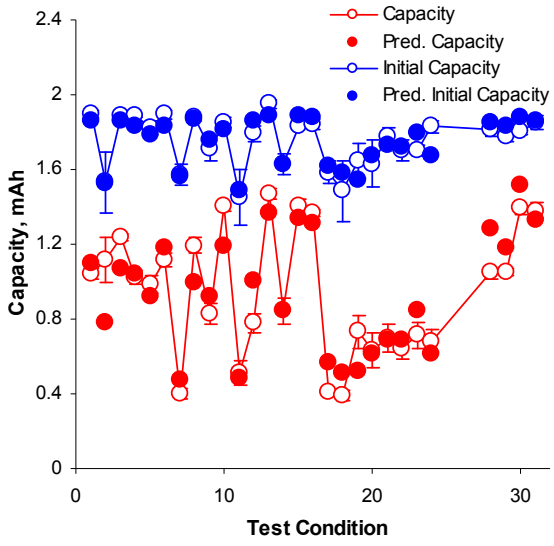	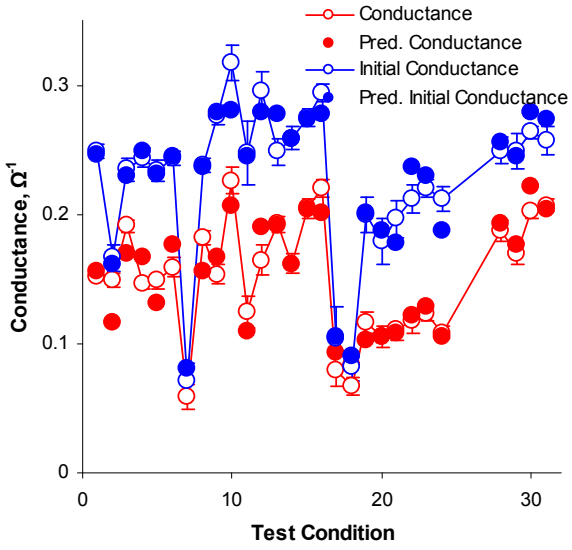
Mean square error for pred. capacity/capacity: 0.0322/ 0.04795 Mean square error for pred. initial capacity/Init. capacity: 0.0253/ 0.05287	Mean square error for pred. conductance/conductance: 0.000551/ 0.007289 Mean square error for pred. initial conductance/ Init. conductance: 0.000979/ 0.010935

Figure IV- 92: Goodness-of-fit for using a sigmoidal-based RVE to render capacity and conductance values for all test conditions.

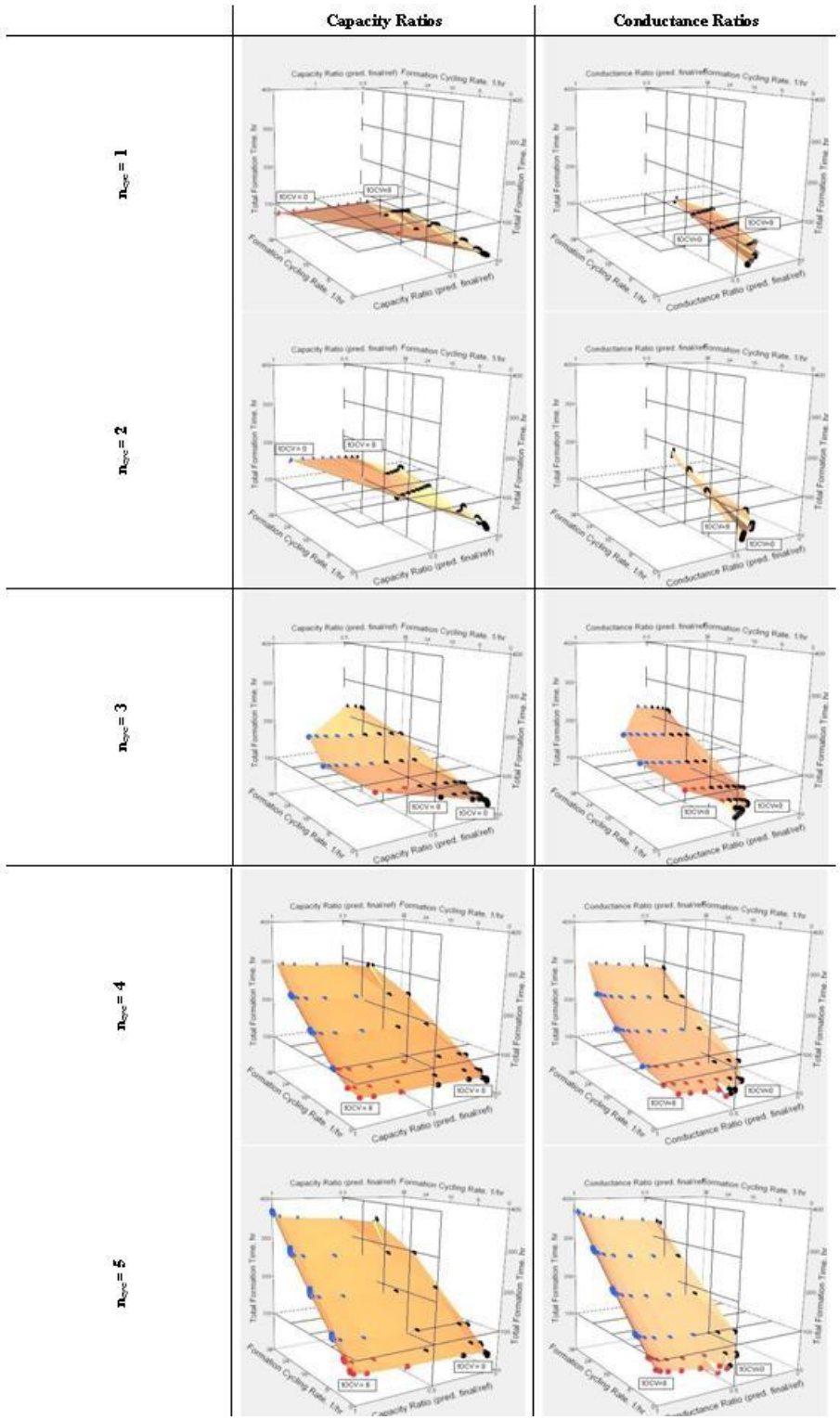

Figure IV- 93: Surface plots of capacity (left column) and conductance (right column) ratios (predicted final to referent) plotted against total formation time and formation cycling rate for all t_{OCV} and for each total number of formation cycles (n_{cyc}).

IV.C.2.3 Key Issues for Electrolytes at Interfacial Regions at Low Temperatures (INL)

Kevin L. Gering, PhD
Idaho National Laboratory (INL)
P. O. Box 1625
Idaho Falls, ID 83415-2209
Phone: (208) 526-4173; Fax: (208) 526-0690
E-mail: Kevin.Gering@inl.gov

Contributors (INL): David Jamison, Sergiy Sazhin

Start Date: October 1, 2003
End Date: September 30, 2009

Objectives

- To gain further understanding of how performance of Li-ion batteries depends on interfacial behavior of electrolytes at open circuit voltage (OCV) and cycling conditions, particularly at low temperatures. This is done to identify plausible mechanisms for performance limitations tied to the battery electrolyte, leading to a more informed mitigation plan based in part on alternative electrode materials and electrolyte components.
- Verify and validate conclusions using multiple laboratory tests and modeling tools.
- This concurs with the stated Programmatic Strategy of the Electrochemical Energy Storage Technical Team Technology Development Roadmap, in the section on enhancing low-temperature performance.

Technical Barriers

Many Li-ion battery systems undergo a marked decrease in performance at low temperatures. Such performance limitations prevent Li-ion technologies from being fully deployed in HEV/PHEV applications for cold climate scenarios. An essential step in mitigating such barriers is to better understand plausible root causes tied to the interfacial behavior of electrolytes that would exist given the physics and thermodynamics of interfacial regions in the cell environment.

Technical Targets

- Design cell testing protocols and laboratory studies that will target low-temperature behavior and isolate root-cause mechanisms for performance loss.
- Develop complementary modeling tools that will facilitate accurate interpretation of test data in terms of thermodynamic and kinetic processes. *Diagnostic testing* provides supporting data toward model validation and identifying probable origins for performance trends.

Accomplishments

- Completed a large matrix study aimed at investigating thermodynamic and kinetics-based limitations of Gen2 Li-ion cells of various aging, considering both charge and discharge conditions.
- Developed an extremely accurate kinetics model that renders various constituent impedance terms over the domains of current, temperature, and pulse duration. This capability lends itself to diagnostic analysis of thermodynamic barriers.
- Developed the theory and modeling tools to investigate field effects on bulk and interfacial behavior of electrolytes in Li-ion cells.
- Other independent studies (DSC, EIS hysteresis, etc.) were performed to investigate thermodynamic processes as they pertain to Li-ion cell materials.
- The infrastructure for applying the Advanced Electrolyte Model (AEM) to cell-level transport modeling (e.g., double layer regions) was improved and expanded.

✧ ✧ ✧ ✧ ✧

Introduction

Broader deployment and acceptance of HEV, PHEV and EV systems based on Li-ion batteries in cold climate regions depends on successful determination and mitigation of the fundamental mechanisms that cause high interfacial impedance and hence lower power at low temperatures. Until recently, however, knowledge has been elusive regarding the fundamental causes of poor low-temperature performance of Li-ion cells. This has been due to conventional testing methods not being amenable or properly adapted to capture the core interactions that emanate from the electrolyte as it resides in the heterogeneous cell environment.

Breakthroughs have been had in this work due to the multidisciplinary approach of considering electrochemical kinetics, thermodynamic energy barriers, diagnostic analysis of cell materials, and field effects at electrolyte-surface interfaces. The key to understanding temperature-related behavior in Li-ion cells is to realize that like all chemical-based systems, Li-ion cells are subject to the laws of thermodynamics and so analysis of performance must include a thermodynamic emphasis.

Approach

- The premise of the collective laboratory and modeling studies is that the heterogeneous Li-ion cell environment, with its complex surface/interfacial features of the electrodes, is a favorable environment for electrolyte-to-surface thermodynamic interactions, particularly at OCV at low temperatures. The consequence of these interactions is higher interfacial impedance and hence, a higher energy barrier for lithium transport through the affected regions.
- A number of laboratory tools and testing techniques were used to investigate this premise: Differential Scanning Calorimetry (DSC), EIS hysteresis, kinetic analysis of constant-current pulses, etc.
- A new kinetics model coupled with various diagnostic testing suggests that apparent kinetic limitations at low temperatures are actually governed by thermodynamically-driven mass transport limitations involving electrolyte solvent located at/near interfacial regions. Electrode surface regions that are occluded by segregated electrolyte phases will in effect have diminished surface availability for Li-ion transport and charge transfer. To facilitate a relevant and accurate evaluation of pulse data, a modified BV expression (denoted θ-BV) was developed that incorporates the effective fraction of electrode surface availability, θ_{eff}, and correction for IR_{ohmic} drop:

$$i = i_o\left[\exp\left(\frac{\theta_{eff}\,\alpha_{a,o}\,F(\eta-\eta_{ohm})}{RT}\right) - \exp\left(\frac{-\theta_{eff}\,\alpha_{c,o}\,F(\eta-\eta_{ohm})}{RT}\right)\right]$$

where the remainder of terms have their usual meanings. This form allows consideration of scenarios wherein there is fouling or occlusion of electrode surfaces, causing the effective transfer coefficient of electrode type i (α_i) to be less than the ideal value ($\alpha_{i,o} = 0.5$), that is, $\alpha_i = \theta_{eff}\,\alpha_{i,o}$. Low α indicate restricted surface availability for the desired reaction, a probable scenario given heterogeneous electrodes. Having both low i_o and low α indicates that electrode kinetics is being impacted by a mass transfer limitation at or very near the electrode surface, hence increasing mass transfer resistance at the surface. Thus, in this way the θ-BV model can help characterize conditions whereby mass transport limitations govern electrode kinetics at low temperatures. Cathode and anode-specific limitations at a given temperature can be surmised by comparing θ_{eff} for discharge and charge conditions.

- Based on the principle of charge-attenuation of permittivity (dielectric depression) and sigmoidally-screened electrostatic functions (SSEF), calculations were also performed that determine the effect of ionic and surface charges on the electrolyte permittivity, field strength, and net repulsive energy between the charged electrode surface and solvent dipoles.
- Electrolyte modeling is based on a molecular-scale chemical physics approach (Associative MSA) that incorporates explicit treatment of ion solvation, ion association, and dielectric depression. Where feasible, a molecular basis has been maintained in the various modeling tools so that the underlying physics is consistent throughout the analyses.

Results

Investigation of Kinetic Limitations in Gen2 cells. A small population of Gen2 18650 cells was utilized to determine their kinetic limitations under charge and discharge conditions over a large matrix of current and temperature. Gen2 cells consist of a lithiated NiCoAl-oxide cathode, a MAG10 carbon anode and an electrolyte EC-EMC (3:7, mass) with 1.2M $LiPF_6$. Considered were cells with approximately 20 and 55% power fade.

At a given low temperature, cells operated at short pulses exhibited a noteworthy drop in total impedance as current increased past the exchange current (Figure IV-94). The impedance drop cannot be solely accounted for by simple joule heating (except in cases of the highest currents), but is explained here by how the field generated by the surface charge density disrupts and reorients solvent dipoles and effectively lowers the energy barrier for lithium transport through the SEI.

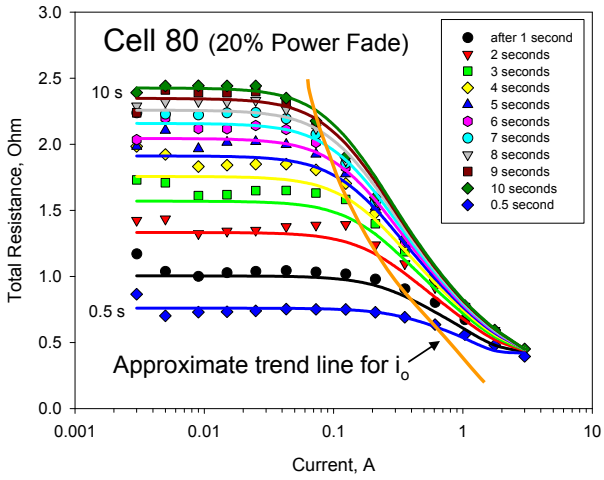

Figure IV- 94: Total impedance at -30°C over pulse timeline for Cell 80 under discharge conditions. The symbols represent data and the solid lines represent model results.

Figure IV- 95 shows the total impedance at the end of ten-second pulses for Cell 80, considering temperatures ranging from -40 to 30 °C. The model fits are exceptional over the entire ranges of current and temperature. Regression of voltage data gave $R^2 \geq 0.999$ in nearly all cases. Data scatter at higher temperatures and low currents is due to extremely small voltage drops (sub-mV) under those conditions, which are recorded with diminished accuracy by the test machinery. Figure IV- 96 shows θ-BV parameter values obtained from regression analysis for cells 14 and 80. The trending is consistent with the difference in aging between these two cells.

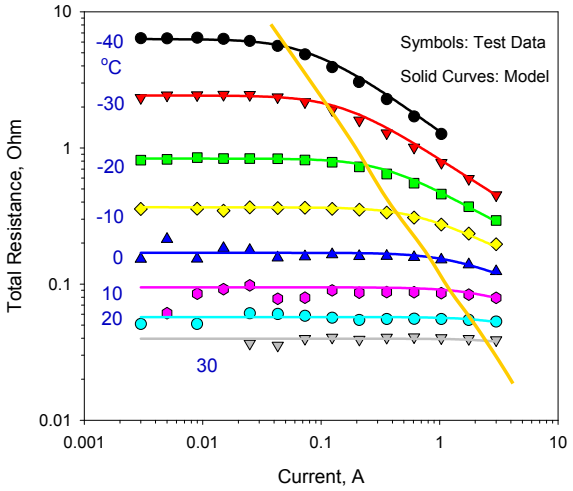

Figure IV- 95: Total impedance for Cell 80 after 10-second discharge pulses over temperature and current.

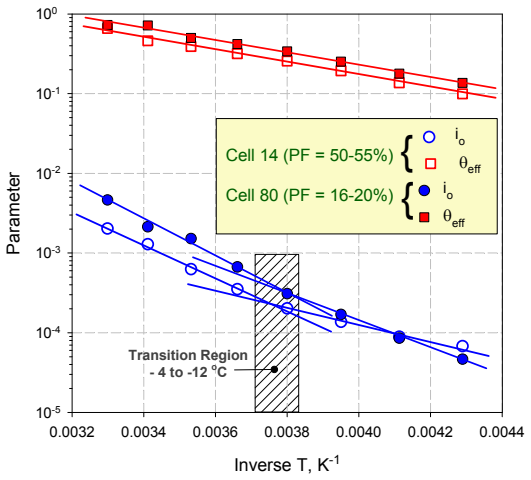

Figure IV- 96: θ-BV parameter values obtained from regression analysis of 4-second pulse data.

A few comments are in order for the figures Figure IV- 94 - Figure IV- 96. First, the exchange current density i_o decreases over elapsed pulse time and with decreasing temperature. This indicates that cells are encountering greater irreversibility in their operation at these conditions. The total impedance starts to plateau by the end of pulse. From Figure IV- 96, both θ_{eff} and i_o decrease at lower temperatures, indicating constrained interfacial transport and greater electrochemical irreversibility. It has been observed that θ_{eff} is relatively invariant over pulse time, while i_o is more variant (Figure IV- 94).

An important quantity that emerges from the overall kinetic analysis is the interfacial thermodynamic energy barrier, ΔE_{int}, which represents the energy required for lithium transport past that required for the ohmic IR drop and charge transfer process. Figure IV- 97 indicates values of this quantity for cell 80 under discharge conditions. Two primary regions are encountered, with a transition temperature of around -4 °C. These results infer one or more thermodynamic processes occur over temperature to increase the interfacial impedance. Mechanisms for this could include increased solvent ordering, rearrangement, adsorption, or phase formation at electrode interfaces and inside porous regions, which are more prone to occur at OCV conditions. Figure IV- 97 is a proto-example of a proper thermodynamic analysis of such data, allowing segregation of electrochemical versus thermodynamic limitations.

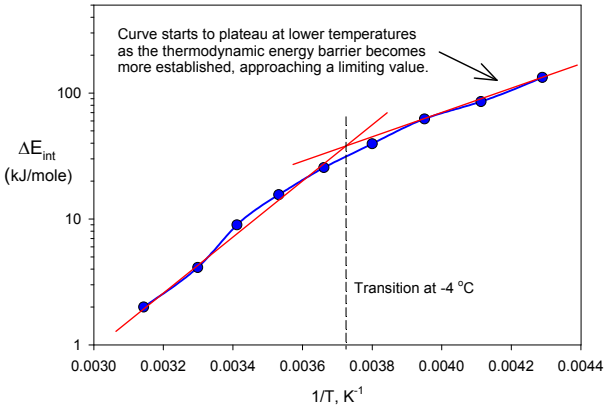

Figure IV- 97: Interfacial energy barrier obtained from analysis of isothermal impedance profiles in concert with θ-BV.

Supporting Laboratory Studies. Ancillary data comes from independent studies involving DSC of harvested Gen2 cell materials and EIS hysteresis of the 18650-type cells.

Figure IV- 98 is a representative thermogram of cell materials taken from room temperature to -60 °C and back again. The amount of heat released is estimated to be *at least three times* that of heat capacity effects (latent heat) of the same materials. Figure IV- 99 shows the EIS hysteresis encountered as the cell was taken through cooling then heating, and allowed to reach thermal equilibrium between each EIS measurement. The hysteresis at each temperature is the difference (here, increase) in the EIS semicircle width, representing the effective increase in interfacial impedance as the cell rests at temperature for prolonged time. Collectively, Figure IV- 98 and Figure IV- 99 bespeak the presence of one or more thermodynamic processes at critical interfaces that are more problematic at lower temperatures. These could include perhaps solvent ordering, rearrangement, adsorption, or self-association at electrode interfaces, SEI, and inside porous regions to a greater extent as the temperature is lowered. Such mechanisms could help explain the high activation energy tied to SEI films, as observed in EIS semi-circle widths over temperature.

Field Effects on Electrolyte Behavior Near Critical Interfaces. As mentioned earlier, it is held that the field generated by the surface charge density disrupts and reorients solvent dipoles and effectively lowers the energy barrier for lithium transport through the SEI. This effect is more pronounced at low temperature, as supported by a higher capacitive effect seen during pulses. Results from model calculations show that the magnitude of field that is generated at higher currents is sufficient to disrupt at least a bi-layer of solvent in close proximity to the charged electrode surface. Figure IV- 100 gives the repulsive coulombic energy between the surface charge (here, at the cathode) and solvent dipoles in the electrolyte as a function of distance from the surface. The Gen2 electrolyte was used for this test case, and the cathode SEI was assumed to have an effective relative permittivity of 10 and a porosity of 30%. The no-SEI case shows greater repulsion nearest the surface, inferring that better low-temperature performance will be had with thinner low-permittivity SEI films. The affected region generally falls within about ten Angstroms, which covers roughly a bi-layer of solvent in this case. Values at sub-molecular scales ($<D_{solvent}$) represent effective averages at those conditions.

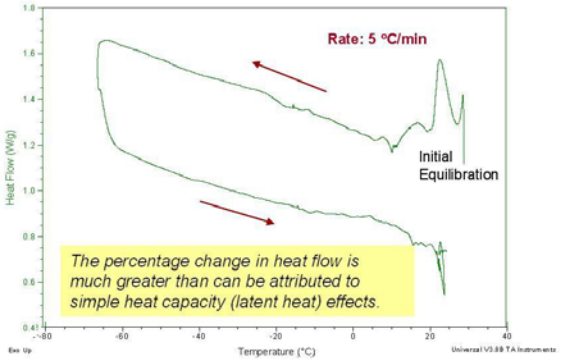

Figure IV- 98: DSC thermogram of harvested Gen2 cell materials with fresh electrolyte.

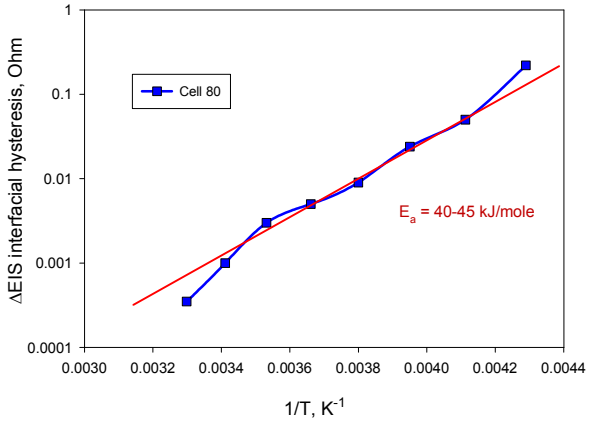

Figure IV- 99: EIS hysteresis of Gen2 cell 80, showing increased interfacial impedance hysteresis at lower temperatures.

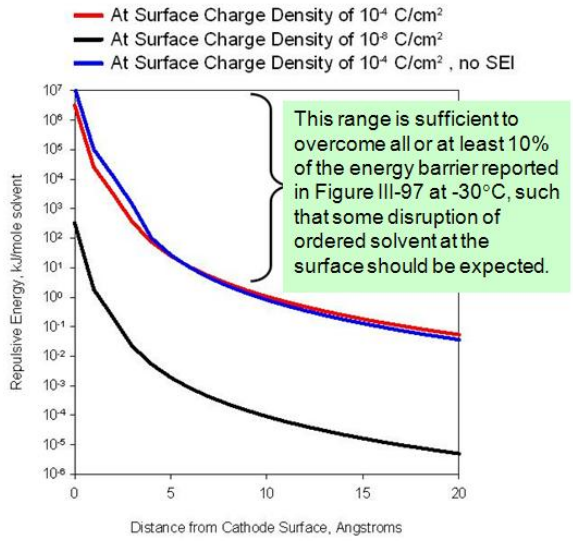

Figure IV- 100: Calculated repulsive coulombic energy between surface charge and solvent dipole over distance from cathode during discharge using charge-attenuated permittivity. All values determined at -30 °C.

Conclusions and Future Directions

Results from multiple independent studies all strongly suggest that one or more thermodynamic processes occur to increase SEI interfacial impedance at lower temperatures, perhaps by increased solvent ordering, rearrangement, adsorption, phase formation, or other electrolyte-surface interactions at electrode interfaces and inside porous regions. The key to future work is continued molecular-scale investigations on species interactions at interfaces, and developing formation protocol to produce thin, compact, low-permittivity SEI films.

FY 2009 Publications/Presentations

1. K. L. Gering, (1) Transport Modeling of Electrolyte Speciation at Electrode-Electrolyte Interfaces for Li-ion Systems, and (2) Kinetic Performance of Li-ion Cells during Short Pulses, with Emphasis on Low Temperature Behavior, 214th Meeting of the Electrochemical Society (October 14 and 17, 2008, Honolulu, HI).
2. K. L. Gering, Key Issues Regarding Electrolytes at Interfacial Regions (subtask low temperature performance), DOE-EERE Merit Review Meeting (May 19, 2009, Arlington, VA).
3. K. L. Gering, Interfacial Processes and Properties that Involve Electrolytes in Lithium-ion Cells, 17th Symposium on Thermophysical Properties (June 25, 2009, Boulder, CO).

IV.C.2.4 Gen 3 HEV Cell Life Testing (ANL, INL)

Ira Bloom
Argonne National Laboratory
9700 S. Cass Ave.
Argonne, IL 60439
Phone: (630) 252-4516; Fax: (630) 252-4176
E-mail: bloom@cmt.anl.gov

Jon P. Christophersen
Idaho National Laboratory
P.O. Box 1625
Idaho Falls, ID 83415
Phone: (208) 526-4280; Fax: (208) 526-0690
E-mail: jon.christophersen@inl.gov

Start Date: March 14, 2007
End Date: April 27, 2009

Objectives

- Provide aged Gen3 cells to diagnostic laboratories with precisely known aging histories to elucidate degradation mechanisms.
- Compare NCA material (Gen2) performance with NMC material (Gen3) performance.

Technical Barriers

Cell testing and diagnostic analysis of multiple chemistries helps to address the barriers limiting the successful commercialization of lithium-ion batteries. These barriers include understanding the life-limiting mechanisms and enhancing life capability.

Technical Targets

- HEV Application: Minimum Power Assist
- Calendar Life: 15 years
- Cycle Life: 300,000 cycles

Accomplishments

- Completed Gen3 cell life testing.
- Shipped requested number of cells to the diagnostic laboratories.

✧ ✧ ✧ ✧ ✧

Introduction

The purpose of the Applied Battery Research Program is to address the barriers that limit the commercialization and implementation of lithium-ion battery technologies, specifically for the automotive industry. Towards that end, prototype cells of various chemistries and configurations are aged using standardized methods. The cells are then subjected to destructive diagnostic analyses to identify failure mechanisms. The second generation of cells (i.e., Gen2 cells) consisted of a nickel-cobalt-aluminum (NCA) mixture, and their performance is described in detail elsewhere [1]. The Gen3 cells consisted of a nickel-manganese-cobalt (NMC) mixture, and life aging has recently been completed.

Approach

The Gen3 HEV cell chemistry is shown in Table IV-6. These NMC cells consisted of a baseline chemistry and a variant chemistry; the Variant A cells included a 2% $LiBF_2C_2O_4$ additive in the electrolyte. Both a pouch cell design (400 mAh) and an 18650-size design (700 mAh) were built for this study.

Table IV-6: Gen3 Cell Chemistry

Positive Electrode	• 8 wt % PVDF binder • 8 wt % Super P carbon black • 84 wt % $Li_{1.05}(Ni_{1/3}Co_{1/3}Mn_{1/3})_{0.95}O_2$
Negative Electrode	• 8 wt % PVDF binder • 92 wt % (MCMB) 10-28
Electrolyte	• 1.2 M $LiPF_6$ in EC:EMC (3:7 wt%) • 2% $LiBF_2C_2O_4$ Additive (Variant A)
Separator	• 25 µm thick PE

The Gen3 life test matrix is shown in Table IV-7, with the cell allocation for both the Baseline (BL) and Variant A (VA) chemistries. The aging sequence mirrored the Gen2 cells, with cycle life groups at 25 and 45°C, and calendar-life groups at 45 and 55°C. All life testing was performed at 60% state-of-charge (SOC). Calendar-life testing consisted of a voltage clamp at the open-circuit voltage corresponding to 60% SOC with a daily pulse profile. Cycle-life testing consisted of continuous pulsing centered at 60% SOC.

The cells were initially characterized, then aged at test temperature with periodic interruptions every four weeks for reference performance tests (RPTs) to gauge degradation in capacity, power, and energy as a function of

test time. The characterization test and subsequent RPTs were performed at 25°C, and consisted of static capacity tests at both the C1/1 and C1/25 rates, a low-current hybrid pulse power characterization (HPPC) test, and electrochemical impedance spectroscopy between 10 kHz and 10 mHz at 60% SOC.

Table IV-7: Gen3 Cell Allocation

	25°C	45°C	55°C
Cal.	-	Pouch: • 2 BL • 5 VA 18650: • 1 BL • 4 VA	Pouch: • 2 BL • 5 VA 18650: • 1 BL • 4 VA
Cyc.	Pouch: • 5 VA	Pouch: • 4 VA 18650: • 3 VA	-

Results

A performance summary of the Gen3 pouch cells is shown in Table IV-8. Clearly, the electrolyte additive in the Variant A cells helps stabilize the Gen3 chemistry and slow down the rate of degradation for both the capacity and power. Additionally, the Variant A cycle-life cells show a slower degradation rate than the corresponding calendar-life cells; the Gen2 cells (NCA material) showed the opposite trend. No data are available for the 18650-size cells since they showed signs of leaking either before testing, or during the initial characterization.

A representative C1/1 discharge curve is shown in Figure IV- 101, and the C1/1 capacity change with respect to test time is shown in Figure IV- 102. These curves display the features typical of using a layered material cathode and a graphite anode. As expected, the C1/1 capacity decreases with cell age and temperature. The corresponding available power and energy curves for a representative cycle-life cell, as determined from the HPPC test, are given in Figure IV- 103. Figure IV- 103 shows that the usable power and energy decline with battery aging as well.

Table IV-8: Pouch Cell Performance Summary

	Temp (°C)	Life Test	C_1/1 Fade (%)	Power Fade (%)	Weeks on Test
BL	45	Cal.	12.9	40.0	20
	55	Cal.	39.9	74.0	12
VA	25	Cyc.	5.95	12.9	80
	45	Cyc.	19.8	50.6	64
	45	Cal.	20.0	53.7	44
	55	Cal.	56.4	62.3	28

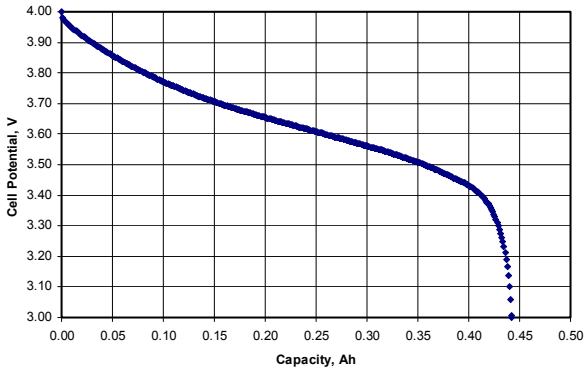

Figure IV- 101: Typical C_1/1 Discharge Curve at Characterization

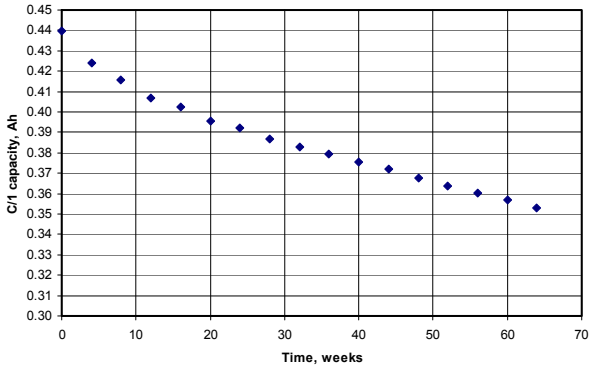

Figure IV- 102: Typical C_1/1 Capacity vs. Time from an Additive Cell that was Cycled at 45°C.

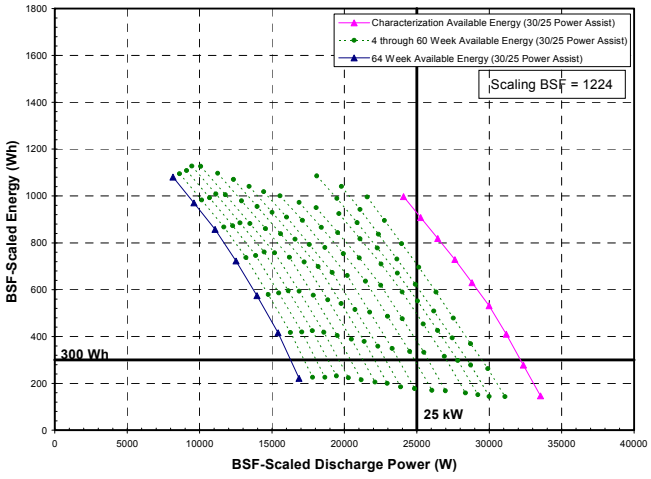

Figure IV- 103: Usable Energy vs. Power as a Function of Test Time.

C1/25 Discharge Data. The initial average C1/25 discharge capacities for the baseline and additive pouch cells were 0.480 and 0.466 Ah, respectively. As expected, the C1/25 capacity also decreases with cell age at all test temperatures. The C1/25 discharge curves from a typical

Variant A calendar-life pouch cell are given in Figure IV-104.

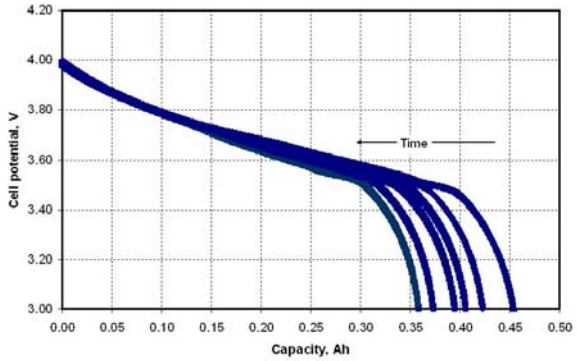

Figure IV- 104: Cell Potential vs. Capacity from a C_1/25 Discharge.

Figure IV- 105 shows the average C1/25 discharge capacity as a function of test time for all pouch cell groups. The relative capacity decline increases with increasing test temperature and time, as expected. Additionally, the rate of relative C1/25 capacity decline in the Baseline cells is higher than those seen in the Variant A cells. Thus, the $LiC_2O_4BF_2$ additive appears to retard C1/25 capacity fade. As with the C1/1 capacity and power fade results, these data also indicate a life test dependence at 45°C, with the calendar-life cells fading faster than the cycle-life cells. The Gen2 cells (NCA material) showed the opposite trend, with cycle-life fading more quickly than calendar-life.

The Gen3 C1/25 discharge capacity data were fit using least-squares techniques, assuming parabolic, diffusion-controlled kinetics, $C = z + kt^{1/2}$, where C is the relative capacity, z is the initial capacity (ideally, $z = 1$), k is the rate constant, and t is time in weeks. These fitting results are shown in Table IV-9, along with the regression coefficient, r^2. The corresponding trendline fits are also shown in Figure IV- 105. These data indicate a very good model fit with a square-root of time dependence, with a regression coefficient of 0.93 or better.

Examining the rate constant (k) values in Table IV-9 shows the expected trends (i.e., the magnitude increases with temperature). Additionally, the magnitude of k is greater for the Baseline cells than the corresponding Variant A cells. For example, the rate of C1/25 discharge capacity decline at 55°C for the Baseline cells is about double the rate for the 55°C Variant A cells. The average fade rate in the Baseline cells is also greater than the Variant A cells. From a practical standpoint, the overall C1/25 capacity fade rates for the Variant A cells was approximately the same as those from the NCA-containing Gen2 Baseline cells [2].

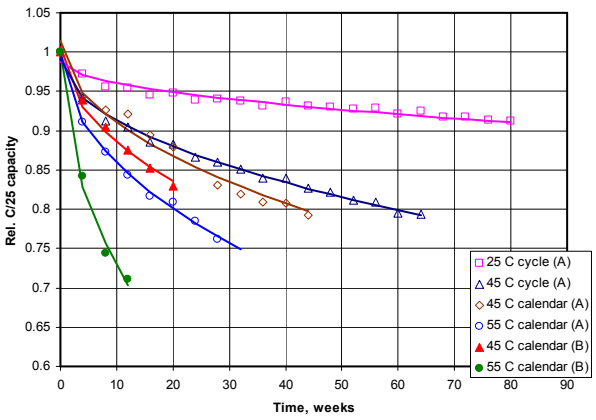

Figure IV- 105: Relative C_1/25 Average Capacity for the Gen3 Pouch Cells.

Conclusions

Cells with and without a $LiC_2O_4BF_2$ additive and that contained NMC positive electrodes were tested for calendar and cycle life at 60% SOC. The temperatures used in these tests were 25 and 45°C (cycle life) and 45 and 55°C (calendar life). It was shown that the electrolyte additive helps reduce the cell degradation rate in the NMC cells. Additionally, the C_1/25 capacity data were shown to degrade with a square root of time dependence.

Table IV-9: Least-Square Fitting Results from the C1/25 Discharge Capacity Data

	Temp (°C)	Life Test	z, Ah (std. error)	k, Ah/Week (std. error)	r^2
BL	45	Cal.	1.00 (6.41×10^{-3})	-3.83×10^{-2} (2.03×10^{-3})	0.99
	55	Cal.	1.00 (1.38×10^{-2})	-8.58×10^{-2} (2.03×10^{-3})	0.99
VA	25	Cyc.	0.99 (3.42×10^{-3})	-8.59×10^{-3} (6.04×10^{-4})	0.93
	45	Cyc.	0.99 (2.70×10^{-4})	-2.50×10^{-2} (4.76×10^{-4})	0.99
	45	Cal.	1.01 (8.41×10^{-3})	-3.27×10^{-2} (1.80×10^{-3})	0.96
	55	Cal.	1.00 (3.30×10^{-3})	-4.42×10^{-2} (8.90×10^{-4})	0.99

FY 2009 Publications/Presentations

1. Presentation to the 2009 DOE Annual Peer Review Meeting.
2. Differential Voltage Analyses of High-Power Lithium-Ion Cells 4. Cells Containing NMC, I. Bloom, L. K. Walker, J. K. Basco, D. P. Abraham, J.

P. Christophersen, and C. D. Ho, J. Power Sources, in press.
3. Using Radial Basis Functions to Approximate Battery Differential Capacity and Differential Voltage, J. P. Christophersen and S. R. Shaw, J. Power Sources, in press.
4. Performance Evaluation of the Advanced Technology Development Gen3 Cells, J. P. Christophersen, K. L. Gering, C. D. Ho, D. P. Abraham, I. Bloom, G. L. Henriksen, Presented at the 214th Meeting of the Electrochemical Society, Honolulu, HI (October 2008).

References

1. Advanced Technology Development Program for Lithium-Ion Batteries: Gen 2 Performance Evaluation Final Report, INL/EXT-05-00913, Jul. 2006.
2. I. Bloom, A. N. Jansen, D. P. Abraham, J. Knuth, S. A. Jones, V. S. Battaglia, and G. L. Henriksen, J. Power Sources, 139 (2005) 295.

IV.D. Abuse Tolerance Studies

The abuse tolerance testing and improvement activities from the previous high power applied research program continue in the ABR program. In particular, researchers aim to characterize the response of materials and cells to abusive conditions using techniques such as DSC and ARC. The objective is to isolate the materials and reactions responsible for the poor abuse tolerance behavior, and to provide input to the materials development teams regarding materials' properties that would result in improved abuse tolerance.

IV.D.1 Develop & Evaluate Materials & Additives that Enhance Thermal & Overcharge Abuse (ANL)

Khalil Amine
Argonne National Laboratory
9700 South Cass Avenue
Argonne, IL 60439
Phone: (630) 252-6551; Fax: (630) 972-4451
E-mail: amine@anl.gov

Start Date: October 1, 2008
Projected End Date: September 30, 2010

Objectives

- Determine the role of cell materials/components in the abuse tolerance of lithium-ion cells.
- Identify and develop more stable materials that will lead to more inherently abuse-tolerant cell chemistries.
- Secure sufficient quantities of these advanced materials (and electrodes) to supply them to Sandia National Laboratories (SNL) for validation and quantification of the safety benefits in 18650-type cells.

Technical Barriers

- Determine role of the solid-electrolyte interface (SEI) layer on carbon anodes in cell safety.
- Determine role of cathode in cell safety.
- Provide overcharge protection of lithium-ion batteries.

Technical Targets

- Understand the response of the SEI layer to thermal abuses.
- Develop functional additives that enhance the stability of the SEI layer.
- Understand the response of cathode materials to thermal abuses.
- Develop functional protection strategies to enhance the thermal stability of batteries.
- Benchmark and develop advanced redox shuttles to improve the overcharge tolerance of lithium-ion batteries.

Accomplishments

- Verified that the stability of the SEI layer is crucial to the life and thermal-abuse tolerance of lithium-ion batteries.
- Measured the activation energy of the SEI decomposition reaction and successfully correlated it with the cycling performance of lithium-ion cells.
- Developed lithium difluoro(oxalato)borate as functional additive that:
  - Improves the thermal stability of lithiated graphite.
  - Enhances the cycle life of lithium-ion cells without sacrificing the power capability.
- Initiated preliminary study on the impact of electrolyte additives on the thermal stability of cathode materials.
- Secured several redox shuttle candidates showing potential application for 4-V lithium-ion batteries. (These candidates are from 3M, Air Products and Chemicals Inc., and Argonne).

✧ ✧ ✧ ✧ ✧

Introduction

The safety of lithium-ion batteries is currently the major technical barrier for their application in hybrid electric vehicles and plug-in hybrid electric vehicles. Understanding the mechanism of thermal runaway reactions is a key to develop advanced technologies that improve the abuse tolerance and mitigate the safety hazard of lithium-ion batteries.

Approach

The following approaches are being taken to tackle the safety issue of lithium-ion batteries:

- Coating cathode particle with stable nano-films of Al oxide or Al fluoride that act as a barrier against electrolyte reactivity with cathodes.
- Exploring new functional electrolyte additives that form stable passivation film at the carbon surface, which can lead to the reduction of the overall heat generated from the SEI breakdown.
- Exploring new redox-shuttle materials to (a) improve the overcharge protection of lithium batteries and (b) achieve automatic capacity balancing of battery packs.
- Quantifying the role of the additives and surface area of carbon on 18650-type cells in collaboration with SNL.

Results

The following reports progress in improving the thermal abuse tolerance and overcharge protection of lithium-ion cells over the last year.

Thermal Stability of Lithiated Graphite.

Figure IV- 106 shows the amount of heat generated when lithiated anodes are reacted with non-aqueous electrolytes. The data clearly show that the lithiated anodes ($Li_{0.81}C_6$, $Li_7Ti_5O_{12}$, and $Li_{0.5}VO_2$) are not stable in the presence of non-aqueous electrolytes with $\Delta H < 0$. Therefore, the long-term compatibility of lithiated anodes with electrolytes can only be kinetically achieved by means of physical barriers that enhance the activation energy of such reactions. In the case of carbon anodes, the physical barrier mentioned is the SEI layer, which prevents the strong reaction between the lithiated carbon and the electrolyte and generally decomposes at a temperature below 100°C, as shown in Figure IV- 107.

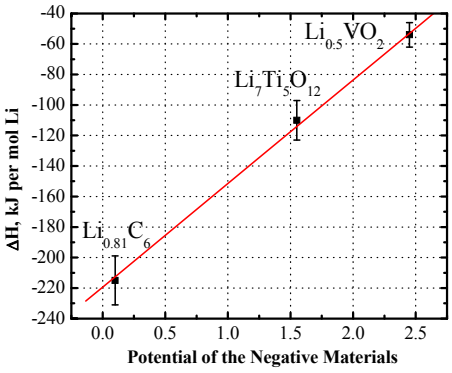

Figure IV- 106: Heat generation of reactions between lithiated anodes and non-aqueous electrolytes showing the thermodynamic instability of lithiated anodes.

Figure IV- 107 shows the differential scanning calorimetry (DSC) of the reaction between lithiated carbon and nonaqueous electrolyte using different heating rates. The electrolyte is 1.2 M $LiPF_6$ in ethylene carbonate (EC)-ethyl methyl carbonate (EMC) (3:7 ratio by weight). Figure IV- 107 clearly shows a long plateau ranging from about 105°C up to onset temperature of the major exothermal reaction at about 250°C. This long plateau is caused by the continuous breakdown/regeneration of a new SEI layer at elevated temperature. A stable SEI layer that decomposes at a higher temperature can certainly improve the thermal stability of lithiated graphite.

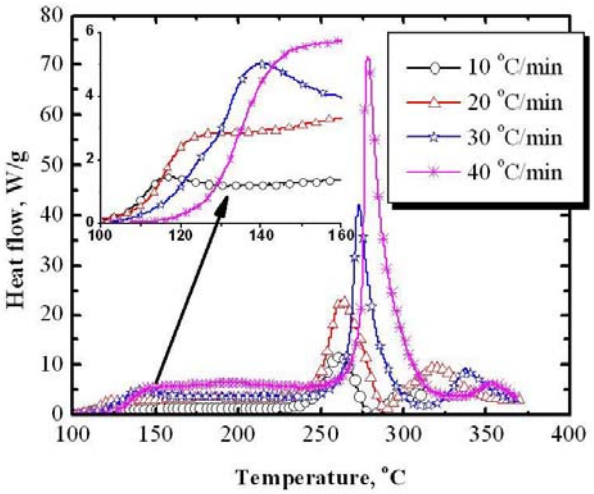

Figure IV- 107: DSC profile of reaction between $Li_{0.81}C_6$ and 1.2 M $LiPF_6$ in 3:7 EC/EMC.

Lithium difluoro(oxalato)borate (LiDFOB) is an electrolyte additive developed at Argonne that can be reduced and polymerized at about 1.7 V vs. Li+/Li during the initial formation of lithium-ion cells. The artificial SEI layer formed with the LiDFOB showed higher stability

than the original SEI layer formed in the control non-aqueous electrolyte (see Figure IV- 108). With the addition of 3 wt% LiDFOB to the electrolyte, the onset temperature of SEI decomposition was pushed to above 150°C, which is about 50oC higher than that for the cell without LiDFOB additive. Figure IV- 109 also shows the activation energy of SEI decomposition as a function of the LiDFOB concentration added to the electrolyte. Apparently, the activation energy for SEI decomposition increases steadily with the concentration of LiDFOB up to 3 wt%.

Figure IV- 110 also shows that the capacity retention of the lithium-ion cells was significantly improved with the addition of LiDFOB because of the stable artificial SEI layer provided by the added LiDFOB.

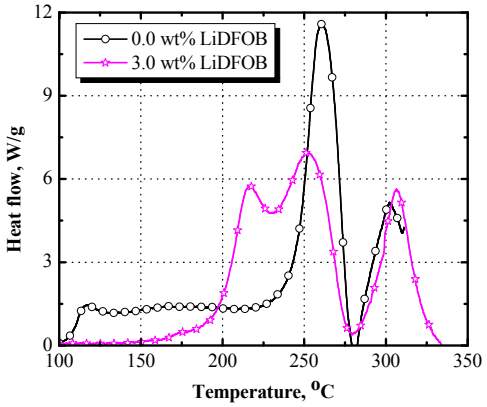

Figure IV- 108: DSC profiles of $Li_{0.81}C_6$ reacted with 1.2 M $LiPF_6$ in EC/EMC (3:7) showing the significant impact of LiDFOB additive on the thermal stability of lithiated graphite.

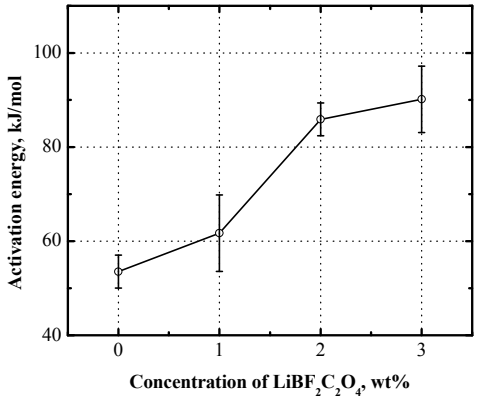

Figure IV- 109: Activation energy of SEI layer decomposition as a function of the concentration of LiDFOB added to the electrolytes.

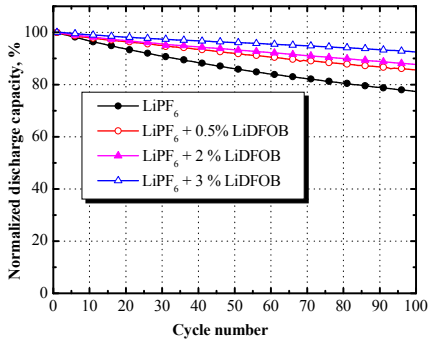

Figure IV- 110: Normalized discharge capacity of mesocarbon microbead (MCMB)/$Li_{1.1}[Mn_{1/3}Ni_{1/3}Co_{1/3}]_{0.9}O_2$ cells showing the positive impact of LiDFOB on the cycle life of the cells. The cells were cycled with a constant current of C/2 at 55°C.

Overcharge protection of lithium-ion cells. Overcharge of lithium-ion batteries can lead to the failure of a battery pack or a fire hazard. A redox shuttle is an electrolyte additive that provides an intrinsic mechanism that enhances the overcharge tolerance of lithium-ion batteries. Moreover, the redox shuttle in lithium-ion batteries can also provide automatic capacity balancing for the battery pack.

Figure IV- 111 shows the cyclic voltammogram (CV) of 10 mM $Li_2B_{12}F_{12}$ and 1.2 M $LiPF_6$ in EC/EMC (3:7) for different scanning rates. The curves clearly show that the onset redox potential of $Li_2B_{12}F_{12}$ is about 4.5 V vs. Li^+/Li, which is higher than the working potential of most cathode materials for lithium-ion batteries. Therefore, $Li_2B_{12}F_{12}$ can serve as a universal redox shuttle to provide overcharge protection for cathode materials.

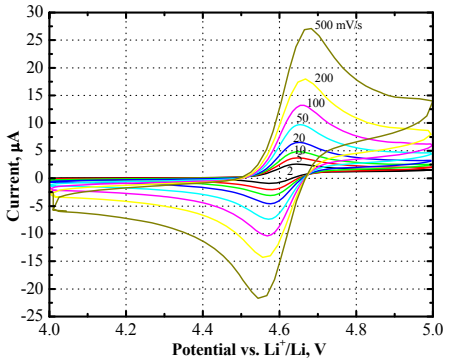

Figure IV- 111: CV of 10 mM $Li_2B_{12}F_{12}$ and 1.2 M $LiPF_6$ in EC/EMC (3:7) in tests using a Pt/Li/Li three-electrode electrochemical cell.

Figure IV- 112 shows charge/discharge capacities of two MCMB/$Li_{1.1}[Mn_{1/3}Ni_{1/3}Co_{1/3}]_{0.9}O_2$ lithium-ion cells during an overcharge test. The cells were first charged for 2.4 mAh under a constant current of 0.5 mA, then discharged with the same constant current. It can be seen that the initial discharge capacity of the cells was about 1.8

mAh, which represents the practical capacity of the cell during normal operation. The difference between the charge capacity and the discharge capacity is the excess charge forced by the charge to overcharge the cells. This portion of excess charge was shuttled through the cells by the redox shuttle, $Li_2B_{12}F_{12}$, without causing chemical or electrochemical decomposition of battery components. Figure IV- 112 also shows that $Li_2B_{12}F_{12}$ provided overcharge protection for up to 80-90 cycles before the charge and discharge capacity dropped dramatically.

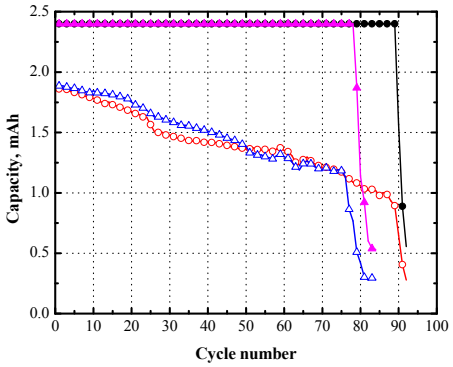

Figure IV- 112: Charge/discharge capacities of two MCMB/$Li_{1.1}[Mn_{1/3}Ni_{1/3}Co_{1/3}]_{0.9}O_2$ lithium-ion cells during overcharge test. The electrolyte used was 0.4 M $Li_2B_{12}F_{12}$ in EC/EMC (3:7) with a proprietary electrolyte additive.

Figure IV- 113 shows the CV of 10 mM 2-(pentafluorophenyl)-tetrafluoro-1,3,2-benzodioxaborole (PFPTFBB) and 1.2 M $LiPF_6$ in ethylene carbonate (EC) with propylene carbonate (PC) and dimethyl carbonate (DMC) (1:1:3 weight ratio) in tests at different scanning rates. The curves clearly show that the onset redox potential of $Li_2B_{12}F_{12}$ is about 4.4 V vs. Li^+/Li, which is high enough to provide overcharge protection for most 4 V-class cathode materials in state-of-the-art lithium-ion batteries.

Figure IV- 114 shows the charge/discharge capacity of a graphite/$LiNi_{0.8}Co_{0.15}Al_{0.05}O_2$ lithium-ion cell containing 5 wt% PFPTFBB in the electrolyte, which was 1.2 M $LiPF_6$ in EC/PC/DMC (1:1:3). The cell was charged and discharged at a constant current of C/10 (0.2 mA). The cell was charged to 4.95 V, or until 4.0 mAh charge was delivered (100% overcharge). The cell was initially tested at 25°C for 20 cycles and was then heated in an oven to 55°C for another 50 cycles to check the stability of the redox shuttle under more aggressive testing. After that, the cell was tested with a higher constant current of C/5. The testing condition for each stage is also labeled in Figure IV- 114. The overcharge protection provided by PFPTFBB failed after 170 cycles of 100% overcharge. **Error! Reference source not found.**Figure IV- 114 also shows that the cell completely lost its capacity after 125 cycles. However, the redox shuttle mechanism remained active for another 50 cycles at 55°C after the cell died.

Therefore, PFPTFBB is believed to be a stable redox shuttle for overcharge protection of 4-V class lithium-ion batteries.

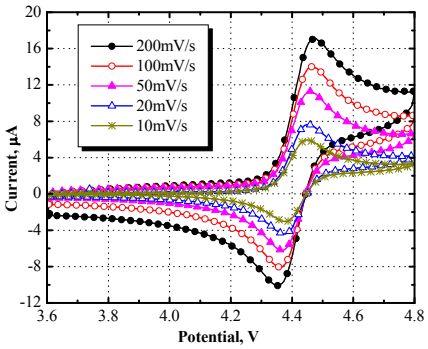

Figure IV- 113: CV of 10 mM 2-(pentafluorophenyl)-tetrafluoro-1,3,2-benzodioxaborole and 1.2 M $LiPF_6$ in EC/PC/DMC (1:1:3) in tests using a Pt/Li/Li three-electrode electrochemical cell.

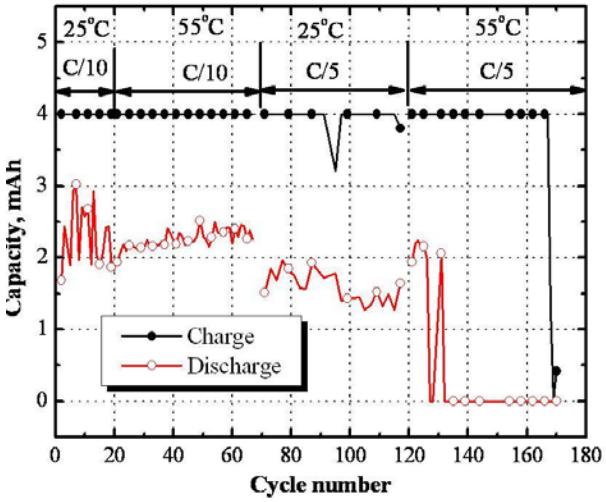

Figure IV- 114: Charge/discharge capacities of two MCMB/$LiNi_{0.8}Co_{0.15}Al_{0.05}O_2$ lithium-ion cells during overcharge test. The electrolyte used was 5 wt% PFPTFBB and 1.2 M $LiPF_6$ in EC/PC/DMC (1:1:3).

FY 2009 Publications/Presentations

1. Z. H. Chen, Y. Qin, and K. Amine, *Electrochimica Acta*, **2009**, 54(24): 5605-5613.
2. Z. H. Chen and K. Amine, *J. Electrochem. Soc.*, **2009**, 156(8): 672-676.
3. Z. H. Chen, Y. Qin, J. Liu, and K. Amine, *Electrochem. Solid-State Lett.*, **2009**, 12 (4): A69-A72.
4. H. B. Kim, B. C. Park, S. T. Myung, K. Amine, J. Prakash, and Y. K. Sun, *J. Power Sources*, **2008**, 179 (1): 347-350.
5. K. Amine, Z. Chen, I. Belharouak, Y. Qin, H. Deng, Z. Zhang, Y. K. Sun and J. Prakash, Abstract #2028, 214 ECS Meeting, October, 2008, Honolulu.

IV.D.2 Diagnostic Studies to Improve Abuse Tolerance and the Synthesis of New Electrolyte Materials (BNL)

Xiao-Qing Yang
Kyung-Wan Nam
Hung-Sui Lee
Xiaojian Wang
Brookhaven National Laboratory
P.O. Box 5000
Upton, NY 11973-5000
Phone: (631) 344-3663; Fax: (631) 344-5815
E-mail: xyang@bnl.gov

Start Date: October 1, 1997
Projected End Date: September 30, 2011

Objectives

- Develop new diagnostic techniques with the ability to distinguish bulk and surface processes, to monitor the degradation processes, to determine the effects of structural changes of electrode materials, the interfacial phenomena, and electrolyte decomposition on the cell capacity and power fading, as well as on the abuse tolerance for safety characteristic related issues
- Using diagnostic techniques to evaluate and screen the new materials and components aimed to improve the performance, calendar and cycling life, and the abuse tolerance of lithium batteries for HEVs, PHEVs, and EV.

Approach

- In-situ X-ray diffraction (XRD) for structural changes during cycling.
- In situ X-ray absorption (XAS) for oxidation state and local structural change study
- Soft X-ray XAS with the capability to distinguish the bulk and surface processes of electrode materials during cycling.
- Time resolved XRD during heating for thermal stability study.

Results

Structural Changes and Thermal Stability of Charged $LiNi_{1/3}Co_{1/3}Mn_{1/3}O_2$ Cathode. Structural changes and their relationship with thermal stability of changed $Li_{0.33}Ni_{1/3}Co_{1/3}Mn_{1/3}O_2$ cathode samples have been studied using time-resolved XRD (TR-XRD) in a wide temperature range from 25 to 600°C with and without electrolyte in comparison with $Li_{0.27}Ni_{0.8}Co_{0.15}Al_{0.05}O_2$ cathodes. Unique phase transition behavior during heating is found for the $Li_{0.33}Ni_{1/3}Co_{1/3}Mn_{1/3}O_2$ cathode: When no electrolyte is present, the initial layered structure changes to a $LiMn_2O_4$ type spinel first, and then to a M_3O_4 type spinel and remains in this structure up to 600°C. For the $Li_{0.33}Ni_{1/3}Co_{1/3}Mn_{1/3}O_2$ cathode sample with electrolyte, additional phase transition from the M_3O_4 type spinel to the MO type rock salt phase takes place from 441 to 600°C together with the formation of metallic phase. The major difference between this type of phase transitions and that for $Li_{0.27}Ni_{0.8}Co_{0.15}Al_{0.05}O_2$ in the presence of electrolyte is the delayed phase transition from the spinel type phase to the rock salt type by stretching the temperature range of spinel phases from about 10°C to 140°C. This unique behavior is considered as the key factor of the better thermal stability of the $Li_{1-x}Ni_{1/3}Co_{1/3}Mn_{1/3}O_2$ cathode materials.

The spectra in Figure IV- 115 provide a good road map for the structural changes of nickel-based cathode materials during heating. As shown in there, when heated from 25 to 450 ˚C, this sample went through a whole series of phase transitions. The structural change starts at about 170˚C. In the temperature range between 180˚C and 210˚C, the (108) and (110) peaks for the original layered structure gradually coalesce into a new peak, indicating the formation of a new structure, the disordered spinel phase. In the temperature range from 220 to 280°C, two new peaks (assigned as (200) and (220) for the rock salt structure of NiO) appear at lower angle sides of the (400) and (440) peaks for the disordered spinel. These two new peaks increase their intensity with increasing temperature, indicating the growing amount of the NiO-like structure at the expense of the disordered spinel phase. A new intermediate structure, Ni_2O_3 phase was also reported in the XRD patterns for $Li_{0.33}NiO_2$ in the temperature range between 220 and 370ºC. From 370 to 450°C, another new phase, the metallic nickel phase forms, grows, and co-exist with the rock salt NiO phase up to 450°C. These phase transitions show clearly that the crystal structure of the sample changes from the layered hexagonal to the disordered spinel cubic and then to the rock-salt cubic by increasing the levels of cation mixing (migration of Li and Ni cations) with increased temperature. The different phase transition behaviors of charged $Li_{0.33}Co_{1/3}Ni_{1/3}Mn_{1/3}O_2$ during heating with or without the presence of electrolyte can be seen in Figure IV- 116 and

Figure IV- 117. Figure IV- 116 (a) shows the TR-XRD patterns of $Li_{0.33}Co_{1/3}Ni_{1/3}Mn_{1/3}O_2$ in the absence of electrolyte as a function of temperature.

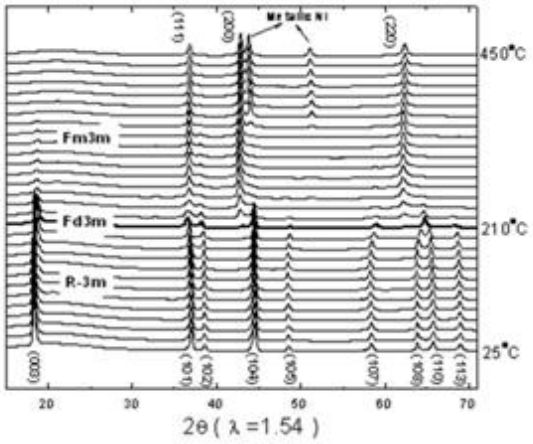

Figure IV- 115: TR-XRD patterns of the charged $Li_{0.33}NiO_2$ in the absence of electrolyte heated from 25°C to 450°C.

The $Li_{0.33}Co_{1/3}Ni_{1/3}Mn_{1/3}O_2$ sample at room temperature shows a hexagonal layered structure with a *R3-m* space group, just like in the $Li_{0.33}NiO_2$ sample. The structural change starts at about 236°C, which is much higher than the 170˚C starting temperature for $Li_{0.33}NiO_2$ shown in Figure IV- 115. In the temperature range from 236°C to 350°C, the coalescence of the original (108) and (110) forms a new peak (marked as (440)), giving clear indication for the formation of a disordered $LiMn_2O_4$ type spinel phase with an unit cell containing 2×2×2 cubic rock salt unit cells. This new peak is indexed as (440) reflection for the cubic structure with a space group of *Fd3m*. The spinel-type cubic symmetry is preserved up to the temperature as high as 600°C, the terminating temperature of the experiment. No further decomposition to MO-type rock salt phase is present at all. However, there are noticeable changes in the diffraction lines in the temperature range from 350 to 600°C. The evolution of the (220) diffraction line at 2θ ~ 31° in the XRD pattern after 350°C shown in Figure IV- 116(a) was used as confirmation of the formation of disordered LiM_2O_4 spinel-type phase in the literature. However, in the spectra for $Li_{0.33}Co_{1/3}Ni_{1/3}Mn_{1/3}O_2$ cathode in Figure IV- 116(a), the appearance and growing of the new (220) peak are concurrent with the appearance and growing of another new peak (422), as well as the disappearance of the old peaks of (331) and (531). This tells us that the spinel structure at the end of heating at 600°C is not the same $LiMn_2O_4$ type spinel, but a completely new phase. Three selected TR-XRD patterns for the sample heated to 350°C, 441°C, and 600°C in Figure IV- 116 (a) are plotted in Figure IV- 116 (b). While the intensity of (220) line gets stronger together with the new (422) diffraction line at 2θ ~ 54 °, the intensity of (331) and (531) peaks gets weaker with increasing temperature towards 600°C.

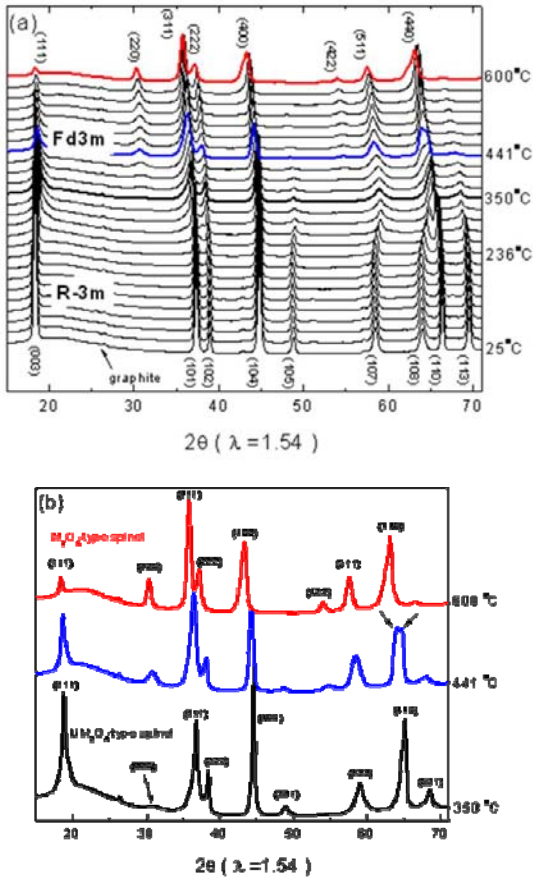

Figure IV- 116: (a) TR-XRD patterns of the charged $Li_{0.33}Co_{1/3}Ni_{1/3}Mn_{1/3}O_2$ in the absence of electrolyte heated from 25°C to 594°C. (b) Three selected XRD patterns from Figure IV- 115 (a) for the sample heated to 345, 424 and 594°C.

The TR-XRD pattern at 600°C can be indexed to the M_3O_4 (e.g., Co_3O_4, JCPDS No. 43-1003) spinel-type structure with the same Fd3m space group as for the disordered LiM_2O_4-type spinel phase. The major differences of these two types of spinel are the different lattice parameters and different cation distribution. The two-phase co-existence region can be seen clearly in the XRD pattern at 441°C in Figure IV- 116 (b): the old (331) and (531) peaks of LiM_2O_4 spinel-type phase co-exist with the new (220) and (422) peaks for M_3O_4 spinel-type phases, in concurrence with the peak splitting of (440) line (marked by two arrows in Figure IV- 115 (b)). It should be noted that the coexistence of two different types of spinel phase during thermal decomposition has not been observed in the nickel based cathodes such as $Li_{1-x}NiO_2$, $Li_{1-x}Ni_{0.89}Al_{0.16}O_2$, and $Li_{1-x}Ni_{0.8}Co_{0.15}Al_{0.05}O_2$. This might be a unique phase transition behavior of Mn containing layered materials only.

Figure IV- 117(a) shows the TR-XRD patterns for $Li_{0.33}Co_{1/3}Ni_{1/3}Mn_{1/3}O_2$ in the presence of electrolyte as a function of temperature. Compared to the sample without

electrolyte, dramatic electrolyte induced structural changes are observed. Although not so much difference of starting temperature for structural change is observed, the completion of phase transition from the layered structure to the disordered $LiMn_2O_4$ type spinel phase is lowered from 340°C to 304°C. In addition, further thermal decomposition from the M_3O_4 type spinel phase to a MO-type rock salt phase (space group: *Fm*3*m*) is observed from 412°C to 440°C. From 440°C to 600°C, new metallic phases (most likely Ni) are formed. These results show that the electrolyte accelerates the thermal decomposition of the charged cathode materials. The presence of the electrolyte changes the paths of the phase transitions and lowers the temperatures of the reactions.

The TR-XRD patterns with smaller temperature steps form 310°C to 441°C are plotted in Figure IV- 117(b). From 310°C to 389°C, the structure transforms from the LiM_2O_4 type-spinel phase to the M_3O_4 type spinel phase as evidenced by the growing intensity of (220) and (422) peaks.

From 389°C to 441°C, new diffraction peaks appear in the left side of the M_3O_4 type-spinel (400) and (440) peaks. These new peaks grow in intensity and get sharper with increased temperature. These two peaks are indexed as (200) and (220) peaks for the MO type phase with rock salt structure. The phase transition from the M_3O_4 type spinel structure to the MO type rock salt structure is completed at 441°C.

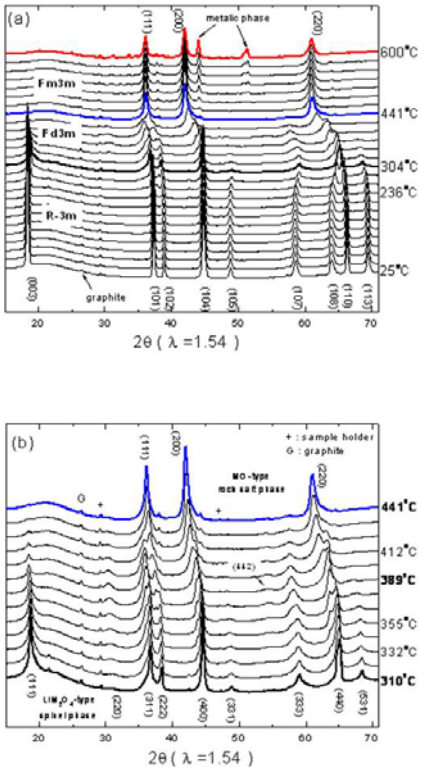

Figure IV- 117: (a) TR-XRD patterns of the charged $Li_{0.33}$ $Co_{1/3}Ni_{1/3}Mn_{1/3}O_2$ in the presence of electrolyte heated from 25°C to 594°C. (b) Same TR-XRD patterns as in Figure IV- 116(b) in temperatures between 304°C and 435°C with smaller temperature step.

In order to compare the thermal decomposition behavior of the $Li_{0.33}$ $Co_{1/3}Ni_{1/3}Mn_{1/3}O_2$ (G3) and the $Li_{0.27}Ni_{0.8}Co_{0.15}Al_{0.05}O_2$ (G2) cathodes in the presence of electrolyte, the TR-XRD patterns for the $Li_{0.27}Ni_{0.8}Co_{0.15}Al_{0.05}O_2$ cathode are plotted in Figure IV-118. Please note that the G2 sample was heated up to 450°C, not 600°C for G3 sample. Decomposition of the layered structure starts at about 200°C. Upon heating, phase transitions from the layered to the spinel-type phase and then to the NiO type rock salt phase are clearly seen. However, there are several noticeable differences between the thermal decomposition behaviors of the $Li_{0.33}Co_{1/3}Ni_{1/3}Mn_{1/3}O_2$ and the $Li_{0.27}Ni_{0.8}Co_{0.15}Al_{0.05}O_2$ cathodes in the presence of electrolyte. Firstly, the $Li_{0.33}Co_{1/3}Ni_{1/3}Mn_{1/3}O_2$ shows higher beginning and ending temperatures of the phase transitions from layered to the spinel, and from spinel to the rock salt type phases than those of the $Li_{0.27}Ni_{0.8}Co_{0.15}Al_{0.05}O_2$, indicating better thermal stability. For $Li_{0.33}Co_{1/3}Ni_{1/3}Mn_{1/3}O_2$, the ending temperature for the transition from layered to spinel-type phase and from spinel-type to rock salt phase in the presence of electrolyte are 304°C and 441°C, while for $Li_{0.27}Ni_{0.8}Co_{0.15}Al_{0.05}O_2$, they are and 280°C and 300°C respectively. These results are consistent with our previously published conclusion about the negative effects

of nickel content on the thermal stability of layered cathode materials. Secondly, the $Li_{0.33}Co_{1/3}Ni_{1/3}Mn_{1/3}O_2$ sample remains in the spinel structures ($LiMn_2O_4$ and M_3O_4 types) in a quite wider temperature range of 140 degrees from 304°C to 441°C. In contrast, for $Li_{0.27}Ni_{0.8}Co_{0.15}Al_{0.05}O_2$, the spinel structure only last in a very narrow temperature range of 10°C before totally converted into the MO type rock salt structure. Since the phase transitions from the spinel-type phase to the rock salt phase are accompanied by oxygen loss, better thermal stability of the $Li_{0.33}Co_{1/3}Ni_{1/3}Mn_{1/3}O_2$ than the $Li_{0.27}Ni_{0.8}Co_{0.15}Al_{0.05}O_2$ in the presence of electrolyte can be attributed to the higher phase transition temperature from spinel-type phase to the rock salt phase during heating. This unique thermal decomposition characteristic of the $Li_{0.33}Co_{1/3}Ni_{1/3}Mn_{1/3}O_2$ cathodes are believed to be originated from the existence of Mn^{4+} ions in the $Li_{0.33}Co_{1/3}Ni_{1/3}Mn_{1/3}O_2$ cathode material.

Synthesis and characterization of novel electrolytes. A novel compound named pentafluorophenylboron oxalate (PFPBO) were designed and synthesized at Brookhaven National Lab. (BNL). PFPBO has a unique molecular structure containing a boron atom center with electron deficiency and an oxalate group as shown in Figure IV- 119.

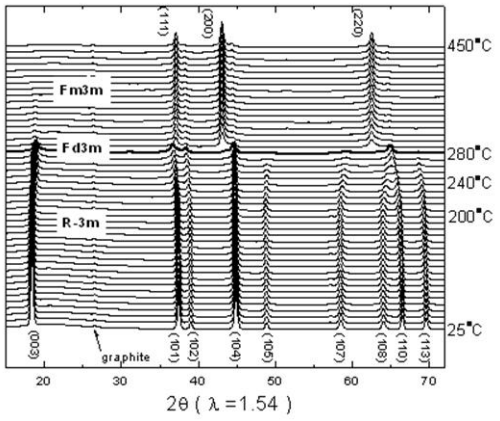

Figure IV- 118: TR-XRD patterns of $Li_{0.27}Ni_{0.8}Co_{0.15}Al_{0.05}O_2$ in the presence of electrolyte, heated from 25°C to 450°C.

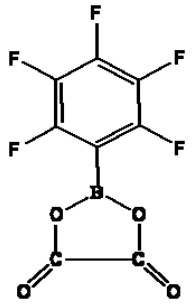

Figure IV- 119: Schematic structure of BNL synthesized new compound pentafluorophenylboron oxalate (PFPBO).

It is found that when PFPBO is used as additive, the solubility of lithium fluoride (LiF) or lithium oxide (Li_2O, Li_2O_2) in propylene carbonate (PC) and dimethyl carbonate (DMC) solvents can be increased dramatically. The new electrolytes show high ionic conductivity, high Li-ion transference number and good compatibility with $LiMn_2O_4$ cathode and MCMB anode. PFPBO was synthesized with the designed structure to act as a bifuncational additive: boron-based anion receptor (BBAR) additive and stable solid electrolyte interphase (SEI) formation additive in PC-based electrolytes. The results show it does process these two desired functionalities. The ionic conductivity and Li-ion transference numbers of electrolytes containing this new compound are listed in Table IV-10.

Table IV-10: Conductivity comparison of various electrolytes at different temperatures and the Li-ion transference number (tLi+) measured at room temperature.

Electrolytes	Conductivity ($mScm^{-1}$)			t_{Li+} (25 °C)	Ea ($kJmol^{-1}$)	
	-30 °C	30 °C	60 °C		Low	High
0.5M PFPOB - PC/DMC	0.1	0.9	1.5	/	20.8	13.3
0.5M PFPOB - 0.5M LiF PC/DMC	0.7	4.4	6.6	0.58	19.9	11.2
0.5M PFPOB - 0.25M Li_2O PC/DMC	0.3	2.0	3.1	0.83	22.1	11.2
0.5M PFPOB - 0.25M Li_2O_2 PC/DMC	0.3	2.0	3.1	0.78	19.6	12.1
0.6M TPFPB - 0.6M LiF PC/DMC[12]	0.8	4.3	6.1	0.71	13.6	13.6
0.4M TPFPB - 0.2M Li_2O PC/DMC[13]	0.3	1.7	2.8	0.78	14.1	6.0
0.4M TPFPB - 0.2M Li_2O_2 PC/DMC[13]	0.4	2.1	3.2	0.74	13.7	5.9

FY 2009 Publications/Presentations

1. Kyung-Wan Nam, Kwang-Heon Kim, Eun-Sung Lee, Won-Sub Yoon, Xiao-Qing Yang, and Kwang-Bum Kim, "Pseudocapacitive Properties of Electrochemically Prepared Nickel Oxides on 3-dimensional Carbon Nanotube Film Substrates", *Journal of Power Sources*, Vol. 182, Iss. 2, pp 642-652 (2008).
2. Kyung-Wan Nam, Chang-Uk Lee, Won-Sub Yoon, Xiao-Qing Yang, and Kwang-Bum Kim, "Electrodeposited Manganese Oxides on 3-dimensional Carbon Nanotube Substrate: Supercapacitive Properties in Aqueous and Organic Electrolytes", *Journal of Power Sources*, Vol. 188, Iss. 1, pp 323-331 (2009).
3. Kyung-Wan Nam, Sang-Bok Ma, Won-Sub Yoon, Xiao-Qing Yang, and Kwang-Bum Kim, "Novel concept of pseudocapacitor using stabilized lithium metal powder and non-lithiated metal oxide electrode in organic electrolyte", *Electrochemistry Communications*, Vol. 11 (6), pp 1166-1169 (2009).
4. G. X. Feng, L. F. Li, J. Y. Liu, N. Liu, H. Li, X. Q. Yang, X. J. Huang, L. Q. Chen, K. W. Nam, and W. S. Yoon, "Enhanced electrochemical lithium storage activity of $LiCrO_2$ by size effect", *Journal of Material Chemistry*, Vol. 19 (19), 2993-2998 (2009).

5. Narah Ominde1, Nick Bartlett1 , Xiao-Qing Yang and Deyang Qu, "The effect of oxygen reduction on activated carbon electrodes loaded with manganese dioxide catalyst", *Journal of Power Sources*, Vol. 185, pp 747-753 (2008).
6. Narah Ominde1, Nick Bartlett1 , Xiao-Qing Yang and Deyang Qu, "Investigation of the Active Sites for Oxygen Reduction on MnO2-loaded Carbon Electrodes", *Applied Catalysis B: Environmental*, submitted.
7. O. Haas, U.F. Vogt, C. Soltmann, A. Braun, W.-S. Yoon, X.Q. Yang, T. Graule "The Fe K-edge X-Ray Absorption Characteristics of $La_{1-x}Sr_xFeO_{3-\delta}$ Prepared by Solid State Reaction Materials", *Material Research Bulletin* Vol. 44 (2009), 1397-1404

Invited presentations

1. X. Q. Yang, X. Wang W-S. Yoon, K. W. Nam, H.S. Lee, J. McBreen, K.zaghib, H. Li, X. Huang, and L. Chen, "Electronic and Crystal Structural change Studies of $LiMPO_4$ (M=Fe, Mn. Co Ni) Cathode Materials during Lithium Intercalation and De-intercalation", **Invited**, presented at the 214th Meeting of the Electrochemical Society, Honolulu, Hawaii, October 12-17, 2008
2. X. Q. Yang, H. S. Lee, W. S. Yoon, K. W. Nam, X. Wang, J. McBreen, Bin Xie, Lifei Li, Hong Li, X. Huang, L. Chen, "New Electrolyte Systems Using LiF, Li_2O or Li_2O_2 with Boron-Based Lewis Acids as Additives and Their Application in High Voltage Lithium-ion Batteries". **Invited**, presented at "Lithium Mobile Power 2008 Meeting", Las Vegas, Nevada, December 8-9, 2008
3. X. Q. Yang, K. W. Nam, X.J. Wang, Y.N. Zhou, H. S. Lee, O. Haas, L. Wu, and Y. Zhu, K. Y. Chung and B. W. Cho, Hong Li, Xuejie Huang and Liquan Chen "Using Synchrotron Based in situ X-ray Techniques and Transmission Electron Microscopy to Study Electrode Materials for Lithium Batteries" **Invited**, Presented at The 4th Southern China Li-ion Battery Top Forum (CLTF2009), May 24-26, 2009, Shenzhen, China
4. X. Q. Yang, X. J. Wang, B. Zhang, K. W. Nam, Y. N. Zhou, J.M. Bai, O. Haas, H. Li, X. J. Huang, "Structural Changes of Nano-sized $LiFePO_4$-$LiMnPO_4$ Solid Solutions Studied by In-situ XRD" **Invited**, presented at The 2009 International Workshop on Nano Materials and Nano Devices, July 2-5, 2009, Beijing, China
5. X. Q. Yang, K. W. Nam, X. J. Wang, Y. N. Zhou, H.S. Lee, O. Haas, L. Wu, and Y. Zhu, "Lithium Battery Research for Vehicle Technology at Brookhaven National Lab." **Invited**, presented at The international Electric Vehicle Power Battery and Motor Seminar, Beijing, China, July 8-9, 2009, Beijing, China
6. X. Q. Yang, K. W. Nam, H.S. Lee, and J. McBreen, "Lithium Batteries—The next Generation of Power Source for Vehicles" **Invited**, presented at The 5th IEEE Vehicle Power and Propulsion Conference (VPPC'09), September 7-11, 2009, Dearborn, MI 48128
7. Won-Sub Yoon, Kisuk Kang, Yun-Sung Lee, Kyung-Wan Nam, Xiao-Qing Yang, "Thermal Behavior of charged Cathode Materials Studied by X-ray Diffraction and Absorption Techniques", **Invited**, presented at The 60th Annual Meeting of the International Society of Electrochemistry, August 16-21, 2009, Beijing, China.

IV.D.3 Li-ion Abuse Model Development (NREL)

Gi-Heon Kim (Principal Investigator)
National Renewable Energy Laboratory
1617 Cole blvd
Golden, CO, 80401
Phone: (303) 275-; Fax: (303) 275-4415
E-mail: gi-heon.kim@nrel.gov

Start Date: October 1, 2009
Projected End Date: September 30, 2010

Objectives

- Develop a model for internal short circuit simulation in Li-ion batteries

Technical Barriers

A major technical barrier to Li-ion adoption in electric drive vehicles is their safety and abuse tolerance due to internal defects and external events.

Technical Targets

- The Li-ion battery system needs to be tolerant to crush, overcharge, over-voltage, heating, external and internal short while meeting all the cost, life, and performance targets.

Accomplishments

- Developed an integrated simulation tool for multi-physics, 3-dimensional modeling of internal short circuit in Li-ion cells by combining NREL's electrochemical, electrothermal, and abuse kinetics reaction models
- Conducted a case study using internal short circuit model simulations
- Revised and validated the existing abuse kinetics model against test data provided by others
- Presented the results at conferences and meetings
- Participated in the newly formed USABC Internal Short Circuit Workgroup.

✧ ✧ ✧ ✧ ✧

Introduction

Thermal runaway in lithium ion (Li-ion) batteries due to internal short circuit (ISC) is a major safety concern. To resolve this concern, it must be understood how a short's nature and various design variables of Li-ion cells impact on thermal/electrical/electrochemical responses of the system during ISC events. However, it is challenging because internal short circuit and its evolution into the thermal runaway of a cell are complex, multi-physics, 3-dimentional phenomena with many sensitive parameters. Initial latent defects leading to later internal shorts may not be easily controlled and evolve into a hard short through various mechanisms; such as separator wear-out, metal dissolution and deposition on the electrode surface, and extraneous metal debris penetration. The thermal behavior of a lithium-ion battery system regarding an internal short-circuit depends on various factors, such as the nature of the short, cell capacity, electrochemical characteristics of a cell, electrical and thermal designs, and system load. The primary focus of this year's work in this area was on developing an integrated simulation tool (Figure IV- 120) for multi-physics, 3-D modeling of ISC in lithium-ion cells by combining NREL's electrochemical, electrothermal, and abuse kinetics reaction models.

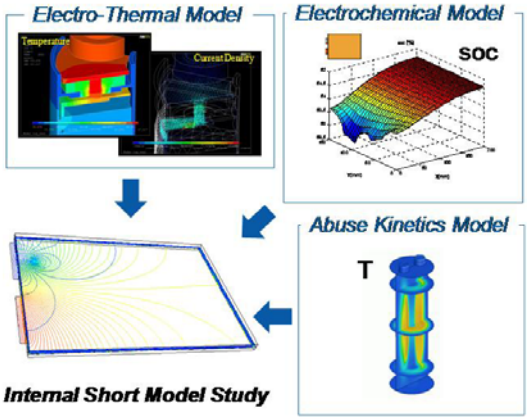

Figure IV- 120: Integrated Multi-Physics Internal Short-Circuit Model

Approach

Various short scenarios were simulated for a case study of prismatic stacked cells. Conditions and cell specifications are shown below:

- 20 Ah
- P/E ration of ~10 h-1
- Stacked prismatic cell
- Form factor: 140 mm x 200 mm x 7.5 mm (Figure IV- 121)
- Layer thicknesses (Al-cathode-separator-anode-Cu): 15 µm-120 µm-20 µm-135 µm-10 µm
- Multi-physics model parameters
- Electrochemistry model: a set evaluated at NREL
- Exothermic kinetics: Hatchard and Dahn (1999)
- Electronic conductivity: Srinivasan and Wang (2003)

The objectives of this model study are to characterize the natures of shorts and to predict cell responses and the onset of thermal runaway. We assume that cells are structurally intact and that the short remains the same during simulated events. Venting and combustion are not considered. The simulation results reasonably reproduced the experimental observations from other research groups and companies and deepened our understanding of complex phenomena by revealing the physics behind them.

Results

ISC Between Metal Current Collector Foils. A short between the positive aluminum current collector and the negative copper current collector was simulated. This type of short could represent metal debris penetration through the electrode and separator layers or contact between the outermost bare aluminum foil and negative-bias container/can. The shorted area size was set as 1 mm by 1 mm in the simulated case. The electrical resistance of the simulated short was calculated as 10 mΩ, and the discharge current flow through the short as 300 A, corresponding to 15 C-rate for the simulated cell. Figure IV- 122(a) shows the electric potential distribution at shorted metal foil layers, and Figure IV- 122(b) and (c) present the diverging current at copper foil and converging current at aluminum foil, respectively. Initial joule heat release is localized for converging current near the short, while cell discharge heat is not as significant as joule heat. As a result, the initial temperature rise is locally observed. The simulation results predict that the cell under the given condition went to thermal runaway eventually, as shown in Figure IV- 123. The abuse kinetic reaction propagates from the short location through the cell volume in less than 1 minute.

ISC Between Electrode. Layers A short between the cathode layer and the anode layer was simulated. This type of short could represent mechanical puncture of the separator or separator wear-out under electrochemical cycling.

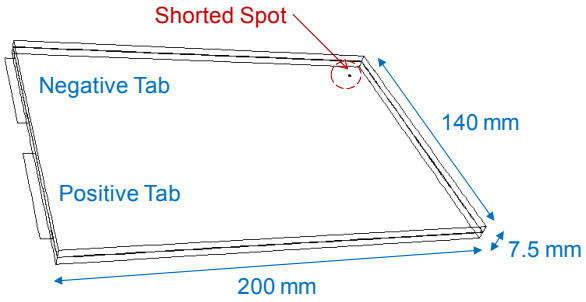

Figure IV- 121: Model Geometry

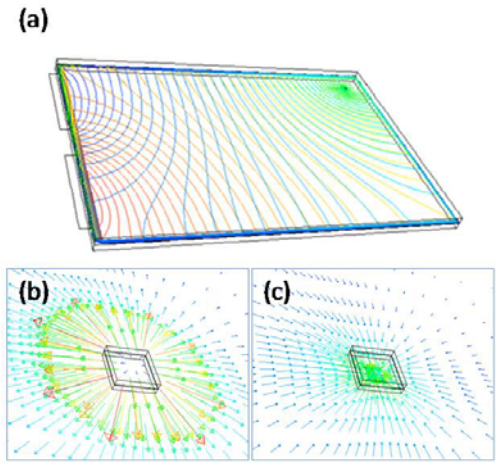

Figure IV- 122: (a) Electric Potential Contour at Shorted Metal Foil Layers, (b) Current Density Vector Plot at Copper Foil, (c) Current Density Vector Plot at Aluminum Foil

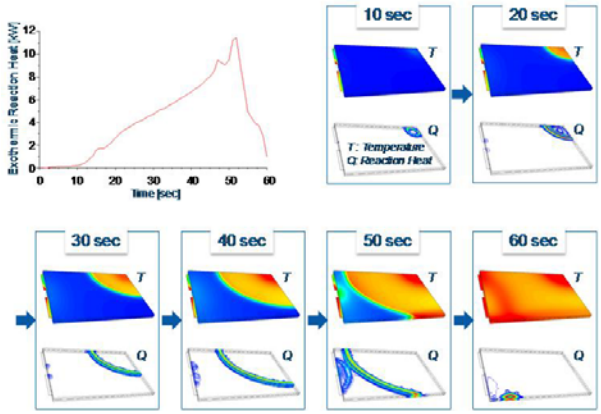

Figure IV- 123: Evolution of Thermal Response of Metal-To-Metal ISC Cell, Exothermic Reaction Heat Release Rate over Time, Temperature and Volumetric Heat Release Rate Contours

The shorted area size was set as 1 mm by 1 mm in the simulated case. The electrical resistance of the simulated short was calculated as 20 Ω, and the discharge current flow through the short was set as 0.16 A, corresponding to less than 0.01 C-rate for the simulated cell. The electron current is still carried mostly by metal current collectors rather than electrode layers. Therefore, the short current should get through resistive electrode layers. The thermal signature of the short is hard to detect from the outer surfaces. The highest temperature appears near the short as 40°C. A short due to a simple separator puncture is not likely to lead to an immediate thermal runaway. Polymer separator film is known to significantly shrink at exposure to high temperatures. Therefore, separator hole propagation due to locally increased temperature near the short could be a concern. A large separator hole (3 cm by 3 cm) short case was simulated. Simulation results show that the electrical resistance of the short is greatly decreased from the small size puncture short to

30 mΩ, and the discharge current flow through the short is 100 A, corresponding to a 5 C-rate for the simulated cell. The cell goes to thermal runaway. This implies that the mechanical integrity of separator could be critical to delay the evolution of an ISC.

ISC Bypassing Cathode Layer. A short between the positive aluminum current collector and the anode layer was simulated. This type of short could represent metal particle inclusion in the cathode slurry or electron conduction path formation between the anode and the bare aluminum foil. The size of the shorted area was set as 1 mm by 1 mm in the simulated case. The electrical resistance of the simulated short was calculated as 2 Ω, and the discharge current flow through the short as 1.8 A, corresponding to less than a 0.1 C-rate for the simulated cell. The model simulation did not predict a thermal runaway, because the short was assumed to remain the same size during the simulation. However, we observed that the temperature at the short quickly reaches over 200°C. It is probable that this type of short would evolve into a hard short in a relatively short time. A short formed through or bypassing a resistive cathode layer would result in a relatively low-resistance short, and it is highly likely to evolve quickly into a more severe short, leading to the thermal runaway of the cell.

Impact of Cell Size (Capacity). A short between a positive aluminum current collector and negative copper current collector is simulated for a small cell of which the capacity is 0.4 Ah. The shorted area size was set as 1 mm by 1 mm in the simulated case, the same as in the 20 Ah cell case. The electrical resistance of the simulated short was calculated as about 7 mΩ, and the discharge current flow through the short as 34 A, corresponding to an 85 C-rate for the simulated cell. When compared with a large cell (20 Ah) for the same type of a short, the current flow through the short in this case is much lower (34 A to 300 A). On the other hand, the C-rate is much higher (85 C-rate vs. 15 C-rate). Therefore, the entire volume of the shorted cell is quickly heated up by high C-rate discharge. The heating pattern tends to be global rather than local. Temperature contours and graphs for volume fraction distribution over the temperatures shown in Figure IV- 124 reveal that the temperature distribution range in a small cell is a tight band. In this type of heating, a shut-down separator thermally triggered to become resistive to ion transfer has a better chance to work. It is difficult to make a shut-down separator function properly in large-capacity systems, however, in which heating under a short condition is highly localized (Figure IV- 125).

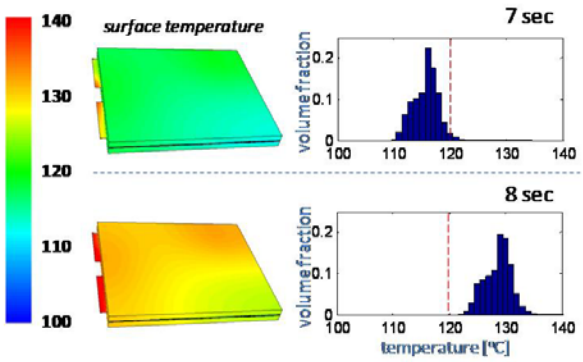

Figure IV- 124: Surface Temperature Contours and Volume Fraction Distribution over Temperatures at 7 Seconds and 8 Seconds after Metal-To-Metal Short in a Small (0.4 Ah) Cell

Impact of Short Location. Shorts between a positive aluminum current collector and a negative copper current collector are compared for different short locations: near-tab short and far-side short. A near-tab short shows more severe initial heating behavior in a large stacked cell. When a low-resistance ISC forms, a near-tab ISC results in a smaller resistance, leading to higher short current and joule heating because of shorter current paths through shorting layers. Near the ISC is a main heating zone of joule heat for short current. However, secondary local heating is observed near tabs in stacked cell structures because of converging current fields. In the near-tab ISC case, these two heating zones are superimposed.

Conclusions and Future Directions

- NREL performed an internal short model simulation study to characterize an internal short circuit and its evolution over time by linking and integrating NREL's electrochemical cell, electro-thermal, and abuse reaction kinetics models.
- The initial heating pattern at short events depends on various physical parameters, such as the nature of the short, cell size, and rate capability.

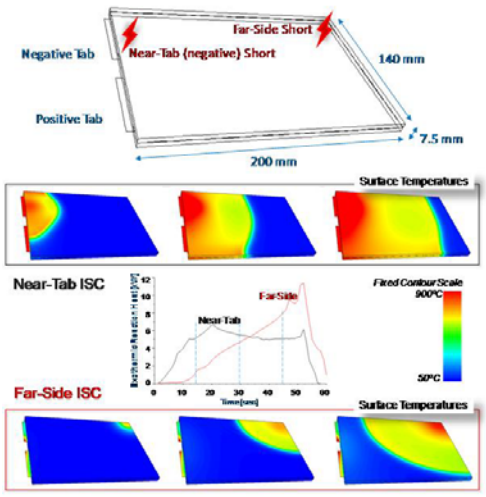

Figure IV- 125: Thermal Response Comparison for Short Location in a Large-Format Stacked Prismatic Cell

- The temperature rise due to the short is localized in large-format cells.
- Electron short current is carried mostly by metal collectors.
- A simple puncture in the separator is not likely to lead to an immediate thermal runaway of a cell.
- Maintaining the integrity of the separator seems critical to delay a short's evolution.
- Metal plating can provide preferable sites for ISC.
- A shutdown separator is difficult to apply in large-capacity and high-voltage systems.
- For low-resistance ISCs, a near-tab short would cause more severe initial heating behavior in a large stacked cell.
- Electrical, thermal, and electrochemical responses of a shorted cell change significantly for different types of internal shorts.

We will perform an in-depth analysis to evaluate recommended safety designs, such as structurally intact separators and a featured shutdown device/strategy in relation to cell design parameters. We will verify and extend the knowledge acquired through the model study by performing carefully designed experiments through inter-laboratory collaborations. We will continue to support the USABC/FreedomCAR Tech Team ISC Workgroup in FY2010,

FY 2009 Publications/Presentations

1. Pesaran, A.; Kim, G.-H.; Smith, K., "Designing Safe Lithium-Ion Battery Packs Using Thermal Abuse Models," Proceedings of the 4th Annual Lithium Mobile Power 2008 Conference, Las Vegas, Nevada, December 8-9, 2008.
2. Smith, K.; Kim, G.-H.; Pesaran, A. "Thermal/Electrical Modeling for Abuse-Tolerant Design of Li-ion Modules," Presented at the NASA Aerospace Battery Workshop Conference, Huntsville, Alabama, November 18-20, 2008.
3. Kim, G.-H.; Smith, K. "Multi-Scale Multi-Dimensional Li-ion Battery Model for Better Design and Management," Presented at PRiME2008, the 214th Electrochemical Society Pacific Rim Meeting, Honolulu, Hawaii, October 12-17, 2008.
4. Gi-Heon Kim, Presentation at Applied Battery Research for Transportation Planning Meeting, Argonne, IL, July 2009
5. Gi-Heon Kim, Kandler Smith, Ahmad Pesaran, Lithium-Ion Battery Safety Study Using Multi-Physics Internal Short-Circuit Model NREL; Presented at 5th International Symposium on Large Li-ion Battery Technology and Application, in conjunction with the 9th Advanced Automotive Battery Conference; Long Beach, CA, June 2009.
6. Presentation at USABC ISC Working Group Meetings, June and September 2009.
7. Presentation at 80th Lithium Battery Technical/Safety Group Meeting, September 2009.

IV.D.4 Impact of Materials on Abuse Response (SNL)

E. Peter Roth
Sandia National Laboratories
PO Box 5800 MS0614
Albuquerque, NM 87109
Phone: (505) 844-3949; Fax: (505) 844-6972
E-mail: eproth@sandia.gov

Start Date Oct. 1, 2008
Projected End Date: September 30, 2010

Objectives

- Identify degradation mechanisms of gas and heat-producing reactions in Li-ion rechargeable cells.
- Identify and develop advanced materials or combination of materials that will minimize the sources of cell degradation during abuse events, thus enhancing safety.
- Build and test full size cells to demonstrate improved abuse tolerance**.**

Technical Barriers

There are several technical barriers to improving Li-ion cell abuse response:

- Develop intrinsically abuse tolerant Li-ion cells and batteries based on low-reactivity materials
- Overcome gas generation and flammability response

Technical Targets

- Quantify thermal runaway response of candidate cell materials in full cell (18650) configuration
- Identify relative effect of cell additives on nominal cell thermal abuse response
- Identify critical cell properties that affect gas generation

Accomplishments

- Quantitatively shown the individual thermal effects of $LiMn_2O_4$ and $LiFePO_4$ cell cathode\anode materials in 18650 cells and shown that anode reactions dominate thermal runaway
- Gas generation during peak runaway normalized by cell capacity has been shown to be independent of cell chemistry and determined primarily by electrolyte quantity
- 18650 cells with 3 wt.% fluorinated LiBOB ($LiC_2O_4BF_2$) electrolyte additive were built and the additive shown to have slight stabilizing effect on $LiMn_2O_4$ cells while causing a slight increase in reactions below 150°C for $LiNi_{1/3}Co_{1/3}Mn_{1/3}O_2$ cells.
- Cells with $LiFePO_4$ and $LiMn_2O_4$ cathodes, though thermally stable, have shown higher heat generation during overcharge compared to other cathode oxides and heat generation starts immediately above 100% state of charge resulting from the low cathode Li level at full SOC.
- Shown that commercial $LiFePO_4$ cells with an ionic liquid flame retardant additive actually showed higher reactivity and flammability of vented gases during high temperature ramp.

✧ ✧ ✧ ✧ ✧

Introduction

The evaluation of materials for improved thermal abuse response requires testing in full cell configurations where material interactions and reaction levels are close to real-world conditions. 18650 cells were built in our laboratory with candidate materials and their abuse response tested using specially developed techniques to quantitatively characterize and compare their response. This year we have concentrated on comparing some of the more stable cathode chemistries and looked at additives designed to improve the thermal and flammability response of those cells.

Approach

The effects of cell materials on thermal runaway were characterized using Accelerating Rate Calorimetry (ARC) to measure the heat and gas generation under ideal adiabatic conditions using specially designed high-pressure cell fixtures. Cells were also tested under more real-world abusive conditions using thermal ramp to high temperatures, overcharge with quantitative heat flow measurement and real-time gas species measurement. Cells were built using coated electrodes with new candidate materials provided in collaboration with the other ABR laboratories. In-house cell building allowed close control of the cell properties for side-by-side comparison of these test cells under the same test conditions. Full cell performance was correlated with basic properties obtained on the cell materials.

Results

Effect of Materials on Thermal Runaway. Much of our studies have concentrated on the most stable cathodes, the $LiMn_2O_4$ spinel and $LiFePO_4$. Previously we have shown that these cathode chemistries have greatly reduced oxygen release at high temperatures and thus have much lower heat generation. We have examined the individual effect of the anode and cathode electrodes on the cell thermal runaway response by removing the electrodes from a fully charged 18650 cell in an argon glove box and resealing the individual electrodes with electrolyte in 18650 cell cans. ARC testing was then performed on each electrode. These individual ARC runs showed that the anode is now the dominant source of heat generation during thermal runaway especially for the $LiFePO_4$ cells. Figure IV- 126 shows the ARC profiles for the MCMB carbon anode and $LiFePO_4$ cathode of a typical 18650 cell. The anode clearly dominates the thermal response during runaway leading to cell failure even for these relatively "safe" cells.

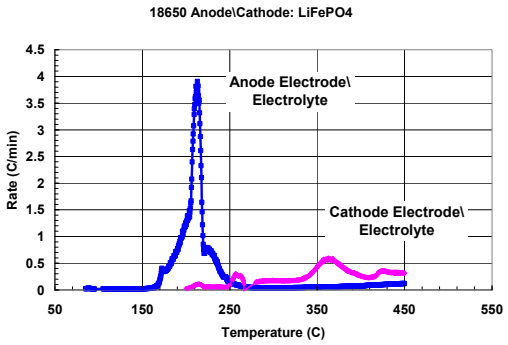

Figure IV- 126: ARC thermal profiles of fully charged 18650 cell electrodes sealed individually in 18650 cans with electrolyte.

Gas generation is also a significant safety concern since vent gas can aerosolize the flammable electrolyte. Figure IV- 127 shows the ARC heat and gas generation profile of a cell during thermal runaway. We have measured the gas generation from 18650 cells with several different cathodes using EC:PC:DMC\1.2M $LiPF_6$ electrolyte. The gas generation at the end of the peak thermal runaway is most significant from a safety aspect. Figure IV- 128 shows that the volume of gas at 350°C normalized for cell capacity was the same for cells with five different cathode chemistries. This data shows that the electrolyte volume is the determining factor for gas volume generation.

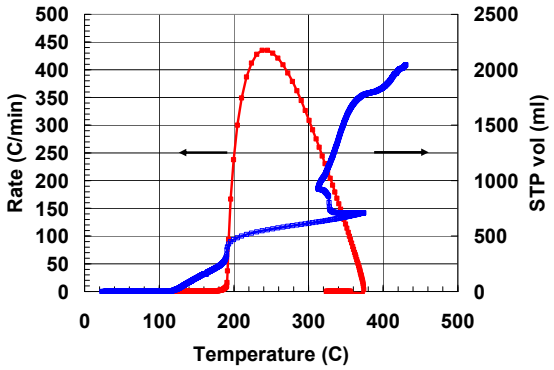

Figure IV- 127: ARC thermal profiles of fully charged 18650 cell showing heat and gas generation.

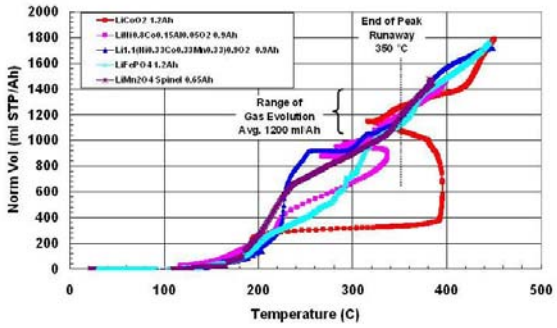

Figure IV- 128: 18650 cell ARC gas generation profiles for 5 different cathode chemistries showing equal gas volumes at end of peak thermal runaway.

Electrolyte Additives. Improvement in cell performance has also been investigated using electrolyte additives. A fluorinated LiBOB ($LiC_2O_4BF_2$) additive was used at the 3 wt.% level in standard EC:PC:DMC\$LiPF_6$ electrolyte with $LiMn_2O_4$ and Gen3 ($LiNi_{1/3}Co_{1/3}Mn_{1/3}O_2$) cathodes. Figure IV- 129 shows the ARC profiles for two cells with the F-LiBOB additive compared with a baseline cell with no additive. For the $LiMn_2O_4$ cathode, a slight reduction in low-temperature reactions was seen possibly associated with SEI reactions at the graphite anode. No effect was observed at the higher temperatures above 300°C where reactions are associated with cathode/binder reactions.

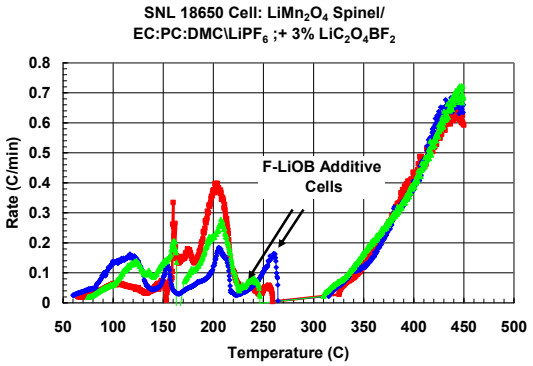

Figure IV- 129: ARC profiles of 18650 cells with $LiMn_2O_4$ cathodes both with and without F-LiBOB electrolyte additive showing only slight low-temperature improvement.

Cells were also tested using Gen3 ($LiNi_{1/3}Co_{1/3}Mn_{1/3}O_2$) cathodes with the electrolyte additive. There was no observable effect during the high temperature runaway as shown in Figure IV- 130 but there was a definite increase in reaction at low temperatures where the SEI layer is reactive as shown in Figure IV- 131.

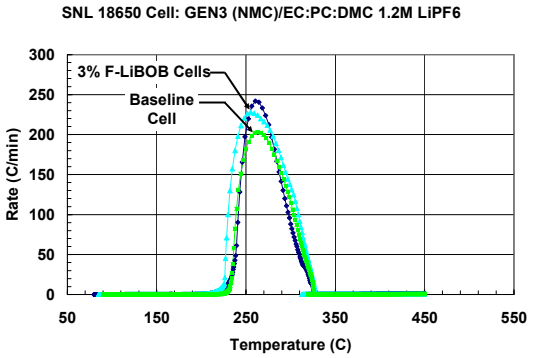

Figure IV- 130: ARC profiles of 18650 cells with $LiNi_{1/3}Co_{1/3}Mn_{1/3}O_2$ cathodes both with and without F-LiBOB electrolyte additive showing no high-temperature effects.

An ionic liquid additive was investigated in commercial 26650 $LiFePO_4$ cells as a possible flame retardant. The 26650 cells contained an ionic liquid additive, 1-Butyl-1-methylpyrrolidinium bis(trifluoromethylsulfonyl)imide (bmpl ntf) at different concentrations. The cells were tested by thermally ramping them to high temperature where they underwent venting and thermal runaway. The cells vented into open air and the flammability was tested by using an external spark ignition source to ignite the vapors as shown in Figure IV- 132. Baseline cells with the standard electrolyte run initially and showed only moderate venting and low-level flames from the vented cells. The cells with the ionic liquid additive showed increased thermal reactions and increased flammability of the vent gases. Figure IV- 133 shows the heating rate profiles of the cells where it is seen that the ionic liquid additive cell heating rates were significantly greater than the baseline cells and resulted in greater temperature excursions. Movies of the thermal ramps showed increased gas generation and flammability. These results reinforce the need for real-world testing of new materials to insure that improved abuse tolerance is actually achieved in full size cells.

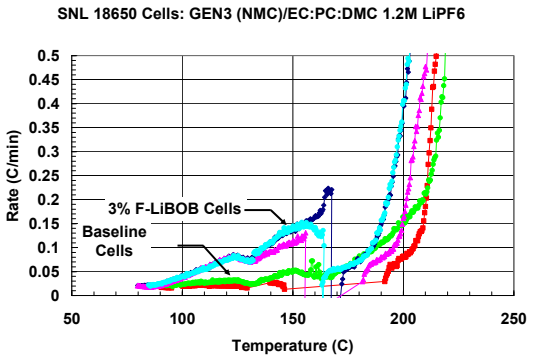

Figure IV- 131: ARC profiles of 18650 cells with $LiNi_{1/3}Co_{1/3}Mn_{1/3}O_2$ cathodes both with and without F-LiBOB electrolyte additive showing increased reaction rate at low-temperatures.

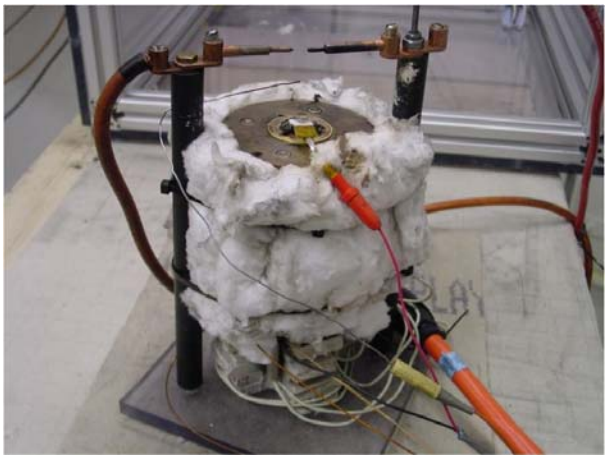

Figure IV- 132: Thermal ramp apparatus for testing thermal runaway and flammability of vent gases.

Overcharge Response. A critical abuse condition for Li-ion cells is overcharge that can result in heat generation, venting and eventual thermal runaway. Overcharge was performed on several 18650 cells with different cathode chemistries. The cells were charged at a 1C rate starting at 100%SOC while monitoring cell temperature. A special fixture was designed that also allowed calculation of the heat generation rate of the cells. Cathodes with high remaining levels of Li at 100%SOC such as LiCoO2 (Li=0.5) and LiNi1/3Co1/3Mn1/3O2 (Li=0.48) did not show a noticeable temperature increase until the cells were at 150%-160% SOC while cathodes such as $LiNi_{0.8}Co_{0.15}Al_{0.05}O_2$ (Li=0.36) showed increased heating at 125%SOC. The increased heat generation was associated the depletion of the Li from the cathode. Cells

with little or no Li remaining at 100%SOCsuch as $LiMn_2O_4$ (Li=0.1) and $LiFePO_4$ (Li=0) showed almost immediate heat generation at the beginning of overcharge. Figure IV- 134 shows the cell temperatures during overcharge.

These results indicate that systems using cells with the safest cathode chemistries ($LiMn_2O_4$, $LiFePO_4$) must also design for sufficient heat removal during possible overcharge to prevent catastrophic thermal runaway.

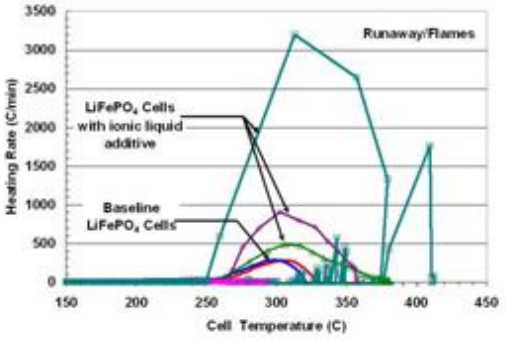

Figure IV- 133: Thermal ramp heating rates of 26650 cells with and without ionic liquid flame retardant. This additive resulted in increased thermal reaction and flammability.

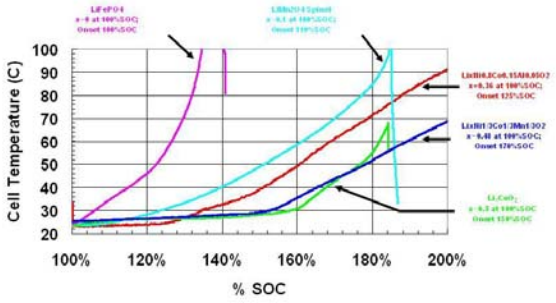

Figure IV- 134: Cell temperature response during overcharging for several different cathode chemistries.

Conclusions and Future Directions

Increased thermal stability has been demonstrated with more stable cathodes ($LiMn_2O_4$ spinel and $LiFePO_4$). The improved stability results from decreased oxygen generation at high temperatures. However, anode reactions are still a significant energy source for thermal runaway and improvements are important to provide better abuse tolerance. Certain additives can reduce thermal reactions under abuse conditions but so far have shown only minor effects on overall abuse response and some can even make the cells more reactive. Electrolyte gas generation and flammability is still a critical issue. All Li-ion cells still contain volatile and flammable organic electrolytes that can result in external fires if abuse of the cells results in venting. Our future research will address the following issues:

- Develop an enhanced stability cell by conducting quantitative cell-level abuse studies to verify material enhancements (e.g. AlF3 coated NMC cathodes).
- Demonstrate improved overcharge abuse tolerance in full cells with new materials and additives.
- Demonstrate reduced electrolyte gas generation under full-cell abuse conditions using non-PF6 salts with increased temperature and voltage stability.
- Support development of an abuse model using measured cell material properties that will allow prediction of cell abuse response for any given cell design and failure mode (e.g. internal short).
- Expand our cell building capabilities by using our commercial electrode coating equipment to fabricate electrodes starting with basic raw materials.

FY 2009 Publications/Presentations

Presentations

1. 214th ECS Meeting (Hawaii), 10/12-17/2008
2. Battery Power 2008 (Dallas, TX), 11/12/2008
3. Power Sources Conf. (Ft. Lauderdale, FL), 3/16-19/2009
4. Space Power Workshop (Manhattan Beach, CA), 4/22-23/2009
5. 215th ECS Meeting, (San Francisco, CA), 5/24-29/2009
6. AABC Battery Safety Conf. (Long Beach, CA), 6/8-12/2009
7. 80th Li Battery Safety Meeting (Denver, CO), 9/1-2/2009
8. 5th IEEE International Vehicle Power and Propulsion Conference (Dearborn, MI), 9/7-8/2009
9. 2009 DOE Annual Peer Review Meeting.

IV.D.5 Impact of Separators on Abuse Response, Internal Short Circuit Simulation (SNL)

Christopher J. Orendorff and E. Peter Roth
Sandia National Laboratories
PO Box 5800-0614
Albuquerque, NM 87185-0614
Phone: (505) 844-5879; Fax: (505) 844-6872
E-mail: corendo@sandia.gov

Start Date: October 1, 2008
Projected End Date: September 30, 2010

Objectives

- Develop an "on-demand" internal short circuit (ISC) approach using an external trigger that does not involve mechanical perturbation or deformation of the cell (crushing, pressing, pinching, etc.).
- To increase our understanding of the role of separator in ISCs and the response of separators under abuse conditions by developing a separator testing platform that mimics cell-like conditions.

Technical Barriers

There are a number of technical barriers to developing an "on-demand" ISC trigger including:

(A) Stimulating ISCs in cells independent of cell chemistry, design, or geometry

(B) Demonstrating normal cell behavior (capacity, cycling, etc.) while the trigger is "off"

(C) Utility of studying the four primary ISC scenarios (active material/foil, foil/foil, etc.).

The technical challenges associated with the separator characterization work include:

(A) Establishing experimental conditions that closely match cell conditions

(B) Developing techniques to determine mechanical and thermal stability

(C) Measuring internal and external cell thermal response to quantitatively evaluate response to different ISCs

Technical Targets

- Identify candidate techniques (defects and triggers) that can be used to cause an "on-demand" ISC
- Demonstrate the utility of these ISC techniques in test platforms (foil electrodes) and in 18650 cells
- Identify the challenges of each technique and potential solutions to be explored next FY.
- Develop a stand-alone separator platform to determine mechanical and thermal performance
- Use this platform to evaluate a variety of commercial separator materials.

Accomplishments

- Demonstrated several approaches for stimulating ISCs in lithium-ion cells, deployed primarily in coin ce1ls. All ISC studies have been for the active material-to-active material ISC scenario.
- Demonstrated "normal" cell behavior in terms of capacity, cycling, charge/discharge profiles for cells containing ISC defects with the trigger in the "off" state.
- Developed experimental techniques to study separator mechanical and thermal stability and performance.
- Demonstrated the use of these separator testing techniques on a variety of commercially available separator materials.

✧ ✧ ✧ ✧ ✧

Introduction

There is significant interest in better understanding and mitigating field failure modes of lithium-ion batteries, especially for internal short circuit in cells related to the transportation industry. To date, there is no suitable, widespread laboratory test for introducing and characterizing an internal short circuit. Moreover, a better understanding of the role and performance of the separator under these conditions could facilitate mitigation of ISCs.

Approach

Current test approaches for internal short circuits all include some degree of battery package deformation. These include the pressure induced internal short circuit (conductive and insulated blunt nail press tests), the Battery Institute of Japan (BAJ) ISC test (blunt nail press on a millimeter-sized defect placed in the cell), and the ISC pinch test by Motorola and ORNL (crush test between two blunt pressure points). Our approach is to generate an ISC in a cell without employing any cell

package deformation and without any significant alteration of the cell performance with the ISC is triggered "off". This approach will include deploying a defect into a cell and trigger that defect by some external stimulus. This FY we have explored the use of various defects including nickel particles (7-50 µm), copper particles (200-500 µm), shape memory (nickel-titanium) wire, and various bismuth/tin alloys. The triggers for these defects have included heat, vibration, and charging current.

Similarly, all characterization techniques for separator integrity (thermal or mechanical) rely on bulk characterization approaches that are not accurate or relevant to the physical environment of a separator in a cell. For example, mechanical integrity of separators is measured by bulk puncture strength and tensile strength in the machine direction (MD) and transverse direction (TD) of the separator. However, these measurements do not test separator strength when it is soaked with electrolyte nor do they measure a separator resistance to puncture for a micro-scale foreign object; conditions that are common place in actually cells. Most of the thermal integrity measurements are based on separator shrinkage as a function of temperature. These measurements do not consider separators that contain electrolyte nor do they account for possible changes in electrical behavior of these materials (e.g. materials may not shrink, but may exhibit significant impedance change). Our approach is to better understand separator performance in cells under thermal and mechanical abuse using a more controlled systematic experimental platform.

Results

ISC Test Method Development. As described above, a considerable amount of effort has been given to evaluating a variety of different ISC defect and trigger combinations in an effort to stimulate ISCs. The approach that received much of the early focus is the nickel particle defect/sonication trigger technique. This involves adding nickel particles (≤ 1 mg of 7-150 µm particles) into cells, typically between anode and separator, and ISCs are triggered by sonication. The proposed mechanism is that the high frequency vibration of the particles inside a cell will cause local damage to the separator and lead to an ISC. This was successfully demonstrated at the coin cell level, however, with significant variability in the results. Figure IV- 135 shows representative plots of voltage and temperature as a function of time for two cells built with nickel particle defects. Each temperature increase is due to heat transfer from discrete sonication pulses. In Figure IV- 135a, the cell develops a soft short after the first pulse which progresses to a hard short after the second pulse. In Figure IV- 135b, after 23 sonication pulses, the cell does not develop an ISC (the voltage drop after the final pulse is due to rupturing the crimp seal of the cell. The variability in the test results along with the inability to trigger an ISC in an 18650 cell has lead to the pursuit of other approaches.

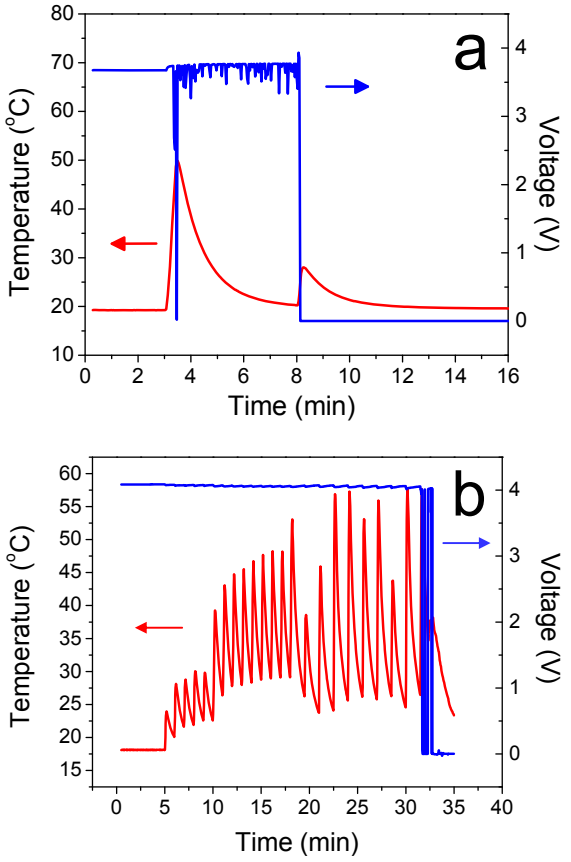

Figure IV- 135: Voltage (blue) and temperature (red) profiles for cells containing nickel particle defects that are triggered by sonication. (a) a cell where a short is triggered after 2 sonication pulses and (b) a cell where a short is not triggered after 23 sonication pulses. Each temperature peak corresponds to a sonicator pulse.

An alternative technique to stimulating ISCs we have developed employs a low melting point metallic alloy defect with a thermal trigger. In this case, the alloy defect is placed between two sheets of separator in a cell. The ISC is stimulated when the alloy melts and leaks through the microporous separator and makes electrical contact between the two electrodes. This has been demonstrated by monitoring the AC impedance between two copper foil electrodes wound in an 18650 configuration and separated by a polyethylene (PE) separator with the alloy defect, shown in Figure IV- 136. Here, the temperature is measured in the core of three foil roll samples and the alloy melting temperature is ~58°C. In all three samples, once the alloy melts, it leaks through the separator, triggering an ISC with a final impedance value of <100 mΩ.

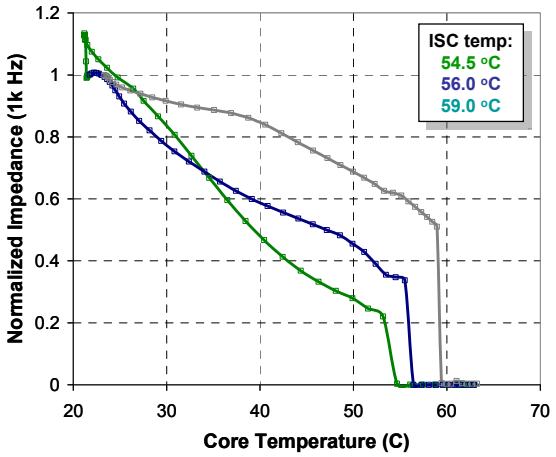

Figure IV- 136: Normalized AC impedance of Celgard 2325 rolled between two copper foil electrodes. The electrodes are shorted together using a Bi/Sn/In/Pb alloy with a melting temperature of 58°C.

In addition to demonstrating the ISC trigger using foil electrodes, we have also successfully triggered ISCs in coin cells. An ISC is triggered at the alloy melt temperature while charging an iron phosphate-based coin cell, shown in Figure IV- 137. The resulting shorted cell voltage drops to < 0.5 V while drawing 100 mA (limit set on the controller).

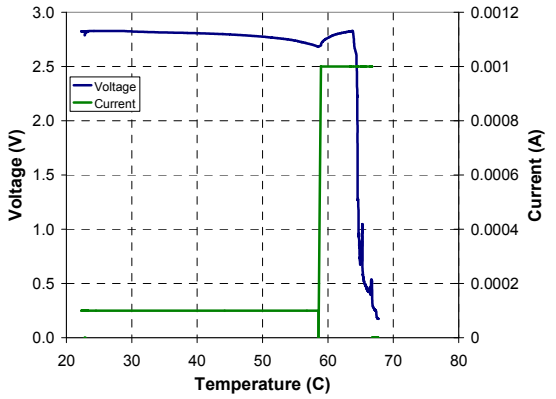

Figure IV- 137: Cell voltage and applied current as a function of temperature for a $LiFePO_4$ coin cell (< 50% SOC) that is shorted using a Bi/Sn/In alloy with a melting temperature of 60°C

Experiments are currently underway to demonstrate the use of this approach to trigger ISCs in 18650 cells not only between active materials but between current collectors and current collector-active materials.

Separator Evaluation Development. In addition to triggering ISCs, we are also interested in understanding how separator performance impacts ISCs. This is of critical importance in high energy and high power battery applications, as in those for EVs and HEVs. For example, under thermal abuse conditions, above the shutdown temperature (>130°C for PE-based separators), shutdown separators can degrade and form pinholes that can develop into ISCs. Moreover, one of the most common field failure modes is the presence of a manufacturing defect particle in cells that can puncture the separator and cause an ISC. To address these issues, we have developed two methods for evaluating separator thermal and mechanical performance *ex-situ*.

Figure IV- 138 shows the normalized AC impedance of two separator materials as a function of temperature. Commercial Celgard 2325 shuts down at ~130°C and the impedance increases by 5 orders of magnitude (not shown on this scale). However, at 175°C the separator completely degrades and the impedance decreases to zero (Figure IV- 138). At temperatures > 130°C, this separator is mechanically unstable and is susceptible to the formation of defects that can lead to a short circuit. Separator "A" and "B" are two adjacent samples from the same roll of a non-shutdown PVdF-based separator. The impedance of each sample is also shown in Figure IV- 138. What is most striking about these data is the significant difference in the thermal integrity between two adjacent sections of the same separator roll. One sample of the separator degrades at 75°C while the other is thermally stable up to 225°C.

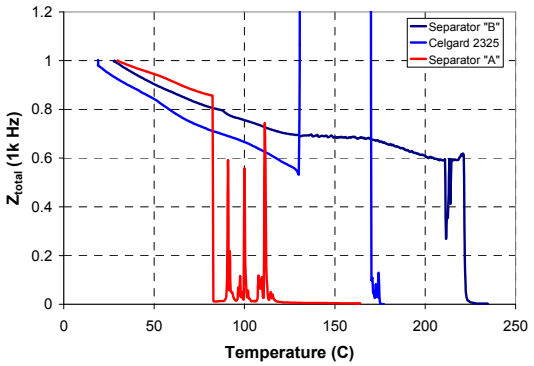

Figure IV- 138: Normalized total AC impedance (50 mV, 1000 Hz) as a function of temperature for a sample of shutdown separator, Celgard 2325 (blue), and for two samples from the same roll of PVdF-based non-shutdown separator (red and navy).

This highlights the importance of reliable and consistent manufacturing processes and the variability that can be observed in separator performance not only from batch to batch but within the same roll.

Mechanical strength, specifically resistance to puncture from a defect metal particle, is also critically important to cell-level separator performance. To study this effect, we have developed a microparticle puncture experiment using our evaluation platform. Samples are prepared by placing metal particles (7-450 µm) onto electrolyte-soaked separators (4 cm^2) and sandwiching them between nickel electrodes and sealing the samples in polyimide tape. The samples are place under increasing mechanical load while monitoring the AC impedance of the separator. The impedance decreases to

zero when the micro particle punctures the separator, causing a short between to two electrodes. The load required to puncture the separator in this experiment is referred to as the load-to-short (LTS) value. Figure IV-139 shows the impedance as a function of applied load for several commercial separators.

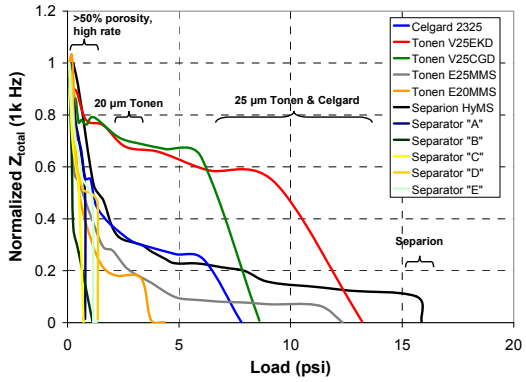

Figure IV- 139: Normalized total impedance (50 mV, 1000 Hz) as a function of applied load to commercial separators punctured with 425 µm copper particles.

It is clear from these data, that the separator puncture response varies widely; where separators are punctured anywhere from <1 to 16 psi. A number of physical properties affect the microparticle puncture strength of these materials including tensile strength, porosity, material hardness, and thickness. Work is in progress to evaluate several more commercial separators and to quantify the relationship of all of these parameters to overall separator mechanical stability. For example, Figure IV- 139 shows the relationship between the LTS values and average tensile strength for Celgard, Tonen, and Separion (Degussa) separators. The average tensile strength plotted in Figure IV- 139 is the average of the MD and TD values and is used to account for the large discrepancy between MD and TD values for certain materials (e.g. Celgard 2325; MD = 1700 kg/cm^2, TD = 150 kg/cm^2).

As the bulk tensile strength of the separator increases, the load required to cause separator puncture increases. While this may seem an obvious result, this work provides quantitative information to the issues of separator puncture by a foreign particle or object for a systematic series of materials.

Conclusions and Future Directions

This work is focused on studying, stimulating and characterizing ISCs. We have demonstrated the ability to stimulate internal short circuits in full coin cells using a number of techniques; however, we have identified the low melting point alloy defect with a thermal trigger to be the most viable approach. This approach has been shown to be the most reproducible and consistent technique studied to date. Future work includes engineering the defect materials to be as small as possible (target dimensions of < 1 mm^2 area and < 100 µm thick) without sacrificing any efficacy, demonstrating the use of this approach to trigger ISCs in 18650 cells, and studying the 4 possible ISC scenarios with this technique. In addition, we will also incorporate these experimental data into the thermal models developed at NREL to more accurately model and predict the cell response to an ISC.

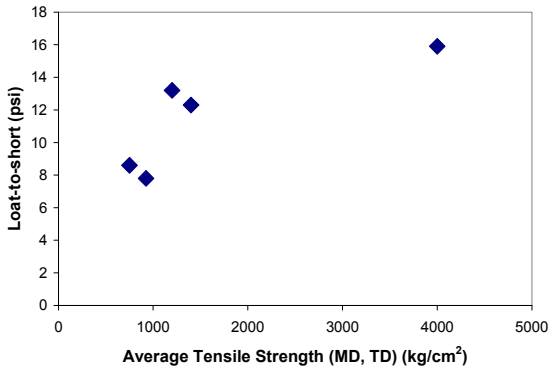

Figure IV- 140: Load-to-short (LTS) values as a function of average tensile strength (MD and TD) for 25 µm thick Celgard, Tonen, and Separion (Degussa) separators.

We have also developed an experimental platform for characterizing separator mechanical and thermal stability. The thermal integrity experiment can differentiate separator shutdown, degradation, and stability by monitoring separator impedance up to temperatures above the onset of thermal runaway (> 180°C). The mechanical integrity experiment uses microparticles and a controlled applied load to puncture separators; simulating a latent defect metal particle or manufacturing flaw that causes an ISC. This technique provides quantitative data on a systematic series of commercial separator mechanical strength under conditions that are more closely related to those in a cell, opposed to a bulk tensile or puncture test.

FY 2009 Publications/Presentations

1. Presentation to the 2009 DOE Annual Peer Review Meeting.
2. Presentation at the Spring 2009 Electrochemical Society (ECS) Meeting
3. Presentation to the 80th Lithium-ion Battery Safety Meeting.

V

FOCUSED FUNDAMENTAL RESEARCH

D.O.E. Project Manager

Tien Q. Duong

Technical Leads

John Newman
Venkat Srinivasan
Lawrence Berkeley National Laboratory

V. FOCUSED FUNDAMENTAL RESEARCH

V.A Introduction

The focused fundamental research program, also called the Batteries for Advanced Transportation Technologies (BATT) program, is supported by the DOE's Vehicle Technologies program (DOE-VT) to research and analyze new materials for high-performance, next generation, rechargeable batteries for use in HEVs, PHEVs, and EVs. The effort in 2009 continued the increased emphasis on high energy materials for PHEV and EV applications.

Background and Program Context

The BATT Program addresses the fundamental problems of chemical and mechanical instabilities that have impeded the development of automotive batteries with acceptable cost, performance, lifetime, and safety. The aim is to identify and better understand cell and material performance and lifetime limitations before initiating battery scale-up and development. Emphasis is placed on the synthesis of components into cells with determination of failure modes, while continuing with materials synthesis and evaluation, advanced diagnostics, and improved model development. Battery chemistries are monitored continuously with timely substitution of more promising components. This is done with advice from within the BATT Program and from outside experts, including consultation with automotive companies and DOE. Also factored into the BATT Program direction is the monitoring of world-wide battery R&D activities. The Program not only supports research that leads to incremental improvements to existing materials, but also into high-risk "leap-frog" technologies that might have a tremendous impact in the marketplace. An overview of the activities and focus of the program is shown in Figure V- 1.

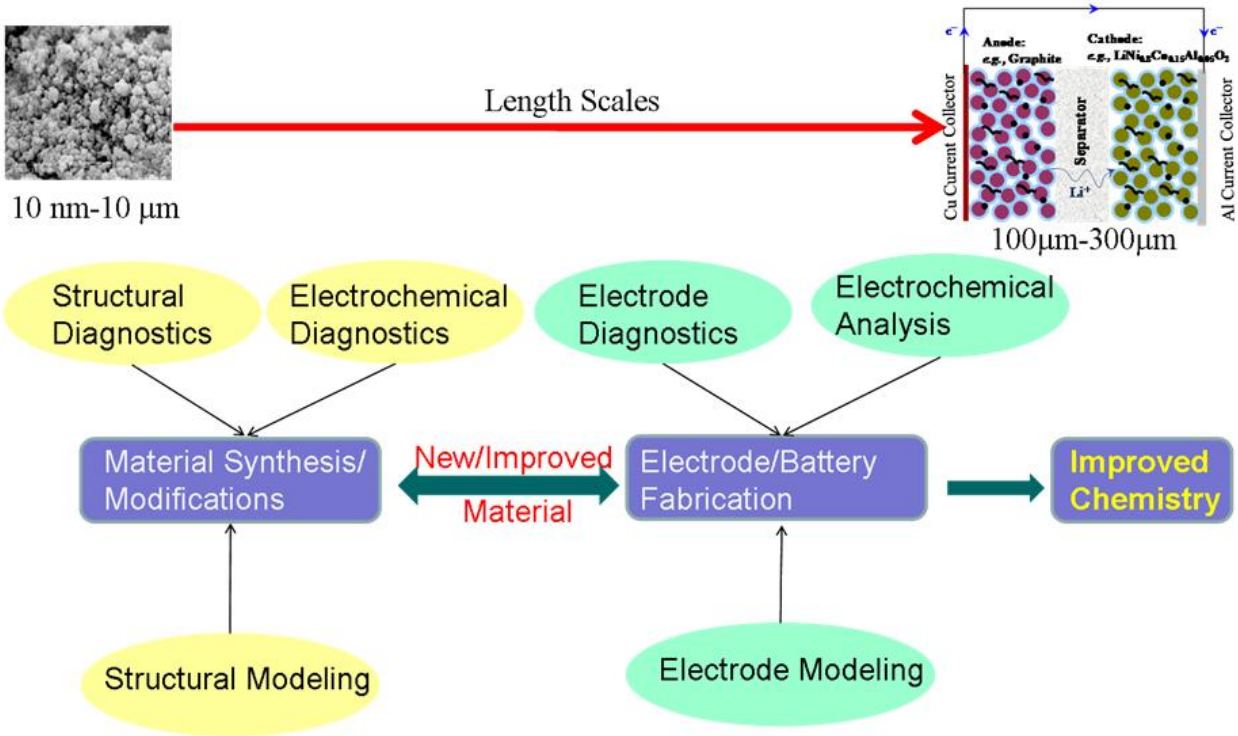

Figure V- 1: BATT Overview

The work is administered by the Lawrence Berkeley National Laboratory (LBNL), with principal researchers from LBNL, five additional laboratories, eleven universities, and one commercial company. The program is organized into the following areas:

- New Cathode Systems, Performance and Limitations
- New Anode Materials
- Novel Electrolytes and their Characterization,
- Li-ion Modeling, Diagnostics, and Cell Analysis

This section summarizes the research activities of this program in FY 2009. The website for the BATT Program is found at http://berc.lbl.gov/BATT/BATT.html. Brief descriptions of each research area are as follows.

The ***New Cathode Materials*** task aims to find improved cathode materials that offer significant improvements in volumetric and specific energy and/or power over current state of the art materials, like $LiCoO_2$. The investigation into phosphate systems includes studies of capacity and power, lower cost synthesis methods, and the impact of processing steps on performance. Work on layered systems includes the $LiNi_{1/3}Mn_{1/3}Co_{1/3}O_2$ (called NMC) cathode material that can be used to produce either a high-energy cell that can be engineered to provide good power. This work aims to understand the failure and degradation modes in NMC and other such systems using cell builds, cell cycling, advanced diagnostics, and modeling. Finally, the work into Mn spinel materials aims to understand the failure and degradation modes using various material doping, cell cycling, and advanced diagnostics. This work also includes the composite, high voltage, high-energy cathode materials that promise a significant increase in both capacity and voltage over current materials.

The ***New Anode Materials*** task aims to find improved anode materials that offer at least twice the volumetric and specific energy of graphite. Researchers are investigating composite negative electrodes containing one (or more) metal components within a graphite matrix, for example C/Sn, C/Si, and C/Sb systems, and nano-composite alloys.

The ***Novel Electrolyte Materials*** task involves several new projects that have begun following the BATT program's solicitation posted in 2008. These five research efforts focus on expanding the temperature range of cells, additives to stabilize the negative and positive interfaces, development of new overcharge shuttles to further stabilize Li-ion cells, new ionic liquids to enable higher voltage windows, and first principles modeling to understand and eventually to construct a more stable SEI.

The ***Modeling, Diagnostics, and Cell Analysis*** tasks involve the use of advanced diagnostics techniques, such as FTIR, X-ray absorption fine structure (XAFS), X-ray diffraction (XRD), nuclear magnetic resonance (NMR) and other techniques to investigate interfacial and other properties in Li-ion batteries. Several modeling approaches are used to understand cell and fundamental material properties, including *ab-initio* calculations, macroscopic cell calculations, and finite element simulations. Finally, standard cell making and testing techniques are developed and applied to provide a common evaluation process for new materials.

V.B Cathode Development

The overall objectives in the cathode area tasks are to understand through theory and experiment the effect of structure on the stability and performance of the phosphate materials, to explore rate limitations and their relation to structure and particle size/morphology, and to use this information to improve the performance of promising phosphate materials. In the layered and composite cathode tasks, the goal is to find lower-cost and higher-capacity cathodes, exceeding 200mAh/g, based on environmentally benign materials, and to investigate surface chemistry and stabilizing additives and their role in long cycle and calendar life. Finally, in the Mn spinel area, researchers are trying to develop low-cost spinel manganese oxides that offer excellent capacity retention at high voltage, high rate, low ICL, and good storage characteristics at elevated temperatures.

V.B.1 First Principles Calculations and NMR Spectroscopy of Electrode Materials (SUNY, MIT)

Clare P. Grey
Chemistry Department
Stony Brook University
Phone: (631) 632-9548; Fax: (631) 632-5731
E-mail: cgrey@notes.cc.sunysb.edu

Gerbrand Ceder
Materials Science and Engineering
Massachusetts Institute of Technology
Phone: (617) 253-1581; Fax: (617) 258-6534
gceder@mit.edu

Start Date: May 2006
Projected End Date: February 2011

Objectives

- Determine the effect of structure on stability and rate capability of cathodes and anodes.
- Explore relationships between electrochemistry and particle size and shape.
- Understand and predict reactivity of anode and cathode electrode materials with electrolytes.
- Develop new materials.

Technical Barriers

- Low rate capabilities, high cost, poor stability of electrode materials.

Technical Targets

- Specific power 300 W/kg, 10 year life, < 20% capacity fade. Low cost.

Accomplishments

- Application of *in situ* NMR methods to investigate self-discharge mechanisms in Silicon, Si lithiation, and the formation of Li dendrites with different electrolytes
- Use of pair distribution function (PDF) and nuclear magnetic resonance (NMR) methods to determine the types of structures present in the amorphous phase of lithiated silicon formed on cycling Si.
- Use of a combination of theory and experiment (NMR, PDF, diffraction) to identify mechanisms for conversion reactions and nano-size effects in Fe-fluorides, Bi-F, Cu-F and Ag-F. Developed a hypothesis/model to explain hysteresis in Fe-F.
- Phosphates: theoretical and experimental (NMR) studies of doping in olivines. Computed quaternary phase diagrams of Li-M-P-O systems with M = Fe, Mn, Ni. Developed $LiFePO_4$ with highest rate capability ever observed. Developed formalism to study mixed metal olivines and applied to $Li(Fe,Mn)PO_4$.
- Developed first principles approach to predict particle morphology as function of environment (in solution and in oxygen) (with K. Persson, BATT, LBNL)

- Investigated surfaces of $LiFePO_4$ and $LiMnPO_4$: structure, potentials, stability and developed theory on the size-dependence of the miscibility gap
- Developed high-throughput computational screening ability to find new electrode materials and experimental characterization of candidate materials.

✧ ✧ ✧ ✧ ✧

Introduction

Achieving DOE goals in this field requires both an understanding of how current materials function – with a view to improving rate, capacity and long-term cycling performance – and the discovery of new materials and new mechanisms by which these materials function. This joint theoretical and experimental program attacks these issues by developing new experimental (and theoretical) tools to investigate battery materials both *in* and *ex situ*, and then applies these to understand relationships between structure and function. One aim is to use these findings to optimize material function and/or develop new materials.

Approach

- Use solid state NMR and diffraction/TEM to characterize local and long range structure as a function of particle size, sample preparation method, state of charge and number of charge cycles (cathodes).
- Use electrochemistry to correlate particle size with rate performance. Continue to develop the use of *in situ* NMR methods to identify structural changes and reactivity in oxides and intermetallics.
- Use first principles calculations (density functional theory) to identify redox-active metals, relative stability of different structures, the effect of structure and particle size on cell voltages and rate capability, and to identify promising cathode materials for BATT applications.

Results

Structure and self-discharge reactions of the negative anode material silicon. A detailed NMR analysis of the amorphous structures that form on lithiation of silicon have been performed. In collaboration with M. Morcrette and J.–M. Tarascon, a series of model crystalline lithium silicides were prepared to establish correlations between Li shifts and local environments. These correlations were then used to help analyze the NMR spectra obtained by *ex-situ* and *in-situ* NMR spectroscopy, the *in-situ* NMR referring to a working battery being monitored inside an NMR coil (Figure V- 2). Pair distribution function (PDF) analysis of XRD data of the anode material, silicon, was performed on the same materials analyzed by NMR. The data has been used to monitor the breakage of the Si-Si bonds, and to investigate the local structure of the amorphous silicon phase that is formed at the end of the 1st charge. A combination of the NMR and PDF results show that small Si clusters are formed along with isolated silicon ions in the 1st discharge plateau; these are broken on the 2nd plateau. NMR experiments have then been used to evaluate the processes that occur on subsequent cycles. The *in-situ* NMR experiments identified a self-discharge process involving side-reactions between the lithiated silicon and the electrolyte. The effect of CMC binder on the self-discharge rates seen for this material was investigated. Particularly at deep discharge, the CMC slowed the self-discharge processes significantly, presumably because it forms a protective coating on the surface of the Si.

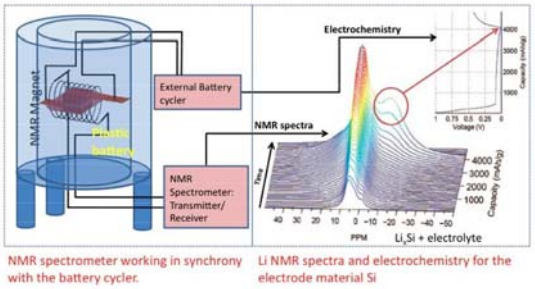

Figure V- 2: A schematic showing the *in situ* NMR set-up and a 7Li NMR spectrum acquired on the 1st discharge of a Si/Li battery.

Conversion reactions. We have used a combination of experiment and theory to provide a deeper understanding of the transformations that occur in conversion reactions, with particular emphasis on the metastable phases formed in these systems, local structures during the reactions and the effect of mobility on the sizes of the (nano)particles and domains formed in these composites. For example, in collaboration with N. Yamakawa (on leave from SONY Corporation), the mechanisms of CuS, CuF_2 and CuO during the electrochemical reaction with Li were studied by solid state 63Cu, 19F, 7Li NMR and XRD.

For CuS, a two-step reaction is observed, which is associated with an insertion reaction involving first limited incorporation of Li into CuS, and then a two phase reaction to form material with approximate composition LiCuS. This is followed by a conversion reaction to form Li_2S and Cu, $Cu_{1.96}S$ being formed as a side product of the decomposition of LiCuS. Evidence for the insertion phases is found from both NMR and XRD. A direct conversion reaction to form LiF and Cu is seen for CuF_2, while the 7Li NMR results indicate that CuO can tolerate a small amount of Li substitution before reacting to form Li_2O and Cu. The mechanisms vary significantly for these three model compounds, depending on the mobilities of the anions and cations in these systems. For example, both

the diffraction and NMR results indicate that the size of the Cu particles formed on discharge is much larger in the CuS system, which is thought to result from the higher $Cu1^+$ mobilities in the intermediate intercalation compounds Li_xCuS. For CuF_2, which is in principle the simplest, Figure V- 3 shows that the conversion even in this system results in the formation of different particles and domains whose sizes vary though out the reaction. After the insertion of only l Li per CuF_2, the CuF_2 phase has totally disappeared by XRD; NMR and diffraction shows the formation of LiF and Cu at this point, and no evidence for Cu(I). This is consistent with the breakage of the CuF_2 particles embedded in LiF and Cu particles/coatings. At this point the potential measured in galvanostatic mode starts to steadily drop, presumably because the diffusion and or tunneling of the electrons over longer distances is required to nucleate and grow the LiF and Cu particles.

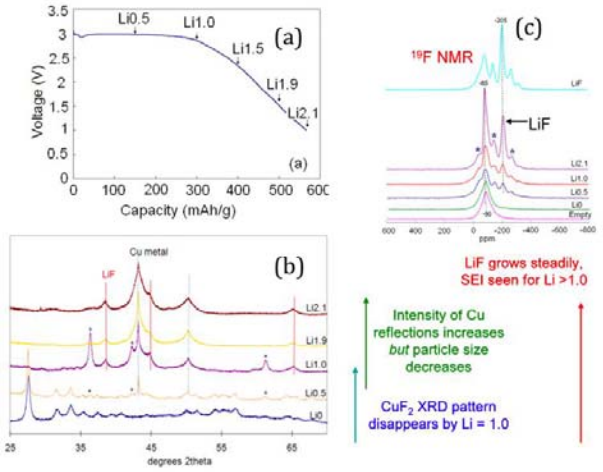

Figure V- 3: The 1st discharge of a CuF_2-carbon nanocomposite (a), studied by synchrotron diffraction (b), and ^{19}F NMR (c).

In FeF_3 both theory and experiment have been used to examine the structural changes that occur on lithiation and during the subsequent conversion reaction, the experiments and theory identifying a series intermediate metastable phase that form on the 1st discharge (before the conversion reaction) and again on charging. The ternary phase diagram of Li-Fe-F was computed (Figure V- 4) and the hysteresis was predicted based on a model that defines different charge and discharge paths in the phase space. The computations also gave insight into why FeF_3 does not return to the same structure upon charge.

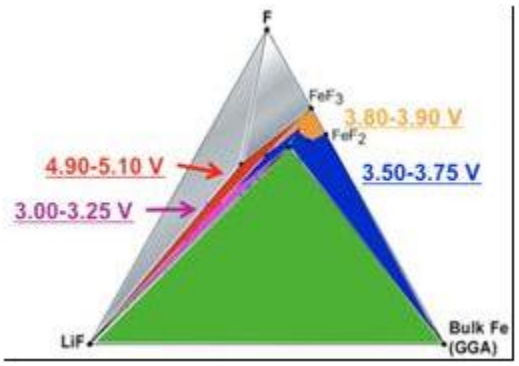

Figure V- 4: Calculated phase diagram of Li-Fe-F and equilibrium potentials in each three-phase section

Olivines. Phase transformations, defects and doping. We investigated several aspects of the olivine systems. For $LiFePO_4$ and $LiMnPO_4$ the quaternary Li-M-O-P phase diagram was computed in order to understand the off-stoichiometry equilibria and optimize a processing sequence that leads to high conducting impurity phases. Using this technique, nano-scale off-stoichiometric $LiFePO_4$ was synthesized which showed exceptional rate performance up to 400C. Further investigations with modified electrodes showed even 1000C capability, in support of earlier theory predictions that the Li mobility in $LiFePO_4$ is unusually high. We have furthermore investigated the surface structure and energy of $LiFePO_4$ and $LiMnPO_4$ in vacuum (clean surfaces) and in solution. This has led to a computational approach which can predict the particle morphology as a function of pH and oxidation strength of the environment. Results of this approach show that upon increasing pH the particle shape of $LiFePO_4$ changes from cubic –with no (010) facets, to thin (010) plates near neutral pH, to columnar crystals at alkaline environment or highly oxidizing conditions. (Figure V- 5). We have also initiated a study of the equilibrium voltage profile and phase transformation behavior of mixed metal olivines, such as $Li(Mn,Fe)PO_4$.

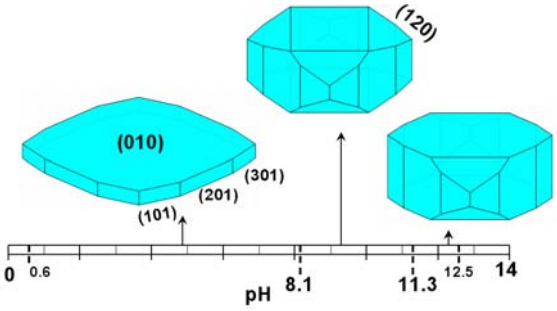

Figure V- 5: Particle shape of $LiFePO_4$ as function of pH under fixed oxidation conditions

NMR experiments have focused on understanding how silicon is incorporated into the phosphate structure, the defects formed on lower temperature synthetic

methods, and on interpreting the NMR spectra of doped olivines.

New Materials. We have developed a high-throughput computational environment in which we can evaluate many relevant electrode properties of existing and new materials. For example, Figure V- 6 shows the calculated capacity/voltage scatter plot for several thousand compounds. This search has already revealed several completely new materials as potential Li-cathode materials, and experiments are currently under way to synthesize and test these materials. In conjunction, NMR experiments have been applied to characterize a wide range of novel electrode materials including organics, metal organic frameworks and oxysulfides.

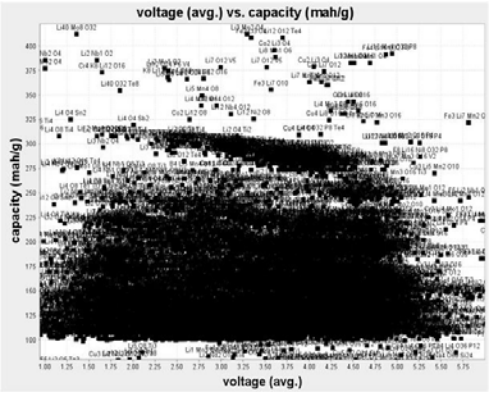

Figure V- 6: Capacity *vs.* voltage for thousands of compounds (calculated).

Conclusions and Future Directions

In conclusion, we have developed a unique *in situ* NMR capability and have utilized this to

- follow structural changes that occur on lithiating the negative electrode material Si;
- identify self-discharge reactions at low voltages in Si;
- identify self-discharge reactions at high voltages for nano-sized layered materials; and
- quantify Li dendrite growth on negative electrode materials.

In conversion reactions and in studies of Si, we have utilized a combination of NMR and diffraction methods to determine reaction mechanisms and identify local structures and clusters present in nanocomposites and in amorphous phases such as Li_xSi. We have developed theoretical approaches to calculate NMR spectra, which we have applied to investigate local structure in phosphates.

In the olivines, we have gained further insight into the rate controlling mechanisms and phase transformation kinetics and have performed experimental work to optimize rate capability. In the area of new materials, we have developed the large computational capability to screen thousands of materials as potential cathode materials and have initiated the synthesis of some promising ones. In conjunction, we have continued to apply our NMR methodologies to help determine structure and lithiation mechanisms in these compounds. Future directions include the implementation of improvements to our in situ NMR experiments to allow us to monitor increasingly rapid processes with improved sensitivity. The methodology will be applied to investigate lithiation mechanisms and side-reactions in a wider range of oxides and intermetallics.

FY 2009 Publications/Presentations

1. Presentation to the 2008 DOE Annual Peer Review Meeting.
2. "Molten Salt Synthesis and High Rate Performance of the "Desert-Rose" form of $LiCoO_2$", H. Chen and C.P. Grey, *Adv. Mater.,* 20, 2206-2210 (2008).
3. "The Formation of a Complete solid solution between the Triphylite and Fayalite Olivine Structures", N. Recham, M. Casas-Cabanas, , J. Cabana, C.P. Grey, J.C. Jumas, M. Armand, & J-M. Tarascon, *Chem. Mat,* 20 (21), 6798-6809, (2008).
4. "Influence of Benzoquinone Sorption on the Structure and Electrochemical Performance of the MIL-53(Fe) Hybrid Porous Material in a Li-ion Battery", G. de Combarieu, M. Morcrette, F. Milange, N. Guillou, J. Cabana, C.P. Grey, I. Margiolaki, G. Ferey, and J.-M. Tarascon, *Chem. Mater.*, 21 (8), 1602-1611, (2009).
5. "Real-time NMR Investigations of Structural Changes in Silicon Electrodes for Lithium-ion Batteries", B. Key, R. Bhattacharyya, M. Morcrette, V. Seznéc, J.-M. Tarascon and C.P. Grey, *J. Am. Chem. Soc.*, 131 (26), 9239-9249, (2009).
6. "Electrochemical and Structural Study of the Layered, "Li-excess" Lithium-Ion Battery Electrode Material $Li[Li_{1/9}Ni_{1/3}Mn_{5/9}]O_2$", M. Jiang, B. Key, Y.S. Meng, C.P. Grey, *Chem. Mater.*,21, 2733-2745, (2009)
7. "Investigation of the Conversion Reaction Mechanisms for Binary Copper (II) Compounds by Solid-State NMR Spectroscopy and X-ray Diffraction", N. Yamakawa, M. Jiang and C.P. Grey, *Chem. Mat, 21* (14), 3162–3176 (2009).
8. "The effects of moderate thermal treatments under air on $LiFePO_4$ -based nano powders", SA. Hamelet, P. Gibot, M. Casas-Cabanas, D. Bonnin, C.P. Grey, J. Cabana, J.-B. Leriche, J. Rodriguez-Carvajal, M. Courty, S. Levasseur, P. Carlach, M. van Thournout, J.-M. Tarascon, C. Masquelier, *J. Mater. Chem.,* 19, (23), 3979-3991 (2009).
9. "A study of the lithium conversion mechanism of iron fluoride in a Li ion battery, by using solid state NMR, XRD and PDF analysis studies", N. Yamakawa, M. Jiang, B. Key and C.P. Grey, *J. Am. Chem. Soc.,* 131 (30), 10525–10536 (2009).

10. "Structural and electrochemical characterization of Li-Mn-Ni-O electrodes with integrated layered-spinel structures for Li-ion batteries", J. Cabana, S.-H. Kang, C.S. Johnson, M.M. Thackeray, and C.P. Grey, *J. Electrochem. Soc.,* 156, (9), A730-A736, (2009).
11. Lithium salt of tetrahydroxybenzoquinone: toward the development of a sustainable Li-ion battery", H. Chen, M. Armand, M. Courty, M. Jiang, C.P. Grey, F. Dolhem, J.-M. Tarascon, and P. Poizot, *J. Am. Chem. Soc.,* 131 (25), 1984-8988, (2009).
12. K. Kang, D. Morgan, G. Ceder, *First Principles Study of Li Diffusion in I-Li2NiO2 Structure*, Phys. Rev. B, Vol. 79, Issue 1, Article Number 014305 (2009).
13. B. Kang, G. Ceder, *Battery Materials for Ultrafast Charging and Discharging*, Nature, Vol. 458, Issue 7235, Pages 190-193 (2009).
14. R.E. Doe, K. Persson, G. Hautier, G. Ceder, *First Principles Study of the Li-Bi-F Phase Diagram and Bismuth Fluoride Conversion Reactions with Lithium*, Electrochemical and Solid-State Letters, 12 (7) A125-A128 (2009).
15. R. Malik, F. Zhou, G. Ceder, *Phase Diagram and Electrochemical Properties of Mixed Olivines from First-Principles Calculation,* Physical Review B, 79, 214201-1 – 214201-7 (2009).
16. K. Tibbetts, R. Doe, G. Ceder, *Polygonal Model for Layered Inorganic Nanotubes*, Physical Review B, 80, 014102-1 – 014102-10 (2009).
17. D. Kramer, G. Ceder, *Tailoring the Morphology of LiCoO2: A First Principles Study*, Chemistry of Materials, 21 (16), pp. 3799 – 3809 (2009).
18. R. Doe, K. Persson, Y.S. Meng, G. Ceder, *First Principles Investigation of the Li-Fe-F Phase Diagram and Equilibrium and Nonequilibrium Conversion Reactions of Iron Fluorides with Lithium*, Chemistry of Materials, 20, 5274-5283 (2008).
19. L. Wang, F. Zhou, G. Ceder. *Ab Initio Study of the Surface Properties and Nanoscale Effects of $LiMnPO_4$*, Electrochemical and Solid-State Letters 11 (6). pp. A94 - A96 (2008).
20. S.P. Ong, L. Wang, B. Kang, G. Ceder, *The Li-Fe-P-O_2 Phase Diagram from First Principles Calculations,* Chemistry of Materials 20 (5), pp. 1798-1807 (2008).

V.B.2 Phase Behavior and Solid State Chemistry in Olivines (LBNL)

Thomas Richardson
Environmental Energy Technologies Division
Lawrence Berkeley National Laboratory
Berkeley, CA 94720
Phone: (510) 486-8619; Fax: (510) 486-8619
E-mail: TJRichardson@lbl.gov

Start Date: October 1, 2008
Projected End Date: September 30, 2010

Objectives

- Synthesize and evaluate new electrode materials with improved energy density.
- Investigate the relationship of structure, morphology and performance of cathode materials, with the emphasis on phosphates.
- Explore kinetic barriers, and utilize the knowledge gained to design and develop cathodes with improved energy density, rate performance and stability.

Technical Barriers

- PHEV: Available energy, cycle life.
- EV: Low energy, poor cycle life.

Technical Targets

- PHEV40: 96 Wh/kg, 5,000 cycles.
- EV: 200 Wh/kg; 1,000 cycles.

Accomplishments

- Identified a previously unreported solid solution regime in the high energy density cathode material, $LiMnPO_4$.
- Proposed the first rational explanation for the poor rate capability and utilization of $LiMnPO_4$ based on the physical decrepitation of particles larger than 25 nm and the absence of a well defined phase boundary due to the solid solution behavior.
- Showed that the thermal instability of "$MnPO_4$" (which may contain residual lithium) results in oxygen loss at fairly low temperatures. The reaction with electrolyte below 200°C, and generating similar amounts of heat to that of $Li_{0.5}CoO_2$, raises concern about the safety of this material.
- The metathesis chemistry of lithium nitride was extended to include the reaction with aluminum, which is an efficient generator of free lithium. This may provide a safe and convenient source of lithium to prelithiate anodes containing carbon or intermetallics.

✧ ✧ ✧ ✧ ✧

Introduction

The dramatic success of $LiFePO_4$ batteries has demonstrated the considerable value of phosphate stabilization. Improvements are needed, however, in energy density. Of the olivine-type phosphates with higher plateau voltages, only $LiMnPO_4$ is within the stability range of commonly used electrolytes. Despite some improvements in particle sizes and morphologies, poor utilization, low energy density, and limited rate capability still block the path to commercial use of the olivine manganese phosphate. Lithium metal phosphates with structures other than olivine will be thoroughly investigated.

Approach

Identify candidate electrode compositions by systematic analysis of phase diagrams and literature reports. Synthesize novel materials and/or unique structures and employ XRD, electron microscopy, vibrational spectroscopies, and electroanalytical techniques to determine their applicability to BATT goals. Characterize known and modified electrode materials (e.g. $LiMnPO_4$) and establish correlations between crystal structure, morphology and performance. Provide guidelines for materials synthesis and electrode fabrication processes.

Results

High energy density cathodes. The team has previously investigated the phase transition mechanism and the behavior of the solid solution phases in large $LiFePO_4$ crystals. Recent work focused on the similar issues in higher energy density $LiMnPO_4$ system. Sub-micron sized hexagonal $LiMnPO_4$ samples with different levels of oxidation were prepared by treating hydrothermally synthesized crystals with varying amounts of NO_2BF_4 for 24 h. *Ex situ* XRD studies showed that both $LiMnPO_4$ and a delithiated phase, Li_yMnPO_4, were present. The lattice parameters and the unit cell volume of the latter phase changed gradually as its concentration increased (Figure V- 7a), indicating the presence of residual Li in the delithiated phase, the amount being closely related to its domain size. A higher concentration of Li can remain in domains that are smaller than 10 nm,

decreasing significantly as the domains grow to above 10 nm. Assuming that the phase formed at $x = 0$ (where x is the mole fraction of $LiMnPO_4$ remaining) is fully delithiated and using Vegard's rule to correlate cell volume with composition, the residual Li (y) when x = 0.93 had its highest observed value of 0.16.

The process was also followed by *ex situ* infrared spectroscopy. Low frequency FTIR patterns of the oxidized samples, along with those of the end members are shown in Figure V- 7b. The peak at 632 cm^{-1} arises from $LiMnPO_4$, while the peak between 650 cm^{-1} and 660 cm^{-1} originates from the delithiated phase, Li_yMnPO_4. Here again, x is used to designate the fraction of $LiMnPO_4$ remaining, while y is the amount of lithium in the delithiated phase. There is a gradual shift towards higher frequency as the amount of the delithiated phase increases, consistent with a decrease in Li content y.

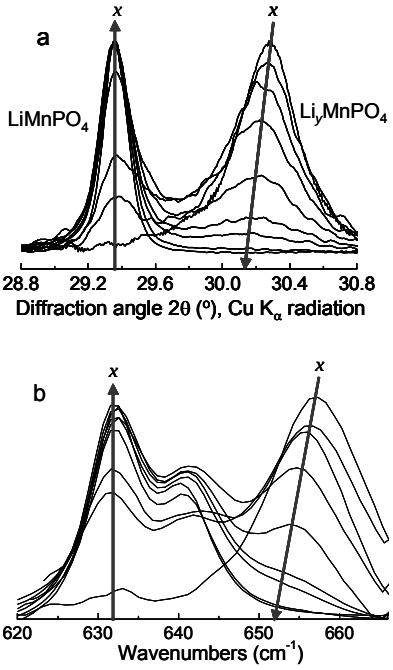

Figure V- 7: XRD patterns (a) and FTIR spectra (b) of xLiMnPO4/(1-x)Li_yMnPO_4 samples. The arrows indicate the trends as x varies.

The formation of Li_yMnPO_4 solid solutions was also observed when $LiMnPO_4$ was electrochemically charged and discharged. During charging, the peak position of the delithiated phase gradually shifted as more lithium is extracted. The cell volume of the delithiated phase decreased from 278.4 $Å^3$ to 275.6 $Å^3$ as the global Li content x decreased from 0.64 to 0.14 (Figure V- 8a). During discharging, again a gradual peak shift of the delithiated phase was observed, and the unit cell volume of the phase increased from 275.6 $Å^3$ at a lithium content of 0.14 to 282.0 $Å^3$ at 0.85 (Figure V- 8b). The cell volume of the lithiated phase, on the other hand, remained constant during both charge and discharge

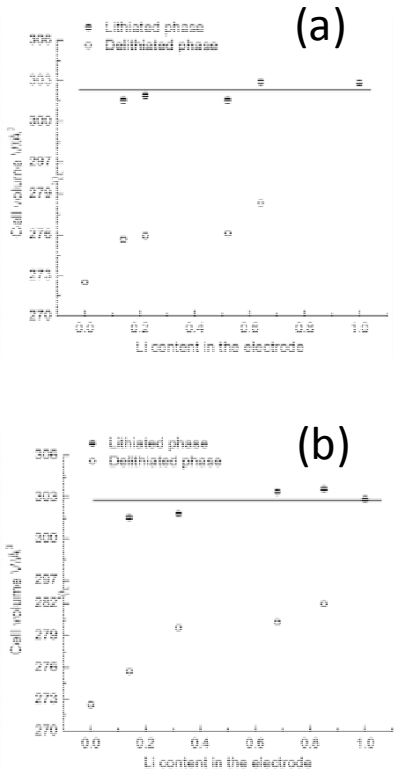

Figure V- 8: The relationship between the unit cell volumes of the phases and the discharge state of the sample: a) charging and b) discharging.

The $LiMnPO_4$ crystals used in the study are sub-micron in size, but well above the range where room temperature $Li_\varepsilon FePO_4$ solid solutions have been reported to exist. The results from these chemical and electrochemical studies indicate that Li_yMnPO_4 solid solutions can form near the end of charge and persist in relatively large particles, provided that the domain size of that phase is small. In contrast to the $LiFePO_4/FePO_4$ system, in which the stable delithiated end member nucleates and grows into large domains quickly, the accumulation of elastic energy in small delithiated $LiMnPO_4$ domains restricts their growth and allows the accommodation of a significant concentration of residual Li in the phase.

The studies have also led to the discovery of thermal instability in olivine $LiMnPO_4/MnPO_4$ system. It is well known that charged oxide cathodes such as Li_xCoO_2, Li_xNiO_2, $Li_xMn_2O_4$, $Li_xNi_{0.8}Co_{0.2}O_2$, $Li_x(Ni_{0.8}Co_{0.15}Al_{0.05})O_2$, and $Li_y[Ni_xCo_{1-2x}Mn_x]O_2$ decompose and release O_2 at elevated temperatures. Olivine-type LiMPO4 (M = Fe, Mn, Co and Ni) compounds have been promoted as safe alternatives, as the strong covalent P-O bonds in the tetrahedral $(PO_4)^{3-}$ anion are believed to inhibit decomposition. Heterosite $FePO_4$ is reportedly stable in air up to 600°C, above which it transforms into quartz-like $FePO_4$ without losing oxygen. Mixtures of $FePO_4$ and $LiFePO_4$ form single-phase solid

solutions when heated in an inert atmosphere. When chemically delithiated (xLiMnPO$_4$/(1-x)Li$_y$MnPO$_4$) samples with x = 0.70 and 0 were heated to 375°C under flowing N_2, the delithiated phase decomposed to form $Mn_2P_2O_7$, characterized by strong diffraction peaks at 29° and 30.5° (Figure V- 9a). The reaction releases O_2 according to Equation 1, with a theoretical weight loss of 5.4%.

$$2MnPO_4 \rightarrow Mn_2P_2O_7 + 0.5O_2 \qquad [1]$$

LiMnPO$_4$ was unaffected by thermal treatment either alone or in mixtures. Single-phase solid solutions were not formed due to the instability of Li$_y$MnPO$_4$.

Thermogravimetric analysis (TGA, Figure V- 9b) supports these conclusions. LiMnPO$_4$ and partially delithiated LiFePO$_4$ lost no weight on heating to 600°C in argon, while both a single-phase delithiated sample (x = 0) and a 0.7LiMnPO$_4$/0.3Li$_y$MnPO$_4$ mixture lost weight between 100°C and 400°C. The total weight loss was larger than expected for $M_2P_2O_7$ formation due to the highly hygroscopic nature of Li$_y$MnPO$_4$.

It is known that O_2 released from the cathode can ignite the organic solvents in the electrolyte and create hazardous conditions including fire and explosion. To evaluate the heat evolution during the thermal decomposition, differential scanning calorimetry (DSC) measurements were carried out in hermetically sealed stainless steel capsules that can withstand an internal pressure up to 150 atmospheres. The pure electrolyte, 1M $LiPF_6$ in PC and EC electrolyte (50:50 by volume and 44:56 by mole ratio), had an exothermic peak centered at 325°C and a total released heat of 280 J/g (Figure V- 10). In the presence of the electrolyte, LiFePO$_4$ and LiMnPO$_4$ had a peak centered at 299 and 294°C, respectively. The heat evolved was only 157 and 154 J/g, consistent with the known low reactivity of these phases.

When chemically delithiated FePO$_4$ alone was heated to 400°C, no heat signal was detected. Three exothermic peaks, centered at 173, 250 and 329°C, were observed for Li$_y$MnPO$_4$. The total heat generated was 200 J/g, corresponding to the exothermic reaction that releases O_2. In the presence of the electrolyte, a series of overlapping peaks with onset temperatures of 250°C and centers at 270, 280 and 315°C were observed for FePO$_4$, accounting for a total heat of 204 J/g. Three exothermic peaks were observed in the profile of Li$_y$MnPO$_4$. The first peak (150 to 210°C) is likely due to the release of O_2 from the phosphate. The combustion of the carbonate solvents then begins at 215°C, the onset temperature of the second exothermic peak. The total heat generated was 884 J/g, with the peak centered at 256°C. This is comparable to the reported data for $LiCoO_2$, $LiNi_{0.8}Co_{0.2}O_2$ and $Li(Ni_{0.8}Co_{0.15}Al_{0.05})O_2$. Surprisingly, the phosphate is more reactive than $LiMn_2O_4$ and the Mn-substituted oxides, $Li(Ni_xCo_{1-2x}Mn_x)O_2$.

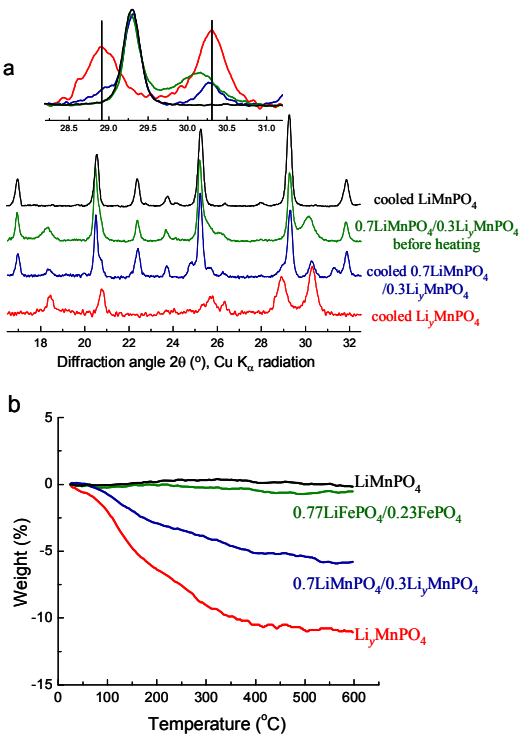

Figure V- 9: a) XRD patterns and b) TGA results for the indicated samples.

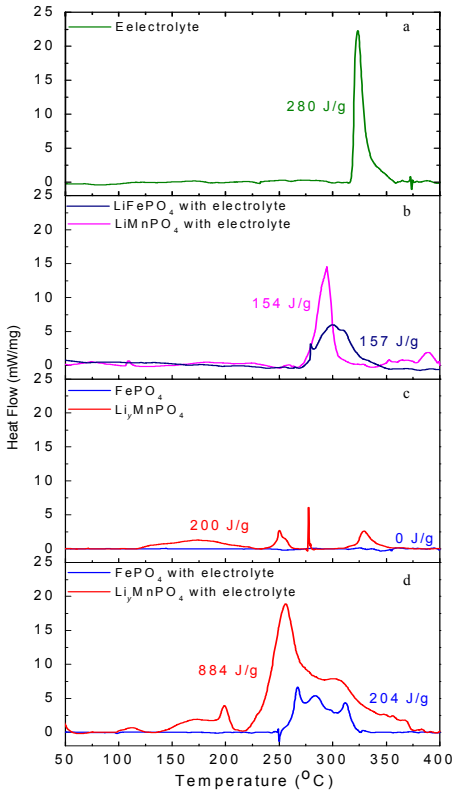

Figure V- 10: DSC comparison of the indicated samples.

It is clear that while $LiFePO_4$ has good thermal characteristics and has been shown to be a safer cathode, $LiMnPO_4$ does not appear to have the same advantage. This instability must be addressed before this cathode material can be commercialized.

High energy density anodes. The preparation of intermetallic lithium compounds of interest as anodes by reaction of Li_3N with metals has been extended to the Li-Al system. Here, as is the case with Mg, the metal nitride AlN is formed along with LiAl and Li_3Al_2 (Figure V- 11).

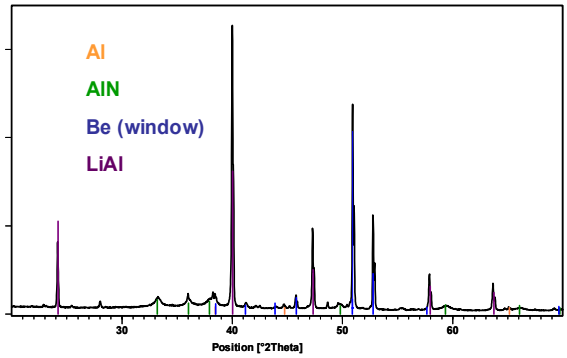

Figure V- 11: XRD pattern of the product of the reaction $Li_3N + 4Al \rightarrow AlN + 3LiAl$.

In addition to providing a convenient route to intermetallic lithium phases with Mg, Si, Al, and Sn, these reactions can also be used to fully or partially lithiate graphite, other carbon anodes, and alternative anodes now being developed including binary and complex intermetallics.

This has been demonstrated using Mg: the lithium powder produced by this reaction reacts with graphite to form LiC_6 and/or LiC_{12}, depending upon the stoichiometry of the mixture (Figure V- 12)

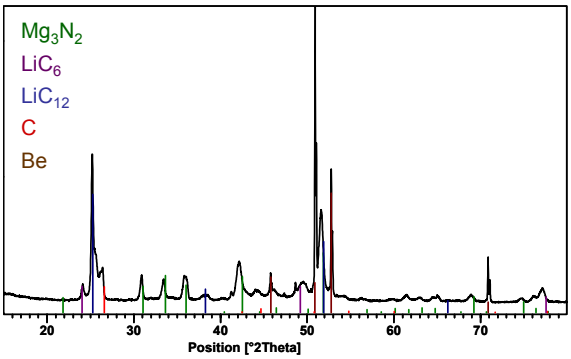

Figure V- 12: XRD pattern of the product of the reaction $2Li_3N + 3Mg \rightarrow 6Li + Mg_3N_2$.

Conclusions and Future Directions

In light of the thermal instability of oxidized $LiMnPO_4$ and its serious implications for its future in commercial batteries, we will conclude our work on this material by completing DSC measurements of the reactivity of partially substituted $LiMnPO_4$ with electrolytes. We have also received some carbon-coated material from HPL, which we will test in the same way. We will continue to pursue novel non-olivine cathode materials along with other promising candidates.

Our experience with Li-Mg alloys has shown that although they have the distinct advantage over Li foil for dendrite suppression, the kinetics of lithium insertion and removal are limited. In addition, the potentials of the Li-Mg solid solution electrodes are too close to those of lithium metal, and result in substantial interactions with the electrolytes. We plan, therefore, to focus our attention on intermetallics with somewhat higher potentials and to use metathesis lithiation where appropriate to reduce early cycle losses of active lithium. We will also synthesize and evaluate some ternary intermetallics containing transition metals and metalloid elements.

FY 2009 Publications/Presentations

1. "Improving the Performance of Lithium Manganese Phosphate through Divalent Cation Substitution", G. Chen, J. D. Wilcox, and T. J. Richardson, *Electrochem. Solid-State Lett.*, **11**, A190 (2008).
2. "Solid Solution Phases in the Olivine-Type $LiMnPO_4/MnPO_4$ System", G. Chen and T. J. Richardson, *J. Electrochem. Soc.*, **156**, A756 (2009).
3. "Thermal instability of Olivine-type $LiMnPO_4$ cathodes", G. Chen and T. J. Richardson, *J. Power Sources*, published online September, 2009.
4. "Phase Transitions, Interfaces, and Stability Relationships in Phosphate Cathodes," presented at the 214th Meeting of the Electrochemical Society, Honolulu, HI, October 14, 2008.
5. "Crystal Chemistry, Reaction Mechanisms and Solid Solution Phases in Li_xMnPO_4," presented at the 4th Lithium Battery Discussions, Arcachon, France, September 21, 2009.
6. "Phase Behavior and Solid State Chemistry in Olivines," presented at the 2009 DOE Hydrogen Program And Vehicle Technologies Annual Merit Review, Washington, DC, May 20, 2009.

V.B.3 Olivines and Substituted Layered Materials (LBNL)

Marca M. Doeff
Lawrence Berkeley National Laboratory
M/S 62R0100
Berkeley, CA 94720
Phone: (510) 486-5821; Fax: (510) 486-4881
E-mail: mmdoeff@lbl.gov

Start Date: October 1, 2008
Projected End Date: September 30, 2010

Objectives

Develop low-cost benign cathode materials having electrochemical characteristics (e.g. cycle life, energy and power densities) consistent with the goals of the USABC and/or FreedomCAR.

Technical Barriers

This project addresses the following technical barriers from the Batteries for Advanced Transportation Technologies program:

(A) Cost

(B) Cycle Life

(C) Energy Density

(D) Power Density

Technical Targets

- Cost: $150/kWh for electric vehicles or $500/system for HEV Low Power Assist battery
- Cycle Life: 1000 cycles to 80% DOD for EVs
- Energy Density/Specific Energy: 150 Wh/kg and 230 Wh/L at C/3 discharge rate for EVs
- Specific Power: 460 W/L for EVs

Accomplishments

- Demonstrated improved rate capability and more stable cycling of Al-substituted layered transition metal compounds.
- Reduced Co content by more than half in NMC compounds by substitution with Al
- Developed potentially lower cost synthesis method for $LiMnPO_4$/C composites.
- Demonstrated improved electrochemical properties of $LiMnPO_4$ made by combustion synthesis.

Introduction

Achieving the DOE cost targets for Li-ion batteries for vehicular applications depends largely on reducing the cost of the cathode materials. Significant savings can be realized by reducing the Co content (Co was $40/lb on a per metals basis in FY2007) in NMC materials (Li[Ni, Co, Mn]O_2 compounds), but this often results in reduced power capability. Increasing the nickel content may also adversely impact thermal abuse tolerance. Partial substitution of cobalt with aluminum reduces cost and is expected to improve the thermal properties. If the aluminum content is kept low, there is little impact on the practical energy density and a significant increase in power capability over the unsubstituted materials.

$LiMnPO_4$ is potentially low-cost and has approximately 20% better energy density than $LiFePO_4$, but suffers from very poor electrochemical performance. To offset its low electronic conductivity, nanostructured particles of $LiMnPO_4$ should be coated with carbon or another conductive material. The solvothermal processes used to make $LiMnPO_4$ currently are expensive, and carbon must be added in a subsequent grinding step, increasing processing costs further. Combustion synthesis allows nanoparticulate $LiMnPO_4$/C composites to be made in one step, starting from inexpensive precursors.

Approach

Cathode materials are synthesized and characterized electrochemically. Relevant physical properties are measured in conjunction with the diagnostics teams. Emphasis is placed on reducing cost and improving electrochemical properties. Some work is directed towards surveying new materials with potential for increased energy density.

Results

Substituted Layered Materials. A series of $Li[Ni_{0.4}Co_{0.2-y}Al_yMn_{0.4}]O_2$, $0 \le y \le 0.2$ compounds were successfully synthesized and found to be phase-pure via X-ray powder diffraction (XRD) experiments (Figure V- 13.) Substitution has no effect on particle size or morphology.

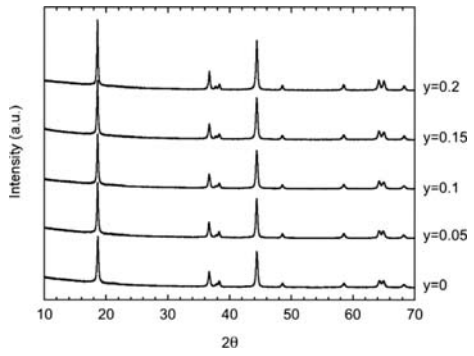

Figure V- 13: XRD powder patterns of $Li[Ni_{0.4}Co_{0.2-y}Al_yMn_{0.4}]O_2$, $0 \le y \le 0.2$ compounds.

Al substitution was found to reduce the electronic conductivity (Figure V- 14) and the practical specific capacity (Figure V- 15), but improves the rate capability and cycling behavior compared to baseline materials. Significantly, there is very little specific energy penalty observed for $Li[Ni_{0.4}Co_{0.15}Al_{0.05}Mn_{0.4}]O_2$ but it has better rate capability than either $Li[Ni_{0.4}Co_{0.2}Mn_{0.4}]O_2$ or $Li[Ni_{1/3}Co_{1/3}Mn_{1/3}]O_2$ in half cell configurations (Figure V- 16).

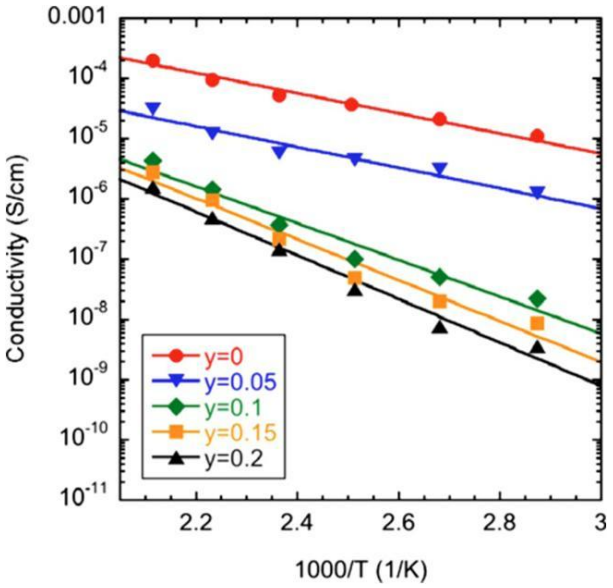

Figure V- 14: Conductivities of $Li[Ni_{0.4}Co_{0.2-y}Al_yMn_{0.4}]O_2$, $0 \le y \le 0.2$ compounds as a function of temperature.

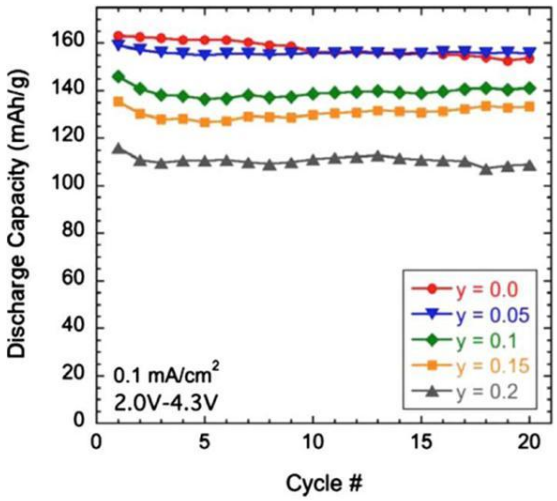

Figure V- 15: Specific capacities as a function of cycle number for lithium half cells containing $Li[Ni_{0.4}Co_{0.2-y}Al_yMn_{0.4}]O_2$, $0 \le y \le 0.2$ compounds discharged at 0.1 mA/cm between 4.3 and 2.0V.

The enhanced electrochemical performance has been attributed to structural effects, by process of elimination. Rietveld refinements on combined XRD and neutron powder diffraction patterns of the $Li[Ni_{0.4}Co_{0.2-y}Al_yMn_{0.4}]O_2$, $0 \le y \le 0.2$ compounds indicate that substitution of the smaller Al ion for Co decreases M-M distances in the transition metal layers and increases the LiO_2 slab spacing ($I(LiO_2)$, Figure V- 17). This increase is associated with improved rates of Li^+ diffusion. Interestingly, the concentration of anti-site defects (Ni in 3a sites) also increases slightly, but the effect of the larger slab spacings offsets any negative effect associated with this.

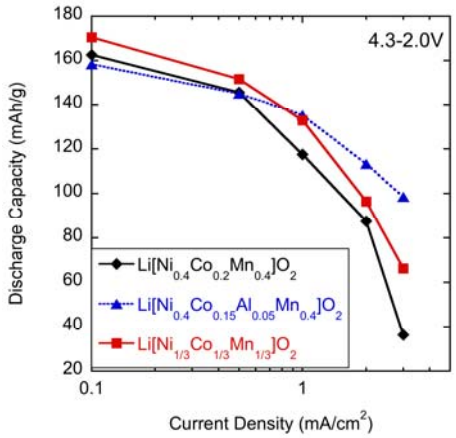

Figure V- 16: Peukert plot showing the discharge capacity as a function of current density for lithium half-cells containing $Li[Ni_{1/3}Co_{1/3}Mn_{1/3}]O_2$, $Li[Ni_{0.4}Co_{0.2}Mn_{0.4}]O_2$, or $Li[Ni_{0.4}Co_{0.15}Al_{0.05}Mn_{0.4}]O_2$.

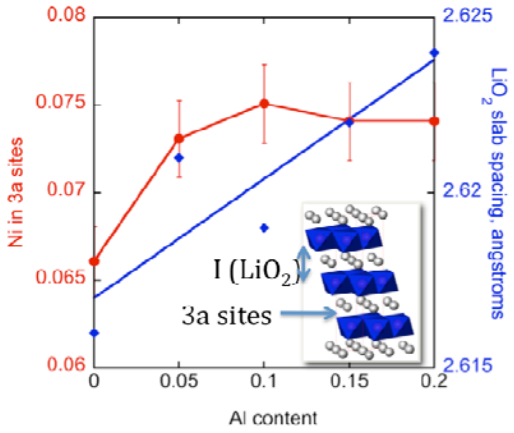

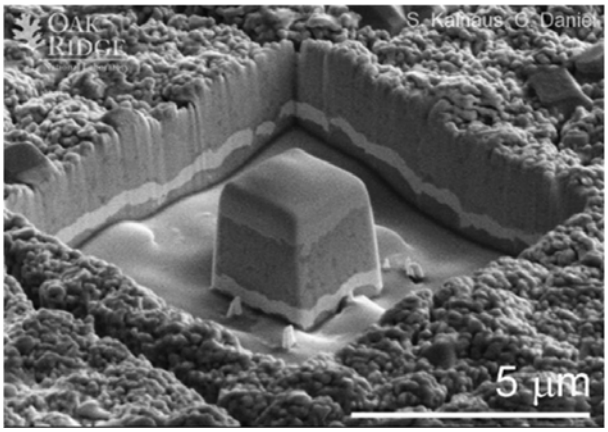

Figure V- 17: Structural parameters obtained from Rietveld refinements of combined XRD and neutron powder patterns on $Li[Ni_{0.4}Co_{0.2-y}Al_yMn_{0.4}]O_2$, $0 \le y \le 0.2$ compounds.

$LiMnPO_4$. $LiMnPO_4$/C and $LiMg_yMn_{1-y}PO_4$/C nanocomposites were synthesized via a combustion process. High resolution transmission electron microscopy (HRTEM) and scanning electron microscopy (SEM) shows that the average particle size is approximately 30-40 nm in diameter (Figure V- 18). The Raman spectra obtained on powders show that the carbon on particle surfaces is disordered.

Although the synthesis is not yet optimized, electrochemical results are encouraging. Cells containing nanocomposite $LiMg_{0.2}Mn_{0.8}PO_4$/C materials discharged nearly 70% of their capacity at C/25 rate at room temperature with very little decrease in utilization as the current was increased (Figure V- 19).

Conclusions and Future Directions

The approach towards reducing Co content by partially replacing it with Al in Li[Ni, Co, Mn]O_2 compounds is encouraging, resulting in enhanced electrochemical performance for certain compositions. Future work will be directed towards deepening the understanding of structural effects of Al substitution on the $Li[Ni_{0.4}Co_{0.2-y}Al_yMn_{0.4}]O_2$, $0 \le y \le 0.2$ series. To this end, magnetic measurements (with Whittingham, SUNY Binghamton) and NMR (with Grey and/or Cabana) are planned, as well as XAS experiments at the Stanford synchroton. It is clear, however, that the amount of Al substitution must be kept low or else energy density is adversely impacted. Thus, further reduction of Co content to contain costs requires adjustment of the Ni and Mn contents instead. In FY10, $Li[Ni_{0.45}Co_{0.1-y}Al_yMn_{0.45}]O_2$ and $Li_{1+x}[Ni_{0.45}Co_{0.1-y}Al_yMn_{0.45}]_{1-x}O_2$ compositions will be synthesized and studied. Although compounds with high Ni content are expected to exhibit increased anti-site mixing, the enlargement of the LiO_2 slab spacing may compensate for any adverse impact on rate capability as with the $Li[Ni_{0.4}Co_{0.2-y}Al_yMn_{0.4}]O_2$, $0 \le y \le 0.2$ series.

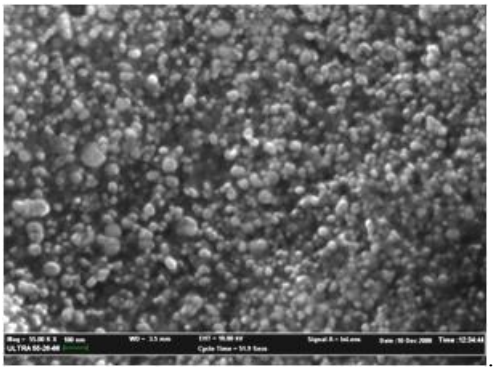

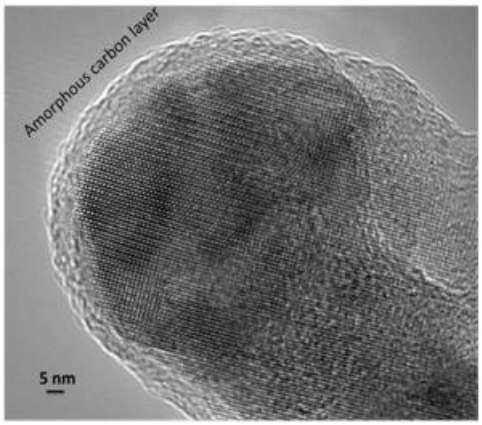

Figure V- 18: SEM (top) and HRTEM (bottom) images of $LiMg_{0.1}Mn_{0.9}PO_4$/C nanocomposites.

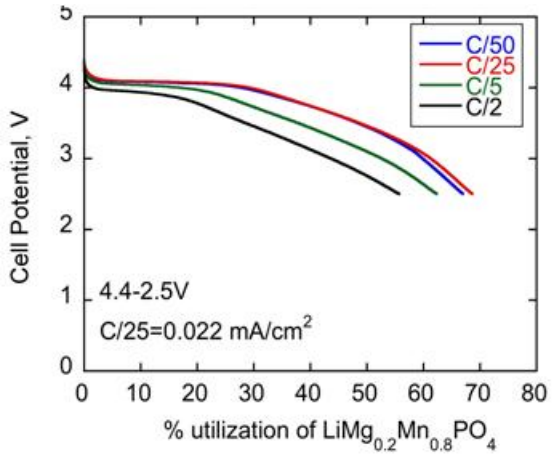

Figure V- 19: Discharges of a Li/$LiMg_{0.2}Mn_{0.8}PO_4$/C nanocomposite cell between 4.4-2.5V at room temperature.

Work on $LiMnPO_4$ and variants will be de-emphasized due to safety and performance concerns. Because the synthesis parameters have been worked out for this system, it will be used to test a spray pyrolysis system now under development in this laboratory. This method is expected to allow production of more homogeneous nanoparticulate composites containing carbon than the current combustion process. Once this has been optimized, this technique will be used to synthesized other polyanionic compounds that currently exhibit poor electrochemical performance, such as $LiMnBO_3$ $LiFeBO_3$, or $Li_2(Mn, Fe)SiO_4$.

FY 2009 Publications/Presentations

1. "Structure and Electrochemistry of $LiNi_{1/3}Co_{1/3-y}M_yMn_{1/3}O_2$ (M=Ti, Al, Fe) Cathode Materials", James Wilcox, Sébastien Patoux, and Marca Doeff, **J. Electrochem. Soc.**, 156, A192 (2009).

2. "Microwave Plasma Chemical Vapor Deposition of Carbon Coatings on $LiNi_{1/3}Co_{1/3}Mn_{1/3}O_2$ for Li-ion Battery Composite Cathodes", M. Marcinek, J. D. Wilcox, M. M. Doeff, and R. Kostecki, **J. Electrochem. Soc.**, 156, A48 (2009).

3. "FTIR and Raman Study of the $Li_xTi_yMn_{1-y}O_2$ (y=0, 0.11) Cathodes in Pyrrolidinium-based Ionic Liquid Electrolyte Systems", L. J. Hardwick, J. A. Saint, I. T. Lucas, M. M. Doeff, and R. Kostecki, **J. Electrochem. Soc.**, 156, A120 (2009).

4. "Electrode Materials with the $Na_{0.44}MnO_2$ Structure: Effect of Titanium Substitution on Physical and Electrochemical Properties", J.A. Saint, J.D. Wilcox, and M.M. Doeff, **Chem. Mater.,** 20**,** 3404 (2008).

5. "Microwave Plasma CVD of Carbon Coatings on $LiNi_{1/3}Co_{1/3}Mn_{1/3}O_2$ for High-Power Li-ion Battery Composite Cathodes" M. L. Marcinek, J.D. Wilcox, M. M. Doeff and R. Kostecki 214th meeting of the Electrochemical Society, October 2008, Honolulu, HI., Abstract 567.

6. "The Origins of the Rate Enhancement in $LiNi_{0.4}Co_{0.2-y}Al_yMn_{0.4}O_2$ ($0<y\leq0.2$) Cathode Materials" James Wilcox and Marca M. Doeff, 214th meeting of the Electrochemical Society, October 2008, Honolulu, HI., Abstract 576.

7. "Comparison of $LiMnPO_4$ made by Combustion and Hydrothermal Syntheses" Jiajun Chen, Marca M. Doeff and Ruigang Wang, 214th meeting of the Electrochemical Society, October 2008, Honolulu, HI., Abstract 583.

8. "Spectroscopic Investigation of the Surface of Li_xMnO_2 and $Li_xTi_{0.11}Mn_{0.89}O_2$ Composite Electrodes in Pyrrolidinium-based Ionic Liquid Electrolyte Systems" L. J. Hardwick, J. Saint, M. M. Doeff and R. Kostecki, 214th meeting of the Electrochemical Society, October 2008, Honolulu, HI., Abstract 718.

9. "Nanostructured Electrode Materials Made by Combustion Synthesis" M. M. Doeff, International Conference on Materials for Advanced Technologies, June 2009, Singapore.

V.B.4 Stabilized Spinels and Nano Olivines (UTA)

Arumugam Manthiram
University of Texas at Austin
Materials Science and Engineering Program
Austin, TX 78712
Phone: (512) 471-1791; Fax: (512) 471-7681
E-mail: rmanth@mail.utexas.edu

Subcontractor: None

Start Date: April 1, 2004
Projected End Date: May 31, 2010

Objectives

- Develop high performance cathodes for Li-ion batteries and a fundamental understanding of their structure-composition-performance relationships.
- Develop low cost spinel manganese oxide compositions exhibiting improved capacity retention at elevated temperatures.
- Develop low cost manufacturing processes for olivine cathodes with controlled size and nanomorphologies.

Technical Barriers

This project addresses the following technical barriers of cathode materials for Li-ion battery technology:

(A) Battery Cost

(B) Cycle Life

(C) Energy and Power Densities

Technical Targets

- Acceptable cycle life for spinel cathodes
- Low manufacturing cost for olivine cathodes
- Increased energy and power densities with spinel cathodes

Accomplishments

- Stabilized spinel cathode compositions exhibiting superior cycle life compared to the conventional spinel cathode have been developed by appropriate cationic and anionic substitutions.
- 5 V spinel cathodes exhibiting improved cycle life, high rate capability, and excellent rate capability retention have been developed by suppressing the formation of solid-electrolyte interface (SEI) layer through surface modification:
- Nanostructured olivine cathodes have been synthesized by novel microwave-assisted solvothermal and hydrothermal approaches with a short reaction time of 5 – 15 minutes at < 300°C without requiring any reducing gas atmospheres, offering the potential to lower the manufacturing cost.

✧ ✧ ✧ ✧ ✧

Introduction

Achieving the DOE targets for transportation applications will require the development of low cost, better performing cathode materials. Accordingly, this project focuses on improving the performance and/or lowering the manufacturing cost of two cathode systems (spinel and olivine) that are known to offer high rate capability and are heavily pursued for vehicle applications.

Approach

To meet the DOE performance and cost targets, our approach is to develop a firm scientific understanding of the factors that control/influence the electrochemical performance of the spinel oxide and olivine cathodes and utilize the knowledge gained to design and develop high performance cathode compositions. In this regard, cationic and anionic substitutions in the spinel lattice, surface modifications, and low cost synthesis of olivine cathodes are being pursued. The materials are characterized by a variety of techniques including X-ray diffraction (XRD), scanning electron microscopy (SEM), transmission electron microscopy (TEM), wet chemical analysis, thermal analysis, Fourier transform infrared (FTIR) spectroscopy, Raman spectroscopy, and X-ray photoelectron spectroscopy (XPS). The electrochemical performances are evaluated in coin cells using charge-discharge, cycle-ability, rate capability, and impedance spectroscopic measurements. Based on the characterization and electrochemical data, an in-depth structure-property-performance relationship is established.

Results

Stabilized 5 V Spinel Cathodes. Spinel oxides based on $LiMn_{1.5}Ni_{0.5}O_4$ provide important advantages compared to the $LiMn_2O_4$ spinel. For example, it offers a higher discharge voltage of ~ 4.8 V (hereafter referred to as 5 V spinel) and much suppressed or little manganese

dissolution as Mn remains as Mn^{4+} throughout the charge-discharge process and only Ni^{2+} ions undergo redox reaction in $LiMn_{1.5}Ni_{0.5}O_4$. However, the major concern with these higher voltage cathodes is the electrolyte instability and possible reaction of the cathode surface with the electrolyte at the higher charge-discharge potential. To develop an understanding of these issues, we have focused on surface modification of the 5 V spinel cathodes and an in-depth characterization of the cathodes before and after surface modification with other materials.

Stabilized, cation-substituted 5 V spinel cathode compositions $LiMn_{1.42}Ni_{0.42}Co_{0.16}O_4$ and $LiMn_{1.5}Ni_{0.42}Zn_{0.08}O_4$ have been surface modified with Al_2O_3, ZnO, Bi_2O_3, and $AlPO_4$ by an electrostatic self-assembly method. High resolution TEM data show that while Al_2O_3, ZnO, and Bi_2O_3 form a continuous, porous, amorphous coating – $AlPO_4$ forms a discrete, dense, crystalline coating. The cycle-ability data given in Figure V- 20 reveal that the surface modified samples show higher capacity and better capacity retention than the bare sample.

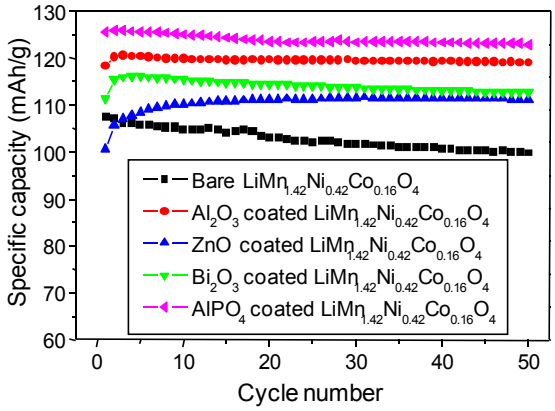

Figure V- 20: Cycling performances of the bare and 2 wt. % Al_2O_3, ZnO, Bi_2O_3, and $AlPO_4$ coated $LiMn_{1.42}Ni_{0.42}Co_{0.16}O_4$.

Figure V- 21 compares the rate capability retention of $LiMn_{1.42}Ni_{0.42}Co_{0.16}O_4$ before and after surface modification with various oxides. The plots in Figure V-21 were obtained by first calculating the percentage capacity retained on going from C/6 to various rates (up to 10C rate) at 3rd and 50th cycles separately and then dividing the latter by the former. For example, surface modification of $LiMn_{1.42}Ni_{0.42}Co_{0.16}O_4$ with Al_2O_3 leads to a rate capability retention of ~ 97 % on going from C/6 to 10C rate while the bare $LiMn_{1.42}Ni_{0.42}Co_{0.16}O_4$ has a rate capability retention of only ~ 55 % under the same conditions. The poor rate capability retention of the bare 5 V cathodes is due to the fast increase in polarization resistance R_P on cycling, which arises from a significant increase in both the SEI layer resistance and electron transfer resistance as indicated by electrochemical impedance spectroscopic analysis. Surface modification slows down the growth of the SEI layer as indicated by the XPS analysis, resulting in a suppression of both the SEI layer resistance and electron transfer resistance. The results suggest that surface modification is an effective way to improve the chemical stability of the 5 V spinel cathodes in contact with the electrolyte and improve their cycle-ability and rate capability during long-term cycling.

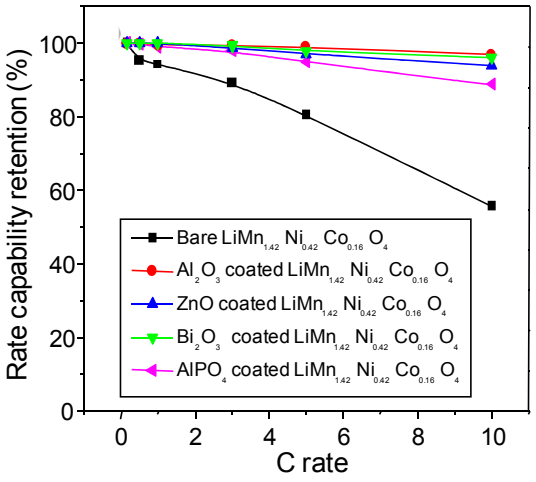

Figure V- 21: Rate capability retention of bare and surface modified $LiMn_{1.42}Ni_{0.42}Co_{0.16}O_4$ cathodes after 50 cycles

Nano Olivines. One of the drawbacks with the olivine $LiMPO_4$ cathode is the poor electronic and lithium ion conductivity and the consequent necessity to synthesize them as nanoparticles and coat with conductive carbon involving heat treatment at > 650°C in a reducing gas atmospheres. This approach leads to high processing cost despite the high abundance and low cost of elements like Fe. To overcome this difficulty, we have developed a microwave-assisted solvothermal (MW-ST) synthesis approach to obtain $LiMPO_4$ (M = Mn, Fe, Co, and Ni) cathodes. The synthesized cathodes have been networked with multi-walled carbon nanotubes (MWCNT) at ambient temperatures as well as coated with conductive carbon by heating the $LiMPO_4$ nanorods synthesized by the MW-ST method with a carbon precursor in a reducing atmosphere at 700°C for a short duration of 1 h. The TEM images shown in Figure V- 22 reveal nano-thumb like shapes with a variation in size and aspect ratio. The phase contrast high-resolution TEM images of the nano-thumb like structures, which are shown in the third column of Figure V- 22, reveal that each nano-thumb is a single crystal for all the four $LiMPO_4$ samples. A more detailed analysis of the high-resolution images and the respective Fast Fourier Transforms (FFT) revealed that all the nano-thumb like $LiMPO_4$ structures exhibit a preferential growth along the *[001]* direction, *i.e.* the long axis of the nano-thumbs. These dimensionally modulated $LiMPO_4$ samples exhibit a unique and favorable morphology since the *b*-axis (the easy lithium diffusion direction) is one of the two short

dimensions of the nanostructures, helping to overcome the poor lithium ion conductivity limitations and enhance the rate capability.

The cycle-ability data given in Figure V- 23 reveal that the $LiFePO_4$-MWCNT nanocomposite exhibits remarkably high rate capability compared to as-prepared $LiFePO_4$ due to the improvement in electronic conduction. Electrochemical performance data collected with different particle sizes of $LiFePO_4$ reveal that both lithium ion conduction and electronic conduction control the performance of olivine cathodes. Our results illustrate that the MW-ST process is a viable low cost manufacturing approach to obtain high performance $LiFePO_4$ cathodes.

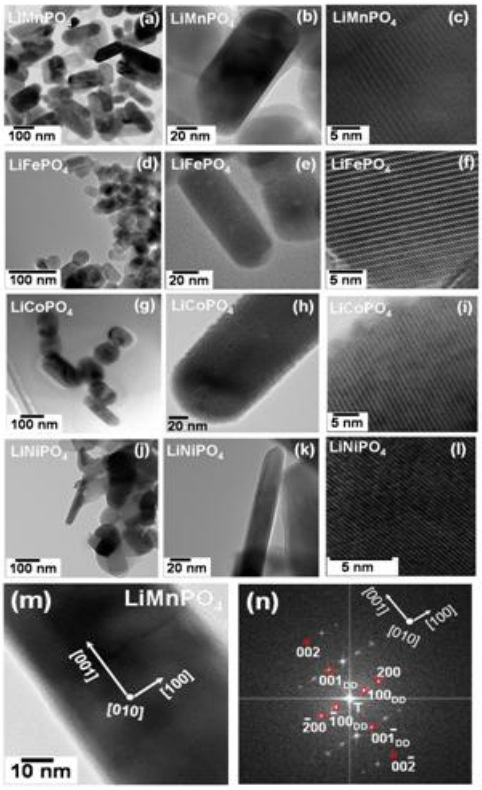

Figure V- 22: TEM images of olivine $LiMPO_4$ (M= Mn, Fe, Co, Ni) prepared by the MW-ST method.

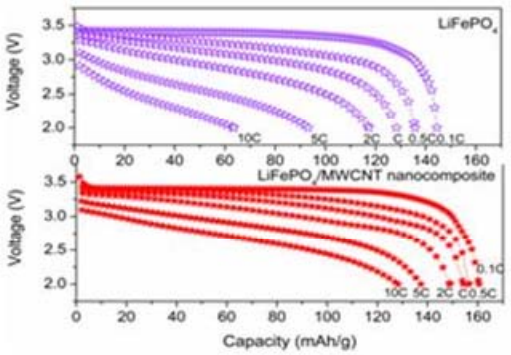

Figure V- 23: Rate capability of $LiFePO_4$ and $LiFePO_4$-MWCNT nanocomposite.

In contrast, both $LiMnPO_4$ and $LiCoPO_4$ exhibit lower capacities than $LiFePO_4$ after networking with MWCNT or coating with carbon, while the electrochemical performance of $LiNiPO_4$ could not be collected due to the electrolyte instability at the high operating voltage of 5.2 V. The inferior performance of $LiMnPO_4$ is due to its poorer electronic conductivity compared to $LiFePO_4$ despite the good Li-ion diffusion achievable with the small nanorods, and our future work will focus on overcoming this problem by ball milling the $LiMnPO_4$ nanorods with conductive carbon. On the other hand, the inferior performance of $LiCoPO_4$ could be due to the reaction of the cathode surface with the electrolyte and the formation of thick SEI layers at the high operating voltage of 4.8 V.

Analogous to the MW-ST process, we have also developed a microwave-assisted hydrothermal (MW-HT) method employing water as a solvent, which offers highly crystalline $LiFePO_4$ nanorods within 15 minutes at 230°C. Additionally, both an *ex situ* carbon coating of the $LiFePO_4$ obtained by the MW-ST method by heating at 700°C with sucrose the $LiFePO_4$ obtained by the MW-ST method and an *in situ* carbon coating by carrying out the MW-HT process in presence of glucose followed by heating at 700°C have been pursued. The MW-HT method offers larger size nanorods (225 nm width and up to 300 nm length) compared to the MW-ST method (25 nm width and up to 100 nm length). Figure V- 24 compares the rate capabilities of the samples obtained by the MW-ST and MW-HT processes. While both the samples exhibit excellent rate capabilities, the MW-ST sample exhibits slightly higher capacity due to smaller particle size compared to the MW-HT sample, illustrating the role of lithium diffusion length on the rate capabilities of olivine cathodes. The data clearly demonstrate that both lithium ion diffusion by controlling the particle size and electronic conductivity by nano-coating or nano-networking play a critical role in determining the electrochemical performance of olivine cathodes.

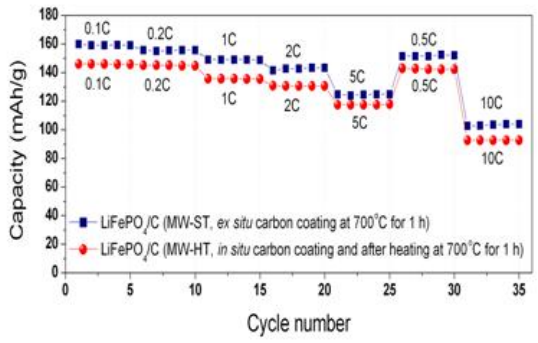

Figure V- 24: Rate performance of the $LiFePO_4$/C nanocomposites.

Conclusions and Future Directions

Surface modification of 5 V spinel cathodes has been found to suppress the growth of SEI layer during cycling, and thereby offers improved capacity retention and rate capability retention during cycling. Based on this understanding, our future efforts will focus on a strategy involving self segregation of certain substituted cations to the surface during the synthesis process. The surface segregating ions are chosen in such a way that they can suppress the growth of SEI layer in contact with the electrolyte and thereby enhance the cycle life and rate capability retention. This approach, if successful, can eliminate the additional chemical surface modification step and offer cost savings.

Nanostructured olivine cathodes with controlled size have been synthesized by a novel microwave-assisted solvothermal synthesis approach with a short reaction time of 5 – 15 minutes at < 300°C without requiring reducing gas atmospheres, offering the potential to lower the manufacturing cost. Our future work will focus on extending this novel approach to obtain solid solutions between different olivine cathodes $LiMPO_4$ (M = Mn, Fe, Co, Ni, and Mg) as well as to access other poly-anion containing cathodes. Having access to nano olivines with controlled size and morphology through our microwave-assisted solvothermal process, we will also focus on understanding the influence of crystallite size and shape as well as defect chemistry on the charge-discharge mechanisms and electrochemical performance.

FY 2009 Publications/Presentations

Journal Articles

1. A. Vadivel Murugan, T. Muraliganth, and A. Manthiram, *Electrochem. Commun.* **10**, 903-906 (2008).
2. A. Vadivel Murugan, T. Muraliganth, and A. Manthiram, *J. Phys. Chem. C* **112**, 14665-14671 (2008).
3. A. Manthiram, A. Vadivel Murugan, A. Sarkar, and T. Muraliganth, *Ener. Environ. Sci.* **1**, 621-638 (2008).
4. T. Muraliganth, A. Vadivel Murugan, and A. Manthiram, *J. Mat. Chem.* **18**, 5661-5668 (2008).
5. J. Liu and A. Manthiram, *J. Electrochem. Soc.* **156**, A66-A72 (2009).
6. A. Vadivel Murugan, T. Muraliganth, and A. Manthiram, *J. Electrochem. Soc.* **156**, A79-A83 (2009).
7. Q. Luo and A. Manthiram, *J. Electrochem. Soc.* **156**, A84-A88 (2009).
8. A. Vadivel Murugan, T. Muraliganth, P. J. Ferreira, and A. Manthiram, *Inorg. Chem.* **48**, 946-952 (2009).
9. Q. Luo, T. Muraliganth, and A. Manthiram, *Solid State Ionics* **180**, 703-707 (2009).
10. J. Liu and A. Manthiram, *Chem. Mater.* **21**, 1695-1707 (2009).

Presentations

1. A. Vadivel Murugan, T. Muraliganth, and A. Manthiram, "Microwave Assisted Solvothermal and Hydrothermal Synthesis of Phospho-olivine Cathodes," *Joint International and 214th Meeting of the Electrochemical Society,* Honolulu, HI, October 12-17, 2008.
2. A. Manthiram, "High Energy Density Cathodes for Next Generation Li-ion Batteries," *International Conference on Electrochemical Power Systems (ICEPS-2008),* Trivandrum, India, November 26-28, 2008 (invited).
3. A. Manthiram, "Stabilized Spinel and Phospho-olivine Cathodes," *2009 Annual Merit Review Meeting of the Office of Vehicle Technologies,* U.S. Department of Energy, Washington, DC, May 19-21, 2008.
4. A. Manthiram, "High Energy Density Cathodes for Next Generation Li-ion Batteries," *Central Regional Meeting of the American Chemical Society (CERMACS),* Cleveland, OH, May 20-23, 2009 (invited).
5. A. Manthiram, "Challenges and Opportunities of Li-ion Battery Technology," *2009 Institute for Materials Research (IMR) Materials Week,* Ohio State University, Columbus, OH, September 1, 2009 (invited).

V.B.5 Synthesis and Characterization of Substituted Olivines and Layered Manganese Oxides (SUNY)

M. Stanley Whittingham (Project Manager)
SUNY at Binghamton
Vestal Parkway East
Binghamton, NY 13902-6000
Phone: (607) 777-4623; Fax: (607) 777-4623
E-mail: stanwhit@binghamton.edu

Start Date: June 1, 2007
Projected End Date: May 31, 2010

Objectives

- Find lower-cost and higher-capacity cathodes, exceeding 200 Ah/kg based on environmentally benign materials
- Find high-rate HEV compatible cathodes based on environmentally benign materials.

Technical Barriers

This project addresses the following technical barriers:

(A) Lower cost materials and processing

(B) Higher power materials

(C) Higher capacity materials

(D) Abuse-tolerant cathodes

Technical Targets

- Characterize the electronically stabilized manganese oxide, determine the rate capability *vs.* Co content, determine the role of Ni and understand its disorder to obtain a stable high rate abuse tolerant cathode (including application to HEVs), determine the optimum composition and compare the best samples with the base case cathodes.
- Determine feasibility of aliovalent doping of olivine, $LiMPO_4$, determine optimum particle size and evaluate other phosphate structures containing Fe and Mn and compare them with high temperature $LiFePO_4$.
- Identify materials that can undergo more than one electron per redox center.

Accomplishments

- Shown for the layered oxides that the composition $LiMn_{0.33}Ni_{0.33}Co_{0.33}O_2$ may not be optimum
  - Lower cobalt contents have the same theoretical capacity, and will be lower cost
  - Lower cobalt content materials appear to have better charging characteristics
  - To achieve capacities over 200 Ah/kg in the layered oxides will require charging voltages over 4.4 volts at RT
  - Manganese contents above 0.5 are deleterious to the electrochemical properties for Li:M = 1 in $LiMO_2$ (where M=Ni+Mn+Co+Al)
- Substitution in $LiFePO_4$ shown to be advantageous:
  - Vanadium substitution on phosphorus site leads to nanostructure
    - Lower cobalt content materials appear to have better charging characteristics
    - To achieve capacities over 200 Ah/kg in the layered oxides will require charging voltages over 4.4 volts at RT
  - Opens up opportunities for $LiMnPO_4$
- Scoping and literature survey underway on two-electron redox active intercalation materials
- Technology transfer accomplished
  - Working with several local battery companies, and many ex-students now in battery companies
  - Students now have positions at BNL, LBNL, NREL, and PNNL

✧ ✧ ✧ ✧ ✧

Introduction

Achieving the DOE energy and power targets for HEV, PHEV and EV batteries will require much higher capacity materials. To meet the DOE cost targets, we are looking at reducing high-cost components, and for power and energy targets at modifying the chemical composition and morphology of the cathode compounds.

Approach

Our cathode approach is to place emphasis on transition metal dioxides and phosphates, both pure and modified with other transition metals, using predominantly low temperature synthesis approaches. These materials will be synthesized, and characterized both structurally and for thermal and chemical stability. All will be evaluated electrochemically in a variety of cell configurations.

One major cost component in the layered oxides is the cobalt. To that end, we are studying the layered compositions, $LiNi_yMn_yCo_{1-2y}O_2$, with a close to stoichiometric Li to transition metal ratio and with values of y of 0.4 and 0.45 leading to a cobalt content of only 10%.

One major challenge facing the use of the olivine class of materials, such as $LiFePO_4$, is their low volumetric energy density, which is exacerbated by the probable need to use nanomaterials. A second challenge is the apparent high cost of making high quality material. Our approach is to form more dense powder structures, using low cost techniques by isovalent substitution on either the iron or phosphorus sites

Results

Layered Transition Metal Oxides. We have formed a range of transition metal oxides of formula $LiNi_yMn_yCo_{1-2y}O_2$ to determine the optimum composition for both energy density and power density. The theoretical capacity was determined by measuring the open circuit voltages, on both lithium removal and lithium insertion. The results are shown in Figure V- 25 for an upper charge limit of 4.3 volts.

Within the voltage regime studied, the voltage curve on lithium removal is higher the lower the cobalt content for all lithium contents less than 0.5; when more than 0.5 lithium is removed for the cobalt-rich compounds the potential increases more rapidly suggesting that the cobalt is becoming involved in the redox reaction. However, the key finding is that the capacity of the material is essentially independent of the cobalt content for the $LiNi_yMn_yCo_{1-2y}O_2$ materials when the charging is limited to 4.3 volts.

The open circuit voltages on lithium insertion, shown in Figure V- 25(bottom) follow the same pattern. However, there is clearly a high polarization at lithium contents close to unity, which prevents all the lithium from being electrochemically cycled when practical cycling rates are used. This is commonly known as the first cycle capacity loss. Thus, we conclude that the maximum capacity of these lithium stoichiometric materials, $LiMO_2$, is 180-186 Ah/kg, when the charging voltage is limited to 4.3 volts. This maximum "theoretical" limit is essentially independent of the cobalt content, but with the 442 composition having marginally the highest capacity.

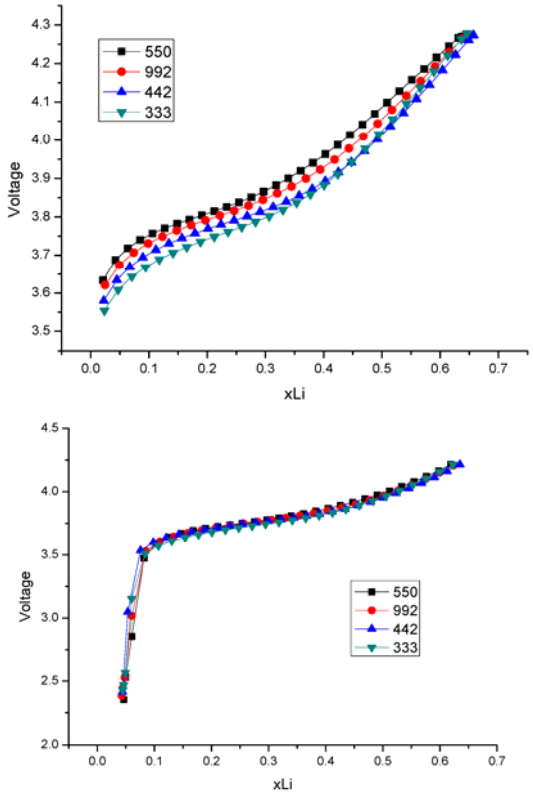

Figure V- 25: Open circuit voltages on (top) charging and (bottom) discharging $Li_{1-x}Ni_yMn_yCo_{1-2y}O_2$, where the composition is represented by the y y 1-2y notation in the graphs (for y=0.45, the notation is 992).

Raising the charging cut-off voltage to 4.4 volts increases the theoretical capacity to 200 Ah/kg, thus indicating that for these NMC stoichiometric materials (1 Li per transition metal) a charging cut-off voltage of over 4.4 volts will be needed to maintain a capacity of 200 Ah/kg considering the expected first cycle capacity loss. The rate capability is much more dependent on the chemical composition, structural disorder and morphology/particle size. Initial measurements suggest that the lower cobalt content compositions such as $LiNi_{0.4}Mn_{0.4}Co_{0.2}O_2$ may have better overall power capabilities. Increasing the manganese content over 0.5 was found to be deleterious to the electrochemical performance.

Structural Modification of $LiFePO_4$. We explored the olivine structure to improve the particle size and morphology so as to optimize the capacity at higher rates by iso-valently substituting in the $LiFePO_4$ structure. We chose to substitute vanadium into the structure, because vanadium forms related structures, such as $VOPO_4$, containing VO_6 octahedra like the FeO_6 octahedra in $LiFePO_4$. A series of compounds were formed and the lattice was found to shrink in size as vanadium was added,

showing that a solid solution was indeed formed. X-ray analysis indicated that the vanadium was on the phosphorus site.

The electrochemical behavior of the 5% substituted sample showed the best behavior and is shown in Figure V- 26. The cycling curves did not show any evidence for electrochemical activity on the vanadium site. The rate capability is superior to our prior hydrothermal data. The observed electrochemistry is almost the same as for $LiFe_{0.95}Mg_{0.05}PO_4$, made by a similar process, suggesting that the role of substitution might be to create strain in the lattice which allows for the more rapid motion of the $LiFePO_4/FePO_4$ interface through the crystallites. [This work was done in collaboration with Professor C. S. Wang at U. Maryland.]

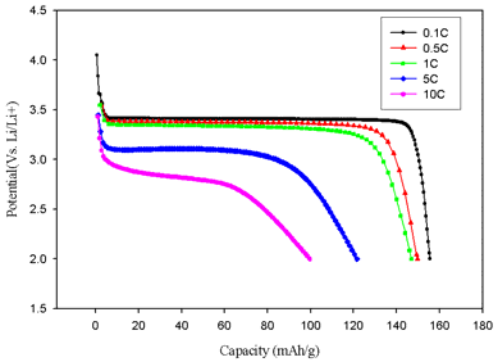

Figure V- 26: Discharge curves of $LiFeP_{0.95}V_{0.05}O_4$ at different rates showing the high rate capability.

The powder structure of this material is comprised of porous particles of around a micron in size, which should allow for a higher packing density than for nanosized powders. These micron-size particles are in turn made up of 50 nm size crystallites, thus giving us the advantage of a nanomaterial without the accompanying disadvantages; as with the SONY anode we have a large particle, stable nanostructured material. As a result the electrochemical rate capability behavior shown below was obtained with 12 wt % of carbon + binder, compared with 23-30 % for comparable $LiFePO_4$ materials shown in Figure V- 27.

.

Conclusions and Future Directions

In order to achieve 200 Ah/kg, the layered oxides will have to be charged in excess of 4.4V irrespective of transition metal composition. The optimum composition and morphology for power capability, both charge and discharge, will be determined next year. The role of aluminum will also be determined (with M. Doeff at LBNL). Iso-valent substitution of the olivine, $LiFePO_4$, allows for a high rate capability with a denser cathode structure, resulting in a higher volumetric and gravimetric energy storage capability. Higher capacities will be attempted by changing the composition and structure of the phosphate. Significantly higher capacities than 200 Ah/kg will require more than one lithium per redox center in an intercalation based battery, and we will continue our search for such materials.

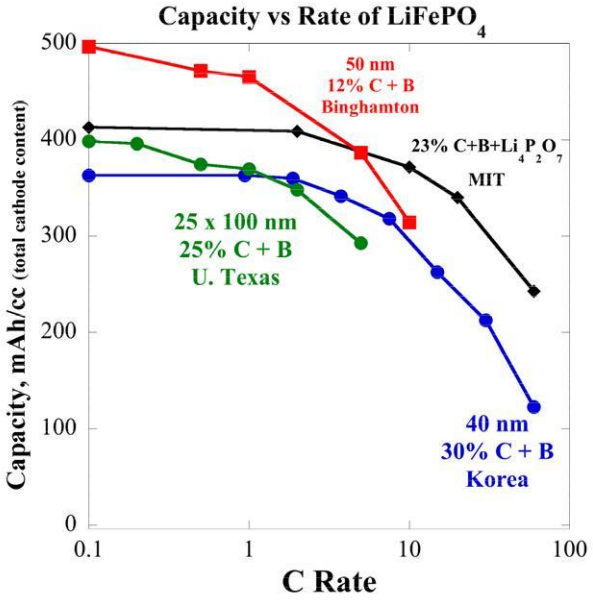

Figure V- 27: Comparison of the capacity in mAh/cc of this material with three other high rate and capacity olivine materials.

FY 2009 Publications/Presentations

1. Presentation to the 2009 DOE Annual Peer Review Meeting, Washington, DC.
2. C. Ban, N. Chernova, M. S. Whittingham, "Electrospun Nano-Vanadium Pentoxide Cathode", Electrochem. Commun., 2009, 11: 522-525.
3. N. A. Chernova, M. Roppolo, A. Dillon and M. S. Whittingham, "Layered vanadium and molybdenum oxides: batteries and electrochromics", J. Mater. Chem., 2009, 19: 2526-2552.
4. J. Xiao, Natasha A. Chernova, and M. S. Whittingham, "Layered Mixed Transition Metal Oxide Cathodes with Reduced Cobalt Content for Li-ion Batteries", Chemistry of Materials, 2008, 20: 7454-7464.
5. J. Hong, C. S. Wang, X. Chen, S. Upreti, and M. Stanley Whittingham, "Vanadium Modified $LiFePO_4$ Cathode for Li-ion Batteries", Electrochem. Solid-State Letters, 2009, 12: A33-A38.
6. Several invited presentations, including:
   - GE, EPRI/CWRU, Dow, Exxon, NYSERDA, Chemical Heritage Foundation
   - IMLB, MRS, ISSI
   - Max-Planck, CSIRO, Brookhaven NL
   - Bath, Columbia, Buffalo, Rochester U.

V.B.6 Low Cost SiO_x-Graphite and Olivine Materials (IREQ)

Karim Zaghib
Hydro-Quebec IREQ.
1800 Lionel Boulet
Varennes, QC, Canada J3X 1S1
Phone: (450) 652-8019; Fax: (450) 652-8424
E-mail: Zaghib.Karim@ireq.ca

Start Date: March 1, 2008
Projected End Date: April 30, 2009

Objectives

- Synthesize and evaluate $LiMnPO_4$ with improved electrochemical characteristics.
- Replace the graphite anode with an alternative anode that meets the requirement for low cost and high energy.
- Continue developing binders for the cathode and alternative anode to understand the properties of the SEI layer that forms.

Technical Barriers

Low energy and poor cycle/calendar life

Technical Targets

- Explore an appropriate technique to produce $LiMnPO_4$ cathode with acceptable reversible capacity.
- Develop an alternative material to the graphite anode based on SiO_x.
- Investigate the interface on SiO_x

Accomplishments

- Different types of graphites were evaluated and the electrode films produced at Hydro-Quebec were sent to investigators in the BATT.
- Evaluated mixed SiO_x-graphite as an alternative anode material.
- The effect of the binder on the performance of the alternative anode (first coulombic efficiency and reversible capacity) was evaluated.
- Different synthesis routes (solid state and hydrothermal and microwave) were investigated to produce $LiMnPO_4$ material.
- Completed study of a new graphite (OMAC from Osaka Gas) and compared its performance with SNG12 (HQ) in standard electrolyte 1M $LiPF_6$–EC/DEC with VC and VEC as additives. Also characterization of electrodes with water-dispersed binder was completed.

✧ ✧ ✧ ✧ ✧

Introduction

Achieving the DOE cost targets will require finding alternative low cost materials, both for the anode and cathode. We are investigating the performance of Mn-based olivine cathodes and alloy anodes. In order to understand the capacity fade of the alloy due to the volume expansion we are studying the SEI layers on this material.

Approach

Different types of graphite will be evaluated to determine the optimal electrode composition. The electrode films produced at Hydro-Quebec will be sent to other BATT investigators involved with SEI analysis using different techniques.

Laminate cathode films and powders will be prepared and sent to BATT investigators for evaluation

Our approach is to develop an appropriate method to synthesis $LiMnPO_4$. The emphasis is to improve electrochemical performance with acceptable carbon content in the electrodes. The effect of particle size on the reversible capacity and cycle life will be investigated.

Different binders with different mechanical properties will be investigated and evaluated with the alternative anode material.

Results

The effect of additives in the electrolyte was investigated in Li/graphite cells to understand their role in SEI layer formation. Vinyl carbonate (VC) and vinyl ethyl carbonate (VEC), and their mixtures, were investigated as additives in the conventional electrolyte 1M-$LiPF_6$-EC/DEC. The performance of the graphite electrodes SNG12 and OMAC-15 were compared.

The performance of SNG12 was sensitive to the additives, and the first coulombic efficiency (CE) was affected when small amount of additives are introduced. The first CE improved to 93% in both cases with the addition of 2%VEC or the mixture (1%VEC + 1%VC) compared to 85% in the cell without additives. However, the reversible capacity is slightly reduced to 345mAh/g and 336mAh/g, respectively, compared to 369mAh/g

without additives. No effect was found when 2%VC is added to the SNG12 cell, yielding the optimum reversible capacity (Table V-1).

Table V-1: Performance of SNG12 and OMAC15

Tab.1	SNG12		OMAC15	
Additives	1st CE (%)	Qrev (mAh/g)	1st CE (%)	Qrev (mAh/g)
No	85	369	93	358
2%VC	86	366	92	355
2%VEC	93	345	92	321
1%VC + 1%VEC	93	336	87	352

When the water soluble binder is used, SNG12 showed better 1st CE (92%) than with PVDF but lower capacity. However, OMAC maintained its 1st CE (95%) and reversible capacity (365mAh/g).

Alternative anode. Experiments were started with Si-based anode alloys - SiO_x with 8-µm average particle size. SiO_x suffers from poor electronic conductivity and dimension variation that limits its performance at high rates and results in capacity fade. To improve performance, we studied carbon-coated SiO_x. Due to the low reversible capacity of SiO_x and its low coulombic efficiency (CE) in the first cycles, we mixed it with graphite - SiO_x/graphite (1:1). To study the SEI layer, we used two binders, PVDF and water dispersed binder (WDB). The first results with these anodes are shown in Figure V- 28 and Figure V- 29. The WDB electrodes show better performance than PVDF electrodes (higher 1st cycle CE - 91% compared to 73%). Also the reversible capacity was 778 mAh/g, 88% of the theoretical capacity, for the WDB electrodes compared to only 394 mAh/g when PVDF is used.

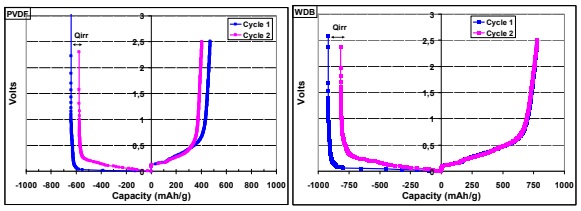

Figure V- 28: First cycles of Li/(SiO_x-graphite) cells in EC-DEC-1M $LiPF_6$ with PVDF and WDB binder

We observed that the performance of anode electrodes improves with the water dispersed binder (WDB). However, the capacity of the anode decreases with cycling. Interfacial studies of cycled cells at different voltages were analysed by SEM (see Figure V- 29). The SEM photos show that the breakdown of SiO_x particles initiates when the anode is discharged at 0.5 V. The disintegration of the SiO_x particles is clearly evident in the selected region in Figure V- 29 after 1.5 cycles at 0 V, which explain the fading capacity of the SiO_x anode.

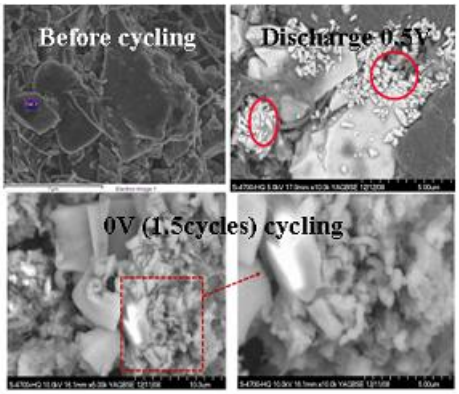

Figure V- 29: SEM of SiO_x-anode at 0 V, 0.5 V and at 0 V (1.5 cycles), EC-DEC-1M $LiPF_6$.

$LiMnPO_4$ cathode material. Hydrothermal and microwave are the common techniques we used to produce $LiMnPO_4$. The material was first evaluated at 25°C in coin-type cells at C/24. The first charge at 4.5 V showed low capacity (29 mAh/g at C/24). When the floating step is added at the end of the charge at 4.5 V, 47 mAh/g is reached with low columbic efficiency 54%. The evaluation of this material at 60°C, showed a dramatic improvement in capacity (Figure V- 30). The first charge at 4.5 V yielded a capacity as high as 159 mAh/g, and 188 mAh/g after floating. The floating step at 4.5 V and 60°C probably resulted in a side reaction, which explains the higher capacity than theoretical. Some decrease in the discharge capacity was noticed in the following cycles; 148 and 146mAh/g, respectively, in the 2end and 3ed cycles. The ionic conductivity of the material is enhanced at 60°C, where the discharge and charge plateaus are well defined.

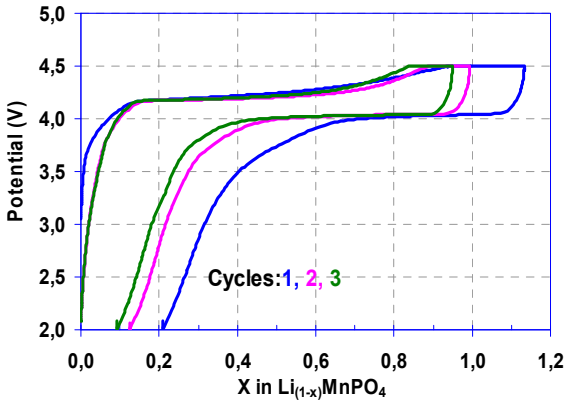

Figure V- 30: First cycles of Li/$LiMnPO_4$ cell EC-DEC-1 M $LiPF_6$ at 60°C

Increasing the temperature has a positive effect on the ionic conductivity of the particles with dimension 0.2-0.5 µm. Thus reducing the particles size below this level is

necessary to improve electrode performance at 25°C. We tried to scale up the production of the material from 10g to 100g using a hydrothermal method. Some parameters were optimized with the scale up process. We evaluated this material before and after wet milling to reduce their particle size. The particle size was reduced to less than 50 nm. At 25°C (Figure V- 31), the first charge of C-$LiMnPO_4$ showed an increasing capacity to 103 mAh/g, with a reversible capacity of 70mAh/g (1st CE = 68%). Compared to the submicron particles (23mAh/g), the reversible capacity is improved by 3 times when the particles were reduced by a factor of 4 (Figure V- 32). We will continue studies of this material to improve its performance at ambient temperature

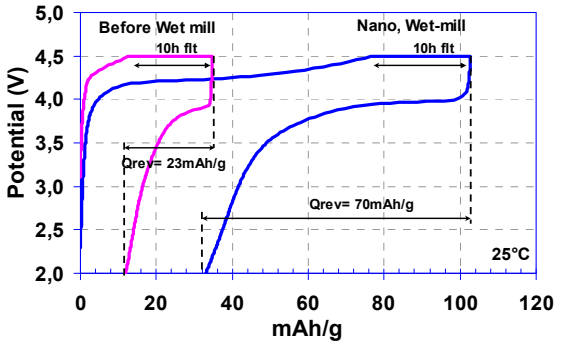

Figure V- 31: First cycles of Li/$LiMnPO_4$ cell EC-DEC-1 M $LiPF_6$ before ant after wet mill at 25°C

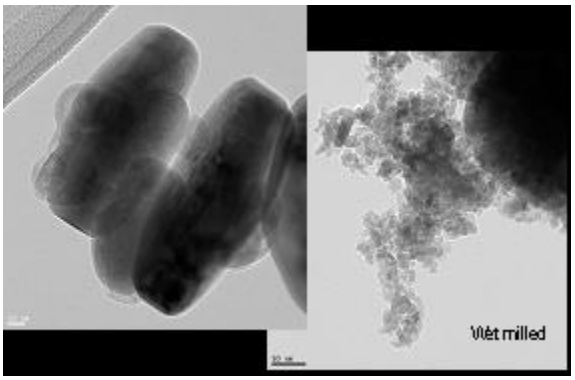

Figure V- 32: SEM photos of $LiMnPO_4$ before and after wet mill.

Conclusions and Future Directions

The new graphite OMAC performs well compared to the base line MCMB and it is a suitable replacement. The water dispersed binder was found to be compatible with the new OMAC graphite.

The SEI layer on the mixed anode, SiO_x:graphite (1:1), was studied by using ex-situ SEM. The breakdown of SiOx particles begins when the anode is discharged at 0.5V, which results in capacity fade.

Efforts will continue on improving the performance of $LiMnPO_4$ at ambient temperature by reducing the particle size to nano scale or by substitution of Mn or P atoms by another metal.

FY 2009 Publications/Presentations

1. Presentation to the 2009 DOE Annual Peer Review Meeting.
2. Presentation at 214th ECS meeting, Honolulu-2008, abstract #582.
3. Presentation at 215th ECS meeting, San Fransisco-2009, abstract #433.

V.B.7 Role of Surface Chemistry on the Cycling and Rate Capability of Lithium Positive Electrode Materials (MIT)

Yang Shao-Horn
Mechanical Engineering and Materials Engineering
Massachusetts Institute of Technology, 3-344
77 Massachusetts Avenue
Cambridge, MA 02139
Phone: (617) 253-2259; Fax: (617) 258-7018
E-mail: shaohorn@mit.edu

Subcontractor:
A.N. Mansour, NSWCCD, West Bethesda, MD

Start Date: April 1, 2009
Projected End Date: March 31, 2010

Objectives

- Develop a fundamental understanding of processes associated with the interfacial instability between active materials and electrolyte.
- Design low cost positive electrodes with stable electrode-electrolyte interface with improved cycling performance and rate capability over wider operating temperatures.

Technical Barriers

This project addresses the following technical barriers in relation to positive electrode materials for lithium-ion batteries:

(A) High Cost

(B) Poor cycle life

(C) Poor calendar life

(D) Abuse tolerance

Technical Targets

- PHEV : Specific energy 56-96 Wh/kg; Specific power 316-750 W/kg; 15-year life (40°C); 3,000-5,000 cycles
- EV : Specific energy 200 Wh/kg; 1,000 cycles

Accomplishments

- Identified changes in the surface chemistry and microstructure of "$AlPO_4$" coated positive electrodes and proposed a mechanism for enhanced capacity retention with cycling and thermal stability relative to uncoated electrodes.
- Collected and analyzed synchrotron based XRD of quenched and annealed $LiNi_{0.5}Mn_{0.5}O_2$ powder material.
- Collected and analyzed X-ray adsorption spectroscopy (XAS) data of quenched and annealed $LiNi_{0.5}Mn_{0.5}O_2$ powder material.
- Collected and analyzed XAS data of surface and bulk structure of $LiNi_{0.5}Mn_{0.5}O_2$ electrodes upon cycling to high voltages.
- Collected and analyzed XPS data of $LiNi_{0.5}Mn_{0.5}O_2$ electrodes upon cycling to high voltages.
- Collected and analyzed STEM data of quenched and annealed $LiNi_{0.5}Mn_{0.5}O_2$ powder material.
- Collected and analyzed STEM data of $LiNi_{0.5}Mn_{0.5}O_2$ electrodes upon cycling to high voltages.

✧ ✧ ✧ ✧ ✧

Introduction

Achieving a fundamental understanding of the roles of coatings and synthesis conditions on the surface chemistry and structural integrity of positive electrode material is necessary to design stable surfaces and structures for Li-ion batteries. The design of chemically and structurally-stable surfaces of Li storage materials is key to the development of low cost, high-energy, high-power, long-life, and thermally-stable Li rechargeable batteries.

Approach

- Probe the surface chemistry of positive electrode materials before and after cycling using surface-sensitive electron microscopy, X-ray photoelectron spectroscopy and electron-yield X-ray adsorption spectroscopy.
- Study the bulk structure of positive electrode materials before and after cycling using synchrotron X-ray diffraction and transmission X-ray absorption spectroscopy.
- Correlate surface chemistry and bulk structure information with electrochemical performance characteristics such as capacity retention and rate capability to determine the origin of surface instability.

Results

Interfacial stability of "$AlPO_4$" Coated $LiCoO_2$. The XPS results have shown that "$AlPO_4$" surface coating promotes the formation of Co and Al-containing fluoride/oxyfluorides and reduce the growth of high-impedance organic layer on the surfaces of the cycled electrodes. Furthermore, we show that the formation of the Co-containing fluorides was further supported by surface sensitive electron yield X-ray absorption spectroscopy. The X-ray absorption near-edge structure (XANES) and the Fourier transforms of EXAFS spectra of pristine and discharged electrodes after 20 cycles for bare and coated $LiCoO_2$ and reference material of CoF_2 are shown in Figure V- 33.

In the XANES region, increased absorption intensity at photon energy around 7720-7725 eV was clearly observed for the coated electrode after 20 cycles, which is consistent with the fact that CoF_2 has higher absorption coefficient in this energy range as shown in Figure V- 33. This result confirms that a thin layer of Co-containing fluorides was formed for the coated electrode after 20 cycles whereas no apparent change of the surface cobalt chemistry was found for the bare electrode after 20 cycles, which is also consistent with the findings by XPS in our previous studies. In addition, the Fourier transforms of EXAFS spectra in Figure V- 33 show that the amplitudes of the first and second Co shells are significantly reduced for the coated electrode after 20 cycles, which is consistent with the simulated results for a mixture of $LiCoO_2$ and CoF_2 (not) shown. It should be noted that the reductions of the FT magnitude for the 1st and 2nd shells were also observed for the bare electrode after 20 cycles, which could be related to the surface structural damage induced upon cycling. Structural damage of cycled bare electrodes has been confirmed based on bulk sensitive synchrotron XRD and XAS studies. Based on the combined XPS and surface sensitive electron yield XAS studies, it is confirmed that "$AlPO_4$" coating can promote the Co and Al-containing fluoride/oxyfluoride formation upon cycling, which serve to protect active particles from further side reactions with the electrolyte, reduce impedance growth and possibly prevent bulk oxygen loss as suggested by synchrotron XRD (not shown). This work has been published in Chemistry of Materials in 2009.

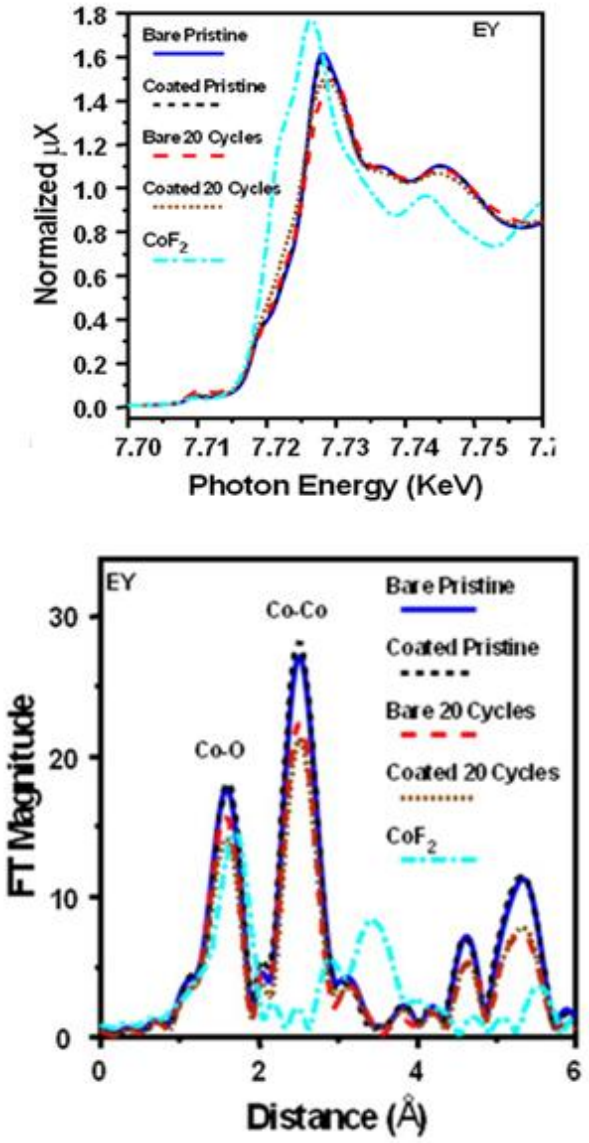

Figure V- 33: Co K-edge XANES (top) and Fourier transforms (bottom) of bare and coated $LiCoO_2$ electrodes in the pristine state and after 20 cycles .and CoF_2 reference.

Synthesis of $LiNi_{0.5}Mn_{0.5}O_2$ Material. In order to examine factors affecting the electrochemical reactivity of $LiNi_{0.5}Mn_{0.5}O_2$, a systematic study of controlling the s***ynthesis*** temperature for $LiNi_{0.5}Mn_{0.5}O_2$ was carried out. The samples were synthesized by heating an appropriate mixture of Li_2CO_3 and $NiMnO_3$ at 10°C/min to 900, 950, and 1000°C, holding at these temperatures for 30 min, and then quenching to room temperature. The samples after the annealing step at 700°C exhibit very good capability at room temperature and very high rate capability at 55°C (~210 mAh/g at 1 C and ~185 mAh/g at 8 C), as shown in Figure V- 34.

The electronic and local structures of Ni and Mn for $LiNi_{0.5}Mn_{0.5}O_2$ synthesized at these temperatures were

examined by X-ray absorption spectroscopy at the Ni and Mn K-edge. A comparison of normalized XANES spectra of the $LiN_{0.5}Mn_{0.5}O_2$ synthesized at 900, 950, and 1000°C with those of NiO and Li_2MnO_3 (not shown) confirmed that Ni is present as Ni^{2+} and Mn as Mn^{4+} regardless of the synthesis temperature. Quantitative analysis of EXAFS spectra and Fourier transforms for the 1st and 2nd coordination shells revealed the following results, which are summarized in Table V-2. The 1st shell coordination number for Mn-O and Ni-O was constrained to equal 6 for an octahedral coordination based on the pre-edge signature in the XANES data. The 2nd shell coordination number was refined to explore the effect of synthesis temperature on cation distribution/disorder. The interatomic distances of Ni-O and Mn-O are approximately 2.07 Å and 1.91 Å respectively, which are comparable to those of the reference materials (2.09 Å for NiO and 1.90 Å for Li_2MnO_3). In addition, the Mn-Ni/Mn coordination number is close to 6 indicating no significant Ni or Mn is residing in Li sites closest to Mn, regardless of the synthesis temperature. However, the Ni-Mn/Ni coordination number is clearly greater than 6 indicating that some Ni or Mn is residing in Li sites closest to Ni. Clearly, as for Ni, a high degree of cation disorder is recognized for all synthesis temperatures. The fact that the Ni-Mn/Ni distance is greater than the Mn-Ni/Mn distance suggests that Ni rather than Mn is most likely to reside in lithium sites and is responsible for cation disorder in the material. This is consistent with the fact that ionic radius for Li^+ is closer to that of Ni^{2+} but is significantly larger than that of Mn^{4+}.

Table V-2: Summary of coordination number (N), distance (R) and disorder (σ^2) for the first and second coordination spheres of Mn and Ni in $LiNi_{0.5}Mn_{0.5}O_2$ as a function of quenching temperature

Quench Temp.	X-Y pair	N	R (Å)	σ^2 (10^{-3}Å^2)
1000°C	Mn-O	6	1.912(4)	3.4(3)
	Mn-Ni	6.4(5)	2.889(5)	6.1(5)
	Ni-O	6	2.062(9)	5.7(7)
	Ni-Mn	7.4(7)	2.937(7)	6.6(8)
950°C	Mn-O	6	1.910(5)	2.4(3)
	Mn-Ni	5.6(5)	2.895(6)	4.3(6)
	Ni-O	6	2.072(6)	5.6(6)
	Ni-Mn	7.8(6)	2.947(5)	7.2(6)
900°C	Mn-O	6	1.912(3)	2.7(3)
	Mn-Ni	6.4(4)	2.884(4)	5.2(4)
	Ni-O	6	2.078(7)	5.1(6)
	Ni-Mn	7.8(6)	2.939(6)	6.9(7)

.

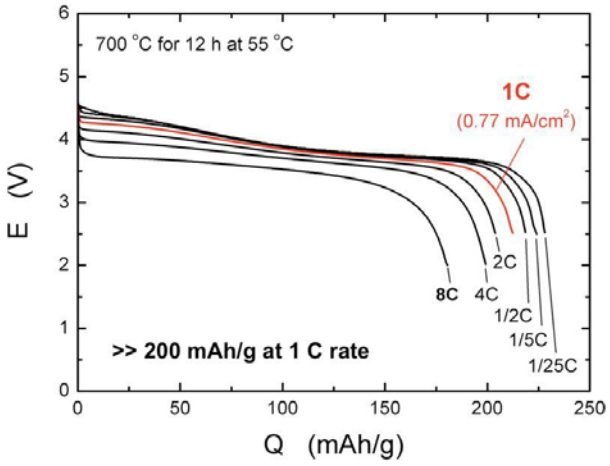

Figure V- 34: Rate capability measurements based on a two-electrode cell.

High-Energy and Power $LiNi_{0.5}Mn_{0.5}O_2$ Cathode. We have used XPS to investigate changes in the surface chemistry of $LiNi_{0.5}Mn_{0.5}O_2$ under different processing and cycling conditions. Changes in the oxidation states and local structures of Ni and Mn, as a function of these heat-treatment and cycling conditions, were also examined by XAS. The XAS measurements were conducted in the transmission (bulk sensitive) and electron yield (surface sensitivity) modes. $LiNi_{0.5}Mn_{0.5}O_2$ from a 1000°C quench followed by a 12hr anneal at 700°C, was tested as a function of the upper potential cutoff value. These electrodes were cycled twenty times at the C/20 rate from 2.5V up to a cutoff value of 4.2, 4.6, and 5.0V with a 2hr hold at the upper voltage limit. Cycled electrodes in the discharge state were analyzed by XPS and XAS. The electron-yield XANES spectra presented in Figure V- 35 show some reduction of Mn takes place in the near surface region upon cycling to high voltage. The degree of reduction appears to increase with increase in the upper voltage limit. The Mn reduction is consistent with the reduction in the amplitude of Fourier transforms (not shown), which could be due to the Jahn-Teller distortion of Mn(III).

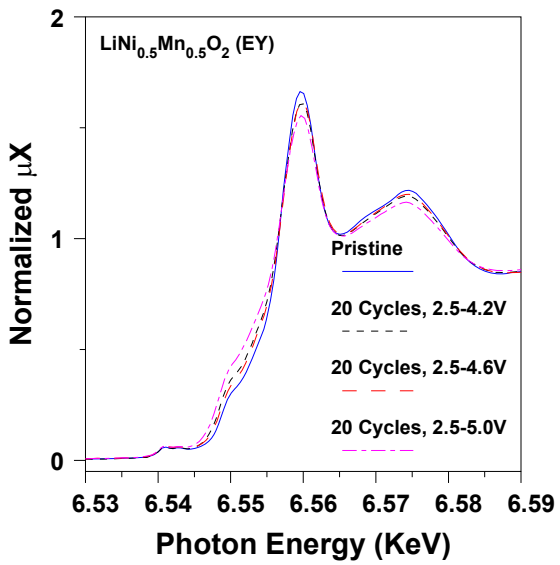

Figure V- 35: Electron yield Mn K-edge XANES for $LiNi_{0.5}Mn_{0.5}O_2$ after 20 cycles to 4.2, 3.6, and 5.0 V.

On the other hand, the Ni K-edge XANES (not shown) indicates that the oxidation state of Ni remains relatively unchanged in the bulk as well as the near surface region regardless of the upper voltage limit. This result suggests that surface Mn^{4+} ions of $LiNi_{0.5}Mn_{0.5}O_2$ may be reduced to Mn^{3+} upon high-voltage cycling. Furthermore, XPS (not shown) revealed that Mn and Ni-containing fluorides were formed on the cycled $LiNi_{0.5}Mn_{0.5}O_2$ electrodes and the surface Mn/Ni ratio is much greater than unity, which implies greater degree of Mn dissolution. Combining XAS and XPS, it is suggested that Ni is relatively stable (less changes of valance state and smaller degree of dissolution) upon cycling compared to Mn.

Conclusions and Future Directions

We used a number of analytical tools such as XPS, XAS, XRD, and STEM to probe the origin of surface instability of Li_xCoO_2 and the enhanced stability associated with "$AlPO_4$" surface coating. We found that surface coating promotes the formation of surface Co-Al-O-F oxyfluorides. These oxyfluorides reduce the amount of resistant surface organic species and LiF, and reduce further Co dissolution and bulk oxygen loss, and thus, lead to enhanced capacity retention during cycling to high voltages.

XPS, XAS, XRD, and STEM were used to probe the effects of synthesis conditions and surface chemistry of on the cycling performance and rate capability of $LiNi_{0.5}Mn_{0.5}O_2$ electrodes. We found that the valence states and local environments for Ni and Mn for $LiNi_{0.5}Mn_{0.5}O_2$ powders are 2+ and 4+, respectively, regardless of quenching at 900, 950, or 1000°C. However, non-uniform in-plane cation distribution was confirmed and is mostly due to Ni residing in lithium sites. Annealed $LiNi_{0.5}Mn_{0.5}O_2$ has much improved capacity retention and rate capability relative to quenched $LiNi_{0.5}Mn_{0.5}O_2$. Electron yield XAS of electrodes confirmed the formation of trivalent Mn upon cycling to 4.6 and 5.0 V. XPS confirmed the formation of Mn and Ni-containing fluorides on the cycled $LiNi_{0.5}Mn_{0.5}O_2$ surface and Mn/Ni ratio is much greater than unity, which suggests larger degree of Mn-dissolution occurred upon cycling.

Our future directions include the following:

- developing angle resolved X-ray photoelectron spectroscopy (ARXPS) to study the surface chemistry of $LiNi_{0.5}Mn_{0.5}O_2$ and $LiCoO_2$ as a function of depth from surface (March 2010)
- applying the fundamental understanding in the relationship between the surface chemistry of $LiNi_{0.5}Mn_{0.5}O_2$ and $LiCoO_2$ and cycle characteristics to design stable surfaces of cycled high-energy cathodes including $LiNi_xMn_xCo_{1-2x}O_2$ (September 2010).

FY2009 Publications/Presentations

Publications

1. Appapillai, A., A. Mansour, J. Cho and Y. Shao-Horn, Microstructure of "$LiCoO_2$" with and without "$AlPO_4$" nanoparticle coating: Combined STEM and XPS Studies, Chem. Mat., 19, 5748-5757 (2007).
2. Yabuuchi N., Y.T. Kim, H.H. Li and Y. Shao-Horn, Structural Instability of $Li_xNi_{0.5}Mn_{0.5}O_2$ upon Heating: An In-Situ Synchrotron X-ray Diffraction Study, Chem. Mat., 20, 4936-3951 (2008).
3. Y.C. Lu, A.N. Mansour. N. Yabuuchi and Y. Shao-Horn, Probing the Origin of Enhanced Stability of "$AlPO_4$" Nanoparticle Coated $LiCoO_2$ during Cycling to High Voltages: An XPS study, Chem. Mat., 21, 4408-4424 (2009).
4. Yabuuchi, N., Y.C. Lu, A. N. Mansour, T. Kawaguchi and Y. Shao-Horn, The Role of Surface Chemistry on the Electrochemical Reactivity of $LiNi_{0.5}Mn_{0.5}O_2$ in Lithium Cells, submitted to Chemistry of Materials (2009).

Presentations

1. Y.-C. Lu, N. Yabuuchi, A. Mansour and Y. Shao-Horn, The Origin of Enhanced Stability of "$AlPO_4$"-Nanoparticle Coated $LiCoO_2$ During Cycling, Abs. No 379, 2008 International Meeting for Lithium Batteries (IMLB2008), Tianjin, China. Jun 22-27 (2008).
2. N. Yabuuchi and Y. Shao-Horn, The Role of Cation Ordering and Segregation in $LiNi_{0.5}Mn_{0.5}O_2$ on the Electrochemical Reactivity, Abs. No 380, 2008

International Meeting for Lithium Batteries (IMLB2008), Tianjin, China. Jun 22-27 (2008).
3. N. Yabuuchi, Y.-T. Kim, H. H. Li and Y. Shao-Horn, Thermal Instability of $Li_xNi_{0.5}Mn_{0.5}O_2$ Electrodes: An In-Situ Synchrotron X-ray Powder Diffraction Study, Abs. No 384, 2008 International Meeting for Lithium Batteries (IMLB2008), Tianjin, China. Jun 22-27 (2008).
4. N. Yabuuchi and Y. Shao-Horn, The Role of Cation Ordering and Segregation in $LiNi_{0.5}Mn_{0.5}O_2$ on the Electrochemical Reactivity, Abs. No 578, 213th Meeting of The Electrochemical Society, Honolulu, HI, Oct 12-18 (2008).
5. Shao-Horn et al., Lithium Reactivity and Stability of $Li_xNi_{0.5}Mn_{0.5}O_2$, invited talk, 2008 International Meeting for Lithium Batteries (IMLB2008), Tianjin, China. Jun 22-27 (2008).

V.B.8 Characterization of New Cathode Materials using Synchrotron-based X-ray Techniques and the Studies of Li-Air Batteries (BNL)

Xiao-Qing Yang
Kyung-Wan Nam
Hung-Sui Lee
Xiaojian Wang
Brookhaven National Laboratory
P.O. Box 5000
Upton, NY 11973-5000
Phone: (631) 344-3663; Fax: (631) 344-5815
E-mail: xyang@bnl.gov

Start Date: October 1, 1997
Projected End Date: September 30, 2011

Objectives

- Develop new diagnostic techniques with ability to distinguish bulk and surface processes, to monitor the degradation processes, to determine the effects of structural changes of electrode materials, the interfacial phenomena, and electrolyte decomposition on the cell capacity and power fading, as well as on the abuse tolerance for safety related issues
- Use diagnostic techniques to evaluate and screen new materials and components aimed to improve the performance, calendar and cycling life, and the abuse tolerance of lithium batteries for HEVs, PHEVs, and EVs.

Approach

- In-situ X-ray diffraction (XRD) for structural changes during cycling.
- In situ X-ray absorption (XAS) for oxidation state and local structural change study
- Soft X-ray XAS with the capability to distinguish the bulk and surface processes of electrode materials during cycling.
- Time resolved XRD during heating for thermal stability study.

Results

Transition metal substituted $LiFe_{1-x}M_xPO_4$ (M=Mn, Co, Ni) cathode materials. Through collaborative studies with Dr. Zaghib at Hydro Quebec and Prof. H. Huang's at the Institute of Physics, Chinese Academy of Sciences, $LiFePO_4$ materials doped with multi transition metal elements have been studied by *in situ* XRD and absorption techniques. Due to the higher voltage plateaus from Mn, Co, and Ni doping, these materials are good candidates as cathode materials for high energy density lithium-ion batteries for PHEVs. Figure V- 36 (a) shows the first charge profile of C-$Li_{1-x}Mn_{0.5}Fe_{0.5}PO_4$ during *in situ* XAS experiments using a slow rate (i.e., C/20 based on theoretical capacity of $168mAhg^{-1}$), which is close to the quasi-equilibrium state. The lithium composition, x in C-$Li_{1-x}Mn_{0.5}Fe_{0.5}PO_4$, was calculated from the elapsed time, current, and mass of the active material in the cathode, by assuming that all the current passed was due to lithium extraction reaction. Two voltage plateaus at around 3.6 and 4.2V marked as I and II are observed in the charge profile. The metal K-edge XAS near edge structure (XANES) spectroscopy is a useful tool in tracking the oxidation states of each element. For each transition metal element, a main edge shift to a higher energy position in its K-edge XANES spectra indicates an increase in the average oxidation state. Therefore, *in situ* XANES spectra was used to study the charge compensation mechanism of these two voltage plateaus and the results at Fe and Mn K-edges are shown in Figure V- 36 (b) and (c). Composition change (Δx) in C-$Li_{1-x}Mn_{0.5}Fe_{0.5}PO_4$ during each scan was ~ 0.01. Figure V- 36 (b) and (c) clearly show that the edge shifts toward higher energy takes place mainly in the Fe K-edge during the first plateau, while the shifts in the Mn K-edge relayed in the second plateau. In the first plateau (I) region at ~3.6V, most of Fe K-edge shift occurs, and then Mn K-edge shifts take over in the second plateau (II) region at ~ 4.2V. Therefore, two voltage plateaus around 3.6 and 4.2V during the first charge are mainly originated from the redox reactions of Fe^{2+}/Fe^{3+} and Mn^{2+}/Mn^{3+}, respectively. This result agrees well with previous *ex situ* XAS studies. However, there are two new interesting findings here. The first one is the existence of two single isosbestic points (marked as red arrows in the insets of Figure V- 36 (b) and (c)) in some Fe and Mn K-edge XANES spectra. The second one is the existence of a narrow composition range (i.e., $\sim 0.4 \leq x \leq \sim 0.5$) where both of the Fe^{2+}/Fe^{3+} and Mn^{2+}/Mn^{3+} redox reactions take place simultaneously.

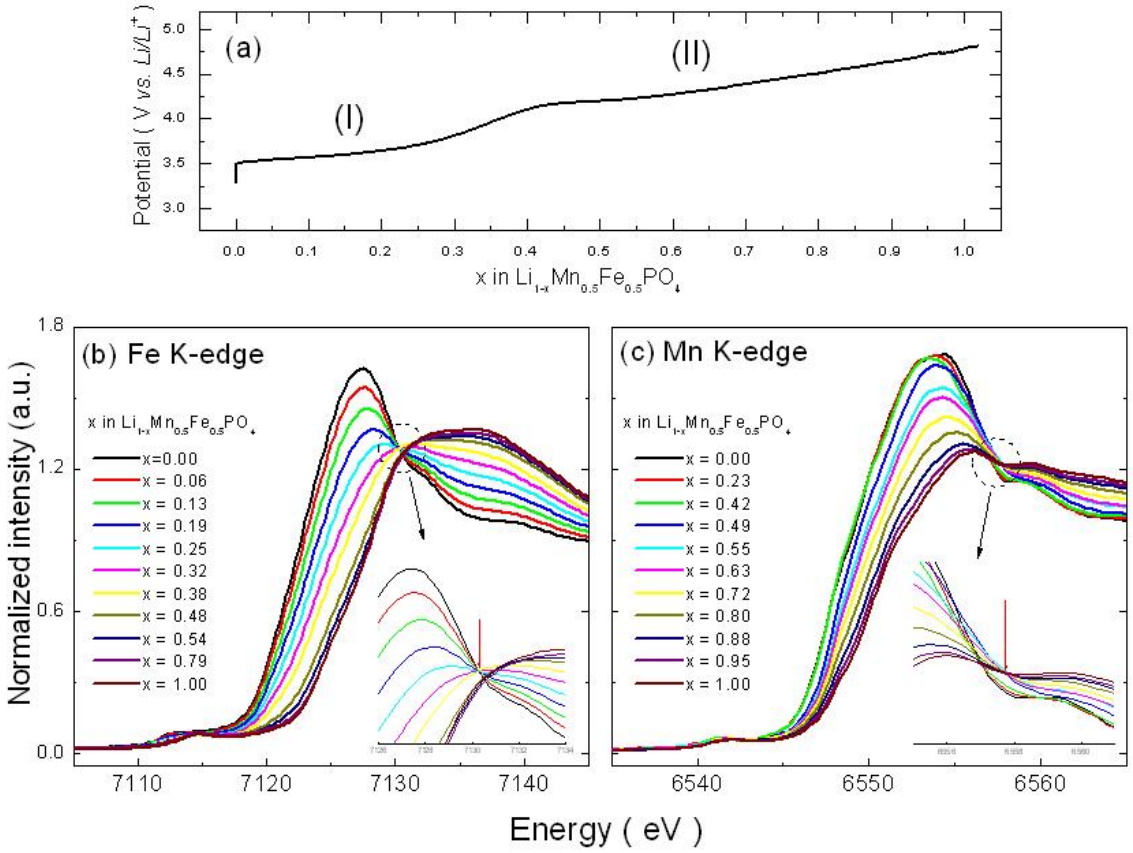

Figure V- 36: (a) First charge curves of C-LiFe$_{0.5}$Mn$_{0.5}$PO$_4$ cathode at a C/20 rate and corresponding *in situ* (b) Fe and (c) Mn K-edge XANES spectra.

The spectra with the composition ranges of 0.00≤x≤ 0.38 for Fe K-edge and 0.49≤x≤ 1.00 for Mn K-edge have single isosbestic points at ~ 7130 and ~ 6558eV, respectively. The presence of an isosbestic point indicates that only two species with changing ratios of their concentration in the mixture contribute to the absorption around the isosbestic point. The normalized Fe and Mn K-edge spectra with an isosbestic point were fitted using principal component analysis (PCA). The spectra for two end members of $Li_{1.00}Mn_{0.5}Fe_{0.5}PO_4$ and $Li_{0.62}Mn_{0.5}Fe_{0.5}PO_4$ (i.e., x=0.00 and 0.38) were used for Fe K-edge spectra fitting whereas the spectra for the $Li_{0.51}Mn_{0.5}Fe_{0.5}PO_4$ and $Li_{0.00}Mn_{0.5}Fe_{0.5}PO_4$ (i.e., x=0.49 and 1.00) were used for Mn K-edge spectra fitting. As shown in Figure V- 37 (a) and (b), excellent fits could be obtained using linear combinations of the spectra for end members at each edge. For example, a PCA result for the Mn K-edge spectrum of $Li_{0.28}Mn_{0.5}Fe_{0.5}PO_4$ (i.e., x=0.72) shown in Figure V- 37 (a) reveals that the observed spectrum is composed of 53% of $Li_{0.51}Mn_{0.5}Fe_{0.5}PO_4$ and 47% of $Li_{0.00}Mn_{0.5}Fe_{0.5}PO_4$. Assuming the ideal two-phase reaction between $Li_{1.00}Mn_{0.5}Fe_{0.5}PO_4$ and $Li_{0.62}Mn_{0.5}Fe_{0.5}PO_4$ within the range of 0.00≤x≤0.38, the theoretical slope for Fe K-edge PCA in Figure V- 37 (b) should be 2.63 (i.e., 1/Δx where Δx=0.38), and this in an excellent agreement with the slope of 2.68 obtained by linear fitting of the PCA results (Figure V- 37 (b)). Likewise, the observed slope of 1.93 for fitting of the Mn K-edge PCA results is also very close to the theoretical value of 1.96 for the ideal two-phase reaction between $Li_{0.51}Mn_{0.5}Fe_{0.5}PO_4$ and $Li_{0.00}Mn_{0.5}Fe_{0.5}PO_4$ (Δx=0.51). The above results and analysis strongly suggest that lithium extraction from C-$Li_{1-x}Mn_{0.5}Fe_{0.5}PO_4$ in the lithium composition ranges of 0.00≤ x≤ 0.38 for Fe^{2+}/Fe^{3+} and of 0.49≤x≤1.00 for Mn^{2+}/Mn^{3+} proceed through a two-phase reaction (i.e., 1st order phase transition).

It should be noted that there is an intermediate region between these two two-phase regions with a narrow composition range of ~0.4≤x≤~0.5 (marked as a boxed region in Figure V- 37 (b)). This region covers from the latter part of the sloppy region in-between two voltage plateaus to the beginning of the second voltage plateau in the charge curve. Interestingly, the simultaneous redox reactions of Fe^{2+}/Fe^{3+} and Mn^{2+}/Mn^{3+} occurs in this region as evidenced by the clear edge shift between the Fe K-edge spectra x=0.62 and x=0.52 (Figure V- 36 (b)) and the Mn K-edge spectra x=0.58 and x=0.51 (Figure V- 36 (c)). In addition, the Fe and Mn K-edge spectra corresponding to

this region do not have a single isosbestic point as shown in the insets of Figure V- 36 (b) and (c), which suggests that the two-phase reaction is no longer valid in this region. Based on the *in situ* XANES results, the lithium extraction in this intermediate region seems to proceed through other reaction mechanism rather than the two-phase reaction mechanism.

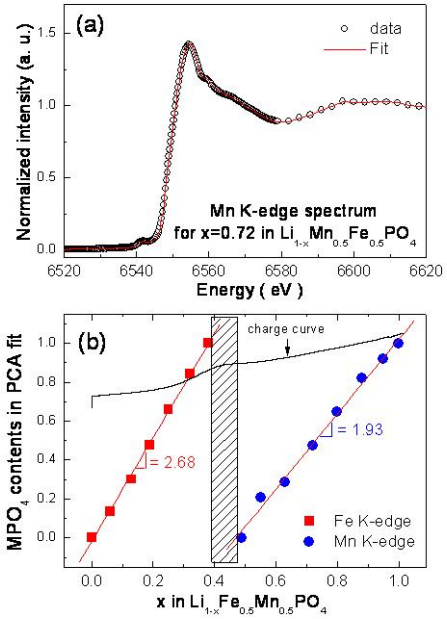

Figure V- 37: (a) Fit of a normalized Mn K-edge spectrum of charged C-$LiFe_{0.5}Mn_{0.5}PO_4$ cathode. The spectrum was fitted using a linear combination of the spectra of the two end members: 53% of $Li_{0.51}Mn_{0.5}Fe_{0.5}PO_4$ contribution and 47% of $Li_{0.00}Mn_{0.5}Fe_{0.5}PO_4$ contribution (b) Variations of MPO_4 ratio in PCA fit as a function of *x*.

In order to study the lithium extraction mechanism in more detail, the structural changes of C-$Li_{1-x}Mn_{0.5}Fe_{0.5}PO_4$ are monitored using *in situ* XRD. Selected *in situ* XRD patterns collected at a C/20 rate during the first charge are shown in Figure V- 38. The charge profile showed almost identical features to that shown in Figure V- 37 (a). The patterns include two 2θ angle ranges with three Brag peaks (indexed based on orthorhombic unit cell with *Pnma* space group): (200), (020) and (301). The corresponding Li composition x in C-$Li_{1-x}Mn_{0.5}Fe_{0.5}PO_4$ is marked beside each pattern. The composition change (Δx) for collecting subsequent diffraction pattern is less than 0.01. The structure marked as *phase 1* is for C-$Li_{1-x}Mn_{0.5}Fe_{0.5}PO_4$ before charge showing the same olivine-structured phase as uncharged $LiFePO_4$. However, upon charging (i.e., lithium extraction), the structure changes of C-$Li_{1-x}Mn_{0.5}Fe_{0.5}PO_4$ are quite different that of $LiFePO_4$. Replacing the pristine phase 1, two new olivine-like phases (i.e., *phases 2* and *3*) are observed during lithium extraction, revealing two two-phase reaction mechanisms in certain lithium composition ranges. At the early state of charge, in the composition range of $0.0 \leq x \leq 0.4$ in C-$Li_{1-x}Mn_{0.5}Fe_{0.5}PO_4$, Brag peaks of a new intermediate *phase 2* appear at slightly higher 2θ values with growing intensities and coexist with the pristine *phase 1*. The Brag peaks from both *phases 1* and *2* are very close to each other, indicating very similar lattice parameters. In the latter region ($0.5 \leq x \leq 1.0$), *phases 2* and *3* coexist and counteract. This result is agrees with the *in situ* XANES result.

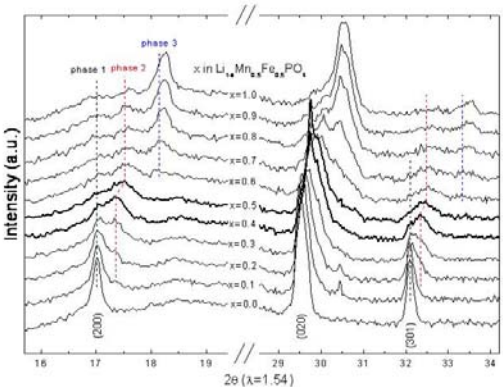

Figure V- 38: *In situ* XRD patterns of C-$LiFe_{0.5}Mn_{0.5}PO_4$ cathode during the first charge.

Investigation of the Gas-Diffusion-Electrode used as Lithium/Air Battery Cathode in Non-aqueous Electrolyte and the Importance of Carbon Material Morphology. The gas-diffusion-electrode (GDE) for Li-air battery cells has been studied in a home-made electrochemical cell. This work has focused on avoiding the passivation of the GDE caused by the deposition of reduction products. It is the first time that the importance of establishing a 3-phase electrochemical interface in non-aqueous electrolyte is demonstrated by creating air-diffusion paths and an air saturated portion for an air-cathode. A model mechanism of electrode passivation by the reaction product is also proposed.

As is well known, lithium oxides formed during O_2 reduction tend to block small pores in the GDE, preventing them from further utilization in the electrochemical reaction. On the other hand, lithium oxides would accumulate inside the large pores during the reduction until the density of oxides becomes high enough to choke-off the mass transfer. For the first time, a near linear relationship between the capacity of GDE in a non-aqueous electrolyte and the average pore diameter was demonstrated, which could be used to estimate the capacity of the GDE quantitatively.

Conventional wisdom tells us that high surface area is desirable for GDEs, but the results in Figure V- 39 indicate that the situation is not so simple. Figure V- 39A, B and C show the relationship between the O_2 reduction capacity and the surface areas of the pores with diameter larger than 5Å, 10Å and 20Å, respectively. The surface area of pores larger than 5Å can be considered as the total surface of the

carbon material, since it is the minimum pore diameter that can be measured using N_2 adsorption isotherm. No correlation can be seen between the surface areas and the discharge capacity, but the discharge capacity is strongly related to the surface area associated with certain size pore sizes. The discharge capacity decreases as the total surface area increases; and the discharge capacity also decreases as the surface area of pores larger than 10 Å increases. However, the trend reverses when the discharge capacity was plotted against the surface area associated with pores larger than 20 Å.

The hypothesis for the mechanism of this phenomenon is illustrated in Figure V- 40. Since both the O_2^{2-} and O^{2-} formed from the reduction of O_2 are insoluble in a non-aqueous electrolyte, solid Li oxides are likely formed near the reaction interface. The interface consists of not only the external surface of carbon particles but also the pore walls inside the porous matrix. The majority of solid Li oxide would be formed inside the micro-, meso-, and macro- pores as shown in Figure V- 40. In order for a GDE to function efficiently, both electrolyte and O_2 have to migrate to the reaction interface. When Li oxide particles are formed near the orifice of a micro-pore as shown in the enlarged inset in Figure V- 40, the micro-pore would be sealed and mass transfer would be blocked because the pore surface becomes inaccessible. Since micro-pores comprise most of the surface area for a carbon material with a very high total surface area, rendering them inaccessible substantially decreases O_2 reduction. The experimental results shown in Figure V- 39, support this hypothesis. On the other hand, at the early stage of O_2 reduction, the density of the Li oxides formed in the meso-pores and macro-pores was low enough to allow both O_2 and electrolyte diffusion at the interface. Since the particle size of the Li oxides was smaller than the meso- and macro-pore sizes, a substantial amount of precipitates can be accommodated in those pores without hindering mass transfer. However, Li oxides kept accumulating inside the pores as O_2 reduction continued. The density of the Li oxides in the large pores kept increasing and mass transfer through the Li oxides became more and more difficult. Eventually, the pores were blocked and the GDE ceased functioning.

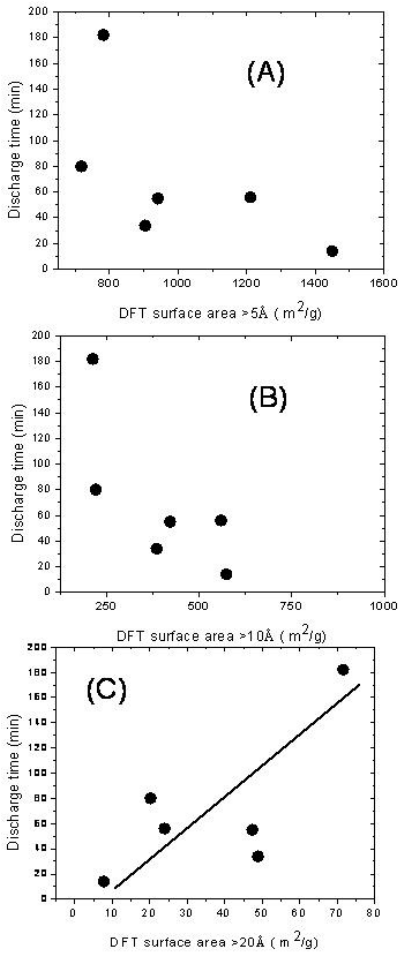

Figure V- 39: The relationship between O2 reduction capacity and DFT surface area of pores with sizes > 5 Å (A), > 10 Å (B) and > 20 Å (C).

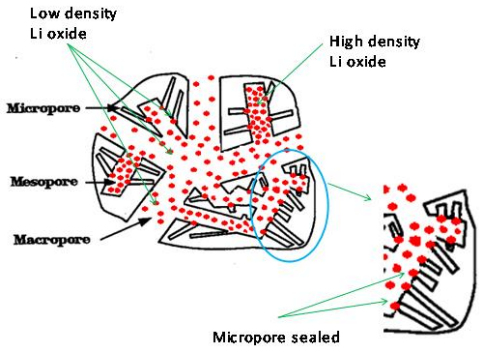

Figure V- 40: Accommodation of Li oxides in the pores of various sizes.

Figure V- 41 provides more evidence for the proposed hypothesis. The large pores in the carbon could accommodate much more Li oxide precipitates than small pores. Thus, the utilization for the surface area in the large pores was much higher than that in the small pores. In

summary, although larger surface area carbon is more desirable for a high rate air-cathode, the discharge capacity may suffer, since most of the surface area inside the smaller pores could not be utilized for O_2 reduction when they become clogged. On the other hand, Li oxides could reside in the pores with a size substantially larger than the solid particle size (for example, those with pore size larger than 20Å) of the Li oxides. The GDE ceases to function only when the density of the oxides becomes high enough to block all mass transfer. Thus the capacity of GDEs used in Li-air cells is determined by the surface area of large pores, not the surface area of total pores.

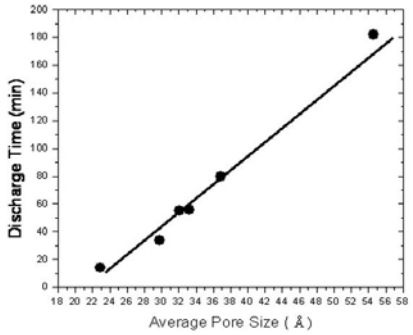

Figure V- 41: Discharge time as a function of average pore diameter.

FY 2009 Publications/Presentations

1. Kyung-Wan Nam, Xiao-Jian Wang, Won-Sub Yoon, Hong Li, Xuejie Huang, and Xiao-Qing Yang, "*In situ* X-ray absorption and diffraction studies of carbon coated $LiFe_{1/4}Mn_{1/4}Co_{1/4}Ni_{1/4}PO_4$ cathode during first charge", *Electrochemistry Communications* Vol. 11, Iss. 4, pp 913-916 (2009).
2. Kyung-Wan Nam, Won-Sub Yoon, Kyung-Yoon Chung, Seungdon Choi and Xiao-Qing Yang, "Structural changes and thermal stability of charged $LiCo_{1/3}Ni_{1/3}Mn_{1/3}O_2$ Cathode material for Li-ion batteries studied by time-resulted XRD", *Journal of Power Sources*, Vol. 189, Iss. 1, pp 515-518 (2009).
3. Kyung-Wan Nam, Won-Sub Yoon, and Xiao-Qing Yang, "*In situ* XRD Studies of Li-ion Cells with Mixed $LiMn_2O_4$ and $LiCo_{1/3}Ni_{1/3}Mn_{1/3}O_2$ Composite Cathode", *Journal of Power Sources* Vol. 192, Iss. 2, pp 652-659 (2009).
4. L. F. Li, B. Xie, H. S. Lee, H. Li, X. Q. Yang, J. McBreen, and X. J. Huang, "Lewis acid additives for Li-ion batteries", *Journal of Power Sources*, Vol. 189, Iss. 1, pp 539-542 (2009).
5. Sang-Bok Ma, Kyung-Wan Nam, Won-Sub Yoon, Seong-Min Bak, Xiao-Qing Yang, Kwang-Bum Kim, "Nano-Sized Lithium Manganese Oxide Dispersed on Carbon Nanotubes for Energy Storage Applications", *Electrochemistry Communications*, Vol. 11, Iss. 8, pp 1575-1578 (2009).
6. Kyung-Wan Nam, Won-Sub Yoon, Kyung-Yoon Chung, and Xiao-Qing Yang, "The phase transition behaviors of $Li_{1-x}Mn_{0.5}Fe_{0.5}PO_4$ during lithium extraction studied by in situ X-ray absorption and diffraction techniques", accepted, *Electrochemistry Communications* (2009)
7. L. F. Li, H. S. Lee, H. Li, X. Q. Yang, and X. J. Huang, "A Pentrafluorophenylboron oxalate Additive in Nonaqueous Electrolytes for Lithium Batteries", submitted to *Electrochemistry Communications* (2009)

Invited presentations

1. X. Q. Yang, X. Wang W-S. Yoon, K. W. Nam, H.S. Lee, J. McBreen, K.zaghib, H. Li, X. Huang, and L. Chen, "Electronic and Crystal Structural change Studies of $LiMPO_4$ (M=Fe, Mn. Co Ni) Cathode Materials during Lithium Intercalation and De-intercalation", **Invited**, presented at the 214th Meeting of the Electrochemical Society, Honolulu, Hawaii, October 12-17, 2008
2. X. Q. Yang, H. S. Lee, W. S. Yoon, K. W. Nam, X. Wang, J. McBreen, Bin Xie, Lifei Li, Hong Li, X. Huang, L. Chen, "New Electrolyte Systems Using LiF, Li_2O or Li_2O_2 with Boron-Based Lewis Acids as Additives and Their Application in High Voltage Lithium-ion Batteries". **Invited**, presented at "Lithium Mobile Power 2008 Meeting", Las Vegas, Nevada, December 8-9, 2008
3. X. Q. Yang, K. W. Nam, X.J. Wang, Y.N. Zhou, H. S. Lee, O. Haas, L. Wu, and Y. Zhu, K. Y. Chung and B. W. Cho, Hong Li, Xuejie Huang and Liquan Chen "Using Synchrotron Based in situ X-ray Techniques and Transmission Electron Microscopy to Study Electrode Materials for Lithium Batteries" **Invited**, Presented at The 4th Southern China Li-ion Battery Top Forum (CLTF2009), May 24-26, 2009, Shenzhen, China
4. X. Q. Yang, X. J. Wang, B. Zhang, K. W. Nam, Y. N. Zhou, J.M. Bai, O. Haas, H. Li, X. J. Huang, "Structural Changes of Nano-sized $LiFePO_4$-$LiMnPO_4$ Solid Solutions Studied by In-situ XRD" **Invited**, presented at The 2009 International Workshop on Nano Materials and Nano Devices, July 2-5, 2009, Beijing, China
5. X. Q. Yang, K. W. Nam, X. J. Wang, Y. N. Zhou, H.S. Lee, O. Haas, L. Wu, and Y. Zhu, "Lithium Battery Research for Vehicle Technology at Brookhaven National Lab." **Invited**, presented at The international Electric Vehicle Power Battery and Motor Seminar, Beijing, China, July 8-9, 2009, Beijing, China
6. X. Q. Yang, K. W. Nam, H.S. Lee, and J. McBreen, "Lithium Batteries—The next Generation of Power Source for Vehicles" **Invited**, presented at The 5th IEEE Vehicle Power and Propulsion Conference

(VPPC'09), September 7-11, 2009, Dearborn, MI 48128

7. Won-Sub Yoon, Kisuk Kang, Yun-Sung Lee, Kyung-Wan Nam, Xiao-Qing Yang, "Thermal Behavior of charged Cathode Materials Studied by X-ray Diffraction and Absorption Techniques", **Invited**, presented at The 60th Annual Meeting of the International Society of Electrochemistry, August 16-21, 2009, Beijing, China.

V.B.9 Layered Cathode Materials (ANL)

Michael Thackeray

Argonne National Laboratory
9700 South Cass Avenue
Argonne, IL 60439
Phone : (630) 252-9184 ; Fax : (630) 252-4176
E-mail: thackeray@anl.gov

Collaborators:

ANL: S.-H. Kang, C. S. Johnson, R. Benedek, C. Lopez
Northwestern University: C. Wolverton, D. Shin

Start Date: October 1, 2008

Projected End Date: September 30, 2011

Objectives

Design high capacity, high-power and low cost cathodes for PHEVs and EVs

- Improve the design, composition and performance of high capacity (>200 mAh/g) Mn-based cathodes at an average voltage 3.5 V vs. Li^0.
- Use theoretical modeling as a guide to identify, design and understand the electrochemical properties of novel cathode structures

Technical Barriers

- Low energy density
- Poor low temperature operation
- Abuse tolerance limitations

Technical Targets (USABC - End of life)

- 142 Wh/kg, 317 W/kg (PHEV 40 mile requirement)
- Cycle life: 5,000 cycles
- Calendar life: 15 years

Accomplishments

- Synthesized and evaluated high-capacity $xLi_2MnO_3\bullet(1-x)LiMO_2$ (M=Mn, Ni, Co) electrodes against Li, C_6, and $Li_4Ti_5O_{12}$ anodes.
- Demonstrated improved rate capability of Li-Ni-PO_4-coated electrodes, which delivered rechargeable capacities of 250 mAh/g (C/11 rate); 200 mAh/g (C/1 rate) and >150 mAh/g (2.5C rate).
- Used theoretical calculations to model the surface structure, and electrochemical/dissolution phenomena of $LiMn_2O_4$ spinel electrodes.

✧ ✧ ✧ ✧ ✧

Introduction

Conventional high potential lithium-ion battery cathodes, such as layered $LiCoO_2$, spinel $LiMn_2O_4$, olivine $LiFePO_4$ and compositional variations thereof, do not deliver sufficient capacity at sufficiently high discharge rates to satisfy the 40+ mile range (energy) requirement for plug-in hybrid-electric vehicles (PHEVs). These electrode materials typically deliver capacities of 100–160 mAh/g between 4.2 and 2.5 V. Considerable progress has been made to increase the capacity of layered electrode systems to 240–250 mAh/g by using Li_2MnO_3-stabilized layered electrodes that can be represented in two-component notation as $xLi_2MnO_3\bullet(1-x)LiMO_2$ (M = Mn, Ni, Co), in which the close-packed Li_2MnO_3 and $LiMO_2$ components are structurally integrated in a highly-complex manner.

In response to calls from industry to increase the rate capability of these high capacity $xLi_2MnO_3\bullet(1-x)LiMO_2$ cathodes for PHEV applications as well as for portable electronic equipment and power tools, we have explored the possibility of protecting the electrode particle surface with a lithium–nickel–phosphate layer. Our study was motivated by the notion that a Li–Ni–PO_4 layer comprised either of olivine $LiNiPO_4$ or a hypothetical defect Li_3PO_4 structure $Li_{3-2x}Ni_xPO_4$ ($0<x<1$) should, in principle, act as a stable lithium-ion conducting solid electrolyte to at least 5 V vs. Li^0.

In parallel studies, we have 1) evaluated the electrochemical performance of $xLi_2MnO_3\bullet(1-x)LiMO_2$ electrodes against $Li_4Ti_5O_{12}$ anodes in 2.5 V (average) Li-ion cells for HEV applications, and 2) used theory to model surface configurations as well as electrochemical and dissolution phenomena of $LiMn_2O_4$ spinel electrodes.

Approach

- Exploit the concept and optimize the performance of structurally-integrated, high-capacity electrodes such as 'layered-layered' $xLi_2MnO_3\bullet(1-x)LiMO_2$ (M=Mn, Ni, Co) electrodes.
- Extend the concept of using integrated bulk electrode structures to surface structures that protect the underlying metal oxide particles from the electrolyte, when charged at high potentials.

- Use computational modeling to aid the design of bulk and surface cathode structures and to understand electrochemical properties.

Results

Layered $xLi_2MnO_3•(1-x)LiMO_2$ Electrodes. During the initial charge, electrochemical extraction of lithium from $xLi_2MnO_3•(1-x)LiMO_2$ electrodes occurs in two steps, as shown in a compositional phase diagram in Figure V- 42. When taken to completion above 4.4 V vs. Li^0, the ideal reactions can be represented:

(1) $LiMO_2 \rightarrow MO_{2-\delta} + Li^+ + \delta/2\ O_2 + (1+2\delta)e$

(2) $Li_2MnO_3 \rightarrow MnO_2 + 2\ Li+ + O_2 + 2e$

The highly oxidizing nature of both the MO_2 and MnO_2 components can result in oxygen loss at the particle surface, particularly when M = Co and/or Ni, thereby damaging the electrode surface; electrolyte oxidation can also occur at these high potentials. These factors limit the rate at which lithium can be reinserted into the charged $xMnO_2•(1-x)MO_2$ electrodes; the electrodes also lose capacity on cycling.

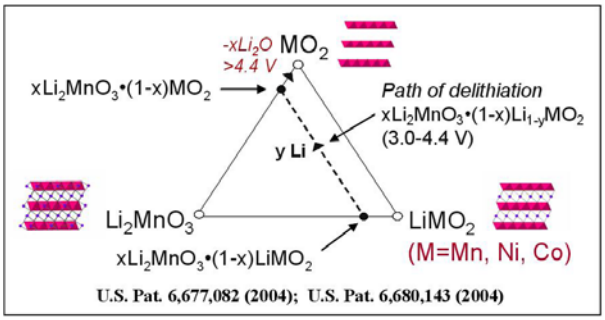

Figure V- 42: Compostional Li_2MnO_3-$LiMO_2$-MO_2 phase diagram.

Li-Ni-PO_4-Coated Electrodes. A $0.5Li_2MnO_3•0.5LiNi_{0.44}Co_{0.25}Mn_{0.31}O_2$ electrode (alternatively, $Li_{1.200}Mn_{0.524}Ni_{0.176}Co_{0.100}O_2$) with a composition of industrial interest, was selected for our investigations. The relative rate capability of untreated and Li–Ni–PO_4-treated electrodes is shown in Figure V-43. The Li–Ni–PO_4-treated electrode is significantly more tolerant to higher discharge currents than the untreated parent $0.5Li_2MnO_3•0.5LiNi_{0.44}Co_{0.25}Mn_{0.31}O_2$ electrode;

In particular, the electrode delivers a rechargeable capacity of 250 mAh/g at a C/11 rate, 225 mAh/g at a C/2 rate, and 200 mAh/g at a C/1 rate.

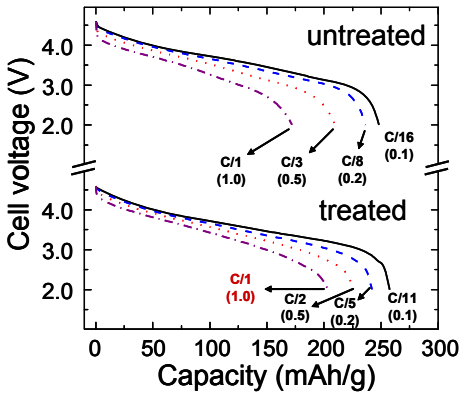

Figure V- 43: Discharge profiles of lithium half cells with untreated and Li–Ni–PO_4-treated $0.5Li_2MnO_3•0.5LiNi_{0.44}Co_{0.25}Mn_{0.31}O_2$ electrodes at various rates

Capacity vs. cycle number plots of these lithium cells, when cycled at C/11 to 2.5C rates, emphasize the superior cycling stability of the Li–Ni–PO_4-treated electrodes (Figure V- 44); such improved performance renders $0.5Li_2MnO_3•0.5LiNi_{0.44}Co_{0.25}Mn_{0.31}O_2$ electrodes attractive for other applications such as cell phones and power tools. The rechargeable capacity of 225 mAh/g at a C/2 rate was validated in a lithium-ion cell (MAG-10 graphite anode) for 40 cycles (data not shown).

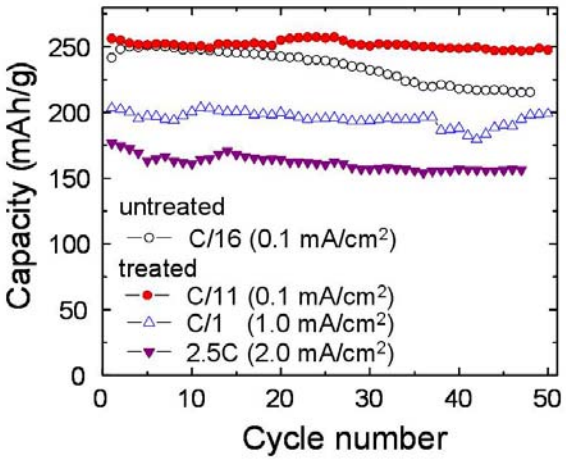

Figure V- 44: Capacity vs. cycle no. of untreated and Li–Ni–PO_4-treated $0.5Li_2MnO_3•0.5LiNi_{0.44}Co_{0.25}Mn_{0.31}O_2$ electrodes (4.6 and 2.0 V).

$Li_4Ti_5O_{12}$/$0.1Li_2MnO_3•0.9LiMn_{0.26}Ni_{0.37}Co_{0.37}O_2$ Cells. During FY09, the utility of $xLi_2MnO_3•(1-x)LiMO_2$ cathodes was also demonstrated in other Li-ion cell configurations:

- blended with spinel to compensate for rate limitations (U.S. Pat. 7,303,840 (2007)).
- used with $Li_4Ti_5O_{12}$ anodes in ~2.5 V cells

The cycling performance of a lithium-ion cell, $Li_4Ti_5O_{12}/0.1Li_2MnO_3\bullet0.9LiMn_{0.26}Ni_{0.37}Co_{0.37}O_2$, cycled between 3.0 and 1.5 V is shown in Figure V- 45.

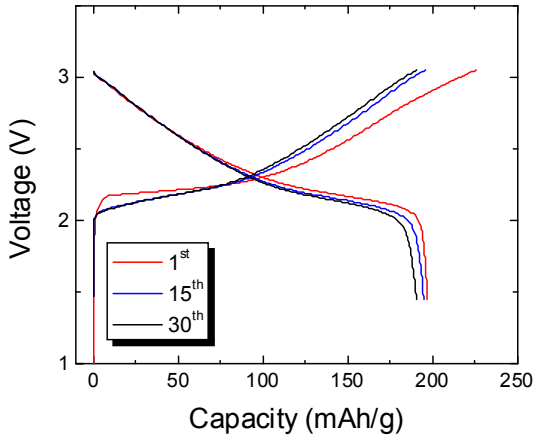

Figure V- 45: Electrochemnical cycling of $Li_4Ti_5O_{12}/ xLi_2MnO_3\bullet(1-x)LiMO_2$ (M=Mn, Ni, Co) lithium-ion cells.

The $0.1Li_2MnO_3\bullet0.9LiMn_{0.26}Ni_{0.37}Co_{0.37}O_2$ composite cathode provides a rechargeable capacity of 190-200 mAh/g and is therefore competitive to $Li_{1+x}Mn_{2-x}O_4$ spinel cathodes (theoretical capacity = 148 mAh/g for x=0) that are being coupled with $Li_4Ti_5O_{12}$ for high-power HEV batteries.

Modeling of $LiMn_2O_4$ Spinel Surfaces. Modeling of metal oxide electrode surfaces with first principles methods has been performed to elucidate the dissolution and surface structure of $LiMn_2O_4$. Calculations of *dissolution-reaction* free energy for lithium-manganese-oxide spinels, following Hunter's classic reaction for the dissolution of $LiMn_2O_4$ in acid:

$$2\ LiMn_2O_4 + 4\ H^+ \rightarrow 3\ MnO_2 + Mn^{2+} + 2\ Li^+ + 2\ H_2O,$$

were analyzed to construct a Pourbaix-like 'spinel dissolution' phase diagram (Figure V- 46). The calculated phase diagram is consistent with the experimentally-observed solubility trends of Mn^{3+} in acidic electrolytes and in Zn/MnO_2 alkaline cells (disproportionation reactions).

In addition, the low energy (111) surface of the $LiMn_2O_4$ structure was modeled, prior to and after a thermalization and quenching step, as were the effects of H_2O at the (111) surface. For these calculations, a Mn-terminated slab (84 atoms) with dimensions of ~6 x 10 x 25 Å and a Mn site occupancy = 0.5 on the termination layers was treated. Our preliminary conclusions are:

- The Mn oxidation state is ~3+ at the Mn-terminated (111) free surface or H_2O interface.
- The Mn coordination number is ~4 at the Mn-terminated (111) free surface; the Mn coordination number is ~5 at the (111) $LiMn_2O_4$ /H_2O interface.
- The O atoms at the (111) $LiMn_2O_4$ /H_2O interface rearrange to encapsulate under-coordinated Mn ions; the Li atoms are drawn in the wake of the O atoms to maintain neutrality; the three top layers form a mixed stoichiometric Li-Mn-O layer at the free surface.

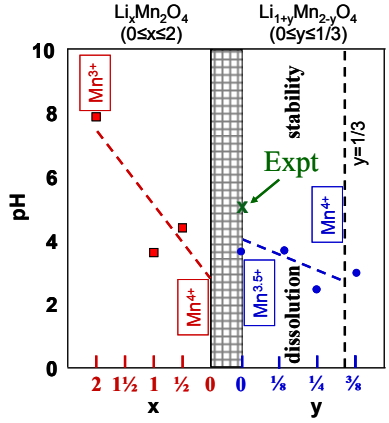

Figure V- 46: 'Spinel Dissolution' Phase Diagram

Conclusions and Future Directions

Conclusions

- Progress was made in stabilizing the surface, and improving the rate capability of high-capacity $xLi_2MnO_3\bullet(1-x)LiMO_2$ electrodes, M=Mn, Ni, Co.
- $xLi_2MnO_3\bullet(1-x)LiMO_2$ electrode materials that provide a rechargeable capacity of 200 mAh/g at C/1 rate are now also under investigation in the ABR program and have the attention of industry. The approach opens the door to fabricating new, stabilizing surface architectures and to advancing electrochemical performance.
- Theoretical modeling of the (111) surface of spinel $LiMn_2O_4$ in the absence and presence of H_2O was used to complement experiments to understand and provide direction for designing stabilized surfaces.

Future Work

- Continue to exploit and optimize $xLi_2MnO_3\bullet(1-x)LiMO_2$ electrode materials (composition and performance) with the particular goal of reaching or exceeding the energy and power goals required for 40-mile PHEVs and EVs.
- Focus on surface studies that will lead to an improved stability and rate capability of metal oxide electrodes at high potentials – continue existing, unfinished thrusts in projects.
- Model interface atomic structure and properties between electrode and protective coating materials
- Explore recently developed autogenic synthesis technique (not discussed in this report) to fabricate

novel cathode materials (optionally carbon coated in one processing step) and architectures.

FY 2009 Publications/Presentations

1. S.-H. Kang and M. M. Thackeray, J. Electrochem. Soc., **155**, A269 (2008).
2. R. Benedek and A. van de Walle, J. Electrochem. Soc., **155**, A711 (2008).
3. N. N. Shukla, S. Shukla, R. Prasad, and R. Benedek, Modeling and Simulation in Materials Science and Engineering, **16 (5)**, Article No. 055008 (2008).
4. C. S. Johnson, N. Li, C. Lefief, J. T. Vaughey and M. M. Thackeray, Chem. Mater. **20**, 6095 (2008).
5. R. Benedek, M. M. Thackeray and A. van de Walle, Chem. Mater. **20**, 5485 (2008).
6. S.-H. Kang and M. M. Thackeray, Electrochem. Comm. **11**, 748 (2009).
7. Presentation to the 2009 DOE Annual Peer Review Meeting in Washington D.C.

V.B.10 Development of High Energy Cathode (PNNL)

Ji-Guang Zhang
Pacific Northwest National Laboratory
902 Battelle Blvd., Mail Stop K3-59
Richland, WA 99352
Phone: (509) 372-6515; Fax: (509) 375-3864
E-mail: jiguang.zhang@pnl.gov

Start Date: Oct. 1, 2008
Projected End Date: December 31, 2009

Objectives

- Develop high energy cathode materials with improved safety.
- Develop a low-cost synthesis route for high-capacity cathodes.

Technical Barriers

Energy density, safety, and cost.

Technical Targets

- Synthesize and characterize olivine structured $LiMPO_4$ (M = Fe, Mn, Co, Ni) cathode materials with improved capacity and cycle-ability.
- Reduce production costs by developing a low-temperature synthesis process.

Accomplishments

The high-voltage cathode material $LiMnPO_4$ has been prepared by several approaches. The surfactant-based solid state reaction was developed to prepare olivine structured cathode materials $LiMPO_4$ (M = Fe, Mn). The effects of ball milling and carbon loading procedures on electrochemical performance of these materials were investigated. The $LiMnPO_4$ sample shows a capacity of ~132 mAh/g when discharged to 2V. Doped $LiMn_{1-x}D_xPO_4$ (e.g. $LiMn_{0.9}Fe_{0.1}PO_4$) has demonstrated a specific capacity of 168mAh/g at C/50 rate. In another effort, a cost effective process was developed to synthesize $LiMnPO_4$ from a $MnPO_4 \cdot H_2O$ precursor precipitated via a spontaneous reaction. These $MnPO_4 \cdot H_2O$ nanoplates react quickly with the lithium source and form a pure phase of $LiMnPO_4$. The samples exhibit a discharge capacity of 115mAh/g at C/20 rate.

✧ ✧ ✧ ✧ ✧

Introduction

The most widely used cathode materials in Li-ion batteries to date are based on lithium transition metal oxide such as $LiCoO_2$, $LiMn_2O_4$, and $LiNi_{1/3}Mn_{1/3}Co_{1/3}O_2$ (NMC). However, these oxide-based cathode materials may release oxygen at high voltage and lead to thermal runaway at elevated temperatures, which raises safety concerns for batteries used in PHEVs. Lithium transition-metal phosphates have attracted much attention in recent years because of their intrinsic structural stability resulted from tightly bonded oxygen in the phosphate anion. Unlike the metal-oxygen (M-O) bonds in the spinel and nickelate cathode materials, the strong P-O bond prevents oxygen release during high-voltage operation and high-temperature abuse. In recent years, nanostructured $LiFePO_4$ cathodes have been successfully used in commercial markets. Further expansion of this success to high-voltage lithium transition-metal phosphates, such as $LiMnPO_4$, can further improve both safety and energy density of Li-ion batteries.

Approach

Olivine-type $LiMnPO_4$ was synthesized using $CH_3CO_2Li \cdot 2H_2O$, metal carbonate/oxalate and $(NH_4)H_2PO_4$ precursors. The precursors were mixed and reacted by high-energy mechanical milling with surfactant for 1hr, followed by heat-treatment under H_2/Ar = 2.7%/97.5% atmosphere at ~500-600°C for 8 hrs to prevent the possible formation of M^{3+} impurities. The obtained $LiMPO_4$ (M = Fe, Mn, Co) powder was subjected to X-ray diffraction, Rietveld refinement, crystallite size, scanning electron microscopy, and high-resolution transmission electron microscopy.

Synthesized $LiMnPO_4$ was carbon coated by planetary ball milling with 20wt% Super P for 4 hours. For electrochemical evaluation, the cathode comprised of active material, Super-P and polyvinylidene fluoride (PVDF) binder, were dispersed in *N*-methylpyrrolidone (NMP) solution in a weight ratio of 80~70%:10~20%:10%, respectively. The $LiMPO_4$ (M = Fe, Mn, Co) cathode was evaluated using coin cells at room temperature. The cells were tested versus Li metal at various rates (*C*/24 to 10*C*).

Another low-cost precipitation method was developed to prepare electrochemically active $LiMnPO_4$ at low temperatures. $MnPO_4 \cdot H_2O$ nanoplates were first precipitated into yarn-ball-like secondary particles. After mixing with a lithium source and carbon, nanosized $LiMnPO_4$ particles formed, which in turn reflected the

homogenous morphology of the precursors. The synthesis parameters were optimized with the information obtained from TGA, XRD, and SEM analysis, as well as electrochemical characterizations.

Results

$LiMnPO_4$ Cathode Materials. SEM images of the synthesized $LiMnPO_4$ nanoplates with a thickness of ~50nm are shown in Figure V- 47. TEM images of $LiMnPO_4$ are shown in Figure V- 48(a). The Li-ion diffusion in olivine is via [010] direction. Therefore, TEM images were taken perpendicular to the $LiMnPO_4$ nanoplates. The diffraction pattern shown in Figure V-48(b) is the same throughout the particles, indicating preferred orientation of $LiMnPO_4$ growth. However, the [010] direction is along the plates with the longest particle lengths.

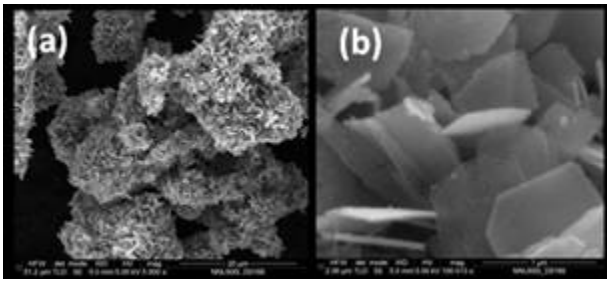

Figure V- 47: SEM images of $LiMnPO_4$ nanoplates

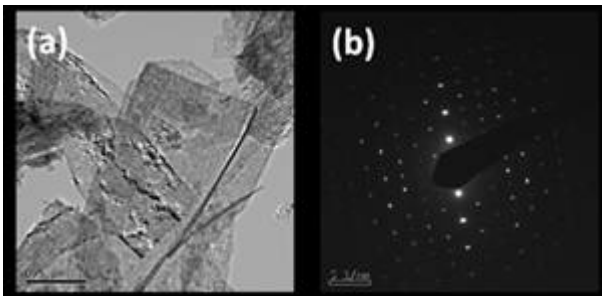

Figure V- 48: TEM images (a) and diffraction pattern (b) of $LiMnPO_4$ synthesized at 550°C under 3%H_2-97%Ar atmosphere

Figure V- 49 shows the specific capacity of $LiMnPO_4$ at various C rates. A specific capacity of 132mAh/g was obtained from $LiMnPO_4$ at C/24 rate. Cycling performance of $LiFePO_4$ and $LiMnPO_4$ at various measured C rates is shown in Figure V- 50. Stable cycling behaviors were obtained for both cathodes.

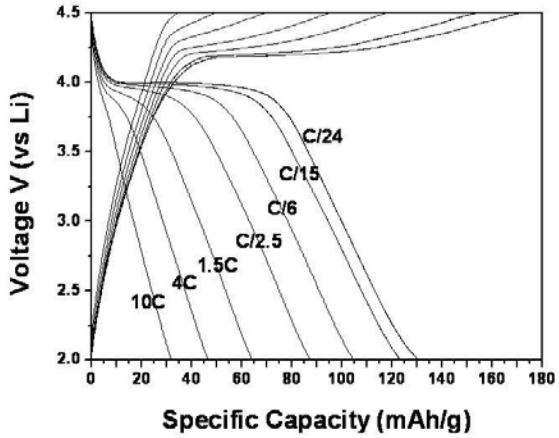

Figure V- 49: Voltage profiles of LiMnPO4 at various measured C rates

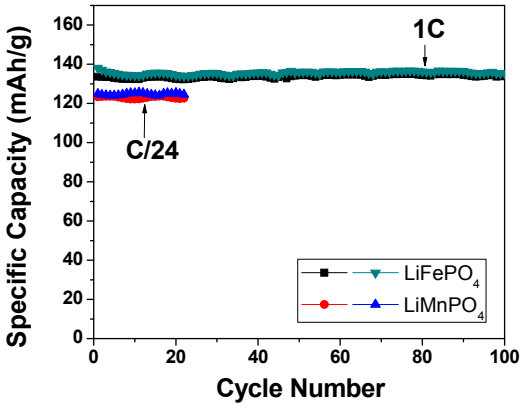

Figure V- 50: Cycling performance $LiFePO_4$ and $LiMnPO_4$ at various measured C rates

Doped Olivine $LiMn_{1-x}D_xPO_4$ (D = Fe, V, Co) Cathode Materials. Doped $LiMn_{1-x}D_xPO_4$ cathode materials were further investigated, where 10% Mn in $LiMnPO_4$ was replaced by Fe, V, or Co. Figure V- 51 shows the voltage profile of $LiMn_{0.9}Fe_{0.1}PO_4$ cycled at C/50 rate. A specific capacity of 168mAh/g was achieved.

$LiMnPO_4$ Prepared by a Low-Temperature Precipitation Method. A novel precipitation method has been developed to prepare electrochemically active $LiMnPO_4$. $LiMnPO_4$ was synthesized from a $MnPO_4 \cdot H_2O$ precursor precipitated via a spontaneous reaction. These $MnPO_4 \cdot H_2O$ nanoplates reacted quickly with the lithium source to form a pure phase of $LiMnPO_4$ with favorable electrochemical properties. Thermogravimetric analysis (TGA) was used to determine the optimum synthesis temperature. We found that the crystallization of $LiMnPO_4$ occurs before 438°C. When the synthesis temperature decreases to 350°C, the particle size of the $LiMnPO_4$ is reduced to 10-50 nm, as shown in Figure V- 52. The reversible capacity of the samples prepared at 350°C is 90

mAh g^{-1}. After full nucleation at 550°C, the samples exhibit a discharge capacity of 115 mAh g^{-1} (C/20 rate, 2.5 to 4.4 V) in the first cycle, as shown in Figure V- 53. The Coulombic efficiency is maintained at near 100 percent after the first few cycles. Further improvement of this precipitation method may lead to a cost-effective approach for manufacturing high-performance $LiMnPO_4$ cathode material.

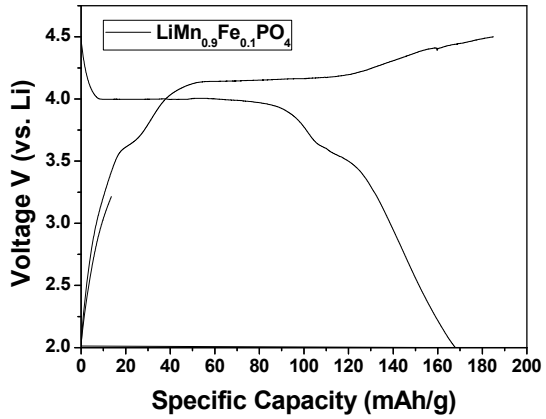

Figure V- 51: (a) XRD pattern and (b) voltage profile of $LiMn_{0.9}Fe_{0.1}PO_4$ at C/50 rate

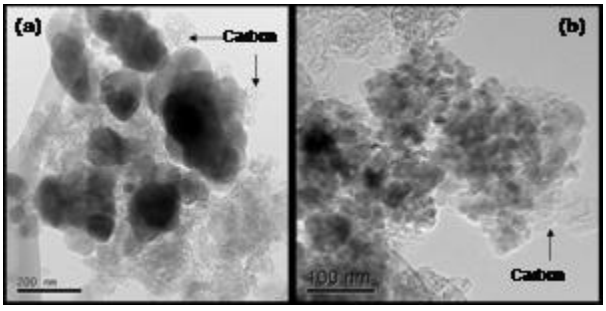

Figure V- 52: TEM images of the $LiMnPO_4$/C composites prepared at (a) 550°C and (b) 350°C

Conclusions and Future Directions

The high-voltage cathode material $LiMnPO_4$ has been prepared by a surfactant-based solid state reaction, which produces uniform nanostructured materials with a capacity of ~132 mAh/g. Planetary ball-milling proved to be effective to improve the rate performance. A doped $LiMn_{1-x}D_xPO_4$ cathode material (e.g. $LiMn_{0.9}Fe_{0.1}PO_4$) demonstrates a specific capacity of 168mAh/g at C/50 rate. A low-temperature process has also been developed to synthesize $LiMnPO_4$ from the $MnPO_4 \cdot H_2O$ precursor precipitated via a spontaneous reaction. The samples exhibit a discharge capacity of 115mAh/g at C/20 rate.

The surfactant-based solid state reaction will be further developed to prepare other olivine structured cathode materials $LiMPO_4$ (M = Fe, Mn, Co, Ni). The effect of ball-milling on electrochemical performance of these materials will be further investigated. In addition, other high-energy cathode materials based on doped lithium metal phosphates and surface-modified inverse spinels ($LiNi_{0.5}Mn_{1.5}O_4$) will be investigated. Polyanions in $LiMnPO_4$ and $LiNiPO_4$ will be partially modified to improve both the conductivity and capacity of high-voltage cathode materials. Novel organic cathode materials will also be investigated to improve their capacity and cycle life.

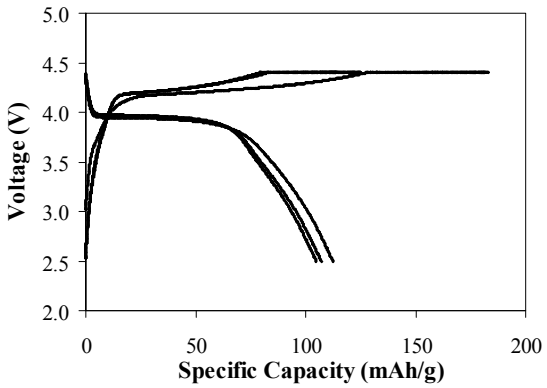

Figure V- 53: Charge-discharge profiles of the $LiMnPO_4$/C synthesized at 550°C during the first three cycles. The rate used was C/20 (7.5 mA g^{-1}) between 2.5 and 4.4 V. CC-CV mode was used for the test.

FY 2009 Publications/Presentations

1. J. Xiao, W. Xu, D. Choi, and J. Zhang, "Synthesis of Lithium Manganese Phosphate by a Novel Precipitation Method", Submitted to *Journal of the Electrochemical Society* (2009).
2. D. Choi, D. Wang, Z Nie, J. Zhang, Z. Yang, and J. Liu, "Nanostructured $LiMPO_4$ (M = Fe, Mn, Co) for Li-ion Cathode by Molten Surfactant Approach", Presented at Electrochemical Society Meeting, May 24-29, 2009, San Francisco, CA.
3. J. Xiao, W. Xu, and J. Zhang, "Synthesis and Characterization of $LiMnPO_4$ as a Cathode Material for Li-ion Batteries, Presented at Electrochemical Society Meeting, May 24-29, 2009, San Francisco, CA.

V.C Anode Development

The primary objective of the anode tasks is to replace carbon materials with inexpensive, high energy, anodes made from environmentally benign materials. The anode should have slightly more positive insertion voltage with respect to Li/Li+ in order to minimize risks of Li plating while charging at high rates and low temperatures. The objective of the intermetallic electrodes work is to search for inexpensive materials with a capacity of at least 400mAh/g (>1500 mAh/ml). The objectives of the Si and Sn alloy research is to understand and reduce the capacity fade of these very high energy materials during cycling. Investigations into nano-scale effects and cycling voltage range are included.

V.C.1 Nanoscale Composite Hetero-structures: Novel High Capacity Reversible Anodes for Lithium-ion Batteries (U Pitt)

Prashant N. Kumta

Swanson School of Engineering,
Departments of Bioengineering, Chemical and Petroleum Engineering, Mechanical Engineering and Materials Science,
University of Pittsburgh, Pittsburgh, PA 15261
Phone: (412)-648-0223 ; Fax : (412) 624-8069
E-mail: pkumta@pitt.edu

Start Date: September 1, 2007
Projected End Date: August 31, 2010

Objectives

- Identify new alternative anode materials to replace synthetic graphite that will provide higher gravimetric and volumetric capacity as well as higher energy density.
- Similar or lower irreversible loss in comparison to synthetic graphite.
- Investigate nano-structured Si based composite or hybrid structured anodes.
- Improve the specific capacity, rate capability and cycle life of nano-structured Si based anode materials.

Technical Barriers

The important technical barriers of alternative anodes for Li-ion batteries to be used in electrical vehicles or hybrid electrical vehicles are the following:

(A) Low energy density

(B) Large first cycle irreversible loss

(C) Poor cycle life

(D) Poor rate capability

(E) Inadequate coulombic efficiencies

Technical Targets

- Synthesize nano-structured Si based anodes using cost effective processing techniques.
- Achieve stable reversible capacity in excess of ~700mAh/g.
- Improve the rate capability.
- Characterize the nano-scale hetero-structures for structure and composition using electron microscopy techniques such as SEM, TEM and HREM.
- Reduce first cycle irreversible loss to less than ~20%.
- Investigate the origin of and characterize the solid electrolyte interphase (SEI) layer.

Accomplishments

- Synthesized Si and C based nano-composite by high energy mechanical milling (HEMM) using polymer additives.
- Identified suitable polymer additives to prevent the formation of non-reactive SiC and reduced the amorphization of graphite during HEMM.
- HEMM derived Si/C nano-composite shows excellent cycle-ability (0.01-0.03% loss per cycle) with specific capacity higher than ~700mAh/g.

- Identified suitable Li-Si alloy and Li-Si/C nano-composite anodes exhibiting excellent cycle-ability, high specific capacity and high energy density.
- Synthesized Si and carbon nanotube (CNT) hybrid nanostructures by cost effective CVD processes.
- Optimized processing parameters to achieve desirable microstructure of Si/CNT hybrid structure.
- The controlled hybrid structures of Si/CNT exhibit specific capacity in excess of ~2,000mAh/g with excellent stability and rate capability.
- The novel Si/C composite and Si/CNT hybrid nanostructures exhibit less than 20% first cycle irreversible loss.

✧ ✧ ✧ ✧ ✧

Introduction

Achieving the DOE-BATT technical targets will require improving the cycling stability and irreversible loss of Si based anodes. Hence it is essential to synthesize Si based composites using economical processes exhibiting excellent mechanical properties to endure the large cycling induced volumetric stresses of Li-Si alloys. In 2008, we conducted a systematic investigation of the electrochemical properties of HEMM derived Si/C based composite anodes. These HEMM derived composite anodes synthesized using polymer additives displayed a reversible capacity ~700mAh/g or higher with a 0.01-0.03% capacity fade per cycle. Scale-up efforts to generate these novel composites are currently in progress; while efforts to further improve the capacities of these systems are also on-going. In addition, collaborative efforts to understand the SEI layers have been initiated with Dr. Kostecki and Dr. Battaglia at LBNL. Although Si/C based composites exhibiting capacity in excess of ~1,000mAh/g have been generated, the system is commercially unsuitable due to capacity fade above 0.1% per cycle.

To improve the capacity stability of Si/C based composite anodes, CNTs have been selected over graphite as a matrix and Si/CNT hybrid structures have been synthesized due to their excellent physical and mechanical properties in comparison to any of the existing systems known to date. They also possess some unparalleled properties such as large aspect ratio, structural flexibility, and tortuosity. Exploitation of these unique CNT attributes combined with its nano-scale dimensions will enable the generation of a nano-scale conductive network improving the electrical contact between the active Si particles. The Si/CNT hybrid structures could thus potentially exhibit high reversible capacity while also displaying excellent cycle-ability.

Approach

To meet the technical targets, our approach is to explore inexpensive Si and C based composite or hybrid nano-structured electrodes exhibiting 1) an electrochemical potential a few hundred mV above the potential of metallic Li, and 2) a capacity of at least ~700mAh/g. To achieve these goals, we focused on exploring novel low cost approaches to generate nano-scale hetero-structures comprising nano-structured Si or Li-Si alloys and a variety of carbons forms derived from graphitic carbon as well as CNT. A detailed study of these Si/C based composite anodes has already been presented at the 2008 DOE annual review.

In 2009, a cost effective simple two-step CVD process has been employed to synthesize hybrid Si/CNT nano-structures. The multi-walled carbon nano-tubes (MWNT) were first synthesized on quartz using xylene and ferrocene serving as the carbon and iron catalyst sources, respectively. Deposition of Si on CNTs has been achieved by cracking SiH_4 in the temperature range of 723K-1023K. Under the experimental conditions used, the CNTs grow perpendicular to quartz covered with Si nano-clusters deposited directly on CNT at defined spacing.

These promising systems were tested in half cells using metallic lithium as both counter and reference electrodes. Rate capability, long-term cycle-ability, including origin and state of the SEI layers, were investigated.

Results

Si/CNT hybrid nanostructure synthesized by CVD techniques. X-ray diffraction patterns of pristine CNTs and the hybrid Si/CNT nanostructures synthesized by the two step CVD processes, shown in Figure V- 54, confirm the presence of nano-crystalline Si (~40nm) along with CNTs. Figure V- 55 (a) and (b) are the SEM and TEM images of the hybrid Si/CNTs, which distinctly show Si nano-particles of ~40nm in diameter adhered to the individual CNT at defined gaps between each other. The average tube diameter of the MWNT is in the range of ~50-80nm. The CNT surface provides the desired sites for Si to nucleate and grow during SiH_4 decomposition with the formation of an interfacial layer of amorphous carbon between the CNT and Si evidenced by HREM and EELS analyses.

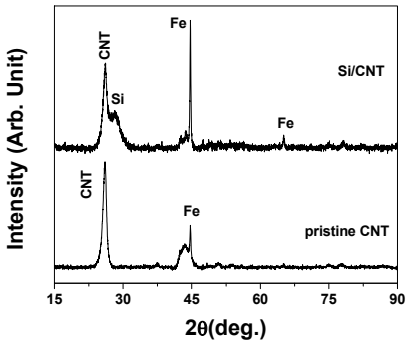

Figure V- 54: XRD of pristine CNTs and hybrid Si/CNTs

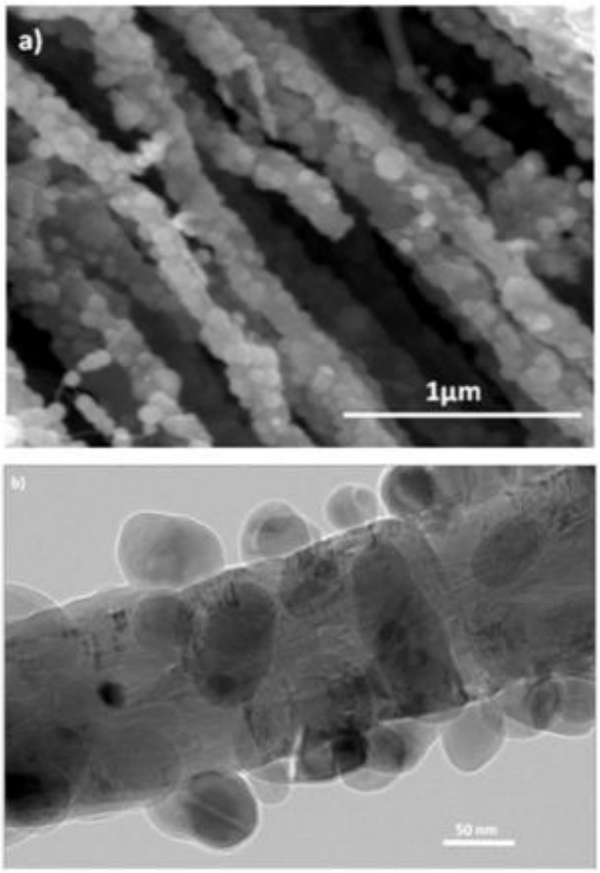

Figure V- 55: (a) SEM image of CNT covered with Si nano-particles and (b) TEM image of a single CNT covered with Si nano-particles with defined spacing to each other.

The variation of specific capacity with cycle number of the hybrid Si/CNT nanostructures is shown in Figure V-56. The 1st discharge and charge capacity are ~2,552mAh/g and ~2,049mAh/g, respectively, an irreversible loss of ~19.7%. In the subsequent cycles, the coulombic efficiency reaches more than 99% and remains nearly constant. The Si/CNT anode exhibits excellent capacity retention with a fade in capacity of only ~ 0.3% per cycle up to 25 cycles. Figure V- 57 shows the capacity at rates of C/10, C/4, C/2, 1.3C and 2.5C. Even at 2.5C, the capacity remains ~1,000mAh/g, which is almost four times higher than the practical capacity observed to be achieved in graphitic anodes, a very much improved rate capability.

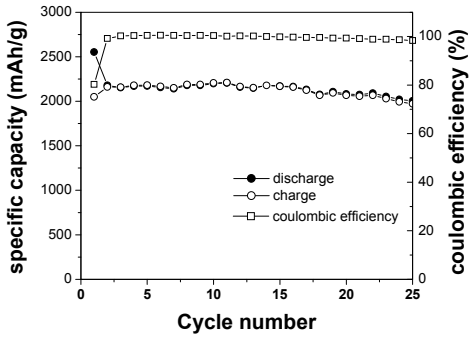

Figure V- 56: Variation of discharge/charge capacity and coulombic efficiency of Si/CNT nanostructure electrode.

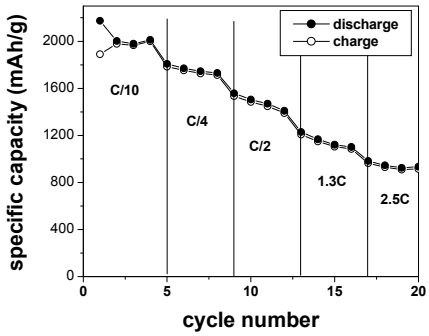

Figure V- 57: Rate capability of Si/CNT electrodes.

The first discharge and charge differential capacity (dQ/dV vs. V) of Si/CNT, shown in Figure V- 58, indicate that the phase formation and transformation reactions occur between Si and *a*-Li_xSi (x=3.5-3.75), bypassing any crystalline phases known to contribute to colossal volume expansion and cracking of electrodes. The excellent cycle-ability of high capacity Si/CNT is likely due to nanoscale Si, and the excellent mechanical and physical properties of CNT.

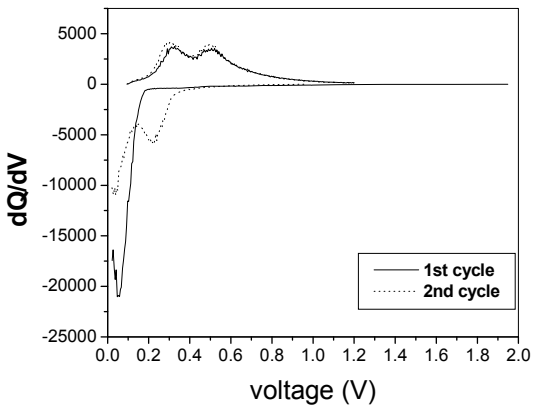

Figure V- 58: Differential capacity with potential showing formation of various phases in Si/CNT hybrid structures.

Conclusions and Future Directions

A unique hybrid Si/CNTs based nano-structure is synthesized using a simple cost effective CVD process in which the CNTs are first synthesized vertically aligned on quartz with defined spacing between each. Subsequently, Si nano-particles are homogeneously deposited on the CNTs. The CNT functions as a flexible mechanical support for strain release offering an efficient conducting channel while the nano-structured Si provide the high capacity. It is demonstrated that the hybrid Si/CNTs exhibit high reversible capacity of ~2,000mAh/g with very little fade in capacity, ~0.3% per cycle over 25 cycles. The proposed approach affords a very facile strategy for the fabrication of next generation anodes exhibiting high energy density and cycle life.

Future work will be dedicated to improve the structural stability of Si/CNT hybrid structures. In this direction a hybrid nano-structure consisting of Si nanowire or nanotube along with CNT will be synthesized directly on copper substrates by the CVD approach to improve the mechanical properties and the electronic conductivity of the hybrid structures. In addition, scale up activities using Si/C composite and Si/CNT hybrid structures will be initiated and performed.

FY 2009 Publications/Presentations

1. W. Wang and P. N. Kumta, “Hybrid Silicon/Carbon Nanotube Heterostructures: Novel Reversible High Capacity Lithium battery anodes”, submitted to Nanoletters.
2. M. K. Datta and P. N. Kumta, “In situ electrochemical synthesis of lithiated silicon-carbon based composites anode materials for Li-ion battery”, J. Power Sources 194 (2009) 1043.
3. J. Nanda, M. K. Datta, J. T. Remillard, A. O’Neill and P. N. Kumta, “In situ Raman microscopy during discharge of a high capacity silicon-carbon composite Li-ion battery negative electrode”, Electrochem. Comm. 11 (2009) 235.
4. M. K. Datta and P. N. Kumta, “Alloy design for long-term cycle-ability of Si based anode materials for Li-ion batteries”, SAE international journal of Materials and Manufacturing, 1 (2009) 285.
5. R. Teki, M. K. Datta, R. Krishnan, T. C. Parker, T. M. Lu, P. N. Kumta and N. Koratkar, “Nanostructured Silicon anodes for Li-ion rechargeable batteries” Small (in press).
6. Presentation at the 2008 DOE Annual Peer Review Meeting.

V.C.2 Interfacial Processes – Diagnostics (LBNL)

Robert Kostecki
Environmental Energy Technologies Division
Lawrence Berkeley National Laboratory
1 Cyclotron Road, MS 70-108B
Berkeley, CA 94720
Phone: (510) 486 6002; Fax: (510) 486 7303
E-mail: r_kostecki@lbl.gov

Start Date: October 1, 2008
Projected End Date: September 30, 2010

Objectives

- Establish direct correlations between BATT baseline electrodes surface chemistry, morphology, topology, interfacial phenomena, and degradation modes of Li-ion cell.
- Evaluate and reduce the capacity and cycle life limitations of intermetallic anodes.
  - Determine physico-chemical properties of the SEI i.e., chemical composition, reaction kinetics, morphology, ionic/electronic conductivity etc.
  - Investigate electrocatalytic behavior of intermetallic anodes in organic electrolytes
  - Characterize degradation modes and improve SEI long-term stability in high-energy Li-ion systems
  - Evaluate the effect of surface composition and architecture on electrochemical behavior of the electrode
  - Provide remedies to interface instability e.g., new alloys and/or structures, electrolyte additives, co-deposition of other metals etc.

Technical Barriers

This project addresses the following technical barriers facing the battery technology development effort in the DOE Office of Vehicle Technologies:

1. Inadequate Li-ion battery energy (related to cost)
2. Poor lithium battery calendar/cycle lifetime for PHEV applications
3. Need for new advanced battery materials with acceptable specific energy, durability, costs, and safety characteristics

Technical Targets

- Cycle life: 3,000 cycles (40 mile).
- Available energy: 96 Wh/kg (40 mile).
- Calendar life: 15 years.

Accomplishments

- Preliminary assessment of interfacial processes on Sn electrode was completed
- *In situ* studies revealed that an effective SEI layer never forms on Sn in EC-based electrolytes
- Effective strategies to suppress unwanted surface reactions on Sn electrodes were proposed

✧ ✧ ✧ ✧ ✧

Introduction

A primary aim of this project is to develop and use advanced diagnostic techniques to characterize basic physico-chemical properties of electrode active and passive components that are being developed for use in PHEV applications. The focus of this task is to correlate fundamental interfacial processes that occur in Li-ion batteries with the electrochemical performance. The diagnostic evaluation of composite and model electrodes are used to determine cell failure mechanisms, anticipate the system lifetime, and to suggest new approaches to design more-stable materials, composites and electrodes.

Approach

Advanced diagnostics are essential to investigate life-limiting and performance-limiting processes in batteries. Powerful and adequate analytic methods must be used to characterize materials and cell components. *In situ* enhanced spectroscopic and microscopic techniques as well as standard post-test analyses are applied to investigate the morphology, structure, and composition changes of electrode materials that accompany cell cycling.

This project employs the following specific research approaches:

1. Adopt and apply an electrochemical cell of the Devanathan-Stachurski type to study the kinetics of lithium alloying and diffusion in intermetallic anodes, and possible correlations with the formation and long-term stability of the SEI layer.
2. Apply *in situ* and *ex situ* Raman and FTIR spectroscopy and microscopy, scanning probe microscopy (SPM), spectroscopic ellipsometry, electron microscopy (SEM, HRTEM), and standard

electrochemical techniques to detect and characterize surface processes in intermetallic anodes, and high-voltage (>4.3V) cathodes.

Results

***In Situ* Studies of Interfacial Processes on a Sn Electrode.** Fundamental diagnostic studies of surface phenomena on tin were carried out to evaluate their impact on the electrochemical performance of Sn anodes in Li-ion systems. We conducted a systematic examination of the electrochemical behavior of a Sn foil electrode in different electrolytes (1M $LiPF_6$ in EC/DEC or PC) and the effect of electrode surface modification with thin-film metallic coatings. The electrochemical behavior of the electrode was investigated in a standard three electrode cell equipped with Li wires as counter and reference electrodes and filled with 1 M $LiPF_6$, either in EC:DEC (1:2 w/w) or PC.

Figure V- 59A shows three initial cyclic voltammograms (CVs) of the pure tin-foil electrode in 1M $LiPF_6$, EC:DEC electrolyte (black trace). The plots reveal an intense irreversible reduction peak at 1.2 V that is attributed to the electrolyte decomposition. A series of complementary potentiometric and *in situ* AFM experiments confirmed that effective SEI layer never forms on Sn in EC:DEC electrolytes. Interestingly, the CV response of the Sn electrode in 1M $LiPF_6$, PC exhibits different behavior. Two irreversible cathodic peaks at 2 V and 1.1 V are still clearly discernible. However, the intensity of these peaks diminishes substantially during the second scan and then they tend to vanish completely in the subsequent scans. Although the electrochemical measurements were carried out in the potential range above Li/Sn-alloying, they provide a clear indication that the PC-base electrolyte tends to form a protective passive layer on Sn and inhibit irreversible capacity losses.

Another effective way of suppressing unwanted cathodic surface processes on Sn electrode was identified by coating Sn with a thin layer of Cu or Ag. Figure V- 59B shows a series of CVs recorded in the 1M $LiPF_6$, EC:DEC (1:2 w/w) electrolyte. The intensity of the cathodic irreversible peaks is greatly reduced and they decrease significantly with cycling.

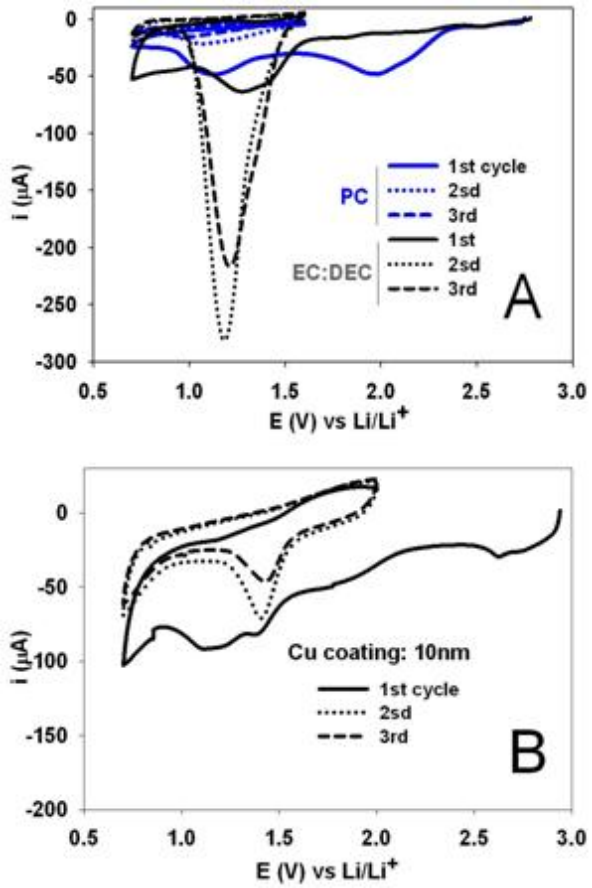

Figure V- 59: (A) CVs (1mVs-1) of Sn foil electrode in 1M LiPF6 EC:DEC (1:2 w/w), (black) and 1M LiPF6, PC (blue). (B) CVs of Sn foil electrode coated with 10 nm of Cu in 1M LiPF6, EC:DEC (1:2 w/w)

Figure V- 60 shows three initial voltammetric cycles (CVs) of the Sn-foil electrode and the corresponding *in situ* AFM images. We confirmed that the surface film forms at potentials >2 V. A series of controlled experiments revealed that dissolved O_2 is not responsible for the early film formation (O_2 reduction occurs at ~1.8 V vs. Li/Li^+ on noble metals). Our results are also in concert with the observed spontaneous decomposition of the electrolyte and formation of the SEI layer upon contact with Sn. The *in situ* AFM images display morphology changes associated with continuous dissolution and reformation of the SEI during cycling. These changes are particularly noticeable at ~1.5 V.

Galvanostatic polarization of the tin foil electrode at different current densities (Figure V- 61) show that the electrode potential tends to stabilize around 1.5 V at i<60 μAcm^{-1}, which indicates continuous electrolyte reduction process(es) without formation of an impervious SEI layer.

Diagnostic Studies of $LiMnPO_4$ Cathodes. A systematic investigation of surface and bulk phenomena of model $LiMnPO_4$ cathodes through spectroscopic observation during charge-discharge processes was

conducted. We used composite $LiMnPO_4$ electrodes from HPL S.A. that exhibit very good electrochemical properties.

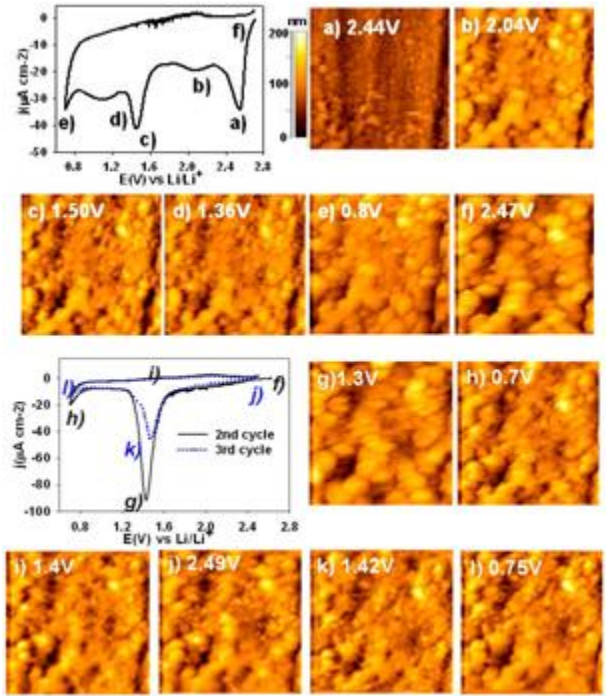

Figure V- 60: *In situ* AFM images (8x8 μm) of Sn in EC: DEC 1:2, 1M $LiPF_6$ ($1mVs^{-1}$) during the initial three CV scans

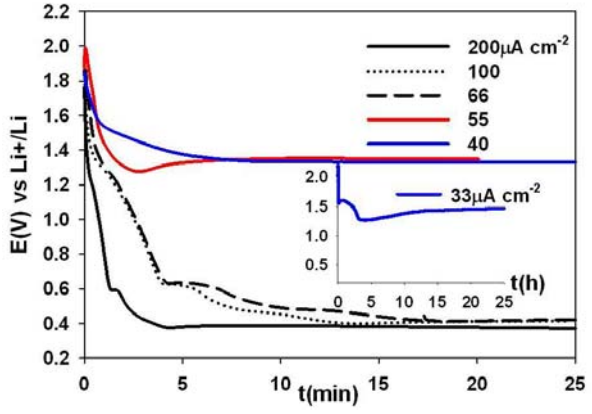

Figure V- 61: Potentiometric response of Sn in EC: DEC 1:2, 1M $LiPF_6$ to galvanostatic polarization at different current densities.

Raman spectra of the pristine composite $LiMnPO_4$ electrode (Figure V- 62c) are dominated by the D and G carbon bands. We observed spectral signatures characteristic of two types of carbon: (i) graphite with a sharp G-band at 1583 cm^{-1} and an overtone band at ca. 2660 cm^{-1}, and (ii) carbon black with a broad D-band at 1335 cm^{-1}. Raman images of the electrode reveal a thick surface layer of conductive carbon additives that prevents detection and characterization of the cathode active material (igure IV- 62a). To overcome this issue, we used O_2- plasma etching to remove surface carbon and expose $LiMnPO_4$ particles, without affecting the electrode's mechanical integrity. After the etching process, the phosphate γ_{sym} peak at 947 cm^{-1} becomes clearly distinguishable and appears in much of the electrode surface (Figure V- 62b).

The etched HPL $LiMnPO_4$ cathode exhibits good charging characteristics (Figure V- 63). However, only carbon D- and G-bands could be positively identified in the spectrum of the charged electrode. Two peak shoulders at ca. 1500 and 1150 cm^{-1} originate from a surface film or are associated with changes in the conductive carbon structure. On the other hand, an intense fluorescent background also clearly indicates the presence of electrolyte decomposition products (Figure V- 63 inset).

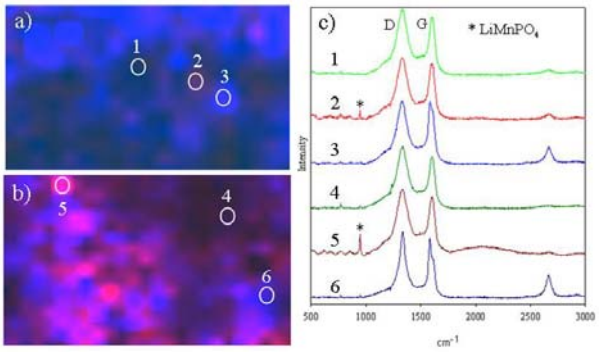

Figure V- 62: Raman images of $LiMnPO_4$ electrodes before (a) and after (b) O_2-plasma etching. Blue areas correspond to carbon additives, red areas represent $LiMnPO_4$. Selected Raman spectra are shown in (c).

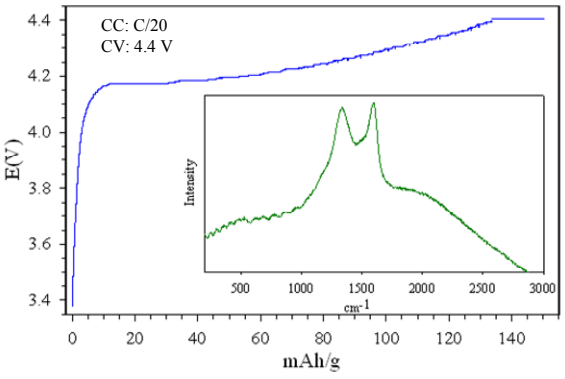

Figure V- 63: Charging curve of an etched $LiMnPO_4$ electrode. (Inset) Raman spectrum of the electrode after charging.

Conclusions and Future Directions

In situ AFM and CVsat potentials > 0.7 V i.e., above the potential of Sn-Li alloying, reveal formation of an unstable SEI at a tin foil electrode in EC-based electrolytes. Initial steps of the SEI formation were

observed at ~ 2.5 V vs. Li/Li^+ followed by gradual film morphology changes at potentials $0.7 < U < 2.5$ V. The SEI layer tends to undergo continuous reformation during the following CV cycles. The surface film on Sn does not effectively prevent electrolyte reduction and a large fraction of the reactions products dissolve in the electrolyte. This interfacial instability is further aggravated by Sn particle decrepitation, which results from large volumetric changes of Sn crystallites upon lithiation-delithiation, and gradual increase of the electrode active surface area, that leads to continuous regeneration of a fresh tin surface, and SEI reformation.

The unstable SEI layer on Sn in EC-based electrolytes may compromise the use of tin-based anodes in Li-ion battery systems unless the interfacial chemistry of the electrode and/or electrolyte is modified. These problems are remedied by (i) careful optimization of the electrolyte composition and use of additives that produce a stable SEI layer, (ii) Sn nanostructuring to prevent particle decrepitation, (iii) tin alloying with metals e.g., Cu that tend to form very thin and stable SEI layer, (iv) protective surface coatings e.g., carbon to prevent direct contact between Sn and the electrolyte.

- Continue studies of mass and charge transfer mechanisms at the electrode-electrolyte interface
- Develop multi-task spectro-electrochemical cell of the Devanathan-Stachurski type to study *in situ* and model kinetics of Li intercalation and diffusion through electrode materials (V. Srinivasan)
- Apply *in situ* and *ex situ* instrumental methods to detect and characterize surface processes in Li-ion intermetallic anodes
- Carry out comprehensive fundamental *in situ* spectroscopic ellipsometry in conjunction with AFM and FTIR/Raman surface analysis studies of the SEI layer formation on Sn and Si electrodes
- Cooperate with the BATT Interfacial Studies Group to investigate the effect of material structure, morphology, and topology on formation of the SEI layer
- Investigate correlations between physico-chemical properties of the SEI layer and long-term electrochemical performance of Li-ion electrodes
- Perform diagnostic evaluation of detrimental phenomena in high-voltage (>4.3V) cathodes
- Apply *in situ* and *ex situ* Raman and FTIR spectroscopy to detect and characterize surface and bulk processes in $LiMePO_4$ cathodes

FY 2009 Publications/Presentations

1. M. Marcinek, J. Wilcox, M. Doeff, R. Kostecki "Microwave Plasma Chemical Vapor Deposition of Carbon Coatings on $LiNi_{1/3}Co_{1/3}Mn_{1/3}O_2$ for Li-ion Battery Composite Cathodes". J. Electrochem. Soc., 156 A48 (2009)
2. L. Hardwick, J. Saint, I. Lucas, M. Doeff, R. Kostecki, "FTIR and Raman Study of the $Li_xTi_yMn_{1-y}O_2$ (y = 0, 0.11) Cathodes in Pyrrolidinium-based Ionic Liquid Electrolyte Systems", J. Electrochem. Soc 156, A120 (2009)
3. L. J. Hardwick, M. Marcinek, L. Beer, J. B. Kerr, R. Kostecki, "An Investigation of the Effect of Graphite Degradation on the Irreversible Capacity in Lithium-ion Cells", J. Electrochem. Soc. 155, A442 (2008)
4. M. M. Doeff, J. D. Wilcox, R. Yu, A. Aumentado, M. Marcinek, R. Kostecki, "Impact of Carbon Structure and Morphology on the Electrochemical Performance of $LiFePO_4$/C Composites", J. Solid State Electrochem., 12, 995, (2008)
5. L. J. Hardwick, Marek Marcinek, Robert Kostecki, "Rechargeable Lithium and Li-ion Batteries", ECS Transactions, Volume 11, 2008
6. R. Kostecki, "Microbatteries for Integrated Autonomous Microdevices", MEPTEC Technical Symposium, February 10, 2009, San Jose, CA (invited talk)
7. R. Kostecki, "Local Interfacial Phenomena in Li-ion Batteries", 1st Annual Workshop on Electrochemistry, Feb. 7-10, 2009, Austin, TX (invited talk)
8. M. Marcinek, J. Wilcox, M. Doeff, R. Kostecki, "Microwave Plasma Chemical Vapor Deposition of Carbon Coatings on LiNi0.33Co0.33Mn0.33O2 for Li-ion Battery Composite Cathodes ", 214th ECS Meeting, Honolulu, HI
9. L.J. Hardwick, J. Saint, M.M. Doeff, R. Kostecki, "Spectroscopic Investigation of the Surface of Li_xMnO_2 and $Li_xTi_{0.11}Mn_{0.89}O_2$ Composite Electrodes in Pyrrolidinium-based Ionic Liquid Electrolyte Systems", 214th ECS Meeting, Honolulu, HI
10. L.J. Hardwick, V. A. Sethuraman V.Srinivasan, R. Kostecki, "A Study of the Mechanism of Graphite Structural Degradation in Lithium-ion Cell Anodes", 214th ECS Meeting, Oct. 12-17, Honolulu, HI
11. R. Kostecki, L. Hardwick, V. Sethuraman, "Carbonaceous Materials for High-rate Anodes in Li-ion Batteries", Invention Disclosure IB-2700
12. R. Kostecki, "Interfacial Processes – Diagnostics", Presentation at the 2009 DOE Annual Peer Review Meeting.

V.C.3 Nanostructured Metal Oxide Anodes (NREL)

Anne C. Dillon
National Renewable Energy Laboratory
1617 Cole Blvd.
Golden, CO 80401
Phone: (303) 384-6607; Fax: (303) 384-6655
E-mail: Anne.Dillon@nrel.gov

Subcontractor:
Prof. Se-Hee Lee, University of Colorado, Boulder

Start Date: 0ctober 1, 2007
Projected End Date: September 30, 2009

Objectives

The ultimate goal of this activity is to develop optimized metal oxide nanostructured electrode materials to enable high-performance, durable, and affordable Li-ion batteries for power-assist HEVs and PHEVs that meet the DOE/FreedomCAR partnership targets.

- Optimize MoO_3 nanoparticle electrodes in coin cell configuration and compare to previous results for electrophoresis deposited thin-film MoO_3 electrodes.
- Demonstrate a full cell with a MoO_3 anode and a state-of-the-art Argonne National Laboratory (ANL) cathode with a high energy density and stable cycling performance.
- Employ first-principles calculations to obtain a better understanding of Li-ion insertion processes as well as to predict new materials.
- Demonstrate the possibility of other metal oxide nanostructures made from less expensive starting materials such as Fe or Mn.
- Develop methods to improve anode volumetric capacity.

Technical Barriers

This project addresses the following technical barriers from the Energy Storage section of the Vehicle Technologies Program Multi-Year Research, Development and Demonstration Plan:

- Cost: develop metal oxide-based anodes from abundant, inexpensive metals
- Energy density: improvements in both gravimetric and volumetric energy densities have been demonstrated
- Safety: metal oxide anodes operate at higher potential relative to Li metal than graphite, eliminating the risk of Li plating.
- Lifetime: Durable and reversible cycling has been achieved.

Accomplishments

- Capacity of the NREL MoO_3 anode has been increased to ~1050 mAh/g by optimizing the coin cell configuration. The theoretical capacity of bulk MoO_3 is 1110 mAh/g.
- Temperature programmed desorption (TPD), thermal gravimetric analysis (TGA), X-ray diffraction (XRD), and infrared (IR) and electron microscopy were employed to facilitate and better understand the coin cell optimization. L. Riley, S-H. Lee, L. Gedvillas and A.C. Dillon, *J. Power Sources* (available online).
- Theoretical calculations were performed to explain the mechanism for the increased Li-insertion observed in the coin cell testing.
- The MoO_3 anode has been successfully paired with two ANL cathodes: $Li_{1.05}M_{0.95}O_2$, M = $Ni_{1/3}$, $Co_{1/3}$, $Mn_{1/3}$ and the state-of-the-art lithium-rich cathode $0.5Li_2MnO_3 \bullet 0.5Li(Mn_{0.31}Ni_{0.44}Co_{0.25})O_2$.
- An atomic layer deposition (ALD) coating was applied to the MoO_3 anode and demonstrated to stabilize the full cell cycling stability.

In the ANL/NREL full coin cell containing MoO_3 and $0.5Li_2MnO_3 \bullet 0.5Li(Mn_{0.31}Ni_{0.44}Co_{0.25})O_2$, the anode has a capacity ~750 mAh/g and the cathode has a capacity of 170 mAh/g with stable cycling for ~50 cycles. The full cell has a capacity of ~140 mAh/g.

The ANL/NREL full cell therefore has the highest overall capacity and represents a remarkable achievement accomplished through a collaborative effort between two national laboratories.

We also report the synthesis of binder-free, high-rate capability Li-ion anodes synthesized by a hydrothermal process and vacuum filtration method. Note that the electrodes contain completely nontoxic and abundant elements, utilizing Fe_3O_4 nanorods as the active lithium storage material and carbon single-wall nanotubes (SWNTs) as the conductive additive. The highest reversible capacity is obtained using 5 wt.% SWNTs, reaching 1000 mAh/g (~2000 mAh/cm^3) at C rate when coupled with a lithium metal electrode, and this high capacity is sustained over 100 cycles. The Fe_3O_4 nanorods/SWNT electrodes exhibit high-rate

capability and stable capacities of 800 mAh/g at 5C and ~600 mAh/g at 10C.

✧ ✧ ✧ ✧ ✧

Introduction

Rechargeable Li-ion batteries have long been considered candidates for high power applications, such as electric vehicles. To realize the full potential of Li-ion batteries, it is essential to develop electrodes that are durable, reversible, nontoxic, and cost effective, with high charge and discharge rate and high volumetric and gravimetric capacity.

Approach

Bulk MoO_3 is a high-capacity Li-insertion compound but suffers from poor reversibility and slow kinetics. The irreversibility is attributed to intolerance to the volume expansion that occurs upon Li-insertion. NREL scientists demonstrated that thin films of MoO_3 nanoparticles have a surprisingly high reversible capacity of 630 mAh/g (*Adv. Mat.* 20 (2008) 3627).

MoO_3 nanoparticles are made at high density with inexpensive hot wire chemical vapor deposition (HWCVD) (*Chem. Phys Lett.* 413 (2005) 88).

The high reversible capacity of the MoO_3 nanoparticles has also been demonstrated for application in thick electrodes (coin cells) that are better suited for HEV or PHEV applications. In FY08 these results were confirmed in collaboration with A123 Systems.

This year we have fabricated Li/MoO_3 coin cells and have achieved ~1050 mAh/g from the MoO_3 electrode, which is almost the theoretical capacity (1110 mAh/g), by optimizing the coin cell configuration. TPD, TGA, XRD, IR and electron microscopy were employed to facilitate and better understand these optimizations. (*J. Power Sources,* available online)

Mo is nontoxic and cheaper than cobalt but is still too expensive to be considered for vehicular applications. Therefore, this year we report the synthesis of binder-free, high-rate capability Li-ion anodes synthesized by an inexpensive hydrothermal process and vacuum filtration method. It is important to note that the electrodes contain completely nontoxic and abundant elements, utilizing Fe_3O_4 nanorods as the active lithium storage material and carbon SWNTs as the conductive additive. The highest reversible capacity is obtained using 5 wt.% SWNTs, reaching 1,000 mAh/g (~2,000 mAh/cm^3) at a C rate when coupled with a lithium metal electrode; this high capacity is sustained over 100 cycles. Furthermore, the electrodes exhibit high-rate capability and stable capacities of 800 mAh/g at 5C and ~600 mAh/g at 10C. (*Nature*, under review).

Results

MoO_3 Coin Cell Optimization. To optimize MoO_3 half-cells, we discovered that polymer-rich electrodes enabled continuous adhesion through the film. Maximum cycling capacity of ~1,050 mAh/g (theoretical 1,110 mAh/g) was achieved at a ratio of 70:10:20 (MoO_3:AB:PVDF), as shown in Figure V-64(top). We also found that the best durable reversible capacity was achieved by heat-treating the electrodes in a glove box at 250˚C overnight, as shown in Figure V-64(bottom).

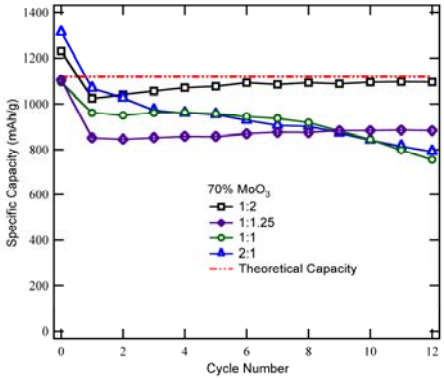

a)

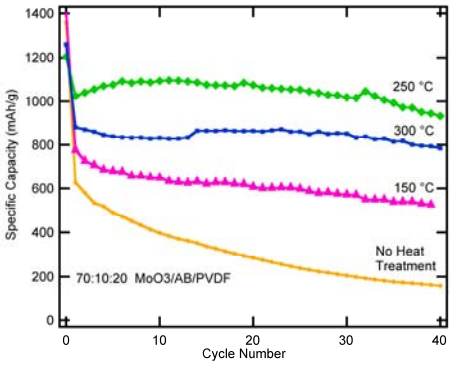

b)

Figure V- 64: Cycling Stability of MoO_3 Coin Cell Half Cells with Varying PVDF:AB (top) and Electrode Heat Treatment

Understanding MoO_3 Coin Cell Optimization. A combination of TPD, TGA, and IR analyses indicate that water and surface hydroxyl groups may be effectively removed at up to 250˚C, while annealing the electrode to 300˚C results in binder decomposition. We believe that each active material will require a unique optimal annealing temperature that can be easily determined through thermal analysis.

Full Cell Fabrication with MoO_3 Anode and ANL Cathodes. A full cell capacity of ~80 mAh/g was achieved when cycling between 4.0 and 1.0 V by coupling with an $Li_{1.05}M_{0.95}O_2$, M = $Ni_{1/3}$,$Co_{1/3}$,$Mn_{1/3}$ cathode from ANL. The coin cell contained 13 mg cathode material and 1.7 mg anode material. In the full cell, MoO_3 had a reversible capacity of ~677 mAh/g and the cathode capacity was 90 mAh/g with a full cell capacity of ~80 mAh/g (commercial capacity is generally ~80 mAh/g). However, a capacity of 140 mAh/g was achieved when cycling the coin cell between 4.0 and 0.01 V as a result of coupling with a state-of-the-art lithium excess cathode (LEC), $0.5Li_2MnO_3 \bullet 0.5Li(Mn_{0.31}Ni_{0.44}Co_{0.25})O_2$ (Figure V- 65).

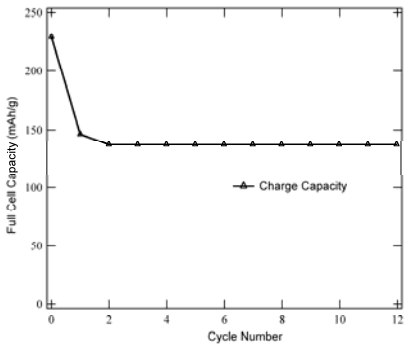

Figure V- 65: Full Coin Cell Cycling Stability Containing MoO_3 Anode and LEC Cathode

The full cell contained 7.4 mg cathode material and 1.6 mg anode material. In the cell the MoO_3 had a capacity of ~776 mAh/g, and cathode capacity was 170 mAh/g. Improved cycling stability was achieved by applying a thin ALD coating on the MoO_3 electrode. In the half-cell, the ALD coating on MoO_3 anode enabled a reversible capacity of ~910 mAh/g when cycled at C/2. An ALD coated MoO_3 anode was then paired with a LEC. Very stable cycling and high coulombic efficiency (Figure V- 66) were obtained for this full cell, suggesting potential for commercial applications.

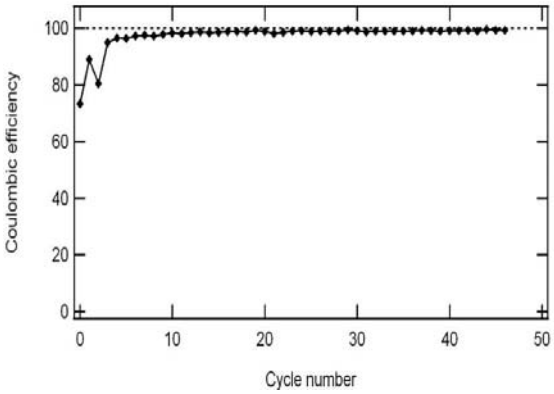

Figure V- 66: Coulombic Efficiency of a Full Coin Cell Containing an ALD-Coated MoO_3 Anode and LEC Cathode

Fabrication of High Gravimetric and Volumetric Capacity with a Binder-free Fe_3O_4 Anode. Li-ion anodes were fabricated with a hydrothermal process to make Fe_3O_4 nanorods as the active lithium storage material and a simple vacuum filtration method to employ carbon SWNTs as the conductive additive. Note that the electrodes contain completely nontoxic and abundant elements, utilizing Fe_3O_4 nanorods as the active lithium storage material. The highest reversible capacity is obtained using 5 wt.% SWNTs, reaching 1000 mAh/g (~2000 mAh/cm^3) at a C rate when coupled with a lithium metal electrode; this high capacity is sustained over 100 cycles. Scanning electron microscopy (SEM) indicates that the low loading of the conductive additive is achieved because Fe_3O_4 nanorods are uniformly suspended in a conductive matrix of SWNTs (Figure V- 67). We expect that our method can be used to achieve other binder-free anodes as well as cathodes with similar high-rate capability.

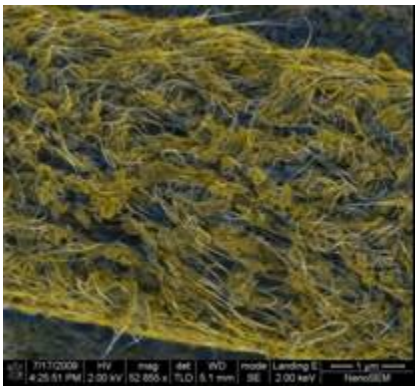

Figure V- 67: Color-Enhanced SEM Image of Fe_2O_3 Nanorods (yellow/blue) in SWNT Net (white)

Demonstration of Durable High-Rate Capability in the Binder-free Electrode. The aforementioned Fe_2O_3/SWNT electrodes were tested at variable rates, as shown in Figure V- 68. The electrodes exhibit high-rate

capability and stable capacities of 800 mAh/g at 5C and ~600 mAh/g at 10C. Furthermore, the cell retained a capacity of 550 mAh/g at 10C (8 Li^+ per formula unit in 6 minutes) after 60 cycles.

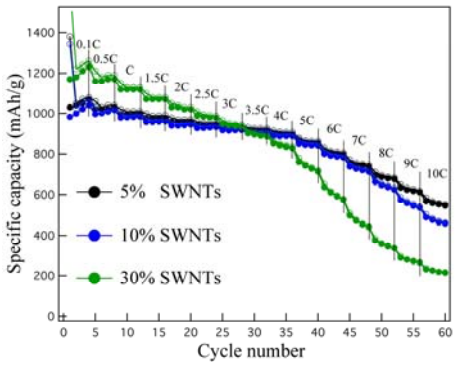

Figure V- 68: Rate Capability for Fe_3O_4 Electrodes with Different SWNT Contents Cycled at Increasing Rate

Conclusions and Future Directions

The capacity of the MoO_3 anode in a coin cell has been increased to ~1050 mAh/g by optimizing the coin cell configuration. TPD, TGA, XRD and IR were employed to facilitate these optimizations. Theoretical calculations were performed to explain the mechanism for the increased Li-insertion observed in the coin cell testing. The MoO_3 anode has been successfully paired with two ANL cathodes: $Li_{1.05}M_{0.95}O_2$, M = $Ni_{1/3}$, $Co_{1/3}$, $Mn_{1/3}$ and the state-of-the-art lithium-rich cathode $0.5Li_2MnO_3 \bullet 0.5Li(Mn_{0.31}Ni_{0.44}Co_{0.25})O_2$. By adding an ALD coating to the MoO_3 anode and coupling to the LEC, a high-capacity stable full cell was achieved, suggesting its potential for commercial application. We also report the synthesis of binder-free, high-rate capability Li-ion anodes synthesized by a hydrothermal process and vacuum filtration method. It is important to note that the electrodes contain completely nontoxic and abundant elements, utilizing Fe_3O_4 nanorods as the active lithium storage material and carbon single-wall nanotubes as the conductive additive. The highest reversible capacity is obtained using 5 wt.% SWNTs, reaching 1,000 mAh/g (~2,000 mAh/cm^3) at a C rate when coupled with a lithium metal electrode, and this high capacity is sustained over 100 cycles. Furthermore, the Fe_3O_4 nanorods/SWNT electrodes exhibit high-rate capability and stable capacities of 800 mAh/g at 5C and ~600 mAh/g at 10C.

We will continue to work with ANL to further optimize full cells with ANL cathodes to improve durable capacity and rate capability. We will also work with Fortu of Switzerland to develop high-voltage cells. We will continue to perform theoretical calculations to understand the hysteresis of the charge/discharge for the MoO_3 nanoparticles and also use theoretical calculations to predict the composition and orientation of economical oxide nanoparticles with more desirable voltage profiles. Finally, we will explore using MnO_2 as an alternate oxide cathode with an anticipated potential of 0.5 relative to lithium metal. In a new effort, we will apply a protective ALD coating on graphite nanoparticles to eliminate surface degradation mechanisms and improve the rate capability.

FY 2009 Publications/Presentations

1. S-H Lee, Y-H. Kim, R. Deshpande, P.A. Parilla, E. Whitney, D.T. Gillaspie, K.M. Jones, A.H. Mahan, S. Zhang, and A.C. Dillon, "Reversible Li-ion Insertion in Molybdenum Oxide Nanoparticles," *Advanced Materials*, 2008 (20), 3627.
2. "Y. S. Jung, S Lee, D Ahn, A C. Dillon, and S.-H. Lee, Electrochemical Reactivity of Ball-milled MoO_{3-y} Powders as Anode for Lithium Secondary Batteries," *J. Power Sources*, 188, 286 (2009).
3. A.C. Dillon, A.H. Mahan, R. Deshpande, P.A. Parilla, K.M. Jones, S-H. Lee, "Metal Oxide Nanoparticles for Improved Electrochromic and Lithium-Ion Battery Technologies," *Thin Solid Films* 516 (5), 794-797 (2008).
4. N.A. Chernova, M. Roppolo, A.C. Dillon, and M.S. Whittingham, "Layered Vanadium and Molybdenum Oxides: Batteries and Electrochromics," *J. Materials Chemistry* (Invited Review) 19 (2009) 2526.
5. L.A. Riley, C. Ban, L. Gedvillas, S-H. Lee, and A.C. Dillon, "Optimization of MoO_3 Li-ion Battery Anodes," *JPC* (available online).
6. C. Ban, Z. Wu, D.T. Gillaspie, Y. Yan, L. Chen, J.L. Blackburn, and A.C. Dillon, "Truly Remarkably High-Rate Capability Li-ion Anodes," *Nature* (under review).
7. A.C. Dillon *et al.*, "Molybdenum Oxide Nanoparticles for Improved Li-ion Battery Technologies" (invited), American Vacuum Society Fall Meeting, Boston, Massachusetts, Oct. 22, 2008.
8. A.C. Dillon *et al.*, "High Energy Metal Oxide Nanoparticle Anodes" (contributed), 1st International Conference on Advanced Lithium Battery for Automotive Applications, Chicago, Sept. 21-23, 2008.
9. A.C. Dillon *et al.*, "Molybdenum Oxide Nanoparticles for Improved Li-ion Battery Technologies" (invited), Rocky Mountain Section of the Materials Research Society Meeting, Boulder, CO, Sept. 3, 2008.
10. A.C. Dillon *et al.*, "Molybdenum Oxide Nanoparticles for Improved Li-ion Battery Technologies" (contributed), Electrochemical

Society Spring Meeting, Phoenix, AZ, May 20, 2008.
11. A.C. Dillon *et al.,* "Metal Oxide Nanostructures for Improved Electrochromic and Battery Applications" (invited), Nanofocus and Oklahoma NSF EPSCoR Annual State Conference, Oklahoma City, OK, March 6-7, 2008.
12. S-H. Lee *et al*., "Metal Oxide Nanoparticles for Advanced Energy Applications" (invited). The Fifth International Conference on Hot-Wire Chemical Vapor Deposition, August 20-24, 2008, Cambridge, MA.
13. L.A. Riley *et al.*, "Optimization of MoO_3 Nanoparticles for Use as Novel Negative-Electrode Material in High-Capacity Lithium-Ion Batteries" (contributed), Electrochemical Society Spring Meeting, San Francisco, CA, May 2009.
14. A.C. Dillon *et al.,* "High Energy Metal Oxide Nanoparticle Anodes" (plenary), Mexican Materials Research Society Meeting, Cancun, Mexico, Aug. 2009.

V.C.4 Search for New Anode Materials (UTA)

John B. Goodenough, PI
Texas Materials Institute
ETC 9.102, University of Texas at Austin
Austin, TX 78712
Phone: (512) 471-1646; Fax: (512) 471-7681
email: jgoodenough@mail.utexas.edu

Start Date: October 30, 2008
Projected End Date: September 30, 2010

Objective

- To identify a non-carbon anode for the Li+-ion rechargeable battery of higher capacity and lower voltage than $Li_4Ti_5O_{12}$ that does not form a passivating SEI layer when used with a carbonate electrolyte.

Technical Barriers

Carbon anodes have a low voltage, V ≈ 0.2 V, versus Li^+/Li and a high capacity, but reduced carbon reacts with a carbonate electrolyte to form a passivating solid/electrolyte interphase (SEI) layer. The SEI layer consumes Li from the cathode, thereby introducing an irreversible loss of cathode capacity. Moreover, during a fast charge, transfer of Li^+ ions across the SEI layer may not be fast enough to prevent plating of Lithium metal on the anode surface. On repeated charge/discharge cycles, the lithium layer becomes mossy and forms dendrites that can short-circuit a cell and set it on fire. Since the capacities of present-day cells are determined by that of the cathode and since safety is a prime concern for the battery of an electric vehicle, the design of an anode of sufficient capacity that can operate safely with a liquid flammable electrolyte is a prime technical target.

Technical Targets

- A non-carbon insertion compound having a capacity in excess of 150 mAh/g at a charge/discharge rate of 2C at a voltage versus Li^+/Li below 1.5 V and does not form an SEI layer in a carbonate electrolyte; it should also have a cycle life of over 1000 cycles

Accomplishments

- Our investigations included sulfides and oxides. We demonstrated the following:
- Framework structures can allow the incorporation of more than one Li per active transition-metal ion, a requirement for a large capacity oxide or sulfide. We inserted reversibly 10 Li/formula unit into $AgTi_2(PS_4)_3$.
- A degenerate redox couple at the bottom of a broad band may consist of itinerant-electron states and therefore allow access to more than one electron per active redox ion without a step in voltage.
- The bottom of the transition-metal M-4s band of the MS monosulfides decreases with increasing atomic number of the M atom; only sulfides of Ti, V, and Cr were found to have a 4s band at a high enough energy for an anode. The Cr(III)/Cr(II) couple of layered $Li_{1+x}CrS_2$ lies above the bottom of the Cr-4s band, which makes Cr(II) inaccessible in the layered sulfide even though CrS exists.
- Changing the electrolyte from $LiClO_4$ in propylene carbonate (PC) to $LiPF_6$ in ethylene carbonate/diethyl carbonate (EC/DEC) gave reversible access to the Ti(III)/Ti(II) and V(III)/V(II) couples in the layered sulfides $Li_{1+x}MS_2$, M = Ti or V. However, an SEI layer formed on both sulfides even though $Li_{1+X}MS_2$ gave a V ≈ 1.0 V versus Li+/Li. Several oxides with a V ≤ 1.0 V were also identified, but all showed formation of an SEI layer at V ≈ 1.0 V versus Li+/Li. These results show that the target anode must give a flat voltage in the narrow range 1.0 -1.5 V versus Li+/Li.
- We obtained a flat V = 1.3 V versus Li+/Li in $Li_xNaLiTi_3O_7$, but a capacity of 80 mAh/g is too low.
- The choice of electrolyte will be critical for improving the performance of a battery that powers an electric vehicle. A non-flammable blend of ionic liquid carbonate electrolyte may allow use of a carbon electrode with suitable connections of balanced cells of a battery pack, but at the expense of a slower rate of discharge/charge.
- We have identified intrinsic voltage limits for electrodes that need to be distinguished from the "window" of a liquid electrolyte, i.e., the limit on an anode voltage due to the lowest unoccupied molecular orbital (LUMO) of the electrolyte and on the cathode voltage by the highest occupied molecular orbital (HOMO) of the electrolyte.
- We have demonstrated the strong influence of a counter cation on the intrinsic voltage limits of an insertion-compound electrode.

✧ ✧ ✧ ✧ ✧

Introduction

The present lithium-ion secondary batteries being designed to power electric vehicles are all based on solid insertion-compound electrodes and a liquid carbonate electrolyte. Critical factors confronting the battery designer are cost, safety, cell capacity, (specific energy), specific power, and service life. At present, the electrolyte of choice is a liquid carbonate that has a window between 1.0 and 4.8 eV below the Fermi energy of elemental Lithium. The carbon anodes presently used have a good capacity with a voltage versus Li^+/Li of about 0.2 V, but the reduced carbon on Li insertion reduces the electrolyte to form a passivating SEI layer. Although this layer is permeable to Li^+ ions, it contains Li^+ ions that come from the cathode during the initial charge. This SEI Li^+ represents a loss of cathode capacity that is *irreversible*, and it is the cathode capacity that limits the specific energy of a cell with a carbon anode. In addition, expansion of the anode on Li insertion breaks the SEI layer; and during a fast charge, the rate at which the SEI layer is healed and Li^+ ions transfer across the layer are both slower than the rate at which elemental Lithium is plated onto the anode surface. On repeated cycling, the plated Li becomes mossy and develops dendrites that can grow across the electrolyte to the cathode to create an internal short-circuit that sets the battery on fire. The spinel $Li_4Ti_5O_{12}$ has its Ti(IV)/Ti(III) couple at 1.5 V versus Li^+/Li, which places it below the LUMO of the electrolyte to make it a thermodynamically stable electrode that operates without an SEI layer. However, its capacity is too low and its voltage versus Li^+/Li too high to make it a viable anode for the battery of an electric vehicle. Therefore, an open question was whether an anode of high specific energy can provide a voltage V < 1.0 V versus Li^+/Li and be kinetically stable in the absence of an SEI layer.

Approach

To investigate this question, we targeted Ti(IV)/Ti(III), V(III)/V(II), Cr(III)/Cr(II), Nb(V)/Nb(IV), and Nb(IV)/Nb(III) redox couples in octahedral sites of oxides and sulfides; these couples promise to provide a voltage ≤ 1.5 V versus Li^+/Li. Although the sulfides are not suitable for cathodes, they are candidates for anodes. We did not consider anodes operating on displacement reactions since these reactions involve too great a volume change.

Results

Anode Redox Couples. Our first task was to determine whether the Madelung energy is strong enough in the sulfides to lift the bottom of the transition-metal 4s band above the Fermi energy of lithium. For this purpose, we monitored the potentials versus Li^+/Li at which the metals M of the monosulfides MS are displaced by Li to form Li_2S + M. The bottom of the 4s band was found to decrease monotonically with increasing M-atom atomic number from just above the E_F of elemental Lithium for TiS to 1.47 eV below it in NiS; it is 0.8 eV below it in CrS. However, we found the Cr(III)/Cr(II) couple is above the bottom of the 4s band in $Li_{1+x}CrS_2$ even though CrS exists; covalent bonding with the Li in $Li_{1+x}CrS_2$ stabilizes the bottom of the 4s band relative to the Cr(III)/Cr(II) couple in $Li_{1+x}CrS_2$. Therefore, we studied Li insertion into the layered sulfides $LiMS_2$ (M = Ti or V). $Li_{1+x}TiS_2$ and $Li_{1+x}VS_2$ gave, respectively, voltages of 0.5 V and 1.0 V versus Li^+/Li. Although early studies had shown the possibility of chemical insertion of Li into $LiVS_2$, electrochemical insertion with $LiClO_4$ in propylene carbonate had proved impossible. With a different electrolyte, *viz.*, $LiPF_6$ in EC/DEC, we were able to insert reversibly one Li per formula unit into $LiMS_2$ (M = Ti or V). However, both $Li_{1+x}TiS_2$ and $Li_{1+x}VS_2$ showed rapid formation of an SEI layer below 0.9 V versus Li^+/Li with an initiation of an SEI layer in $Li_{1+x}VS_2$ even at 1.0 V. We also found a similar SEI layer formation on all our oxides that provide a V ≤ 1.0 V versus Li^+/Li. Moreover, we found that although we could insert reversibly 10 Li per formula unit into $AgTi_2(PS_4)_3$, this framework structure dissolves in our electrolyte, and even more rapidly with V substituted for Ti. From these experiments we draw the following conclusions:

- The choice of electrolyte is critical to the realization of a commercially viable rechargeable battery for powering an electric vehicle.
- With a liquid electrolyte that contains a carbonate to provide a low viscosity as well as a large solubility of a Li^+-ion salt, any anode providing a voltage V ≤ 1.0 V versus Li^+/Li will form an SEI layer, which means it must compete with the carbon anode.
- With a carbonate component in a liquid electrolyte, an insertion-compound anode must provide a flat voltage in the range 1.0 to 1.5 V versus Li^+/Li and have a capacity in excess of 150 mAh/g if it is to be competitive with $Li_4Ti_5O_{12}$.

We studied several oxides with Ti(IV)/Ti(III) and Nb(V)/Nb(IV) couples, all of which provided a V ≤ 1.5 V versus Li^+/Li. Our best was $Li_xNaLiTi_3O_7$, which gave a flat V ≈ 1.3 V versus Li^+/Li, but its capacity of 80 mAh/g is too small.

Intrinsic Voltage Limits. In the course of our work, we also explored the intrinsic voltage limits of a battery electrode as against the limitations imposed by the electrolyte window. For the anode, the intrinsic limit is the overlap by a broad conduction band of a *d*-orbital redox energy as we demonstrated with $Li_{1+x}CrS_2$ as against CrS. For a cathode, sulfides are not competitive with oxides because the top of the S-3p bands is at too high an energy. In the oxides, the Ni(III)/Ni(II) couple is at the top of the O-2p bands. The Ni(II):$3d^8$ configuration is localized

because the addition of another *d* electron to create a Ni^{+} ion costs an additional energy associated with the crystal-field splitting. However, in the perovskite $LaNiO_3$, oxidation of an octahedral-site Ni(II) leads to a low-spin Ni(III) having σ-bond *d* electrons occupying a narrow σ* band of itinerant-electron states because the σ-bonding states of the Ni(III) ion contain a large fraction of O-2p character. As a redox couple crosses the top of the anion-p bands of an oxide or chalcogenide, the Fermi energy becomes pinned as the fraction of anion-p states admixed into the antibonding states of a couple change from primarily cation-*d* to primarily anion-*p*. Where the anion-*p* character becomes too large, holes in the couple become trapped in anion-anion antibonding *p* states. Pinning of E_F in $Li_{1-x}NiO_2$ allows access to the Ni(IV)/Ni(III) couple to x ≈ 0.8, above which peroxide ions are formed at the surface with a subsequent loss of oxygen. In the spinel $Li[Ni_{0.5}Mn_{1.5}]O_4$, both the Ni(III)/Ni(II) and Ni(IV)/Ni(III) couples can be accessed at a V = 4.7-4.8 V versus Li^{+}/Li without loss of oxygen whereas layered $Li_{1-x}NiO_2$ only has a V ≈ 3.8 V. In the spinel, the top of the O-2p bands is lowered by 1 eV because the Li are in tetrahedral versus octahedral sites, and the pinned E_F of the redox couple is similarly stabilized. We showed a similar pinning of E_F for the V(V)/V(IV) and V(IV)/V(III) couples in the thiospinels. On the other hand, we could not access the Ni(III)/Ni(II) couple in $Li[Ni_{0.5}Ti_{1.5}]O_4$, which shows that the influence of a counter cation can be important for stabilization of a pinned redox couple.

Conclusions and Future Directions

Our data show that any anode that gives a voltage $V \leq$ 1.0 V will form an SEI passivation layer in a cell that uses a non-aqueous carbonate electrolyte. Since formation of an SEI layer restricts the rate at which a cell can be charged without plating of lithium on its surface, it is now evident that with the existing electrolytes, a rapid charge can only be achieved if the anode gives a voltage $V > 1.0$ V versus lithium. Moreover, the capacity of a cell with available solid cathode materials is limited by the capacity of the cathode, and this capacity suffers an irreversible loss on the initial charge by capture of Li in the SEI layer of any anode giving a $V \leq 1.0$ V versus lithium. Therefore, in order to have a rapid charge that is safe, the anode must give a $V > 1.0$ V versus lithium. At present, the best such anode insertion compound is the spinel $Li_4Ti_5O_{12}$, which gives a $V = 1.5$ V versus lithium, but it has a limited capacity. In the present fiscal year, we will provide an anode oxide insertion compound with twice the capacity of $Li_4Ti_5O_{12}$ that gives a voltage in the range $1.2 < V < 1.6$ V.

FY 2009 Publications/Presentations

1. Y.-S. Kim and J.B. Goodenough, " Lithium Intercalation into $ATi_2(PS_4)_3$ (A = Li, Na, Ag) *Electrochemistry Communications* **10**, 497-501 (2008)
2. Youngsik Kim and John B. Goodenough, "Lithium Insertion into Transition Metal Monosulfides: Tuning the Position of the Metal 4s Band," *J. Phys. Chem. C.* **112**, 15060 (2008)
3. Y. Huang and J.B. Goodenough, "High-rate $LiFePO_4$ lithium rechargeable battery promoted by electrochemically-active polymers," *Chem. Mater.* **20**, 7237-7241 (2008)
4. Y. Kim and J.B. Goodenough, "Reinvestigation of $Li_{1-x}Ti_yV_{1-y}S_2$ Electrodes in Suitable Electrolyte: Highly Improved Electrochemical Properties," *Electrochem. Solid-State Lett.* **12**, A73 (2009)
5. J.B. Goodenough, K. Park, S. Song, and J. Han, "Access to M^{3+}/M^{2+} Redox Couples in Layered $LiMS_2$ Sulfides (M = Ti, V, Cr) as Anodes for Li-ion Battery," *J. Electrochem. Soc.* **156**, A703-A708 (2009)
6. Presentation to the 2008 DOE Annual Peer Review Meeting.

V.C.5 Intermetallic Anodes (ANL)

Michael Thackeray
Argonne National Laboratory
9700 South Cass Avenue
Argonne, IL 60439
Phone : (630) 252-9184 ; Fax : (630) 252-4176
E-mail: thackeray@anl.gov

Collaborators:
J. T. Vaughey, Argonne National Laboratory
L. Trahey, Argonne National Laboratory
V. Pol, Argonne National Laboratory
C. Wolverton, Northwestern University
D. Shin, Northwestern University

Start Date: October 1, 2008
Projected End Date: September 30, 2010

Objectives

Design high capacity metal, semi-metal or intermetallic anodes that will provide electrochemical couples to meet the 40-mile range requirement of PHEVs

- Improve the design and performance of Sn- and Si-based intermetallic electrodes
- Use theoretical modeling as a guide to identify, design and understand the electrochemical properties of novel intermetallic electrode system

Technical Barriers

- Low energy density
- Poor low temperature operation
- Abuse tolerance limitations

Technical Targets (USABC - End of life)

- 142 Wh/kg, 317 W/kg (PHEV40 requirement)
- Cycle life: 5,000 cycles
- Calendar life: 15 years

Accomplishments

- Synthesized copper foam substrates and Cu_6Sn_5/Sn electrodes by electrodeposition.
- Evaluated various copper-tin electrodes. A rechargeable capacity of 670mAh/g was achieved which is significantly greater than that obtained previously from Cu_6Sn_5 electrodes alone.
- Completed an experimental/theoretical study of $LaSn_3$ electrodes. Used computational first-principles methods to determine a likely mechanism for the reaction of lithium with $LaSn_3$.

✧ ✧ ✧ ✧ ✧

Introduction

A search for an alternative anode to replace graphite in lithium-ion batteries has been conducted for many years. Various classes of materials have been investigated, notably: i) metals, ii) metalloids, iii) intermetallic compounds, and iv) metal oxides. Metals (e.g., Sn), metalloids (e.g., Si) and intermetallic compounds (e.g., Cu_6Sn_5) are of particular interest because they offer significantly higher theoretical volumetric and gravimetric capacities compared to graphite (372 mAh/g and 818 mAh/ml), and because they react with lithium several hundred millivolts above the potential of metallic lithium. However, these materials have densely packed structures and therefore expand considerably on reaction with lithium.

The major objective of our work is to design a three-dimensional, microporous copper architecture that can act as a current collector and substrate for copper-based intermetallic electrodes, such as Cu_6Sn_5, that will provide a sufficient void volume to accommodate the volumetric expansion associated with the reaction of the intermetallic compound with lithium. Such a design has already been successfully used in high temperature Na/$NiCl_2$ cells; in this case, a porous, sintered nickel current collector is used as the substrate for the electrochemically deposited nickel particles generated during discharge of cells. The displacement reaction:

$$2\,Na + NiCl_2 \leftrightarrow 2\,NaCl + Ni \qquad (1)$$

which is accompanied by a 64% increase in volume at the cathode, and is fully reversible at 300 °C. In principle, therefore, it seems that it should be possible to design an analogous copper current collecting architecture and substrate for intermetallic electrodes that operate by lithium insertion/copper displacement reactions and to improve the reversibility of such reactions. We have used this approach to fabricate, evaluate and characterize three-dimensional, composite Cu_6Sn_5-Sn electrode architectures in which a sintered, microporous copper foam substrate acts as the current collector.

We have also investigated the highly Sn-rich compound, $LaSn_3$, as an anode material.

Approach

- Search for, and design, inexpensive intermetallic electrode materials that provide an electrochemical potential several hundred mV above Li^0, notably Sn-based materials, and a capacity of at least 400 mAh/g.
- Focus on compounds in which there is a strong structural relationship between the parent and product to minimize lithium diffusion distances.
- Use high surface area copper foam current collectors and electrodeposited Cu_6Sn_5 and Sn.
- Use computational modeling to aid the design and understanding of electrode structures on reaction with lithium, e.g., $LaSn_3$ with a high Sn content.

Results

Electrodeposition of Cu_6Sn_5/Sn. Electrodeposited Cu_6Sn_5-Sn products with appreciable concentrations of Cu_6Sn_5 and Sn and without the production of inactive Cu-Sn phases, such as Cu_4Sn, and Cu_3Sn) could be produced when solutions of $CuCl_2$ and $SnCl_2$ heavily rich in Sn were used. For our experiments, a 100:1 ratio of Sn:Cu was selected. Electrodeposition was carried out using a potential square wave in a scanner loop program. The X-ray diffraction pattern of a product, electrodeposited on copper foil from a 0.002 M $CuCl_2 \cdot 2H_2O$, 0.2 M $SnCl_2$, 12 vol.% HCl solution, confirmed that a tin-rich composite of Sn and Cu_6Sn_5 had been formed (Figure V- 69a). Annealing the product at 150°C under argon, increased the crystallization of the Cu_6Sn_5 component significantly, as evident from the growth and improved resolution of the Cu_6Sn_5 XRD peaks in Figure V- 69b.

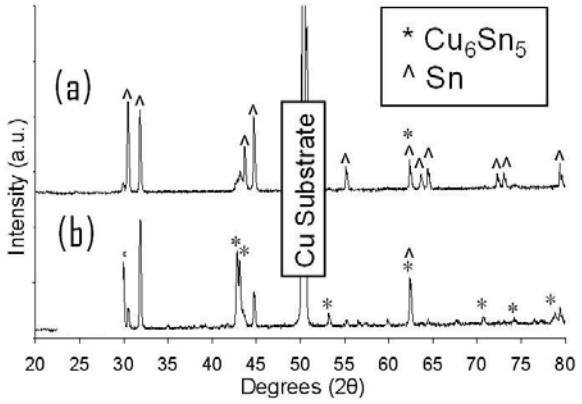

Figure V- 69: XRD patterns of (a) electrodeposited Cu_6Sn_5-Sn product (as-grown) on Cu foil; (b) after annealing at 150 °C

Electrodeposition of Cu_6Sn_5/Sn on Cu Foam. An SEM image of a copper foam substrate produced by the electrodeposition of copper onto copper foil is shown in Figure V- 70a. The as-grown foam is brittle and powdery. Therefore, in order to strengthen the foam and its contact to the underlying copper foil, the substrate was sintered at 500°C under argon for 45 hours. The resulting morphology change is notable (Figure V- 70b). Although the foam lost some porosity, the intrinsic strength of the three-dimensional copper architecture increased significantly and provided a sufficiently robust substrate for depositing the active Cu_6Sn_5-Sn electrode material. A SEM micrograph of the final Cu_6Sn_5-Sn on Cu electrode architecture, after annealing at 150°C, is shown in Figure V- 70c.

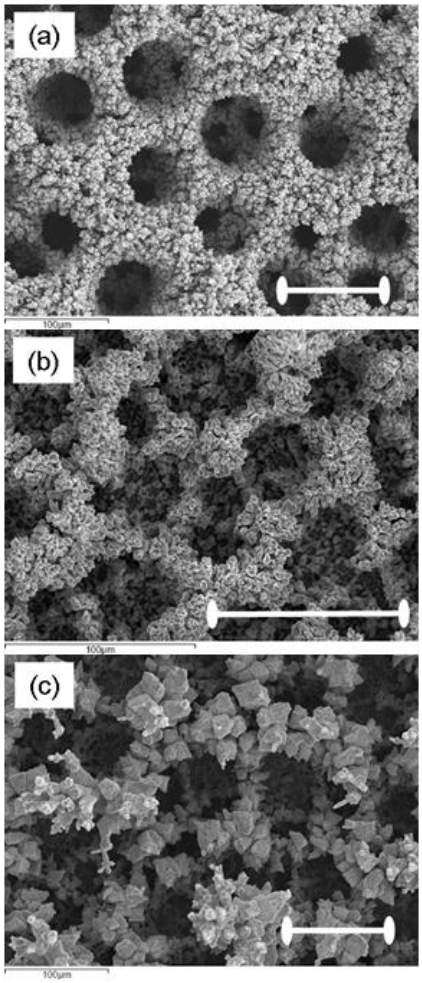

Figure V- 70: SEM micrographs of (a) copper foam, as grown, (b) sintered copper foam (500°C), and (c) electrodeposited Cu_6Sn_5-Sn film on sintered copper foam. All scale bars represent 100 µm.

Electrochemistry. A capacity vs. cycle number plot for the first 54 cycles of a Li/Cu_6Sn_5-Sn, Cu-foam coin cell is shown in Figure V- 71. Four break-in cycles, during which the capacity dropped steadily from an initial value of ~1020 mAh/g, were necessary before the capacity steadied at ~670 mAh/g for the next 26 cycles. The significant irreversible capacity loss that occurs during the break-in cycles is typical for metal and intermetallic electrodes, and is attributed largely to irreversible reactions

with the electrolyte that form a solid electrolyte interphase (SEI) layer on the active copper-tin particles. The discharge capacity delivered by the reaction of lithium with the Cu_6Sn_5-Sn electrode of the Li/Cu_6Sn_5-Sn cell is slightly larger than the charge capacity; this behavior is attributed to the use of lithium as the counter electrode and that our cycling conditions did not allow the Cu_6Sn_5-Sn electrode to come to equilibrium and fully utilize all of the available capacity of the electrode during the electrochemical discharge reactions.

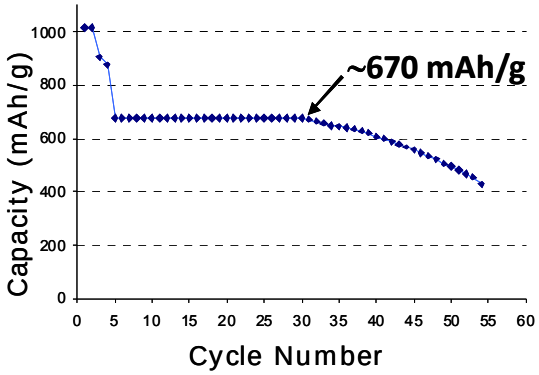

Figure V- 71: Discharge capacity vs. cycle number of a Li/Cu_6Sn_5-Sn, Cu-foam coin cell.

The experimental capacity of ~670 mAh/g obtained from the composite Cu_6Sn_5-Sn electrode is significantly higher than that achieved from Cu_6Sn_5 electrodes alone, as expected. By contrast, ball-milled Cu_6Sn_5 electrodes have been reported to yield a rechargeable capacity of ~200 mAh/g, whereas sputtered thin film Cu_6Sn_5 electrodes yield a rechargeable capacity of ~350 mAh/g. Although the electrochemically-deposited Cu_6Sn_5-Sn composite electrode delivered an impressive capacity during the early cycles, there was an abrupt onset of capacity fade at cycle 30 (Figure V- 71), the exact reasons for which have not yet been determined.

$LaSn_3$ Electrodes. In our search for new anode materials for lithium-ion batteries, we have undertaken investigations of $LaSn_3$ and isostructural $LaSn_{2.7}In_{0.3}$. $LaSn_3$ has an intermetallic "defect perovskite-type" structure; it is an interesting candidate anode material because 1) it has a high tin content and therefore a high theoretical specific capacity (677 mAh/g), and 2) the possibility exists that it might accommodate some lithium within its structure.

Despite its high Sn content, $LaSn_3$ electrodes were found to deliver only 225-250 mAh/g (or 33-36% of theoretical capacity). We therefore used computational first-principles calculations of various reactions to predict the preferred mechanism of lithium reaction with $LaSn_3$ as well as the likely reaction products. Table V-3 provides formation enthalpies and theoretical capacities derived from a $LaSn_3$ electrode for various competing reactions.

Table V-3: Formation enthalpies and $LaSn_3$ capacities for competing reactions

Reaction type	Reactions		Theor. Cap. (mAh/g)	ΔH (meV/Li)
Insertion	$Li + LaSn_3 \rightarrow LiLaSn_3$	(1)	54	864
	$12\ Li + LaSn_3 \rightarrow Li_{12}LaSn_3$	(2)	650	3232
Displacement	$66\ Li + 5\ LaSn_3 \rightarrow 5\ La + 3\ Li_{22}Sn_5$	(3)	715	-252
	$51\ Li + 4\ LaSn_3 \rightarrow 4\ La + 3\ Li_{17}Sn_4$	(4)	690	-275
	$88\ Li + 15\ LaSn_3 \rightarrow 5\ La_3Sn_5 + 4\ Li_{22}Sn_5$	(5)	318	-368
	$17\ Li + 3\ LaSn_3 \rightarrow La_3Sn_5 + Li_{17}Sn_4$	(6)	307	-395

Reactions (1) and (2) are insertion-type reactions. In reaction (1), the vacant octahedral site of the $LaSn_3$ defect perovskite structure is filled with Li to form hypothetical $LiLaSn_3$. In reaction (2), all the octahedral and tetrahedral interstitial sites in $LaSn_3$ are filled to form hypothetical $Li_{12}LaSn_3$. reactions (3)-(6) involve Sn displacement from the $LaSn_3$ structure and complete lithiation of the displaced Sn; both $Li_{17}Sn_4$ ($Li_{4.25}Sn$) and $Li_{22}Sn_5$ ($Li_{4.40}Sn$) compositions were considered as the fully lithiated Sn product. In reactions 3 and 4, complete displacement of Sn takes place to yield La metal, whereas in reactions 5 and 6, partial displacement of Sn yields La_3Sn_5. From Table V-3, we can draw the following conclusions: (i) lithium insertion reactions with $LaSn_3$ are energetically unfavorable and unlikely to occur; (ii) $Li_{17}Sn_4$ ($Li_{4.17}Sn$) is energetically more favored than the previously reported composition $Li_{22}Sn_5$ ($Li_{4.4}Sn$); (iii) the reaction in which Sn is partially displaced from $LaSn_3$ to yield La_3Sn_5 and $Li_{17}Sn_4$ is energetically preferred to complete displacement and lithiation of Sn (La and $Li_{17}Sn_4$).

Conclusions and Future Directions

- The project on $LaSn_3$ was completed.
- A significant improvement in the electrochemical properties of Cu_6Sn_5 was achieved by electrochemically co-depositing Cu_6Sn_5 and Sn onto a three-dimensional, high surface area copper foam current-collecting substrate. Excellent cycling stability was obtained during early operation (30 cycles) before the onset of capacity fade. This promising approach has opened the door for investigations of other electrodeposited intermetallic systems in FY2010.
- Preliminary studies (not discussed in this report) have shown that a recently-developed autogenic synthesis process shows promise for fabricating novel nano-composite and carbon-coated Si-C, intermetallic-C and metal-oxide-C anode materials. This technique for preparing materials with novel architectures will be a new research thrust in FY2010.

FY 2009 Publications/Presentations

1. L. Trahey, J. T. Vaughey, D. W. Dees, H. H. Kung and Michael M. Thackeray, J. Electrochem. Soc. **156,** A385 (2009).
2. J. T. Vaughey, M. M. Thackeray, D. Shin and C. Wolverton, J. Electrochem. Soc. (2009). **156,** A536 (2009).
3. Presentation to the 2009 DOE Annual Peer Review Meeting in Washington D.C.

V.C.6 Nanostructured Materials as Anodes (SUNY)

M. Stanley Whittingham (Project Manager)
SUNY at Binghamton
Vestal Parkway East
Binghamton, NY 13902-6000
Phone: (607) 777-4623; Fax: (607) 777-4623
E-mail: stanwhit@binghamton.edu

Start Date: June 1, 2007
Projected End Date: May 31, 2011

Objectives

- Replace the presently used carbon anodes with safer materials that will be compatible with low cost manganese oxide and phosphate cathodes and the associated electrolyte.

Technical Barriers

This project addresses the following technical barriers facing the use of lithium-ion batteries in PHEVs and all-electric vehicles:

(A) Materials and manufacturing cost of lithium-ion batteries

(B) Safety of lithium-ion batteries

(C) Volumetric capacity limitations of lithium-ion batteries

Technical Targets

- Determine and understand impact of depth of cycling on capacity fade (HEV *vs.* EV) for both crystalline and amorphous Sn
- Identify the structural and surface changes of Sn anodes during cycling
- Explore nano-size Sn/Si alloys and metal oxides to identify their cycling characteristics
- Explore Co-free alloys

Accomplishments

- Shown that bulk tin, in the form of foil, whether shallow or deep cycled, loses capacity at all depths of discharge.
- SEI film is not protective, and increases continuously in resistance
- Shown that amorphous nano-size tin does not lose capacity whether shallow or deep cycled.
  - Shows high rates for lithium release
  - Shown that this material is charge-limited, that is lithium insertion is slow
- Technology transfer accomplished.
  - Working with several local battery companies, and many ex-students now in battery companies
  - Students now have positions at BNL, LBNL, NREL, and PNNL

✧ ✧ ✧ ✧ ✧

Introduction

Achieving the DOE cost and energy/power density targets will require improved anode materials that have higher volumetric energy densities than carbon, and have lower cost production methods. At the same time the material must have higher lithium diffusion rates than carbon and preferably be at a slightly higher potential to improve the safety.

Approach

Our anode approach is to explore, synthesize, characterize and develop inexpensive materials that have a potential around 500 mV above that of pure lithium (to minimize risk of Li plating and thus enhance safety) and have higher volumetric energy densities than carbon. We are placing emphasis on simple metal alloys/composites from bulk to nano-size, to determine the impact of size; all present indications are indicating that nano is the way to go. The materials are evaluated electrochemically in a variety of cell configurations, and for thermal, kinetic and structural stability to gain an understanding of their behavior.

Results

Bulk Tin Foil Anodes. We have shown previously that, though pure tin foil has a very high rate of reaction with lithium, its capacity falls precipitously after ten to twelve deep cycles. We showed that the electrical resistance of these cells increases dramatically as the capacity fades. This is due to the continuous formation of the SEI layer as the tin expands and contracts on reaction with the lithium. In our anode collaboration, Robert Kostecki at LBNL has this year shown that the SEI layer formed on tin in the carbonate electrolytes in non-protective.

Reducing the depth of discharge of crystalline tin foil did not significantly increase the lifetime of the anode, as measured by total lithium plated, over that of deep cycling. The tin was cycled over the central portion of its capacity, that is around the 50% level. The results are shown in Figure V- 72, and show that the equivalent of 10-12 complete utilizations of the tin can be obtained before the capacity falls off.

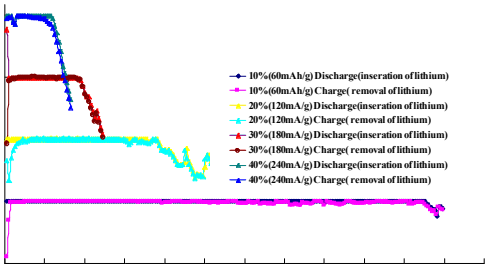

Figure V- 72: Cycling of tin foil at 1 mA/cm^2 at 10 – 40 % depth of discharge.

Amorphous Nano-Sized Tin. We have continued our understanding of the capabilities of the amorphous tin anode developed by SONY. We showed earlier that this material is a 1:1 alloy of tin and cobalt buried in a carbon matrix; the tin-cobalt particles are around 5-6 nm in size and amorphous to X-rays. A collaboration with P. Chupas at Argonne National Laboratory determined the local structure.

We have determined the cycle-ability of this material as a function of depth of discharge. The results are shown in Figure V- 73. At all depths of discharge studied, from 10% to 40%, the amorphous anode showed no loss of capacity in direct contrast to the crystalline tin foil. The electrodes were cycled at the fairly high rate of 1 mA/cm^2 on both charge and discharge; no top-up charging was used. These results are a clear indication that tin at the nano-size and in amorphous form can be cycled repetitively without capacity loss, and gives clear direction for future work on tin-based systems. However, this anode material, from the SONY cells, contains equal amounts of tin and cobalt, and thus is not viable for large-scale batteries because of the cost. We still must clearly show whether nano or amorphous is the more important parameter. Our earlier work on the nano-oxides, that are partially crystalline suggest that nano is the more important parameter.

Limitations to Amorphous Nano-Sized Tin. We set-out to determine the rate-capability on both lithium insertion and removal. The results are shown in Figure IV- 74. Figure IV- 74a shows the lithium insertion curve, which is the charging of the battery using this material as an anode. Figure IV- 74b shows the capacity as a percentage of the capacity at 0.1 mA/cm^2; for each data point, the lithium was first removed at the low rate of 0.1 mA/cm^2. It can be immediately seen that at the high rates used, the capacity falls off very rapidly. At a rate of 2 mA/cm^2 50% of the capacity is lost. In contrast, the capacity on lithium removal is maintained even at high rates; for example, around 70% of the capacity is retained at 10 mA/cm^2 (2.5C rate). Thus, this anode material can sustain high discharge rates but is more limited on charging. This could create problems with the fast charging needs of PHEV batteries, and has been reported for other metal alloys.

Other Anode Materials. We have shown that that the highly insulating behavior of the titanium oxide spinel anode can be alleviated by forming the oxide in a slightly reducing atmosphere. The resistance dropped from over 10^{12} ohm-cm to 10^6 ohm-cm. We have some clues that aluminum, when in a composite, may yet work as an anode in carbonate-based electrolytes – capacities of over 600 mAh/g have been maintained for over 12 cycles.

Conclusions and Future Directions

A clear result from our study of understanding the cycling behavior of tin anode materials is that nano/amorphous materials work, and that bulk materials with their high expansion on lithium reaction do not and are therefore unsuitable for batteries. In this particular case the nano material is protected from the electrolyte by a carbon coating, which also probably helps in keeping the tin nano on cycling and during formation. We do not yet know whether in this case nano and amorphous are both needed.

The cobalt in this particular anode material must be replaced and our future efforts will emphasize related compounds, including those of silicon that have minimal content of rare/expensive elements such as cobalt. We will also maintain a small effort to find other materials with a reaction voltage between 0.5 and 1.0 volts, that may exhibit the stability and high rates of the titanium oxide spinel without the associated 1.5 volt penalty.

FY 2009 Publications/Presentations

1. Presentation to the 2009 DOE Annual Peer Review Meeting.
2. M. S. Whittingham, “Materials Challenges Facing Electrical Energy Storage”, Mater. Res. Soc. Bulletin, 2008, 33: 411-420.
3. M. S. Whittingham, “Inorganic Nano-Materials for Batteries”, 2008, 5425-5431.
4. Many invited presentations, including:
   - GE, EPRI/CWRU, Dow, Exxon, NYSERDA, Chemical Heritage Foundation
   - IMLB, MRS, ISSI
   - Max-Planck, CSIRO, Brookhaven NL

- Bath, Columbia, Buffalo, Rochester U.
- Local outreach.

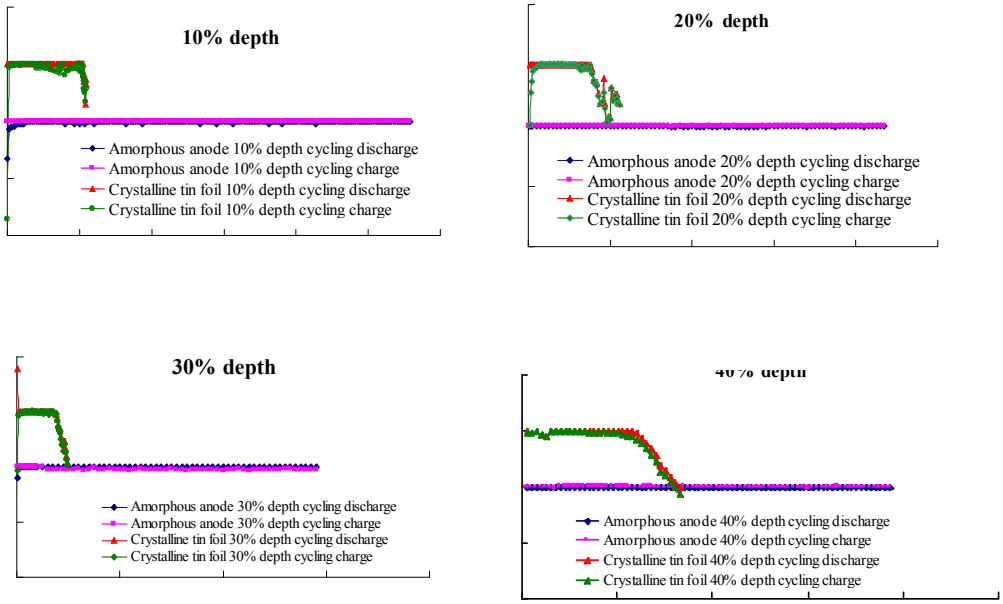

Figure V- 73: Shallow cycling of amorphous tin anode compared with that of crystalline tin foil.

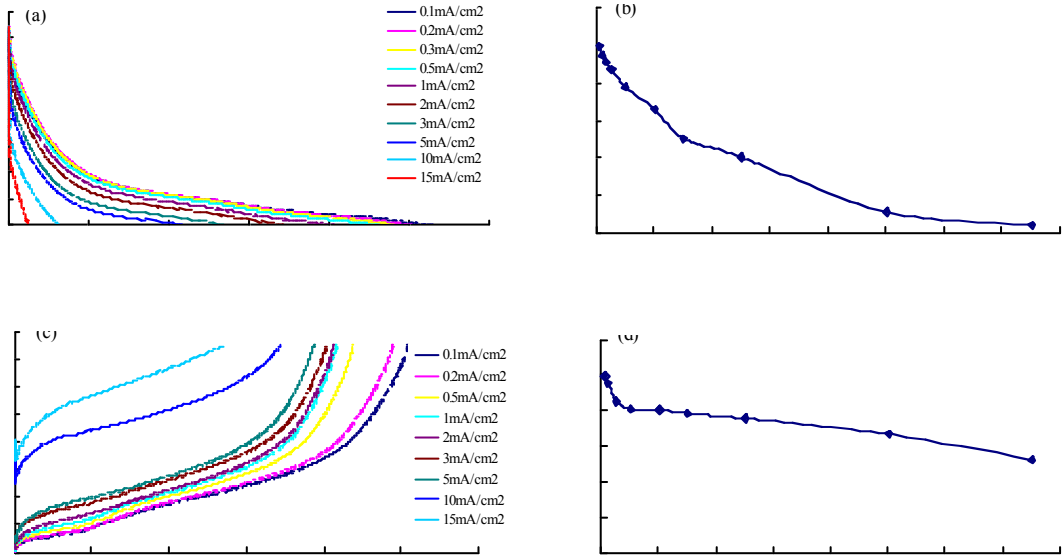

Figure V- 74: (a) The lithium insertion curves of amorphous Sn-Co anode cycled between 0 and 1.5V at different rates, and (b) rate capability; (c) the lithium removal curves at different rates, and (d) rate capability. [C rate is ≈ 4 mA/cm^2]

V.C.7 Development of High Capacity Anodes (PNNL)

Jun Liu, Ji-Guang Zhang
Pacific Northwest National Laboratory
902 Battelle Blvd., Mail Stop K3-59
Richland, WA 99352
Phone: (509) 375-4443; Fax: (509) 375-3864
E-mail: jun.liu@pnl.gov; jiguang.zhang@pnl.gov

Start Date: Oct. 1, 2008
Projected End Date: December 31, 2009

Objectives

- Develop high capacity anode materials with improved stability.
- Develop a low-cost synthesis route for high-capacity anodes.

Technical Barriers

Energy density, stability, and cost.

Technical Targets

- Synthesize well-controlled nanocomposite materials with improved conductivity and stability.
- Increase power rate of new anode materials.

Accomplishments

We developed a multiphase self-assembly approach using graphene as a fundamental building block to construct controlled graphene nanocomposites with SnO_2 and Si as active materials. A new class of layered nanocomposites is formed containing stable, ordered alternating layers of nanocrystalline metal oxide and graphene sheets from SnO_2. The self-assembly method can also be used to fabricate free standing, flexible graphene nanocomposite films and electrodes. The SnO_2-graphene nanocomposite films can achieve near theoretical specific energy density without significant charge/discharge degradation. A similar method is used for Si-graphene nanocomposites. We also used CVD to coat carbon on porous Si which exhibits a capacity of 1700 mAh/g in 30 cycles.

Introduction

Si and SnO_2 are good high capacity anode materials for Li-ion batteries, but usually show rapid capacity fading during charge/discharge cycles due to large volume expansion and phase transformation upon lithiation and de-lithiation. For example, high capacity has been reported in SnO_2/C composites, but capacity fading is still significant in these studies. Good capacity retention could be obtained by only using a much larger amount of carbon (above 60 wt %) in the electrode. Low conductivity and poor stability of such materials usually require the addition of conductive phases to enhance electron transport and electrical contact of the active materials in the electrode of Li-ion battery. In most of these studies, the approach has been used to prepare the composite materials by mixing metal oxides and conductive materials such as amorphous carbon, carbon nanotubes, and graphene, resulting poor distribution of the different components.

Approach

We developed novel ordered metal oxide-graphene nanocomposites by ternary self-assembly of metal oxides, surfactants and graphene sheets. We prefer to work with surfactants since they can not only assist the dispersion of graphene in aqueous media but also direct the self-assembly of metal oxides as structural agents into nanostructures. The anionic surfactants first adsorb onto the graphene sheets to ensure that the graphene sheets are dispersed in the hydrophobic domains of the surfactant micelles. The surfactant micelles with the graphene sheets then become the fundamental building blocks for self-assembly. The surfactants bind to the metal cations and self-assemble with the graphene sheet to form an ordered nanocomposite. Subsequently, the metal oxides are crystallized between the graphene sheets, producing a new class of nanocomposites in which alternating layers of graphene sheets and metal oxide nanocrystals are assembled into layered nanostructures.

In another effort, porous silicon (VESTA Ceramics Inc.) has been investigated as an anode material for Li-ion batteries. A thin layer of carbon was coated on the surface and within the pores in the porous Si by CVD method. The content of the carbon in the Si/C composite is about 6 % according to the weight gain.

Results

SnO_2/graphene nanocomposites. The structures of the nanocomposites were characterized by transmission electron microscopy (TEM). Figure V- 75 shows the cross-sectional TEM results of the nanostructures of alternating layers of metal oxides and graphene sheets in a SnO_2-graphene composite prepared in powder form. The cross-sectional TEM image of the calcined SnO_2-graphene composite clearly shows the regular multilayers (Figure V-75A). Each layer is about 3 to 5 nm thick and is rather uniform. A selected area electron diffraction (SAED, inset in Figure V- 75A) pattern suggests a typical crystal structure of cassiterite SnO_2 (JCPDS No. 000-0024), which is consistent with the X-ray diffraction (XRD) results. The corresponding dark-field image from the (211) reflection of SnO_2 (Figure V- 76B) confirms that the SnO_2 layer is made out of 4-nm crystals. Two symmetrical but diffuse diffraction spots are also observed on top of the (110) diffraction ring of the SnO_2, which are attributed to the (0002) diffraction of graphite-like multilayer graphene sheets. The dark-field image (Figure V- 75C) from the (0002) diffraction indeed reveals some band structures of the multilayer graphene sheets separated by SnO_2. A high-magnification TEM image (Figure V- 75D) reveals that the SnO_2 nanoparticles are connected to one another within the layer but separated from layer to layer by graphene sheets. Lattice fringes of both the (110) plane in 4-nm-diameter nanocrystalline SnO_2 and the (0002) plane in multilayer graphene sheets are observed in the high-resolution TEM image (Figure V- 75E).

The charge/discharge properties of the SnO_2-graphene nanocomposite film were investigated. The free-standing SnO_2-graphene nanocomposite electrodes (see Figure V-76(A) and Figure V- 76(B)) were studied using a half cell design without using other carbon additive, polymer binder or a metal current collector. The voltage-capacity profiles (see Figure V- 76C) of the SnO_2-graphene nanocomposite electrode at different current densities indicate good charge/discharge reversibility. The increase in specific capacity during the initial 10 cycles is attributed to improvement in electrolyte wetting of dense SnO_2-graphene nanocomposite electrode. As the electrode is well wetted by the electrolyte, a steady specific capacity of SnO_2 (625 mAh/g) is obtained at a current density of 0.01 A/g. A steady specific capacity of 760 mAh/g for the nanocomposite electrode can be obtained at a current density of 0.008 A/g, close to the theoretical capacity of SnO_2 (780 mAh/g). The specific capacities of 225 and 550 mAh/g are obtained at current densities of 0.08 and 0.02 A/g, respectively.

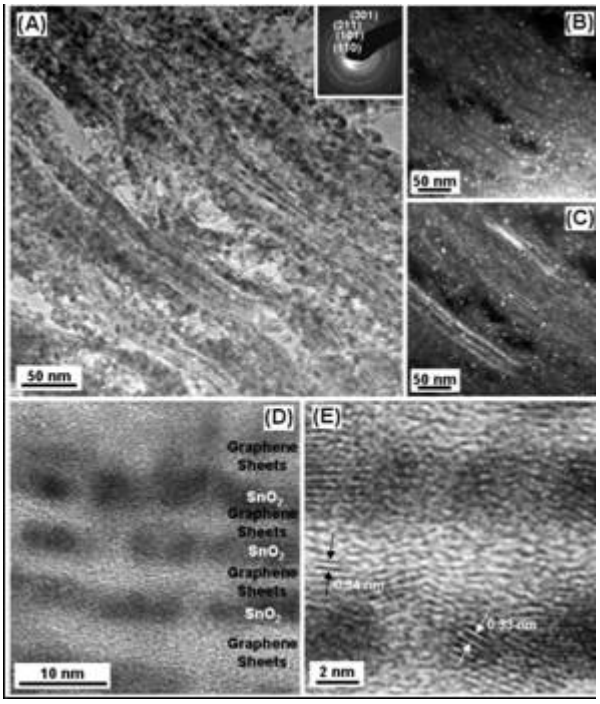

Figure V- 75: TEM images of calcined SnO_2-graphene nanocomposites. (A) Bright-field cross-sectional TEM image of the SnO_2-graphene nanocomposite powder showing layered structures. The inset is the corresponding SAED pattern. The ring pattern of diffraction shows polycrystalline cassiterite SnO_2. (B) Dark-field TEM image obtained from the (211) diffraction ring of SnO_2. (C) Dark-field TEM image obtained from the bright (002) diffraction spots of the graphene sheets. (D) High-magnification TEM of SnO_2-graphene nanocomposites in (A). The layered structure of SnO_2 is composed of connected nanocrystalline SnO_2 with a 4-5 nm diameter interspaced by graphene sheets. (E) High-resolution TEM image of the layered nanostructure of SnO_2-graphene nanocomposites in (D). Lattice fringes of 0.33 nm corresponding to the (110) plane of SnO_2 and lattice fringes of 0.34 nm corresponding to the (002) multilayer graphene sheets are marked in each layer.

Si/graphene nanocomposites. The Si-graphene nanocomposite was prepared using similar method as in the SnO_2/graphene nanocomposites, but using Si nanoparticles. The electrode was tested for cycling performance at C/65 and C/6 rate as shown in Figure V-77. Carbon content was 66wt% including graphene. A stable specific capacity of ~1000mAh/g for Si is obtained, which is more stable than traditional Si- carbon electrode.

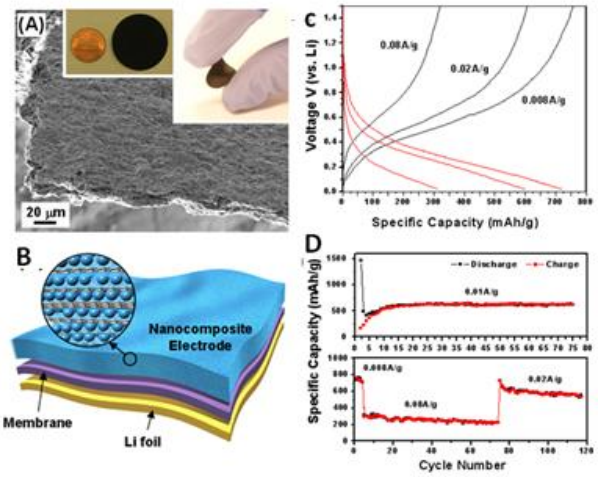

Figure V- 76: (A) Side-view SEM image of a self-assembled free-standing SnO_2-graphene nanocomposite (40 wt% graphene sheets) electrode 15-μm thick. Photographs in the insert show a disk-like 3-cm-diameter SnO_2-graphene nanocomposite electrode on the left and a folded electrode on the right. (B) A Li-ion battery configuration directly using a free-standing metal oxide-graphene nanocomposite film as an electrode. The graphene sheets in the layered nanostructures functions as both current collector and conductive additives in the anode. (C) Charge/discharge profiles of a SnO_2-graphene nanocomposite electrode (40 wt% graphene sheets) between 0.02 V and 1.5 V at a current density of 0.008 A/g, 0.02A/g and 0.08 A/g, respectively. (D) Top: Specific capacity of SnO_2 as a function of charge/discharge cycles in the SnO_2-graphene nanocomposite electrode at a current density of 0.01 A/g. Bottom: Specific capacity of SnO_2 as a function of charge/discharge cycles in the SnO_2-graphene nanocomposite at different charge/discharge current densities of 0.008 A/g, 0.08 A/g and 0.02 A/g, respectively.

Carbon coated Porous Si. Figure V- 78 compares XRD pattern of porous Si before and after carbon coating. No significant change in the XRD patterns were observed before and after carbon was coated on porous Si by CVD. This suggests that the coated carbon is amorphous. The pore size of the original porous silicon is around 5 nm as shown in Figure V- 79. During the CVD coating process, carbon was coated inside of porous Si. This uniform coating of carbon is expected to form a durable conductive layer and absorb the volume expansion of Si during lithium insertion and thus stabilizes the cycling performance of Si.

The cycling abilities of the porous Si are shown in Figure V- 80. Both pure porous Si and carbon-coated porous Si show very high initial capacities at ~ 4000 mAh/g. The capacity of pure porous Si decays to ~500 mAh/g quickly after 20 cycles. After CVD coating, the Si electrode shows a stable cycling with a high capacity of 1700 mAh/g up to 30 cycles. The coated amorphous carbon closely contacts with micro-sized Si particle (> 4 μm) increasing its electronic conductivity while the three dimensional porous structure of silicon itself facilitates the lithium transport and alleviates the huge volume expansion during cycling.

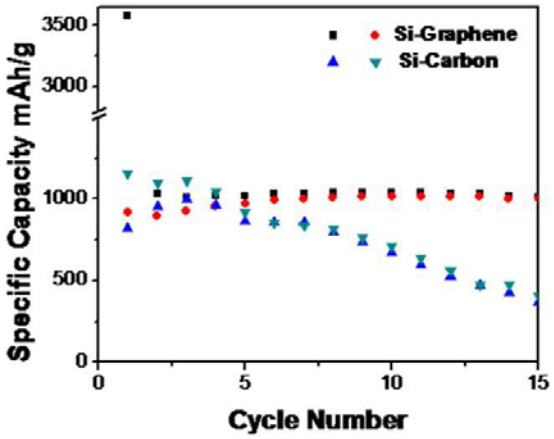

Figure V- 77: Comparison of specific capacity of Si-graphene nanocomposite and traditional Si-carbon electrode.

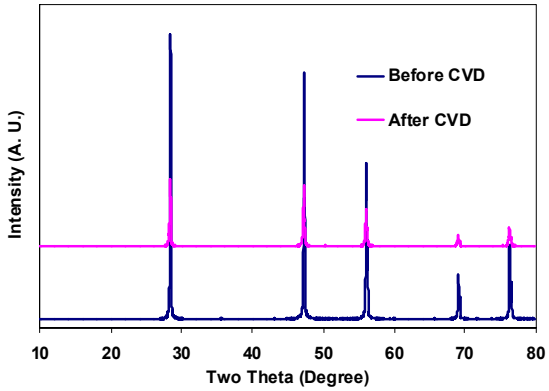

Figure V- 78: XRD pattern of porous Si before and after CVD coating.

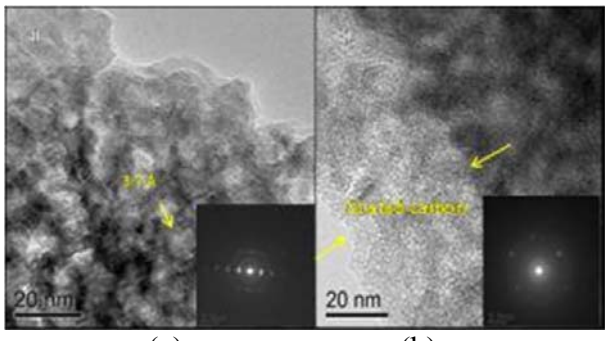

(a) (b)

Figure V- 79: TEM images of porous Si (a) before and (b) after carbon coating by CVD.

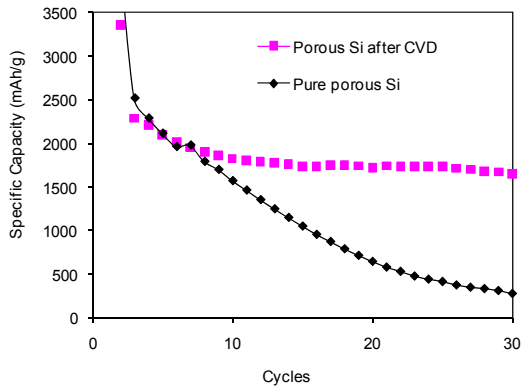

Figure V- 80: Comparison of cycling abilities of porous Si before and after CVD at 100 mA/g.

Conclusions and Future Directions

The SnO_2-graphene nanocomposite showed significantly increased stability. The nanocomposite structure, in particular the dimension and chemistry of the graphene materials, will be optimized to improve the high charge rate properties. For Si nanocomposite, the main focus will be on improving the binding between the Si and the carbon material. Carbon coated porous Si will be combined with graphene to improve their electrical conductivity, strengthen their three-dimensional architectures, and to increase their long-term cycling stability.

FY 2009 Publications/Presentations

1. D. Wang, D. Choi, J. Li, Z. Yang, Z. Nie, R. Kou, D. Hu, C. Wang, L. V. Saraf, J. Zhang, I. A. Aksay, J. Liu, "Self-Assembled TiO_2-Graphene Hybrid Nanostructures for Enhanced Li-ion Insertion," ACS Nano, ***cover article***, 3, 907-914, 2009.
2. Jun Liu, "Synthesis and Self-assembly of Nanostructured Materials for Energy", the Electrochemical Society 215th Meeting, San Francisco, May 24 to May 29, 2009. Invited.
3. Jun Liu, "Multifunctional Materials from Self-Assembly for Energy Storage", the University of Washington's Annual IGERT Nanotechnology Conference jointly with Japan's National Institute for Material Science (NIMS), panel talk, Seattle, June 9 to June 11, 2009. Invited.
4. Jun Liu, "Multiphase Self-Assembly Approaches for Advanced Energy Storage", 13th IACIS International Conference on Surface and Colloid Science and the 83rd ACS Colloid & Surface Science Symposium, panel talk, New York, June 13 to June 20, 2009. Invited.
5. Jun Liu, "Self-Assembled Nanocomposites", the Seventeenth Annual International Conference on COMPOSITES/NANO ENGINEERING, Honolulu, Hawaii, July 23 to August 1, 2009. Invited.
6. Jun Liu, "Nanostructured Materials for Energy Conversion and Storage", Nano and Giga Challenges in Electronics, Photonics and Renewable Energy and the 14th Canadian Semiconductor Technology Conference." Ontario, Canada, August 8 to August 16, 2009. Invited.
7. Jun Liu, "Multiphase Self-Assembly Approaches for Advanced Energy Storage", Micro Nano Breakthrough Conference 2009, Portland, September 21-23Oregon, 2009. Invited.
8. Ji-Guang Zhang, Jun Liu, Gary Z. Yang, Guan-Guang Xia, Daiwon Choi, Donghai Wang Chongmin Wang, Larry Pederson, and Gordon Graff, "Large-Scale Production of Si-Nanowires for Li-ion Battery Applications," presented on 214th ECS meeting in Honolulu, HI on Oct. 13-17, 2008.

V.D Electrolyte Development

In the electrolytes area, researchers are studying the stability of Polystyrene (PS)- Poly(ethylene oxide) (PEO)/LiTFSI electrolytes against Li electrodes, testing their properties against Li-metal anodes and $LiFePO_4$ cathodes, and investigating the use of block copolymers as separators with liquid electrolytes. Another team is determining the role of electrolyte structure upon the intrinsic electrochemical kinetics and how it contributes to the interfacial impedance and determining how bulk and electrode reactions of electrolytes contribute to impedance growth and lead to battery failure.

In addition, researchers are using molecular dynamics to explore the ability of reactive force fields to predict SEI layer composition and structure on graphite in contact with ethylene carbonate solvent, and to gain molecular level understanding of Li^+ transport mechanisms in ionic liquids, SEI layers and the process of Li intercalation/deintercalation from/into graphite, and from cathodes into/from liquid electrolytes. Finally, several new electrolyte projects have begun mid-way through 2009. Those projects are investigating: new additives for both anodic and cathodic stability; additives for overcharge protection; new materials conferring flame retardant properties; quantum chemical modeling to find good additives for SEI formation followed by constructing and testing of the most promising materials, and development of new salts other than $LiPF_6$.

V.D.1 Polymer Electrolytes for Advanced Lithium Batteries (LBNL)

Nitash P. Balsara

Lawrence Berkeley National Laboratory
1 Cyclotron Road
Berkeley, CA 94720
Phone: (510) 642-8973; Fax: (510) 642-4778
E-mail: NPBalsara@lbl.gov

Start Date: October 1, 2008
Projected End Date: September 30, 2010

Objectives

- Synthesize polystyrene-polyethyleneoxide-polystyrene (PS-PEO-PS) triblock copolymers with varying molecular weights and compositions to obtain polymer electrolytes with high ionic conductivity and shear modulus.
- Electrochemically characterize salt doped PS-PEO-PS electrolytes against Li-metal anodes in symmetric cells, with planar $LiCoO_2$ cathodes, and with sulfur cathodes.
- Synthesize polystyrene-polyethylene-polystyrene (PS-PE-PS) triblock copolymers for use as mesoporous battery separators.

Technical Barriers

This project examines the following technical barriers for the application of polymer electrolytes in batteries:

(A) Poor ion transport and low power, particularly at low temperatures

(B) Short life due to power and capacity fade

(C) Safety concerns due to the formation of dendrites when using lithium metal anodes

(D) Lithium polysulfide reaction intermediates (Li_2S_x $3 \leq x \leq 8$) are soluble in traditional battery electrolytes resulting in capacity fading

(E) Battery separators for liquid electrolytes need to maintain high ambient conductivity (>0.1 mS/cm) while the pore diameter decreases significantly (<50 nm)

Technical Targets

- 30 ohm-cm^2 area-specific impedance
- 300,000 shallow discharge cycles
- Abuse tolerance to cell overcharge and short circuit
- Electric vehicle (EV) application goals are a specific energy of 150 Wh/kg and a specific power of 300 W/kg

Accomplishments

- Measured PS-PEO conductivities with $Li[N(SO_2CF_3)_2]$ (LiTFSI) salt across broad molecular weight ranges, salt concentrations, and temperature ranges.
  - Found that conductivity in PS-PEO block copolymers increases with increasing PEO molecular weight
  - Determined optimum salt concentration of LiTFSI salt for conductivity (r=0.085)
  - Found that conductivity follows an Arrhenius relationship with temperature
- Measured salt diffusion coefficient in PS-PEO/LiTFSI systems across broad molecular weight ranges, salt concentrations, and temperature ranges
  - Found that salt diffusion coefficient increases with increasing PEO molecular weight in PS-PEO block copolymers
  - Salt diffusion coefficient does not depend strongly on salt concentration in this system
- Battery cycling experiments with Li-Li electrodes show that the lifespan of lithium metal batteries is increased by using PS-PEO, which contains a hard polystyrene phase. This is consistent with expectations.
- Initiated study of lithium polysulfide solubility in PEO and PS-PEO polymers
- Synthesized porous battery separators using PS-PE-PS block copolymers

✧ ✧ ✧ ✧ ✧

Introduction

Achieving the DOE goals for energy and power densities for EV applications will require dramatic improvements in electrolyte materials. We are currently taking three different approaches toward improving battery electrolytes. Each of these approaches addresses a unique concern and applies to different electrode systems.

Approach

To meet DOE energy and power density requirements for EV applications, electrolyte materials with high ionic conductivity and shear modulus must be synthesized. Solid polymer electrolytes will enable the use of lithium metal anodes in secondary batteries, which have much higher energy densities than traditional intercalation anodes. Homopolymer PEO doped with LiTFSI salt has been shown to have high ionic conductivity, even at low temperatures, which is essential for high specific power. However, PEO cannot suppress the formation of lithium dendrites that form in lithium metal systems. Work by Monroe and Newman, *J. Electrochemical Soc.* **2003**, 150 (10) has suggested that by increasing the modulus of the electrolyte material, lithium dendrite growth can be suppressed. We are therefore synthesizing PS-PEO-PS block copolymers, where PS, which has a large modulus, acts as a hard structural phase and PEO is a lithium ion conducting phase. It is necessary to understand the fundamental transport properties of lithium ions in these block copolymers. We will measure the conductivity, salt diffusion coefficient, and lithium transference number for these systems.

The use of sulfur as a cathode material can greatly increase the specific energy of a battery system. Most lithium polysulfide species (Li_2S_x $3 \leq x \leq 8$) that form during cycling are soluble in electrolytes. However, the most reduced species (Li_2S and Li_2S_2) are insoluble. This dissolution of lithium sulfides leads to decreases in capacity. Our initial studies examine the solubility of various lithium sulfur complexes in PS-PEO block copolymers. We are attempting to design a block copolymer electrolyte that will not dissolve these polysulfide intermediates.

Recent developments in battery technology have led to the use of electrode materials that are tens of nanometers in diameter for higher specific power. Block copolymers that can self-assemble into features on the order of tens of nanometers are being studied as potential battery separator materials for these electrode materials. These mesoporous separators are expected to have issues with wettability. PS wets the studied liquid electrolyte more favorably than PE. PS is partially soluble in traditional liquid electrolytes, which necessitates a structural PE block. PS-PE-PS block copolymers are being synthesized for these battery separator applications.

Results

Ionic Conductivity of PS-PEO/LiTFSI Systems. In order to achieve high specific power, electrolytes with high ionic conductivity are necessary. We have measured the conductivity of our PS-PEO/LiTFSI system as a function of salt concentration and molecular weight. In Figure V-81, the conductivity reaches a maximum at a salt concentration of r = 0.085, where r is the molar ratio of lithium to ethylene oxide repeat units. As molecular weight increases, the conductivity also increases. Conductivities as high as 1.1 mS/cm have been achieved at 120°C. These experiments have led to a recent publication[1].

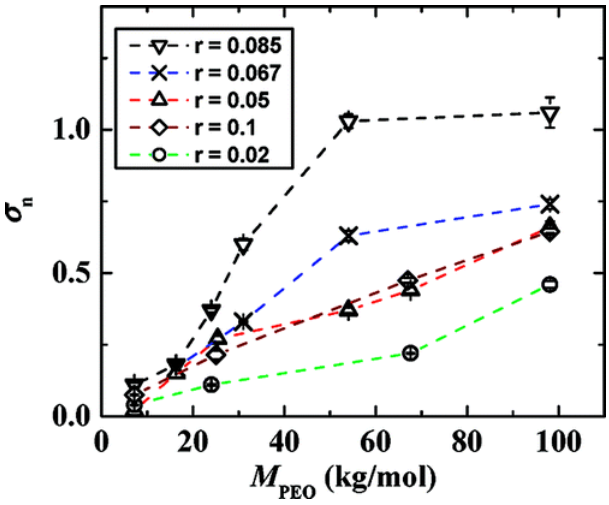

Figure V- 81: Temperature averaged normalized conductivity, σ_n, versus M_{PEO} for r = 0.02 – 0.10.

Salt Diffusion. We have measured the salt diffusion coefficients in a series of PS-PEO block copolymers using the restricted diffusion method. The initial measurements suggest that the diffusion coefficient does not depend strongly on the salt concentration. We do find, however, that the salt diffusion coefficient increases with the molecular weight of PEO block (Figure V- 82). We further find that the diffusion coefficient is about an order of magnitude less than that of PEO.

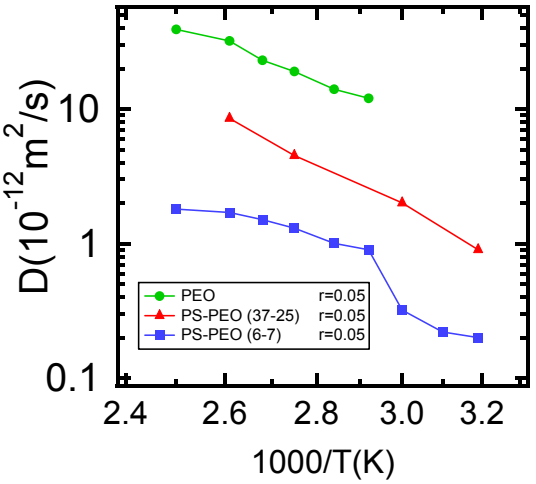

Figure V- 82: Salt diffusion coefficient for PEO and PS-PEO over a range of temperatures.

Increased Battery Lifespan with Higher Modulus Polymer Electrolytes. We have performed cycling experiments on PS-PEO/LiTFSI electrolytes using symmetric lithium electrodes (Figure V- 83). As expected, the block copolymer electrolyte batteries exhibited a much higher lifespan than homopolymer PEO based electrolytes, in which the battery lifespan is represented as the total current passed before failure. Battery failure is the point where a dendrite penetrates the electrolyte and shorts the cell when it reaches the opposite electrode. Batteries run near their limiting current tend to form dendrites and short more rapidly. This work is funded by the BATT program (EERE) and the Soft Matter Electron Microscopy program (BES).

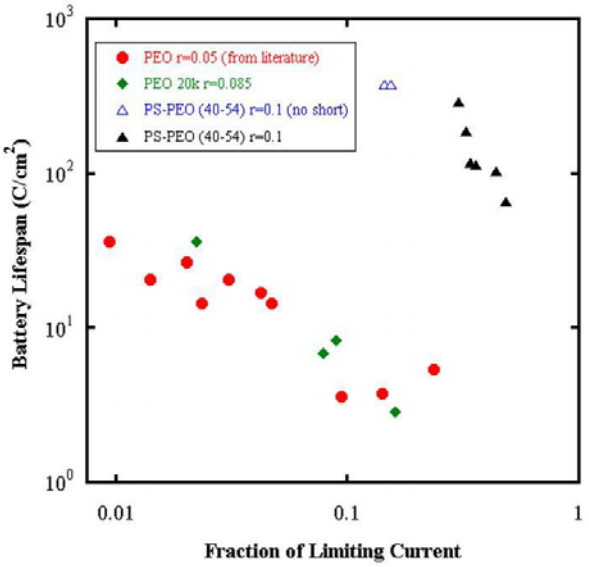

Figure V- 83: Battery lifespan for symmetric lithium-lithium cells containing either homopolymer PEO or block copolymer PS-PEO

Porous Battery Separators from PS-PE-PS Block Copolymers. We have synthesized porous battery separator materials from PS-PE-PS triblock copolymers. By blending homopolymer PS with these block copolymers, we can generate holes by removing the homopolymer using a selective solvent. A scanning electron micrograph of a separator material with a porosity of 29% made by this method confirms the porous nature of the material (Figure V- 84).

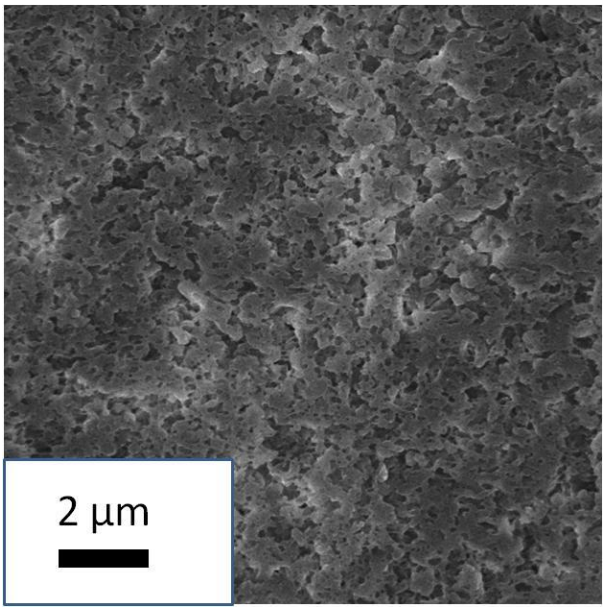

Figure V- 84: SEM of porous PS-PE-PS battery separator

Conclusions and Future Directions

The diblock copolymer PS-PEO was studied extensively and the results were presented in this report. Conductivity, salt diffusion, and symmetric lithium-lithium battery cycling data were presented. An optimum salt concentration was determined and the effect of PEO molecular weight shown. Salt diffusion data suggest that PEO molecular weight has an effect on the diffusion coefficient. Lithium-lithium battery cycling experiments showed that the higher modulus PS-PEO/LiTFSI electrolytes resisted the formation of dendrites much better than homopolymer PEO. The present study is being expanded to examine PS-PEO-PS triblock copolymers to improve mechanical properties. These polymers are currently being synthesized. The transport properties – conductivity, salt diffusion coefficient, and lithium transference number – will be measured for these systems, in addition to battery cycling experiments.

The solubility of the lithium polysulfides in PS-PEO and PS-PEO-PS is being studied. Light scattering and X-ray diffraction experiments will be used to study the solubility of these complexes in polymers at different temperatures. Different polymer systems will be explored to identify candidates for lithium sulfur battery electrolytes.

The triblock copolymer PS-PE-PS has been synthesized by hydrogenation of commercial polymers. The porous nature of these materials has been verified using SEM. Conductivity experiments using liquid electrolytes have been initiated with these battery separator materials. Conductivity and pore geometry of these polymers at varying molecular weights and volume fractions will be studied.

FY 2009 Publications/Presentations

1. Panday, A.; Mullin, S.; Gomez, E.D.; Wanakule, N.; Chen, V.L.; Hexemer, A.; Pople, J.; Balsara, N.P. *Macromolecules* **2009**, 42, 4632-4637.
2. Wanakule, N.S.; Panday, A.; Mullin, S.A.; Gann, E.; Hexemer, A.; Balsara, N.P. *Macromolecules* **2009**, 42, 5642-5651.
3. Mullin, S.A.; Panday, A.; Balsara, N.P., Presentation to the American Physical Society March Meeting, Pittsburgh, PA, "Ion Transport Through Block Copolymer Electrolytes," March 16th, 2009.
4. Wanakule, N.S.; Panday, A.; Mullin, S.A.; Balsara, N.P. Presentation to the American Physical Society March Meeting, Pittsburgh, PA, "Ionic Conductivity of Poly(ethylene oxide)-Containing Block Copolymers at Order-Disorder and Order-Order Transitions," March 19th, 2009.
5. Mullin, S.A.; Panday, A.; Balsara, N.P., Presentation to The Electrochemical Society 215th Meeting, San Francisco, CA, "Transport in a Microstructured Polymer Electrolyte for Secondary Lithium Batteries," May 25th, 2009.
6. Wanakule, N.S.; Panday, A.; Mullin, S.A.; Balsara, N.P. Presentation to The Electrochemical Society 215th Meeting, San Francisco, CA, "Ionic Conductivity of Poly(ethylene oxide)-Containing Block Copolymer Electrolytes," May 26th, 2009.

V.D.2 Interfacial Behavior of Electrolytes (LBNL)

John B. Kerr
Lawrence Berkeley National Laboratory,
MS 62R0203, 1 Cvclotron Road,
Berkeley, CA 94720
Phone: (510) 486-6279; Fax: (510) 486-4995
E-mail: jbkerr@lbl.gov

Start Date: October 1, 2008
Projected End Date: September 30, 2010

Objectives

FY09

- Determine the role of electrolyte structure upon the intrinsic electrochemical kinetics and how it contributes to the interfacial impedance.
- Determine how bulk and electrode reactions of electrolytes contribute to impedance growth and lead to battery failure.

FY08

- Investigate the feasibility of pre-forming SEI layers on both anodes and cathodes by use of electrolyte additives, chemical modification of the electrode particles and coating with single-ion conductor polymers.
- Determine whether the interfacial impedance of single-ion conductors can be reduced to practical values (< 20 $\Omega.cm^2$ at RT).
- Evaluate the use of very high rate polymer electrodes and redox active binders.

Technical Barriers

This project addresses the following technical barriers

- Poor cycle and calendar life.
- Low power and energy densities.
- High manufacturing cost.
- Safety

Technical Targets

- Determine the feasibility of pre-forming electrode SEI layers using additives, chemical modifications and single-ion conductor polymer coatings.
- Complete the evaluation of the impedance characteristics of single ion conductor electrolytes and binders at composite electrodes.
- Complete evaluation of the interfacial behavior of at least three anode materials.
- Complete evaluation of the interfacial behavior of three cathode materials.
- Determine the contribution to the interfacial impedance of the SEI layers versus intrinsic electrode kinetics.

Accomplishments

- Prepared larger quantities of single ion conductor materials for use in interfacial experiments. Prepared materials useful for low voltage (<3.6V) and high voltage (>4V) operations.
- Developed three-electrode cell testing system that provides insight into interfacial behavior of an electrode without interference of other electrodes.
- Continued to characterize effects of impurities on electrolyte reactivity.

✧ ✧ ✧ ✧ ✧

Introduction

The presence of large interfacial resistances is a critical barrier to the deployment of Li-ion batteries in traction vehicles. Inherent reactivity of presently available electrolytes results in poor rate and energy density capabilities over time resulting in poor lifetime. This effect of reactivity is in addition to the intrinsic safety issues. Single-ion polyelectrolyte lithium conductors possess the potential solution for many of the problems with present electrolytes. They can be used with no liquid electrolyte thereby reducing the safety problem. They can be prepared and deployed in ways that avoid many of the reactivity issues both in the bulk of the electrolytes and at the interfaces. Because they possess a unity transference number, there is no concentration polarization through the composite electrodes. Thus, provided the conductivity is in excess of 10^{-4} S/cm, the single ion conductors (SIC) can facilitate the use of thicker composite electrodes thereby leading to higher energy and power densities. In past years, this group has demonstrated that SIC materials, both dry and as gels, possess the bulk transport properties required. However, the interfacial behavior of these materials has exhibited disastrously high impedances rendering the SIC materials unusable. It is imperative that the source of this

impedance be elucidated and reduced to manageable values and hence the whole goal of the work is to elucidate the mechanisms that lead to interfacial impedance so that this critical factor may be minimized.

There is considerable continuing discussion in the literature about the effect of the solid electrolyte interphase (SEI) upon the interfacial impedance of Li-ion battery electrodes. Growth of the impedance is one mode of failure that limits the calendar and cycle life of Li-ion batteries. From studies of a variety of electrolytes ranging from single ion polyelectrolyte Li-ion conductors through binary salt polymer electrolytes, polymer gels, ionic liquids and liquid electrolytes it has been noted that the properties of the electrolyte have a significant impact on the apparent intrinsic rates of electrode reactions quite apart from their reactions to form side products that may form the SEI layer. To separate out these effects we have attempted to study a variety of electrodes with a variety of electrolytes that can allow the separation of the effect of side reactions from that of intrinsic kinetics. Needless to say, the effects of trace impurities and intrinsic instabilities in both the electrolytes and the electrodes can have a major impact upon the interfacial behavior and considerable effort is still required to properly characterize the materials for reproducible results.

Approach

A physical organic chemistry approach is taken to electrolyte design, where the molecular structure is varied to provide insight into the processes that may affect the performance of the battery. These processes include transport properties, electrochemical kinetics, electrode side-reactions, thermal stability of the bulk material and interfacial behavior. The work involves use of model compounds as well as new synthesis of materials to test hypotheses which may explain battery behavior. Examples include:

- Different solvents and salts, including polymer gels.
- Electrode materials with different reaction potentials.
- Single-ion conductor polyelectrolyte gels.
- Functionalized surfaces for electrode components.

To accomplish this work requires collaboration with other groups in BATT.

- Surface analysis groups to identify side reaction products and reactive intermediates by combination of spectroscopy and product distribution analysis,
- MD and electrochemical systems modeling groups to provide experimental data.
- Deliver promising materials to cell testing group.

Results

Preparation of Single Ion Conductor Materials. Synthetic procedures have been developed under other programs to prepare polymer structures similar to the one shown in Figure V- 85. The anionic groups (Y) may be grafted on to the polymer in any appropriate concentration to optimize the properties.

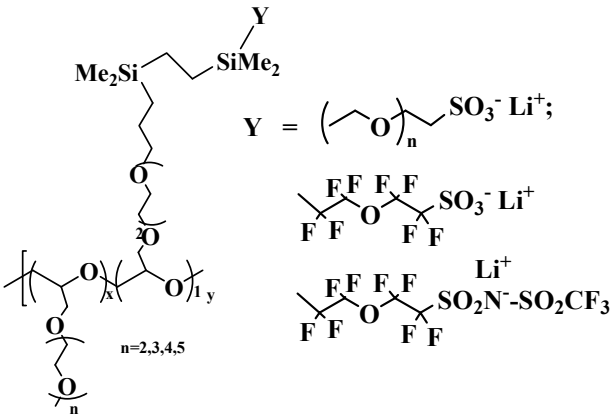

Figure V- 85: General structure of polyelectrolyte single ion conductors

These polyelectrolytes are based upon polyethers and have shown encouraging bulk conductivities of 10^{-5}S/cm at room temperature in the dry state and very much higher conductivities when gelled with solvents such as propylene and ethylene carbonate. The bulk lithium ion transport properties are therefore suitable for use in electric vehicles. However, these materials demonstrate very large interfacial impedances (> 1000 Ω.cm^2 at 80°C) at lithium metal and composite electrodes. In order to study the source of the impedance it has been necessary to prepare larger batches of quality material in order to study the interfacial behavior. The synthesis of these materials is achieved largely through co-operation with programs funded by the Office of Fuel Cell Technologies.

The materials shown in Figure V- 85 are not suitable for use with high voltage cathodes with voltages above 4V. Again, in cooperation with the fuel cell program, new polyelectrolytes have been synthesized which are stable to > 4V vs. Li^0. These are shown in Figure V- 86 where the Y groups may be selected from those listed in Figure V- 85. The high voltage materials are those where the Y group is perfluorinated. These materials are not so suitable for anode structures but the ability to choose the structural features for a particular electrode application is attractive. These materials show interesting properties particularly with respect to interfacial properties.

The grafting technique that attaches the Y groups to the polymers may also be used to attaché ionic groups to solid components of the composite electrodes. For example the carbon black conductivity additive that is often used in composite electrodes may be modified with these Y groups to provide a means of altering the local concentrations of ions in the electrodes close to the actual surface of the active electrode materials since the conductivity additives are often nano-scale. The developed

synthetic methods are being applied to this concept and results should be available early in FY10.

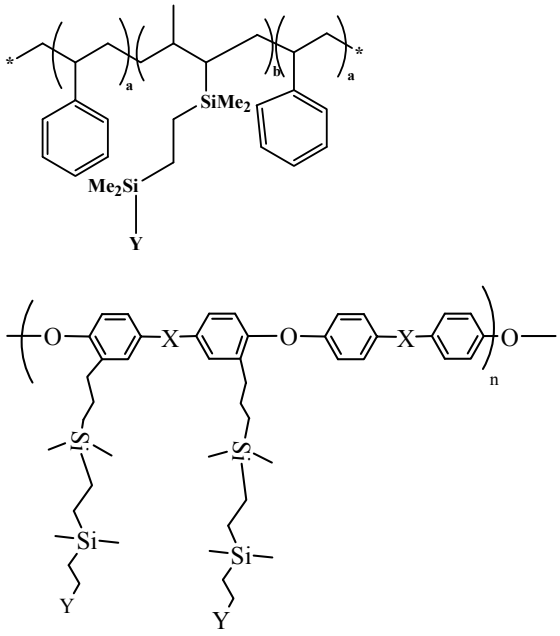

Figure V- 86: New polyelectrolyte materials for high voltage cathodes (>4Vvs. Li^0). Y is chosen from the list in Figure IV- 85.

Interfacial studies of conventional Li-ion battery electrolytes. Our initial primary goals included the provision of a reproducible test electrolyte system that could be used with presently available electrolytes as well as new ones. For this, the liquid electrolyte system consisting of mixtures of ethylene carbonate (EC) and ethyl methyl carbonate (EMC) with $LiPF_6$ and LiTFSI (TFSI = bis(trifluoromethylsulfonyl)imide). The LiTFSI salt was used as a control since the PF_6 material is known to possess considerable reactivity that influences the interfacial behavior. A part of this reactivity involves water impurities where it is though that PF_5 formed from the $LiPF_6$ reacts with water to form HF and PF_3O. These Lewis acid species are known to react with the electrolyte solvents as well as electrode surfaces.

Considerable effort has been expended to prepare totally dry electrolytes that have no water present as measured by Karl-Fischer (K-F) titration. It should be noted that measurement of water content of electrolytes is no guarantee that the electrolyte was not contaminated by water. Figure V- 87 shows the measurements of water content of electrolytes over several days at various temperatures. It can be seen that the water content drops to zero quickly for the PF_6 electrolytes which is consistent with the production of HF from the PF_6. It was noted that the presence of 50mM LiF in the solution did not prevent the disappearance of the water. Even more puzzling was the reduction of water content with LiTFSI. It was suspected that the purity of the LiTFSI was responsible but measurements with 3M HQ115 LiTFSI also showed the same behavior. It is conjectured that the water may hydrolyze the carbonate solvents and that this is catalyzed by the presence of Li^+. Experiments are currently being carried out to confirm this. However, these results indicate that the presence of lithium metal in a test cell can alter the electrolyte behavior compared to a real Li-ion cell.

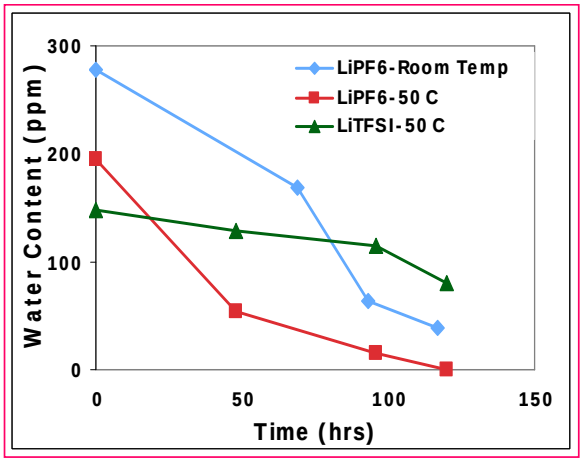

Figure V- 87: K-F titration measures of water content of EC/EMC solutions of $LiPF_6$ and LiTFSI over time at different temperatures.

A further example of this problem is shown in Figure V- 88 which shows the exchange current density values obtained from impedance measurements for Gen 3 anodes (MCMB graphite) and Gen 3 cathodes ($Li_{1.1}Ni_{1/3}Co_{1/3}Mn_{1/3}O_{2+y}$) where the impedance measurements are made against a lithium counter electrode (2-electrode cell) and a lithium reference electrode(three electrode cell). It can be seen that the two electrode cells show identical behavior indicating that the cell is dominated by the lithium counter electrode. The three-electrode measurements for the Gen 3 cathode show a different activation energy than the lithium metal dominated cells. From the discussion above it is clearly necessary to carry out the interfacial measurements in the absence of lithium metal and hence properly balanced cells must be built with a non-lithium metal reference electrode to provide meaningful data. Experiments with Ag/AgCl reference electrodes have shown promising results and experiments with the lithiated Sn electrodes reported by Argonne National Lab will be carried out for comparison.

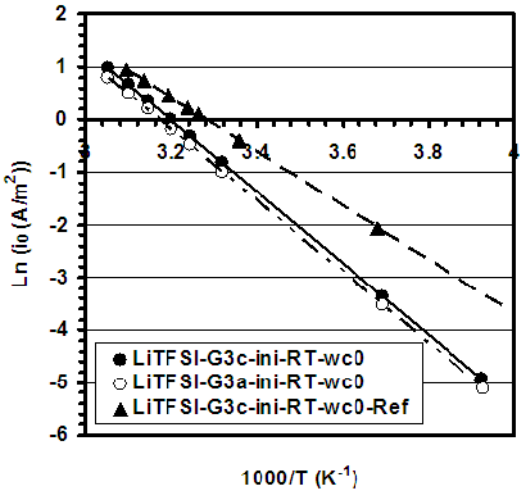

Figure V- 88: Exchange current density values as a function of temperature for Gen 3 anodes and cathodes in 2-electrode and 3-electrode (Li metal reference) configurations. EC/EMC- LiTFSI (1M) totally dry(wc0).

FY 2009 Publications/Presentations

1. Presentation to the 2009 DOE Annual Peer Review Meeting. ES39.
2. Shin, J. H., Basak, P., Kerr, J. B. & Cairns, E. J. Rechargeable Li/$LiFePO_4$ cells using N-methyl-N-butyl pyrrolidinium bis(trifluoromethane sulfonyl)imide-LiTFSI electrolyte incorporating polymer additives. *Electrochimica Acta* **54**, 410-414 (2008).
3. Hardwick, L. J., Marcinek, M., Beer, L., Kerr, J. B. & Kostecki, R. An investigation of the effect of graphite degradation on irreversible capacity in lithium-ion cells. *Journal of the Electrochemical Society* **155**, A442-A447 (2008).
4. Basak, P., Fink, D., Beer, L, Kerr, J.B., "The Impact of Li-ion Battery Electrolyte Impurities on Performance Decline and Self-discharge". 214th ECS Meeting on Electrochemical and Solid State Science, Honolulu, Hawaii, October 12-7, 2008.

V.D.3 Molecular Dynamic Simulation Studies of Electrolytes and Electrolyte/Electrode Interfaces (UU)

Grant D. Smith

Department of Materials Science & Engineering, 122 S. Central Campus Dr, Rm. 304, University of Utah, Salt Lake City, UT 84112-0560
phone: (801) 585-3381
E-mail: gsmith2@gibbon.mse.utah.edu

Start Date: October 1, 2008
Projected End Date: September 30, 2010

Objectives

Our primary objective is to gain molecular level understanding of the structure and Li^+ cation transport mechanisms in bulk electrolytes, in SEI layers and through electrode/electrolyte interfaces. This molecular level information comes from atomistic molecular dynamics (MD) simulations with and without chemical reactions, and will provide guidance for design of electrolytes with improved Li^+ transport and reduced interfacial resistance.

Technical Barriers

- poor low-temperature operations
- poor transport through SEI layers
- high interfacial transport resistance

Technical Targets

- 10 s discharge power: 750 W/kg (10 mile) and 316 W/kg (40 mile)

Accomplishments

- Extensive MD simulations using reactive force fields (ReaxFF) have been conducted to investigate pathways of electrolyte decomposition and SEI formation.
- Simulations of the interface between $LiFePO_4$ and representative organic liquid and ionic liquid electrolytes have been performed in order to better understand interfacial charge transfer resistance.
- An electroactive interface MD method has been developed and implemented that allows for control of the electrode potential during simulations.
- A many-body polarizable force field has been developed for trimethyl phosphate (TMP) and triethyl phosphate (TEP) solvents interacting with $LiPF_6$. MD simulations have been performed on TMP doped with 1 M $LiPF_6$.
- MD simulations of FSI-based ionic liquids have been performed.

✧ ✧ ✧ ✧ ✧

Introduction

The interfaces between electrodes and the bulk electrolyte in secondary lithium batteries are complex. Often in direct contact with the anode is the solid electrolyte interphase (SEI) comprised of species formed primarily by the electrochemical decomposition of the electrolyte, salt, and additives. The SEI layer in turn is in contact with the electrolyte (solvent + salt) whose structure and dynamics are likely strongly perturbed by the presence of the interfaces. Electrode/electrolyte interfaces influence cell performance in numerous ways. For example, the SEI layer, particularly at the anode but perhaps also at the cathode, stabilizes the electrode against solvent intercalation/dissolution and stabilizes the electrolyte against electrochemical decomposition but can result in high interfacial transport resistance, particularly at lower temperatures. Formation of SEI layers with good transport properties, good mechanical properties and electrochemical stability is of paramount importance in obtaining good cell performance and cycle-ability. While we continue in our efforts to understand Li^+ solvation and transport in bulk electrolytes such as mixed carbonate electrolytes, TMP, TEP and ionic liquids, much of our efforts are centered on predicting and understanding transport at electrode/electrolyte interfaces.

Approach

Our approach to simulation of bulk electrolytes, SEI layers, and electrode/electrolyte interfaces is three-pronged. First, where possible and appropriate, we utilize quantum-chemistry based force fields and non-reactive simulation methods. These studies include bulk electrolytes, model SEI layers and electrode/electrolyte interfaces. Second, we utilize an electroactive interface model to study electrolyte structure and charge transfer processes at electrode/electrolyte interfaces where control of electrode potential is paramount. Finally, to develop a

simulation framework (simulation software, analysis tools, and force fields) that allows efficient investigation of chemical pathways of SEI formation we utilized atomistic MD simulations with ReaxFF, a reactive force field developed by Adri van Duin and William Goddard at Caltech. This simulation method combines accuracy in modeling reaction energies and barriers with capability to simulate systems large enough and over sufficiently long time to capture the diffusive properties of molecules necessary to adequately capture important chemical and structural reorganization during SEI formation. The ReaxFF is an empirical potential which is parameterized to reproduce results from quantum chemistry calculations.

Results

1. Electrolyte Reduction Using Reactive MD Simulations. To ensure accurate predictions by simulations with ReaxFF a set of parameters has to be determined for the specific system of interest. In collaboration with Adri van Duin (PennState) we continued to refine and validate ReaxFF against high level quantum chemistry (QC) calculations. We have confirmed that ReaxFF adequately captures energetics of radical recombination and polymerization reactions reported previously in the literature and as obtained from our own QC calculations. Specifically, the ReaxFF predicts that formation of lithium butylene dicarbonate is energetically the most favorable product of two EC linear radicals recombination, consistent with QC results; as well as polymerization reaction initiated by the EC radical with VC has very small barrier. The current version of the ReaxFF also accurately captures energy barriers and relative energy difference of reaction products predicted by quantum chemistry calculations for various reaction paths of EC and VC reduction. Using this validated and updated version of ReaxFF we have conducted extensive simulations of EC and VC decomposition on Li metal surface. Consistent with experimental observations extensive two-electron reduction of EC and VC is observed resulting in formation of lithium carbonates and gas products such as ethylene (for EC), acetylene (for VC) and carbon mono- and dioxide. As the layer of formed lithium carbonates thickens the reduction of electrolyte slows down and switches primarily to single-electron reduction mechanisms.

2. Interfacial Properties with Fixed Electrode Charge. The experimentally measured charge transfer resistance commonly includes contributions associated with the lithium desolvation from the electrolyte and its intercalation into outer part of SEI or cathode. MD simulations have been performed on liquid carbonate electrolytes and ionic liquid electrolytes doped with lithium salts next to graphite and $LiFePO_4$ surfaces in order to better understand the structure of the electrolyte near the electrode interface and the transport of Li^+ from the bulk electrolyte to the electrode surface

Electrolytes next to Graphite. MD simulations of EC/$LiPF_6$ and EC:DMC(3:7)/$LiPF_6$ at 1 M salt concentration next to graphite that were started in 2008 were finalized in FY2009. Due to the high barrier (high energy) for desolvation of Li^+, standard equilibrium MD simulations are not well suited for determining the free energy profile $\Delta G(z)$, i.e., the free energy of a Li^+ cation as a function of position relative to the graphite/electrolyte interface.

Instead we calculated $\Delta G(z)$ using a constrained force technique, in which a Li^+ is constrained at a certain position relative to the surface and the constraining force is calculated. The simulations were 6-12 ns for each constrained distance. The integral of the constrained force gives a free energy profile that is shown in Figure V- 89. The free energy profile $\Delta G(z)$ shows a local minimum of -0.5 kcal/mol (relative to the bulk electrolyte) at ~ 5Å from the graphite. The free energy sharply increases as the lithium approaches graphite and is forced to desolvate from electrolyte at distances closer than 4 Å from graphite.

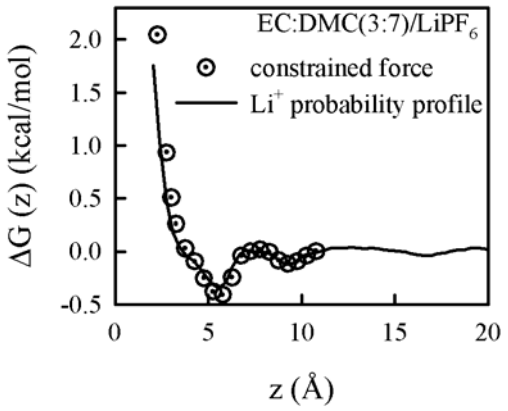

Figure V- 89: The free energy profile for the lithium cation desolvation from EC:DMC(3:7)/$LiPF_6$ at 1 M electrolyte at 298 K calculated using the Li^+ distribution profile from equilibrium MD simulations and the integration of the constrained force method. Z = 0 corresponds to the position of hydrogen atoms of graphite.

The local lithium diffusion coefficients (along z direction, perpendicular to graphite layer) have been calculated and is shown in Figure V- 90. Good agreement is found between D_z away from graphite and the lithium diffusion coefficient obtained from equilibrium simulations of bulk electrolytes, 1.44 x 10^{-10} m^2/s for EC/$LiPF_6$ 1 M and 3.2 x 10^{-10} m^2/s for EC:DMC(3:7)/$LiPF_6$ 1 M at 298 K. Figure V- 90 shows that the local diffusion coefficient changes only within a factor of 3 as lithium approaches graphite and disolvates.

We conclude by stating that MD simulations of EC/$LiPF_6$ and EC:DMC(3:7)/$LiPF_6$ 1 M electrolytes near graphite showed a similar barrier $\Delta G(z)$ for lithium desolvation in accord with the experimental evidence. If

one assumes that the charge-transfer reaction occurs when a Li^+ is located between outer layer carbon and hydrogen atoms then a value of ΔG(z) around 12-19 kcal/mol is obtained.

$LiFePO_4$/electrolyte interfaces. During 2008/2009 we made significant progress in developing a molecular model for $LiFePO_4$ and the interface between $LiFePO_4$ and both liquid and ionic liquid electrolytes. The developed model and the resulting simulations represent a significant advancement in our ability to model this complex system, allowing us to accurately predict the barrier/energetics associated with bringing the cation up to the surface of the cathode.

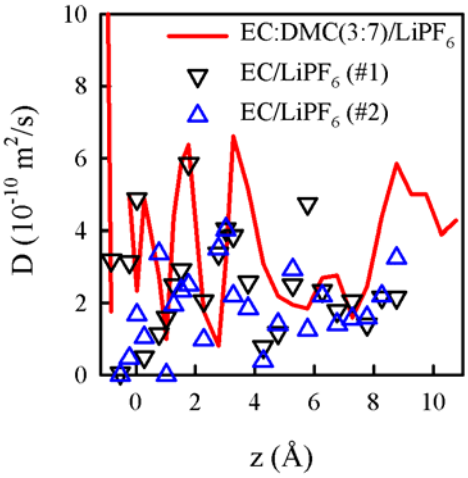

Figure V- 90: The local lithium self-diffusion coefficient as a function of the z-coordinate perpendicular to graphite layers.

MD simulations of the interface between a $LiFePO_4$ cathode and two electrolytes: a liquid electrolyte comprised of EC/DMC + $LiPF_6$ and an ionic liquid electrolyte comprised of $EMIM^+/FSI^-$ + LiFSI, were performed. This study was conducted using our polarizable force field augmented to include the $LiFePO_4$ cathode. Simulations reveal the electrolyte/electrode interface to be highly structured as shown in Figure V- 91 up to distances about 1 nm from the cathode surface. Simulations also reveal a potential barrier for Li^+ transport to the surface and a large negative potential at the electrode surface. The ionic liquid/electrode interface is even more structured than that for the EC/DMC electrolyte with a larger potential barrier for Li^+ transport to the surface and a less negative potential at the electrode surface. These features are due to the ability of the positively charged ionic liquid cations to coordinate strongly with the exposed negatively charged oxygen atoms on the cathode surface.

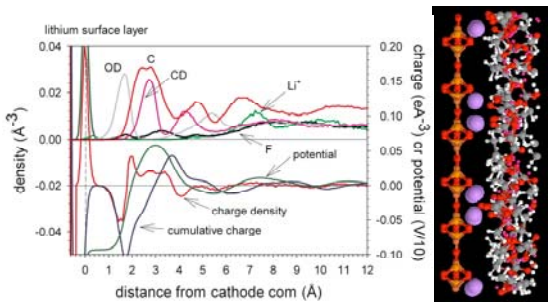

Figure V- 91: Atom density profile charge density and electrostatic potential near the $LiFePO_4$ cathode an EC/DMC electrolyte. Figure on the right shows the electrolyte structure near at the cathode/electrolyte interface.

3. Electroactive Interface with Electron Transfer. One of the main purposes of this project has been to investigate and understand at molecular level the processes occurring at electrodes in batteries during charging and discharging processes, the interfacial structure of electrode-electrolyte interface, and quantitative predictions regarding of several relevant macroscopic properties (free energy, electrode capacitance). The development of this task involves three stages: i) the implementation of an efficient treatment of electroactive interfaces within the MD simulation framework, ii) validation and verification the implemented framework, iii) a systematic investigation of interfaces relevant to batteries and supercapacitor applications. At this stage of the project we successfully implemented the fundamentals of the methodology and have tested our framework for molten salts (LiCl, KCl), SPC-water and SPC-water + NaCl.

4. Simulations of Bulk Ionic Liquids and Liquid Electrolytes. Molecular dynamics simulations have been performed on a number of pure ionic liquids and ionic liquids doped with Li salts that are of potential interest as electrolytes for lithium batteries. An improved force field that incorporates extended force centers on FSI^- anion has been used. A number of correlations between the heat of vaporization, cation-anion binding energy, molar volume and transport properties of a large number of ionic liquids have been investigated. A correlation between the ion self-diffusion coefficient, conductivity, the diffusion coefficient activation energy with the heat of vaporization was found, while no correlations were found between the diffusion coefficient and molecular volume and the diffusion coefficient and cation/anion binding energy.

In published experimental results, alkyl phosphate electrolytes have shown some advantages over carbonate electrolytes, for example, addition of trimethyl phosphate (TMP) to PC-$LiBF_4$ solutions resulted in improved ion dissociation and electrolyte conductivity. Our MD simulations have been performed on trimethyl phosphate (TMP) doped with 1 M $LiPF_6$ salt at 363 K and 298 K. We observed a high fraction of free ions (solvent separated ion

pairs) of 61% has been found for TMP doped 1 M $LiPF_6$ electrolyte compared to 38% found for EC doped with 1 M $LiPF_6$.

Conclusions and Future Directions

Our recent simulations of bulk electrolytes and electrode/electrolyte interfaces have provided valuable insight into structure and transport in systems of direct relevance to the development of lithium batteries with improved energy and rate capabilities. Most important for our future simulation studies is the incorporation of capabilities to study reduction processes at the anode surface and to control electrode potential during our simulations. These capabilities will allow us to predict SEI structure and transport properties, to understand the role of electrode potential on interfacial structure and dynamics, and to study the complete intercalation/deintercalation process of Li^+.

FY 2009 Publications/Presentations

1. Smith, G. D.; Borodin, O.; Salvy, R.; Rees, R.; Hollenkamp, A. F. "A Molecular Dynamics Simulation Study of $LiFePO_4$/Electrolyte Interfaces: Structure and Li^+ Transport in Carbonate and Ionic Liquid Electrolytes" Chem. Phys. Phys. Chem. 2009, DOI: 10.1039/b912820d
2. Borodin, O. A Relation Between Heat of Vaporization, Ion Transport, Molar Volume and Cation-Anion Binding Energy for Ionic Liquids. J. Phys. Chem. B, 2009, 113, 12353-12357.
3. Borodin, O. Polarizable Force Field Development and Molecular Dynamics Simulations of Ionic Liquids. J. Phys. Chem. B 2009, 113, 11463-11478.
4. Vatamanu, J.; Borodin, O.; Smith, G. D. "Molecular Dynamics Simulations of Atomically Flat and Nanoporous Electrodes with a Molten Salt Electrolyte" Chem. Phys. Phys. Chem. 2009 (in press)
5. Borodin, O.; Smith, G. D. "Molecular Dynamics and Quantum Chemistry Study of Li^+ Solvation in Dimethyl Carbonate/Ethylene Carbonate Doped $LiPF_6$ Electrolytes" J. Phys. Chem. B 2009, 113, 1763–1776
6. Borodin, O.; Smith, G. D.; Kim, H. "Viscosity of a Room Temperature Ionic Liquid: Predictions from Non-equilibrium and Equilibrium Molecular Dynamics Simulations" J. Phys. Chem. B, 2009, 113, 4771-4774.
7. Gomas, E.; Panday, A, Feng. E.; Chen. V.; Stone. G.; Minor, A.; Kisielowski, C.; Downing, K.; Borodin, O.; Smith, G. D.; Balsara, N. "Effect of Ion Distribution on Conductivity of Block Copolymer Electrolytes" Nano Letters, 2009, 9, 1212-1216.
8. Borodin, O.; Smith, G. "Interfacial Structure and Interfacial Resistance of EC:DMC/LiPF6 and Ionic Liquid Electrolytes at Graphite and $LiFePO_4$" 216th ECS Meeting - Vienna, Austria, 2009

V.D.4 Bi-functional Electrolytes for Li-ion Batteries (CWRU)

Daniel A. Scherson (Principal Investigator)
Department of Chemistry
Case Western Reserve University
Cleveland, OH 44106-7078
Phone: (216) 368-5186, Fax: (216) 368-3006
E-mail: Daniel.Scherson@case.edu

John D. Protasiewicz (Co-Principal Investigator)
Department of Chemistry
Case Western Reserve University
Cleveland, OH 44106-7078
Phone: (216) 368-5060, Fax: (216) 368-3006
E-mail: protasiewicz@case.edu

Start Date: April 1, 2009
Projected End Date: March 30, 2013

Objectives

- Design, synthesize, and characterize the physical, electrochemical, and interfacial characteristics of functionalized Li salt anions containing phosphorous moieties known to impart materials with flame retardant properties
- Develop bifunctional electrolytes to allow species to support charge transport through the electrolyte and to provide flame retardant properties (FRIONS) and/or overcharge protection.
- Implement in situ methods to correlate Li passive film structure to performance

Technical Barriers

This project addresses issues relating to abuse tolerance which is regarded as a major technical barrier toward commercialization of Li batteries for automotive and other large scale applications.

Technical Targets

- Synthesize, purify and characterize new Li-ion salt anions with flame retardant and overcharge protection attributes.
- Design and construct an electrochemical cell for in situ attenuated total reflection ATR-FTIR studies using a special device that incorporates a diamond window.
- Seek correlations between the composition of the electrolyte and the passive film formed at high energy density cathodes and anodes using ATR-FTIR as a function of their state of charge.

✧ ✧ ✧ ✧ ✧

Introduction

As the reach of Li batteries expands into vehicular transport applications and the consumer market at large, safety issues are increasingly becoming the focus of major concern. Relatively few isolated accidents, amply publicized by the media, have led to major recalls, not only afflicting manufacturers with major financial losses, but creating a public perception of unreliability and imminent danger. At the heart of the matter is the intrinsic flammability of the solvents currently in use, which for some systems by themselves would not pose a serious threat, except when sudden heating generated by internal shorts or other causes leads to ignition. One of the most promising avenues toward tackling this complex problem is the incorporation of flame retardants into the electrolyte; not surprisingly, a few reports implementing this specific tactic have been published over the past few years both in scientific and technical journals and the patent literature as well. Although this strategy provides a viable route toward meeting safety considerations, materials must be selected judiciously to avoid impairing otherwise critical aspects of the electrochemical device performance from energy storage and power delivery standpoints.

Approach

Design and synthesize multifunctional materials for battery applications. Evaluate materials' performance and fundamental physical properties of relevance to battery applications. Build a database of fundamental knowledge on this chemistry. Impart electrolyte, i.e., solvent and salt, bifunctionality, by incorporating covalently linked groups to anions known to display high conductivity and stability with flame retardant and/or overcharge protection characteristics.

Results

Our synthetic efforts in the first few months of the project have thus far concentrated on the preparation of M-BOP-Ph salts (Figure V- 92). Although we succeeded in generating compound **Na-4a**, the same pathway failed to yield a stable Li analogue. Reactions of compound **Na-4a** with BCl_3 to yield the Na-BOP-Ph salt have also proven unsatisfactory, suggesting that an electron transfer/decarboxylation process occurs to produce the

phosphinic acid PhP(O)(OH)H. Other boron reagents are now being explored in order to overcome these hurdles.

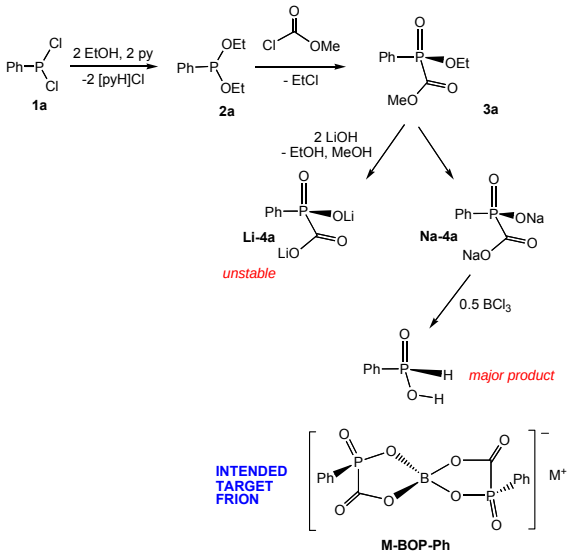

Figure V- 92: The Preparation of M-BOP-Ph salts

Conclusions and Future Directions

We are now redirecting efforts toward the synthesis on three new FRION compounds (Figure V- 93). The first, M-BOP-^{t}Bu, will feature a *tert*-butyl group, instead of the phenyl group. It is anticipated that a large change in the nature of the alkyl group will allow the desired synthesis to occur. The other two new targets represent hybrids between the known LiBOB salt and organophosphorus compounds.

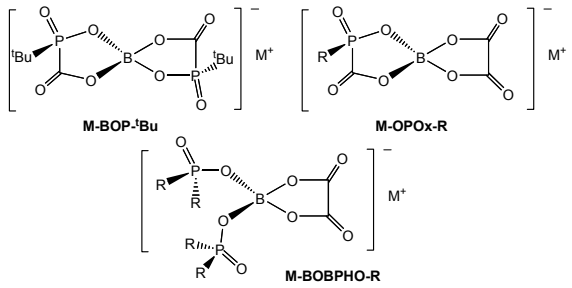

Figure V- 93: The synthesis of three new FRION compounds

FY 2009 Publications/Presentations

1. Presentation to the 2009 DOE Annual Peer Review Meeting.

V.D.5 Advanced Electrolyte and Electrolyte Additives (ANL)

Khalil Amine (Project Manager Name)
Chemical Sciences and Engineering Division
Argonne National Laboratory
Argonne, IL 60439
Phone: (630) 252-3838; Fax: (630) 252-4672
E-mail: amine@anl.gov

Start Date: Jan 1, 2010
Projected End Date: Dee. 30, 2011

Objectives

- Develop an advanced quantum chemical model to predict functional additives that form stable Solid Electrolyte Interface (SEI) on carbon anode and cathodes.
- Expand the model to predict how additives interact with the surface of anode and cathode during the initial charging.
- Synthesize suitable additives predicted by the modeling, characterize them and carry out extensive cycle and calendar life test.

Technical Barriers

This project addresses the following technical barriers in Li-ion battery technology

(a) Cycle/calendar life

(b) Abuse tolerance

Technical Targets

- New additives that form stable film formation on anodes and cathodes
- Increased cycle life
- Improved safety
- A quantum model that help identify new and stable additives

Accomplishments

- Developed an improved quantum chemical model for the calculation of reduction and oxidation potentials of potential additive molecules. This uses improved basis sets and an improved continuum model for the solvation effects.
- Initiated screening of potential additives for their potential to form a protective film on the anode.
- Initiated synthesis and testing of new candidate additives that are likely to form protective films.
- Developed a model for the graphite surface for investigation of formation of protective films.
- Initiated investigation of lithium carbonate adsorbates on graphite surface.

✧ ✧ ✧ ✧ ✧

Introduction

The stabilization of the interface of Li-ion batteries is needed to prevent detrimental decomposition of the electrodes. We are investigating functional electrolyte additives that can be added to the electrolyte and that can either polymerize or be reduced at voltages higher than 1.1 V during the initial formation charging to prevent any conventional passivation film from forming at the anode. In the case of the cathode, the additive must be oxidized at voltages above 4V to allow for stable film formation at the interface of the cathode. These additives must form a thin and uniform film made of one stable single component that protects the interface of both electrodes.

Approach

We are using a joint theoretical/experimental approach to design and discover new electrolyte additives that react in a preferential manner to prevent detrimental decomposition of cell components. We use quantum chemical screening to predict oxidation and reduction potentials and decomposition pathways that form desirable coatings. We use density functional studies of graphite surface reactions to determine mechanisms for protective film formation from additives. Synthesis of the new additives and testing of them is done to determine the cycle life of the batteries. Investigation of the SEI is done to determine structure and formation through both and experiment and theory.

Results

Quantum chemical model for prediction of reduction and oxidation potentials. We have developed an improved quantum chemical model for the calculation of reduction and oxidation potentials of possible additive molecules. This work uses improved basis sets for calculation of geometries, improved methods for calculation of ionization potentials and electron affinities, and an improved continuum model for the solvation effects.

Screening and testing of potential additives. Using this model we have initiated screening of candidate additives. In addition, for those candidates that meet the screening criteria, we are investigating their decomposition pathways to determine if the additive is likely to lead to a protective film such as lithium carbonate or a polymer film. The candidates that have passed the screening criteria are being synthesized for testing.

Model for graphite surface. We have developed a model for the graphite surface for investigation of the adsorption of electrolyte decomposition products using density functional calculations. The graphite model has hydrogen terminated surfaces with no defects and hydrogen terminated surfaces with defects (i.e., missing hydrogen atoms from the C-H bonds). The model thus represents the edge of a graphite crystal where adsorption is likely to occur at an anode. A periodic model of the graphite surface is used in the density functional calculations with a unit cell of 128 carbon atoms. The surface is shown in Figure V- 94. The structure of the graphite surface using this model was relaxed using plane-wave density functional theory with the PW91 functional allowing for relaxation of the C-H bond distances and the distance between the planes. The optimized distance between planes is 3.4 Å, which is in good agreement with theory.

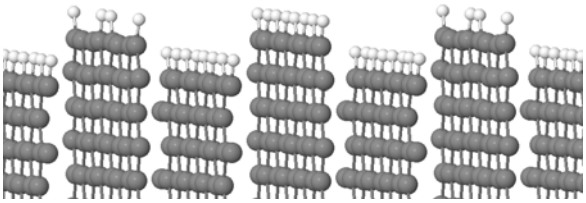

Figure V- 94: Model of graphite surface for use in study of film growth and adsorbates.

Adsorbates on graphite surface. We are initially using the graphite model to investigate the adsorption of a Li_2CO_3 monomer on the surface with both a perfect surface and on a defect site. The latter exhibits a much stronger binding of the monomer and is the likely site for nucleation of lithium carbonate. Studies will also be done to investigate Li_2CO_3 dimers and larger clusters on the graphite surface to understand the structure and growth mechanisms. The results will be used to understand growth mechanisms and structure of the SEI in conjunction with experimental studies.

Polymerization modeling. We have initiated studies of several model systems for assessing the feasibility of polymerization of electrolyte additives. Polymerization can create a protective film on the electrode surface the same as lithium carbonate. The initial work involves investigation of spin densities on radical cations and radical anions resulting from oxidation and reduction of potential additives. The molecules are being investigated to see if the spin densities correlate with dimerization.

V.D.6 Inexpensive, Non-fluorinated Anions for Lithium Salts and Ionic Liquids for Lithium Battery Electrolytes (NCSU)

Wesley A. Henderson
North Carolina State University
Department of Chemical & Biomolecular Engineering
911 Partners Way
Raleigh, NC 27695
Phone: (919) 513-2917; Fax: (919) 515-3465
E-mail: whender@ncsu.edu

Start Date: August 1, 2009
Projected End Date: July 31, 2011

Objectives

- Develop new anions as replacements for PF_6^- or as additives for electrolytes

Technical Barriers

Low cost cell materials, abuse tolerance, low temperature performance

Technical Targets

- Available energy: 56 Wh/kg (10 mile) and 96 Wh/kg (40 mile)
- 10 s Discharge power: 750 W/kg (10 mile) and 316 W/kg (40 mile)
- Cycle life: 5000 cycles (10 mile) and 3000 cycles (40 mile)
- Calendar life: 15 years (at 40°C)
- Cold cranking capability to -30°C
- Abuse tolerance

Accomplishments

- Synthesized the organoborate salt lithium bis(α-hydroxyisobutyro)borate.
- Determined the phase behavior using DSC of LiBOB with EC and $LiBF_4$ with EC, γ-valerolactone (GVL), DMC, DEC and ethyl acetate (EA).
- Examined the thermal stability (mass loss) using TGA of LiBOB or $LiBF_4$ with EC to aid in explaining the solubility differences between the salts.

✧ ✧ ✧ ✧ ✧

Introduction

Electrolyte materials are a key component in terms of both the cost and performance of a battery. The properties of salts (either lithium salts or ionic liquids) containing new anions are being explored to determine their utility for lithium battery applications.

Approach

To explore new anions for alternative salts to $LiPF_6$, ionic liquids and electrolyte additives, two classes of nonfluorinated anions: 1) chelated and non-chelated organoborate anions (related to bis(oxalate) borate or BOB^-), and 2) Hückle-type anions in which the charge is stabilized on a 5-member azole ring and noncyclic cyanocarbanions are being synthesize and characterized. The physical properties of these new anions, incorporated in both lithium salts and ionic liquids, will be examined including the thermal phase behavior (phase diagrams); thermal, chemical and electrochemical stability; transport properties; interfacial properties; molecular interactions and cell performance. These salts will be compared with current salts of interest such as $LiBF_4$, $LiPF_6$ and LiBOB and ionic liquids based upon the bis(trifluoromethane-sulfonyl)imide anion.

Results

Salt Synthesis. The salt lithium bis(α-hydroxyiso-butyro)borate (LiHIBB) has been synthesized and the crystal structure of the monohydrate determined (Figure V-95) (the anhydrous salt is a powder). This salt was prepared for comparison with LiBOB to determine how the solubility of LiHIBB compares with that of LiBOB as most of the known lithium organoborate salts have poor solubility in aprotic solvents. Whereas LiBOB is soluble to >10 mol% in EC and GBL, the anhydrous LiHIBB has a very low solubility of <0.5 mol%.

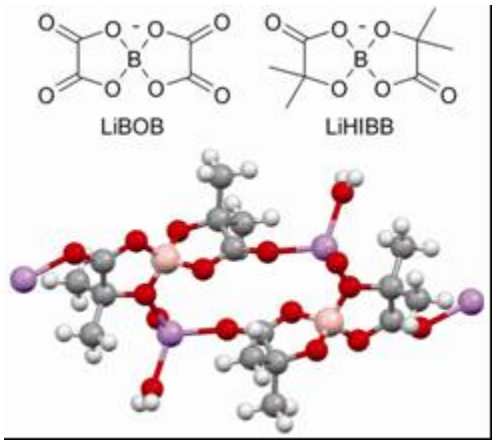

Figure V- 95: (top) Comparison of the structures of LiBOB and LiHIBB and (bottom) a portion of the crystal structure of LiHIBB·H_2O (Li - purple; O - red; B - tan)

The synthesis of a number of other organoborate salts has been attempted with a variety of organic ligands, but no new lithium salts have yet been confirmed from these efforts. Alternative synthesis techniques are now underway to identify the reason for this.

The synthesis of lithium 1,2,3-triazole-4,5-dicarbonitrile (LiTADC):

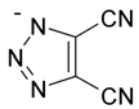

is being scaled up to produce a large enough quantity of this salt (>100 g) for full characterization as well as the synthesis of ionic liquids containing this anion.

Solvent-LiBOB and $LiBF_4$ Characterization. The thermal phase behavior and stability of LiBOB and $LiBF_4$ solutions with a variety of aprotic solvents is being determined. This will provide a foundation for comparison as the properties of the newly prepared salts are determined.

DSC heating traces for (1-x) EC-(x) LiX (where x is the mol fraction) mixtures with either LiBOB or $LiBF_4$ are shown in Figure V- 96. In EC, LiBOB displays a maximum solubility of just over 11.5 mol% (x = 0.115) after which it is not possible to dissolve further salt by stirring at room or elevated temperature. This is an intriguing observation since a crystal structure has been reported in the literature for a $(EC)_4$:LiBOB phase (x = 0.20). In sharp contrast, $LiBF_4$ can be dissolved to a concentration approaching 0.50 (a 1:1 mole ration of solvent to lithium salt) (Figure V- 96) with complete dissolution of the salt at elevated temperature. The DSC data indicates that $(EC)_4$:$LiBF_4$ (x = 0.20), $(EC)_2$:$LiBF_4$ (x = 0.33) and $(EC)_1$:$LiBF_4$ (x = 0.50) crystalline phases form, although confirmation of these phases from powder XRD is necessary. The phase behavior of $LiBF_4$ with DEC indicates the formation of a $(DEC)_2$:$LiBF_4$ (x = 0.33) crystalline phase in dilute mixtures, whereas no crystalline solvate phase is found with DMC, EA and GVL (for x < 0.20).

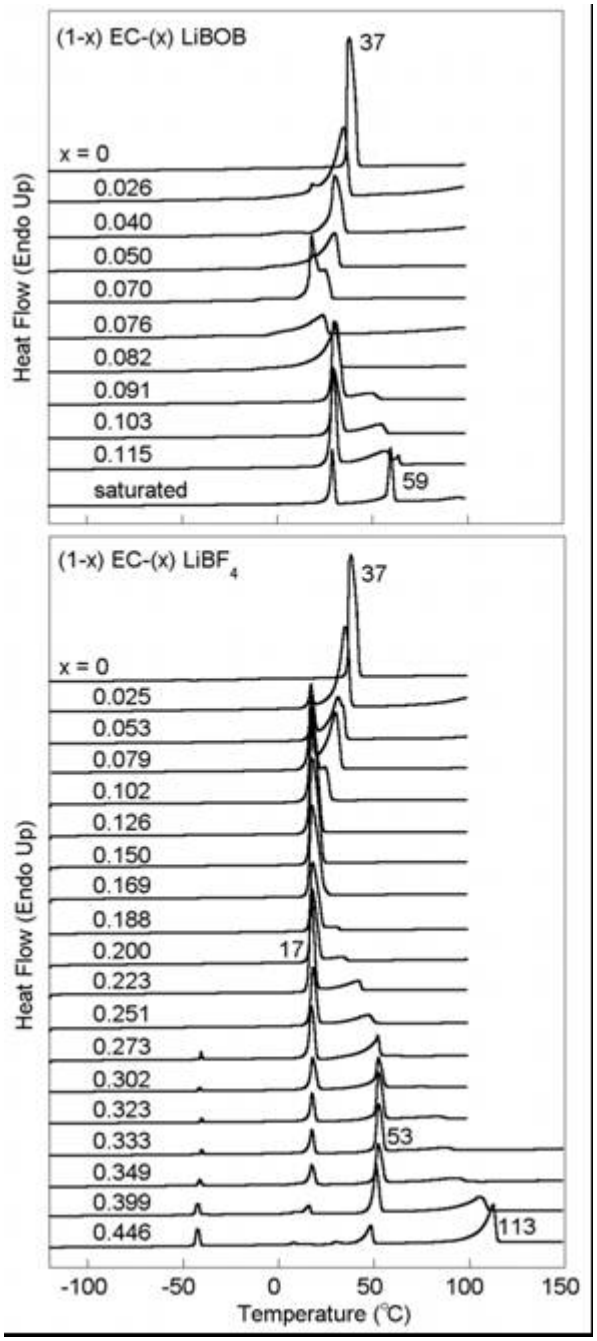

Figure V- 96: DSC Heating traces (5°C/min) of (top) (1-x) EC-(x) LiBOB and (bottom) (1-x) EC-(x) $LiBF_4$ mixtures

TGA heating traces for (1-x) EC-(x) LiX mixtures are shown in Figure V- 97. These data provide important clues regarding why the LiBOB and $LiBF_4$ salts display such markedly different solubility with EC. Although the reported boiling point (T_b) of EC is 248°C, all of the EC

volatilizes under the experimental conditions (flowing N_2) by 150°C with the onset of mass loss near 25°C. The neat LiBOB salt has a much higher thermal stability than $LiBF_4$. For the LiBOB samples up to x = 0.15 (a salt saturated sample), all of the EC is lost at approximately the same temperature as for bulk EC, in contrast with the $LiBF_4$ samples, indicating that the solvent has a much weaker interaction with the Li^+ cations in the presence of the BOB^- anions than is found with the BF_4^- anions at elevated temperature. This may be due to a significant increase in the aggregation of the ions in the LiBOB samples with increasing temperature (a "salting out" effect) thus explaining the limited solubility of this salt relative to $LiBF_4$.

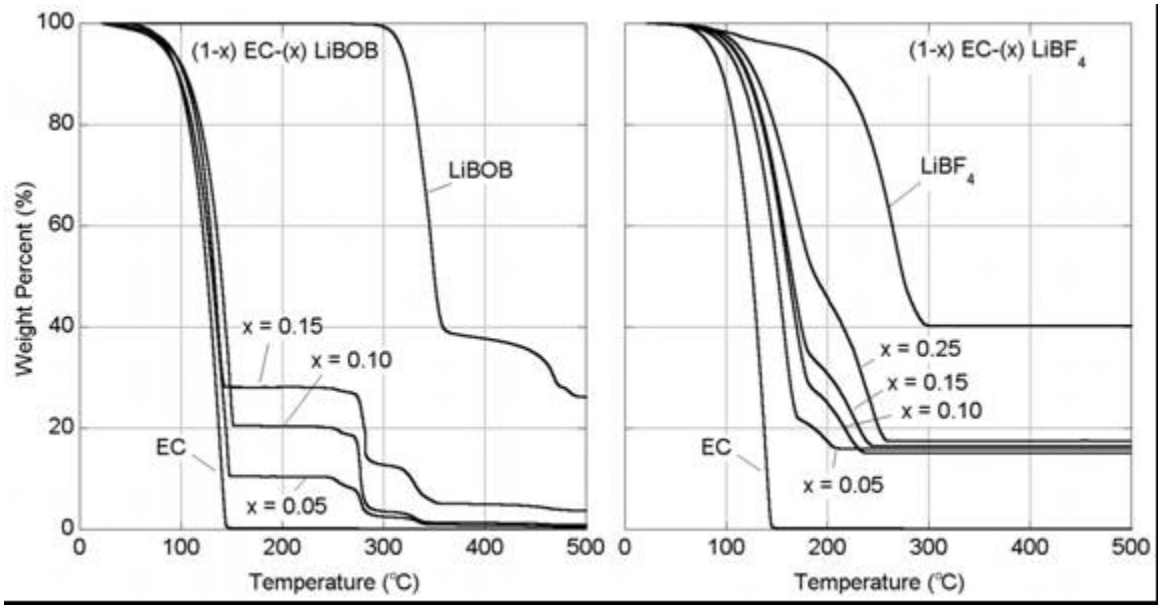

Figure V- 97: TGA heating traces (5°C/min) of (1-x) EC-(x) LiX mixtures

Conclusions and Future Directions

Dramatic difference are noted between the solvent interactions with the LiBOB and $LiBF_4$ salts. The explanation for the greatly reduced solubility (relative to LiBOB) of the newly synthesized LiHIBB salt is not yet known. The solvent interactions with the different salts will continue to be characterized to gain a better understanding of how these interactions govern the properties of the electrolytes.

FY 2009 Publications/Presentations

1. Presentation to the 2009 DOE Annual Peer Review Meeting.

V.D.7 Development of Electrolytes for Li-ion Batteries (URI)

Brett L. Lucht
University of Rhode Island
Department of Chemistry
51 Lower College Rd., Pastore
Phone: (401) 874-5071; Fax: (401) 874-5072
E-mail: blucht@chm.uri.edu

Start Date: April 1, 2009
Projected End Date: March 31, 2014

Objectives

- Develop novel electrolytes or electrolyte/additive combinations that will facilitate a more stable SEI on the anode.
- Develop additives that allow for formation of protective coatings on the cathode, i.e., a cathode SEI, and enhance electrochemical stability above 4.3 V.
- Improve the thermal stability and calendar life of Li-ion batteries via improvements of the electrolyte

Technical Barriers

This project addresses the following technical barriers from the Batteries for Advanced Transportation Technologies Research & Development Plan regarding electrolytes.

(A) Improve cell performance, life and cost

(B) Improve calendar Life

(C) Expand survival temperature range

Technical Targets

- Calendar life: 15 yrs
- Survival Temp Range: -46 to 66°C
- Cold cranking power at -30°C
- Cycle life, 5,000 charge depleting cycles

Accomplishments

- Developed a novel electrolyte for Li-ion batteries, $LiPF_4(C_2O_4)$. Conducted initial testing of $LiPF_4(C_2O_4)$ electrolytes in Li-ion coin cells.
- Produced approximately 100 g of $LiPF_4(C_2O_4)$ for testing. The material produced was utilized for internal testing of the novel salt, provided to three different potential electrolyte producers under confidential non-disclosure, analyzed by our industrial partner Yardney Technical Products/Lithion, and provided to a BATT partner (Battaglia).
- Investigated combinations of film forming additives with thermal stabilizing additives in Li-ion cells. Developed combinations of additives that have superior performance to standard electrolytes in MCMB/$LiCoNiO_2$ cells after accelerated aging experiments.

✧ ✧ ✧ ✧ ✧

Introduction

While commercial lithium-ion batteries (LIBs) perform well for most home electronic applications, currently available LIB technology does not satisfy some of the performance goals for Plug-in Hybrid Electric Vehicles (PHEV). In particular, currently available LIB technology does not meet the 15 year calendar life requirement set by the United States Advanced Battery Consortium (USABC).

The most extensively used LIB electrolytes are composed of $LiPF_6$ dissolved in organic carbonates. However, $LiPF_6$ based electrolytes have poor thermal stability and performance when cycled to high voltage (> 4.5 V vs. Li). Significant energy fading occurs after several years at room temperature and over only a few months the moderately elevated survival temperature of 66°C required by the USABC. While there are several different factors that limit the thermal stability, calendar life and voltage window of LIBs, the reactions of the electrolyte with the surface of the electrode materials are frequently reported to be the most important.

Approach

Develop novel electrolytes for Li-ion batteries to improve performance and lifetime. Investigate properties of $LiPF_4C_2O_4$/carbonate electrolytes in small (coin or pouch) Li-ion cells. Develop commercially viable low-cost synthetic method for production of $LiPF_4(C_2O_4)$ and produce high purity $LiPF_4(C_2O_4)$ for additional testing. Study Lewis basic thermal stabilizing additives for $LiPF_6$/carbonate electrolytes which prevent degradation of the anode SEI. Investigate combinations of thermal stabilizing additives and anode film forming additives in $LiPF_6$/carbonate electrolytes. Investigate cathode film forming additives which will allow the use of cathodes above 4.3 V. Investigate the surface of cycled cathodes and anodes with novel electrolytes or electrolyte / additive combinations to develop a mechanistic understanding of

SEI formation and degradation. Use the mechanistic information to design superior electrolytes and additives for Li-ion batteries.

Results

$LiPF_4(C_2O_4)$ Electrolyte Development. A novel salt, lithium tetrafluorooxalatophosphate ($LiPF_4(C_2O_4)$), was prepared and its properties as a Li-ion battery electrolyte were investigated. The conductivity, electrochemical stability, and cycling performance of 1.0 M $LiPF_4(C_2O_4)$ in 1:1:1 ethylene carbonate : dimethyl carbonate:diethyl carbonate are comparable to the industry standard $LiPF_6$ electrolyte. While the reversible capacity of the first cycle is lower than $LiPF_6$ based electrolytes, the reversible cycling efficiency is equivalent (Figure V- 98). Electrochemical impedance spectroscopy and electrode surface analysis suggest that the primary differences between $LiPF_6$ and $LiPF_4(C_2O_4)$ are thicker electrode surface films containing oxalates. The differences are most likely related to trace oxalate containing impurities in $LiPF_4(C_2O_4)$. The performance characteristics and ease of preparation suggest that $LiPF_4(C_2O_4)$/carbonate electrolytes are a promising alternative for lithium-ion batteries in PHEV applications.

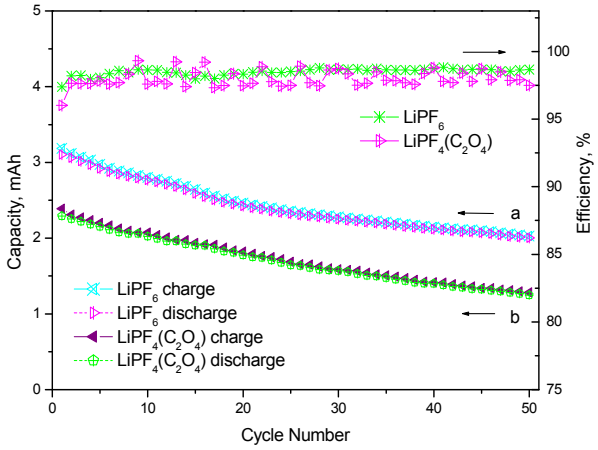

Figure V- 98: Cycling performance of Li-ion cells with 1 M $LiPF_6$ 1/1/1 EC/DEC/DMC (vol) electrolyte (a), and 1 M $LiPF_4(C_2O_4)$ 1/1/1 EC/DEC/DMC (vol) electrolyte (b).

We have produced approximately 100 g of $LiPF_4(C_2O_4)$. Several batches of this material have been sent to industrial collaborators for incorporation into commercial cells for testing. While the first few large batches of $LiPF_4(C_2O_4)$ had inferior cycling efficiencies to the batches prepared for coin cells, with the assistance of our corporate partners, we were able to identify the source of the problems as residual solvent used during salt purification. Upon generating higher purity salt, we provided the high purity salt to corporate partners for testing in 18650 cells. The results obtained from the commercial 18650 cells (Graphite/$LiNi_xCo_{1-2x}Mn_xO_2$) support our initial investigations with coin cells.

Upon preparation of larger quantities (> 10 g) of high purity $LiPF_4(C_2O_4)$, we initiated investigations of the thermal stability of the pure salt and the electrolyte solutions. The thermal stability of solid $LiPF_4(C_2O_4)$ compared to solid $LiPF_6$ is provided in Figure V- 99. The thermal gravimetric analysis for both samples is very similar suggesting similar thermal stabilities of the solids. However, investigation of the thermal stability of liquid $LiPF_4(C_2O_4)$/carbonate electrolyte suggest dramatically superior thermal stability to $LiPF_6$/carbonate electrolytes. Storage of $LiPF_4(C_2O_4)$ in 1:1:1 EC/DEC/DMC at 85°C for two weeks results in minimal decomposition of the electrolyte (Less than 1 %). Comparable storage of $LiPF_6$ in 1:1:1 EC/DEC/DMC results in nearly quantitative decomposition of the electrolyte. These results suggest that the thermal stability of the solid lithium salts and the related liquid electrolytes may not have a direct correlation.

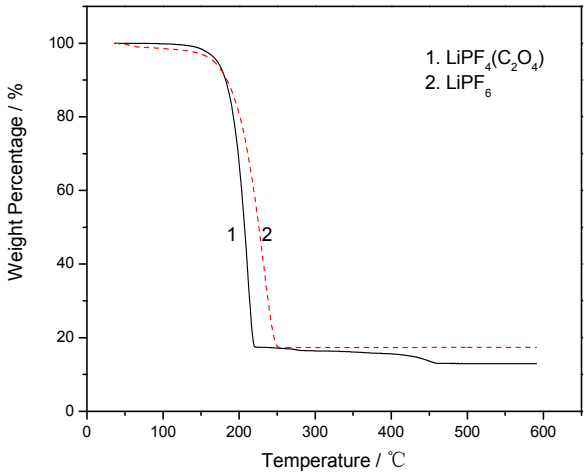

Figure V- 99: Thermogravimetric analysis of $LiPF_6$ and $LiPF_4(C_2O_4)$.

Development of Lewis Basic Additives. We have conducted an investigation of the effect of combinations of thermal stabilizing additives, including dimethyl acetamide (DMAc), vinylene carbonate (VC), and lithium bis(oxalato) borate (LiBOB), on the performance of Li-ion batteries stored at 70°C for one month. The reactions of the lithium hexafluorophosphate/carbonate electrolyte, with and without electrolyte additives, with the surface of the electrodes after initial formation cycling have been analyzed via a combination of IR-ATR and XPS. The combinations of additives have an additive effect on cell performance suggesting that the different types of additives can work together to generate a greater benefit than is observed with a single additive.

Conclusions and Future Directions

We have investigated a new salt for Li-ion batteries, $LiPF_4(C_2O_4)$ in graphite/$LiNiCoO_2$ coin cells. $LiPF_4(C_2O_4)$ electrolytes have comparable performance to $LiPF_6$ electrolytes. We have prepared 100 g of $LiPF_4(C_2O_4)$ for additional testing. Some of this material has been provided to commercial partners and some has been provided to BATT collaborators (Battaglia). We have also shown $LiPF_6$ electrolytes containing combinations of additives, thermal stabilizing and anode film forming, can provide cells with superior high temperature resilience to cells containing a single additive.

Our future efforts will be directed towards improving the calendar life, survival temperature range, cycle life of Li-ion batteries via modifications of the electrolyte. We will focus on the development of cathode film forming additives that improve the cycling performance of graphite/$LiNi_xCo_{1-2x}Mn_xO_2$ cells cycled to high voltage (4.9V vs Li). We will also expand our investigation of the novel salt $LiPF_4(C_2O_4)$ by testing in coin cells under accelerated aging conditions, graphite/$LiMn_2O_4$ electrodes, and electrolytes containing PC.

FY 2009 Publications/Presentations

1. Presentation to the 2008 DOE Annual Peer Review Meeting.
2. *Electrochem. & Solid State Lett.* **2009**, *12,* A155-A158.
3. *J. Power Sources,* **2009**, *194* 1053–1060.
4. Presentation at the 60th Annual Meeting of the International Society of Electrochemistry.

V.E Cell Analysis and Modeling

The objectives of the Cell Analysis and Modeling task areas are to provide a comprehensive and independent assessment of promising materials developed in the BATT program and to bring fundamental understanding to the area of electrode fabrication. Also, researchers are aiming to improve battery power and life through novel electrode structures and to increase our understanding of how electrode morphology influences performance.

V.E.1 Electrode Construction and Analysis (LBNL)

Vince Battaglia
Lawrence Berkeley National Laboratory
1 Cyclotron Road
Berkeley, CA 94720
Phone: (510) 486-71721; Fax: (510) 486-4260
E-mail: vsbattaglia@lbl.gov

Start Date: October 1, 2007
Projected End Date: September 30, 2012

Objectives

- Understand the role of the inactive materials and the processing steps in the fabrication and performance of electrodes.
- Identify and understand the sources of limited energy density and cell life.

Technical Barriers

This project addresses the following technical barriers from the Energy Storage section of the Vehicle Technologies Program Multi-Year Research, Development and Demonstration Plan:

(A) Cost

(B) Energy density

(C) Calendar and cycle life

Technical Targets

- EV
  - $150/kWh
  - 230 Wh/dm^3
  - 1,000, 80%-capacity, discharge cycles.
  - 10-year system life
- PHEV 40-mile
  - $220/kWh
  - 193 Wh/dm^3
  - 2750, 75%-capacity, discharge cycles + 80,000 HEV cycles
  - 15-year system life

Accomplishments

- Determined that a large amount of binder is needed in anodes of MCMB active material to improve cycle life.
- Determined that more binder is better with regard to improved lamination to the copper current collector on the anode.
- Determined that for PHEV applications, the MCMB-1028 anode is rate performance limiting when matched with a $LiNi_{1/3}Co_{1/3}Mn_{1/3}O_2$-based oxide (NCM) from Seimi (L333).
- Determined that the discharge rate of MCMB-1028 is very dependent on the electrode-thickness.
- Determined that the discharge rate of L333 is not very dependent on thickness and is limited to around 3C.
- Found we could improve a cell's energy density by 10% without affecting cycle-ability by reducing the amount of binder from 8% to 2%.
- Found we could make cells capable of 600, P/2, 70%-discharge cycles with just a 4% loss of energy.
- Determined that the coulombic inefficiency of the anode during C/10 cycling is an order of magnitude too high.

- Determined that the capacity of cells is very dependent on the amount of vinylene carbonate, VC, added.
- Found that VC addition to the electrolyte had very little effect on the coulombic efficiency, independent of the formation process.
- Developed a new polymer for Si-based anodes that allows Si-nanoparticles to cycle

✧ ✧ ✧ ✧ ✧

Introduction

Achieving the DOE energy and cost targets will require materials of higher capacity and/or voltage and improved coulombic efficiency compared to the current MCMB/NCM couple. We are making electrodes of good cycle-ability in order to test new materials from the BATT program that may lead to higher energy density cells. In making good electrodes we are trying to understand the role of the inactive materials and the processing steps on all battery performance metrics.

Approach

To meet the DOE cost targets, the battery must be improved both in terms of energy density and life. Achieving these targets will require new materials and a complete evaluation of their energy density, rate capability, and cycle-ability in full cells. Our group focuses on making good electrodes so that we may evaluate these properties in half- and full-cells.

We use a combination of trial-and-error research and systematic design of experiments, and collaborations in diagnostics and modeling to improve electrode performance. We have a procedure for making good laminates arrived at mostly through trial and error. We are now investigating the impact of the variables in each step in the process, including the levels of inactive and active materials, the order of mixing, and the rate of drying. After electrodes are made, we evaluate their electrochemical and mechanical performance and attempt to correlate them with each other and with the properties of the starting materials. We work closely with diagnostic and modeling experts to elucidate the fundamental underpinnings of our results.

Results

Anode Development. We have been working with MCMB as the baseline anode material since Argonne National Lab identified this as the baseline graphite for their Gen 3 cells. We have been trying to make good electrodes that cycle well, without excess binder and conductive additive. We tested a series of cells with different levels of binder, from 2 to 15%, and different ratios of binder to conductive additive, from 5:0 to 5:5. In the end we found that the cells with 15% binder and 5:1 binder to conductive additive gave the best overall cycle-ability: see Figure V- 100.

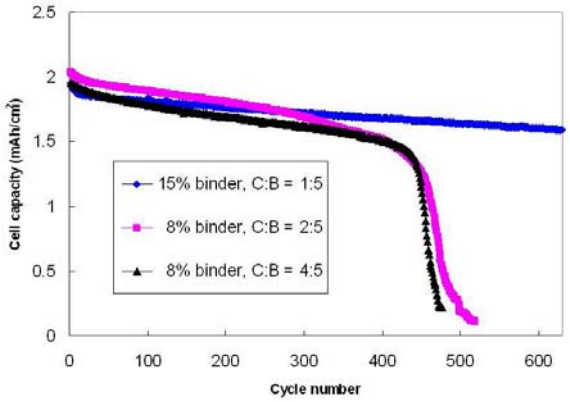

Figure V- 100: Cycling capability of MCMB with different levels of binder and conductive additive.

Assessing Sources of Delamination. In our efforts to make good anodes we found that delamination of the anode laminate was much more prevalent than in cathode electrodes. We decided to perform a partial factorial, resolution III design of experiments (DOEx) to identify parameters that improve adherence to the current collector. We tested seven different parameters: binder type, carbon to binder ratio, total binder content, laminate thickness, heating under lamps *vs*. not heating, calendaring, and thickness of the current collector. The results indicated that increased levels of binder and increased levels of binder to conductive additive significantly improved the force needed to peel the laminate from the current collector. This result was consistent with our improved anode cycle-ability, although it is not clear that this is a casual relationship.

Determining the Proper PHEV Cell Design. Once the proper amount of binder and conductive additive needed for making MCMB-1028 cycleable was determined, we evaluated rate capability. Electrodes of different thicknesses calendered to 35% porosity were fabricated. They were each tested for constant discharge rate capability by discharging them at C/10, /5, /2, 1, 2, 5, and 10. The capacity density was plotted *vs.* the current density. The point at which just before the capacity density started to drop as a result of current density was identified. The capacity and current density just before drop-off for each laminate was then re-plotted on another graph of area specific capacity *vs.* area specific current for the anodes. A similar process was repeated for cathodes of L333 of different thicknesses. A plot of these two curves is shown in Figure V- 101.

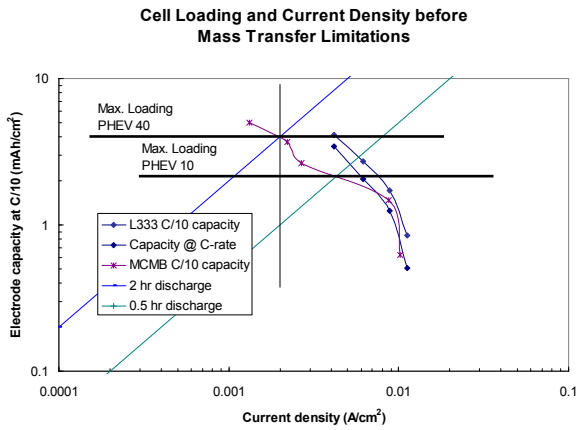

Figure V- 101: Electrode capacity as a function of the current density just before mass transfer limitations set in.

Also plotted are the diagonals that represent C/2 and 2C, which are the approximate discharge rates of a PHEV40 and PHEV10, respectively. As one can see, for both the PHEV10 and the PHEV 40, the anode is the rate limiting electrode. As the figure shows, a PHEV40 should be built with a capacity loading of 4 mAh/cm^2, and a PHEV10 with a loading of no more than 2 mAh/cm^2.

Testing of Full Cells. In the previous year we went through a similar process as was described for the anodes of determining the best combination of active and inactive material contents for the cathode. In the end of that study, we found that electrodes of binder to conductive additive of 5:2 cycled the best, but electrodes of different binder content could not be tested as they were limited by the cycle-ability of the anode. Now, with an improved anode formulation in hand and the proper loading to make electrodes for PHEVs, we tested our best cathode laminates again. Two cathodes, one of 8% and the other of 2% binder with a binder to conductive additive ratio of 5:2 were matched against anodes and assembled in coin cells for their PHEV cycle-ability. The capacity of the cells was measured at C/2. The amount of energy between 4.3 V and 70% of the total cell capacity was determined. Cells were then discharged at P/2 to 70% discharge of the capacity and charged at C/4. (P/2 is a constant power discharge equivalent to the energy divided by 2 hours.) The result of this analysis was that the cycle-ability of the two cells was equivalent: see Figure V- 102 the cells lost approximately 4% of their energy after 600 P/2 cycles. An interesting note is that the cell with a cathode with 6% less binder has 10% higher energy density than the cell with more binder.

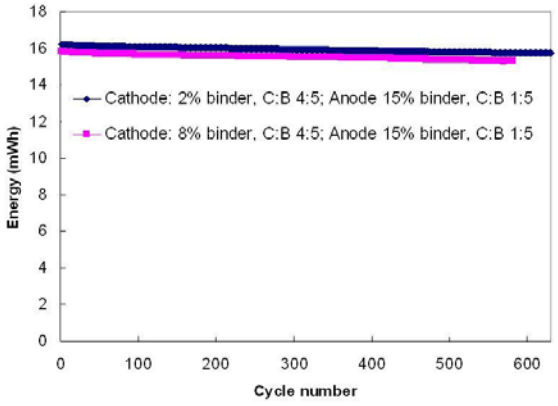

Figure V- 102: Energy *versus* cycle number of two cells with different binder content in the cathode cycled at P/2 discharge to 70% of its C/2 capacity and charged at C/4 to 4.3 V.

Effect of VC on Coulombic Efficiency. Most of the cells we have constructed lose capacity as a result of irreversible consumption of lithium at the anode. We believe this to be a critical problem for cells that undergo large swings in S.O.C. as expected for batteries for PHEV applications. We thought that the addition of VC was going to solve this problem, so we attempted to determine the right amount of VC and the right formation process.

To study this effect, we used electrodes of SNG-12 graphite from Hydro Quebec, which demonstrates a large amount of first cycle irreversible capacity loss and poor cycling efficiency. We set up cells to perform cyclic voltamograms and slow constant current discharges. We found that the VC is reduced at a higher potential than ethylene carbonate but at a slower rate. For this reason we believed that the rate at which a cell is formed when VC was present would affect the composition of the solid electrolyte interface, SEI, layer and the resulting coulombic efficiency. Unfortunately, we found that although the rate of intercalating the cell did have an effect on the composition of the SEI, it did not significantly improve the cycling efficiency of the electrode.

New Binder for Si-nanoparticles. This year we started a new project under the guidance of Gao Liu to develop a binder that would improve the cycle-ability of Si. It is presently understood that metals such as Si can be successfully lithiated and delithated for several cycles if it is nano size, otherwise it breaks apart and forms isolated islands. Researchers have found ways to cycle this material either as nanowires grown directly from a substrate or as encapsulated nanoparticles in solid-conductive matrices. Both methods lead to reduced capacity densities. Our approach is to use a binder that we developed specifically for this material. We cannot say much more about this binder as we are going through the patent process. Some performance data are provided in Figure V- 103. Also provided in the figure is cycling data

using poly vinylidene difluoride, PVDF, and PVDF with acetylene black as the binders.

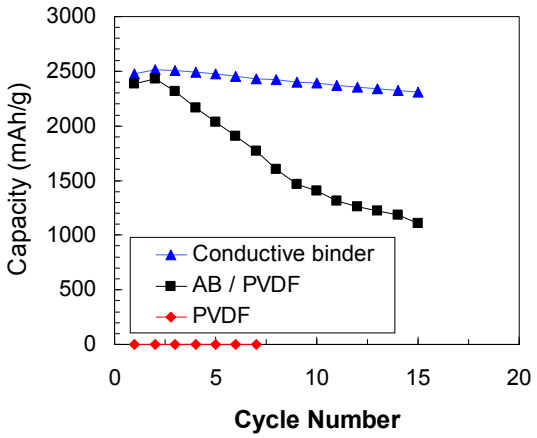

Figure V- 103: The cycle-ability of Si-nanoparticles with our binder, PVDF, and PVDF w/acetylene black.

Conclusions and Future Directions

After this year's effort we can consistently fabricate good cathodes and anodes of NCM and MCMB, respectively. We know that more binder helps to prevent delamination of the anode from the copper current collector. We know that the proper loading for a PHEV40 is 4 mAh/cm^2 and for a PHEV10, 2 mAh/cm^2, as dictated by the rate of discharge of the MCMB. We also know we can make cells that cycle 600 times with just 4% energy fade. We know that coulombic efficiency is critical for long cycle life and that VC does not appear to fix this problem. Finally, we have developed a binder that allows for 2,500 mAh/g of cycle-ability of Si-nanoparticles.

In the future we intend to complete our assessment of graphites for PHEVs, and look into the performance of SBR-CMC binders for anodes. Now that we can make good electrodes, we hope to investigate the processing parameters for their effect on electrode performance. We hope to make cells with reference electrodes that cycle as well as our coin cells. We will begin to focus on the upper cut-off limit of NCM and other new, higher energy materials from the BATT program. We also hope to improve on our present binder for Si-nanoparticles, improving the first cycle irreversibility and the coulombic efficiency during cycling.

FY 2009 Publications/Presentations

1. Presentation to the 2009 D.O.E. Annual Peer Review Meeting.

V.E.2 Microscale Electrode Design Using Coupled Kinetic, Thermal and Mechanical Modeling (UM)

Ann Marie Sastry
University of Michigan
2350 Hayward St.
Ann Arbor, MI 48109
Phone: (734) 998-0006; Fax: (734) 998-0028
E-mail: amsastry@umich.edu

Start Date: October 1, 2008
Projected End Date: September 30, 2010

Objectives

- Determine optimal particle blends for high power and long lifetime for both energy- and power-dense systems via coupled multiphysics modeling and experiments on baseline materials.
- Identify and predict failure mechanisms in baseline cells, considering coupled electrochemical and mechanical effects.
- Determine fundamental properties of SEI layers, and model their effects on performance, in addition to self-assembly in particulate systems.

Technical Barriers

Inadequate power and life in systems for PHEVs:

Technical Targets

- Available energy: 56 Wh/kg (10 mile) and 96 Wh/kg (40 mile)
- 10 s discharge power: 750 W/kg (10 mile) and 316 W/kg (40 mile)
- Cycle life: 5,000 cycles
- Calendar life: 15 years

Accomplishments

- Realistic mechanical loads and porosities (30-50%) will be used to specify composites with required conductive and mechanical properties. Elimination of unnecessary mass will be achieved for high-power systems.
- Materials fabricated according to computational modeling results will be created and tested; importantly, new models will have been extended to account for mechanics, electrochemistry (kinetics), and thermal effects, in addition to alterations in diffusive properties for SEI layers, for particulate electrodes.

✧ ✧ ✧ ✧ ✧

Introduction

Failure mechanisms such as mechanical and thermal failure have to be understood and minimized to improve battery performances. In this study, 3D Finite Element Model (FEM) simulations were conducted to study the stress and heat generation, coupled with electrochemistry, inside single electrode particles. This model was further extended to consider these phenomena in electrode microstructure consisting of particle clusters.

Approach

Advanced FE simulations, in collaboration with continuum modeling (V. Srinivasan, LBNL) will be advanced to understand critical failure mechanisms and their interactions. Optimized electrode design and fabrication (with V. Battaglia, LBNL) will be accomplished using developed simulation tools. Self-assembly of conductive additives will be considered as a mechanism in simulations of conduction and in order to reduce inactive mass.

Results

Modeling—Stress and Heat Generation. We have been working on the cathode particle modeling considering intercalation-induced stress and heat generation inside single cathode particles under potentiodynamic control by considering the diffusion process, electrochemical kinetics and the intercalation-induced lattice expansion. Resistive heat was identified as the heating source of greatest importance. The surrogate-based analysis approach showed that both intercalation-induced stress and time-averaged resistive heat generation rate increase with increasing equivalent particle radius and potential sweep rate; intercalation-induced stress increases first, then decreases, as aspect ratio of an ellipsoidal particle increases, while averaged resistive heat generation rate decreases as aspect ratio increases. The surrogate-based analysis conducted suggested that ellipsoidal particles with larger aspect ratios were preferred over spherical particles,

in improving battery performance when stress and heat generation were the only factors considered.

We proposed a multiscale framework to model Li-ion batteries. In this framework, closure terms for macroscopic modeling of cells are obtained directly from microscopic scale simulations of electrode microstructure. As a part of the framework, we conducted full 3D finite element modeling of electrode materials including a solid active material phase (consisting of multiple ellipsoidal particles) and liquid electrolyte phase. The ellipsoidal particle microstructure in the electrode was generated by a collision-driven molecular dynamics algorithm. The coupled physical processes of ion/electron transport and electrochemical reaction were implemented using COMSOL Multiphysics. Representative simulation results for Li-ion concentration in both solid and liquid phases are shown in Figure V- 104. We will use this tool to study the effect of microstructure and extend the current implementation to include stress analysis.

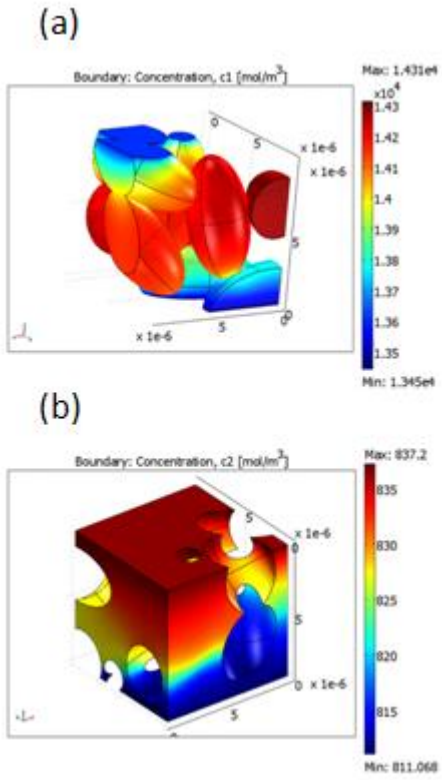

Figure V- 104: Li-ion Concentration in (a) Solid Active Material and (b) Liquid Electrolyte Phases

Modeling—Self-Assembly and Fracture. As for the modeling of self-assembly of conductive additives, we investigated the aggregation kinetics in cathodes. Governing equations and parameters were found for convection effect of homogenization process as well as diffusivity of particles in the settling process in cathode fabrication. The on-off probability of cluster-cluster sticking upon contact was also found. A cluster-cluster aggregation simulation algorithm was formulated.

Brownian dynamic simulation was used to model the aggregation of cathode particles. Parameters such as surface charge can be modified to study their influence on the geometry of aggregated clusters. The geometry of a cluster was characterized using radius of gyration and main chain length. The whole aggregated system that contains all clusters was characterized by averaged number of contacting neighbors. Figure V- 105 shows an aggregated cluster generated from simulation and the influence of surface charge on cluster geometry, statistically.

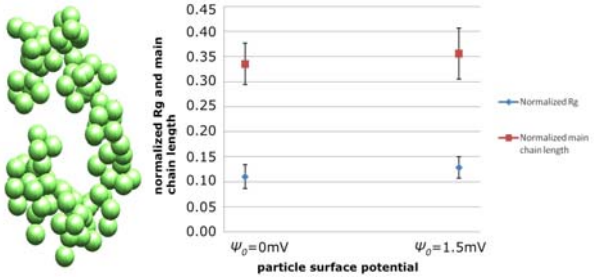

Figure V- 105: Aggregated Cluster Generated from Simulation and the Influence of Surface Charge on Cluster Geometry

Finite element analysis was performed using ABAQUS 6.8 to simulate crack propagation in an active material particle. The loading condition was the intercalation induced stress field determined by COMSOL multiphysics software and imported into ABAQUS using a Matlab script. A Virtual Crack Closure Technique (VCCT) criterion, which is suitable to simulate brittle material was used to determine the condition in which crack propagates. An initial crack was also required. The accurate material properties used in the fracture simulation were measured using nanoindentation on thin films or simulated. Figure V- 106 shows stress distribution in ABAQUS model and the opening of a pre-existing crack.

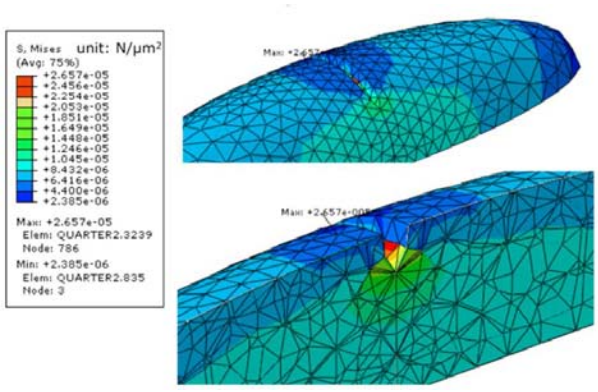

Figure V- 106: Stress Distribution in Cathode Model and Opening of a Pre-existing Crack

Experiment / Modeling—Diffusion Properties and Particle Geometry. We have also been working on the extension of cathode modeling to utilize measured diffusion properties in 3D-FE simulations. Dispersed single particle electrodes have been developed as an experimental model for the measurement to generate realistic 3D particle geometric models and concentration-dependent diffusion coefficient profile. Diffusion coefficients of cathode particles as well as their geometry were implemented into our 3D-FE simulations. Simulation results from these experimental inputs are shown in Figure V- 107 with higher maximum stress due to the lower diffusion coefficients and local stress concentration at the grain boundaries compared to theoretical oblate shape with a similar aspect ratio.

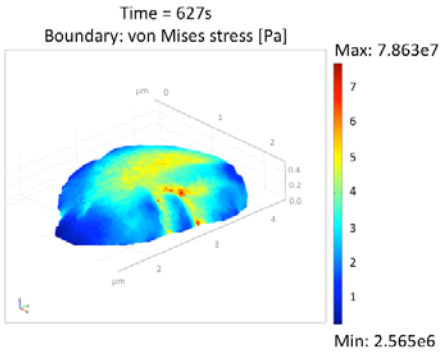

Figure V- 107: Simulated Stress Distribution on Actual Particle Surface with Stress Concentration at the Grain Boundary

Conclusions and Future Directions

3D FEM simulations of single electrode particles showed that ellipsoidal particles with larger aspect ratios are preferred to reduce stress and heat generation. This single particle model was extended to electrode microstructure consisting of solid active material and liquid electrolyte phases. The species transport and electrochemistry equations were implemented which enables the stress and heat generation modeling inside electrode microstructure in the near future. Meanwhile, the mechanics of aggregation and fracture analysis for electrode particle clusters were also studied. All these efforts pave the way toward 3D FEM mesoscale modeling of mechanical, thermal, electrochemical effects inside electrode architecture.

FY 2009 Publications/Presentations

1. Presentation to the 2008 DOE Annual Peer Review Meeting.
2. Sastry, A.M., “Advanced Batteries: Enabling Simulations for the Drivetrain of the Future”, Invited Presentation, ASME 2009 Conference on Smart Materials, Adaptive Structures & Intelligent Systems, Oxnard, California, September 21-23, 2009
3. Zhang, X., Sastry, A.M. and Shyy, W., “Multiscale modeling of thermal and stress characteristics of lithium-ion batteries”, SIAM Conference on Computational Science and Engineering, Miami, FL, March 2, 2009.
4. Zhang X., Shyy W. and Sastry A.M., “Particle- to Electrode-Scale Heat and Stress Generation Simulation and Optimization for Li-ion Batteries”, 215th ECS Meeting, San Francisco, CA, May 24-29, 2009.
5. Chung M.D., Zhang X., “Experimental Study of Diffusion Coefficients in Single LiMn2O4 Particles”, 215th ECS Meeting, San Francisco, CA, May 24-29, 2009.

V.E.3 FIB Micromachined Electrodes (ORNL, UM)

Claus Daniel

Oak Ridge National Laboratory
1 Bethel Valley Road
P.O. Box 2008, MS-6083
Oak Ridge, TN 37831-6083
Phone: (865) 241-9521; Fax: (865) 241-5531
E-mail: danielc@ornl.gov

Subcontractor : Ann Marie Sastry

University of Michigan, Ann Arbor
2350 Hayward St., Ann Arbor, MI 48109-2125
Phone: (734) 764-3061; Fax: (734) 647-3170
E-mail: amsastry@umich.edu

Start Date: Sept. 2009
Projected End Date: Sept. 2010

Objectives

- Develop a fundamental understanding of deformation processes and stress generation during Li intercalation/ deintercalation from active cathode materials via experimental work on micromachined samples.
- Develop and validate a coupled kinetic, thermal, and mechanical model based on the experimental results.

Introduction

It is commonly accepted that Li-ion battery life is limited by the process of degradation of electrode materials with repeated charging and discharging. During battery operation, Li-ions are shuttled between cathode and anode when the battery is being charged and discharged. One of the degradation mechanisms is related to the development of internal stresses in electrode particles due to repeated lithium insertion and removal. The stresses ultimately result in cracks in and fracture of particles. The current project targets the fundamental understanding, description through mathematical modeling, and controlled experimental validation of internal stress generation in and morphology change of electrode particles in Li-ion batteries.

Approach

Since the goal of the project is rather fundamental, the experiments are being performed on model systems represented by microscopic specimens of electrode material. The modeling work is being done on preselected geometries of specimens to validate the constitutive approach. Different electrode materials are being investigated, including $LiCoO_2$, $LiMn_2O_4$, and $Li_4Ti_5O_{12}$.

The specific distribution of tasks is as follows. Thin-film battery systems with thicknesses suitable for Focused Ion Beam (FIB) machining will be synthesized at ORNL. Subsequent micromachining of electrode samples will be done at ORNL using a dual-beam FIB Scanning Electron Beam (SEM). Samples will then be tested in half-cell setup at the University of Michigan. The setup is equipped with an atomic force microscope. Its tip serves as a current collector, which allows for simultaneous cycling and investigation of morphology change of the specimen. X-ray diffraction under a protective atmosphere will be performed at ORNL. Comparison between behaviors of different electrode materials will allow for material classification based on internal stress development and cycling stability. The experimental results will be used to validate the proposed coupled kinetic, thermal, and mechanical model.

Results

Physical Vapor Deposition (PVD) of Thin Film Systems. At the first stage, a sample thin-film system with a $LiCoO_2$ cathode was prepared by PVD in the thin-film battery laboratory at ORNL (Nancy Dudney). The deposition of layers was done on an Al_2O_3 substrate. The $LiCoO_2$ cathode was deposited over a thin layer of gold, which acts as a current collector. The system was covered by Lipon, which acts as a solid electrolyte. The cross section of the system is shown in Figure V- 108.

Micromachined Electrodes. Sample electrode specimens were micromachined from the PVD layer of $LiCoO_2$ on the gold current collector. The average grain size of the deposited cathode material was 100 nm. Fabrication of samples was performed using a Hitachi NB5000 dual-beam FIB/SEM. A surface protecting tungsten coating was applied prior to specimen micromachining or cross-sectioning. Two samples, one circular and another square in cross section, were milled. SEM pictures of the milled samples are shown in Figure V- 109.

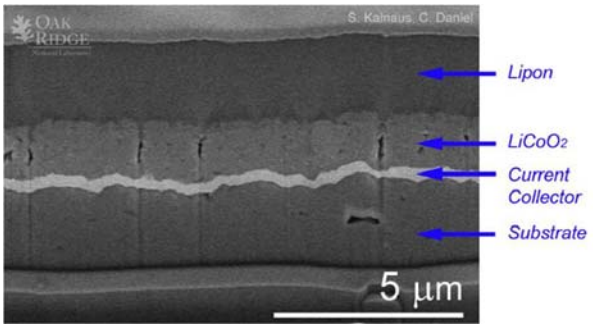

Figure V- 108: Cross-section view of PVD fabricated thin film system

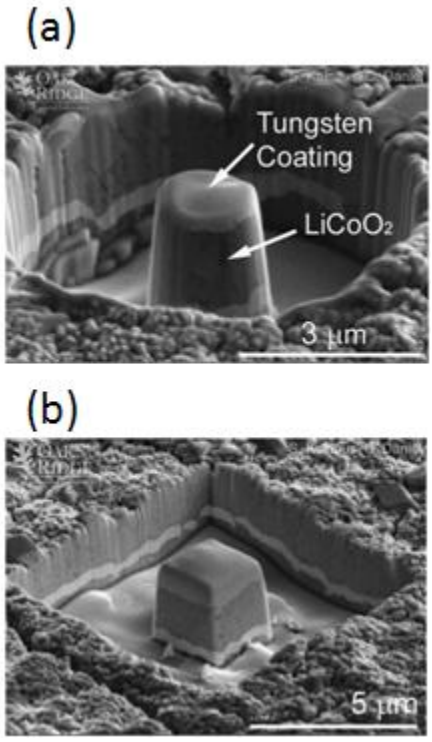

Figure V- 109: FIB machined specimens with: (a) circle and (b) square as a base shape

Computational Modeling of Internal Stress Generation. Preliminary results were obtained based on a cylindrical homogenous $LiMn_2O_4$ particle. Intercalation-induced stresses during a discharge process (current density $i = 2A/m^2$) were simulated using a stress-diffusion coupling model. Three cases were considered to quantify the stress level (Figure V- 110): (a) a single particle, (b) two agglomerated particles, and (c) two particles combined by a PVdF binder.

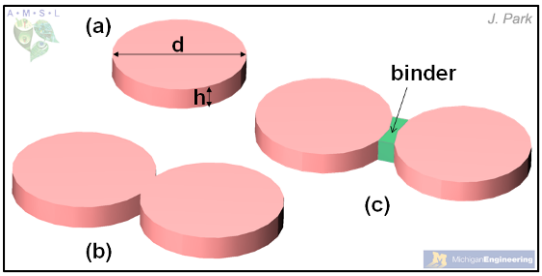

Figure V- 110: Schematic diagram of cylindrical lithium-manganese-oxide particles (a) a single cylindrical particle (d: 30 μm, h: 5 μm) (b), two agglomerated particles, and (c) combined two particles through a binder (PVdF)

Figure V- 111 shows the Li-ion concentration distribution. In all cases, the concentration is maximized along the upper edge of the cylinders. In the (c) case, the concentration is zero in the binder because lithium ions cannot enter into the binder. Figure V- 112 shows the von Mises stress distribution at the end of the discharge process, where the maximum concentration reaches the stoichiometric maximum. In a single particle, the stress is larger along the upper edge, where the gradient of lattice spacing is more severe. In case (b), there is a stress concentration at the connection between two particles. This is caused by an abrupt change in the geometry. However, in the (c) case, there is no concentration around that connection. The stress level and distribution are similar to the case of a single particle. In the binder there is no intercalation of lithium ions; as a result, the (c) case may be similar to two isolated particles.

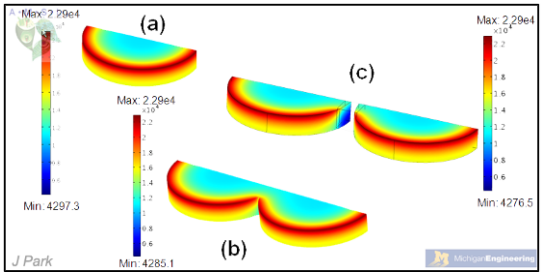

Figure V- 111: Lithium-ion concentration distribution (mol/m^3) when the surface concentration reaches the stoichiometric maximum value (2.29e4 mol/m^3)

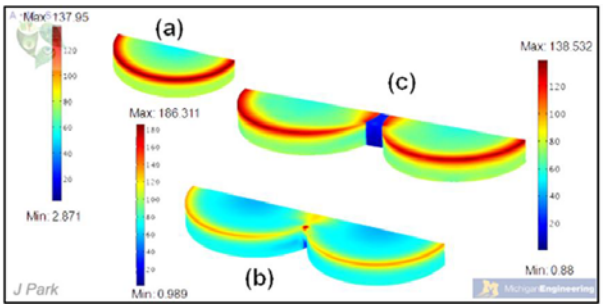

Figure V- 112: Von Mises stress distribution (MPa) when the surface concentration reaches the stoichiometric maximum value

Conclusions and Future Directions

The diffusion-stress coupling model shows the capability of internal stress predictions in electrode particles. The model will be validated using experimental data obtained from electrochemical cycling of electrode samples. Also, the simulation will be improved using realistic particle agglomerations and particle shapes to predict behavior more accurately. In the initial stage, the work will be concentrated primarily on cylindrical specimens. Experimentation with FIB techniques will continue in order to improve the machining technique and to produce samples with more complicated geometries. Experimental work on stress generation during cycling will create a connection between the magnitudes of shape and stress induced in the specimens.

Acknowledgment

This research at Oak Ridge National Laboratory, managed by UT Battelle, LLC, for the U.S. Department of Energy under contract DE-AC05-00OR22725, and at the University of Michigan was sponsored by the Vehicle Technologies Program for the Office of Energy Efficiency and Renewable Energy. Parts of this research were performed at the Shared Research Equipment Collaborative Research Center, sponsored by the Office of Science, Basic Energy Sciences Program.

V.E.4 Investigations of Electrode Interface and Architecture (LBNL)

Venkat Srinivasan
Lawrence Berkeley National Laboratory
1 Cyclotron Road, MS 70-0108B
Berkeley, CA 94720
Phone: (510) 593-5787; Fax: (510) 486-4260
E-mail: VSrinivasan@lbl.gov

Start Date: October 1, 2008
Projected End Date: September 30, 2009

Objectives

- Quantify the usefulness of alloy anodes for use in PHEVs with larger focus on silicon anodes for this fiscal year. The specific objectives include: (a) understand and mathematically describe potential hysteresis and quantify the energy efficiency under rates relevant for vehicular applications, (b) quantify the impact of electrolyte solvents and additives on the potential hysteresis, 1st cycle loss, and steady-state efficiency to enable higher energy and longer life; (c) quantify impact of potential hysteresis on small state-of-charge cycling, especially on the energy efficiency; (d) evaluate the impact of surface coatings in order to minimize side reactions and enable better cycling characteristics to improve life; (e) extend the kinetic model for silicon anodes to include phase behavior and transport in order to predict conditions under which life-limiting crystalline phases form.
- Understand behavior and suggest means to enhance performance of high-energy phosphates (e.g., $LiMnPO_4$).
- Provide modeling support in the determination of diffusion coefficient in carbon anodes.

Technical Barriers

This project addresses the following technical barriers: high cost (or low energy) of lithium-ion batteries for PHEV applications.

Technical Targets

- Relevant USABC goals: Available energy: 56 Wh/kg (10 mile) and 96 Wh/kg (40 mile); 10 s discharge power: 750 W/kg (10 mile) and 316 W/kg (40 mile).

Accomplishments

- Experimentally quantified the kinetic limitations in silicon anodes and developed a model that predicts polarization losses and time constants.
- Estimated kinetic parameters for lithiation and delithiation reactions as well as side reactions in silicon anode for different electrolytes.
- Estimated activation energies for lithiation/delithiation reaction and side reactions.
- Extracted kinetic parameters on porous electrodes fabricated with Si nanoparticles and compared the results with those obtained on thin films.
- Developed a model for a single particle of silicon that accounts for volume change and allows for predictions of conditions where specific phases form.

✧ ✧ ✧ ✧ ✧ ✧

Introduction

Novel lithium-ion chemistries for use in HEVs and PHEVs need to be understood, characterized and evaluated in lab-scale systems before they can be scaled up for use in real-world applications. An integral component of this process is the use of mathematical models to test the capabilities of these chemistries from the context of where they will be used. Among novel lithium-ion chemistries, alloy anodes are widely considered to be a replacement for the present-day graphite anodes due to their high-theoretical capacity and attractive rate-capability features.

Approach

Develop mathematical models for candidate Li-ion chemistries to quantify their ability to meet DOE/USABC performance goals for use in HEV and PHEV applications. This is accomplished by designing experiments to estimate thermodynamic, kinetic and transport properties for a particular chemistry. These properties are then be used to test theoretical predictions and provide guidance to material-synthesis and cell-development PIs. Overall, the approach is to connect fundamental material properties to practical performance requirements.

Results

Kinetic Limitations in Silicon Electrodes. In the previous fiscal year (*i.e.,* 2008), we studied the electrochemical lithiation and delithiation behavior on both crystalline and amorphous thin-film Si anodes. These

films were obtained respectively through pulse-laser deposition (PLD) and magnetron sputtering techniques. The films were cycled galvanostatically between 0 and 1.2 V *vs.* Li/Li^+. The difference between lithiation and delithiation capacities between the cutoff potentials, which results in the cycle-to-cycle marching seen in this system (as well as the departure from 100% cycling efficiency) was attributed to solvent reduction and solid-electrolyte-interphase (SEI) formation, and is a persistent problem with all Si electrodes. In addition to this, the large potential offset between the lithiation and delithiation curves lowers the energy efficiency between charge and discharge during a PHEV operation. We presented a complete understanding of these features using mathematical modeling of main and side reactions (in conjunction with galvanostatic and open circuit potential relaxation experiments) to quantify the various losses if Si anodes were to be used in PHEVs.

Effect of Solvents and Additives on Side Reactions. In this fiscal year, these studies were extended to include the effect of solvents and additives on the above-mentioned characteristic features exhibited by Si electrodes. While the addition of propylene carbonate (PC) resulted is marginally better performance of these electrodes, the addition of fluoro ethylene carbonate (FEC) resulted in significant improvements (Figure V- 113). Though the effect of this additive has been documented in patent literature, we were able to confirm this using careful experimentation and mathematical analysis (*i.e.,* estimated side-reaction rates were an order of magnitude smaller than without this additive) and more importantly, this enabled us to move closer towards an accurate estimation of equilibrium potential as a function of state-of-charge for silicon.

The kinetic parameters corresponding to the main and side reactions for all of the electrolyte compositions studied have been reported in the BATT quarterly reports submitted during this fiscal year. There was however no significant change in the hysteresis behavior between the various electrolytes studied.

Activation Energy Estimation. The kinetic experiments were performed as a function of temperature between 5 and 50°C. The potential hysteresis appears to decrease with increasing temperature and an extrapolation suggests that this may disappear in the neighborhood of 200°C (see Figure V- 114). The reaction rate constants corresponding to lithiation at 50% state-of-charge were estimated using this data. The apparent activation energies for the main and the side reactions for the EC:DEC (3:7) with 10% FEC electrolyte were estimated to be 26.05 (lithiation), 29.64 (delithiation) and 20.2 kcal/mol (side reaction).

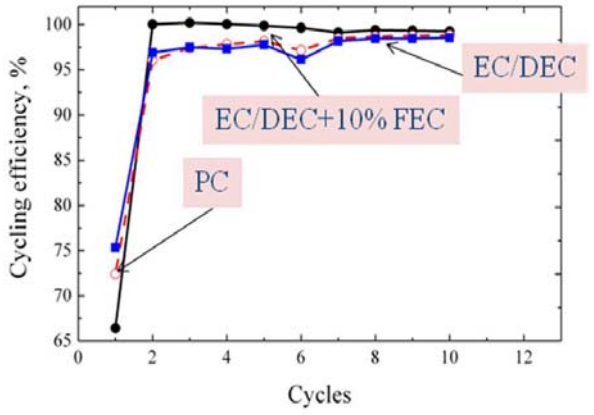

Figure V- 113: Cycling efficiency shown as a function of cycle number for three different electrolyte compositions

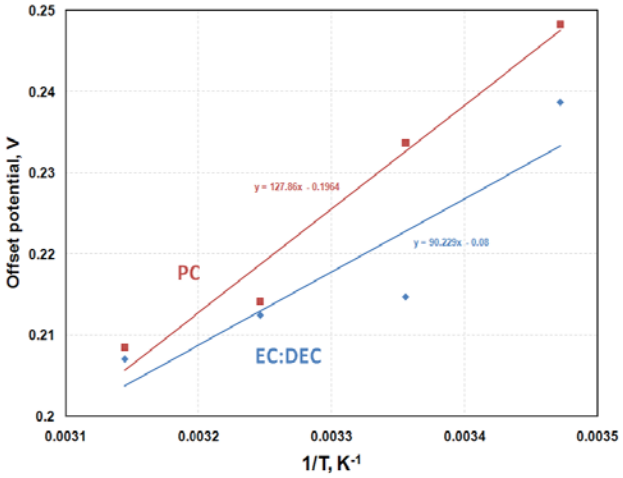

Figure V- 114: Offset potential measured between lithiation and delithiation potentials vs. Li/Li^+ at 50% state-of-charge is measured as a function of temperature.

Modeling Mass Transport in Silicon. A single-particle model that accounts for volume expansion with lithiation was developed. This model describes the lithiation behavior of silicon on a formed electrode and helps describe transport limitations in silicon anodes. The model is used to identify conditions under which the crystalline phases form (which is thought to be highly detrimental to cycling) with emphasis on PHEV operation. Analyses were performed for cycling in the amorphous regime after the first cycle lithiation. Figure V- 115 describes the utilization that can be obtained at a specified rate before the $Li_{15}Si_4$ phase formation occurs in a dimensionless form. In order to connect this data to PHEV performance, an estimation of the diffusion coefficient of lithium in silicon is needed. We found a wide disparity in reported values of diffusion coefficient and the results shown in the figure (points for C/2 and 2C) are representative of a smaller value of the diffusion

coefficient (10^{-12} cm^2/s) and for a particle size of 5 microns. This model suggests that silicon electrodes could have rate limitations when used in PHEVs but a more accurate estimate of diffusion coefficient of lithium in this system is needed. For this purpose, we intend to do a careful estimation of the diffusion coefficient in the future.

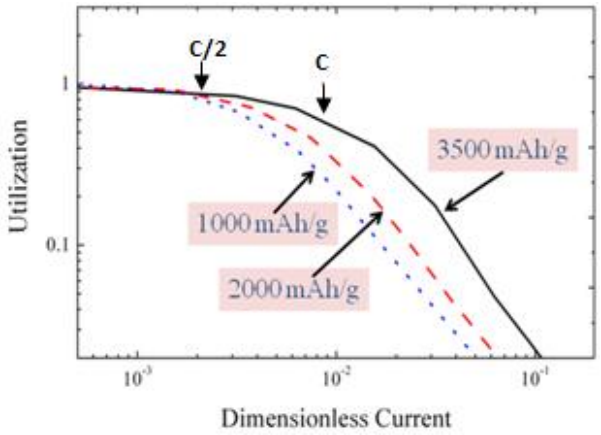

Figure V- 115: Results from a single-particle diffusion model that accounts for volume expansion with lithiation of silicon. C and C/2 represent lithiation rates at 25°C.

Studies on Composite Si Electrodes. Composite electrodes were made with 30 nm Si particles (Sigma-Aldrich) and a proprietary binder developed at LBNL. The electrodes were obtained from the Cell Analysis group (Battaglia) and experimentation was done to measure key lithiation/delithiation characteristics of this system. Using parameters obtained from the thin film Si electrodes, we carried out simulations for a porous-electrode (using dual-foil model developed by Prof. Newman). The model results indicated uniform reaction distribution across the composite electrode under normal operating conditions, owing to the poor kinetics. A direct consequence of this is that the parameter-estimation procedure on a kinetic model that was used on the thin-film system can now be used for the composite electrode. We therefore estimated the relevant kinetic parameters at 50% state-of-charge on two different composite electrodes along with the side reaction rate and cycling efficiency values. Results were seen to be comparable to those extracted from thin-film studies (see BATT quarterly report in Q3 - FY 2009).

Studies on Copper-coated Silicon. The role of copper coating on silicon electrodes was evaluated for possible improvements in cycling efficiency and rate capability. Figure V- 116 shows the enhanced cycling capability of using a nano coating of copper to cover the silicon thin films. However, the amount of copper covering the surface impacts the rate capability of this system by, presumably, decreasing the access of the electrolyte to the reaction site. Therefore a critical amount of copper is required to enhance the cycle-ability of silicon electrode without compromising capacity. We are extending this preliminary study into the next fiscal year towards the optimization of coating thickness and whether or not a porous coating will help the overall performance for this particular system.

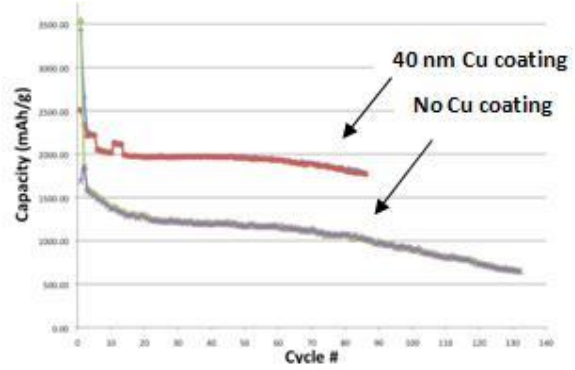

Figure V- 116: Cycling of silicon thin films with and without a copper coating. Note the lowered capacity loss and better efficiency with a 40nm copper coating.

Conclusions and Future Directions

In the next fiscal year, we intend to accomplish the following: (1) Incorporate the kinetic and mass transfer models into a porous electrode model and simulate the performance of a NMC/Si cell under PHEV conditions, (2) Work with Cell Analysis group to obtain experimental data on silicon powders to compare to the model (3) Complete the study on the copper-coated silicon samples and develop a mathematical model that accounts for the decreased area for reaction and increasing diffusion length on PHEV operation and (4) Develop a model for $LiMnPO_4$ that incorporates the recent understanding of phase behavior obtained in $LiFePO_4$.

FY 2009 Publications/Presentations

1. Optimizing the Performance of Lithium Titanate Spinel Paired with Activated Carbon or Iron Phosphate, *J. Electrochem. Soc.*, **155,** A253 (2008).
2. A Combined Model for Determining Capacity Usage and Battery Size for Hybrid and Plug-in Hybrid Electric Vehicles, *Journal of Power Sources,* **183,** 771 (2008).
3. Modeling the Performance of Lithium-Ion Batteries and Capacitors during Hybrid-Electric-Vehicle Operation, *J. Electrochem. Soc.,* **155,** A664 (2008).
4. A Study of the Mechanism of Graphite Structural Degradation in Lithium-ion Cell Anodes, *Meet. Abstr. - Electrochem. Soc.,* **802,** 1162 (2008).
5. Hysteresis during Cycling of Lithiated Silicon Electrode, *Meet. Abstr. - Electrochem. Soc.,* **802,** 1189 (2008).

6. Analysis of the Charge/Discharge Behavior of Silicon Anodes, *Meet. Abstr. - Electrochem. Soc.*, **802,** 607 (2008)
7. Annual Merit Review, Office of Vehicle Technologies, 2009.

V.E.5 Analysis and Simulation of Electrochemical Energy Systems (LBNL)

John Newman
Lawrence Berkeley National Laboratory
306 Gilman Hall
University of California, Berkeley
Berkeley, CA 94720
Phone: (510) 642-4063; Fax: (510) 642-4778
E-mail: newman@newman.cchem.berkeley.edu

Start Date: October 1, 2008
Projected End Date: September 30, 2010

Objectives

- Develop experimental methods for measuring transport, thermodynamic, and kinetic properties.
- Model electrochemical systems to optimize performance, identify limiting factors, and mitigate failure mechanisms.

Technical Barriers

This project addresses the following technical barriers from the USABC:

(A) Capacity and power fade

(B) Safety and overcharge protection

Technical Targets

This project contributes to the USABC requirements of end of life energy storage systems for PHEVs and EVs:

- 300,000 shallow discharge cycles
- 15 year calendar life

Accomplishments

- Completed and published theoretical study on the effects of two-dimensional geometry on lithium deposition on graphite electrodes
- Implemented redox shuttles in the porous-electrode model Dualfoil to consider the how material properties of a redox shuttle affect tradeoffs between overcharge protection and system performance.
- Designed experiments to investigate how redox shuttles are reduced through the SEI and demonstrated proof-of-concept for the reduction of ferrocenium to ferrocene.

✧ ✧ ✧ ✧ ✧

Introduction

Achieving the DOE targets for cycle life and calendar life requires improved understanding of side reactions in Li-ion batteries, both detrimental and beneficial. Models can explain why side reactions occur in certain situations and predict methods to control them. In FY09, we worked on modeling several side reactions. The first, lithium deposition, is a detrimental side reaction that causes capacity fade, power fade, and safety issues. The second, a redox shuttle, is a beneficial side reaction that provides overcharge protection but can present tradeoffs in performance. Finally, we began work on an experimental project involving SEI-forming side reactions, which are both detrimental and beneficial to battery lifetime.

Approach

- Develop two-dimensional model that explains edge effects on lithium deposition during charging and how physical properties (conductivity, rate constants) and design parameters (geometry, capacity ratio) affect results.
- Apply a combination of experiments and simulations to study the ability of redox shuttles to provide overcharge protection. A simplified zero-dimensional model can provide basic insights, while a detailed battery model can examine complexities.
- Utilize classical electrochemistry experiments to understand the interaction of redox shuttles and the SEI. Measure shuttle reduction kinetics in the presence and absence of passivating films to determine the relative transport and kinetic inhibitions to reaction.

Results

Effects of 2-D Geometry on Lithium Deposition. In last year's report, we showed that extending the negative electrode relative to the positive can prevent lithium deposition by providing excess capacity where it is needed most, thus reducing overpotential at the electrode. Because of the non-uniform current distribution in the battery, extending the negative electrode prevents deposition more effectively than making it thicker does. In FY09 we expanded on this work to determine how various physical and design parameters affect the results. The results for one of those parameters, the electrolyte conductivity, are shown below in Figure V- 117. More details can be found in our publications on this subject [2, 3].

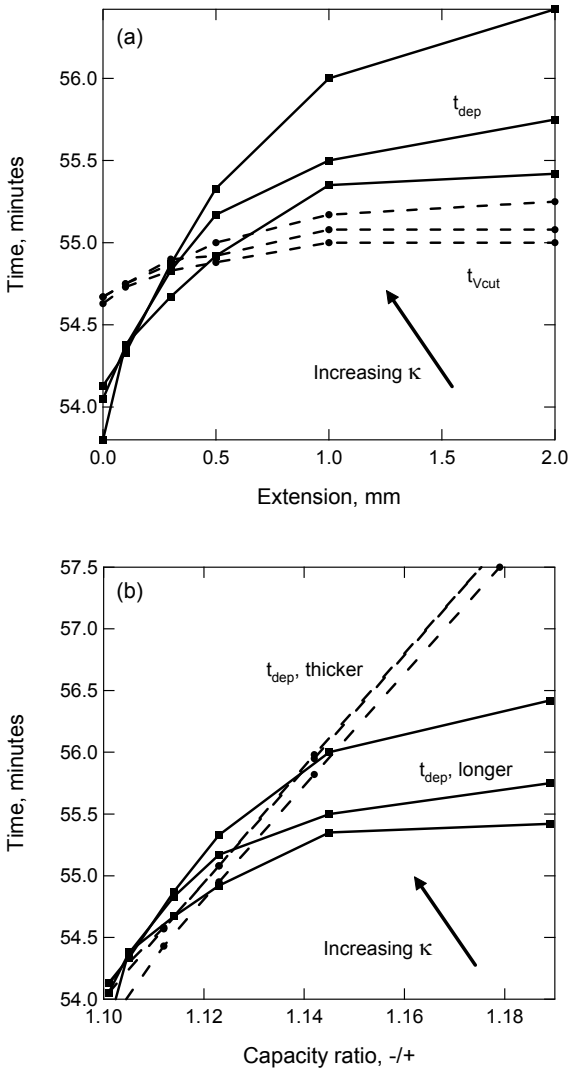

Figure V- 117: (a) Time to reach deposition (t_{dep}, solid lines) and cutoff potential (t_{Vcut}, dashed lines) as the electrode is extended, for κ_{eff} = 0.33, 0.533 (baseline), and 1.3 S m^{-1}. (b) Time to reach deposition as electrode is either extended (solid lines) or thickened (dashed lines), for the same values of κ_{eff}. As the conductivity increases, there is less ohmic resistance through the separator to the extension and thus extending the electrode becomes more effective at preventing deposition. Neither the time to reach the cutoff potential nor the time to reach deposition is strongly affected when the electrode is made thicker.

System Modeling of Redox Shuttles.

Implementation of redox shuttles in macroscopic battery models has shown qualitative agreement with literature results. Some results from the simplified, zero-dimensional model are shown in Figure V- 118 and Figure V- 119. Figure V- 118 shows the simulated potential versus time in a lithium/ lithium nickel-cobalt-manganese oxide (L333) cell with 0.2 M of the molecule 2-(pentafluorophenyl)-tetrafluoro-1,3,2-benzodioxaborole as the overcharge current is increased from 0.017 mA/cm^2 to 3.4 mA/cm^2 (0.01 C to 2.0 C). Cell potential increases with the overcharge rate, and shoots up when the shuttle can no longer maintain the applied current. Increasing either the shuttle diffusivity or concentration would allow a higher overcharge current to be applied.

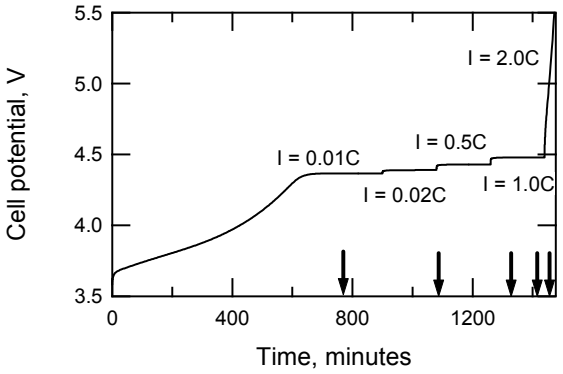

Figure V- 118: Simulated overcharge protection in a Li/$LiNi_{1/3}Co_{1/3}Mn_{1/3}$cell at increasing values of the overcharge current. The cell potential increases with increasing charge rate until the limiting current of the shuttle is reached. Black arrows indicate where concentration profiles are plotted in Figure V- 119.

Figure V- 119 shows the concentration profile of the shuttle cation versus cell sandwich position at different times. At low overcharge currents, the shuttle can carry the current with a very small concentration gradient.

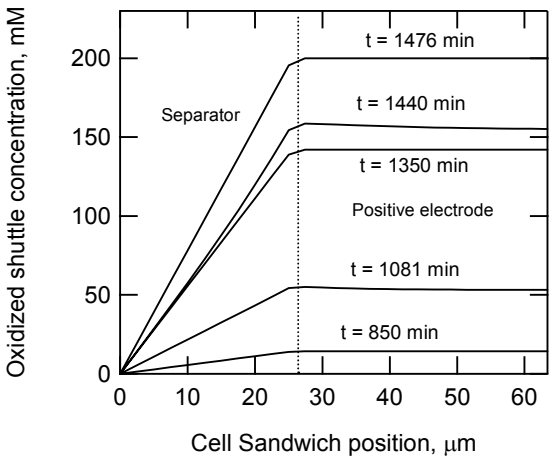

Figure V- 119: Concentration profile of shuttle cation versus cell position at different times, as indicated by black arrows in Figure V- 118. The concentration is initially zero, but as cell potential rises, the cation is generated and diffuses across the separator. Concentration is zero in the negative electrode because the reaction is at the limiting current.

As the rate increases, a larger gradient is required, and more of the total shuttle concentration exists as the charged species. Before steady-state is reached after each current change, the concentration decreases from the front to the

back of the positive electrode. This is because the kinetics of the shuttle reaction is fast, causing a non-uniform reaction distribution within the porous electrode. The non-uniformity of the reaction distribution suggests that electrode parameters such as thickness, porosity, and particle size will not be relevant to the application of redox shuttles in commercial cells.

Interactions between Redox Shuttles and the SEI. We have begun to work on explaining how a redox shuttle can be reduced across the SEI, which is supposed to block electron transfer. Our approach is to measure shuttle kinetics in the presence and absence of passivating films using the rotating-disk-electrode (RDE). Preliminary experimental results on ferrocene, a model redox shuttle, are shown in Figure V- 119. The intercept of the bottom line in this Koutecky-Levich plot is zero, showing that in the absence of surface films, the ferrocenium reduction is reversible. The other three lines in Figure V- 120 are measured at different voltages after sweeping the electrode to potentials that caused reduction of the supporting electrolyte. The intercept of the Koutecky-Levich lines becomes non-zero, showing kinetic inhibitions to the ferrocenium reduction. More work is required to obtain accurate and reproducible results.

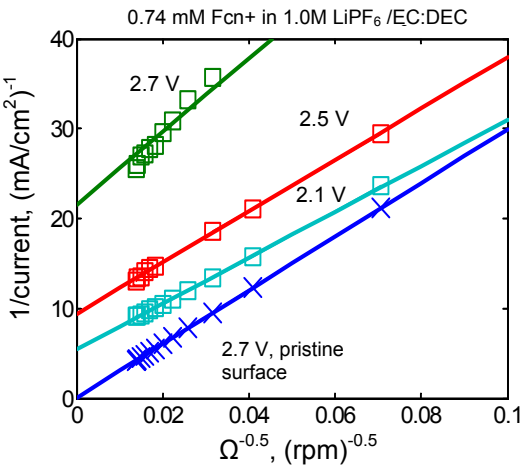

Figure V- 120: Koutecky-Levich plot of inverse current vs. the reciprocal of the square root of rotation speed for ferrocenium reduction. After reducing the supporting electrolyte on the surface, the reaction is slowed, as evidenced by the nonzero intercept of the lines.

Conclusions and Future Directions

1. Modeling of Failure Mechanisms due to Impurities. We next plan to extend our work on lithium deposition on carbon electrodes to include other materials in order to understand what happens when impurities such as iron and manganese ions enter the system. We will look at how fast these species could react, where reaction is likely to occur, and how electrode construction could prevent reactions when impurities enter the manufacturing stream. Along with simulations, we plan to include experimental work to validate the results of the model. The goal of this project is to improve the understanding of impurities in order to develop a long-life battery with adequate power and energy.

2. System Modeling of Redox Shuttles. Future work will continue investigation of tradeoffs among overcharge protection and cell performance. We will incorporate overcharge side reactions at the positive electrode and consider side reactions at the negative electrode as well. Temperature effects will be modeled, because during overcharge, no net reaction takes place; thus, all current is converted entirely to heat. This causes a rise in cell temperature, which accelerates overcharge reactions but also decreases the resistance of the cell.

3. Interactions between Redox Shuttles and the SEI RDE studies on the reduction of ferrocenium will continue. The first step is to establish accurate and reproducible experimental methods. The next step will test different shuttle molecules, electrolytes, and electrodes to develop correlations between material properties and the amount of passivation occurring. Modeling to corroborate and explain experimental results will continue in parallel. If necessary, characterization of electrode surfaces via collaborations with colleagues at Lawrence Berkeley National Laboratory will take place. Determining the mechanism of shuttle reduction will contribute to understanding of electron transport in the SEI and allow improvements in battery chemistry and design.

FY 2009 Publications/Presentations

1. Presentation to the 2008 DOE Annual Peer Review Meeting, May 2009.
2. M. Tang, P Albertus, and J. Newman, *ECS Meeting Abstracts*, **802**, 1290 (2008).
3. M. Tang, P. Albertus, and J. Newman. *J. Electrochem. Soc.* **156**, A390 (2009).

V.E.6 Carbon Fiber and Foam Current Collectors (ORNL)

Nancy J. Dudney
Oak Ridge National Laboratory
Material Science and Technology Division
Building 4500S MS6124
PO Box 2008
Oak Ridge, TN 37831-6030
Phone: (865) 576-4874
E-mail: dudneynj@ornl.gov

Start Date: July, 2007
Projected End Date: September 30, 2010

Objectives

- Investigate the use of highly-conductive graphite as the current collector and skeleton for Li-ion battery cathodes.

Technical Barriers

This project addresses the following technical barriers for development of plug in hybrid electric vehicle technologies:

(A) Cycle and calendar life, 5,000 cycles for PHEV; 300,000 cycles HEV; 15 year life

(B) Abuse tolerance

(C) Much higher energy density (40 mile system: 11.6 kWh; 120 kg; 80 liter)

Technical Targets

- Cathode composites with a specific energy and volumetric energy density as good as current commercial cathode plus metal current collector sheets.
- Cathode sheets up to 1mm thick with larger capacity per area to reduce the volume and mass associated with the electrolyte and anode components.
- Cycling of 100-1,000 cycles with little capacity fade due to the cathode.

Accomplishments

- Achieved >100 cycles with multiple battery half cells using $LiFePO_4$ and carbon fibers.
- Compared energy and power performance for distinctly different fiber and foam carbon structures
- Identified where the loading of active material in the fiber skeleton begins to impede high rate performance.
- Determined that the thermal conductivity of the composite cathode is the same as the carbon skeleton.

✧ ✧ ✧ ✧ ✧

Introduction

Cycling performance for PHEV batteries is extremely demanding. Although the multiple degradation processes have not been fully characterized, it is clear that both the organic binder and the metal foil current collector of typical electrode sheets are not innocent materials but contribute to degradation through corrosion, side reactions, or lost connectivity. Also, degradation is promoted by local variations in the current density and the local heating, and perhaps also flaws introduced by pressing the electrode compact. With novel electrode architecture and a binder-free assembly, we expect to generate proof of principle for use of conductive carbon fibers or open cell foams distributed throughout the electrode in order to provide a high surface area collector for the current and heat transport.

Approach

A variety of conductive carbon fiber and foam structures are infiltrated with a slurry of LiFePO4 particles with ~3 wt.% added aromatic resin pitch. The carbon structures provide at least 20-fold higher surface area for the current collector relative to the foot print. Heat treatment at 700ºC results in a carbon bonded composite, such as that shown schematically in

Figure V- 121. The cathodes are tested in lithium half cells with both coin cell and prismatic constructions at ORNL and LBNL. Microstructure is characterized by SEM and X-ray tomography. Thermal diffusion is measured using a LaserPIT technique. Results are used to estimate the volume and weight required for the cathode of an 18650 cell for comparison with commercial Li-ion batteries. Concerns about the cost of the carbon fibers, strength of the composite, and tab attachment are addressed.

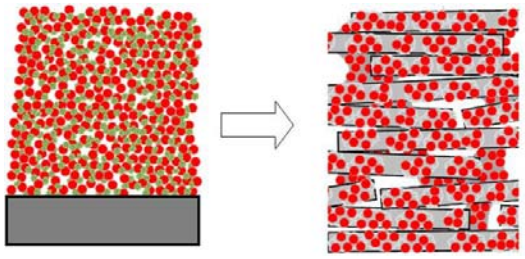

Figure V- 121: Replacement of standard particle coating on a metal foil (left) with particles coating a carbon fiber skeleton to form a composite (right).

Results

Specific energy and power of the cathode composite, including the carbon skeleton, depends on the openness of the carbon structure, thickness, and density. Examples are shown in Figure V- 122. Fiber mats and papers performed better than graphite foams and a 1mm thick sheet of carbon bonded carbon fibers (CBCF) with fibers preferentially aligned normal to the sheet showed particularly good performance. Toray carbon fiber papers with most fibers aligned in-plane were overall easiest to handle and convenient to fabricate with several thicknesses.

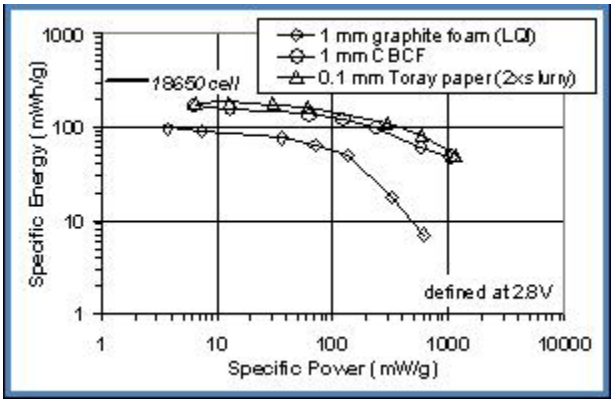

Figure V- 122: Specific energy and power performance for several composite cathodes. The mass includes the carbon current collector, $LiFePO_4$ and carbon binder.

A number of the 0.1 and 0.4mm thick cathodes with Toray fibers cycled with little loss of capacity for >100 cycles, such as the results shown in Figure V- 123. This shows that robust $LiFePO_4$-fiber bonds are formed by the 700ºC treatment.

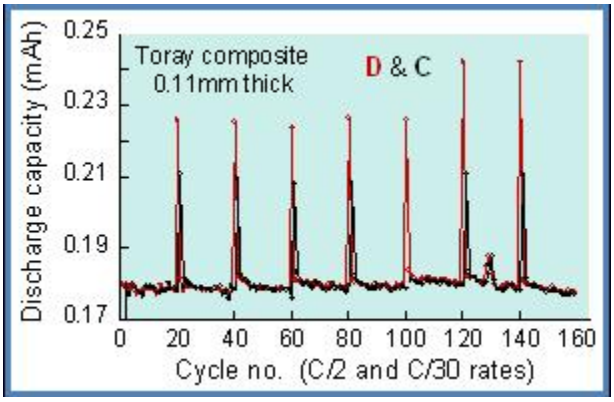

Figure V- 123: Discharge and charge capacity for 0.7 cm^2 disk with C/2 rates with a slow C/30 every 20 cycles.

SEM and X-ray tomography (Figure V- 124) show that the active material is distributed evenly throughout the thickness of the carbon fiber sheet. Weight loading ($LiFePO_4$:total) ranged from 35 to 65%. However, even for the higher $LiFePO_4$ loading, there are still large regions void of active material. The slurry tends to bridge smaller spans of the fiber web. A large fraction of the fiber surface is not coated with active material, so fibers are not fully utilized with current composites. Improvement in the electrochemical performance is anticipated with better control of the pore distribution and full coating of carbon skeleton.

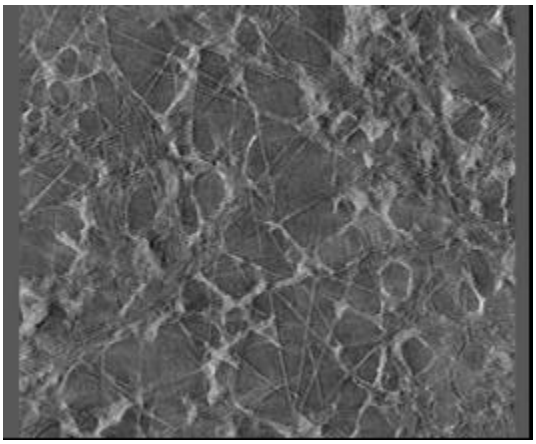

Figure V- 124: Lateral midsection of a 0.4mm Toray sheet with xx % weight loading of $LiFePO_4$ as viewed using X-ray tomography. For scale, fibers are 8µm in diameter.

In-plane thermal diffusivity results, measured by scanning a pulsed laser along the sample, indicate that the heat transfer is through the carbon fiber network and matches that expected for the highly conductive fibers. Future work will separate the thermal transport of the coating and compare this with commercial electrodes on Al foils.

Conclusions and Future Directions

Composites of $LiFePO_4$ and conductive carbon fibers formed by thermal processing have been shown to have promising cycle life, capacity utilization, and power performance, although the structure is far from optimized. Future work will attempt to increase the loading of active material and reduce the volume porosity while maintaining a good interconnected carbon skeleton. Targets for the weight loading and volume porosity are 70% and 30% respectively. Key to controlling the structure will be improving the wetting and adhesion of the carbon fibers by the slurry, notoriously difficult for the carbon interface, and engineering the porosity such that a denser structure will still afford good access of the liquid electrolyte into the composite structure.

Studies of the thermal properties will continue as improved thermal uniformity and thermal management are expected to be key advantages for this electrode architecture. These properties need to be quantified by tests that accurately and fairly compare the carbon skeleton electrode structure with typical cathode coatings on foil.

Choice of materials for future work will include commercial $LiFePO_4$ and $Li(Mn_xNi_yCo_z)O_2$ powders, and low-cost carbon fibers being developed at ORNL. The carbon fibers are prepared from a low-cost lignin precursor and incorporate a few percent of carbon nanotubes for strength and improved transport. With well integrated fiber coating and calcination processes, the cathode materials may be cost effective. Experiments to metalize the electrodes or fibers will be undertaken to facilitate fabrication of electrode tabs for incorporation of these electrode by LBNL into pouch battery structures.

Fabrication and characterization of the thermal, electrochemical and structural properties of the electrodes will be carried out with colleagues at ORNL, particularly through the High Temperature Materials Laboratory. $LiFePO_4$ and other active materials will be obtained from HydroQuebec and BATT colleagues. Fabrication of full and larger-scale pouch cells utilizing these cathodes will be performed along with LBNL researchers.

FY 2009 Publications/Presentations

1. Presentation to the 2009 DOE Annual Peer Review Meeting.
2. A. K. Kercher, N.J. Dudney, J. O. Kiggans, and J. W. Klett, “Coated porous carbon cathodes for Li-ion batteries,” ECS Transactions, Vol.13, no.19 (2008) pg.109.

Acknowledgment

This research at Oak Ridge National Laboratory, managed by UT Battelle, LLC, for the U.S. Department of Energy under contract DE-AC05-00OR22725, was sponsored by the Vehicle Technologies Program for the Office of Energy Efficiency and Renewable Energy. Parts of this research were performed at the High Temperature Materials Laboratory, a National User Facility sponsored by the same office.

Appendix A: American Recovery and Reinvestment Act (ARRA) Awards

RECOVERY ACT AWARDS FOR ELECTRIC DRIVE VEHICLE BATTERY AND COMPONENT MANUFACTURING INITIATIVE			
Applicant	**DOE Award (Dollars in Millions)**	**Project Locations**	**Technology**
Cell, Battery, and Materials Manufacturing Facilities			
Johnson Controls, Inc.	$299.2	Holland, MI Lebanon, OR (Entek)	Production of nickel-cobalt-metal battery cells and packs, as well as production of battery separators (by partner Entek) for hybrid and electric vehicles.
A123 Systems, Inc.	$249.1	Romulus, MI Brownstown, MI	Manufacturing of nano-iron phosphate cathode powder and electrode coatings; fabrication of battery cells and modules; and assembly of complete battery pack systems for hybrid and electric vehicles.
KD ABG MI, LLC (Dow Kokam)	$161	Midland, MI	Production of manganese oxide cathode / graphite lithium-ion batteries for hybrid and electric vehicles.
Compact Power, Inc. (on behalf of LG Chem, Ltd.)	$151.4	St. Clair, MI Pontiac, MI Holland, MI	Production of lithium-ion polymer battery cells for the GM Volt using a manganese-based cathode material and a proprietary separator.
EnerDel, Inc.	$118.5	Indianapolis, IN	Production of lithium-ion cells and packs for hybrid and electric vehicles. Primary lithium chemistries include: manganese spinel cathode and lithium titanate anode for high power applications, as well as manganese spinel cathode and amorphous carbon for high energy applications.
General Motors Corporation	$105.9	Brownstown, MI	Production of high-volume battery packs for the GM Volt. Cells will be from LG Chem, Ltd. and other cell providers to be named.
Saft America, Inc.	$95.5	Jacksonville, FL	Production of lithium-ion cells, modules, and battery packs for industrial and agricultural vehicles and defense application markets. Primary lithium chemistries include nickel-cobalt-metal and iron phosphate.
Exide Technologies with Axion Power International	$34.3	Bristol, TN Columbus, GA	Production of advanced lead-acid batteries, using lead-carbon electrodes for micro and mild hybrid applications.
East Penn Manufacturing Co.	$32.5	Lyon Station, PA	Production of the UltraBattery (lead-acid battery with a carbon supercapacitor combination) for micro and mild hybrid applications.
Advanced Battery Supplier Manufacturing Facilities			
Celgard, LLC, a subsidiary of Polypore	$49.2	Charlotte, NC Aiken, SC	Production of polymer separator material for lithium-ion batteries.
Toda America, Inc.	$35	Goose Creek, SC	Production of nickel-cobalt-metal cathode material for lithium-ion batteries.
Chemetall Foote Corp.	$28.4	Silver Peak, NV Kings Mtn., NC	Production of battery-grade lithium carbonate and lithium hydroxide.
Honeywell International Inc.	$27.3	Buffalo, NY Metropolis, IL	Production of electrolyte salt (lithium hexafluorophosphate (LiPF6)) for lithium-ion batteries.
BASF Catalysts, LLC	$24.6	Elyria, OH	Production of nickel-cobalt-metal cathode material for lithium-ion batteries.
EnerG2, Inc.	$21	Albany, OR	Production of high energy density nano-carbon for ultracapacitors.
Novolyte Technologies, Inc.	$20.6	Zachary, LA	Production of electrolytes for lithium-ion batteries.
FutureFuel Chemical	$12.6	Batesville, AR	Production of high-temperature graphitized precursor

RECOVERY ACT AWARDS FOR ELECTRIC DRIVE VEHICLE BATTERY AND COMPONENT MANUFACTURING INITIATIVE			
Applicant	**DOE Award (Dollars in Millions)**	**Project Locations**	**Technology**
Company			anode material for lithium-ion batteries.
Pyrotek, Inc.	$11.3	Sanborn, NY	Production of carbon powder anode material for lithium-ion batteries.
H&T Waterbury DBA Bouffard Metal Goods	$5	Waterbury, CT	Manufacturing of precision aluminum casings for cylindrical cells.
Advanced Lithium-Ion Battery Recycling Facilities			
TOXCO Incorporated	$9.5	Lancaster, OH	Hydrothermal recycling of lithium-ion batteries.

Appendix B: List of Contributors and Research Collaborators

Contributor/Collaborator	Affiliation	Annual Progress Report Section(s)
Abkemeier, Kristin	New West Technologies	II
Abraham, Daniel P.	Argonne National Laboratory	IV.B.2, IV.C.1.1, IV.C.2.2, IV.B.5.1, IV.C.1.2, IV.C.1.3
Alamgir, Mohamed	Compact Power, Inc.	III.A.1.3
Allen, Jan L.	U.S. Army Research Laboratory	IV.B.5.3
Amine, Khalil	Argonne National Laboratory	IV.B.1, IV.B.3.1, IV.B.3.4, IV.B.4.1, IV.B.4.2, IV.B.5.2, IV.D.1, V.D.5
Andrew, Jansen	Argonne National Laboratory	IV.B.2
Arsenault, Renata	United States Advanced Battery Consortium	III.A.1.1
Ashtiani, Cyrus N.	Enerdel, Inc.	III.A.1.2, III.A.2.1
Balasubramanian, M.	Argonne National Laboratory	IV.B.4.3, IV.B.4.4, IV.C.1.3
Balsara, Nitash P.	Lawrence Berkeley National Laboratory	V.D.1
Bareno, J.	Argonne National Laboratory	IV.C.1.3
Barnes, James A.	Naval Surface Warfare Center/Department of Energy	II, III.A.3.8, III.D
Barnett, Brian	TIAX LLC	III.B.1
Basco, John	Argonne National Laboratory	III.C.1
Battaglia, Vince	Lawrence Berkeley National Laboratory	V.E.1
Belharouak, Ilias	Argonne National Laboratory	IV.B.4.5
Belt, Jeffrey R.	Idaho National Laboratory	III.C.2
Benedek, R.	Argonne National Laboratory	V.B.9
Bernardi, Dawn	United States Advanced Battery Consortium	III.A.1.2
Bloom, Ira	Argonne National Laboratory	III.C.1, IV.C.2.4
Ceder, Gerbrand	Massachusetts Institute of Technology	V.B.1
Christophersen, Jon P.	Idaho National Laboratory	IV.C.2.4
Cresce, Arthur von	U.S. Army Research Laboratory	IV.B.5.3
Daniel, Claus	Oak Ridge National Laboratory	IV.C.1.5, V.E.3
Dees, D.	Argonne National Laboratory	IV.C.1.2
Dees, Dennis	Argonne National Laboratory	IV.B.1, IV.B.2, IV.B.3.2, IV.C.2.1
Dees, Dennis W.	Argonne National Laboratory	IV.B.3.3, IV.C.1.1
Deppe, John B.	Deppe Consulting	All
Dillon, Anne C.	National Renewable Energy Laboratory	V.C.3
Doeff, Marca M.	Lawrence Berkeley National Laboratory	V.B.3
Dudney, Nancy J.	Oak Ridge National Laboratory	V.E.6
Duong, Tien Q.	U.S. Department of Energy	V
Einerson, Jeffrey	Idaho National Laboratory	IV.C.2.2
Elder, Ron	United States Advanced Battery Consortium	III.A.1.4, III.A.2.2
Emanuel, J.	ENTEK Membranes LLC	III.A.3.2
Engstrom, Scott	Johnson Controls-Saft, Inc.	III.A.1.1
Gaines, Linda	Argonne National Laboratory	III.B.6
Galusha, Jeremy	U.S. Department of Energy	IV
Gao, Yuan	FMC Corporation	III.A.3.5
Gering, Kevin L.	Idaho National Laboratory	IV.C.1.1, IV.C.2.2, IV.C.2.3
Gonder, Jeff	National Renewable Energy Laboratory	III.B.7
Goguen, Stephen	U.S. Department of Energy	II
Goodenough, John B.	University of Texas at Austin	V.C.4
Grey , Clare P.	Stony Brook University	V.B.1
Henderson, Wesley A.	North Carolina State University	V.D.6
Henriksen, Gary	Argonne National Laboratory	IV.B.1
Howell, David	U.S. Department of Energy	All
Jamison, David	Idaho National Laboratory	IV.C.2.3

Contributor/Collaborator	Affiliation	Annual Progress Report Section(s)
Jansen, Andrew N.	Argonne National Laboratory	IV.B.1, IV.B.3.2, IV.C.1.1, IV.C.1.2, IV.C.2.1
Jiang, Junwei	3M	III.A.3.3
Johnson, Chris	National Energy Technology Laboratory	III.A.3.4, III.A.3.5, III.A.3.6, III.A.3.7
Johnson, Christopher S.	Argonne National Laboratory	IV.B.4.3, IV.B.4.4, V.B.9
Jow, T. Richard	U.S. Army Research Laboratory	IV.B.5.3
Joyce, Chris	Argonne National Laboratory	IV.B.3.2, IV.C.2.1
Kang, Sun-Ho	Argonne National Laboratory	IV.B.1, IV.B.2, IV.B.4.3, IV.B.4.4, IV.C.1.1, IV.C.1.2, IV.C.1.3, IV.C.2.1, V.B.9
Karan, N.	University of Puerto-Rico	IV.C.1.3
Kerr, John B.	Lawrence Berkeley National Laboratory,	V.D.2
Keyser, Matt	National Renewable Energy Laboratory	III.C.4
Kim, Gi-Heon	National Renewable Energy Laboratory	IV.D.3
Kostecki, Robert	Lawrence Berkeley National Laboratory	V.C.2
Kumar, Bijayendra	Energetics, Incorporated	All
Kumta , Prashant N.	University of Pittsburgh	V.C.1
Lee, Hung-Sui	Brookhaven National Laboratory	IV.D.2, V.B.8
Lee, Se-Hee	University of Colorado, Boulder	V.C.4
Liu, Jun	Pacific Northwest National Laboratory	V.C.7
Lopez, Carmen M.	Argonne National Laboratory	IV.B.3.3, V.B.9
Lu, Wenquan	Argonne National Laboratory	IV.B.1, IV.B.2, IV.C.1.1, IV.C.2.1
Lucht , Brett L.	University of Rhode Island	IV.B.5.1, IV.C.1.2, V.D.7
Mansour, A. N.	Naval Surface Warfare Center	V.B.7
Manthiram, Arumugam	University of Texas at Austin	V.B.4
McLarnon, Frank	Lawrence Berkeley National Laboratory	IV.C.1.4
Mikhaylik, Yuriy	Sion Power	III.A.3.6
Nam, Kyung-Wan	Brookhaven National Laboratory	IV.D.2, V.B.8
Nelson, Paul	Argonne National Laboratory	IV.B.3.2, IV.C.2.1
Newman, John	Lawrence Berkeley National Laboratory	V.E.5
O'Keefe, Michael P.	National Renewable Energy Laboratory	III.B.4
Obrovac, Mark	3M	III.A.3.4
Orendorff, Christopher J.	Sandia National Laboratories	IV.D.5
Paik, Amy	United States Advanced Battery Consortium	III.A.3.1
Pekala, R.W.	ENTEK Membranes LLC	III.A.3.2
Pesaran, Ahmad	National Renewable Energy Laboratory	III.B.5, III.B.7
Petrov, I.	University of Illinois at Urbana-Champaign	IV.C.1.2, IV.C.1.3
Pham, Binh	Idaho National Laboratory	IV.C.2.2
Pinnell, Leslie	A123Systems	III.A.1.4
Pol, S. V.	Argonne National Laboratory	IV.B.4.3
Pol, Vilas G.	Argonne National Laboratory	IV.B.4.4, V.C.5
Prezas, Panos	Argonne National Laboratory	III.C.1
Protasiewicz, John D.	Case Western Reserve University	V.D.4
Richardson, Thomas	Lawrence Berkeley National Laboratory	V.B.2
Roth, E. Peter	Sandia National Laboratories	III.C.3, IV.D.4, IV.D.5
Sacco, Terri	A123Systems	III.A.2.2
Santini, Danilo J.	Argonne National Laboratory	III.B.2
Sastry, Ann Marie	University of Michigan	V.E.2, V.E.3
Sazhin, Sergiy	Idaho National Laboratory	IV.C.2.3
Scherson, Daniel A.	Case Western Reserve University	V.D.4
Shao-Horn, Yang	Massachusetts Institute of Technology	V.B.7
Shin, D.	Northwestern University	V.B.9, V.C.5

Contributor/Collaborator	Affiliation	Annual Progress Report Section(s)
Singh, Dileep	Argonne National Laboratory	IV.B.3.2
Smart , Marshall C.	Jet Propulsion Laboratory	IV.B.5.4
Smith, Grant D.	University of Utah	V.D.3
Smith, Kandler	National Renewable Energy Laboratory	III.
Smith, Ron	Celgard, LLC.	III.A.3.1
Srinivasan, Venkat	Lawrence Berkeley National Laboratory	V.E.4
Stamos, Euthemios	United States Advanced Battery Consortium	III.A.2.1
Tataria, Harshad	United States Advanced Battery Consortium	III.A.1.3, III.A.3.2, III.A.3.3
Thackeray, Michael	Argonne National Laboratory	IV.B.4.3, IV.B.4.4, V.B.9, V.C.5
Thurston, Anthony M.	BASF Catalysts, LLC	III.A.3.7
Trahey, L.	Argonne National Laboratory	V.C.5
Vaughey, John T.	Argonne National Laboratory	IV.B.3.2, IV.B.3.3, V.C.5
Veselka, Nick	Argonne National Laboratory	IV.B.3.2
Walker, Lee	Argonne National Laboratory	III.C.1
Wang, Xiaojian	Brookhaven National Laboratory	IV.D.2, V.B.8
Waterhouse, R.	ENTEK Membranes LLC	III.A.3.2
Weinstock, Irwin M.	Sentech, Inc.	I.B.2, V
Whittingham, M. Stanley	SUNY at Binghamton	V.B.5, V.C.6
Wolverton, C.	Northwestern University	V.B.9, V.C.5
Xu, Kang	U.S. Army Research Laboratory	IV.B.5.3
Yakovleva, Marina	FMC Corporation	III.A.3.5
Yang, Xiao-Qing	Brookhaven National Laboratory	IV.D.2, V.B.8
Zaghib, Karim	Hydro-Quebec IREQ.	V.B.6
Zhang, Ji-Guang	Pacific Northwest National Laboratory	V.B.10, V.C.7

Appendix C: Acronyms

AAS	Atomic absorption spectroscopy
ABCD	Advanced Battery Coalition for Drivetrains
ABR	Applied Battery Research for Transportation
AC	Alternating Current
ACN	Acetonitrile
ACS	American Chemical Society
AE	Available energy
AER	All electric range
AGM	Absorbed Glass Mat
ALD	Atomic layer deposition
ANL	Argonne National Laboratory
APS	Advanced Photon Source
ARC	Accelerated rate calorimetry
ARL	Army Research Laboratory
ARRA	American Recovery & Reinvestment Act
ARXPS	Angle resolved X-ray photoelectron spectroscopy
ASI	Area specific impedance
ASME	American Society of Mechanical Engineers
ATD	Advanced Technology Development
ATR	Attenuated total reflection
BAJ	Battery Institute of Japan
BATT	Batteries for Advanced Transportation Technologies
BBAR	boron based anion receptors
BCF	Binder and carbon free
BDS	Battery Design Studio
BET	Brunauer, Emmett, and Teller surface area
BF	Binder free
BL	Base line
BM	Bending magnet beamline
BNL	Brookhaven National Laboratory
BOB-	bis(oxalate) borate
BSF	Battery scaling factor
CBCF	Carbon bonded carbon fibers
CBED	Convergent beam electron diffraction
C_{ch}	Charge rate
CD	Charge depleting
C_{dis}	Discharge rate
CE	Counter electrode
CID	Current interrupt device
CLTF2009	Southern China Li-ion Battery Top Forum 2009
CMC	Sodium Carboxy Methyl Cellulose
COGS	Cost of goods sold
COP	ConocoPhillips
CPI	Compact Power Inc.
CRADA	Cooperative research and development agreement
CS	Charge-sustaining
CV	Cyclic voltammogram
CVD	Chemical vapor deposition
CWRU	Case Western Reserve University
DEC	Diethyl carbonate
DFT	Density function theory
DHF	dihydrofuran

DMC	Dimethyl carbonate
DOD	Depth-of-discharge
DOE	Department of Energy
DOEx	Design of experiment
DOH	Degree of hybridization
DPA	Destructive physical analysis
DSC	Differential scanning calorimetry
DT	Diagnostic Testing
DVP&R	Design, validation, plan, and report
EC	Ethylene carbonate
ECS	Electrochemical Society
EDLC	Electrical double layer capacitor
EDS	Energy dispersive spectroscopy
EDV	Electric Drive Vehicle
EIA	Energy Information Administration
EIS	Electrochemical impedance spectroscopy
EMC	Ethyl methyl carbonate
EMIM	1-ethyl-3-methyl imidizolium
EMI-TFSI	1-ethyl-3-methylimidazolium - Bis(fluorosulfonyl)imide
EOL	End of life
EPD	Electrophoretic deposition
EPMA	electron-probe X-ray micro-analysis
EPR	Electron paramagnetic resonance
EPRI	Electric Power Research Institute
EREV	Extended range electric vehicle
ESS	Energy storage system
EUCAR	European Council for Automotive Research and Development
EV	Electric vehicle
EXAFS	Extended X-ray absorption fine structure
FCV	Fuel cell vehicle
FE	Finite element
FEC	fluoro ethylene carbonate
FEM	Finite Element Model
FFCC	FutureFuel Chemical Company
FFT	Fast Fourier Transforms
FIB	Focused Ion Beam
FLC	Federal Laboratory Consortium for Technology Transfer
FSI	(fluorosulfonyl)-imide
FT	Fourier Transform
FTIR	Fourier transform infrared
FVM	Finite volume method
GC	Gas chromatography
GDE	gas-diffusion-electrodes
GHG	Green house gases
GITT	Galvanostatic intermittent titration technique
GM	General Motors
GPC	Gel-permeation chromatography
GVL	γ-valerolactone
HAADF	High angle annular dark field
HDPE	High density polyethylene
HEMM	High energy mechanical milling
HEV	Hybrid electric vehicle

HF	Hydrofluoric acid
HHV	High heating value
HOPG	Highly oriented pyrolytic graphite
HPL	High Power Lithium
HPPC	Hybrid pulse power characterization
HQ	Hydro-Québec
HRTEM	High resolution transmission electron microscopy
HTMI	High temperature melt integrity
HVAC	Heating, ventilation, and air-conditioning
HWCVD	Hot-wire chemical vapor deposition
IACIS	International Conference on Surface and Colloid Science
IA-HEV	Implementing Agreement - hybrid electric vehicles
IBA	International Battery Materials Association
ICE	Internal combustion engine
ICEPS	International Conference on Electrochemical Power Systems
ICL	Irreversible capacity loss
ICP	Inductively coupled plasma
IEA	International Energy Agency
IEEE	Institute of Electrical and Electronics Engineers
IL	Ionic liquids
IMLB	International Meeting on Lithium Batteries
IMPRES	Innovative Materials for Processes in Energy Systems
INL	Idaho National Laboratory
IR	Infra-red
JCI	Johnson Controls, Incorporated
JCPDS	Joint Committee on Power Diffraction System
JCS	Johnson Controls - Saft
JECS	Journal of the Electrochemical Society
JPL	Jet Propulsion Laboratory
JPS	Journal of Power Sources
JR	Jelly Roll
kHz	kilo-Hertz
kW	kilo-Watt
kWh	kilo-Watt Hour
LBNL	Lawrence Berkeley National Laboratory
LCC	Linear cyclic carbonate
LCR	Inductance, capacitance, and resistance
LDV	Light-duty vehicle
LEC	Lithium excess cathode
LFP	Li iron phosphate
LFP-G	Li iron phosphate - graphite
LIB	Lithium-ion battery
LiBOB	Lithium bis(oxolato)borate
LIC	Lithium-ion capacitor
LiTFSI	Lithium bis(trifluoromethane-sulfonyl)imide
LMNO	Lithium manganese nickel oxide
LMNO/LTO	Lithium manganese nickel oxide/Lithium Titatate
LMO	Lithium manganese oxide
LMO-G	Lithium manganese oxide - graphite
LTO	Lithium titanate, $Li_4Ti_5O_{12}$
LTS	Load-to-short
LUMO	Lowest unoccupied molecular orbital

MAC	methyl allyl carbonate
MAG	Massive activated graphite
MAS	methyl allyl sulfone
MBB	Module Balance Board
MCMB	Mesocarbon micro beads
MD	Molecular dynamics
MEK	Methyl ethyl ketone
MES	Mitsui Engineering Shipbuilding
MF	Morphology factor
MHz	Megahertz
MIT	Massachusetts Institute of Technology
M-O	Metal - oxygen
MPC	methyl propargyl carbonate
MPPC	Minimum pulse power characterization
MPS	methyl propargyl sulfone
MRS	Materials Research Society
MS	Mass spectroscopy
MSA	mean spherical approximation
MSMD	Multi-scale, multi-dimensional
MW	Molecular weight
MWCNT	Multi-walled carbon nanotubes
MW-HT	Microwave-hydrothermal method
MW-ST	Microwave-solvothermal
NASA	National Aeronautics and Space Administration
NCA	$LiNi_{0.8}Co_{0.15}Al_{0.05}O_2$
NCA-G	$LiNi_{0.8}Co_{0.15}Al_{0.05}O_2$ - graphite
NCM	$Li_{1+w}[Ni_xCo_yMn_z]1\text{-}wO_2$
NCS	Nanocomposite separator
NCSU	North Carolina State University
n_{cyc}	Net number of complete formation cycles per cell
NETL	National Energy Technology Laboratory
NG	Natural gas
NHTS	National Household Travel Survey
NIMS	National Institute for Material Science (Japan)
NIST	National Institute of Standards and Technology
NMC	$LiNi_{1/3}Co_{1/3}Mn_{1/3}O_2$
NMP	N-methylpyrrolidone
NMR	Nuclear magnetic resonance
NREL	National Renewable Energy Laboratory
NSF	National Science Foundation
NYSERDA	New York State Energy Research and Development Authority
OCP	Open circuit potential
OCV	Open circuit voltage
OECD	Organization for Economic Cooperation and Development
OEM	Original equipment manufacturer
OFD	Oregon Freeze Dry
ORNL	Oak Ridge National Laboratory
OTS	off the shelf
OVT	Office of Vehicle Technologies
PAAH	poly acrylic acid polymer
PAn	Polyaniline
PC	Propylene carbonate

PCA	Principal component analysis
PDF	Pair distribution function
PE	polyethylene
PEDOT	p-toluene sulfonic acid (p-TSA) doped poly(3,4-ethylenedioxythiophene)
PEO	Poly(ethylene oxide)
PEY	Partial electron yield
PFPBO	pentafluorophenylboron oxalate
PFPTFBB	pentafluorophenyl)-tetrafluoro-1,3,2-benzodioxaborole
PHEV	Plug-in hybrid electric vehicle
PLD	Pulse laser deposition
PNGV	Partnership for a new generation of vehicles
PNNL	Pacific Northwest National Laboratory
PP/PE	Polypropylene/Polyethylene
PPT	Porous Power Technologies
PS	Polystyrene
PSAT	Powertrain System Analysis Toolkit
PVD	Physical Vapor Deposition
PVdF	Poly(vinylidene fluoride)
QM/MM	Quantum Mechanical / Molecular Mechanical
R&D	Research and development
RDE	Rotating-disk-electrode
RE	Reference electrode
RMS	Root mean square
RTIL	room-temperature ionic-liquid
RVE	Response variable expressions
SAD	Selected area diffraction
SAED	Selected area electrode diffraction
SBIR	Small Business Innovative Research
SBIR/STTR	Small Business Innovative Research/Small Business Technology Transfer
SCE	Saturated calomel electrode
SCFM	Standard cubic feet per minute.
SEI	Solid electrolyte interphase
SEM	Scanning electron microscopy
SENB	Single Edged Notched Bend
SIC	Single ion conducting
SIMS	Secondary ion mass spectrometry
SLMP	stabilized lithium metal powder
SLPB	Superior Lithium Polymer Battery
SMG	Surface modified graphite
SNL	Sandia National Laboratories
SOC	State of charge
SPE	Solid polymer electrolytes
SRPT	Stored Response Pattern Tester
SRS	Safety Reinforcing Separator
SSEF	Sigmoidally-screened electrostatic function
STEM	Scanning transmission electron microscope
STTR	Small Business Technology Transfer Program
SUNY	State University of New York
SWNT	Single-walled nanotube
T	Temperature
TD	Transverse direction
TEM	Transmission electron microscopy

TFSI	bis(trifluoromethanesulfonyl)imide
TGA	Thermal gravimetric analysis
TLVT	Technology life verification test
TM	Transition metal
t_{ocv}	Time at open circuit potential
TOF-SIMS	Time of flight secondary ion mass spectrometry
TPD	Temperature programmed desorption
TPFPB	tris(pentafluorophenyl) borane
TR-XRD	time-resolved X-ray diffraction
UCV	Upper cutoff voltage
UDDS	Urban Dynamometer Driving Schedule
UHMWPE	Ultrahigh molecular weight polyethylene
UM	University of Michigan
UN	United Nations
UN/DOT	United Nations/Department of Transportation
URI	University of Rhode Island
U.S.	United States
USABC	United States Advanced Battery Consortium
USCAR	United States Council for Automotive Research
USGS	United States Geological Survey
UTA	University of Texas at Austin
UU	University of Utah
VC	Vinylene carbonate
VCCT	Virtual Crack Closure Technique
VEC	Vinyl ethylene carbonate
VMT	Vehicle miles travelled
VPPC	Vehicle Power and Propulsion Conference
VRLA	Valve Regulated Lead-Acid
VS	Vinylene triacetoxyvinylsilane
VT	Vehicle Technologies
WDB	Water dispersed binder
WTW	Well to wheels
XAFS	X-Ray absorption fine structure
XANES	X-Ray absorption near edge structure
XAS	X-Ray absorption spectroscopy
XLHDPE	Cross linkable polyethylene
XMD	Cross-machine direction
XPS	X-ray photoelectron spectroscopy
XRD	X-ray diffraction

EPARTMENT OF ENERGY | Energy Ef ı ıency & Renewable Energy

For more information
1-877-EERE-INF (1.877.337.3463)
programname.energy.gov